VOL. 691 NOS. 1 + 2 3 FEBRUARY 1995
COMPLETE IN ONE ISSUE

18th International Symposium on Column Liquid Chromatography Minneapolis, MN, 8–13 May 1994 Part I

JOURNAL OF CHROMATOGRAPHY A

INCLUDING ELECTROPHORESIS AND OTHER SEPARATION METHODS

ELSEVIER

JOURNAL OF CHROMATOGRAPHY A

INCLUDING ELECTROPHORESIS AND OTHER SEPARATION METHODS

Scope. The *Journal of Chromatography A* publishes papers on all aspects of **chromatography, electrophoresis** and related methods. Contributions consist mainly of research papers dealing with chromatographic theory, instrumental developments and their applications. In the *Symposium volumes*, which are under separate editorship, proceedings of symposia on chromatography, electrophoresis and related methods are published. *Journal of Chromatography B: Biomedical Applications* —This journal, which is under separate editorship, deals with the following aspects: developments in and applications of chromatographic and electrophoretic techniques related to clinical diagnosis or alterations during medical treatment; screening and profiling of body fluids or tissues related to the analysis of active substances and to metabolic disorders; drug level monitoring and pharmacokinetic studies; clinical toxicology; forensic medicine; veterinary medicine; occupational medicine; results from basic medical research with direct consequences in clinical practice.

Submission of Papers. The preferred medium of submission is on disk with accompanying manuscript (see *Electronic manuscripts* in the Instructions to Authors, which can be obtained from the publisher, Elsevier Science B.V., P.O. Box 330, 1000 AH Amsterdam, Netherlands). Manuscripts (in English; *four* copies are required) should be submitted to: Editorial Office of *Journal of Chromatography A*, P.O. Box 681, 1000 AR Amsterdam, Netherlands, Telefax (+31-20) 485 2304, or to: The Editor of *Journal of Chromatography B: Biomedical Applications*, P.O. Box 681, 1000 AR Amsterdam, Netherlands. Review articles are invited or proposed in writing to the Editors who welcome suggestions for subjects. An outline of the proposed review should first be forwarded to the Editors for preliminary discussion prior to preparation. Submission of an article is understood to imply that the article is original and unpublished and is not being considered for publication elsewhere. For copyright regulations, see below.

Publication information. *Journal of Chromatography A* (ISSN 0021-9673): for 1995 Vols. 683–714 are scheduled for publication. *Journal of Chromatography B: Biomedical Applications* (ISSN 0378-4347): for 1995 Vols. 663–674 are scheduled for publication. Subscription prices for *Journal of Chromatography A*, *Journal of Chromatography B: Biomedical Applications* or a combined subscription are available upon request from the publisher. Subscriptions are accepted on a prepaid basis only and are entered on a calendar year basis. Issues are sent by surface mail except to the following countries where air delivery via SAL is ensured: Argentina, Australia, Brazil, Canada, China, Hong Kong, India, Israel, Japan, Malaysia, Mexico, New Zealand, Pakistan, Singapore, South Africa, South Korea, Taiwan, Thailand, USA. For all other countries airmail rates are available upon request. Claims for missing issues must be made within six months of our publication (mailing) date. Please address all your requests regarding orders and subscription queries to: Elsevier Science B.V., Journal Department, P.O. Box 211, 1000 AE Amsterdam, Netherlands. Tel.: (+31-20) 485 3642; Fax: (+31-20) 485 3598. Customers in the USA and Canada wishing information on this and other Elsevier journals, please contact Journal Information Center, Elsevier Science Inc., 655 Avenue of the Americas, New York, NY 10010, USA, Tel. (+1-212) 633 3750, Telefax (+1-212) 633 3764.

Abstracts/Contents Lists published in Analytical Abstracts, Biochemical Abstracts, Biological Abstracts, Chemical Abstracts, Chemical Titles, Chromatography Abstracts, Current Awareness in Biological Sciences (CABS), Current Contents/Life Sciences, Current Contents/Physical, Chemical & Earth Sciences, Deep-Sea Research/Part B: Oceanographic Literature Review, Excerpta Medica, Index Medicus, Mass Spectrometry Bulletin, PASCAL-CNRS, Referativnyi Zhurnal, Research Alert and Science Citation Index.

US Mailing Notice. *Journal of Chromatography A* (ISSN 0021-9673) is published weekly (total 52 issues) by Elsevier Science B.V., (Sara Burgerhartstraat 25, P.O. Box 211, 1000 AE Amsterdam, Netherlands). Annual subscription price in the USA US$ 5389.00 (US$ price valid in North, Central and South America only) including air speed delivery. Second class postage paid at Jamaica, NY 11431. **USA POSTMASTERS**: Send address changes to *Journal of Chromatography A*, Publications Expediting, Inc., 200 Meacham Avenue, Elmont, NY 11003. Airfreight and mailing in the USA by Publications Expediting.

See inside back cover for Publication Schedule, Information for Authors and information on Advertisements.

0021-9673/95/$09.50

Printed in the Netherlands

For Contents see p. VII.

JOURNAL OF CHROMATOGRAPHY A

VOL. 691 (1995)

JOURNAL OF CHROMATOGRAPHY A

INCLUDING ELECTROPHORESIS AND OTHER SEPARATION METHODS

ELSEVIER

Amsterdam – Lausanne – New York – Oxford – Shannon – Tokyo

0021-9673/95/$09.50

SYMPOSIUM VOLUME

18TH INTERNATIONAL SYMPOSIUM ON COLUMN LIQUID CHROMATOGRAPHY

PART I

Minneapolis, MN (USA), 8–13 May 1994

Guest Editor

L.D. BOWERS
(Indianapolis, IN, USA)

The papers submitted for the Symposium Volumes on the *18th International Symposium on Column Liquid Chromatography* are published in two consecutive Volumes of the *Journal of Chromatography A*, Vols. 691 and 692 (1995). The Foreword only appears in Vol. 691. A combined Author Index to both Vols. 691 and 692 only appears in Vol. 692.

VOL. 691, NOS. 1 + 2 JOURNAL OF CHROMATOGRAPHY A 3 FEBRUARY 1995

CONTENTS

(Abstracts/Contents Lists published in Analytical Abstracts, Biochemical Abstracts, Biological Abstracts, Chemical Abstracts, Chemical Titles, Chromatography Abstracts, Current Awareness in Biological Sciences (CABS), Current Contents/Life Sciences, Current Contents/Physical, Chemical & Earth Sciences, Deep-Sea Research/Part B: Oceanographic Literature Review, Excerpta Medica, Index Medicus, Mass Spectrometry Bulletin, PASCAL-CNRS, Referativnyi Zhurnal, Research Alert and Science Citation Index)

18TH INTERNATIONAL SYMPOSIUM ON COLUMN LIQUID CHROMATOGRAPHY, MINNEAPOLIS, MN, USA, 8–13 MAY 1994

GENERAL, THEORY AND DETECTION

SORBENTS, COLUMNS, PROCEDURES CHIRAL SEPARATIONS

ELSEVIER

Journal of Chromatography A, 691 (1995) 1

JOURNAL OF CHROMATOGRAPHY A

Foreword

It seems appropriate that the *18th International Symposium on Column Liquid Chromatography* (HPLC '94) was held in the Twin Cities of Minneapolis/St. Paul, MN, USA, on the 30th anniversary of the discovery of high-performance liquid chromatography (HPLC). Professor L.S. Palmer, who spent much of his professional career on the faculty of the University of Minnesota, is widely credited with popularizing column liquid chromatography in the USA. More recently, the Minnesota Chromatography Forum was one of the more active chromatography discussion groups in the USA. So when over 800 delegates gathered in the Twin Cities on May 9–13, 1994 to attend some of the 96 oral presentations and to view the more than 350 posters on display, it added one more chapter to the history of chromatography.

The commercial chromatography community is owed another round of thanks for their support of the latest in this series of meetings. Not only did they exhibit their wares in 96 booths in the midst of the posters, but they supplied much needed financial support for many of the important aspects of the meeting. Twelve of the companies presented scientific workshops, a well-received new feature at HPLC '94, on state-of-the-art products and accessories.

Making a meeting like HPLC '94 a scientific success requires the work of many dedicated individuals. Professor Peter Carr, Program Chairman, and the Scientific Committee contributed greatly to the flow and the excellence of the program. Our goal to encourage personal interactions as well as more formal exchanges was by all accounts successful. Professor Barry Karger was very supportive during an unexpected medical emergency. I would also like to recognize Mr. Peter Johnson who was always willing to complete a critical task. The Education Committee of the MCF ably organized the details of the four short courses. The members of the Permanent Scientific Committee contributed invaluable insight at various crucial stages of the meeting planning.

Organization of such a symposium would be impossible without the assistance of an experienced professional. From the early planning stages, through registration, to assuring that delegates had a wonderful experience on site, Janet Cunningham of Barr Enterprises had a large role in the smooth operation of the meeting. It was a pleasure to work with her and her staff.

I want to express particular thanks to the graduate students from Professor Peter Carr's and my research groups. Many of the details which contribute to the seemingly effortless flow of the scientific sessions were handled by these individuals. Particular recognition must be given to Christopher Dunlap and Paul Jackson who went beyond the call of duty. The manuscripts that follow summarize the science of HPLC '94. We cannot reproduce here the wonderful weather, the solar eclipse, the magnificent music, and the fellowship which were its soul. I thank the Permanent Committee and the attendees for providing me with such a memorable professional opportunity.

Indianapolis, IN, USA Larry D. Bowers
General Chairman, HPLC '94

SSDI 0021-9673(94)01266-0

ELSEVIER

Journal of Chromatography A, 691 (1995) 3–19

JOURNAL OF CHROMATOGRAPHY A

High pH mobile phase effects on silica-based reversed-phase high-performance liquid chromatographic columns

J.J. Kirkland[a,*], M.A. van Straten[b], H.A. Claessens[b]

[a]*Rockland Technologies, Inc., 538 First State Boulevard, Newport, DE 19804, USA*

[b]*Eindhoven University of Technology, Department of Chemistry, P.O. Box 513, 5600 MB Eindhoven, Netherlands*

Abstract

Aqueous mobile phases above pH 8 often cause premature column failure, limiting the utility of silica-based columns for applications requiring high pH. Previous studies suggest that covalently bound silane ligands are hydrolyzed and removed by high-pH mobile phases. However, we found that the siloxane bonds for certain monomeric silanes are hydrolyzed very slowly from silica supports at pH 9–10. Therefore, bonded-phase packing degradation at high pH is a result mainly of silica support dissolution. The rate of column degradation for C_{18} columns is influenced not only by the type and purity of silica support, but also by the nature of the silane stationary phase. We found different rates of degradation for several commercial C_{18} columns. The relative rates of silica dissolution for these packings were determined by chemically measuring the silicate formed during column purging at high pH. The type and concentration of mobile phase organic modifier also significantly influences column degradation at high pH. Certain silica-based C_{18} packings can be used for long periods at pH 9 without significant changes in chromatographic properties. Results of this study better define the practical utility and limitations of silica-based columns in high pH environments.

1. Introduction

Based mainly on manufacturers recommendations, most workers do not attempt reversed-phase separations on silica-based bonded-phase columns with mobile phases above pH 8. This practice apparently is based on early studies with columns of certain silica supports [1,2]. These early studies showed that the rate of column degradation was dependent on the type of base and the concentration of organic modifier used in the mobile phase. Other workers also found that the rate of silica dissolution for untreated silica at pH 9–10 was reduced in high concentrations of organic modifier, especially when ammonia was the source of hydroxyl ions [3,4]. Another study showed that dissolution of unmodified chromatographic silica was affected by the type and concentration of salts in the mobile phase [5]. Vigorous treatment of unmodified chromatographic silicas with certain bases also caused significant changes in surface areas and pore structure [6]. More recently, work with a specific untreated chromatographic silica showed that this material could be used for extended periods with pH 9.2 methanol–buffer mobile phase for good results, provided the column inlet was repacked when performance decreased [7].

The study herein reported provides additional insight regarding the utility of silica-based bond-

* Corresponding author.

0021-9673/95/$09.50
SSDI 0021-9673(94)00631-8

ed-phase column packings in high-pH aqueous mobile phases. Although basic compounds often are separated at low pH [8,9] or with ion-pairing agents [9], there are instances when reversed-phase operation at high pH is preferred. Previous studies have not defined how differences in the silica support and different stationary phases influence column stabilities at high pH. Also, the reasons for the degradation of silica-based, bonded-phase columns under various operating conditions were not verified. Therefore, a wider range of information was needed to better define the potential utility of silica-based column packings for reversed-phase HPLC.

2. Experimental

2.1. Chromatographic columns

All 15 × 0.46 cm I.D. Zorbax columns were prepared by Rockland Technologies. Comparable Zorbax SB-C_8 (diisopropyl-C_8), Zorbax Rx-C_{18} (dimethyl-C_{18}), Zorbax SB-C_{18} (diisobutyl-C_{18}), and Zorbax-ODS (dimethyl-C_{18}) columns are available from Mac-Mod Analytical (Chadds Ford, PA, USA). The 15 × 0.39 cm I.D. Novapak C_{18} column was from Waters Assoc. (part No. 86344; lot No. T-32451; Milford, MA, USA). 15 × 0.46 cm I.D. Hypersil ODS (cat. No. 9875; SN 93091196) and Nucleosil C_{18} (cat. No. 89161; SN 93091195) columns were obtained from Alltech (Deerfield, IL, USA). LiChrosorb C_{18} columns were packed at Eindhoven Technical University using packing obtained from Merck (Darmstadt, Germany). Typical physical characteristics of the silicas used in these columns are summarized in Table 1. In Table 1, Type A refers to more acidic, less purified silica supports, while Types B are the less acidic, highly purified silicas [6].

The purity of the silica supports used for the alkyl-bonded phase columns tested is summarized in Table 2. Absolute silica purity suggested by these results may not be totally comparable, since analyses may have been conducted by methods with different levels of detectability for the various elements.

2.2. Silica support solubility study

Apparatus and reagents

Columns were purged with a Model 100A pump (Beckman, Fullerton, CA, USA). Eluent fractions were collected with a Waters P/N 37040 fraction collector (Waters, Milford, MA, USA).

Table 1
Typical physical properties of silica supports for C_{18} columns studied

Column name	Silica type[a]	Pore size (nm)	Surface area (m^2/g)	% Volume porosity[b] (ml/ml)	Ref.
Hypersil ODS	A	12	170	57	10
LiChrosorb C_{18}	A	10	355	71	11
Novapak C_{18}	A/B	6	N/A[c]	N/A	12
Nucleosil C_{18}	B	10	350	69	10
Zorbax-ODS	A	6	300	55	10
Zorbax Rx-C_{18}	B	8	180	50	13
Zorbax SB-C_8, C_{18}	B	8	180	50	13

[a] Based on data in Refs. [9,13].
[b] Calculated as in Ref. [14].
[c] N/A = not available.

Table 2
Typical impurity levels in silica supports

Silica	Na	K	Mg	Al	Ca	Ti	Fe	Zr	Cu	Cr	Zn	Ref.
Hypersil	2900	N/A	40	300	38	65	230	N/A	N/A	N/A	N/A	27
Nucleosil	56	N/A	N/A	nd	130	57	76	nd	N/A	N/A	nd	16
Zorbax-SIL	17	nd	nd	57	9	32	21	88	<1	nd	88	15
Zorbax Rx-SIL	10	<3	4	1.5	2	nd	3	nd	nd	nd	1	13,15

Metal concentration, ppm. Data for impurity levels in LiChrosorb and Novapak were not available. N/A = not available. nd = Not detected by the analytical method used.

Absorbance measurements were with a Zeiss MM 12 UV–Vis spectrophotometer (Carl Zeiss, Oberkocken/Württemberg, Germany). All chemicals and solvents were of analytical grade from Merck. Silicate standard solutions also were from Merck. Buffers and reagent solutions were prepared from deionized water from a MILLI-Q purification system (Millipore, Bedford, MA, USA): eluent I: methanol–0.1 *M* sodium carbonate/bicarbonate buffer, pH 10.0 (50:50, v/v) (overall buffer concentration 0.05 *M*); eluent II: acetonitrile–0.084 *M* sodium carbonate/bicarbonate buffer pH 10.0 (40.6:59.4, v/v) (overall buffer concentration 0.05 *M*).

Different concentrations of methanol and acetonitrile were used in these tests to maintain equal-strength mobile phases for the tests —acetonitrile is a stronger modifier [9].

Procedures

Columns were continuously purged at 1.0 ml/min with eluents I or II. To maintain an equivalent linear velocity, a flow-rate of 0.72 ml/min was used for the NovaPak column. To simulate usual chromatographic practice, mobile phases were *not* recycled. Tests were at ambient temperature (about 22°C). All columns were flushed for 10 min with a mixture of methanol–water (1:1) prior to the dissolution experiments. After a specific dissolution experiment was begun, the column effluent was sampled after 1 h. After that, the column effluent was sampled every 8–10 h using a fraction collector. Column effluent samples for silicate analysis were collected for a 5-min period (total: 5 ml; for the Novapak column: 3.6 ml).

We measured silica concentrations colorimetrically in collected fractions using the well-known silicomolybdate complex method [18]. Absorbance was measured at 410 nm in 1-cm cuvets. For the silica measurement, standard silicate mixtures were prepared in the concentration range of 1.0 to 20.0 mg Si/l. These standard mixtures were prepared in the corresponding buffer–modifier purge solutions used in the dissolution studies. Absorbance values were measured using blank solutions as reference. Results were plotted of the silica concentration in the column effluent as a function of the volume of effluent. The total silica dissolved from the column was first determined by using the silica average of two consecutive fractions. Then, the corresponding intermediate eluent volume was calculated. By multiplying these values and summing the mass of silica over the total effluent volume, cumulative plots then were obtained which represented the mass of silica which had been removed as a function of eluent volume flushed through the column.

2.3. Chromatographic column degradation studies

Apparatus and reagents

Analytical-grade methanol, sodium hydroxide and Na_2HPO_4 were from Baker (Phillipsburg, NJ, USA). EM Science (Gibbstown, NJ, USA) supplied HPLC-grade methanol and acetonitrile for chromatographic measurements. Test solutes were from Chem Service (West Chester, PA,

USA). Column purging ("ageing") studies at pH 9 were performed with a Shimadzu Model LC-600 pump. Column testing for the pH 9 study was with a DuPont Model 860 pump and Model 860 UV absorbance detector. Column ageing and testing at pH 12.3 used a Hewlett-Packard Model 1050 pump/detector system (Wilmington, DE, USA). Chromatographic samples were injected with a Rheodyne Model 7125 sampling valve (Cotati, CA, USA).

Column ageing procedures

For the pH 9 study, methanol–0.01 *M* phosphate solution (60:40) or acetonitrile–0.01 *M* phosphate solution (50:50) was continuously pumped through each column at a flow-rate of 1.0 ml/min at ambient temperature (ca. 22°C). As in the silica solubility study, to simulate actual chromatographic usage, the mobile phase purge was not recycled. The different organic modifier concentrations in both the silica support dissolution and column ageing studies were used to maintain solvent strength approximately constant, according to published solvent strength relationships [9]. The phosphate solution was made by adjusting 0.01 *M* Na_2HPO_4 to pH 9.0 with 4 *M* sodium hydroxide solution. (Note: phosphate solutions do not buffer strongly at pH 9.) Periodically during this purging routine, the columns were flushed with at least 20 column volumes of methanol–water (60:40), and 5 μl of a test solution chromatographed. This test mixture consisted of 0.02, 0.10, 0.033, 0.033, 0.20, 0.20 mg/ml each of uracil (t_0 marker), benzamide, 4-bromoacetanilide, N,N′-dimethylaniline, naphthalene, and N,N′-diethylaniline, respectively, in methanol–water (50:50).

For pH 12.3 tests, methanol–0.02 *M* sodium hydroxide (50:50) was continuously purged through a column of dimethyl-C_{18} (Zorbax Rx-C_{18}) at ambient temperature (ca. 22°C). Periodically the column was injected with 5 μl of a test solution consisting of 0.05, 0.5, 0.01, and 1.0 mg/ml each of uracil (t_0 marker), phenol, N,N′-dimethylaniline, and toluene, respectively, in methanol–water (50:50).

3. Results and discussion

Previous studies have shown that silica-based columns at high pH resulted in eventual deterioration of the silica support [1–5]. However, the rate and extent of degradation appeared to vary, depending on the silica, mobile phase and other conditions. Our interest was to better define the factors controlling deterioration of the silica support for bonded-phase packings at high pH. With more information, it was anticipated that a wider utility of silica-based packings in higher pH environments might be feasible.

We used two different experimental approaches to obtain information on the stability of silica-based bonded-phase packings. First, columns of various packings were continuously purged with pH 10 aqueous–organic mobile phases. The resulting dissolved silicate was measured with the well-known molybdate color reaction. Second, columns were continuously purged with organic-modified pH 9.0 and 12.3 mobile phases, and packed-bed stability and change in bonded stationary phase measured chromatographically. In both approaches, we found that the mobile phase organic modifier, silica support type, and the type of silane bonded phase all can affect the rate of silica support degradation.

3.1. Silica support solubility studies

The repeatability of experiments to measure the rate of silica dissolution was tested by performing duplicate experiments with columns of a monomeric dimethyl-C_{18} bonded-phase on a highly purified silica support (Zorbax Rx-C_{18}). Two columns each were tested with both methanol- and acetonitrile-modified pH 10 mobile phases. The pH 10 environment was chosen to ensure sufficient solubility of the silica supports for precise and meaningful measurements of silica in the collected fractions. Fig. 1 shows the amount of silica dissolved from these four different columns as a function of the volume of eluted mobile phase. These results confirm that

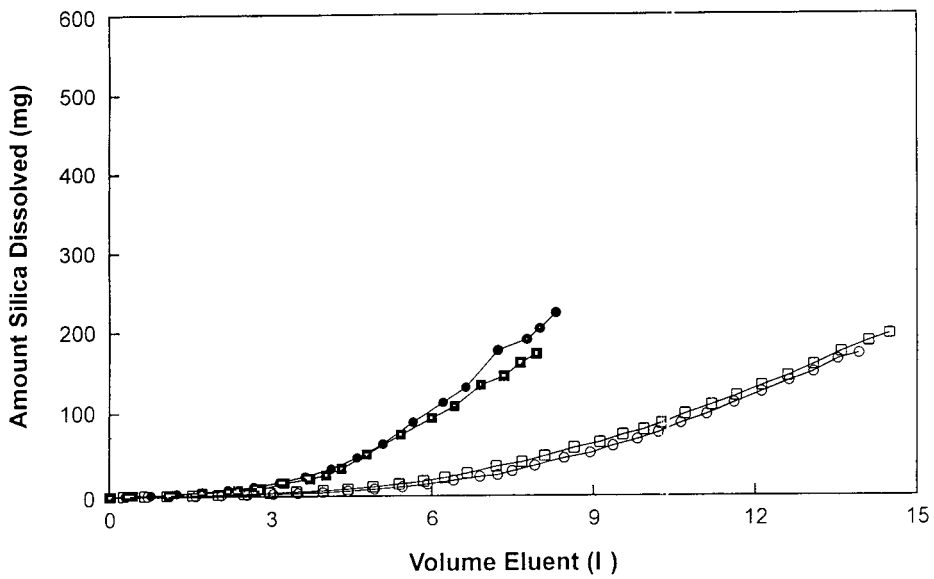

Fig. 1. Reproducibility of tests for silica support dissolution. Columns (A = ○; B = □): 15 × 0.46 cm I.D. Zorbax Rx-C_{18} (dimethyl-C_{18}); duplicate tests with mobile phases: methanol–sodium carbonate/bicarbonate (0.1 *M*) buffer pH 10.0 (50:50, v/v) (solid symbols) and acetonitrile–sodium carbonate/bicarbonate buffer (0.084 *M*) buffer pH 10.0 (40.6:59.4, v/v) (open symbols); flow-rate: 1.0 ml/min; ambient temperature; molybdate colorimetric analysis for dissolved silicate.

the test and analytical measurements method are repeatable. All four experiments were concluded when the columns clogged and exhibited very high back pressures. The data in Fig. 1 further demonstrate that silica support solubility can be considerably higher in methanol compared to acetonitrile.

However, for a sterically protected silane stationary phase with bulky side groups, a different silica solubility pattern occurred. Fig. 2 shows that two columns of a highly purified silica support with a monomeric diisopropyl-C_8 stationary phase gave essentially the same solubility pattern for methanol and acetonitrile mobile phase modifiers. Unfortunately, tests had to be discontinued after about 5.6 l of acetonitrile–buffer purge, since the column bed clogged. (The resultant high column bed back pressure might reflect the precipitation of sodium silicate because of the lower solubility in acetonitrile, compared to methanol modifier). For methanol- or acetonitrile-modified mobile phases, the solubility of the diisopropyl C_8-modified silica was significantly higher than that for the same silica modified with dimethyl-C_{18} groups, shown on Fig. 2 for the two solvents. From this, one might conclude that the type of stationary phase can influence the solubility of a silica support and the ultimate stability of a column at higher pH.

Fig. 3 shows the silica dissolution found for several representative commercial C_{18} columns when continuously purged with a methanol–pH 10 buffer (50:50) mixture. Nucleosil C_{18} showed the highest rate of silica dissolved. This silica previously was shown to be weaker than some other silicas tested in column packing and crush-test studies [6,19]. The silica from LiChrosorb C_{18} also dissolved quickly, but at a somewhat slower rate than Nucleosil. Silicas from Novapak C_{18}, Zorbax Rx-C_{18}, Zorbax-ODS and Hypersil C_{18} dissolved more slowly, with the latter showing the slowest rate of those columns tested. Again, all experiments were terminated when columns clogged and exhibited very high back pressures.

Three factors probably dictate the differences

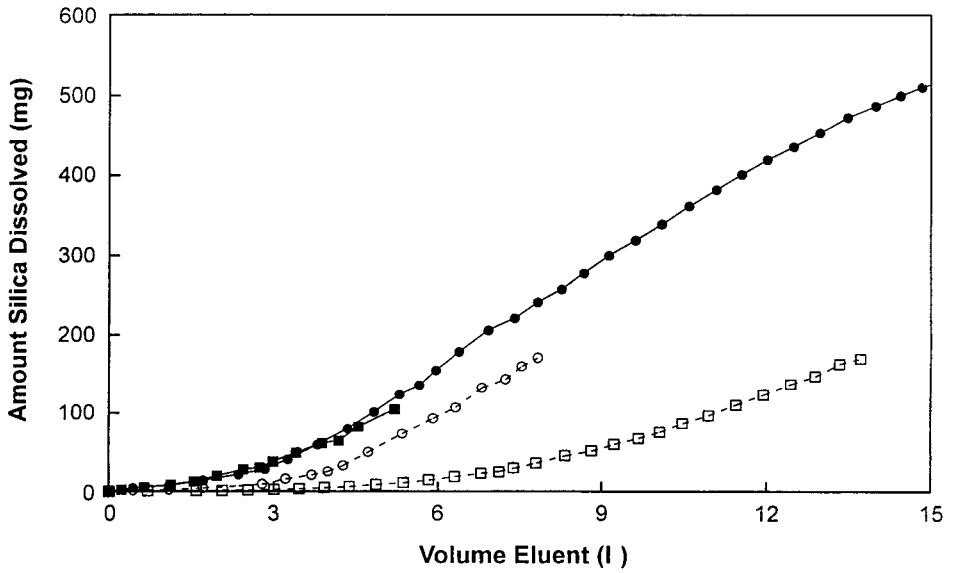

Fig. 2. Silica support dissolution for diisopropyl-C_8 column. Columns: 15 × 0.46 cm I.D. Zorbax SB-C_8 (diisopropyl-C_8; solid symbols) and Zorbax Rx-C_{18} (dimethyl-C_{18}; open symbols); same mobile phases and pH 10 buffer conditions as in Fig. 1. ○ = Methanol, □ = acetonitrile.

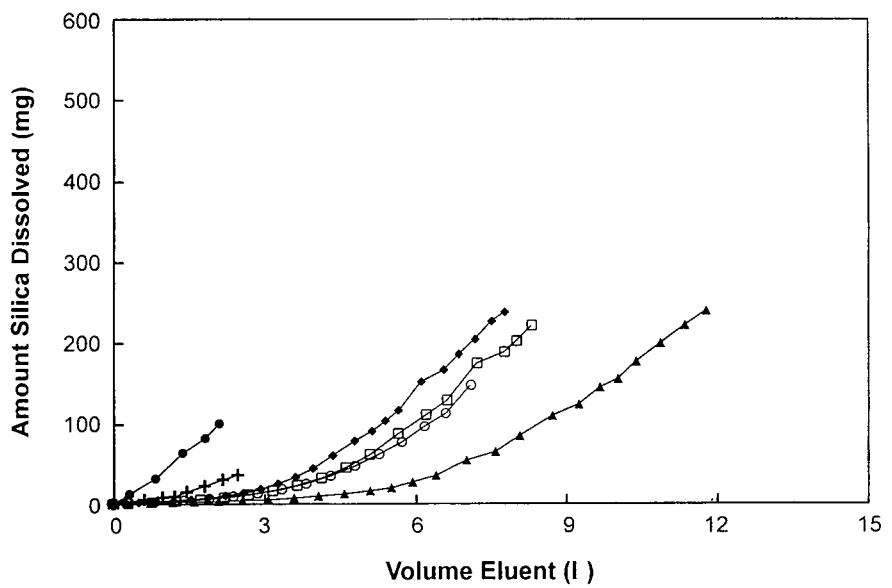

Fig. 3. Comparison of silica support dissolution for some commercial C_{18} columns. Columns: 15 × 0.46 cm I.D., except 15 × 0.39 cm I.D. for Novapak C_{18}; conditions of Fig. 1, except methanol–pH 10 buffer mobile phase and flow-rate 0.72 ml/min for the Novapak column. ● = Nucleosil C_{18}; ▲ = Hypersil ODS; ◆ = Novapak C_{18}; + = LiChrosorb C_{18}; ○ = Zorbax-ODS; □ = Zorbax Rx-C_{18}.

in silica dissolution rates shown in Fig. 3: silica pore structure, silica purity, and nature of the stationary phase. We believe that both of the silicas showing highest dissolution rates (Nucleosil, LiChrosorb) are made by a xerogel process [20], resulting in high surface areas (Table 1) and pores with variable wall thicknesses. The silicas with slower dissolution rates (e.g., Zorbax, Hypersil) are made by silica sol-gel or silica sol coacervation methods [20]. These silicas all have lower surface areas, but more importantly, the walls of the pores are quite thick. Particles formed from silica sols have cusp-shaped pores, whose walls are formed by neighboring silica sol particles. The result is that the degradation of pores within these particles requires a much larger amount of dissolved silica than particles having pores with thinner, more randomly shaped walls.

We speculate that differences in the dissolution rates from particles formed from silica sols also may be related to silica purity. It is well-known that silicas containing even small quantities of certain elements such as aluminum, iron, etc. show much lower solubility in aqueous systems than comparable highly purified silica [21]. These contaminating elements not only affect solubility, but they also increase the acidity of the silica surface [6,22,23]. Based on chromatographic properties and the published specifications in Table 2, the sol-based silica supports for Hypersil ODS and Zorbax-ODS are less pure; silicas for Nucleosil C_{18} and Zorbax Rx-C_{18} more highly purified [13,15,17]. Therefore, bonded phases from these more highly purified silicas contain less solubility inhibiting impurities and might be expected to dissolve more readily at high pH. This general trend appears to be supported by data in Fig. 3, where Hypersil column with the highest impurity levels of Al, Fe, etc., shows the lowest level of solubility. However, this effect is complicated by the fact that the type of stationary phase also may influence the silica support solubility (see following discussion). Silica support particle size, pore size and bonded phase type and concentration probably also affect silica support solubility.

The effect of stationary phase type on silica support solubility is more difficult to determine. Stationary phases for the columns in Fig. 3 probably were variously monomeric or polymeric, depending on the manufacturer. Published specifications are incomplete, but our NMR measurements showed that Nucleosil C_{18} and Hypersil-ODS are bonded with trifunctional silanes and end-capped. NMR measurements also revealed that LiChrosorb C_{18} is difunctionally modified. The rest of the stationary phases in Fig. 3 are monomeric, including the Zorbax products. While Zorbax ODS with the less-purified silica shows lower solubility than Zorbax Rx-C_{18} with highly purified silica, Zorbax ODS is end-capped while Zorbax Rx-C_{18} is not. Therefore, from the tests reported in Fig. 3, it is difficult to isolate effects of pore structure and particle purity from effects solely due to stationary phase differences.

To gain information regarding the effect of stationary phase type, a series of solubility tests were conducted on the same silica with four densely covering monomeric stationary phases, three with conformational differences. Fig. 4 shows dissolution results with the methanol–pH 10 buffer (50:50) purge. The rate of silica solubility was slowest for columns with dimethyl-C_{18} stationary bonded phases. The silica for the dimethyl-C_{18} column on the Type A silica (Zorbax-ODS) appears to be similarly solubilized than for the highly purified Type B silica (Zorbax Rx-C_{18}) with the same stationary phase. However, the effect again may be complicated in that Zorbax-ODS is end-capped, while Zorbax Rx-C_{18} is not. Support solubility rates in Fig. 4 were comparable for silicas with sterically protected diisopropyl-C_8 (Zorbax SB-C_8) and diisobutyl-C_{18} (Zorbax SB-C_{18}) bonded phases.

These results suggest that the bulky side groups of the sterically protected bonded silanes affect the posture of the organic stationary phase. Packings with these bulky side groups apparently leave a larger surface area of unmodified silica support exposed for dissolution at high pH, compared to that for the dimethyl-C_{18} bonded phases. Presumably, densely bonded dimethyl-C_{18} groups more effectively cover the surface of the silica support. This outcome is in

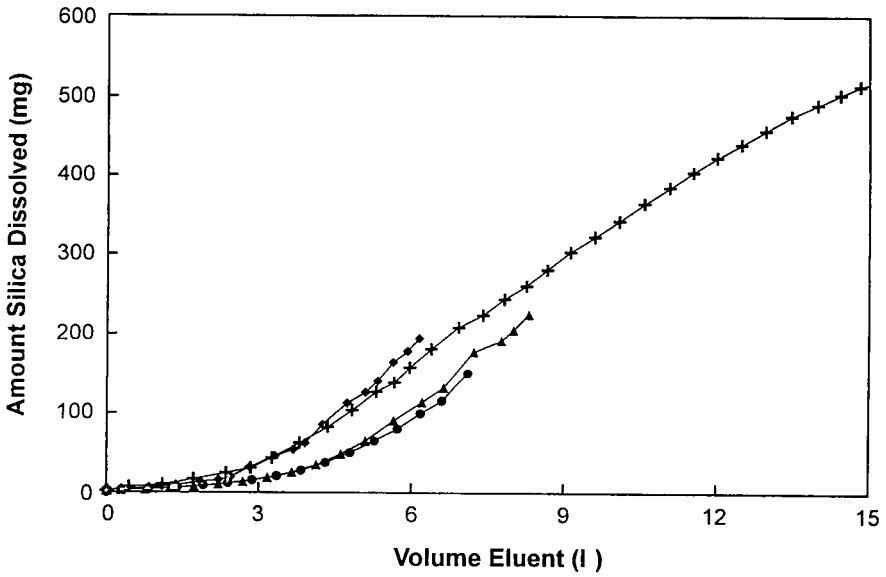

Fig. 4. Effect of bonded stationary phase type on silica support dissolution: methanol modifier. Columns: 15 × 0.46 cm I.D., (○) Zorbax-ODS (dimethyl-C_{18}; Type A silica), (▲) Zorbax Rx-C_{18} (dimethyl-C_{18}; Type B silica), (◆) Zorbax SB-C_{18} (diisobutyl-C_{18}; Type B silica) and (+) Zorbax SB-C_8 (diisopropyl-C_8; Type B silica); conditions of Fig. 1, except methanol–pH 10 buffer mobile phase.

strong contrast to low pH effects where bulky side groups much more effectively protect the bonded phase-connecting siloxane group against hydrolysis [24,25]. It also is likely that the essentially equivalent solubility for packings with the two sterically protected stationary phases occurs because the concentration of organic groups on the surface is essentially the same; steric effects from the bulky side groups limit and define the concentration of densely bonded ligands [26]. The results in Fig. 4 suggest that the nature of the stationary phase affects silica support solubility at high pH. However, the purity of the underlying silica support also may be a factor.

Previous studies have indicated that bare silica support dissolves more quickly than silica bonded with alkyl-silane functional groups [17]. With bonded phases, the concentration of the organic modifier also has a significant effect on chromatographic silica solubility [2–4]. However, the influence of the nature of the organic modifier on silica support dissolution has not been previously totally clarified. Data in Fig. 1 showed that the silica support for a dimethyl-C_{18} column (Zorbax Rx-C_{18}) was much more rapidly dissolved with methanol than with acetonitrile. Conversely, Fig. 2 showed that the silica support solubility for a diisopropyl-C_8 column with the same silica support (Zorbax SB-C_8) was only slightly less for the acetonitrile organic modifier. These limited results suggest that the stationary phase type can influence whether the silica support displays differences in solubility with different organic modifiers.

On the other hand, data in Figs. 4 and 5 suggest that stationary phase functionality causes larger silica solubility differences when acetonitrile is the mobile phase modifier, compared to methanol. With acetonitrile modifier, larger differences in silica solubility occurred for the dimethyl-substituted C_{18} packings than for the packings with bulky side groups, compared to results with methanol modifier (Fig. 4). These results suggest that use of acetonitrile modifier can reduce silica support solubility, especially for certain stationary phase functionalities.

Following the silica support dissolution tests,

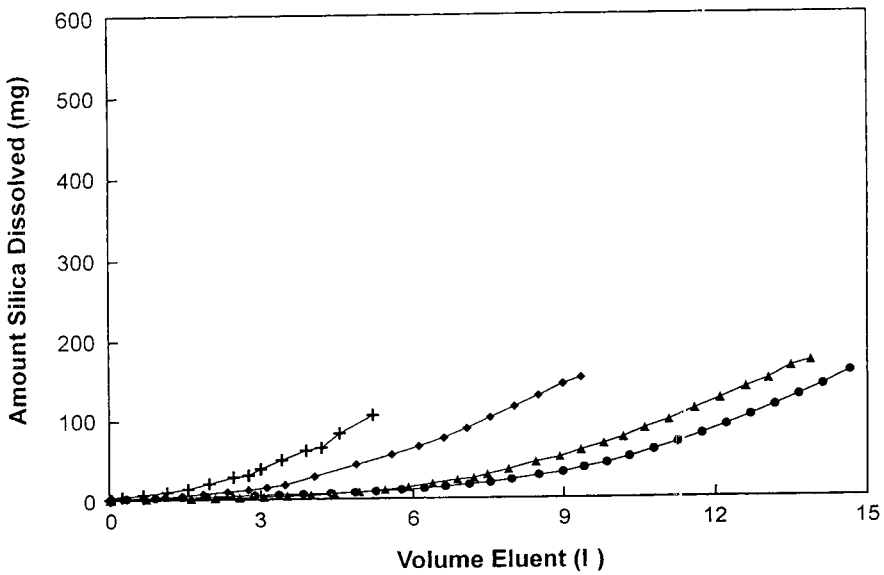

Fig. 5. Effect of bonded stationary phase type on silica support dissolution: acetonitrile modifier. Same conditions as Fig. 4, except acetonitrile–pH 10 buffer mobile phase of Fig. 1.

certain column packings were extruded from columns and thoroughly washed with methanol–water prior to elemental analysis. Table 3 shows carbon analysis results obtained in the silica dissolution tests, compared to % carbon present on the starting packing material. Also, for some columns, the inlet, middle and outlet one-third portions were separately extruded and sampled for elemental analysis. In all cases for the C_{18} columns, the % carbon after ageing actually is higher than for the original packing. We believe that this is due to significant dissolution of the silica under these aggressive conditions, leaving the organic coating essentially intact (as indicated by virtually unchanged k' values —see later data such as in Fig. 6). This increase in the organic–silica ratio with resultant decrease in particle density, increases the weight % carbon in the elemental analysis. This result is additional evidence that the Si–O–Si bond binding the silane to the silica is not significantly hydrolyzed at pH 10.

Table 3 also shows that the % carbon values actually decreased for the diisopropyl-C_8 columns in the pH 10 tests, especially when acetonitrile was used as the organic modifier. This effect is counter to the increase in % carbon for the diisobutyl-C_{18} packing, which displayed essentially identical solubility characteristics in methanol–pH 10 buffer (Fig. 4). Consequently, a change in the density of the support does not explain this trend. We speculate that the loss in carbon is a function of the shorter C_8 ligand. The % carbon decrease may involve a faster spalling off and subsequent elution of bonded silane than a decrease in support density can describe. Or, the decrease in % carbon may reflect a cleavage of the Si–O–Si bond connecting the shorter-chain silane to the silica support. Such effects were not seen for the longer-chain diisobutyl-C_{18} packing.

Finally, from the data in Table 3 for the inlet, middle and outlet samples from the aged columns, it is clear that the rates of silica dissolution and ligand hydrolysis are different for the packings investigated. For example, compare the results for Zorbax ODS with those for Nucleosil C_{18}, Hypersil ODS and Novapak C_{18}. Zorbax ODS shows little change in carbon content along the aged column, while the others exhibit changes that often are large. These differences probably are associated with the type of bonded

Table 3
Elemental analysis of column packings from silica support dissolution tests

Column type	Mobile phase purge	Carbon content (%, w/w)				
		Initial	After test			
			Final	Inlet	Middle	Outlet
Dimethyl-C_{18} (Zorbax Rx-C_{18})						
Column A	MeOH/pH 10	12.30	16.17	N/A	N/A	N/A
Column B	MeOH/pH 10	12.30	14.52	N/A	N/A	N/A
Dimethyl-C_{18} (Zorbax Rx-C_{18})						
Column A	ACN/pH 10	12.30	13.66	N/A	N/A	N/A
Column B	ACN/pH 10	12.30	14.73	N/A	N/A	N/A
Diisobutyl-C_{18}	MeOH/pH 10	10.07	12.38	N/A	N/A	N/A
(Zorbax SB-C_{18})	ACN/pH 10	10.07	11.03	N/A	N/A	N/A
Dimethyl-C_{18}	MeOH/pH 10	16.84	20.30	19.92	20.67	20.31
(Zorbax-ODS)	ACN/pH 10	16.84	20.18	19.75	20.61	20.18
Diisopropyl-C_8	MeOH/pH 10	6.28	5.98	N/A	N/A	N/A
(Zorbax SB-C_8)	ACN/pH 10	6.28	5.06	N/A	N/A	N/A
Nucleosil-C_{18}	MeOH/pH 10	N/A	N/A	17.86	14.14	13.23
Hypersil ODS	MeOH/pH 10	N/A	N/A	14.47	13.58	12.19
Novapak C_{18}	MeOH/pH 10	N/A	N/A	13.72	10.54	9.43
LiChrosorb C_{18}	MeOH/pH 10	20.18	21.07	N/A	N/A	N/A

N/A = Not available.

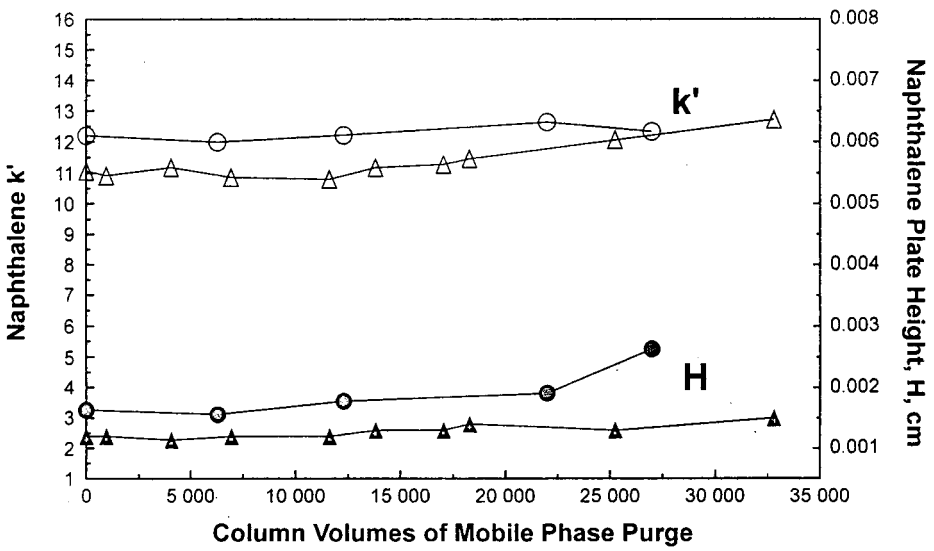

Fig. 6. Repeatability of chromatographic column pH 9 ageing tests. Columns: duplicate 15 × 0.46 cm I.D. Zorbax Rx-C_{18} (dimethyl-C_{18}); mobile phase purge: methanol–0.01 *M* phosphate, pH 9.0 (60:40); flow-rate: 1.0 ml/min; solute: naphthalene; ambient temperature.

phase used (i.e., monomeric, polyfunctional), and differences in the pore configuration and purity of the silica support.

3.2. Chromatographic column ageing tests

We also studied the degradation of silica-based, bonded-phase packings using chromatographic ageing tests. As given in Experimental, columns were continuously purged with pH 9.0 phosphate solution and periodically tested chromatographically for changes in retention, peak shape and column efficiency. Both neutral and basic solute probes were used in these tests. Naphthalene was used as the neutral solute to measure the loss of organic reversed-phase ligands from the silica surface; k' values for neutral solutes are related to the amount of bonded organic stationary phase [24]. The basic solute, N,N'-dimethylaniline (DMA) was selected as a solute to detect possible changes in the acidity and the type and number of residual silanols of the silica support. Data from the other test solutes used are not presented, since they gave no additional insights over the results herein given.

Fig. 6 data illustrate the repeatability of the chromatographic degradation tests. In June 1992 and October 1992 dimethyl-C_{18} columns with the same silica support were continuously purged with methanol–0.01 *M* pH 9.0 phosphate solution (50:50), and tested periodically. The neutral solute, naphthalene was plotted as the test solute, but similar results were seen for the other compounds in the test mixture. The June 92 column showed essentially no change for about 25 000 column volumes of purge, then suddenly failed. The October 92 column remained stable for more than 34 000 column volumes when the stability test was arbitrarily terminated. Plate height comparisons for the two columns indicate that the October 92 column was better packed, suggesting the reason for the better stability during the tests. Slight differences in the k' values are ascribed to different instruments and mobile phases used for the experiments after a four-month delay.

The data in Fig. 6 suggest that this dimethyl-C_{18} column packing can be safely used at pH 9 for method development. These results also indicate that well-packed columns of this material should be useful for more than 100 8-h work days, providing other conditions (contaminations, etc.) are not limiting. As discussed below, depending on bonded-phase functionality and silica support type, other packings may not provide this level of stability.

Results in Fig. 7 show striking differences in the stability of column packings with different bonded-phase functionalities. After about 12 000 column volumes of pH 9 purge, both the diisopropyl-C_8 and the diisobutyl-C_{18} columns failed almost simultaneously. This compares to the $>34\,000$ column volumes of stability exhibited by the dimethyl-C_{18} column. These results also suggest, however, that the diisopropyl-C_8 and diisobutyl-C_{18} columns could be used at pH 9 without problems for more than 30 8-h working days, compared to >100 days for the dimethyl-C_{18} packing.

Fig. 8 shows the effect of methanol and acetonitrile modifiers on k' values in pH 9 mobile phase with diisobutyl-C_{18} and dimethyl-C_{18} columns (same Type B silica support). Values for naphthalene k' slowly and continuously decreased at about the same rate for the diisobutyl-C_{18} column with both organic modifiers, indicating a slow loss in stationary phase. This decrease in k' is largely attributed to a loss in organic stationary phase as the silica support is eroded by the basic mobile phase [26]. (Absolute differences in k' values for the two columns is because of imperfections in adjusting % organic volume for the two organic modifiers to obtain the same k' values —acetonitrile is a stronger modifier [9]). After about 27 000 column volumes of purge, the k' values had decreased only about 10% from initial for columns tested with both organic modifiers. At this point the diisobutyl-C_{18} column k' test was discontinued.

Also shown in Fig. 8 is that the naphthalene k' values for the dimethyl-C_{18} are unchanged after almost 35 000 column volumes of pH 9.0 buffer with methanol and $>33\,000$ column volumes for acetonitrile (tests arbitrarily terminated). These results again suggest that the bonded dimethyl-

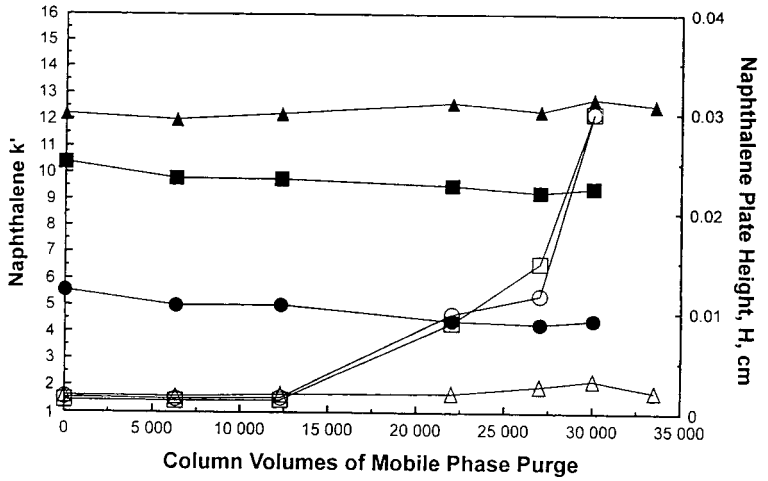

Fig. 7. Effect of stationary type on column ageing at pH 9. Columns: 15 × 0.46 cm I.D. Zorbax SB-C_8 (diisopropyl-C_8, ○), Zorbax SB-C_{18} (diisobutyl-C_{18}, □) and Zorbax Rx-C_{18} (dimethyl-C_{18}, △); open symbols, H; solid symbols, k'; conditions as in Fig. 6.

C_{18}-substituted silane protects the silica support from attack better than the diisobutyl-C_{18} phase. This postulation is directly in keeping with the silica solubility results given in Figs. 4 and 5, and the chromatographic results of Fig. 7.

Fig. 9 shows the same packing degradation tests with DMA as the test solute. Opposite to the retention pattern for the neutral solute, naphthalene, in Fig. 8, the retention pattern for the basic solute, DMA, is controlled by the number and acidity of accessible silanol groups. Again, the diisobutyl-C_{18} column exhibits a continuous slow decrease in k' values for DMA over the test period, just as in Fig. 8 for the

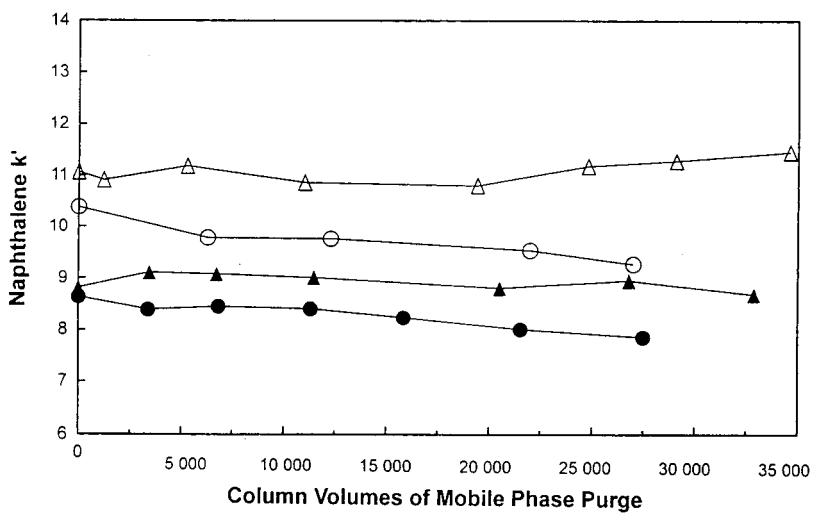

Fig. 8. Effect of organic modifier on k' for column ageing at pH 9: naphthalene solute. Columns: 15 × 0.46 cm I.D. Zorbax SB-C_{18} (diisobutyl-C_{18}, ○) and Zorbax Rx-C_{18} (dimethyl-C_{18}, △); mobile phase purge: methanol–0.01 M phosphate, pH 9.0 (60:40); flow-rate: 1.0 ml/min; solute: naphthalene; ambient temperature. Open symbols, methanol; closed symbols, acetonitrile.

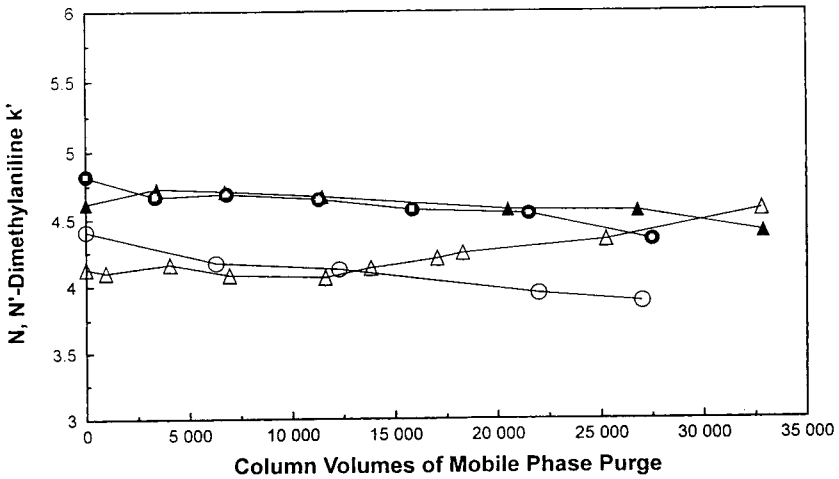

Fig. 9. Effect of organic modifier on k' for column ageing at pH 9: N,N'-dimethylaniline solute. Conditions and symbols as in Fig. 8, except solute: N,N'-dimethylaniline.

neutral solute, naphthalene. The final k' values for DMA again were about 10% below initial for both organic modifiers. With the dimethyl-C_{18} packing, however, a different pattern is evident. For about 20 000 column volumes of purge, k' values were constant. Afterwards, these values slightly increased over the remaining test period. We speculate that this trend could be due to changes in the silica support surface by this treatment, perhaps in the arrangement of silanol groups that influence retention of the basic solute. Finally, it should be noted that absolute k' values for N,N'-dimethylaniline were comparable for both the dimethyl-C_{18} and diisobutyl-C_{18} columns.

Plate height data for the dimethyl-C_{18} and diisobutyl-C_{18} columns at pH 9 with methanol and acetonitrile modifiers give a somewhat different picture of packing stability, as shown in Fig. 10. The dimethyl-C_{18} packing showed little loss in efficiency after $>33\,000$ column volumes of purge with methanol, and only a slightly

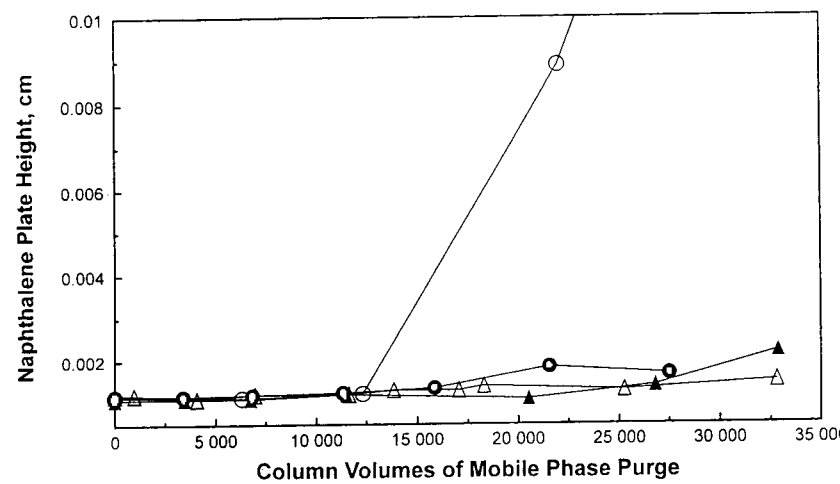

Fig. 10. Effect of organic modifier on plate height for column ageing at pH 9. Columns, conditions and symbols as for Fig. 8.

greater efficiency loss after >27 000 column volumes of purge with acetonitrile as organic modifier. In contrast, the diisobutyl-C_{18} column failed after about 12 000 column volumes of purge with methanol–pH 9 buffer, but remained stable for >27 000 column volumes when purged with acetonitrile-modified mobile phase. However, since only one column was tested in methanol, the earlier failure may have been due to a more poorly packed bed, rather than bed degradation because of silica support dissolution (see data in Fig. 4).

Peak asymmetry data also is useful for defining when packed bed stability is compromised. However, information on peak symmetry degradation closely follows that of plate height data. Therefore, although available for all studies, peak symmetries generally are not reported since results are redundant with plate height data.

Several commercial C_{18} columns were tested with the phosphate pH 9–acetonitrile system for stability, with the results shown in Fig. 11. As described previously in Figs. 8 and 9, Zorbax Rx-C_{18} (dimethyl-C_{18}) packing exhibits stability for >27 000 column volumes of purge. Here, plate height data suggest that this column fails after about 30 000 column volumes under the test conditions used. Tests with other commercial columns produced similar results. Hypersil ODS showed higher stability (wider pores? —see Table 1), while Novapak C_{18} was only slightly less stable, based on plate height data. But, Nucleosil quickly failed in this test. This result is in strong contrast to previous tests on laboratory-synthesized bonded phases made with this silica [17]. It also should be noted, however, that packing stability is a strong function of silica type and purity, as discussed above. Therefore, it is difficult to isolate the influence of bonded phase type when the type of silica support is varied.

3.3. Sodium hydroxide column-flush studies

Workers analyzing protein and peptides often like to flush their columns periodically with high-pH (>12) sodium hydroxide solution to purge strongly retained extraneous material from the separating system. Zorbax Rx-C_{18} (dimethyl-C_{18}) columns have demonstrated interesting characteristics for analyzing peptides and small proteins with conditions normally used for separating these materials. Therefore, we were interested in determining the stability of this column with sodium hydroxide washing procedures that might be required for some applica-

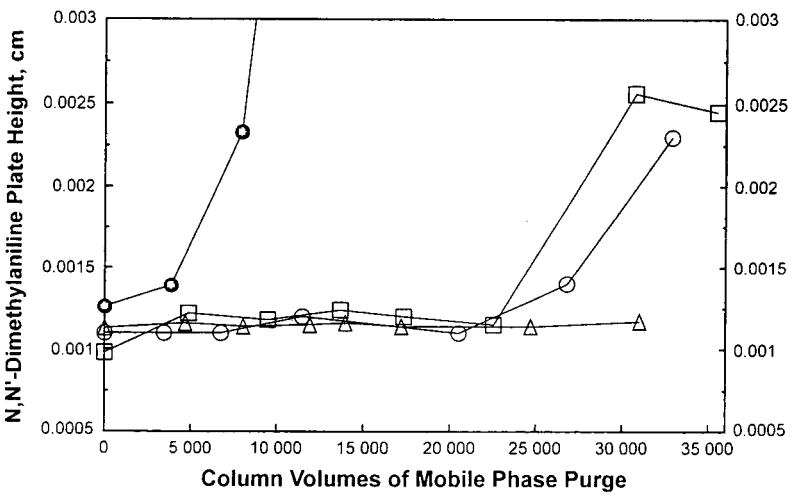

Fig. 11. Comparison of ageing at pH 9 for some commercial dimethyl-C_{18} columns. Columns: 15 × 0.46 cm I.D. Zorbax Rx-C_{18} (○, k' = 4.3), Hypersil ODS (△, k' = 4.3), and Nucleosil C_{18} (●, k' = 4.5); 15 × 0.39 cm I.D. Novapak C_{18} (□; k' = 4.1); mobile phase purge: acetonitrile–0.01 *M* phosphate, pH 9.0 (50:50); solute: N,N'-dimethylaniline.

tions. Accordingly, a 1:1 mixture of methanol–0.02 *M* sodium hydroxide (pH 12.3) was passed continuously through a Zorbax Rx-C_{18} column at 1.0 ml/min. Periodically, k' values, plate heights and peak asymmetry values (not shown) were measured for a neutral solute, toluene, and a basic solute, N,N′-dimethylaniline. The plots in Fig. 12 indicate that the packed bed was unchanged after about 15 h of this continuous treatment (ca. 900 ml). The column then exhibited a modest change, then stabilized in performance for an additional 17 h before apparent bed collapse. Inspection of the column after removing the frit showed about a 1-mm void at the column inlet. This pH 12.3 study suggests that a column of this silica and functional group type probably could be purged more than 60 times with ten column volumes (15 ml total) of pH 12.3 sodium hydroxide solution without objectionable dissolution of the silica support. Previously, such a treatment for silica-based columns was believed to invite an early catastrophic column failure.

Table 4 gives % carbon analysis data for certain column packings analyzed after various chromatographic ageing studies. Little loss in carbon for the bonded-phase columns was found as a result of the pH 9 tests, which is in keeping with the k' data in Figs. 6–9. Contrary to results at pH 10 (Table 3), % carbon values did not increase —the density of the silica particles does not appear to have been significantly altered at pH 9. The packing for the dimethyl-C_{18} column aged at pH 12.3 was extruded so that the top, middle and bottom third could be analyzed separately. The total carbon content of the packing was unchanged by this treatment, as suggested by the constant k' values in Fig. 12. But, higher carbon values were found down the bed, suggesting that silane removed from the top was captured by the stationary phase as it passed down the column.

4. Conclusions

Several important conclusions can be derived from these high-pH chromatographic and dissolution tests. First, densely bonded monomeric dimethyl-C_{18} ligands better protect the silica support from dissolution than bulky diisopropyl- and diisobutyl-substituted bonded silanes. These results suggest that the silica support is more exposed when bulky groups are used on the

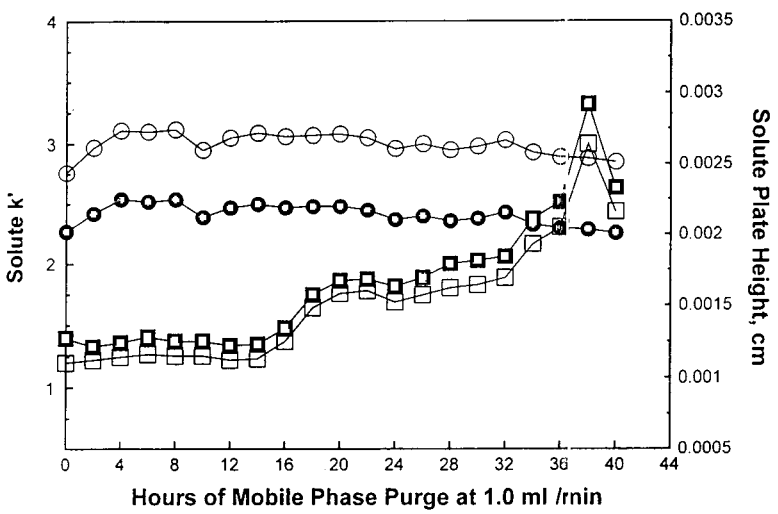

Fig. 12. Stability of dimethyl-C_{18} column at pH 12.3. Column: Zorbax Rx-C_{18}; mobile phase: methanol–0.02 *M* sodium hydroxide, pH 12.3 (50:50); flow-rate: 1.0 ml/min; ambient temperature; solutes: toluene (open symbols) and N,N′-dimethylaniline Solid symbols). ○ = k'; □ = H.

Table 4
Carbon analysis of column packings from chromatographic ageing tests[a]

Column type	Mobile phase purge	Initial % carbon	Final % carbon	After tests, % carbon		
				Inlet third	Middle third	Outlet third
Diisopropyl-C_8 (Zorbax SB-C_8)	pH 9	5.91	5.56	N/A	N/A	N/A
Diisobutyl-C_{18} (Zorbax SB-C_{18})	pH 9	9.90	9.30	N/A	N/A	N/A
Dimethyl-C_{18} (Zorbax Rx-C_{18})	pH 9	12.77	12.12	N/A	N/A	N/A
Dimethyl-C_{18} (Zorbax Rx-C_{18})	pH 12.3	12.21	12.29	12.03	12.39	12.49

Mobile phases with 50% methanol modifier. N/A = Not available.
[a] Average of duplicate values.

silane; the dimethyl-substituted silane groups apparently are more tightly arranged on the surface. This feature is indirectly supported by studies which showed superior peak shapes and column efficiency with diisopropyl- and diisobutyl-C_{18} packings for highly basic drugs whose retention at pH 7 is largely based on interaction with silanol groups [26]. Here, the densely reacted dimethyl-C_{18} phase on highly purified, low-acidity silica support produced poorer results, presumably because a smaller number of surface silanol groups were available for needed interaction with basic drugs ionized at this pH.

Second, failure of silica-based columns at high pH is a direct result of solubilizing the silica support, with ultimate collapse of the packed bed. Columns tested during the pH 10 silica-dissolution studies often showed several centimeters of void at the inlet after the tests. But, after bed failure of columns in the pH 9 chromatographic tests, only a small decrease in k' values (ca. 10%) for solutes was observed. This result confirms that column failure results from loss of silica support, and *not* in the hydrolysis of the Si–O–Si siloxane bond of the bonded silane as has been proposed [2]. This is contrary to effects at low pH, where hydrolysis of the covalently bonding Si–O–Si group is the mechanism of bonded-phase column degradation. Here, bonded phases with bulky, sterically protecting groups show excellent stability at low pH and high temperatures [24,25].

Third, the nature of the bonded C_{18} stationary phase (whether monomeric or polymeric) does not significantly influence column degradation at high pH. The dominating feature is the nature of the silica support, since siloxane (Si–O–Si) hydrolysis for the C_{18} bonded silane either does not occur, or occurs very slowly at high pH. Loss of bonded phase (and retention) at high pH likely is a result of silica dissolving around the covalently attached silane, eventually causing mechanical attrition and a spalling off of the bonded organic phase.

Fourth, the rate of silica dissolution is a strong function of the nature of the porous silica support. All three of the more stable columns in Fig. 11 apparently were prepared from silicas made by consolidating silica sols, although by different methods. Here, the similar pore structure is a series of cusp-shaped passages, with thick outer walls represented by the outer surface of neighboring individual sol particles. Pore volumes of these more stable silicas also are somewhat comparable. Conversely, some silica supports apparently are prepared by a two-phase xerogel process that does not start with a silica sol. The resultant material has a higher pore volume and differently shaped pores. These

silicas apparently have a more random pore structure containing a high population of pores with thin walls that are readily dissolved at high pH. Rapid dissolution apparently causes individual particles to break down, then the whole packed bed to collapse.

Fifth, purity of the support affects the stability of silica-based bonded-phase packings. More highly purified less-acidic Type B silicas dissolve more rapidly; less-pure Type A silicas with significant contamination from aluminum, iron, zinc and other elements appear to solubilize more slowly and are more stable at high pH. In keeping with a previous studies [2,7], these results suggest that certain C_{18} bonded-phase column packings prepared from silica sols are useful at pH 9 operation. C_{18} packings with less-pure Type A silicas made from silica sols appear most stable; pH 10 operation seems feasible for some of these materials. *In all cases, however, potential lifetime of silica-based bonded-phase packings will always be reduced with high aqueous pH operation.* Use of a precolumn of silica support (located between the pump and sample injector) could enhance column lifetime. Such a precolumn would partially saturate the mobile phase with silica, diminishing the tendency of the silica in the separating column to dissolve. However, use of such a precolumn would make gradient elution impractical.

Sixth, in keeping with previous studies, we found that acetonitrile organic modifier often prolongs column life at high pH compared to methanol. Other reports have shown that silica support dissolution is reduced with increasing organic modifier concentrations.

Finally, certain silica-based C_{18} columns can be safely purged with 0.02 *M* sodium hydroxide solution to clean unwanted highly retained materials from the column bed. Bed stability under these conditions is strongly influenced by the type and purity of silica support and the type of C_{18} bonded-phase functionality.

Acknowledgements

We thank C.H. Dilks, Jr. for his expert assistance with the chromatographic ageing experiments. We also gratefully acknowledge J.W. de Haan and L.J.M. van de Ven for NMR measurements and their interpretation of the data.

References

[1] Cs. Horvath, W. Melander and I. Molnar, *Anal. Chem.*, 49 (1977) 142.
[2] A. Wehrli, J C. Hildenbrand, H.P. Keller, R. Stampfli and R.W. Frei, *J. Chromatogr.*, 149 (1978) 199.
[3] J.G. Atwood, G.J. Schmidt and W. Slavin, *J. Chromatogr.*, 171 (1979) 109.
[4] B. Wheals, *J. Chromatogr.*, 187 (1980) 65.
[5] P.E. Barker, B.W. Hatt and S.R. Holding, *J. Chromatogr.*, 206 (1981) 27.
[6] J. Köhler and J.J. Kirkland, *J. Chromatogr.*, 385 (1987) 125.
[7] B. Law and P.F. Chan, *J. Chromatogr.*, 467 (1989) 267.
[8] M.A. Stadalius, J.S. Berus and L.R. Snyder, *LC–GC*, 6 (1988) 494.
[9] L.R. Snyder, J.L. Glajch and J.J. Kirkland, *Practical HPLC Method Development*, John Wiley, New York, 1988, Ch. 3–6.
[10] A. Berthod, *J. Chromatogr.*, 549 (1991) 1.
[11] K.K. Unger, K.D. Lork, B. Pfleiderer, K. Albert and E. Bayer, *J. Chromatogr.*, 556 (1991) 395.
[12] *Millipore Catalog*, Millipore, Medford, MA, 1991–1992.
[13] J.J. Kirkland, C.H. Dilks, Jr. and J.J. DeStefano, *J. Chromatogr.*, 635 (1993) 19.
[14] J.J. Kirkland, *J. Chromatogr.*, 125 (1976) 231.
[15] J.J. DeStefano, Rockland Technologies, *personal communication*, July 1992.
[16] G.B. Cox, *J. Chromatogr. A*, 656 (1993) 353.
[17] M. Hetem, L. van de Ven, J. de Haan, C. Cramers, K. Albert and E. Bayer, *J. Chromatogr.*, 479 (1989) 269.
[18] R.K. Iler, *The Chemistry of Silica*, John Wiley, New York, 1979, p. 97.
[19] J. Köhler, D.B. Chase, R.D. Farlee, A.J. Vega and J.J. Kirkland, *J. Chromatogr.*, 352 (1986) 275.
[20] K.K. Unger, *Porous Silica*, Elsevier, Amsterdam, 1979, Ch. 2.
[21] R.K. Iler, *The Chemistry of Silica*, John Wiley, New York, 1979, Chapt. 2.
[22] R.K. Iler, *The Chemistry of Silica*, John Wiley, New York, 1979, Chapt. 6.
[23] J. Nawrocki, *Chromatographia*, 31 (1991) 177–205.
[24] J.J. Kirkland, J.L. Glajch and R.D. Farlee, *Anal. Chem.*, 61 (1988) 2.
[25] B.E. Boyes and J.J. Kirkland, *Pept. Res.*, 5 (1993) 249.
[26] J.J. Kirkland and J.W. Henderson, *J. Chromatogr. Sci.*, (1994) in press.
[27] H.J. Ritchie, Shandon Southern Products, Cheshire, *personal communication*, 1994.

ELSEVIER

Journal of Chromatography A, 691 (1995) 21–27

JOURNAL OF CHROMATOGRAPHY A

Use of chromatographic system peaks for continuous quantitative analysis

Nira Mizrotsky, Luba Kristol, Eli Grushka*

Department of Inorganic and Analytical Chemistry, The Hebrew University, 91904 Jerusalem, Israel

Abstract

A study was made to establish whether the size of system peaks, which occur in chromatography with multi-component mobile phases, is a linear function of the concentration of the components. In the two chromatographic systems studied, it was found that the size of the system peaks is proportional to concentration. Using the fact that the injection of concentrations lower than that in the mobile phase results in negative system peaks whereas the injection of higher concentrations yields positive peaks, a simple method to determine the concentration of the components in the mobile phase is described. The approach seems to be robust although the retention times of some mobile phase components might be affected by the concentration of other components. The results presented indicate that system peaks can be used to monitor continuously various streams such as rivers, waste waters and physiological fluids.

1. Introduction

System peaks occur in chromatographic systems whenever the mobile phase contains more than one component. They are observed when at least one of the mobile phase components is detected by the detector. System peaks are not directly related to the injected solutes; they are a thermodynamic phenomenon, resulting from the perturbation in the chemical equilibrium at the column inlet which occurs when a sample of different composition to the bulk mobile phase enters the column. At the onset of this perturbation of equilibrium, the chromatographic system (i.e., column and stationary and mobile phases) begin to relax towards a new state of equilibrium by transferring mobile phase components, in addition to solutes, between the two phases. The net effect of the relaxation to a new state of equilibrium is the appearance of system peaks. System peaks move through the column as if they were injected solutes, i.e., they have definite capacity factors and peak shapes and they exhibit conventional adsorption isotherms that can be linear, Langmuir or of any other type normally encountered in chromatography.

System peaks have been studied extensively over the past decade or so. For example, Riedo and Kováts [1,2] developed the fundamental theory for the formation of system peaks. Melander et al. [3] also examined the process of system peak development. Knox and Kaliszan [4] used system peaks to obtain a better estimate of a column's void volume. Levin and Grushka [5–7] used experimentally determined system peaks to extract several chromatographic quantities such as void volumes and capacity factors. Arvidsson et al. [8] examined system peaks in ion-pair

* Corresponding author.

0021-9673/95/$09.50
SSDI 0021-9673(94)00767-5

chromatography. Golshan-Shirazi and Guiochon [9] solved numerically the mass balance equations relating to system peaks in linear chromatography. Levin and Abu-Lafi used system peaks to characterize the chromatographic behaviour of enantiomers in chiral liquid chromatography [10] and to study the distribution of several hydroxylated benzenes [11].

All of the above papers deal with fundamental aspects of system peaks. Very few publications can be found describing the use of system peaks. Phillips and McIlwrick [12] used system peaks in gas chromatography to characterize a catalytic bed. In another attempt, Westerlund and coworkers [14–17] demonstrated the use of system peaks to generate, in situ, mobile phase gradients which can produce sharper solute peaks.

In this work, we stress the practical utilization of system peaks. From a conceptual point of view it is of no, or little, consequence whether the sample is injected into the chromatograph in a small volume of the mobile phase, or whether it is passed through the column as part of the mobile phase and pure mobile phase (i.e., without the components to be separated) is injected. In both instances a chromatogram will be generated. However, from a practical point of view, the possibility of continuously passing the sample to be separated through the column opens the door to new modes of chromatographic operations. For example, a portion of a flowing stream, such as running waste effluents in factories, rivers and physiological fluids, can be diverted to pass continuously through the chromatographic column. At predetermined time intervals, a neat solvent is injected into the column, resulting in system peaks belonging to the components in the stream. In this manner, the stream can be monitored continuously, and automatically, for the level of one or more of the components in the stream.

To be a viable analysis method, the system peak approach must be analytically sound; it must be robust, precise and accurate. In this work, we investigated the dependence of system peak areas on the concentration of the solutes in the mobile phase and on the concentration of the same solutes which are injected into the column. This dependence establishes the quality of calibration lines that can be obtained for system peaks. The results also indicate the interrelationships between mobile phase components and thus the robustness of the analytical approach for the system concerned.

2. Experimental

2.1. Instrumentation

Two chromatographic systems were used. (A) A Perkin-Elmer (Norwalk, CT, USA) Series 4 liquid chromatograph equipped with a 10-μl loop injection valve (Rheodyne, Cotati, CA, USA), a Perkin-Elmer Model 85B variable-wavelength spectrophotometric detector having a 1.4-μl flow cell and a D-2000 integrator (Merck–Hitachi, Darmstadt, Germany) was used. The detector was operated at 254 nm. (B) A Merck–Hitachi liquid chromatograph with a variable-wavelength detector and a 20-μl injection loop was used. The detector was operated at 235 nm. The detector was connected to a Merck–Hitachi D-2000 integrator. Two columns were used, 25-cm and 12.5-cm LiChrosorb RP-18 cartridges, held by a Hiber manual holder. The columns were thermostated with the aid of a laboratory-built water-bath.

2.2. Materials

Two mobile phases were prepared: (A) acetate buffer (0.02 *M*, pH 5.6) containing 0.001 *M* heptanesulphonate, $4 \cdot 10^{-4}$ *M* copper acetate and various concentrations of valine (Val), histidine (His), hydroxyproline (Hyp) and glycine (Gly); and (B) phosphate buffer (sodium dihydrogenphosphate and disodium hydrogenphosphate, 0.01 *M*, pH 6) containing various concentrations of tyrosine (Tyr) and phenylalanine (Phe). All amino acids were purchased from Sigma (Tel-Aviv, Israel).

2.3. Procedure

Four batches of mobile phase A were prepared containing the amino acids at concentra-

tions of 0.02, 0.04, 0.06 and 0.072 m*M*. Into each mobile phase was injected the same buffer containing various concentrations of the four amino acids.

With mobile phase B we prepared fifteen combinations of tyrosine and phenylalanine concentrations. Three phenylalanine concentrations were used, $5 \cdot 10^{-4}$, $1 \cdot 10^{-3}$ and $5 \cdot 10^{-3}$ *M*. At each phenylalanine concentration, five tyrosine concentrations were prepared: $1 \cdot 10^{-5}$, $5 \cdot 10^{-5}$, $1 \cdot 10^{-4}$, $2.5 \cdot 10^{-4}$ and $5 \cdot 10^{-4}$ *M*. The injected samples consisted either of pure buffer or buffers containing any of the above combinations of the two amino acids.

Owing to noisy detector signals, resulting from the use of strongly UV-absorbing mobile phases, it was decided to measure peak heights rather than peak areas.

3. Results and discussion

3.1. Behaviour of mobile phase A

The first system examined was with mobile phase A. Although a complicated system, we chose it for our initial studies owing to our familiarity with its behaviour [5–8]. The Cu–amino acid complexes absorb radiation at 235 nm, so we can monitor the behaviour of all amino acids.

Fig. 1a shows a chromatogram resulting from the injection of a pure buffer into the column equilibrated with mobile phase A containing 0.02 m*M* of Gly, Hyp, His and Val. The chromatogram has four negative peaks, one for each amino acid. The identification of these peaks was established by injecting the amino acids at higher concentrations than that in the mobile phase. Fig. 1b shows the chromatogram obtained from the injection of 0.05 m*M* of the four amino acids. The two positive peaks in Fig. 1a are system peaks belonging to other components of the mobile phase.

The injection of the amino acids gives either positive or negative peaks depending on whether the concentrations of the injected amino acids are higher or lower than those in the mobile phase. An example of the dependence of peak size and direction on the concentration of the injected amino acid is shown in Fig. 2 for valine. Similar behaviour was observed for all four amino acids.

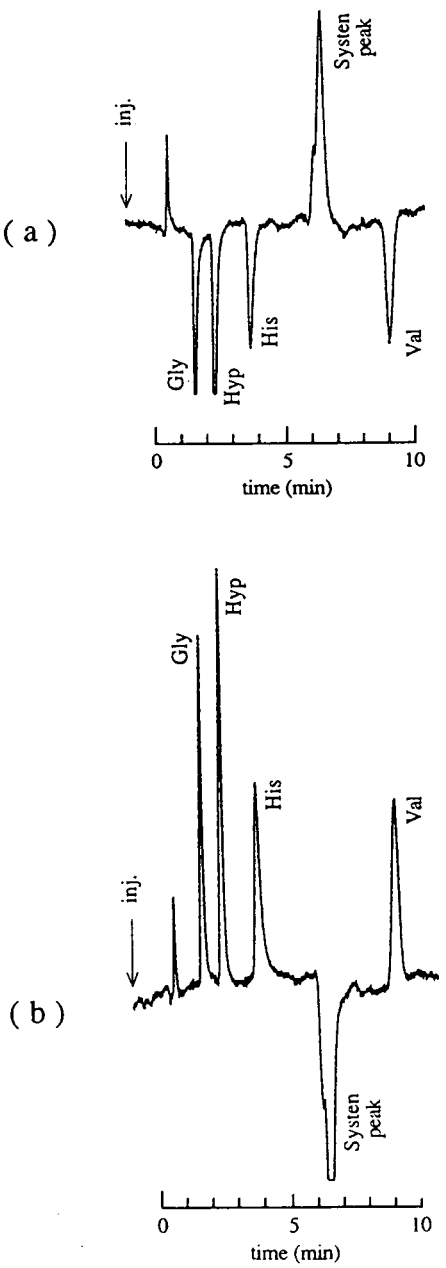

Fig. 1. System peaks resulting from the injection of (a) neat buffer and of (b) buffer and 0.05 m*M* Gly, His, Hyp and Val. Mobile phase, mobile phase A containing 0.02 m*M* Gly, His, Hyp and Val.

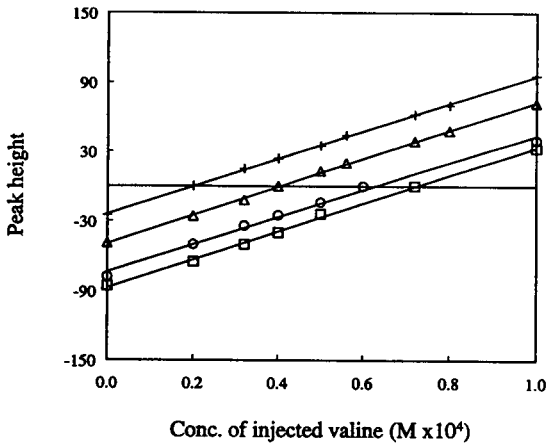

Fig. 2. Calibration lines obtained by injecting various concentrations of Val into mobile phase A. Each line corresponds to a different concentration of Val in the mobile phase: + = $2.0 \cdot 10^{-5}$; △ = $4.0 \cdot 10^{-5}$; ○ = $6.0 \cdot 10^{-5}$; □ = $7.2 \cdot 10^{-5}$ *M*. Peak heights are in arbitrary (integrator) units.

Each line in Fig. 2 represents a different concentration of the amino acid (valine in this instance) in the mobile phase. The linear dependence of the peak height on the concentration of the injected amino acid is not a function of the concentration of the same amino acid in the mobile phase. Each line is a calibration-type line that can be used to measure the concentration of the amino acid. The zero-height crossing point for each line occurs when the amino acid concentration in the injected sample equals the concentration in the mobile phase. Note also that as the concentration of the amino acid in the mobile phase is increased, the peak resulting from the injection of neat buffer is higher (more negative).

The linear dependence of the system peak height on the concentration coupled with the fact that each line crosses the zero-height line is of great practical importance. To characterize the amount of a solute in a stream all that we need to do is to divert a part of the stream through a chromatographic column and make two injections. One injection is of the stream effluent without the solute. This injection will result in a negative system peak associated with the solute. The second injection will include the solute at a relatively high concentration which will result in a positive peak. Interpolation between the two peak heights will give a line that will cross the zero-height line at the concentrations of the solute in the stream.

To check the linearity of the chromatographic system, some of the data in Fig. 2 were replotted so that the peak height was now a function of the concentration of Val in the mobile phase (Fig. 3). Each line in Fig. 3 belongs to a different injected concentration of the amino acids. Although each line has only four experimental points, the linearity is very good, with correlation coefficients of 0.999 and above. The bottom line is due to the injection of pure buffer without any Val. The extrapolation of that line to zero Val in the mobile phase shows, as expected, that the system peak vanishes. Extrapolation of all other lines to zero Val in the mobile phase gives positive peaks that would result from the injection of various concentrations of Val into a neat buffer. The extrapolated peaks heights should be the same as the absolute value of the system peak heights resulting from the injection of a neat buffer into mobile phases containing the same concentration of the amino acid, i.e., the absolute values of the points on the bottom line. Fig. 3 shows that such is the case. For

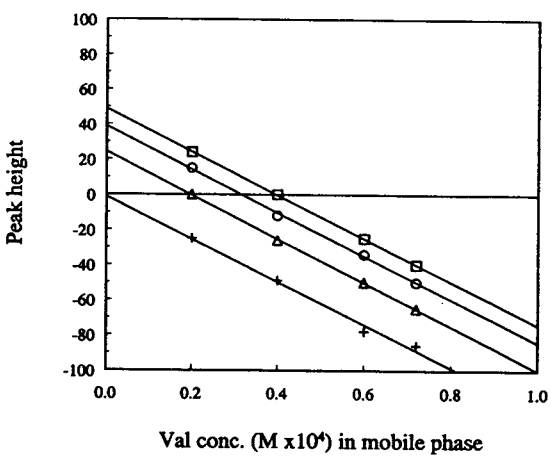

Fig. 3. Heights of Val system peak as a function of Val concentration in mobile phase A. Each line belongs to a different concentration of Val in the injected buffer: + = 0; △ = $2.0 \cdot 10^{-5}$; ○ = $3.2 \cdot 10^{-5}$; □ = $4.0 \cdot 10^{-5}$ *M*. Peak heights are in arbitrary (integrator) units.

example, the peak height resulting from the extrapolation of the line belonging to an injected concentration of 0.04 m*M* (top line) is 48.9 cm. The absolute value of the peak height resulting from the injection of a neat buffer into a mobile phase containing 0.04 m*M* Val is 49 cm. Hence system peaks can be calibrated and, therefore, can be used to determine species in the mobile phase.

3.2. Behaviour of mobile phase B

The mobile phase discussed above presents a very complex chromatographic system. To examine the feasibility of using system peaks with conventional mobile phases, we prepared a simple phosphate buffer and added to it Tyr and Phe. Injection of the neat phosphate buffer gave the system peaks associated with Tyr and Phe. Typical calibration lines resulting from the injection of various concentrations of Tyr in the phosphate buffer are shown in Fig. 4. Each line belongs to different concentrations of Tyr in the mobile phase. In all instances, the concentration of Phe was $5 \cdot 10^{-3}$ *M*. As in Section 3.1, the calibration lines cross the zero-height line when the concentrations of the injected Tyr were identical with those in the mobile phase. Extrapolation of each line to zero injected Tyr gives the system peak that would result from the injection of a neat buffer.

Fig. 5 shows the system peak heights as a function of Tyr concentration in the mobile phase. Each line corresponds to a different concentration of the injected Tyr. Again, in all instances the concentration of Phe in the mobile phase was $5 \cdot 10^{-3}$ *M*. The extrapolation of each line to zero Tyr concentration in the mobile phase gives the Tyr peak that would result from the injection of tyrosine into a mobile phase made up of the phosphate buffer and $5 \cdot 10^{-3}$ *M* Phe. The absolute values of the extrapolated peak heights discussed in connection with Fig. 4 should be identical with the extrapolated peak heights in Fig. 5. Table 1 gives the extrapolated peak heights. Also given in Table 1 are the absolute value of the actual Tyr system peak obtained from the injection of a neat buffer into each of the mobile phases containing various amounts of Tyr. All three values are very close, indicating the robustness of the approach; quantitative information about components of the

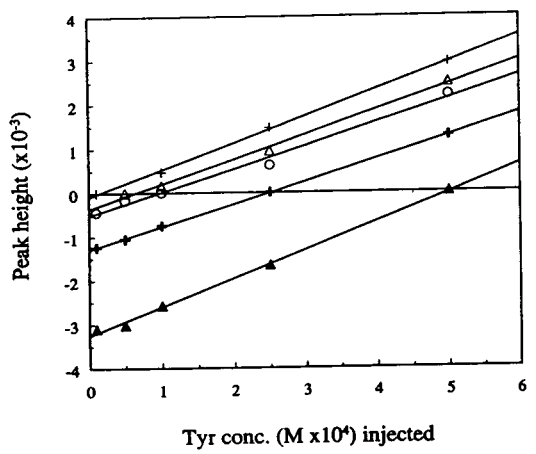

Fig. 4. Calibration lines obtained by injecting various concentrations of Tyr into mobile phase B containing Tyr and 0.005 *M* Phe. Each line corresponds to a different concentration of Tyr in mobile phase B: + = $1.0 \cdot 10^{-5}$; △ = $5.0 \cdot 10^{-5}$; ○ = $1.0 \cdot 10^{-4}$; + = $2.5 \cdot 10^{-4}$; ▲ = $5.0 \cdot 10^{-4}$ *M*. Peak heights are in arbitrary (integrator) units.

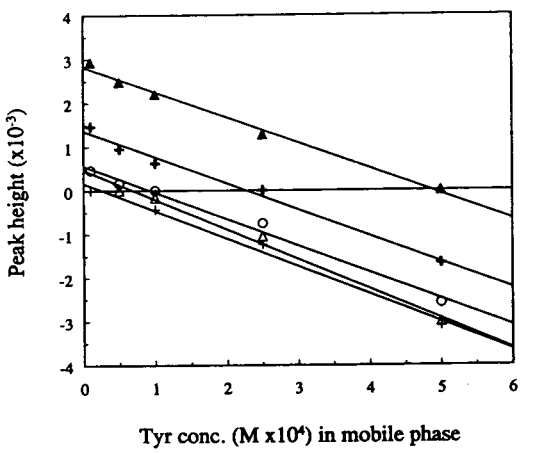

Fig. 5. Heights of Tyr system peak as a function of Tyr concentration in mobile phase B containing 0.005 *M* Phe. Each line belongs to a different concentration of Tyr in the injected buffer: + = $1.0 \cdot 10^{-5}$; △ = $5.0 \cdot 10^{-5}$; ○ = $1.0 \cdot 10^{-4}$; + = $2.5 \cdot 10^{-4}$; ▲ = $5.0 \cdot 10^{-4}$ *M*. Peak heights are in arbitrary (integrator) units.

Table 1
Heights of extrapolated system peaks from Figs. 4 and 5 and from injection of neat buffer

Tyr concentration either in mobile phase or injected (10^{-4} M)	Extrapolated peak height to zero Tyr in injected sample (Fig. 4)	Extrapolated peak height to zero Tyr in mobile phase (Fig. 5)	Peak height resulting from neat buffer injection
0.1	85	175	0
0.5	359	475	236
1.0	512	571	468
2.5	1288	1366	1417
5.0	3246	2828	3127

mobile phase can indeed be obtained via their system peaks.

We examined two other sets of mobile phase, each with a different concentration of Phe, to see if different concentrations of mobile phase components affect the peak height of Tyr. Table 2 shows that a ten-ten fold increase in Phe changes the Tyr peak height by at worst 30%. Hence the determination of Tyr by system peaks can be carried out without the need to control closely the concentration of Phe in the mobile phase.

The discussion up to this point was centred on the size of the peaks which were generated from various combinations of Tyr in the mobile phase and in the injected sample. In addition to peak size, the question of retention time stability is also of great importance. If the retention times are a strong function of concentration, then we might have difficulty with the actual identification of a peak. Fig. 6 shows plots of the capacity factor of Tyr as a function of injected Tyr concentration when the mobile phase contains $2.5 \cdot 10^{-4}$ M of the same amino acid. Each line corresponds to a different Phe concentration in the mobile phase. Similar results were obtained for other Tyr concentrations in the mobile phase. To a good approximation, the capacity factor is independent of the amount of Tyr injected. However, the concentration of Phe does have an effect of the retention of Tyr. As the concentration of Phe in the mobile phase is increased, the retention of Tyr becomes smaller, possibly because of the more successful competition of the former compound for the interaction sites in the stationary phase. At the higher concentrations Phe acts like a weak mobile phase modifier. Thus, although Phe does not have a large effect

Table 2
Effect of Phe concentration in mobile phase B on the height of the Tyr system peak

Injected Tyr concentration (M)	Phe concentration in mobile phase (M)		
	0.0005	0.001	0.005
$1.0 \cdot 10^{-5}$	−1692	−1385	−1240
$5.0 \cdot 10^{-5}$	−1324	−1151	−1053
$1.0 \cdot 10^{-4}$	−818	−866	−754
$2.5 \cdot 10^{-4}$	0	0	0
$5.0 \cdot 10^{-4}$	1726	1439	1269

The mobile phase contained $2.5 \cdot 10^{-4}$ M Tyr.

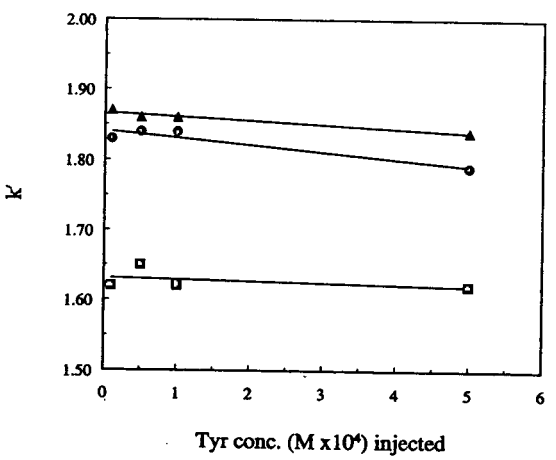

Fig. 6. Capacity factors of Tyr as a function of injected Tyr concentration. Mobile phase B contained $2.5 \cdot 10^{-4}$ M Tyr and Phe. Each line corresponds to a different Phe concentration: ▲ = $5.0 \cdot 10^{-4}$; ○ = $1.0 \cdot 10^{-3}$; □ = $5.0 \cdot 10^{-3}$ M.

on the peak size, it does have an appreciable influence on the retention of Tyr. If the amount of Phe in the mobile phase is not maintained over a narrow concentration range, the Tyr peak might be outside the time window of the integrator, and a misidentification might occur.

4. Conclusions

The size of system peaks is related to the amounts of the components responsible for these peaks. Hence system peaks can be used to monitor the concentration of the components in the mobile phase. This fact opens up the possibility of using the solutions to be analysed as the mobile phase. Injection of neat solutions, or of controlled concentrations of the components of interest, will give quantitative information about the concentrations of these components in the mobile phase. The attraction of this approach lies in the fact that the sample to be analysed can be passed continuously through the column and the analysis is carried out periodically by the injection of neat solvents. There is no need to remove samples for off-line analysis. The approach can be automated very easily. It can be utilized for continuous stream monitoring and also for continuous, on-line process control. We are applying the system peak method to monitor the progress of chemical reactions. Subsequent publications will describe the monitoring of an on-line titration and of a hydrolysis reaction.

References

[1] F. Riedo and E. Kováts, *J. Chromatogr.*, 239 (1982) 1–28.
[2] F. Riedo and E. Kováts, in F. Dondi and G. Guiochon (Editors), *Theoretical Advancement in Chromatography and Related Techniques (NATO ASI Series)*, Kluwer, Dordrecht, 1992, pp. 211–226.
[3] W.R. Melander, J.F. Erad and Cs. Horváth, *J. Chromatogr.*, 282 (1983) 229–248.
[4] J.H. Knox and R. Kaliszan, *J. Chromatogr.*, 349 (1985) 211–234.
[5] S. Levin and E. Grushka, *Anal. Chem.*, 58 (1986) 1602–1607.
[6] S. Levin and E. Grushka, *Anal. Chem.*, 59 (1987) 1157–1164.
[7] S. Levin and E. Grushka, *Anal. Chem.*, 61 (1989) 2428–2433.
[8] E. Arvidsson, J. Crommen, G. Schill and D. Westerlund, *J. Chromatogr.*, 461 (1989) 429–441.
[9] S. Golshan-Shirazi and G. Guiochon, *Anal. Chem.*, 62 (1990) 923–932.
[10] S. Levin and S. Abu-Lafi, *Chirality*, 6 (1994) 148–156.
[11] S. Levin and S. Abu-Lafi, *J. Chromatogr. A*, in press.
[12] C.S.G. Phillips and C.R. McIlwrick, *Anal. Chem.*, 45 (1973) 782–786.
[13] A. Sokolowski, T. Fornstedt and D. Westerlund, *J. Liq. Chromatogr.*, 10 (1987) 1629–1662.
[14] T. Fornstedt, D. Westerlund and A. Sokolowski, *J. Liq. Chromatogr.*, 11 (1988) 2645–2684.
[15] T. Fornstedt, D. Westerlund and A. Sokolowski, *J. Chromatogr.*, 506 (1990) 61–74.
[16] T. Fornstedt, D. Westerlund and A. Sokolowski, *J. Chromatogr.*, 535 (1990) 93–110.
[17] T. Fornstedt and D. Westerlund, *J. Chromatogr.*, 648 (1993) 315–324.

ELSEVIER

Journal of Chromatography A, 691 (1995) 29–35

JOURNAL OF CHROMATOGRAPHY A

Microdialysis sampling coupled on-line to fast microbore liquid chromatography

Anqing Chen, Craig E. Lunte*

Department of Chemistry and Center for Bioanalytical Research, University of Kansas, Lawrence, KS 66045, USA

Abstract

A system which combines intravenous microdialysis sampling on-line with fast microbore liquid chromatographic analysis is described. Using a 14 mm × 1 mm I.D. ODS column, caffeine, theobromine and paraxanthine could be resolved in under 1 min and acetaminophen and its two main metabolites, the glucuronide and sulfate conjugates, could be resolved in 30 s. This fast separation allowed on-line microdialysis sampling to be conducted with a 1-min sampling interval. The system was evaluated by monitoring the pharmacokinetics following intravenous administration of acetaminophen and caffeine.

1. Introduction

Microdialysis sampling has been shown to be a powerful technique for pharmacokinetic investigations [1–5]. Liquid chromatography is commonly used for the analysis of microdialysis samples. The microdialysis sample is protein-free allowing direct injection into the chromatographic system. However, while microdialysis sampling is a continuous sampling method, liquid chromatography requires discrete samples. For chromatographic analysis, the dialysate is collected over some fixed time interval to provide the required sample volume. The high temporal resolution of microdialysis is therefore lost and becomes dependent upon the sample requirements of the chromatographic system. To minimize the sample volume required and therefore increase the temporal resolution of the experiment, microbore chromatographic systems are often employed with microdialysis sampling [1,2,4,6,7].

A difficulty encountered with microdialysis sampling is collection and injection of the small sample volumes. Using microbore chromatographic systems samples of 1 μl or less are common. With such small volumes loss from evaporation and sample transfer are major limitations requiring sophisticated sample collectors and autosamplers. That microdialysis samples are protein-free provides the potential for direct coupling of the microdialysis system to the chromatographic system because no sample clean-up is necessary. Such an on-line system also eliminates the problems associated with evaporation and sample transfer. On-line coupling of microdialysis sampling with microbore liquid chromatographic analysis has previously been reported [6–8]. The major limitation of these systems is that the temporal resolution of the sampling system is a function of the analysis time of the chromatographic system. The next sample cannot be injected until the previous one has

* Corresponding author.

0021-9673/95/$09.50
SSDI 0021-9673(94)00634-2

been completely eluted as no provision for sample storage is possible. This report describes the coupling of microdialysis sampling to fast microbore liquid chromatography to provide analysis times of less than 1 min and therefore 1-min temporal resolution for the pharmacokinetic experiment. This on-line system provides a near real-time response to multiple chemical species in an awake, freely moving experimental animal.

2. Experimental

2.1. Materials

Caffeine, paraxanthine, theobromine, theophylline and acetaminophen (APAP) were purchased from Sigma (St. Louis, MO, USA). Acetaminophen-4-O-sulfate (APAP-S) was prepared by the procedure of Feigenbaum and Neuberg [9]. Acetaminophen-4-O-glucuronide (APAP-G) was isolated from human urine. HPLC-grade acetonitrile was obtained from Fisher Scientific (Fair Lawn, NJ, USA). All other chemicals were reagent grade or better and were used as received.

2.2. Microdialysis system

Microdialysis sampling was performed using a CMA/100 microinjection pump from Bioanalytical Systems (BAS)/Carnegie Medicine (West Lafayette, IN, USA). The microdialysis pump was connected to a flexible cannula-style microdialysis probe which was inserted into the jugular vein of a rat. The microdialysis probe was constructed from dialysis tubing of regenerated cellulose with an inner diameter of 220 μm, a wall thickness of 22 μm and a molecular mass cutoff of 15 000 as described previously [4]. All connections from the pump to the microdialysis probe and from the microdialysis probe outlet to the injection valve were made with 0.1 mm I.D. FEP (Teflon) tubing. The perfusion solution was a Ringer's solution consisting of 155 m*M* NaCl, 5.5 m*M* KCl and 2.3 m*M* $CaCl_2$. A perfusion rate of 1.5 μl/min was used for all experiments. The experimental animal was housed in an awake animal containment system as described previously [4]. A two-channel liquid swivel was positioned in the flow path to provide a liquid connection that allowed free movement of the animal without tangling of the tubing.

2.3. Chromatographic system

The HPLC system consisted of a PM-60 LC pump (BAS, West Lafayette, IN, USA), a SPD-6A UV absorbance detector (Shimadzu, Columbia, MD, USA), and an electrically actuated HPLC injection valve with a 0.5-μl internal sample loop (Model E90; Valco Instruments, Houston, TX, USA). The injector switching rate and injection time were controlled by a personal computer. The dialysate was flushed directly into the injection valve. A schematic of the complete on-line microdialysis sampling–microbore chromatography analysis system is shown in Fig. 1.

Separation was achieved using a 14 mm × 1

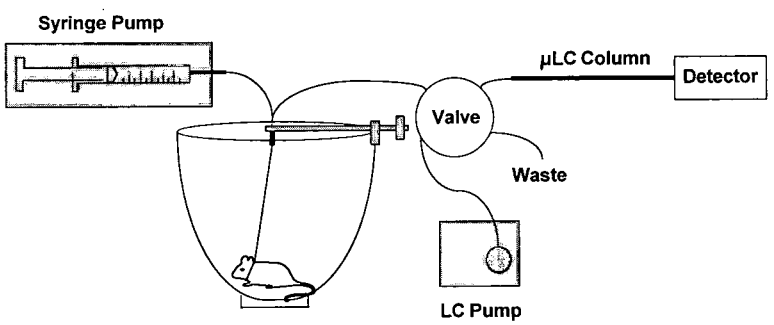

Fig. 1. Schematic diagram of the on-line microdialysis sampling–fast microbore chromatographic analysis system.

mm microbore BAS Sep-Stik column packed with 3-μm ODS material. The mobile phase for APAP and its metabolites was 0.05 *M* ammonium acetate buffer, pH 5.0. For caffeine and its metabolites the mobile phase was 0.05 *M* ammonium phosphate buffer, pH 2.5, with 5% (v/v) acetonitrile. A flow-rate of 200 μl/min was used for all experiments. For detection of APAP and its two metabolites the UV detector was operated at 250 nm. For detection of caffeine and its two metabolites the UV detector was operated at 273 nm.

2.4. *In vitro experiments*

For characterization of the on-line injection and chromatographic analysis system, the sample was directly introduced into the injection valve in a continuous manner. This was accomplished by directly connecting the microperfusion pump to the injection valve with the microdialysis probe replaced by a liquid switch. For these experiments the perfusion fluid was a Ringer's solution containing the desired concentration of APAP and its metabolites or caffeine and its metabolites. Up to three syringes can be controlled by a single microinfusion pump and therefore a blank Ringer's solution and two different concentrations of the analytes could be tested without stopping the system.

The response of the on-line microdialysis sampling–microbore chromatographic analysis system was also evaluated in the microdialysis sampling mode. In this case the microdialysis probe was placed in a beaker containing a stirred Ringer's solution. Concentration steps were achieved by quickly moving the microdialysis probe to beakers containing various concentrations of the analytes.

2.5. *Pharmacokinetic experiments*

Male Sprague-Dawley rates weighing between 300 and 400 g were used. The rat was anesthetized using a mixture of ketamine and xylazine (140 mg/kg ketamine, 12 mg/kg xylazine) given as intramuscular injection. The animal's body temperature was maintained with a heating pad beneath its body during surgery. The microdialysis probe and dosing cannula were implanted into the right jugular vein as previously described [4]. Animals were allowed 24 h to recover from surgery prior to a pharmacokinetic experiment. Microdialysis sampling was initiated at least 1 h prior to dosing the animal. For both APAP and caffeine, a 30 mg/kg dose of the drug in 1 ml of Ringer's solution was administered intravenously (i.v.). Microdialysis sampling was continued until the parent compound was no longer detectable in the dialysate, typically 2 h for APAP and 6 h for caffeine.

3. Results and discussion

3.1. *System characterization*

Using the system in the direct on-line injection mode the separations were optimized and the linearity and precision were determined. For APAP and its metabolites the elution order was APAP-G at 10 s, APAP-S at 19 s and APAP at 29 s, with resolutions of 2.43 and 1.59, respectively (Fig. 2). The response for all three compounds was linear from 0.3 to 20 μg/ml (Table

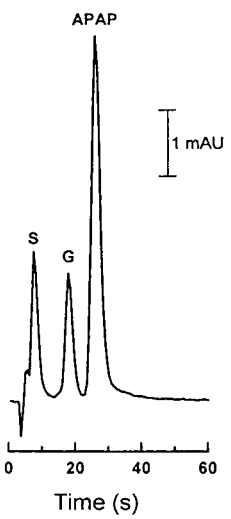

Fig. 2. Chromatogram of direct on-line injection of APAP and metabolites standard. Peaks: APAP = acetaminophen; S = acetaminophen-4-O-sulfate; G = acetaminophen-4-O-glucuronide.

Table 1
Linearity and detection limits

Compound	Range (μg/ml)	Slope (mAU μg^{-1} ml^{-1})	Intercept (AU)	r	Detection limit (μg/ml)[a]
APAP	0.3–20	0.0797	−0.023	0.9994	1.25
APAP-G	0.3–20	0.540	−0.035	0.9998	0.3
APAP-S	0.3–20	0.107	−0.026	0.9992	0.3
Caffeine	0.3–25	0.278	−0.001	0.9997	0.3
Theobromine	0.3–25	0.956	0.035	0.9993	0.3
Paraxanthine	0.3–25	0.831	−0.004	0.9998	0.3

[a]At $S/N = 3$.

1). For caffeine and its metabolites the elution order was theobromine at 13 s, paraxanthine at 21 s and caffeine at 46 s, with resolutions of 1.37 and 3.94, respectively (Fig. 3). Again the response for all three compounds was linear from 0.3 to 25 μg/ml (Table 1). The precision of multiple injections was about 2% R.S.D. in all cases, whether by direct injection or following microdialysis sampling. The precision appears slightly worse for microdialysis sampling relative to direct injection although in no case is the difference statistically significant.

The system response time was then evaluated by making step changes to the sample concentration. The response time was evaluated using both direct on-line injection and on-line microdialysis sampling. Typical responses to step changes in APAP concentration are shown in Fig. 4. There is no difference in the response to direct sample injection and on-line microdialysis sampling. Even with a 1-min sampling interval

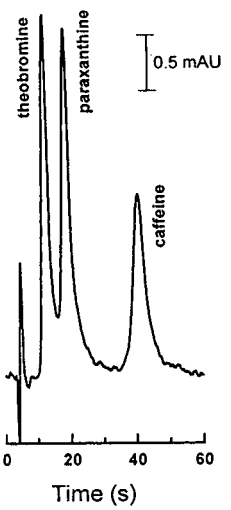

Fig. 3. Chromatogram of direct on-line injection of caffeine and metabolites standard.

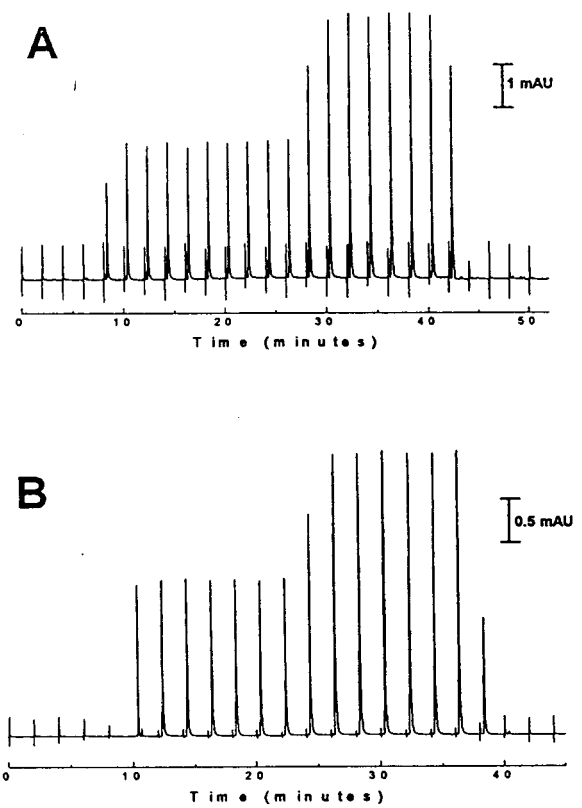

Fig. 4. System response to a step change in sample concentration of APAP. (A) Direct on-line injection; (B) on-line microdialysis sampling.

the microdialysis response can accurately monitor the sample concentration. It can be seen in Fig. 2 that the first sample following a step change in concentration does not give the new sample concentration. This is because the dialysate which is analyzed is of finite volume and reflects the time-averaged concentration of the sample over the sampling interval. For a step change in concentration, the sampling interval rarely begins just at the step and therefore the first dialysate represents some time at the initial concentration and some time at the final concentration. Fortunately, real processes are seldom instantaneous and this phenomena therefore does not result in a distortion of the response. Sampling intervals as short as 30 s have shown no distortion of the response due to slow sampling through the microdialysis probe. These results are in agreement with those recently reported by Newton and Justice [7] and of Hogan et al. [10].

3.2. Intravenous sampling

The performance of the on-line microdialysis sampling–fast microbore LC analysis system was initially evaluated in vivo using APAP. Representative chromatograms of a dialysate prior to dosing and after administration of 30 mg/kg APAP i.v. are shown in Fig. 5. The blank is clean except for a void peak due to endogenous unretained hydrophilic compounds. APAP and APAP-S are well resolved in 30 s in the dialysate following dosing with APAP. Unfortunately, APAP-G is very near the void which limits its quantification. The resulting pharmacokinetic curve for APAP is shown in Fig. 6. The results are plotted as a bar graph because each dialysate sample represents the time-averaged concentration in vivo over the sampling interval. This system provided for near real-time monitoring of the plasma concentrations of unbound APAP and APAP-S with a 1-min temporal resolution. Microdialysis samples the unbound fraction of the drug in plasma as proteins, and therefore protein-bound drugs, are excluded by the membrane. The pharmacokinetic curve shown in Fig. 6 is for free APAP. These results can be converted to total drug concentrations if the degree of protein binding is known. Alternatively, the in vivo binding can be determined by simultaneously withdrawing a whole blood sample from which to determine the total drug concentration.

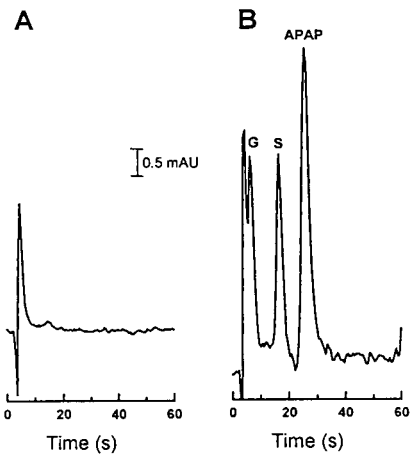

Fig. 5. Chromatograms of on-line intravenous dialysates. (A) Prior to administration; (B) 40 min after administration of 30 mg/kg APAP i.v.

The pharmacokinetics of caffeine were also examined using the on-line microdialysis sampling–fast microbore LC analysis system. Representative chromatograms of a dialysate prior to

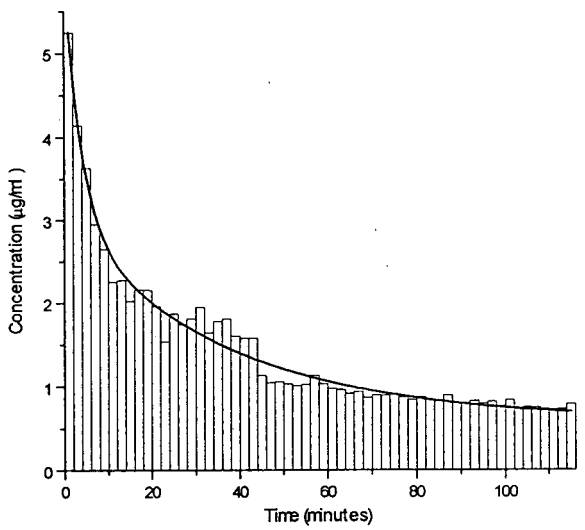

Fig. 6. Pharmacokinetic curve for APAP generated by intravenous microdialysis sampling coupled on-line to fast microbore HPLC.

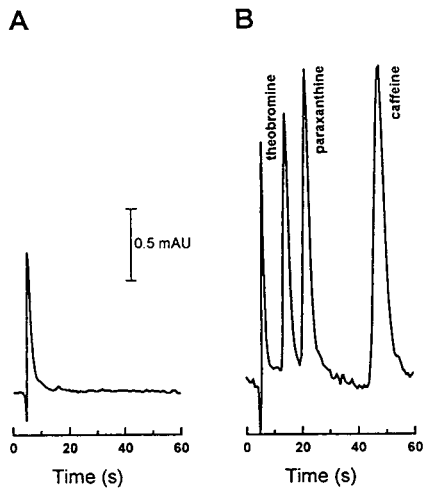

Fig. 7. Chromatograms of on-line intravenous dialysates. (A) Prior to administration; (B) 70 min after administration of 30 mg/kg caffeine i.v.

dosing and after administration of 30 mg/kg caffeine i.v. are shown in Fig. 7. In this case, caffeine and its two major metabolites, theobromine and paraxanthine, are all resolved from each other and the void in 50 s. The chromatographic results from a pharmacokinetic experiment using caffeine are shown in Fig. 8. The inset shows the individual chromatograms which constitute the curve in more detail. As can be

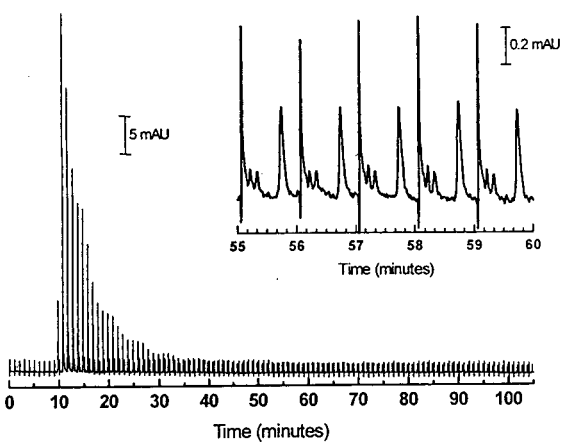

Fig. 8. Detector output from the on-line microdialysis sampling–fast microbore HPLC system following the plasma concentration of caffeine and its main metabolites. Caffeine was administered i.v. (30 mg/kg) at 10 min. The inset shows an expanded scale of the output from 55 to 60 min.

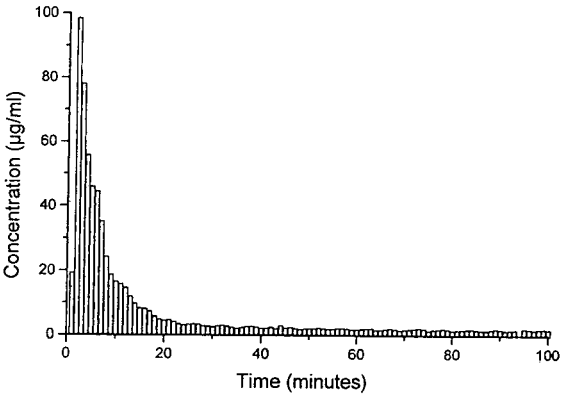

Fig. 9. Pharmacokinetic curve for caffeine generated by intravenous microdialysis sampling coupled on-line to fast microbore HPLC.

seen, the metabolites as well as caffeine can be detected in these dialysates. The resulting pharmacokinetic curve for caffeine is shown in Fig. 9.

4. Conclusions

Microdialysis sampling coupled on-line to fast microbore LC analysis provides near real-time monitoring of the in vivo concentration of multiple analytes with temporal resolutions of less than 1 min. The response time of the system is less than 1 min and a function of the sample volume needed for chromatographic analysis. This provides the possibility of building feedback into the system such that data from the current experiment can be used to modify that experiment. It may ultimately be possible to use an on-line sampling–analysis system such as this to provide therapeutic drug monitoring of multiple drugs and metabolites simultaneously.

Acknowledgements

The authors acknowledge the financial support of the National Institutes of Health through grant R01-GM44990 and the Center for Bioanalytical Research at the University of Kansas.

References

[1] K.L. Steele, D.O. Scott and C.E. Lunte, *Anal. Chim. Acta*, 246 (1991) 181–186.
[2] D.O. Scott, L.R. Sorensen, K.L. Steele, D.L Puckett and C.E. Lunte, *Pharm. Res.*, 8 (1991) 389–392.
[3] P. Lönnroth, J. Carlsten, L. Johnson and U. Smith, *J. Chromatogr.*, 568 (1991) 419–425.
[4] M. Telting-Diaz, D.O. Scott and C.E. Lunte, *Anal. Chem.*, 64 (1992) 806–810.
[5] P. Sjoberg, I.-M. Olofsson and T. Lundqvist, *Pharm. Res.*, 9 (1992) 1592–1598.
[6] S.A. Wages, W.H. Church and J.B. Justice, Jr., *Anal. Chem.*, 58 (1986) 1649–1656.
[7] A.P. Newton and J.B. Justice, Jr., *Anal. Chem.*, 66 (1994) 1468–1472.
[8] K.L. Steele, *M.S. Thesis*, University of Kansas, Lawrence, KS, 1993.
[9] J. Feigenbaum and C.A. Neuberg, *J. Am. Chem. Soc.*, 63 (1941) 3529–3533.
[10] B. Hogan, S.M. Lunte, J.F. Stobaugh and C.E. Lunte, *Anal. Chem.*, 66 (1994) 596–602.

ELSEVIER

Journal of Chromatography A, 691 (1995) 37–53

JOURNAL OF CHROMATOGRAPHY A

Optical properties of axial-illumination flow cells for simultaneous absorbance–fluorescence detection in micro liquid chromatography

Ahmad A. Abbas, Dennis C. Shelly*

Department of Chemistry and Biochemistry, Texas Tech University, Lubbock, TX 79409-1061, USA

Abstract

Simultaneous measurements of absorbance and fluorescence are possible with axial-illuminated flow cells, fashioned with a unique bend geometry. The optical properties of these flow cells have been studied. Effects of variations in lumen refractive index, capillary wall thickness and physical pathlength have been examined. A theoretical understanding of the various light propagation modes and of light intensity distributions in these modes, based upon lumen refractive index, has been attained. Of more practical significance, optical pathlengths from <1 cm to 6 cm are simply attained by positioning the inlet optical fiber along the capillary axis with respect to the bend. The flow cell volumes obtained with different combinations of capillary I.D. and optical pathlength make the flow cell and resulting detector compatible with conventional HPLC and microscale separations. Also, studies have been performed to determine the effects of increased optical pathlength on overall analytical separation efficiency and detectability in the analysis of polynuclear aromatic hydrocarbons using laser-induced fluorescence micro-LC.

1. Introduction

Microcolumn separation techniques, such as micro-LC and capillary electrophoresis, have gained considerable interest during the past decade [1–3]. These techniques have provided extremely high separation efficiencies and rapid analyses, compared to conventional methods. In order to exploit these advantages, it is necessary to minimize extracolumn dispersion, particularly in connecting tubes and at the detector. "On-column" detection techniques [4–6], utilizing cross-capillary illumination of the actual micro-column, provide the lowest extracolumn dispersion. Also, post-column, cross-capillary illumination has provided acceptable performance for UV absorbance [7,8] and fluorescence [9,10] detection in micro-LC. Various flow cell and illumination options for laser-induced fluorescence detection have been reviewed [11,12]. Though quite reasonable detection limits have been reported with these detection schemes, the small optical pathlengths (50–250 μm) result in very small illuminated volumes. This limits absorbance and fluorescence signal intensities and prevents detection of solutions with low concentrations, e.g. high concentration limits of detection.

Illuminating a capillary flow cell along its axis (axial illumination) is one way to increase the pathlength for optical detection [13–27]. It is achieved by focussing light with a lens (convex lens, ball lens, etc) [13,16–22,25,26] or inserting

* Corresponding author.

0021-9673/95/$09.50
SSDI 0021-9673(94)01036-6

a light-guiding optical fiber directly into the capillary flow cell [14,24]. Once light enters the capillary, it propagates by total internal reflection, external reflection and refraction at the wall–air and/or wall–lumen interface, thus confining its energy within the outer wall boundaries of the capillary [28]. A lensless, externally mirrored capillary flow cell has been reported [27].

Various axial-illumination flow cell designs have recently been developed in order to improve the concentration sensitivity of detectors for micro-LC and capillary electrophoresis. The importance of eliminating mechanical vibrations and the necessity for smooth coupling of source light into the capillary flow cells (50–250 μm I.D) are some of the most important design considerations. Abbas and Shelly [25] coupled laser light inside a 150 μm I.D capillary flow cell (pathlength 1 cm) using a convex lens with a unique nebulizer orifice. This device eliminated solvent droplet formation at the exit end of the flow cell, enabling efficient coupling of incident laser light into the capillary and approximately $1 \cdot 10^{-10}$ M concentration detectability for aflatoxins. Also, Chervet and co-workers [16,22] constructed a capillary "Z shaped" flow cell (pathlength 3 mm) for micro-LC with UV absorbance detection. The "Z" cell was merely interposed between the source and the transducer. There was no "coupling" in actuality [16,22]. This produced very low light transmission in the flow cell capillary, mainly due to the large fraction of light refracting out of the capillary, before reaching the detector. This resulted in high background noise and low signal-to-noise ratio (S/N). Moring and Reel [26] reported improvements in the absorbance S/N (minimum detectable concentration, MDC, of 10^{-8} M), by coupling light with sapphire ball optics into the "Z" cell. Taylor and Yeung [24] inserted a 46-μm light-guiding optical fiber into a 75 μm I.D. capillary for laser-induced fluorescence detection in capillary electrophoresis. Concentration detection limits ($S/N = 3$) of between $1 \cdot 10^{-11}$ and $6 \cdot 10^{-12}$ M were reported for Rhodamine 6G. A 7-nl multireflection flow cell has been developed by Wang et al. [27]. In this device, a straight externally mirrored capillary is illuminated through the wall at an angle sufficient to cause multiple cross-capillary reflections, over a total linear distance of less than 1.5 mm. Substantial increases in sensitivity (40 ×) and pathlength (44 ×) were reported for absorbance detection in capillary electrophoresis. A concentration limit of detection of $3 \cdot 10^{-7}$ M for Brilliant Green was reported.

Most of this micro-LC detector development work has resulted in flow cells/detectors that enable single-parameter measurement. This does not fully utilize the available optical information. Also, many analytes may not be detected under optimum conditions in single-parameter sensing. Consequently, there is a need for simultaneous measurement of more than one signal (absorbance, fluorescence, refractive index, etc.). Consider the TriDet, trifunctional detector for conventional HPLC [29], which permits simultaneous absorbance, fluorescence and conductivity measurements. Multiparameter detection can provide much greater overall detectability and also generate more information about a particular analyte in a single chromatographic experiment. To the best of our knowledge, there has only been one report of multiparameter optical detection for miniaturized LC, namely simultaneous absorbance, fluorescence and refractive index microbore LC [30] using a "rather large" 1-μl flow cell.

In this paper we show how light-propagation characteristics of a unique bent capillary flow cell can be exploited for multiparameter optical detection. A description of the design and operation of the simultaneous absorbance–fluorescence capillary flow cell and detector are presented. The dependence of absorbance and fluorescence signal intensities on lumen refractive index ($n_1 = 1.3587$–1.4940), physical pathlength (1–5.8 cm) and capillary wall thickness (65–271 μm) are discussed in detail. Finally, we examine the combined influence of fluorescence optical window length on detectability and separation efficiencies for a model reversed-phase micro-LC separation of polynuclear aromatic hydrocarbons.

2. Theory

In order to obtain a large optical signal (absorbance, fluorescence, etc), the analyte must interact with most of the incident light energy. For capillaries, this is possible if most of the incident light is present in the lumen, as opposed to the wall of the capillary. Light distribution in the wall and the lumen depend on various factors such as the method used to introduce light into the capillary (as discussed in the Introduction), ratio of the lumen and wall refractive indices and lumen and wall thicknesses. Tsunoda and coworkers [14,15] used statistical methods such as Markov chain and Monte Carlo simulations to show that a propagating photon (ray) will spend half of its time in the lumen and half in the wall, for a particular capillary dimension (wall and lumen thickness) and lumen/wall refractive indices. In our previous work [25] we used a ray trace diagram approach to analyze the light propagating pathways inside a capillary flow cell. Results obtained therein, using Snell's law and simple trigonometric functions, showed the effects of lumen refractive index on effective pathlength, for any propagating ray. We also found that the calculated effective pathlength was smaller than the physical pathlength of the capillary flow cell, when ray propagation occurred via pathway C (light propagation in the capillary wall *and* lumen), under the conditions used. The effective pathlength would exceed the physical pathlength *only* when pathway B (light propagation only in the capillary lumen) was the major light propagating pathway. We also observed that effective numerical aperture of the capillary increased with lumen refractive index and we concluded that this was partly responsible for increased fluorescence signals for higher mobile phase refractive indices. Strictly speaking, this change in numerical aperture is justified only for point source illumination at the lumen face. Since the lens defined the entrance cone to be smaller than this aperture, there must have been a different reason for these observations. Also, a complete description of light propagation was not achieved, as neither the angular distribution of incident light rays nor the complicating influence of lumen refractive index were taken into account.

In the present paper we have used Fresnel's equations [28] to obtain the values of reflectance and transmittance of a light ray at the lumen–wall and wall–air interfaces. In this scenario externally reflected rays remain within the lumen and refracted rays are transmitted out of the lumen. These equations provide a means for determining the fraction of a light ray that is distributed in the wall and the lumen of the capillary after striking such an interface. Eqs. 1 and 2 are Fresnel's equations for a lumen-propagating light ray, incident at the lumen–wall interface;

$$r_{sl} = -\sin(\phi_L - \phi_w)/\sin(\phi_L + \phi_w) \quad (1)$$

$$r_{pl} = \tan(\phi_L - \phi_w)/\tan(\phi_L + \phi_w) \quad (2)$$

where r_{sl} and r_{pl} are the reflection coefficients for the perpendicular and parallel components of light approaching the lumen/wall interface from the lumen and ϕ_L and ϕ_w are the angles as shown in Fig. 1. When a light ray approaches the lumen–wall interface, after propagating in the wall, the reflection coefficients for the perpendicular and parallel components are given as r_{sw} and r_{pw}, respectively, as shown below

$$r_{sw} = \{\cos(\phi_w) - [(n_l/n_w)^2 - \sin(\phi_w)^2]^{1/2}\}/\{\cos(\phi_w) + [(n_l/n_w)^2 + \sin(\phi_w)^2]^{1/2}\} \quad (3)$$

$$r_{pw} = \{(n_l/n_w)^2 \cos(\phi_w) - [(n_l/n_w)^2 - \sin^2(\phi_w)]^{1/2}\}/\{(n_l/n_w)^2 \cos(\phi_w) + [(n_l/n_w)^2 - \sin^2(\phi_w)]^{1/2}\} \quad (4)$$

where n_l and n_w are the lumen and the wall refractive indices, respectively. Since we used an unpolarized light source, the reflectance, R, of a particular light ray is the average reflectance of

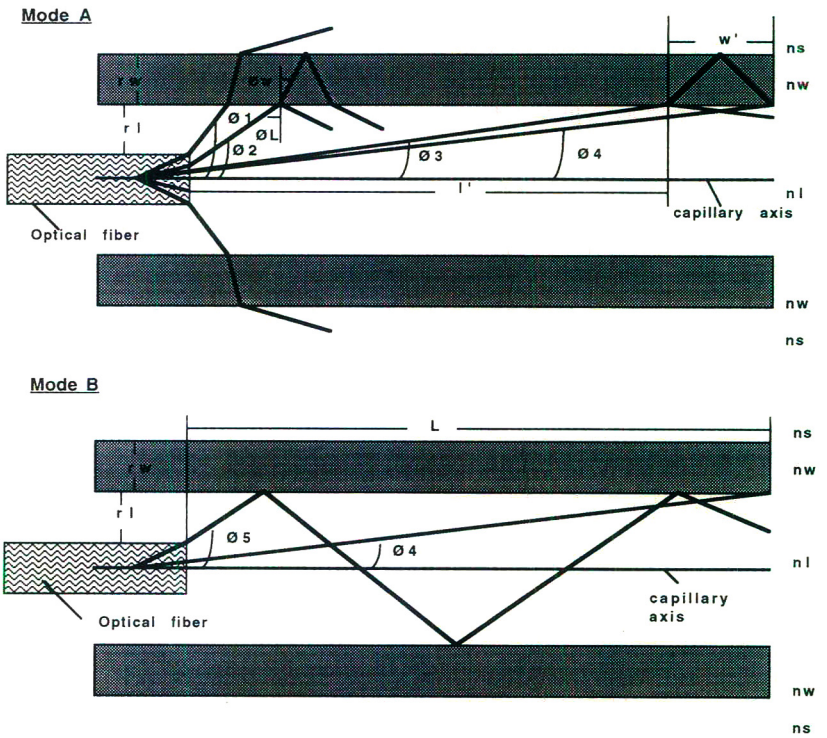

Fig. 1. Light propagation modes inside a capillary. n_s, n_w and n_l are the refractive indices of the medium surrounding the capillary, capillary wall and the lumen, respectively. r_l and r_w are half the lumen and wall thickness, respectively. The dark lines represent the different angled rays of light incident inside the capillary. l', w' and L are the distances as shown.

the parallel and the perpendicular components [28] and is given as

$$R_l = 0.5\left(r_{sl}^2 + r_{pl}^2\right) \quad (5)$$

$$R_w = 0.5\left(r_{sw}^2 + r_{pw}^2\right) \quad (6)$$

Fig. 1 shows ray trace diagrams for the different types of light propagation modes that are present in an axial-illumination capillary flow cell. These are correctly grouped into two categories, mode A and mode B, which exist according to inequalities 7 and 8 as

$$\text{Mode A: } n_l < n_w/\sin\,\phi_L \quad (7)$$

$$\text{Mode B: } n_l > n_w/\sin\,\phi_L \quad (8)$$

As shown in Fig. 1, at any instant in time, light energy is completely confined to the lumen if mode B is the light-propagating mode or light is distributed in both the wall and the lumen if mode A is observed. Let us consider each mode individually.

2.1. Mode A

This mode of light propagation can be divided into four submodes. Each submode is defined by finite angular light ray distributions according to the boundary conditions:

Mode A1: $\phi_1 \geq \phi > \phi_2$

Mode A2: $\phi_2 \geq \phi > \phi_3$

Mode A3: $\phi_3 \geq \phi > \phi_4$

Mode A4: $\phi_4 \geq \phi \geq 0$

Mode A1

For most chromatographic mobile phase (refractive indices, n_1, >1.2) and optical fiber (numerical aperture, NA, ≤ 0.8) combinations this mode does not exist. In this mode light rays refract out of the capillary at the wall–air interface since the angle that all light rays make at this interface (ϕ_w) will always be less than ϕ_{wc}, the critical angle for light to internally reflect at the wall–air interface. Obviously, this is a "lossy" mode. With proper selection of lumen refractive index and fiber numerical aperture, this mode can be completely eliminated. Using Snells law (see [28]) ϕ_{wc}, ϕ_1 and ϕ_2 can be calculated as shown below.

$$\phi_{wc} = \sin^{-1} (n_s/n_w) \quad (9)$$

$$\phi_1 = \sin^{-1} (NA/n_1) \quad (10)$$

$$\phi_2 = \pi/2 - \sin^{-1} (n_s/n_1) \quad (11)$$

where n_s is the refractive index of the medium surrounding the capillary (air). Unlike mode A1, modes A2–A4 are the capillary-confined modes.

Mode A2

Mode A2 is the main light propagating mode (containing 97–98% of total light energy) when $n_1 < n_w$. When a ray of light that is within the confined angular boundaries supporting this mode (see above), is incident on the lumen–wall interface, two optical phenomena occur simultaneously. The light ray is refracted into the wall and externally reflected back into the lumen, as noted above using Fresnel's theory. Similarly, when a ray of light in the wall is incident on the lumen–wall interface, external reflection at the wall and refraction into the lumen occur simultaneously. Unlike mode A1 all the light rays incident at the wall–air interface are internally reflected back into the capillary. These processes repeat as the light ray propagates along the capillary. Variation of lumen refractive index will alter the fraction of light energy that is refracted and externally reflected at each interface. Fortunately, this can be calculated using Eqs. 1–6. The lower angular cutoff for mode A2 is an angle less than ϕ_3, where ϕ_3 is the angle for which $l' + w' = L$. Here, the propagating light ray, after penetrating the wall, will never reenter the lumen. l' and w' are given in Eqs. 12 and 13.

$$l' = r_1/\tan \phi_3 \quad (12)$$

$$w' = 2r_w \tan \left[\sin^{-1} (n_1/n_w \cos \phi_3)\right] \quad (13)$$

where r_1 and r_w are half the lumen and the wall thicknesses, respectively.

Modes A3 and A4

When n_1 is small compared to n_w only a very small fraction of light energy will propagate in mode A3. The angular distribution of light rays in mode A3 increases with lumen refractive index. Fresnel's equations can be used to find the fraction of light externally reflected in the lumen and refracted into the wall, for mode A3. Mode A4 is a single pass mode and is strictly dependent on r_1 and L (physical pathlength of the capillary flow cell). It is composed of a very small fraction of the total light rays. ϕ_4 defines the upper boundary and is given by Eq. 14

$$\phi_4 = \tan^{-1} (r_1/L) \quad (14)$$

2.2. Mode B

When light is incident at the lumen–wall interface, having been launched from an optical fiber with numerical aperture NA, and inequality 8 is satisfied, light will propagate as mode B (see Fig. 1). The angle at which *all* light is reflected back into the lumen (total internal reflection) is defined as ϕ_c. ϕ_c is given by inequality 15.

$$\phi_c \geq \sin^{-1} (n_w/n_1) \quad (15)$$

We can define an angle $\phi_{1'}$ such that $\phi_{1'} = \pi/2 - \phi_1$. ϕ_1 is defined in Eq. 10 and represents the largest angle of the light ray emitted by the fiber. For mode B to occur $\phi_{1'}$ must be greater than or equal to ϕ_c. Using a graphical mathematical computing program, MathCAD (Mathsoft, Seattle, WA, USA), we found that the lumen refractive index at which mode B occurs lies between

1.471 and 1.472. The numerical aperture for these calculations was chosen to be 0.2. The number of reflections in the lumen is maximized when n_l is at least equal to $n_w/\sin \phi_L$ and decreases as the lumen refractive index increases further.

Fig. 2 is a graphic representation of the behavior of Fresnel's equations over a wide range of lumen refractive indices, satisfying mode A. The variation of reflectance (R_l) and transmittance ($T_l = 1 - R_l$) of a light ray at the lumen–wall interface for n_l from 1.359 to 1.494 is shown in Fig. 2. Reflectance decreases with n_l up to 1.458, where it equals zero. Here, $n_l = n_w$. Thus a hollow cylindrical lightguide (capillary flow cell) behaves as a solid cylindrical lightguide (step index optical fiber). Further increases in n_l lead to a much higher reflectivity, hence a larger distribution of light in the lumen. This continues until $n_l \geq n_w/\sin \phi_L$ where light is totally reflected back into the lumen. At this point a transformation of the externally reflected mode (of mode A2) to the totally internally reflected mode (mode B) occurs (not shown in figure).

Consider that a beam of light is actually composed of a large number of rays incident at the interface and that each ray will have some fraction of its light distributed in the wall and the lumen of the capillary, determined by Fresnel's equations. Rays with small inclination, with respect to the capillary axis, will distribute more of their incident light into the externally reflected mode, compared to the refracted mode. As the angle increases, the fraction of light in the externally reflected mode decreases (decreasing reflectance). This confirms that axial-illumination flow cells are highly directional under optimal conditions suitable for reversed-phase micro-LC.

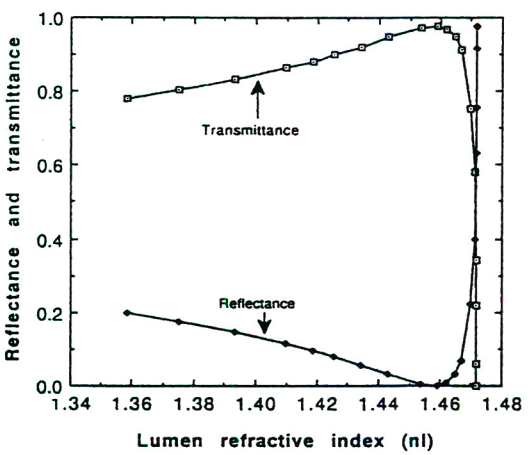

Fig. 2. Theoretically generated curve for reflectance and transmittance at the lumen–wall interface. For computation NA = 0.2 and $n_w = 1.458$.

3. Experimental

3.1. Capillary flow cell

Two types of bent flow cells were fabricated using fused-silica capillaries (Polymicro Technologies, Phoenix, AZ, USA). Fig. 3 shows photographs of the bend geometries, eccentric (a) and 90° (b) immediately after bend formation. A jig, containing a razer blade that was attached to metal clamps, and a butane microtorch were used to reproducibly bend the fused-silica capillaries. Fig. 3c and d shows light exiting at the bends of water-filled capillaries. These photographs were obtained with a 35 mm camera that was equipped with a $f/1.2$ lens. Water vapor from a dry ice–water bath was used to visualize the He–Ne laser (Melles Griot, Irvine, CA, USA) light Each of the two straight portions of the flow cells were about 7 cm long.

3.2. Simultaneous absorbance–fluorescence detector

Fig. 4 is a diagram that illustrates the operating principles of the simultaneous absorbance and fluorescence detector flow cell. Note the overall flow cell geometry, as described above. A block diagram of the entire instrument is shown in Fig. 5. A Model 487C Xenon cold fountain lamp (Karl Storz Endoscopy-America, Los Angeles, CA, USA) was used as the optical source. Wavelength selection was achieved with a $f/3.5$ grating monochromator (Optical Technology Devices, Elmsford, NY, USA). Light from the monochromator was focused into two 116-μm core diameter optical fibers (Polymicro

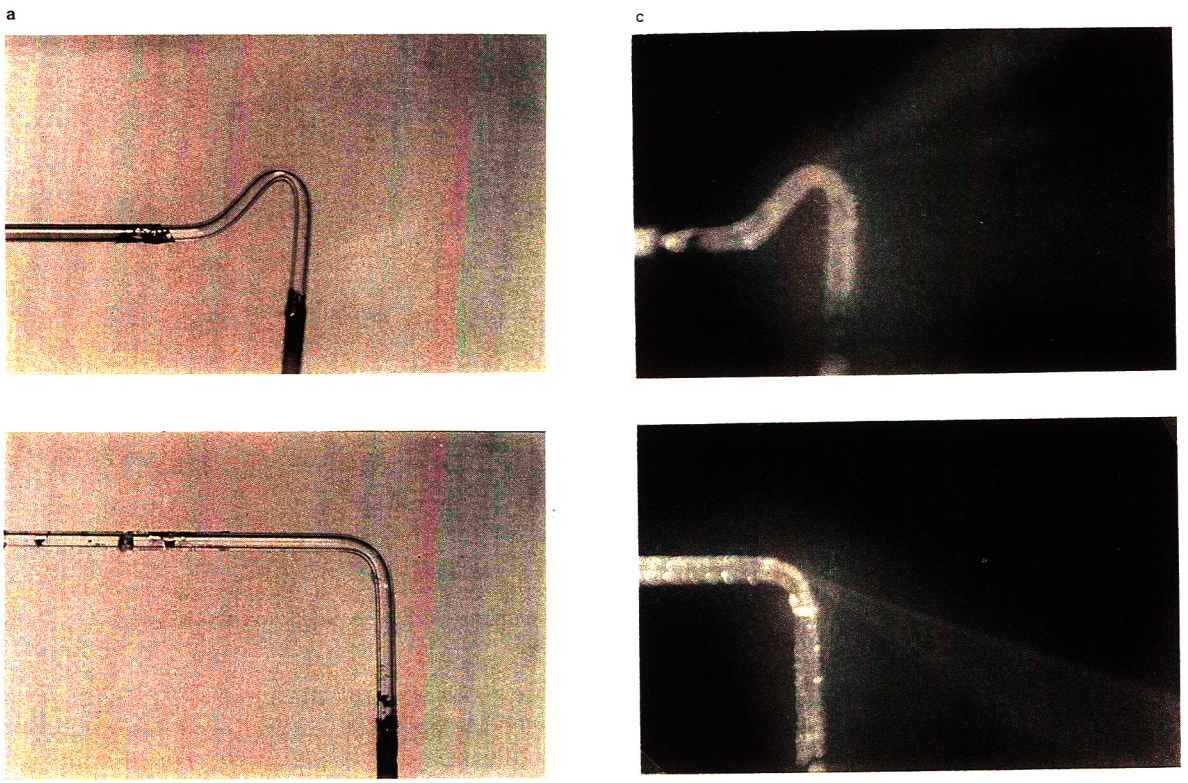

Fig. 3. Photographs of bent fused-silica capillaries (250 μm I.D. × 345 μm O.D.). (a) and (b) represent the eccentric and the 90° bend capillary flow cells, respectively. He–Ne laser light decoupled at the eccentric and 90° bend capillaries are shown in (c) and (d), respectively. In all cases the lumen contained water.

Technology) using a biconvex lens (Edmund Scientific, Barrington, NJ, USA). Two, nearly identical, 250 μm I.D, fused-silica eccentric bend capillaries were used as sample and reference cells. The optical fibers were inserted inside these capillaries, as shown in Fig. 4, and the pathlength of the detector window was adjusted by simply moving the optical fiber inside the capillary. Note that mobile phase enters at the arm opposite to that of the optical fiber; therefore, the optical fiber enters at the mobile phase exit of the capillary cell. Silicon photocells (Electronic Goldmine, Scottsdale, AZ, USA) were used as absorbance detector optical transducers. The capillary bends were positioned 1.5 mm from each detector, such that the exiting cone of light illuminated the entire face of the photocells. The fluorescence optical window was formed by removing the polyimide coating from a 2.4-cm length portion adjacent to the bend, using hot concentrated sulfuric acid. Fluorescence from this optical window was then imaged onto a Model R928 photomultiplier tube (PMT) (Hamamatsu, Bridgewater, NJ, USA), operated at 900 V. The emission optics consisted of a $f/1.5$ cylindrical lens (Melles Griot) and plastic sheet-type long-pass (>480 nm) cut-off filters (Roscolux, Port Chester, NY, USA). The mounting of optics and optoelectronics was accomplished by glueing Lego blocks of various shapes (Lego Systems, Enfield, CT, USA) into the appropriate geometries. Both photocells were electronically connected to a Model 757N log ratio amplifier (Analog Devices, Norwood, MA, USA) whose output was then digitized by a Model DT-2805 A/D board (Data Translation, Marlboro, MA,

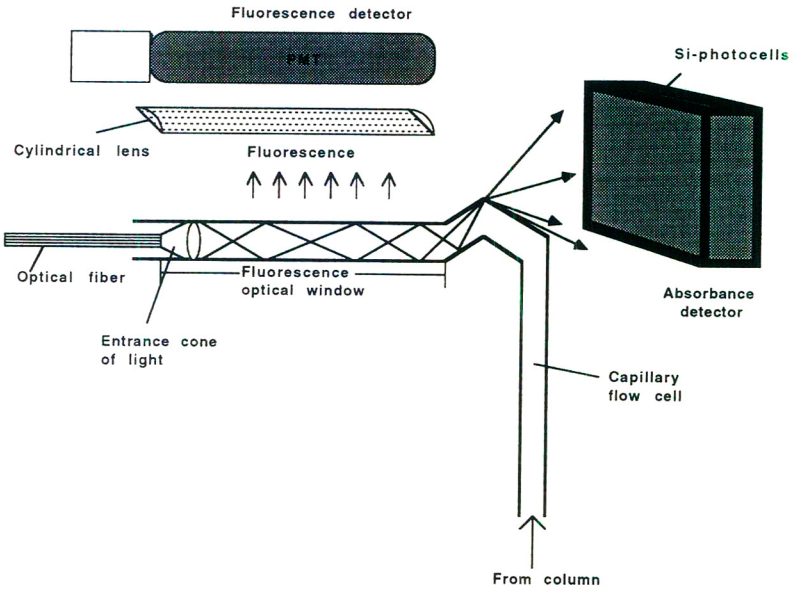

Fig. 4. Functional diagram of the simultaneous absorbance–fluorescence detector flow cell.

USA) and stored in a XT-class computer for further data analysis. Similarly for fluorescence, the analog output from the PMT was amplified with the electrometer from an Aminco Fluoromonitor HPLC detector (SLM-Aminco, Urbana, IL, USA) and digitized with a separate A/D–computer combination.

3.3. Micro-LC

Seven component polynuclear aromatic hydrocarbon mixtures were separated using reversed-phase micro-LC. A 250 μm I.D. fused-silica capillary (Polymicro Technologies), was packed with Spherisorb ODS2 (5 μm) particles (Alltech, Deerfield, IL, USA) using a computer controlled pump [31]. The length of the column used was 45 cm. A Model 8500 syringe pump (Varian Associates, Walnut Creek, CA, USA) was used for mobile phase delivery; 10-s sample injections were performed using a C14W microinjector (Valco, Houston, TX, USA) that was equipped with a 100-nl internal loop. All injections were of the moving loop type. The polynuclear aromatic hydrocarbon mixture was prepared by dissolving the sample in filtered (0.2-μm membrane) mobile phase (acetonitrile–water, 92:8). A Model 4412 B UV (325 nm) He–Cd laser (Liconix, Sunnyvale, CA, USA) was coupled with a 50-μm core diameter optical fiber using a $f/1.9$ planoconvex quartz lens (Oriel, Stanford, CT, USA) and an optical fiber positioner (Newport, Irvine, CA, USA). The other end of this fiber was then inserted into a low-volume capillary flow cell (99 μm I.D., 66 μm wall thickness), transferring approximately 40 μW (5.2 mW total laser power) into the flow cell. Fluorescence was measured with the R928 PMT, operated at 900 V. A 2-cm pathlength liquid filter, containing saturated aqueous cobalt sulfate, was used to minimize continuous emission from the laser. A 380-nm long-pass filter, a 385–488-nm band pass filter (both from Oriel) and a cylindrical lens ($f/1.5$, Melles Griot) were used as emission optics.

3.4. Data analysis

All chromatographic signals were analyzed using DADiSP 32 (DSP Development, Cambridge, MA, USA) digital signal processing software. Various operations, such as determination

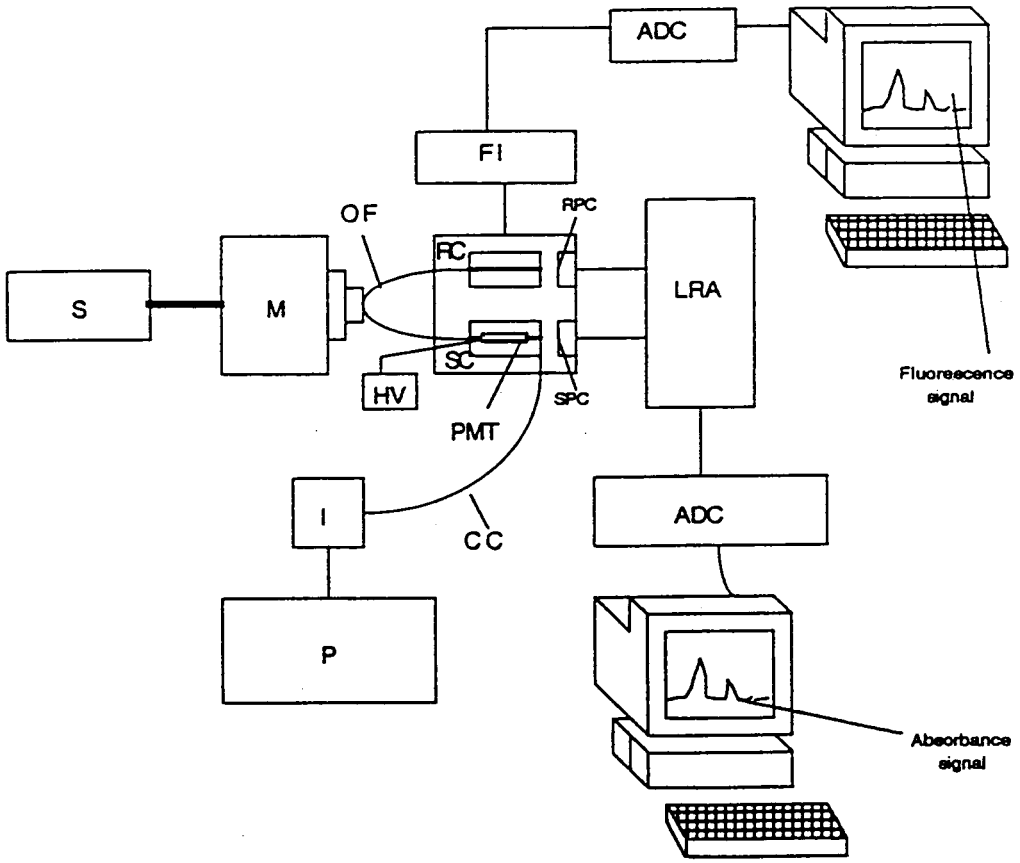

Fig. 5. Experimental setup for simultaneous absorbance and fluorescence measurements. S = Source; M = monochromator; OF = optical fiber; SC and RC = sample and reference cell, respectively; SPC and RPC = sample photocell and reference photocell, respectively; LRA = log ratio amplifier; Fl = fluorometer; PMT = photomultiplier tube; HV = high voltage to the PMT; CC = capillary column; I = injector; P = pump; ADC = analog-to-digital converter.

of noise from a baseline and peak height, were easily performed with this software.

3.5. Chemicals and reagents

Non-chromatographic mobile phases included absolute ethanol (AAPER Alcohol and Chemical Co., Shelbyville, KY, USA), chlorobenzene (MCB Reagents, Cincinnati, OH, USA) and mixtures (with different v/v ratios) of ethanol and chlorobenzene. All mobile phases were reagent grade and were used without further purification. The chromatographic mobile phase consisted of a 92:8 mixture of acetonitrile (Burdick & Jackson Labs., Muskegon, MI, USA) and water (Nanopure, Barnstead, Boston, MA, USA). Perylene and Rhodamine 6G were purchased from Aldrich (Milwauke, WI, USA) and the polynuclear aromatic hydrocarbons were obtained from Chem Services (West Chester, PA, USA).

3.6. Additional instrumentation

All solution refractive indices were measured using a Bausch & Lomb refractometer (Rochester, NY, USA). The absorbance and fluorescence (1 cm pathlength) of Rhodamine 6G solutions were recorded on a Model UV-265 UV–Vis spectrophotometer (Shimadzu Scientific Instru-

ments, Columbia, MD, USA) and a Model 4800C spectrofluorometer (SLM-Aminco), respectively. A Harvard Apparatus (Natick, MA, USA) syringe pump was a substitute for the Varian pump for all of the non-chromatographic flow cell evaluation work.

4. Results and discussion

4.1. Comparison of bend geometries

Three important optical phenomena can be used to characterize the bend geometries. Differences in beam divergence and angular deviation were noted at various mobile phase refractive indices (data not shown). Fig. 3c and d show light decoupling from water-filled lumens in the eccentric and 90° bends, respectively. Note the differences in direction of this decoupled beam for the two bend geometries. Note also differences in beam divergence and light distribution within the beams. While these two phenomena are critical to a complete understanding of flow cell operation, we considered them to be secondary to the ability to efficiently decouple light at the bend. Thus, this third phenomenon (light decoupling) became the most important design consideration for simultaneous absorbance–fluorescence sensing. The eccentric bend capillary flow cell was chosen for all optical and chromatographic evaluations in this work due to its enhanced light decoupling efficiency for a wide range of mobile phase refractive indices. Comparative performance studies of these two flow cell geometries is the subject of a separate publication.

4.2. Detection limits and linearity

The performance of the detector can be judged from its ability to measure small concentrations of analytes and the concentration range over which the detector gives a linear response. We fabricated a variable-pathlength flow cell, whose detection window could be varied by moving the optical fiber (core 116 μm, clad 140 μm, jacket 162 μm) inside the capillary. An eccentric bend capillary with a 250 μm I.D. was used as the flow cell.

Absorbance

Rhodamine 6G solutions ($5 \cdot 10^{-7}$ to $1 \cdot 10^{-4}$ M) were injected into a stream of ethanol through a 60 cm × 250 μm I.D. capillary at a flow-rate of 20.6 μl/min. Visible light at 530 nm and a 5-cm optical pathlength were used for these absorbance measurements. Fig. 6 shows the behavior of absorbance S/N over this range in injected concentration. The injected concentration limit of detection was $1.62 \cdot 10^{-7}$ M ($S/N = 3$) and it was linear over 2.5 orders of magnitude (response index of 0.9716). The sensitivity of the measurement appeared to be shot noise limited. Electronic noise corresponding to ± 0.5 milliabsorbance units (mAU) levels was recorded. These were at least two orders of magnitude higher than those obtainable with commercial detectors. However, the concentration limit of detection is comparable to that reported in the literature for Rhodamine 6G. Planned improvement in this detector design include use of low dark current UV-sensitive photodiodes and a configuration that will allow us to keep the photodetectors as close as possible to the electronics module.

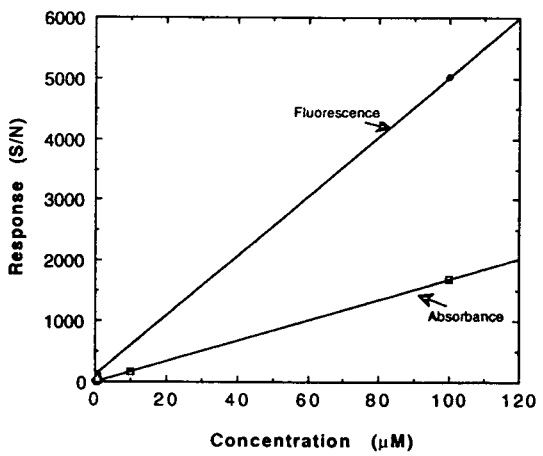

Fig. 6. Variation of absorbance and fluorescence response (S/N) with concentration.

Fluorescence

Perylene solutions from $5 \cdot 10^{-8}$ to $1 \cdot 10^{-4}$ M were injected into ethanol at 20.6 μl/min. A cylindrical lens collected fluorescence light from a 2.4-cm region, one edge of which was just outside the fluorescence optical window (see Fig. 4). This placement helped to minimize specular reflections from the optical fiber and scattering effects from the capillary wall. Fluorescence optical window position was optimized for maximum fluorescence signal by making fluorescence measurements at different optical fiber positions inside the capillary flow cell. Fluorescence response for the concentration range studied is also shown in Fig. 6. The concentration limit of detection was $15 \cdot 10^{-9}$ M and the response index was 0.8313 for the 3.5 orders of magnitude. Non linear response in fluorescence signal intensity at high fluorophore concentration ($1 \cdot 10^{-4}$ M) was observed. We attribute this is to preabsorption filtering along the length of the capillary, i.e. decreasing incident light intensity with increasing distance from the optical fiber. At low analyte concentration this effect is negligible due to very small analyte absorbance. However, as analyte concentration increases propagating incident light decreases exponentially with pathlength as a fundamental consequence of Beer's law.

4.3. Variation of absorbance and fluorescence with flow cell physical pathlength

Absorbance versus pathlength

The pathlength was varied from 1 to 5.8 cm by simply moving the optical fiber relative to the bend. All concentrations of Rhodamine 6G (listed above) were injected for each fixed optical pathlength and the absorbance S/N was plotted as a function of analyte concentration. Sensitivity versus pathlength is plotted in Fig. 7a. The slopes of the response curves (sensitivities) increased from $2.9 \cdot 10^{6}$ mAU/M for 1 cm pathlength to $19.5 \cdot 10^{6}$ mAU/M for 5.8 cm pathlength, an seven-fold increase in sensitivity for a five-fold increase in pathlength. The slope of a log–log plot (not shown) was found to be 1.093. These results clearly indicate that absorbance increases linearly with pathlength, over the range

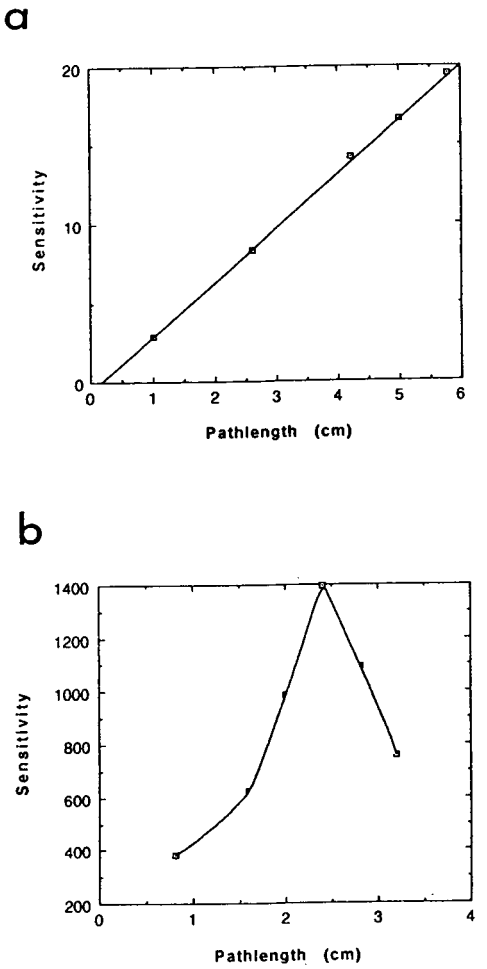

Fig. 7. Variation of detection sensitivity for absorbance (a) and fluorescence (b) with changes in optical pathlength.

of pathlength studied. This experiment indicates Beer's law behavior for small-I.D. axially illuminated capillary flow cells and also verifies that large pathlengths can be used without deviation from linearity neglecting refractive index artifacts. This is not particularly surprising considering that the major light propagation pathway, mode A2, is highly directional (see Theory) and coincident upon the cell's physical pathlength.

Fluorescence versus pathlength

The total fluorescence pathlength that could be obtained was limited to 2.4 cm because of

experimental constraints, i.e. PMT photocathode dimensions and cylindrical lens. Different pathlengths were obtained by moving the optical fiber from 0.8 cm within the fluorescence optical window to 3.2 cm or 0.8 cm beyond that segment of the capillary seen by the PMT. These locations corresponded to distances of 1.8–4.2 cm, relative to the bend. Fluorescence signals for $1 \cdot 10^{-6}$, $1 \cdot 10^{-5}$ and $1 \cdot 10^{-4}$ M Rhodamine 6G solutions at each pathlength were obtained. A plot of sensitivity versus pathlength is shown in Fig. 7b. We see that fluorescence sensitivity increases with pathlength from 0.8 to 2.4 cm and then decreases up to 3.2 cm. This decrease in signal is due to the fact that the incident light intensity reaching the fluorophore at the fluorescence optical window is less than the light intensity at the face of the optical fiber. This self absorption phenomenon [32] is more prominent at higher fluorophore concentrations.

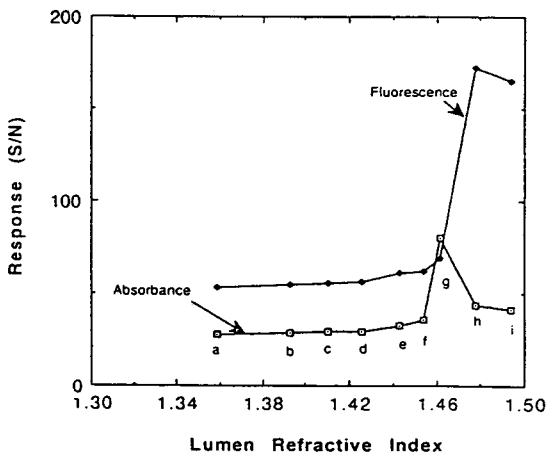

Fig. 8. Variation of absorbance and fluorescence response (S/N) with changes in lumen refractive index. Mobile phase refractive indexes: a = 1.3587; b = 1.3930; c = 1.4184; d = 1.4256; e = 1.4340; f = 1.4538; g = 1.4620; h = 1.4774; i = 1.4940.

4.4. Variation of absorbance and fluorescence with lumen refractive index

Ethanol (refractive index 1.3587) and chlorobenzene (refractive index 1.5241) were mixed in various v/v ratios to make nine solutions with refractive indices from 1.3587 to 1.494. A stock solution of $1 \cdot 10^{-3}$ M Rhodamine 6G was prepared in ethanol and $1.123 \cdot 10^{-5}$ M working solutions were then obtained by diluting the stock solution with the different refractive index diluent solutions (ethanol–chlorobenzene mixtures). Varying concentrations of Rhodamine 6G were injected into each of the nine different refractive index diluent solutions (as mobile phases) in order to study lumen refractive index effects. To isolate these effects on absorbance and fluorescence S/N, we divided our capillary flow cell/detector data with normalized optical signals, obtained from standard UV–Vis spectrophotometer and spectrofluorometer measurements, respectively.

Fluorescence

Fig. 8 shows the behavior of absorbance and fluorescence S/N over the range of lumen refractive indices studied. The Rhodamine 6G concentration for these measurements was $1.12 \cdot 10^{-5}$ M. Notice the gradual increase in S/N with refractive index from 1.359 to about 1.462 followed by a rather sharp increase in S/N for refractive index 1.4774. Further increases in mobile phase refractive index yielded a small, but significant, decrease in fluorescence S/N. The computed value of n_1 (see Theory) for which all light energy would be lumen-confined was found to be 1.4716. For all solutions up to refractive index 1.462 light propagates via mode A where maximum light energy is contained in the capillary wall and lumen. For the 1.4774 and 1.494 refractive index solutions mode B is the primary light propagating mode. The mode transition point, at refractive index 1.4716, is highly correlated with the sharp increase in fluorescence S/N. Light-scattering effects in the capillary wall can contribute to the overall S/N when mode A predominates over mode B. We have examined the noise data for these measurements and there does appear to be less noise for the two highest refractive index mobile phases. Thus, mode B generates more efficient photonic interactions, since higher signals result from greater incident

light propagation in the lumen and lower noise is present due to less scattering from wall losses associated with mode A. However, less S/N can be seen at mobile phase refractive index significantly greater than 1.4716, as shown in Fig. 8. This is rationally explained as a decrease in the solid angle (see Eq. 10) of light that is emitted from the optical fiber which leads to a decrease in effective pathlength.

Absorbance

A maximum absorbance S/N was recorded for a mobile phase refractive index of 1.4620. Notice the gradual increase in S/N for mobile phases with lower refractive index and the decrease in S/N for mobile phase refractive indexes greater than this value. Compare this decrease in absorbance S/N to the increasing fluorescence S/N in this region of the refractive index scale. Greater fluorescence clearly suggests that the analyte molecules absorbed more light and therefore should have had higher absorbance, as well. We attribute this discrepancy to non-linear photometric phenomena, as follows. If the analyte is a fluorophore and the capillary is a perfect lightguide, deviations from Beer's law can occur [33]. Let

$$A_m = \log (I_r/I_m) \quad (16)$$

and

$$A_s = \log (I_r/I_s) \quad (17)$$

where A_s and A_m are the absorbance readings with and without the sample in the flow cell, respectively. I_r is the light intensity incident on the reference photocell, and I_s and I_m are the light intensities falling on the sample photocell with and without the sample, respectively. The difference, ΔA, or $(A_s - A_m)$ is the absorbance signal due to the sample *only* and is given by

$$\Delta A = \log (I_m/I_s) \quad (18)$$

This equation shows that ΔA will decrease with an increase in I_s. If the flow cell is a perfect lightguide and if the sample is fluorescing and/or scattering, Eq. 18 is written as

$$\Delta A = \log [I_m/(I_s + I_{s'} + I_f)] \quad (19)$$

where $I_{s'}$ and I_f are the light intensities due to scattering and fluorescing, respectively, that strike the sample photocell. In our experiments $I_{s'}$ is considered to be negligible and I_f can be disregarded unless large amounts of fluorescence reach the sample photocell, presumably when the flow cell is a perfect lightguide. Normally, incident light energy that interacts with the fluorophore at the bend is small and the fluorescence signal is negligible. However, when $n_l >$ 1.4716, the capillary acts as a perfect lightguide and large amounts of fluorophore molecules are excited in the bend region. This results in a non-negligible value of I_f and a concomitant *decrease* in absorbance.

Fig. 9 is a plot of the baseline absorbance signal as a function of n_l. Notice the negative values on the ordinate. The absolute absorbance values are not nearly as important as the overall trend. More negative baseline absorbances indicate greater amounts of light exiting at the bend. Since incident light intensity is fixed, a higher light intensity at the sample photocell is possible

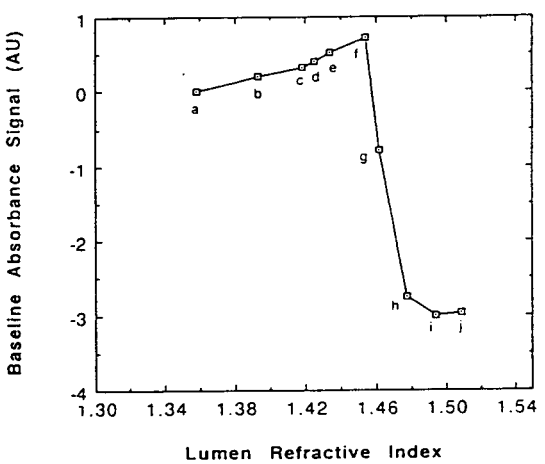

Fig. 9. Baseline absorbance signal (AU) as a function of lumen refractive index. Mobile phase refractive indexes as in Fig. 8 plus j = 1.5087.

only if more light actually propagates from the optical fiber to the bend and completely decouples at the bend. In the region from lumen refractive indexes of 1.359 to 1.454 a gradual increase in baseline absorbance is seen. This corresponds to *less* light arriving at the sample photocell which we correlate with the fact that the capillary actually becomes a less-efficient lightguide as n_l approaches n_w (1.458) due to more light escaping into the wall. Recall that $R = 0$ when $n_l = n_w$. At $n_l = 1.462$, n_w is exceeded and significantly negative baseline absorbance readings are observed. Here, there is an improvement in lightguiding capability of the capillary flow cell. This trend continues, dramatically up to $n_l = 1.4774$ and much less dramatically up to 1.494. Better flow cell performance is indicated within the 1.49 to 1.50 refractive index range since the combined effects of more efficient lightguiding within the capillary and significant light decoupling at the bend can explain the features in this region of the plot. A slight increase in baseline absorbance is observed at $n_l = 1.509$. This is likely due to the fact that some light rays are now able to travel across the bend, therefore less light strikes the sample photocell and the absorbance is higher.

The results shown in Fig. 9 present important implications regarding absorbance detection for gradient micro-LC. If the mobile phase refractive index varies from 1.359 to 1.4538 there will be a baseline shift in the absorbance signal that follows two trends, points a to c and points c to f. In the first region the slope is 5.4 mAU/mRIU (millirefractive index units) and the slope is 11.3 mAU/mRIU in the second region. These features probably represent a single exponential curve, within the precision of the experiment. For a typical 0 to 100% acetonitrile/water gradient, the refractive index change is approximately 10 mRIU (data not shown.) Therefore, such a gradient would produce a baseline change of about 54 mAU, a significant amount indeed compared to amplitudes of typical analyte peaks at low concentration. The specific optical effects responsible for this artifact have been identified and discussed above. Logically, then, there are optical techniques which might be employed to minimize their impact. This is the subject of our current research in this area.

4.5. Influence of capillary wall thickness on absorbance and fluorescence signals

Two capillary flow cells, with similar inner diameter (approximately 100 μm) but different wall thicknesses (67 and 261 μm), were evaluated. Solutions of Rhodamine 6G ($1.12 \cdot 10^{-4}$, $1.12 \cdot 10^{-5}$ and $1.12 \cdot 10^{-6}$ M) were used for absorbance and solutions of perylene ($1 \cdot 10^{-4}$, $1 \cdot 10^{-5}$ and $1 \cdot 10^{-6}$ M) were used for fluorescence measurements. An ethanol mobile phase was pumped at 20 μl/min in all cases. Absorbance measurements were performed at 530 nm and 434 nm excitation light was used for fluorescence measurements. For both wavelengths, light was launched into the flow cell capillaries with a 50-μm core diameter optical fiber. Fig. 10 shows plots of detector response versus analyte concentration for both types of measurements and detector flow cells. Compare the slopes of the response plots for each of the measurement types and wall thicknesses. Absorbance sensitivity increased by a factor of 1.16 as the wall thickness decreased from 261 to 67 μm. Similarly, fluorescence sensitivity increased by a factor of 1.21 for the same wall thickness

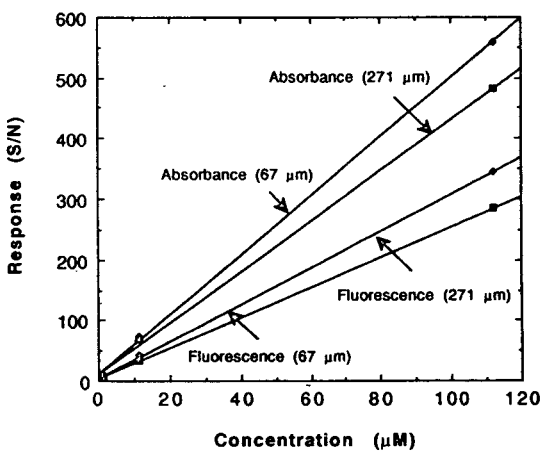

Fig. 10. Absorbance and fluorescence response (S/N) for 100 μm I.D. capillaries with two different wall thickness, 76 and 271 μm.

values. Even though this is not a significant sensitivity enhancement with decreasing wall thickness, a higher S/N is achieved for *both* absorbance and fluorescence. A smaller wall thickness results in less wall propagation, reducing the contributions of losses in the wall (such as scattering and absorption).

4.6. Polynuclear aromatic hydrocarbon micro-LC

A reversed-phase micro-LC separation of a seven-component polynuclear aromatic hydrocarbon mixture was used to further illustrate utility of the flow cell. The mobile phase, acetonitrile–water (92:8), was pumped at a flow-rate of 5 μl/min. A 2.2-cm optical pathlength was used to generate the fluorescence chromatogram shown in Fig. 11. Only fluorescence measurements were made since the silicon photocells had very poor UV response. The inset of Fig. 11 shows a chromatogram close to the detection limit. The analytical figures of merit for these polynuclear aromatic hydrocarbons are listed in Table 1. These concentrations (at $S/N = 3$) are two orders of magnitude better than what we have achieved in the past [34], using cross-beam illumination, photon-counting electronics and higher laser power at the flow cell (1 mW). The peak labelled c in Fig. 11 is due to two coeluting analytes (chrysene and 1,2-benzanthracene). Peak identifications were confirmed by spiking a low concentration (10^{-8} M) mixture with individual analytes of higher concentration (10^{-5} M). We also studied the effect of optical detector window length on overall detectability in polynuclear aromatic hydrocarbon separation. The optical window length was varied from 0.09 to 2.2 cm. The resulting chromatograms are shown in Fig. 12. With increasing length of the fluorescence window, the detectability for pyrene and

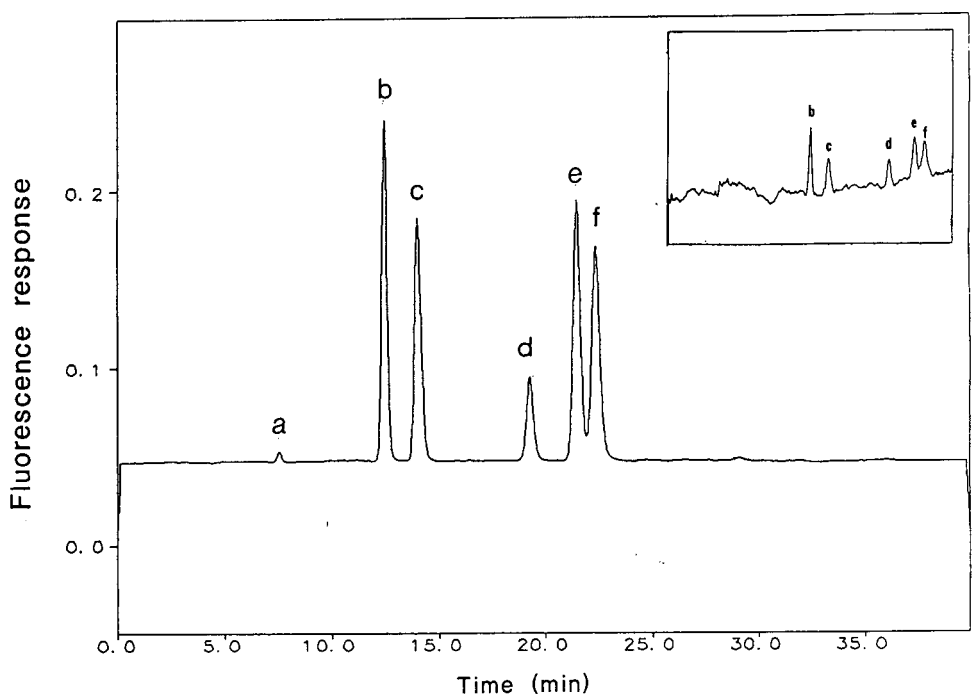

Fig. 11. Laser-induced fluorescence micro-LC chromatograms of a seven-component mixture of polynuclear aromatic hydrocarbons. Peaks: a = 1,2-benzofluorene; b = pyrene; c = chrysene and 1,2-benzanthracene; d = perylene; e = 1,2-benzopyrene; f = 1,2,5,6-dibenzanthracene. Inset shows chromatogram close to the detection limit.

Table 1
Analytical figures of merit for polynuclear aromatic hydrocarbons

Polynuclear aromatic hydrocarbons	MIC (M)	MIQ (g)
1,2-Benzofluorene	$4.8 \cdot 10^{-7}$	$10.4 \cdot 10^{-12}$
Pyrene	$2.1 \cdot 10^{-8}$	$433 \cdot 10^{-15}$
Perylene	$1.4 \cdot 10^{-8}$	$343 \cdot 10^{-15}$
1,2-Benzopyrene	$1.6 \cdot 10^{-8}$	$406 \cdot 10^{-15}$
1,2,5,6-Dibenzanthracene	$1.6 \cdot 10^{-8}$	$456 \cdot 10^{-15}$

MIC and MIQ are the minimum injected concentration and minimum injected quantity, respectively, at $S/N = 3$.

perylene increased by a factor of 4 while their separation efficiencies decreased by factors of only 1.2 and 1.1 for pyrene and perylene, respectively. Obviously the chromatographic peak width is greater than the largest detector volume represented. This flow cell design allows such changes (optical window length) to be easily made, enabling optimum performance to be achieved for a given capillary volume and analytical separation.

5. Conclusions

We have shown some of the optical sensing capabilities of a unique eccentric bend axial-illumination capillary flow cell. The light-propagation pathways in such a device have been evaluated as a function of lumen refractive index and capillary wall thickness. At low mobile phase refractive index, typical of reversed-phase LC, light propagation in the flow cell is highly

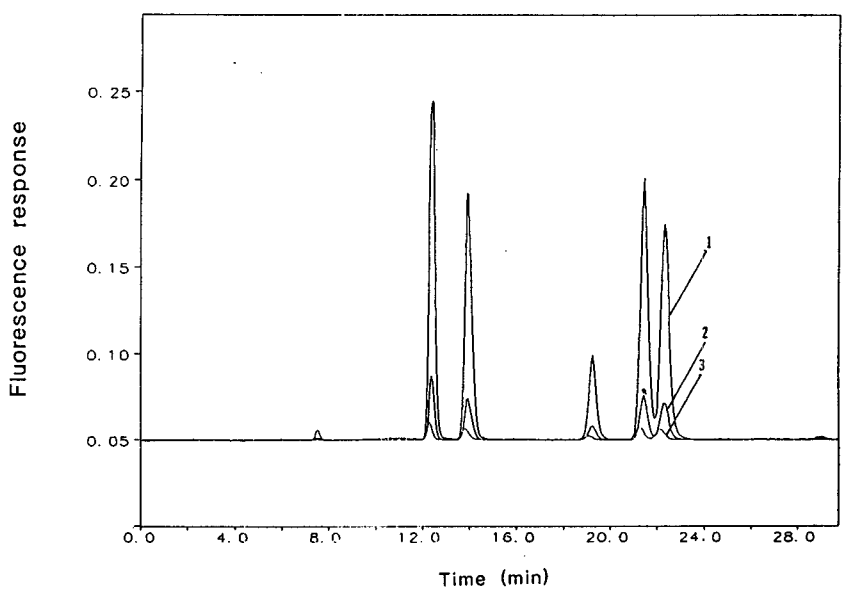

Fig. 12. Laser-induced fluorescence micro-LC chromatograms with three different optical window lengths. Window lengths: 1 = 2.2 cm; 2 = 0.27 cm; 3 = 0.09 cm.

directional and light can be very efficiently decoupled at the bend. Both absorbance and fluorescence sensing, with extended pathlengths, are possible with this design. Pathlengths up to 5 cm and enhanced detection sensitivities have been demonstrated. The flow cell is compatible with micro-LC and analytical performance is two orders of magnitude better than our previous results [34]. With a volume of 173 nl, the 2.2 cm long × 100 μm I.D. cell is far too large for capillary electrophoresis. Smaller versions are possible, however, using smaller optical fiber–capillary combinations as well as shorter pathlengths. Perhaps this design will also enable refractive index sensing. Work is underway to verify this. The potential for simultaneous absorbance, fluorescence and refractive index detection for micro-LC is alluring.

Acknowledgements

We gratefully acknowledge the assistance of Harvey Bellamy in obtaining the flow cell photographs in Fig. 3. We also thank Professor Dominick Casadonte for use of the plastic sheet cut-off filters. Travel support for A.A. Abbas was provided by the Embassy of the United Arab Emirates. Support for poster preparation was partially provided by a grant from Westinghouse-Hanford Co., Richland, WA, USA.

References

[1] M.V. Novotny and D. Ishii (Editors), *Microcolumn Separations —Columns, Instrumentation and Ancillary Techniques*, Elsevier, Amsterdam, New York, 1985.
[2] D. Ishii, *Introduction to Microscale High-Performance Liquid Chromatography*, VCH, New York, 1988.
[3] K. Jinno and C. Fujimoto, *LC·GC*, 7 (1989) 328.
[4] F. Yang, *J. High Resolut. Chromatogr. Chromatogr. Commun.*, 4 (1981) 83.
[5] E.J. Guthrie and J.W. Jorgensen, *Anal. Chem.*, 56 (1984) 483.
[6] S. Einarsson, S. Folestad, B. Josefsson and S. Lagerkvist, *Anal. Chem.*, 58 (1986) 1638.
[7] F. Yang, *J. Chromatogr.*, 236 (1982) 265.
[8] M. Janecek, F. Foret, K. Šlais and P. Boček, *Chromatographia*, 25 (1988) 815.
[9] Y. Hirata and M. Novotny, *J. Chromatogr.*, 186 (1979) 521.
[10] C. Borra, D. Wiesler and M. Novotny, *Anal. Chem.*, 59 (1987) 339.
[11] V.L. McGuffin, in P. Sandra and W. Bertsch (Editors), *Proceedings of the 6th International Symposium on Capillary Chromatography*, Hüthig, Heielberg, 1985, p. 800.
[12] T.J. Edkins and D.C. Shelly, in G. Patonay (Editor), *HPLC Detection: Newer Methods*, VCH, New York, 1992, p. 13.
[13] K. Fujiwara, J.B. Simeonsson, B.W. Smith and J.D. Winefordner, *Anal. Chem.*, 60 (1988) 1065.
[14] K. Tsunoda, A. Nomura, J. Yamada and S. Nishi, *Appl. Spectrosc.*, 43 (1989) 49.
[15] K. Tsunoda, A. Nomura, J. Yamada, S. Nishi and I. Kojima, *Nippon Kaguka Kaishi*, 1989 (1989) 233.
[16] J.P. Chervet, M. Ursem, J.P. Salzmann and R.W. Vannoort, *J. High Resolut. Chromatogr., Chromatogr. Commun.*, 12 (1989) 278.
[17] I.H. Grant and W. Steuer, *J. Microcol. Sep.*, 2 (1990) 74.
[18] X. Xi and E.S. Yeung, *Anal. Chem.*, 62 (1990) 1580.
[19] X. Xi and E.S. Yeung, *Appl. Spectrosc.*, 45 (1991) 1199.
[20] J. Taylor and E.S. Yeung, *J. Chromatogr.*, 550 (1991) 831.
[21] J.V. Sweedler, J.B. Shear, H.A. Fishman and R.N. Zare, *Anal. Chem.*, 63 (1991) 496.
[22] J.P. Chervet, R.E.J. van Soest and M. Ursem, *J. Chromatogr.*, 543 (1991) 439.
[23] K. Fujiwara, S. Riekojyo, H. Tsubota and R.L. Carter, *Appl. Spectrosc.*, 46 (1992) 1032.
[24] J.A. Taylor and E.S. Yeung, *Anal. Chem.*, 64 (1992) 1741.
[25] A.A. Abbas and D.C. Shelly, *J. Chromatogr.*, 631 (1993) 133.
[26] S.E. Moring and R.T. Reel, *Anal. Chem.*, 65 (1993) 3454.
[27] T. Wang, J.H. Aiken, C.W. Huie and R.A. Hartwick, *Anal. Chem.*, 63 (1991) 1373.
[28] E. Hecht, *Optics*, Wesley, Reading, MA, 1987, Ch. 4, p. 79.
[29] J.R. Gant and P.A. Perrone, *Am. Lab.*, 17 (1985) 104.
[30] S.A. Wilson and E.S. Yeung, *Anal. Chem.*, 57 (1985) 2611.
[31] T.J. Edkins and D.C. Shelly, *J. Chromatogr.*, 411 (1987) 185.
[32] D.C. Harris, *Quantitative Chemical Analysis*, Freeman, New York, 1987, Ch. 20, p 524.
[33] J.R. Lackowicz, *Principles of Fluorescence Spectroscopy*, Plenum, New York, 1983, Ch. 2, p. 48.
[34] T.J. Edkins and D.C. Shelly, *J. Chromatogr.*, 459 (1988) 109.

ELSEVIER

Journal of Chromatography A, 691 (1995) 55–65

JOURNAL OF CHROMATOGRAPHY A

Amperostatic–potentiometric detection for micro high-performance liquid chromatography

Aftab Siddiqui, Dennis C. Shelly*

Department of Chemistry and Biochemistry, Texas Tech University, Lubbock, TX 79409-1061, USA

Abstract

Constant current is applied to a microelectrode which is "bathed" in the effluent from a micro-LC column. A micro indicator electrode senses the potential as electroactive solutes undergo electron transfer at the working electrode surface. In the absence of analyte, mobile phase components (principally water) are reduced or oxidized, generating a significant working electrode potential. Because the measured signal (potential or charge density) is significant near the detection limit, detection sensitivity may, under optimum conditions, be higher than for conventional amperometric detection. We report on the design, fabrication and evaluation of amperostatic–potentiometric (ASPEN) detection for micro-LC. The determination of phenol, *o*-chlorophenol, 2,4-dimethylphenol and *p*-benzylphenol, each at the femtomole level (injected amount), has been performed with a packed fused-silica capillary (250 μm I.D.), operating in the reversed-phase mode. The real and apparent limitations to this technique will be presented.

1. Introduction

1.1. Micro-LC with electrochemical detection

Microcolumn high-performance liquid chromatography (micro-LC), using capillaries with less than 500 μm I.D., is characterized by several fundamental measurement and practical analytical advantages. With dramatically reduced column dimensions the quantities of sample, mobile phase and packing material are reduced [1]. Micro-LC is ideal for the analysis of such unique samples as exotic physiological fluids and single cells [2,3]. Good kinetic performance is also characteristic of micro-LC [4]. Significant gains in detection limits can be realized by the enhanced mass sensitivity of coupled concentration-sensitive detectors [5]. Detector development has been problematic, however, due to stringent volumetric requirements.

Amperometry

One of the most suitable detection techniques for such small columns is microelectrochemical detection in the amperometric mode [6]. Amperometric detection currently provides the best detectability among the various electrochemical detection techniques [6–14]. The primary advantage of electrochemical detection for micro-LC lies in the fact that electrochemical processes take place at the surface of a microelectrode, resulting in very high detection efficiency, "virtually coulometric in the case where electroactive analytes are contained in the very thin annular

* Corresponding author.

0021-9673/95/$09.50
SSDI 0021-9673(94)00985-6

flow region between the electrode and capillary wall" [11]. The unique compatibility between micro-LC and microelectrochemical detection is largely due to the fundamental features of microelectrodes. A relatively large current *density* at the microelectrode is achievable at low applied current and enhanced mass transport to and from the electrode surface is seen (both due to the small size and surface area). The use of carbon fiber working electrodes for microvoltammetric micro-LC detection was first demonstrated by Knecht et al. [10] in 1984 and has been steadily refined [6].

In the normal amperometric mode a constant potential is applied to the auxiliary reference electrode pair and the working electrode remains at virtual ground [15]. Current flows along the working electrode signal pathway to "earth" ground through a current-to-voltage converter and is amplified in the process. The magnitude of this current is proportional to the mass flux of electroactive species to the working electrode surface plus background contributions. Double layer capacitance and reaction (adsorption/desorption) of the electrolyte/mobile phase impurities at the working electrode surface contribute to the background current. Fluctuations in these, stimulated by surges in fluid flow, generally give small current and noise levels [16]. However, as one approaches the limit of detection (i.e less and less analyte mass flux), vanishingly small analyte current becomes indistinguishable from the background. In other words, at the detection limit analyte detection *sensitivity* is low with amperometric sensing.

The disadvantages of fixed potential detection are poor selectivity and generation of rather limited electrochemical information. Selective detection using a differential pulse amperometric technique has been demonstrated [11]. Though improved detection limits were also shown the technique does not give general information about the electroactive species in the sample.

Voltammetry

Potential scanning methods (voltammetry) give increased information content but they are usually less sensitive than amperometric techniques, largely due to the charging current associated with the rapid scan rates necessary for real-time chromatographic detection. By discriminating against background current, square-wave voltammetric detection [17,18] has been used to improve sensitivity and yet maintain the inherent selectivity of the potential scanning technique. Square-wave voltammetry is well suited to mercury because the relaxation of the charged double layer, induced by the pulses, is reproducible. Staircase voltammetry has demonstrated reasonable results at solid electrodes in chromatography at around 1 V/s sweep rate [7]. The coulostatic electrochemical technique discriminates against double layer charging current and is largely immune from solution resistance effects [19,20]. In this technique pulses are used to charge the double layer capacitor, changing the electrode-solution potential. White et al. [7] used a scanning microvoltammetric detector for on-column detection in open tubular liquid chromatography. It was noted that an advantage of microvoltammetric electrodes is the reduced double layer capacitance that permits rapid scanning of the electrode potential.

Potentiometry

Potentiometric electrochemical detection has been performed with capillary liquid chromatography. A micro ion-selective electrode has been used for potentiometric detection with micro-LC–electrochemical detection [21,22]. The utility of potentiometric detection with microanalytical separations has recently been addressed. For both direct and differential potentiometric detection, the ideal voltage measurement is necessary, i.e. no induced current flow. No change in electrical charge during transduction and amplification can be tolerated. Though this ideal is not perfectly attainable, modern electronic devices can allow very small absolute and differential voltage measurements to be made.

1.2. The amperostatic–potentiometric (ASPEN) measurement

If an appropriate constant current is applied between a working electrode and a counter

electrode, a potential gradient is generated by the mass flux of electroactive species, to the working electrode. If this working electrode is a microelectrode it is reasonable to expect that the potential gradient would be significant in the same way that current density is significant for such an electrode in amperometry. This potential can be measured with an "indicating" electrode, using a high-impedance electrometer. Negligible charge is expected to flow if a suitable microelectrode like Ag/AgCl is used. In the constant-current mode, unlike the constant potential mode, solvent components react at the micro working electrode generating a background potential gradient. When a more easily electrolyzed species passes over the microelectrode it will preferentially react at the electrode surface, changing the potential such that this signal (potential gradient) would be related to the amount of analyte reacting at the electrode surface. At vanishingly small analyte concentration, there would be a comparatively large background signal level. However, the noise component will be present as a very small portion of this large signal. Our ability to detect smaller and smaller amounts of analyte becomes limited only by our ability to distinguish between smaller and smaller *differences* in the large signals. Thus, ASPEN detection may offer enhanced detectability at the lower limit of detection. ASPEN detection can, thus, be viewed as a simple modification of these familiar measurements. In its basic configuration, a two-electrode galvanostat would be coupled with a high-impedance electrometer (in the voltage mode) through a suitable indicator electrode. Alternatively, an indicator–reference electrode pair could be used for differential measurement of working electrode charge.

2. Experimental

2.1. Galvanostat/potentiostat

The instrumental set-up for ASPEN detection is shown in Fig. 1. An EG & G Princeton Applied Research (Princeton, NJ, USA) Model 273 potentiostat/galvanostat was used to apply constant current to the cell. The electrochemically generated potential was measured with a Keithley Instruments (Cleveland, OH, USA) Model 610C solid-state electrometer. Data acquisition was accomplished with a IBM PC computer system. The cell was shielded in a laboratory-made Faraday cage. The offset circuit was made in the departmental electronic shop. The lowest current that the galvanostat could apply was 25 pA. A current divider could not be used to reach lower currents because a constant-current condition could not be maintained.

2.2. Micro-LC

A Model 8500 syringe pump (Varian, Walnut Creek, CA, USA) and a Model CI4W injection valve (Valco, Houston, TX, USA) were used for all micro-LC experiments. The volume of injection valve was 80 nl. Slurry-packed capillary columns, 75 cm × 0.25 mm I.D., were prepared using published procedures [23]. Micro-LC was performed with microcolumns which contained Spherisorb ODS2 reversed-phase packing (Alltech, Deerfield, IL, USA) and an acetonitrile–phosphate buffer (65:35) mobile phase. The aqueous portion had a pH of 4.8 and was 0.02 *M* in total phosphate and $1 \cdot 10^{-4}$ *M* in EDTA. This mobile phase was degassed by vacuum ultrasonication and used for all transport and chromatographic studies, unless otherwise stated. All chromatograms were analyzed using DADiSP (DSP Development, Cambridge, MA, USA), digital signal processing software. All noise analysis was done using this system.

2.3. Reagents and chemicals

Acetonitrile (Optima grade), potassium phosphate (monobasic and dibasic) and hydroquinone were obtained from Fisher Chemical (Pittsburgh, PA, USA). EDTA was obtained from J.T. Baker (Phillipsburg, NJ, USA). Phenol, *o*-chlorophenol, 2,4-dimethylphenol and *p*-benzylphenol were obtained from Aldrich (Milwaukee, WI, USA). All the above chemicals were used without further purification.

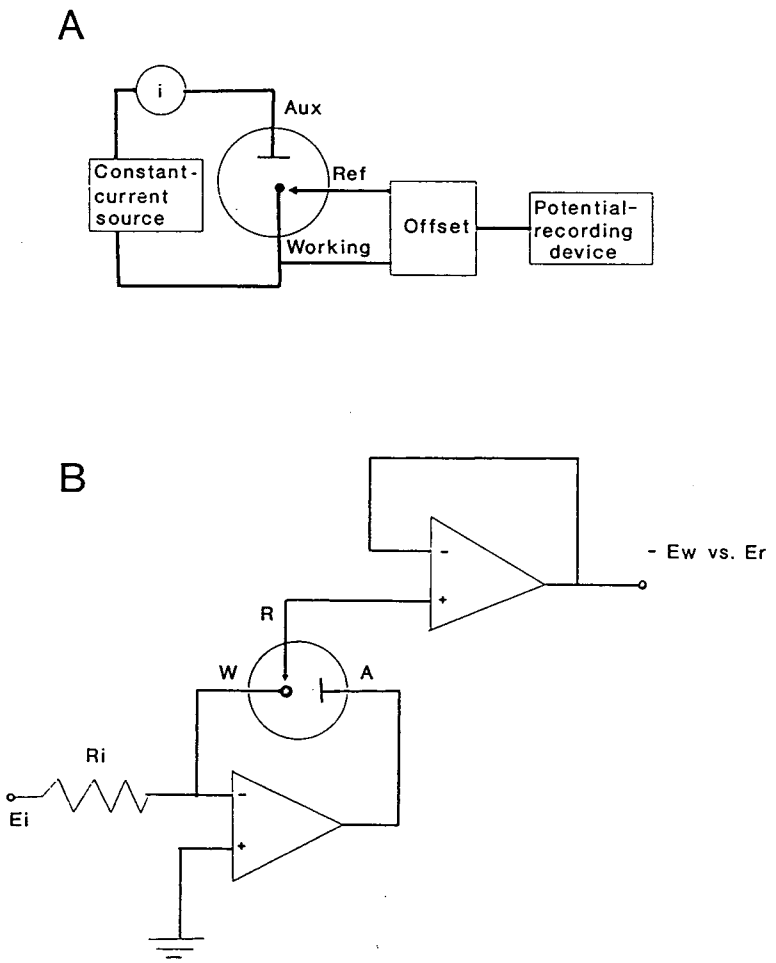

Fig. 1. (A) Simplified block diagram of ASPEN measurement apparatus; (B) simplified schematic of three-electrode cell in amperostatic (galvanostatic) mode. Aux (A), Ref (R) and Working (W) = Auxiliary, reference and working electrodes, respectively; i = current; E_i = input voltage; R_i = input resistance ($i = E_i/R_i$); E_w and E_r = working electrode and reference electrode potentials, respectively.

2.4. Construction of electrodes

In order to make a carbon fiber working electrode, 7 μm diameter Magnamite Type AS-4 carbon fiber, obtained from Hercules, was cleaned by soaking in hot (80–90°C) concentrated sulfuric acid for several hours. It was rinsed in distilled water, then methanol and finally dried in ambient air. A single carbon fiber was then inserted into a 530 μm I.D. capillary so that 2 to 3 mm was protruding outside the capillary and then it was glued with optical adhesive (No. 63) which was obtained from Norland Products (New Brunswick, NJ, USA). Mercury and copper or tin wire were used for electrical connection.

Ag/AgCl reference electrodes were made by soldering a 5 mm length of 0.215 mm diameter silver wire (Aldrich) to an aluminum or copper lead. The lead was then sealed in a 530 μm I.D. capillary, leaving about 3 mm of silver wire exposed. The silver surface was cleaned by placing only the protruding portion in a 3 *M* nitric acid solution, for 1 h. It was then im-

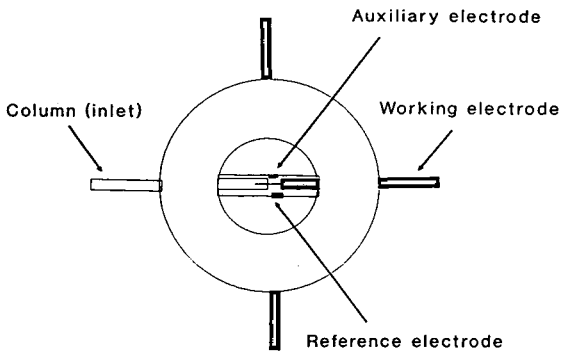

Fig. 2. Drawing of flow-through cell.

mersed in a 1 *M* potassium chloride (with few drops of HCl) solution and the potential was held at 1.0 V for about 24 h.

2.5. Construction of electrochemical cell

A polyether ether ketone (PEEK) "tee" connector from Alltech was used to fabricate the flow-through cell. Holes of 0.035 in. (1 in. = 2.54 cm) diameter were drilled through the long axis of 1/4 × 28 T.P.I. (threads per inch) nylon plugs; the electrodes were inserted through these holes and into the "tee", as shown in Fig. 2. For one pair of holes, oriented at 180°, a carbon fiber microelectrode was inserted into the lumen of a fused-silica capillary. Reference and auxiliary electrodes were inserted through the other holes. An observation hole had been bored in the exact center of the "tee", through the top surface, to enable viewing with a microscope. This hole also served as an outlet for mobile phase. The reference electrode was placed as close as possible to the working electrode surface.

3. Results and discussion

3.1. Background signal and noise characteristics

One of the first studies was directed to examining the importance of inlet capillary inner diameter on detector performance. Fig. 3 shows a plot of background potential as a function of applied current for inlet fused-silica capillary

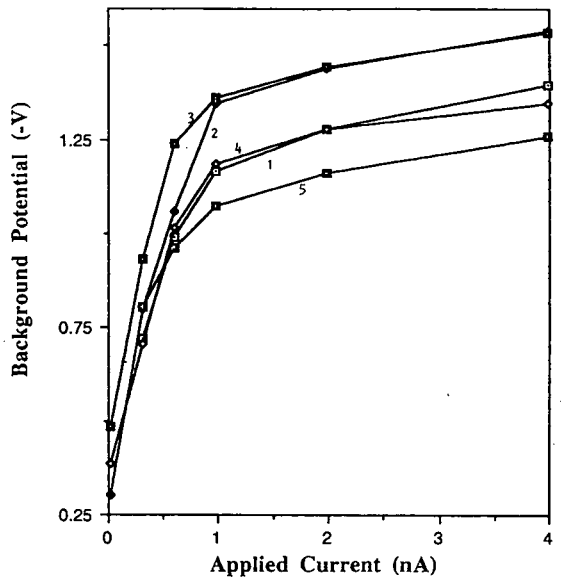

Fig. 3. Plot of background potential (−V) versus applied current (nA) for capillaries of various internal diameters. Capillary I.D.: 1 = 15 μm; 2 = 19 μm; 3 = 50 μm; 4 = 73 μm; 5 = 98 μm.

I.D.s of 15, 19, 50, 73 and 98 μm. In each case, the carbon fiber working electrode was inserted to a depth of 2 mm into the capillary and the mobile phase solution flowed at approximately 5 μl/min across the electrode. The measured background potential becomes more negative with increasing applied current. A "limiting potential" condition is attained in this controlled-current mode just as a limiting current is achieved in controlled-potential experiments. Application of an anodic current between the working and auxiliary electrodes implies that the working electrode potential should be positive. The measured background potential is equal to $-E_w$ versus E_r (where E_w and E_r are the working electrode and reference electrode potentials, respectively) because these potentials were measured relative to earth ground. Therefore, a negative value of background potential corresponds to a positive working electrode potential. There does not appear to be a trend to the limiting background potentials, in terms of inlet capillary inner diameter.

With an applied current, the working elec-

trode potential increases in order to pass this current. Electroactive mobile phase components will undergo electron transfer and the working electrode will take on a potential, dependent on the magnitude of the applied current and the nature and concentration of the available electroactive species. With an anodic bias and an aqueous mobile phase, water oxidation:

$$2H_2O \rightarrow O_{2(g)} + 4H^+ + 4e^-$$

will be the predominant electrochemical reaction at the working electrode. This probably explains the plateau of 1.4 V (versus ground potential) at >1 nA applied current.

When the working electrode potential exceeds the standard potential for water, application of higher currents does not increase the working electrode potential significantly, since solution resistance probably accounts for the remaining current dissipation. The potential (electrode surface charge) depends on the current density at the working electrode and the cell resistance. Due to its very small surface area, the current density for the microelectrode is high, hence there tends to be a rather high background potential for a very small applied current. For example, the surface area of the carbon fiber working electrode ranges from about $4 \cdot 10^{-4}$ cm^2 to $7 \cdot 10^{-4}$ cm^2. At an applied current of 250 pA the current density would be 0.62 to 0.28 μA/cm^2. Since the carbon fiber was of the same dimensions in each of our experiments, we would not expect the current density to be affected by inlet capillary inner diameter. On the other hand, the resistance of the flow-through cell is very high and would likely cause the cell resistance to be higher for capillaries of smaller diameters. Therefore, a higher background potential would be expected with the 15 and 19 μm I.D. capillaries, irrespective of the applied current. This is not seen in Fig. 3. One possible explanation for this is variation in fiber placement inside the inlet capillaries, which would be more problematic with the smaller-I.D. capillaries This would cause rather drastic differences in cell resistance. Another explanation lies in the differences between linear velocity and volumetric flow. Since each of the cells was operated at constant volumetric flow-rate, a much higher mobile phase linear velocity would accompany the smaller-I.D. inlet capillary. The measured noise did not appear to signal such changes in linear velocity as the noise ($3 \cdot 10^{-4}$ V) remained within a factor of two at the different applied currents used in this study. Drift in the background signal was observed, especially at 600 pA. Drift *decreases* tremendously when currents exceeding 600 pA were applied. The sloping baseline showed some resemblance to a potential–time profile of a charging capacitor. A possible source of drift is the gradual dissolution of the thick AgCl film on the reference electrode.

3.2. Relationship of applied current and potential in ASPEN detection

Hydroquinone (HQ) was used as an oxidizable analyte for evaluation of the applied current–potential relationship. Here, a constant anodic current was applied and the peak height of an injected solute was measured. In the absence of analyte, water would give the background potential, as discussed above. Since HQ is more easily oxidized than water, the potential at the working electrode decreases during HQ elution and reaction at the working electrode. In order to record the small changes in potential accompanying the presence of electroactive analytes, an offset circuit was used. This device applied a reverse polarity signal to the electrometer output in order to maintain a "0" response voltage. This response signal is plotted against applied current for several concentrations of HQ in Fig. 4. As shown, the response increases with applied current for nearly all the HQ concentrations up to a maximum applied current level of about 0.600 nA. At higher applied current dramatic decreases in response are seen. Even though each concentration represents different injected masses of HQ, the point at which no more HQ results in higher response occurs at nearly the same applied current. This may be attributable to oxygen evolution at the working electrode. Molecular oxygen would hinder transport of electroactive species to the electrode and may also

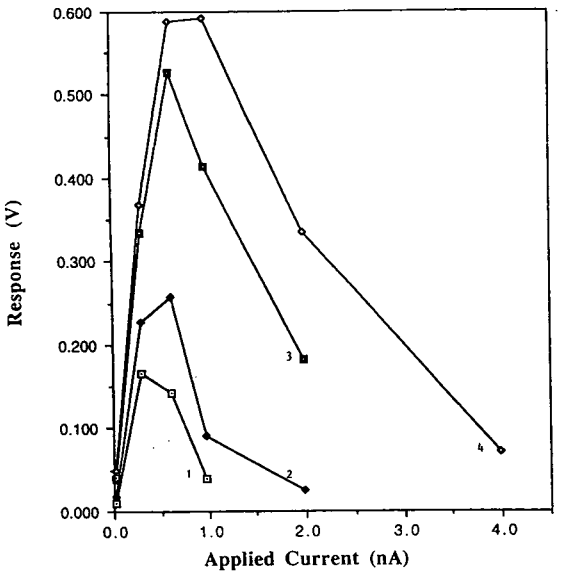

Fig. 4. Plot of ASPEN detector response (V) versus applied current (nA) at various hydroquinone concentrations. HQ concentrations: $1 = 5.10 \cdot 10^{-6}$ M; $2 = 1.02 \cdot 10^{-5}$ M; $3 = 2.60 \cdot 10^{-5}$ M; $4 = 5.10 \cdot 10^{-5}$ M.

contribute to preoxidation of HQ. The 0.600 nA threshold is not distinct, however. Note that $1.02 \cdot 10^{-6}$ M HQ reaches a maximum response at an applied current of 0.300 nA and there is a gradual shift in the current threshold to almost 1.0 nA at $5.10 \cdot 10^{-5}$ M. This shows that a somewhat greater response can be obtained for low analyte concentrations by applying lower currents. Another interesting conclusion stems from the slopes of these curves at currents < 0.5 nA. Since the HQ concentrations are different (by virtue of the different injected masses) yet the slopes in these regions are almost the same, it is reasonable to conclude that the response in this region is not transport-dependent, but rather kinetically limited. To our knowledge, this a totally unique situation for microelectrochemical detection.

3.3. Response and sensitivity

Classically speaking, the concentration response function is linear for amperometric detectors and logarithmic for potentiometric detectors. Table 1 is a compilation of response versus log of HQ concentration at the various applied currents and inlet capillary diameters tested. The linear regression slopes and correlation coefficients are also shown. Note the high correlation coefficient (R^2) values. With the lowest value of 0.92, these results suggest that most of the available data are accurately represented by the model. Note also that the slopes of the response curves increase with applied current up to 1.975 nA. Compare these results to those of Table 2. Table 2 is a list of linear regression data for response versus HQ concentration, again at various applied currents and inlet capillary I.D.s. Apart from the much higher slope values, there is generally much poorer correlation of data with this model, as evidenced by the lower R^2 values.

Further evidence of "anomalous" detector response is seen in actual plots of these data.

Table 1
Linear regression data summary from ASPEN detector response versus log HQ concentration for capillaries of different I.D.

Capillary diameter (μm)	Current applied (pA)	Slope	R^2
15	300	0.1422	1.00
	600	0.2268	0.99
	975	0.351	0.98
	1975	0.677	0.97
19	300	0.1053	0.99
	600	0.2725	0.97
	975	0.3056	0.92
	1975	0.2283	0.97
50	300	0.1937	0.99
	600	0.3542	0.96
	975	0.5882	0.98
	1975	0.4364	1.00
73	300	0.1127	0.99
	600	0.2547	1.00
	975	0.3447	0.98
	1975	0.6747	0.97
98	300	0.1299	1.00
	600	0.2362	0.99
	975	0.3234	0.98
	1975	0.5787	0.97

Table 2
Linear regression data summary from ASPEN detector response versus HQ concentration for capillaries of different I.D.

Capillary diameter (μm)	Current applied (pA)	Slope	R^2
15	300	3994.65	0.87
	600	6221.61	0.85
	975	$1.007 \cdot 10^4$	0.87
	1975	$1.367 \cdot 10^4$	0.92
19	300	3055.46	0.89
	600	8295.79	0.92
	975	$1.020 \cdot 10^4$	0.96
	1975	5005.97	0.99
50	300	5572.17	0.89
	600	$1.100 \cdot 10^4$	0.93
	975	$1.246 \cdot 10^4$	0.97
	1975	7398.96	0.99
73	300	3381.47	0.92
	600	6344.45	0.83
	975	9815.82	0.87
	1975	$1.339 \cdot 10^4$	0.90
98	300	3653.39	0.87
	600	6522.45	0.84
	975	9077.44	0.86
	1975	$1.141 \cdot 10^4$	0.90

Fig. 5 shows plots of detector response versus HQ concentration at several different applied currents for a 50 μm I.D. inlet capillary. Note that the greatest response level is achieved at 0.600 nA applied current throughout the concentration range. The greatest sensitivity (slope) is found at 0.975 nA applied current, as confirmed by the results of Table 1. The range of concentrations included in Fig. 5 is very narrow and is meant to show calibration plots rather than the entire response curves.

We look again at the aspect of inlet capillary I.D. Table 1 shows that inlet capillary has no clear influence on response sensitivity. An examination of the noise data from these measurements (data not shown) indicates, at most, a two-fold variation over the range 15–98 μm I.D. This is quite different from typical behavior for amperometric detection [24]. If the response

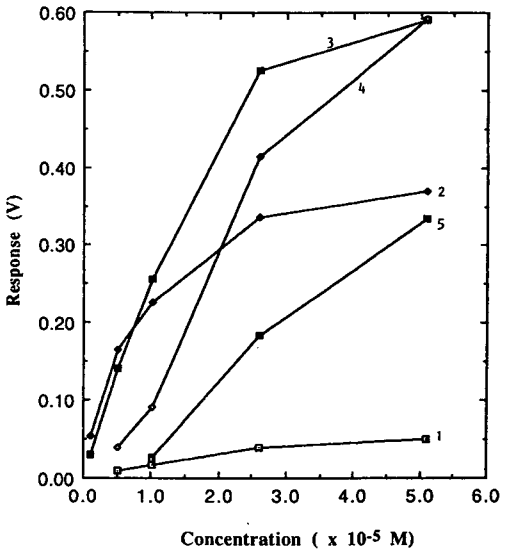

Fig. 5. Plot of ASPEN detector response (V) versus HQ concentration at various applied currents. Applied current: 1 = 0.025 nA; 2 = 0.30 nA; 3 = 0.60 nA; 4 = 0.975 nA; 5 = 1.975 nA.

were mass-transport limited there would have been an optimum or, at least, some effect of inlet capillary diameter. Our data show no influence of inlet capillary diameter on response sensitivity, detection limits or background noise. It is quite possible that without a careful noise analysis [25] such effects have been overlooked. Admittedly, we have not proven superior detection sensitivity near the detection limit, compared to microamperometric detection. However, we have not pushed the instrumentation or measurement to its limits in this preliminary study. Therefore, we can conclude from these results that ASPEN detection is not characterized by a mass-transport limited analytical signal as is microamperometric detection. Obviously, design flexibility and versatility are inherent in this conclusion and positive attributes of ASPEN detection.

3.4. ASPEN detection of phenols

A four-component mixture of phenols (phenol, *o*-chlorophenol, 2,4-dimethylphenol and *p*-benzylphenol) was analyzed by micro-LC.

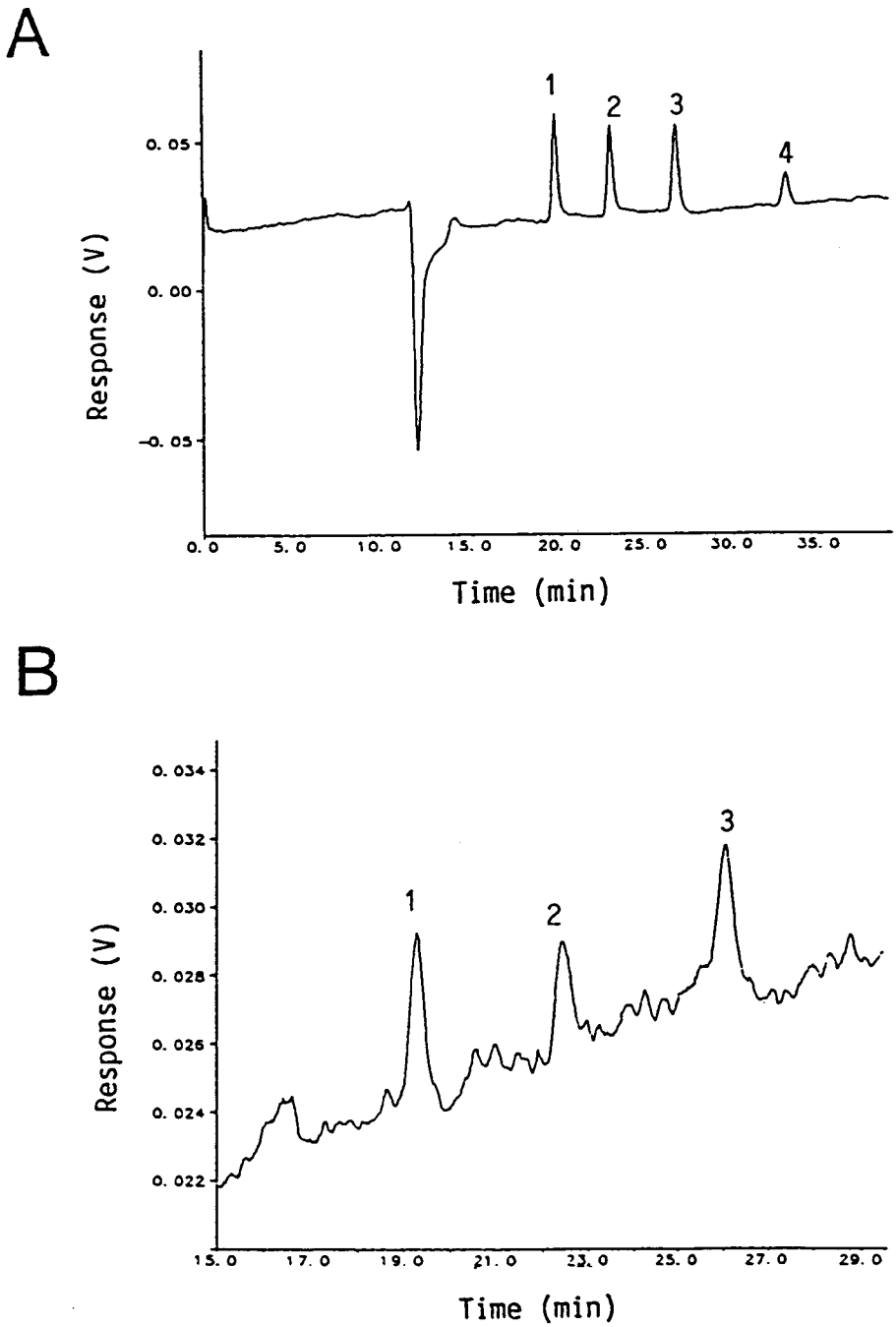

Fig. 6. (A) Chromatogram of phenol mixture: 1 = 0.714 pmol phenol; 2 = 0.80 pmol *o*-chlorophenol; 3 = 0.80 pmol 2,4-dimethylphenol; 4 = 0.756 pmol *p*-benzylphenol. (B) Chromatogram of a ten-fold dilution of mixture as in (A).

Fig. 6 shows two chromatograms of this mixture, each obtained at 0.600 nA applied current and a 50 μm I.D. inlet capillary. Fig. 6A represents an injection of 0.714 pmol phenol, 0.80 pmol *o*-chlorophenol, 0.80 pmol 2,4-dimethylphenol and 0.756 pmol of *p*-benzylphenol. Fig. 6B is an injection of a ten-fold dilution of that shown in Fig. 6A. *p*-Benzylphenol was not seen in the signal for Fig. 6B. Fig. 7 shows the peak heights of each component plotted against the applied current, now in the range of 0.1 to 4 nA. Note that for each analyte except 2,4-dimethylphenol a limiting response occurs between 1 and 2 nA. The response for 2,4-dimethylphenol is maximum at 0.300 nA and it steadily decreases with applied current. This can be attributed to the almost 200 mV lower half wave potential for 2,4-dimethylphenol [26], compared to phenol and *o*-chlorophenol, as shown in Table 3. Mass detectabilities, as limits of detection, for each phenol are also shown in Table 3. It is reasonable to conclude that an applied current of 0.600 nA for the chromatograms of Fig. 6 represents nearly optimum detection response for *all* these analytes. Had microamperometric detection been employed, detection selectivity, due to

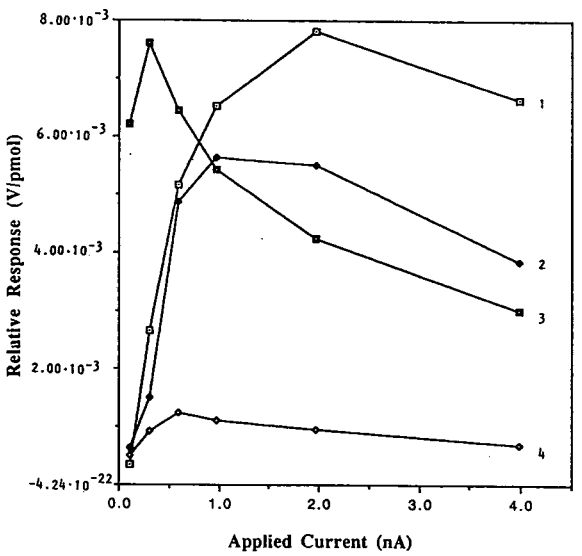

Fig. 7. Plot of relative response (V/pmol) versus applied current (nA) for the phenols. 1 = Phenol; 2 = *o*-chlorophenol; 3 = 2,4-dimethylphenol; 4 = *p*-benzylphenol.

Table 3
Analytical data for phenols

Analyte	$E_{1/2}$ vs. SCE (V)	LOD (fmol)
Phenol	0.633	70
o-Chlorophenol	0.625	76
2,4-Dimethylphenol	0.459	76
p-Benzylphenol	–	76

$E_{1/2}$ = Half-wave potential; SCE = saturated calomel electrode; LOD = limit of detection. See Ref. [26] for $E_{1/2}$ data.

constant applied potential, may have excluded 2,4-dimethylphenol from detection. ASPEN detection appears, then, to be a more universal type of microelectrochemical detection technique than conventional amperometry, voltammetry or coulometry. Much more evaluation work remains before this can be confirmed.

4. Conclusions

ASPEN detection appears to be a feasible microelectrochemical detection technique. With a constant applied current (in the 0.2–2 nA range) a surface charge is created on a carbon fiber working electrode in response to the concentration and identity of electroactive species flowing past the electrode surface. In the absence of more easily oxidized species, the surface charge depends on mobile phase (water oxidation) components. When an easily oxidized electroactive eluite flows by, the electrode's surface charge changes only enough to allow the applied current to pass. This modulation of surface charge or potential can be easily detected and has been shown to be proportional to analyte mass. Theoretically, this combination of effects should give ASPEN detection certain advantages for trace-level sensing. Unfortunately, these advantages were not seen in this preliminary study.

More work is needed before a thorough understanding of this technique is attained. Studies of response sensitivity at the limit of analyte detection are planned. A thorough noise analysis is needed. The influence of applied current upon detection efficiency is warranted, because slow

electrode kinetics may alter detection temporal performance at low applied current. Substantial reductions in limit of detection may result from further minimization of noise, as in a dual-channel–differential sensing mode.

Acknowledgements

We gratefully acknowledge the support of HPLC'94 in providing registration expenses for A.S. We are also grateful to the Texas Tech Graduate School for summer support during 1991. Assistance by Westinghouse-Hanford Co. as partial support of poster preparation expenses, was also provided. We also thank John K. Foley, Ph.D. for many helpful discussions regarding the theoretical principles of this technique.

References

[1] M.V. Novotny and D. Ishii (Editors), *Microcolumn Separations —Columns, Instrumentation and Ancillary Techniques*, Elsevier, Amsterdam, 1985.
[2] T.M. Olefirowicz and A.G. Ewing, *Anal. Chem.*, 62 (1990) 1872.
[3] B.R. Cooper, J.A. Jankowski, D.J. Leszczyszyn, R.M. Wightman and J.W. Jorgenson, *Anal. Chem.*, 64 (1992) 691.
[4] G. Guichon and H. Colin, in P. Kucera (Editor), *Microcolumn High-Performance Liquid Chromatography*, Elsevier, Amsterdam, 1984, pp. 1–38.
[5] M.V. Novotny, *Anal. Chem.*, 53 (1981) 1294A.
[6] A.G. Ewing, J.M. Mesaros and P.F. Gavin, *Anal. Chem.*, 66 (1994) 527A.
[7] J.G. White, R.L. St. Claire III and J.W. Jorgenson, *Anal. Chem.*, 58 (1986) 293.
[8] M. Goto, E. Sakura and D. Ishii, *J. Chromatogr.*, 238 (1982) 357.
[9] K. Slais and D. Kourilova, *J Chromatogr.*, 258 (1983) 57.
[10] L.A. Knecht, E.J. Guthrie and J.W. Jorgenson, *Anal. Chem.*, 56 (1984) 479.
[11] R.L. St. Claire III and J.W. Jorgenson, *J. Chromatogr. Sci.*, 23 (1985) 186.
[12] K. Slais and M. Krejci, *J. Chromatogr.*, 235 (1982) 21.
[13] Y. Hirata, P.T. Lin, M V. Novotny and R.M. Wightman, *J. Chromatogr.*, 181 (1980) 287.
[14] M. Goto, Y. Koyangi and D. Ishii, *J. Chromatogr.*, 208 (1981) 261.
[15] P.T. Kissinger, *Laboratory Techniques in Electroanalytical Chemistry*, Marcel Dekker, New York, 1984, p. 163.
[16] D.M. Morgan and S.G. Weber, *Anal. Chem.*, 56 (1984) 2560.
[17] R. Samuelson, J. O'Dea and J. Osteryoung, *Anal. Chem.*, 52 (1980) 2215.
[18] J. Wang, E. Ouziel, C. Yarnitzky and M. Ariel, *Anal. Chim. Acta*, 102 (1978) 99.
[19] T.A. Last, *Anal. Chem.*, 55 (1983) 1509.
[20] A.C. Barnes and T.A. Nieman, *Anal. Chem.*, 55 (1983) 2309.
[21] A. Mant and W. Simon, *J. Chromatogr. Sci.*, 21 (1983) 326.
[22] S.R. Muller, W. Simon, H.M. Widmer, K. Grolimund, G. Schomburg and P. Kolla, *Anal. Chem.*, 61 (1989) 2747.
[23] D.C. Shelly, V.L. Antonucci, T.J. Edkins and T.J. Dalton, *J. Chromatogr.*, 458 (1989) 267.
[24] S.G. Weber and W.C. Purdy, *Anal. Chim. Acta*, 100 (1978) 531.
[25] S.G. Weber and J.T. Long, *Anal. Chem.*, 60 (1988) 223.
[26] L. Meites and P. Zuman (Editors), *Electrochemical Data*, Part 1, Vol. A, Wiley, New York, 1974.

ELSEVIER

Journal of Chromatography A, 691 (1995) 67–79

JOURNAL OF CHROMATOGRAPHY A

Multivariate visualization in the size-exclusion chromatography and pattern recognition of biological samples

R.D. Ricker[a,*], L.A. Sandoval[a], J.D. Justice[b], F.O. Geiser[c]

[a]*Rockland Technologies, Inc., 538 First State Boulevard, Newport, DE 19804, USA*
[b]*Justice Innovations, Inc., 1240 L'Avenida Avenue, Suite A, Mountain View, CA 94043, USA*
[c]*Geiser Scientific, Inc., 287-A Wilson Avenue, Glen Mills, PA 19342, USA*

Abstract

A principal-component technique that maps highly correlated data by the use of non-orthogonal vectors has been described by Geiser et al. [*J. Chromatogr.* 631 (1993) 1–13]. As many as 35 chromatographic variables were simultaneously visualized in a single three-dimensional map, using cosines of the correlation coefficients as vector angles. Applications included the validation of system-suitability parameters and the elucidation of biomolecular structure–activity relationships. In this paper, the mapping technique was extended to the chemometric analysis of data for the size-exclusion chromatography of biological samples. The study was to characterize protein–packing interactions for 25 molecules at nine mobile phase concentrations. Using this chemometric technique, the relationships between all of the data points could be viewed in a single graph. Analysis of the graph revealed mapping regions for proteins demonstrating hydrophobic characteristics, ionic characteristics, a combination of hydrophobic and ionic characteristics, or little interaction with the packing. The optimal mobile phase concentration for ideal size-exclusion chromatography in this system could also be identified from the graph.

1. Introduction

The trend in high-performance liquid chromatography (HPLC) is towards faster and improved chromatography. This is being accomplished in several ways. First, highly purified, low-acidity silica is being used to provide better peak shapes and higher resolution [1,2]. In addition, highly stable bonded phases have been developed that can withstand high-temperature and low-pH operation, reducing separation time by sharpening peaks, and lowering viscosity [3]. Carefully controlled particle-size distributions allow the use of small-particle-size columns having shorter lengths, with no loss in efficiency [4]. Improvements in the unattended operation of HPLC instrumentation and data collection have also increased the number of chromatographic runs that can be performed. Using these advancements, one can easily generate more data than can be readily analyzed and interpreted. With the resulting increase in ability to generate data, and strong demands for faster analyses, chemometrics is becoming an increasingly popular tool [5–9]. Chemometrics is designed to reduce the dimensionality of a multivariate dataset so that patterns in the data might be more easily viewed and interpreted by the human mind. While many of the variables of chromatographic data are highly correlated, the information becomes very complex with the introduction of biological sam-

* Corresponding author.

0021-9673/95/$09.50
SSDI 0021-9673(94)01136-2

ples, different mobile phases and different stationary phases.

We have used a unique chemometric program (DataMax) for visualization and partial quantitation of differences in the interactions between 21 proteins and the column packing during size-exclusion chromatography (SEC) on the Zorbax (registered trademark of DuPont) BioSeries GF-250. Interpretation of these interaction data is especially complicated in SEC because the chromatography is normally carried out under conditions such that the sample is in its native state. The chemometric software (DataMax) maps the correlations of all the attributes (mobile phase concentrations) and all the objects (proteins) of this system, in a single, non-orthogonal, three-dimensional graph (MultiGraf; registered trademark of Echo Data). Reports of the actual statistical values and mapping coordinates are also available. DataMax allowed us to determine the best of our mobile phase concentrations for performing ideal SEC in this system. The technique also provided a means of grouping proteins by their relative hydrophobicities and ionic character, as determined by the extent of their interaction with the column-packing surface.

2. Experimental

2.1. Instrumentation

HPLC was carried out using a Ti-Series 1050 liquid chromatograph equipped with a four-solvent pump, autosampler and variable-wavelength UV detector, all from Hewlett-Packard (Valley Forge, PA, USA). HPLC was also carried out with an LKB 2150 pump (Pharmacia LKB, Piscataway, NJ, USA), DuPont 8800 Series multiwavelength detector (DuPont, Wilmington, DE, USA), and a 9125 injector from Rheodyne (Cotati, CA, USA). Data were collected with an IBM-compatible 80486 computer running ChromPerfect Direct 4I chromatography analysis software (Justice Innovations, Mountain View, CA, USA), using a DT2804 data-acquisition card, all from Geiser Scientific (Glen Mills, PA, USA). Multivariate maps of log M_r vs. relative retention volume were prepared using DataMax software (ECHO Data, Orem, UT, USA). The final graphics were exported as HPGL files and enhanced using CorelDraw 4.0 (Corel, Ottawa, Canada).

2.2. Columns

The columns used were Zorbax BioSeries GF-250, obtained from Mac-Mod Analytical (Chadds Ford, PA, USA). The columns had dimensions of 250 × 9.4 mm, with 5 μm particle diameter and 150 Å pore size.

2.3. Chemicals and proteins

All proteins and low-molecular-mass markers used in this study were of 90% purity or better, purchased from Sigma (St. Louis, MO, USA). Sodium phosphate, monobasic, ultrapure bioreagent, and analytical-grade sodium hydroxide were obtained from VWR Scientific (Bridgeport, NJ, USA). Samples and buffers were made with de-ionized water filtered through a 0.22-μm hydrophilic filter (Millipore, Bedford, MA, USA).

2.4. Procedures

Protein stock solutions were prepared individually at 10 mg/ml. The stock solutions were prepared in de-ionized prefiltered water, with the exception of bovine insulin (INS), which contained 0.05% trifluoroacetic acid (HPLC Spectro-grade, Pierce, Rockford, IL, USA) for its solubilization. Sample mixtures containing 1–3 proteins were prepared for injection by diluting the stock solutions. This was typically a 10-fold dilution with 0.20 *M* sodium phosphate adjusted to a pH of 7.0 with 10 *M* NaOH. In cases where the relative retention volume (K_d) was greater than 1, individual protein concentrations were increased to 2–3 mg/ml to facilitate detection. Sample mixtures were prepared fresh daily. Detection was carried out at 230 nm with a flow-rate of 2 ml/min and ambient temperature.

2.5. Theoretical

Relative retention volume (K_d)

Retention times, t_R, for each protein were determined in mobile phase containing sodium phosphate buffer (pH 7.0) at concentrations from 50 to 1000 m*M*. To reduce experiment time, flow-rates were 2 ml/min. V_R values were used to calculate K_d, defined here as $K_d = \{V_R / V_m\}$, where V_R is the retention volume of the solute and V_m is the column volume of the mobile phase, or total permeation volume of the column (determined as the retention volume of the solute sodium azide at 200 m*M* sodium phosphate, pH 7.0). This use of K_d is simply $k' + 1$, and is useful in this context because it indicates whether a particular solute elutes within the SEC separation range of the column ($V_R < 1$).

Log K_d and regression analysis

For the approximation of missing retention values, regression analyses of log K_d values were carried out using a Hewlett-Packard HP-42S calculator. By restricting the log K_d values used to those obtained at lower mobile phase concentrations, correlation values were kept greater than 0.95 in each case. The resulting extrapolated log K_d values were then converted back to standard K_d.

3. Results and discussion

3.1. Solute–packing interactions in SEC

SEC is one of the few chromatographic methods in which biomolecules may be separated in their native state. However, all columns have surface characteristics that can adversely affect the retention of solute molecules [10,11]. This is especially true in SEC, where the mobile phase is often designed to provide a good environment for the protein and not necessarily for the best performance of the column. A considerable number of column types and mobile phases have been used to better understand and predict protein–packing interactions, and achieve ideal size-exclusion behavior [12–16]. The column used in this study was silica-based and is surface-stabilized with zirconia to withstand operation at higher pH (up to pH 8). Zorbax silica particles have extreme physical stability, allowing high flow-rates and operational pressures. The particles are coated with a bonded monolayer of silane containing a diol functionality. The result is a highly consistent coverage of the particle with the bonded phase. This surface is very hydrophilic and some interaction of proteins with unreacted silanol groups may occur because of this hydrophilic nature. Other SEC supports are made by coating the entire surface of a silica particle with a polymeric bonded phase. While solutes are completely shielded from the silanol groups of these column packings, this surface is not likely to be as reproducible as a monolayer coating and can have more hydrophobic character. Additionally, size-exclusion columns can be made from cross-linked polysaccharide particles. While being very hydrophilic, these packings are relatively soft and can undergo electrostatic interactions with some solutes. Because of this wide variability in synthesis of size-exclusion columns, the chromatographer should have an understanding of solute–column packing interactions before using a particular column type. (See [17] for a recent review of SEC.)

This study reports this type of information for the Zorbax BioSeries GF-250 column. The current results are only one set of a large number of experiments that might be performed to better understand chromatography on a column packing. We intend to complete a more rigorous treatment of this topic, that will include the use of different mobile phase types buffered to higher and lower pH values. These parameters are known to have a dramatic effect on the interaction of proteins with the packing surface. However, with the addition of just four different buffers and three different pH values for these 21 proteins, conclusions would require the analysis of more than 2000 data points. We have, therefore, spent time looking for a tool that would allow rapid visualization of these results, and the work became more focused on learning about the non-orthogonal vector-plotting charac-

teristics of DataMax and introducing it as a valuable tool for this kind of study.

Once all of the data has been entered into the DataMax table, versatile analysis is allowed. Provisions are made for selecting and de-selecting any of the attributes and objects, and making comparisons with external data. A corresponding change is made to the statistical report. The DataMax MultiGraf may be rotated to any orientation to simplify determination of the alignment between any of its objects. In these experiments, it was useful to orient the MultiGraf so that the log M_r axis was vertical and neither angled forward nor backward. This provided a fixed axis for comparison of other attributes to those of "ideal" SEC.

3.2. Extrapolation of K_d values

Data are entered into DataMax using a standard table format —the columns are the attributes (mobile phase concentration) and the rows are individual objects (proteins). Because of the statistical calculations involved, the data table must be completely filled. In this type of study, as in many others, this is not always possible. Many of the proteins were simply not detectable at very low mobile phase concentration. The missing numbers can be determined by extrapolation using linear or curvilinear regression, in systems where this is meaningful. A very similar MultiGraf is created when the estimated values are removed (50, 70 and 80 m*M* data). Once an initial trend is generated by the data, DataMax seems to properly interpret and represent that trend.

In the case of electrostatic and hydrophobic interactions, a great deal of theory is known. In both cases, linear maps are produced when the logarithm of the retention factor is plotted against logarithm of salt concentration or reciprocal salt concentration.

Specifically, for ion exchange [18,19],

$$\log k = 2z \log [1/(X^{+u}Y^{-v})] + \log K_z$$

where k = capacity factor; X^{+u} = concentration of displacing ion; Y^{-v} = concentration of counter ion; z = the number of charges interacting between the solute and the surface; K_z = a constant.

For hydrophobic interactions [20],

$$\log k = (1/2.303)Sm + \log K_w$$

or

$$\ln k = Sm + \ln K_w$$

where m = the molality of the salt; $K_w = k$ when water is the mobile phase; S = parameter that varies with ion and solute type.

When these treatments are applied to SEC K_d values, the data should be linearized, simplifying the approximation of missing values. In DataMax, when data increase logarithmically, the position of data points with smaller values becomes compressed to the center of the graph. In preliminary application of the logarithm calculations, an important additional benefit was found. The MultiGraf "opened up"; many data points were moved out from the center of the map to group more closely with other objects of similar type, and the amount of information visualized was markedly increased. It should be kept in mind that linearization should only be applied to the attributes for which it is valid. In this case, log K_d and log (1/[sodium phosphate]) should be used for the lower-ionic-strength data. The log K_d and log [sodium phosphate] should be applied only to the higher-ionic-strength data. These topics will be discussed further in a following paper.

3.3. Raw SEC data

The characterization of solute interactions with the surface of a size-exclusion column packing is often carried out by an analysis of retention volumes of the sample molecules over a wide range of ionic strengths, pH, and mobile phase type [10–16]. These interactions were characterized for proteins eluting from a Zorbax BioSeries GF-250 column using sodium phosphate, pH 7.0 as a mobile phase. Sodium phosphate is a very common biological buffer and is the mobile phase currently suggested for use by the column manufacturer. The relative retention volumes (K_d) for the proteins at various mobile phase concentrations are shown in Table 1, along

Table 1
Relative retention volumes (K_d) for the 21 proteins and 4 low-molecular-mass markers

Sample name	p*I*	M_r	K_d of sample at listed concentration of sodium phosphate, pH 7.0								
			50 m*M*	70 m*M*	80 m*M*	100 m*M*	150 m*M*	200 m*M*	400 m*M*	600 m*M*	1000 m*M*
Thyroglobulin	5.1	669 000	0.54	0.54	0.54	0.54	0.54	0.53	0.55	0.55	0.60
Ferritin	4.2	440 000	0.67	0.63	0.64	0.65	0.64	0.64	0.67	0.73	0.88
Catalase	5.4	250 000	0.68	0.68	0.68	0.69	0.68	0.68	0.71	0.74	**1.54**
β-Amylase	4.8	200 000	0.64	0.63	0.63	0.64	0.64	0.64	0.65	0.66	0.78
Alcohol dehydrogenase	6.8	150 000	0.66	0.66	0.66	0.67	0.67	0.67	0.67	0.68	0.72
BSA dimer	5.4	132 000	0.64	0.63	0.64	0.64	0.64	0.64	0.65	0.66	0.72
BSA	5.1	66 430	0.70	0.70	0.70	0.70	0.70	0.70	0.72	0.73	0.79
Ovalbumin	4.6	44 000	0.75	0.74	0.75	0.75	0.75	0.75	0.78	0.79	0.89
Peroxidase	9.0	44 000	0.73	0.73	0.73	0.73	0.73	0.73	0.73	0.75	0.88
Pepsin	2.0	35 000	0.92	0.82	0.81	0.80	0.81	0.81	0.92	**1.16**	**1.70**
Carbonic anhydrase	5.9	29 000	0.91	0.85	0.85	0.83	0.82	0.82	0.83	0.85	0.97
Chymotrypsinogen A	9.3	25 000	**2.51**	**1.16**	**1.00**	0.88	0.84	0.83	0.83	0.90	**1.23**
Trypsinogen	9.3	23 977	0.87	0.84	0.83	0.82	0.80	0.82	0.83	0.85	0.89
Trypsin	10.5	23 280	0.93[a]	0.90	0.87	0.85	0.83	0.83	0.85	0.86	0.95
α-Chymotrypsin	8.8	21 600	**2.10**	**1.09**	0.96	0.86	0.82	0.82	0.83	0.84	0.92
Myoglobin	7.2	17 600	0.82	0.82	0.82	0.82	0.82	0.82	0.83	0.83	0.87
Lysozyme	10.0	14 300	**2.10**[a]	**1.59**	**1.33**	**1.02**	0.94	0.95	0.95	**1.00**	**1.38**
Ribonuclease A	7.8	13 700	**4.25**[a]	**2.74**	**1.82**	**1.78**	0.96	0.85	0.86	0.87	0.91
Cytochrome *c*	9.6	12 400	**6.47**[a]	**4.90**[a]	**4.26**[a]	**3.72**	**1.20**	0.92	0.85	0.84	0.85
Aprotinin	10.5	6 500	**2.75**[a]	**2.18**	**1.72**	**1.11**	0.96	0.94	0.93	0.96	**1.10**
Insulin	5.7	6 000	0.97	0.97	0.97	0.95	0.96	0.97	**1.09**	**1.34**	**2.92**
Vitamin B_{12}	–	1 355	0.95	0.96	0.95	0.95	0.96	0.99	**1.04**	**1.19**	**1.44**
Uridine	–	244	0.95	0.99	0.95	0.94	0.95	0.96	0.97	0.97	**1.03**
Uracil	–	122	0.99	0.99	0.99	0.98	0.99	**1.00**	**1.01**	**1.01**	**1.02**
Sodium azide	–	67	0.99	0.99	**1.00**	**1.00**	**1.00**	**1.00**	**1.01**	**1.02**	**1.05**

Protein samples (1 mg/ml) were chromatographed on a GF-250 size-exclusion column at 2 ml/min. Numbers in bold type are retention volumes greater than V_R for sodium azide at 200 m*M* sodium phosphate, pH 7.0. All p*I* values and molecular masses were obtained from Sigma and Refs. [22] and [23].

[a] Values approximated by linear regression as described under Experimental.

with values for the low-molecular-mass markers. Although only one mobile phase type was used, the number of data points needed to perform an adequate characterization was quite large. However, by careful analysis of the resulting K_d values (Table 1), certain patterns can be recognized. At mobile phase concentrations of 70 to 100 m*M*, several proteins had a $K_d > 1$. In fact, trypsin, lysozyme, RNase A, cytochrome *c* and aprotinin were not detected, even at run times of 40 min. These proteins are known to have relatively high isoelectric points (p*I*) (p$I > 8$) and carry an overall positive charge at the pH of the mobile phase (pH 7.0). It is also possible to pick out proteins that elute with $K_d > 1$ at very high mobile phase concentrations —notably, catalase, pepsin, chymotrypsinogen A, lysozyme, aprotinin and insulin. Table 1 shows that the proteins elute at different retention volumes that change at dramatically different rates towards the extremes of high or low mobile phase ionic strength. K_d values were, therefore, estimated using regression analysis. These estimated values appear in bold type, followed with a superscript "a".

Although various characteristics can be surmised from the table, it is difficult to visualize, all-at-once, how they interrelate. If one views the data using traditional x–y plots of K_d versus mobile phase concentration, or as log M_r versus K_d, the result is numerous, slightly differing curves plotted over one another. Placing them in separate graphs makes comparison and presentation difficult. Individual graphs of log M_r plotted

against K_d (traditional calibration curves) are not quantitative and limit the comparison of data for different mobile phase strengths.

3.4. The DataMax statistical report

Table 2 is a statistical report exported directly from DataMax using the data in Table 1. The report first shows the amount of variance in the data accounted for in one, two and three dimensions of the MultiGraf. In this case, 97.729% of the total variance was accounted for in the three-dimensional map (Fig. 1). This indicates that the angles between the attributes (correlations between mobile phase, ionic strength data) add up to somewhat more than what can be represented in a three-dimensional sphere. The more correlated the attributes, the smaller the angles between the axes; hence, more axes (attributes) can be mapped in the same three-dimensional sphere.

In the second section of its report, DataMax lists the correlations between the attributes. This is reported as a matrix of correlations; one for each attribute calculated against every other. In SEC, one expects the elution volume to increase as log M_r decreases (negative correlation). Therefore, the mobile phase concentration with the greatest negative value represents the best mobile phase in this study for ideal SEC. It can be seen in the table "Correlations between attributes" section of Table 2 that 200 mM sodium phosphate has the highest negative correlation (-0.88914) with log M_r. Correlation values close to zero indicate attributes that are not correlated to each other.

The DataMax report continues with a table of the actual x, y and z coordinates (normalized between $+1$ and -1) for mapping the high end of the axes (attributes) on the sphere. The mean of each data set is placed at the center of the MultiGraf. At the right middle of the DataMax report, communalities are listed for the first three factors of the factor analysis. These values indicate the variance of each attribute accounted for in each of the 1st, 2nd and 3rd dimensions of the graph. At the far right appear the totals of variance accounted for in all three dimensions; as these totals approach 1, the MultiGraf better depicts the entire data set.

Each of the factors represents a characteristic of the system. It can be seen in this section of Table 2 that the middle mobile phase concentrations (150, 200 and 400 mM) make up a large percentage of the first factor. The second factor is largely accounted for by characteristics of the 50, 70, 80, 100, 400 and 600 mM mobile phase concentrations. The third factor is almost exclusively made up by the characteristics of the 1000 mM mobile phase concentration. More than 97% of the system characteristics were attributable to these first three factors. SEC systems are well defined; therefore, it seems appropriate to assign actual characteristics to these three factors. The first factor is most likely related to separation of the molecules by size (hydrodynamic volume); it occurred at medium ion strengths and correlated most negatively with log M_r. The second factor is best described by ion exchange of solute with the column packing; it occurred at high and low ionic strengths (except where SEC dominated). The third factor is strongly associated with hydrophobic interaction of solute with the column packing; it occurred only at the highest ionic strength used.

At the end of the report, DataMax lists the actual x, y and z coordinates for placement of the objects within the three-dimensional sphere (MultiGraf). When these objects are mapped, they appear perpendicular from their proper, relative position on each axis. As a result of this type plotting, the attributes and objects are pushed out into three dimensions, and group into different regions of the sphere.

3.5. The DataMax MultiGraf

The DataMax MultiGraf of chromatographic data from Table 1 is shown in Fig. 1. The MultiGraf may be rotated in any direction. In Fig. 1, the sphere graph has been rotated so that the log M_r axis runs vertically through the center of the sphere. The label for the attribute is always near the high end of the axis. (Larger molecular mass values are toward the top of the graph, and lower masses are near the bottom.) It

Table 2
DataMax statistics and plotting parameters generated from Table 1

Correlations between attributes:

	50 m*M*	70 m*M*	80 m*M*	100 m*M*	150 m*M*	200 m*M*	400 m*M*	600 m*M*	1000 m*M*	Log M_r
50 m*M*	1.0000	0.9721	0.9385	0.9188	0.6676	0.3569	0.2078	0.1059	−0.0494	−0.1413
70 m*M*	0.9721	1.0000	0.9866	0.9684	0.7156	0.3979	0.2472	0.1361	−0.0351	−0.1939
80 m*M*	0.9385	0.9866	1.0000	0.9852	0.7279	0.4103	0.2588	0.1505	−0.0191	−0.2151
100 m*M*	0.9188	0.9684	0.9852	1.0000	0.7183	0.3897	0.2475	0.1429	−0.0247	−0.2250
150 m*M*	0.6676	0.7156	0.7279	0.7183	1.0000	0.9191	0.8335	0.6888	0.3257	−0.7708
200 m*M*	0.3569	0.3979	0.4103	0.3897	0.9191	1.0000	0.9662	0.8358	0.4489	−0.8894
400 m*M*	0.2078	0.2472	0.2588	0.2475	0.8335	0.9662	1.0000	0.9406	0.6174	−0.8488
600 m*M*	0.1059	0.1361	0.1505	0.1429	0.6888	0.8358	0.9406	1.0000	0.7971	−0.6695
1000 m*M*	−0.0494	−0.0351	−0.0191	−0.0247	0.3257	0.4489	0.6174	0.7971	1.0000	−0.2277
Log M_r	−0.1413	−0.1939	−0.2151	−0.2250	−0.7708	−0.8894	−0.8488	−0.6695	−0.2277	1.0000

Attribute coordinates: Attribute name	*X*	*Y*	*Z*	*Communalities:* 1 D	2 D	3 D	Total
50 m*M*	0.13	0.79	−0.56	0.518	0.417	0.011	0.9461
70 m*M*	0.18	0.80	−0.57	0.583	0.402	0.007	0.9926
80 m*M*	0.19	0.79	−0.57	0.597	0.381	0.007	0.9844
100 m*M*	0.19	0.79	−0.55	0.580	0.379	0.005	0.9635
150 m*M*	0.78	0.36	−0.51	0.980	0.002	0.014	0.9963
200 m*M*	0.92	0.03	−0.37	0.777	0.169	0.037	0.9829
400 m*M*	0.88	−0.19	−0.43	0.653	0.337	0.002	0.9928
600 m*M*	0.70	−0.39	−0.58	0.487	0.431	0.052	0.9701
1000 m*M*	0.22	−0.61	−0.74	0.146	0.365	0.468	0.9783
Log M_r	−0.98	−0.02	0.01	0.492	0.220	0.254	0.9657

Object coordinates: Data point name	*X*	*Y*	*Z*
Thyroglobulin	−0.414	−0.031	0.211
Ferritin	−0.290	0.050	0.072
Catalase	−0.292	0.165	−0.107
β-Amylase	−0.260	0.004	0.152
Alcohol dehydrogenase	−0.211	−0.012	0.169
BSA dimer	−0.236	−0.012	0.183
BSA	−0.141	0.004	0.154
Ovalbumin	−0.071	0.028	0.112
Peroxidase	−0.106	0.014	0.132
Pepsin	−0.021	0.280	−0.246
Carbonic anhydrase	0.008	0.032	0.069
α-Chymotrypsin	−0.025	0.010	−0.085
Trypsin	0.020	0.021	0.101
Trypsinogen	0.033	0.025	0.073
Chymotrypsinogen A	0.005	−0.043	0.045
Myoglobin	0.039	0.010	0.126
Lysozyme	0.113	0.027	−0.166
Ribobuclease A	0.016	−0.329	−0.169
Cytochrome *c*	−0.002	−0.860	−0.511
Aprotinin	0.143	−0.131	−0.114
Insulin	0.114	0.521	−0.615
Vitamin B_{12}	0.310	0.181	−0.086
Uridine	0.362	0.017	0.158
Uracil	0.439	0.014	0.167
Sodium azide	0.466	0.014	0.175

Total variance accounted for: in one dimension: 58.134%; in two dimensions: 89.158%; in three dimensions: 97.729%.

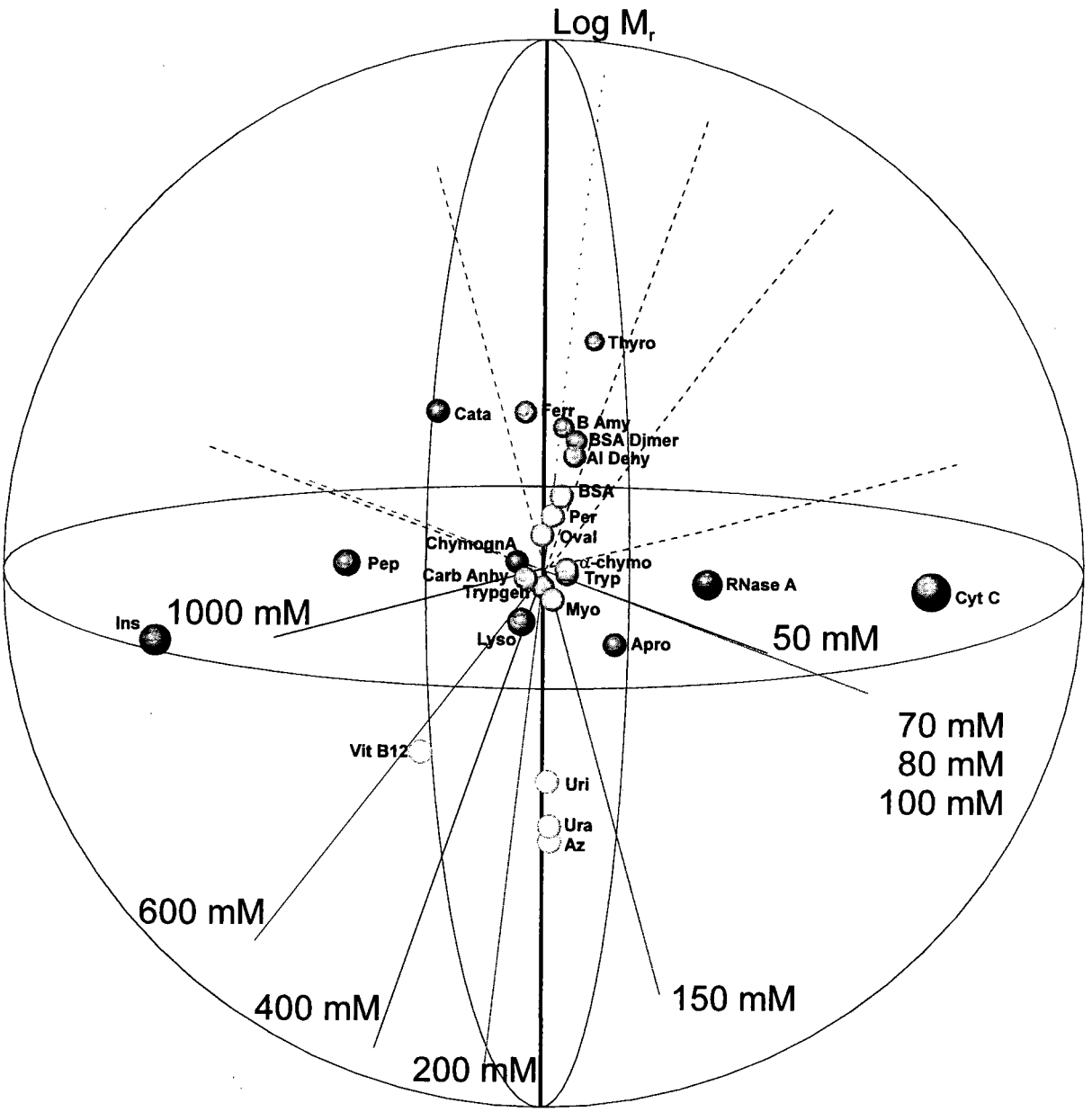

Fig. 1. Analysis of protein–packing interactions in SEC by multivariate non-orthogonal plotting. DataMax map of all relative retention volumes (K_d) for 21 proteins and 4 small molecules determined at 9 sodium phosphate concentrations (pH 7.0). Column: Zorbax GF-250 (250 × 9.4 mm), flow-rate 2 ml/min.

can be seen that the axis of the 200 mM mobile phase concentration lies nearly anti-parallel to that of the log M_r —with its low-value end tilted slightly back. Solid lines indicate that the end of the axis extends towards the front of the graph, while dashed lines indicate extension towards the back. This MultiGraf shows that each of the mobile phase concentrations are consistently

correlated with each other, from low concentrations, which are grouped tightly at the right, to the 1000 m*M* data on the left. The DataMax report was used to reduce these data for a graph that adequately represents only the three principal factors. The mobile phase concentrations chosen, by their correlations and communalities, were 100, 200 and 1000 m*M*. The resulting MultiGraf appears in Fig. 2. In the front view (Fig. 2a), it is seen that the majority of the proteins lie along the 200 m*M* and log M_r axes. In the side view (Fig. 2b) it is possible to see the deviations of the objects from these two axes. To account for the correlation between the attributes, these axes are placed at nearly 90° from each other and those of the 200 m*M* and log M_r. Again, data values that deviate from their relative position on the 200 m*M* axis are pushed out into the sphere at a point perpendicular to their relative value on each axis. The high retention times for cytochrome *c* and RNase A may be readily visualized in the MultiGraf. These large K_d values are attributable to electrostatic interactions. The non-ideal retention of insulin is also readily apparent, being mapped at the high end of the 1000 m*M* axis, indicating hydrophobic interactions. Two proteins, lysozyme and aprotinin, have a tendency towards both ionic and hydrophobic interactions. These objects appear between the 100 and 1000 m*M* axes. By comparing the front and side views of the MultiGraf (Fig. 2a and b), it can be seen that the majority of the proteins fall along the log M_r axis and are undergoing ideal size separation at these various conditions. It appears that larger molecules cannot sample as much of the packing surface as a small molecule. As a result, these larger molecules should have less interaction with the packing and exhibit little deviation from their proper elution volume.

3.6. Chromatographic examples

Through the use of the DataMax MultiGraf, three objects (proteins) were chosen to demonstrate their different interactions with the column packing at various mobile phase concentrations. By showing the actual chromatograms, one can more easily see the dramatic differences that change of mobile phase has on the chromatography of these proteins. Cytochrome *c* was positioned in Figs. 1 and 2 at the high end of the 100 m*M* axis, at the edge of the MultiGraf. This protein was chosen to show the elution characteristics of a molecule that undergoes electrostatic interactions with the column packing (Fig. 3). Cytochrome *c* has a high p*I* (Table 1) and is known to have positive charges at its surface under native conditions and pH 7.0 [21]. At low mobile phase ionic strengths, these cations can undergo ion exchange with silanol groups on the surface, causing the peak to be retained and broadened. Higher mobile phase ionic strengths tend to shield these interactions. Fig. 4 shows the elution characteristics of a relatively hydrophobic protein, insulin. This protein is very sensitive to hydrophobic interactions and maps on the edge of the MultiGraf at the high end of the 1000 m*M* axis. It is retained past the total permeation volume at mobile phase concentrations as low as 400 m*M* sodium phosphate, pH 7.0. Extensive band broadening is observed at this mobile phase concentration. Finally, Fig. 5 shows the elution profile for lysozyme, a protein that exhibits both electrostatic and hydrophobic tendencies [18]. This duality is made possible by discrete domains of the protein (e.g., certain folding, amino acids, and conformational changes, allow two adjacent areas of the protein surface to be completely different). It should be noted that the extents of these protein interactions with the column packing are relative. At lower ionic strengths, the interactions of all the proteins with the packing becomes exaggerated. In addition, these proteins can change their conformation as a result of mobile phase changes, and may consequently mask or display different surface characteristics.

4. Conclusions

DataMax allowed visualization of large amounts of SEC data, through principal-component analysis and non-orthogonal-plotting techniques (a MultiGraf). The relationships between log M_r and the retention volumes for all

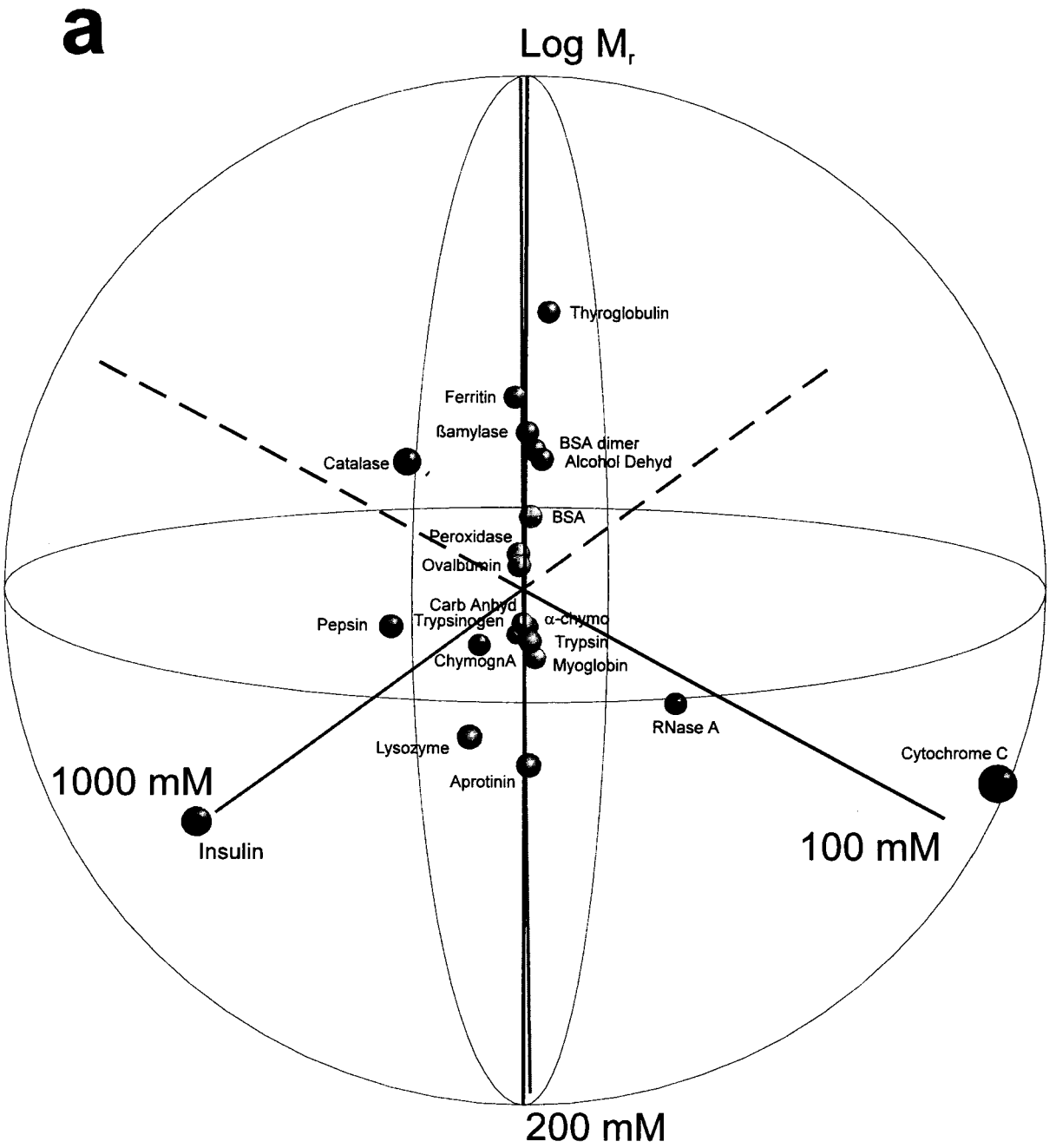

Fig. 2.

the proteins at different mobile phase concentrations were visualized in a single graph. As a result, a mobile phase could be selected for achieving the most-ideal SEC in this system —200 m*M* sodium phosphate (pH 7.0). DataMax also provided a means of viewing the grouping proteins by their relative hydrophobicities and ionic character, as determined by the

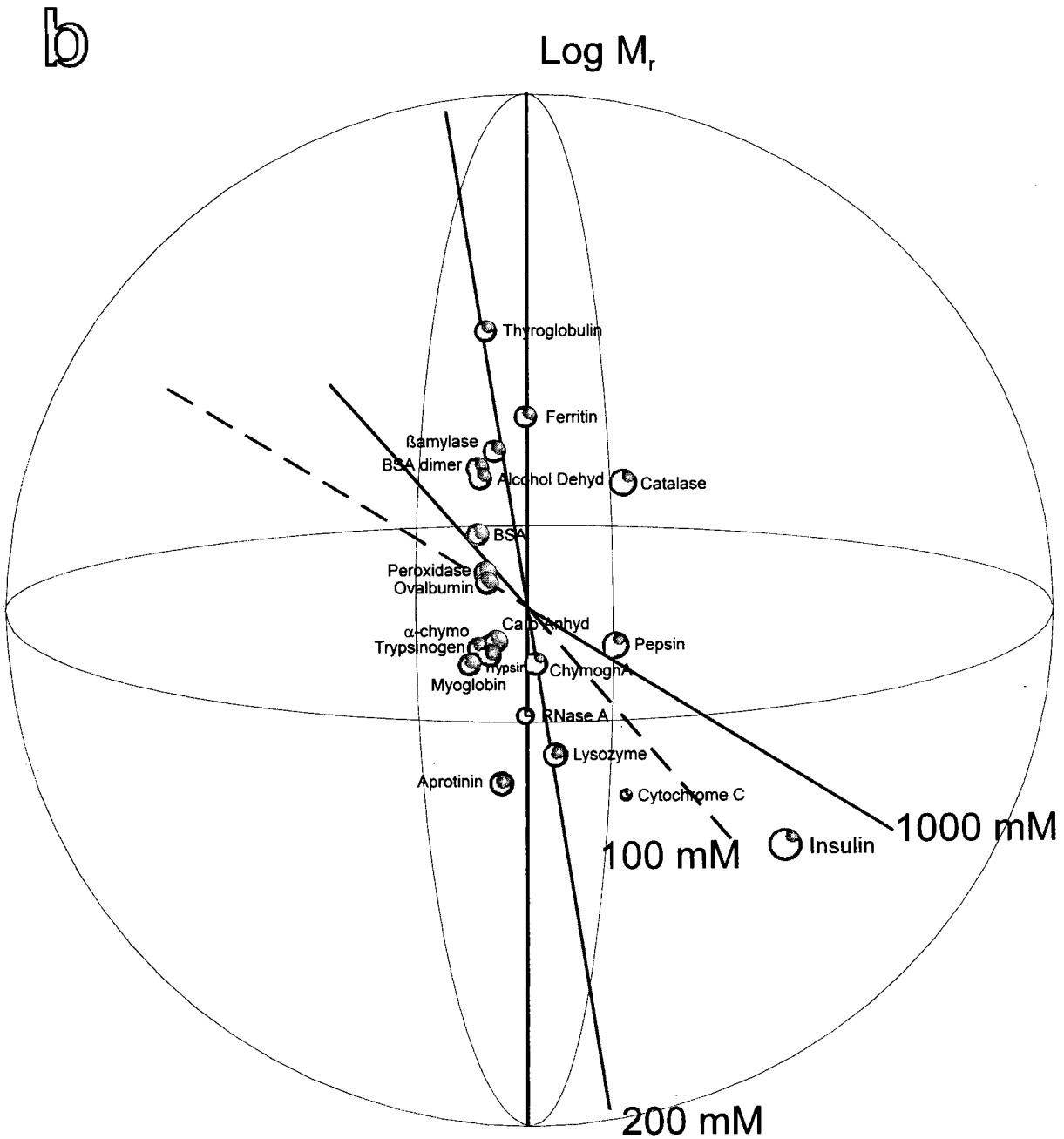

Fig. 2. Analysis of protein–packing interactions in SEC by multivariate non-orthogonal plotting. Reduction of data in Fig. 1 to emphasize the major attributes (mobile phase concentration) and objects (proteins). (a) Front view; (b) is (a) spun 90° around its log M_r axis.

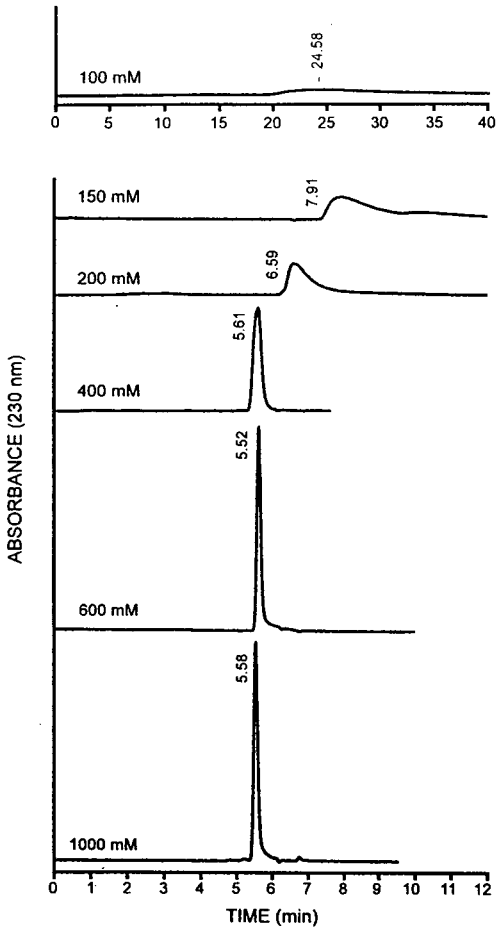

Fig. 3. Characteristic elution profiles of cytochrome *c*, identified in Figs. 1 and 2 to undergo electrostatic-type interactions. Actual chromatograms showing change in retention volume and peak shape. Conditions as in Fig. 1.

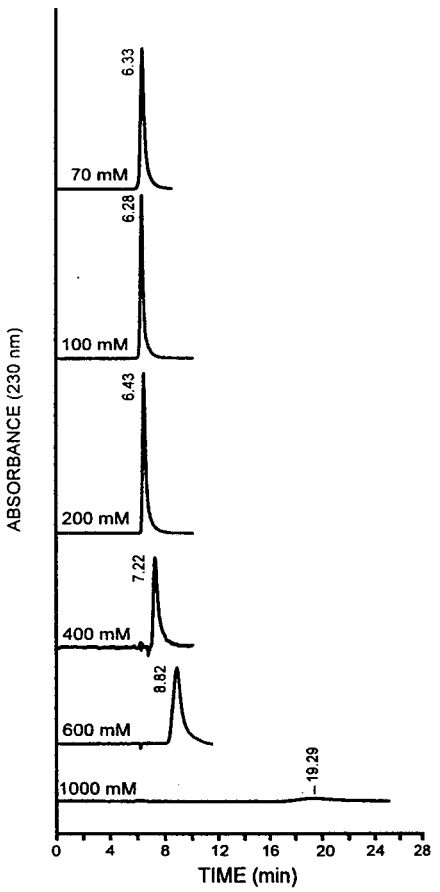

Fig. 4. Characteristic elution profiles of insulin, identified in Figs. 1 and 2 to undergo hydrophobic interactions. Actual chromatograms showing change in retention volume and peak shape. Conditions as in Fig. 1.

extent of their interaction with the column-packing surface. Proteins, including cytochrome *c* and ribonuclease A, grouped in a region of the MultiGraf that indicates electrostatic interactions as a major characteristic. Catalase, pepsin, chymotrypsinogen A, insulin and vitamin B_{12} mapped in an area indicating that they undergo hydrophobic interaction with the column packing. Aprotinin and lysozyme had a tendency towards both types of interaction, and were mapped between the hydrophobic and electrostatic objects on the MultiGraf. Principal-component analysis has been used in a similar way to study reversed-phase systems [24], but the MultiGraf allows improved visualization of the data. DataMax would be a useful aid in demonstrating the hydrophobic and ionic characteristics of an unknown protein. Alternatively, optimal mobile phase conditions could be suggested for a protein of known characteristics. We plan to extend these analyses in the future, providing a more rigorous analysis of non-ideal SEC. It is clear, however, that the ability to visualize *all* of the data from an experiment, through non-orthogonal plotting and techniques such as linearizing data through their logarithms, make DataMax a powerful chemometric tool, especially in SEC.

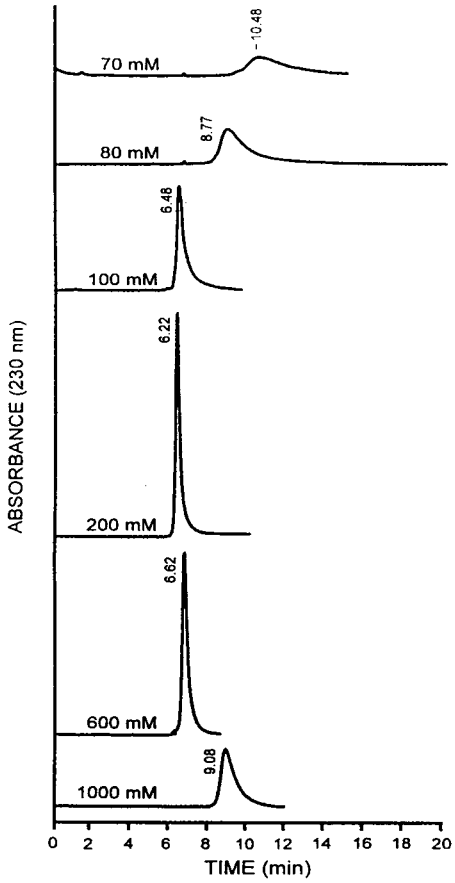

Fig. 5. Characteristic elution profiles of lysozyme. Lysozyme was identified in Figs. 1 and 2 to undergo both electrostatic and hydrophobic interactions. Actual chromatograms showing change in retention volume and peak shape. Conditions as in Fig. 1.

Acknowledgement

The authors would like to thank J.J. DeStefano for many helpful discussions and critical reading of the manuscript.

References

[1] J.J. Kirkland, C.H. Dilks, Jr. and J.J. DeStefano, *J. Chromatogr.*, 635 (1993) 19.
[2] J.J. Kirkland, C.H. Dilks, Jr. and J.E. Henderson, *LC·GC*, 11 (1993) 290.
[3] B.E. Boyes and J.J. Kirkland, *Peptide Res.*, 6 (1993) 249.
[4] J.J. Kirkland, *J. Chromatogr. Sci.*, 31 (1993) 493.
[5] L. Morin-Allory and B. Herbreteau, *J. Chromatogr.*, 590 (1992) 203.
[6] P.J. Bailey and B.G. Rohrback, *Food Technol.*, 48, No. 4 (1994) 69.
[7] F.O. Geiser, C. Golt, L. Kung, Jr., J.D. Justice and B.L. Brown, *J. Chromatogr.*, 631 (1993) 1.
[8] S.J. Schmitz, H. Zwanziger and H. Engelhardt, *J. Chromatogr.*, 544 (1991) 381.
[9] P. Karsnas and T. Lindblom, *J. Chromatogr.*, 599 (1992) 131.
[10] Y. Kato and T. Hashimoto, *J. High Resolut. Chromatogr. Chromatogr. Commun.*, 6 (1983) 324.
[11] W. Kopaciewicz and F.E. Regnier, *Anal. Biochem.*, 126 (1982) 8.
[12] M. Potschka, *J. Chromatogr.*, 441 (1988) 239.
[13] F. Hefti, *Anal. Biochem.*, 121 (1982) 378.
[14] M. LeMaire, A. Ghazi, J.V. Moller and L.P. Aggerbeck, *Biochem. J.*, 243 (1987) 399.
[15] M. LeMaire, L.P. Aggerbeck, C. Monteilhet, J.P. Andersen and J.V. Moller, *Anal. Biochem.*, 154 (1986) 525.
[16] P.L. Dubin and J.M. Principi, *Macromolecules*, 22 (1989) 1891.
[17] H.G. Barth, B.E. Boyes and C. Jackson, *Anal. Chem.*, 66 (1994) 595R.
[18] R.W. Stout, S.I. Sivakoff, R.D. Ricker, H.C. Palmer, M.A. Jackson and T.J. Odiorne, *J. Chromatogr.*, 352 (1986) 381.
[19] W. Kopaciewicz, M.A. Rounds, J. Fausnaugh and F.E. Regnier, *J. Chromatogr.*, 266 (1983) 3.
[20] G. Rippel and L. Szepesy, *J. Chromatogr. A*, 664 (1994) 27
[21] O.-W. Reif, V. Nier, U. Bahr and R. Freitag, *J. Chromatogr. A*, 664 (1994) 13.
[22] P.G. Righetti and C. Tiziana, *J. Chromatogr.*, 127 (1976) 1.
[23] D.W. Darnell, in G.D. Fasman (Editor), *CRC Practical Handbook of Biochemistry and Molecular Biology*, CRC Press, Boca Raton, FL, 1989, p. 158.
[24] M.C. Pietrogrande, M.I. Turnes Carou and F. Dondi, *Analusis*, 20 (1992) 111.

ELSEVIER

Journal of Chromatography A, 691 (1995) 81–89

JOURNAL OF CHROMATOGRAPHY A

Characterization of a new reversed-phase chromatographic column on a 2-μm porous microspherical silica gel

Hiroyuki Moriyama*, Masakazu Anegayama, Katsuo Komiya, Yoshio Kato

Separation Centre, Tosoh Co., Kaisei-cho 4560, Shinnanyo, Yamaguchi 746, Japan

Abstract

The physical and chromatographic properties of a reversed-phase column based on a 2-μm porous silica gel, TSKgel Super-ODS, were investigated. The Super-ODS column reveals higher column efficiencies (over 200 000 theoretical plates/m) at a higher flow-rate than that on a conventional column. High selectivity for a planar compound on Super-ODS implies that it possesses a polymeric ODS layer. Employing pure silica and a full end-capping procedure resulted in sharp peaks for basic and chelating compounds. To avoid the loss of column efficiency, the void volumes in an operating system such as connecting tubes, cell volume and sample volume, should be minimized as much as possible. The time constant of the detector also affected the column efficiency. The separation of peptides was achieved within 4 min.

1. Introduction

Octadecylsilylated silica gel (ODS) has been widely employed for separating many compounds. In general, the particle sizes utilized for fast LC and conventional columns are around 3 and 5 μm, respectively. The column efficiencies on these columns range from ca. 60 000 to 150 000 theoretical plates (TP)/m.

In the last decade, many researchers have emphasized the advantages of the use of small particles 1.5–3 μm in diameter [1–4]. These columns, based on non-porous materials, allow fast separations and good resolution for biological samples such as proteins and DNAs in several separation modes [5–7]. It is assumed that no diffusion of a solute into pores results in the avoidance of peak broadening. However, these columns show a low capacity for low-molecular-mass compounds because of the small surface area. On the other hand, Danielson and Kirkland [8] suggested the use of a short reversed-phase (RP) column packed with porous microparticles for separating large molecules such as peptides and proteins. They stressed that their short column was a useful tool for analysing biological macromolecules and reported high column efficiencies more than 130 000 TP/m).

Recently, a new reversed-phase chromatographic column, TSKgel Super-ODS, based on 2-μm silica gel, became commercially available from Tosoh (Tokyo, Japan). In this paper, we report the characterization of this RP column in comparison with conventional and fast LC ODS columns.

* Corresponding author.

0021-9673/95/$09.50
SSDI 0021-9673(94)00744-6

Table 1
HPLC columns employed

Column	Supplier	Column size (mm × mm I.D.)	Particle size (μm)	Functionality	End-capping
TSKgel Super-ODS	Tosoh	50 and 100 × 4.6	2	Polymeric C_{18}	Yes
TSKgel ODS-80Ts	Tosoh	150 × 4.6	5	Monomeric C_{18}	Yes
TSKgel Octadecyl-NPR	Tosoh	35 × 4.6	2.5	–	No
YMC-FL-ODS-3	YMC	50 and 100 × 4.6	3	Monomeric C_{18}	Yes
Capcell Pak $3C_{18}$	Shiseido	50 and 100 × 4.6	3	Monomeric C_{18}	Yes
Cosmosil $3C_{18}$	Nacalai Tesque	50 and 100 × 4.6	3	Monomeric C_{18}	Yes
Develosil ODS-K-3	Nomura Chemicals	50 × 4.6	3	Monomeric C_{18}	Yes

2. Experimental

2.1. Chemicals and materials

Perchloric acid, phosphoric acid and NaH_2Po_4 of guaranteed grade were purchased from Wako (Osaka, Japan). Organic solvents (methanol and acetonitrile) of HPLC grade were obtained from Kanto Chemicals (Tokyo, Japan). Peptides were purchased from the Peptide Institute (Kyoto, Japan) and antibacterial chemicals from Sigma (St. Louis, MO, USA). The HPLC columns (from LCC, Yamaguchi, Japan) are listed in Table 1 with regard to column size, supplier, particle size, functionality and end-capping procedure. Mobile phases were prepared by mixing deionized water obtained with a Milli-Q system (Millipore, Bedford, MA, USA) and an HPLC-grade organic solvent. Perchloric acid was added directly to an aqueous solution. Phosphate buffer was made by using NaH_2PO_4 (pH 6.8 adjusted with concentrated H_3PO_4). For peptide separations and determination of antibacterial chemicals, linear gradient elution was adopted.

2.2. Instrumentation

The HPLC system consisted of a Model CCPM-II dual computer-controlled multi-pump (Tosoh), a UV-8020 variable-wavelength UV detector equipped with a 2-μl microflow cell or a Model UV-8010 detector equipped with 10 μl flow cells with and without a heat-sink coil (Tosoh) and Model MCPD-3600 Spectro multichannel photodiode-array detector (Tosoh).

The physical properties of Super-ODS and ODS-80Ts were measured using an Autoscan-60 mercury penetration apparatus (Quantachrome, Syosset, NY, USA) and a JSM-5300 scanning electron microscope (Jeol, Tokyo, Japan).

3. Results and discussion

Table 2 gives the physical data for Super-ODS and ODS-80Ts gels measured by the mercury penetration method and scanning electron microscopy. Whereas ODS-80Ts has granules, Super-ODS possesses a smaller pore volume and

Table 2
Physical properties of ODS gels

Column	Pore volume (ml/g)	Specific surface area (m^2/g)	Mean pore diameter (nm)	Particle size ±S.D. (μm)
TSKgel Super-ODS	0.25	96.8	11.2	2.29 ± 0.27
TSKgel ODS-80Ts	0.63	312.8	8.2	5.06 ± 0.87

surface area. The small S.D. on Super-ODS (0.27 μm) implies that the Super-ODS gel is more uniformly sized than with ODS-80Ts (S.D. 0.87 μm). Fig. 1A and B show scanning electron micrographs of Super-ODS with different magnifications. Tables 3 and 4 give the column efficiencies on Super-ODS and commercial fast LC columns under the same conditions. For each column size, Super-ODS shows greater efficiency (over 200 000 TP/m) than the fast LC columns (110 000–170 000 TP/m). In spite of the high column performance with Super-ODS, the operating pressure drops were lower than those on the fast LC columns. It seems that the narrow particle distribution of the Super-ODS gel contributes to lowering the operating pressure drops. With respect to the retention ability, solutes on Super-ODS were eluted earlier than on the other columns. This is consistent with a small surface area of the base silica gel.

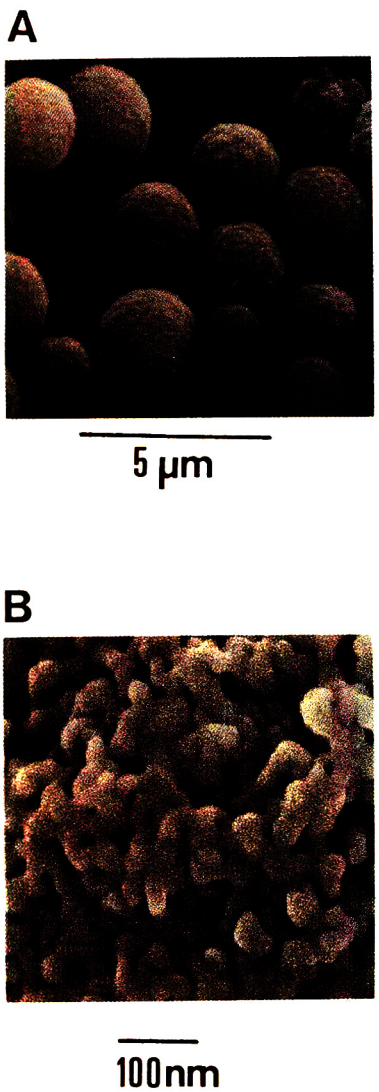

Fig. 1. Scanning electron micrographs of Super-ODS. Magnification: (A) ×5000; (B) ×100 000.

Fig. 2 shows a comparison of the elution profiles of a basic compound, pyridine, on Super-ODS and ODS-80Ts. In general, incompletely end-capped ODS gels give poor peak shapes for basic compounds owing to the strong adsorption [9,10]. The sharp peaks of pyridine on each column imply the existence of fewer ionic sites on each ODS surface contributing to the ionic interaction. Fig. 3 also demonstrates the inertness of the Super-ODS gel as a chelating reagent. Metal impurities on ODS gels affect on the elution profiles of chelating [11–13] and oxidizing compounds [14] owing to the formation of chelating complexes or to conversion into an oxidized form in an ODS column by an redox reaction. Consequently, the use of a purified silica gel containing a smaller amount of metal impurities leads to better peak shapes and reproducible chromatographic results.

Jinno and Kawasaki [15] emphasized that the selectivity for planar compounds relates to the manner of the introduction of a functional group on the silica surface, which is a monomeric and polymeric ODS layer. The separation factor, α(OT/TR), between *o*-terphenyl (OT) and triphenylene (TR) on a polymeric ODS column is generally greater than that on a monomeric ODS. As indicated in Table 5, the Super-ODS gel possesses a polymeric layer because it has a large α(OT/TR) of 1.98, whereas ODS-80Ts gel has a monomeric layer owing to the small α(OT/TR) of 1.27.

To obtain a high efficiency on a short column, there are a few factors to be considered, such as the void volume and the time constant, ν, of the detector [16]. The former factor consists of

Table 3
Comparison of column efficiencies on ODS columns

Column	Fluorene		Separation factor, α(NAP/FLU)	Pressure drop (MPa)
	Retention time (min)	TP/column		
TSKgel Super-ODS	3.71	10728	2.30	9.8
YMC-FL-ODS-3	6.10	7453	2.38	9.9
Capcell Pak $3C_{18}$	4.70	8701	2.27	12.6
Cosmosil $3C_{18}$	6.58	5893	2.39	11.8
Develosil ODS-K-3	6.61	7652	2.38	9.5

Mobile phase, methanol–water (70:30); detection, UV at 254 nm (detector equipped with a 2 μl flow cell); sample, naphthalene (NAP)–fluorene (FLU); flow-rate, 1 ml/min; column size, 50 mm × 4.6 mm I.D.

Table 4
Comparison of ODS column efficiencies

Column	Naphthalene		Pressure drop (MPa)
	Retention time (min)	TP/column	
TSKgel Super-ODS	4.06	20612	19.4
Capcell Pak $3C_{18}$	4.46	10651	26.5
Cosmosil $3C_{18}$	3.47	11685	19.4

Sample, naphthalene; column size, 100 mm × 4.6 mm I.D.; other conditions as in Table 3.

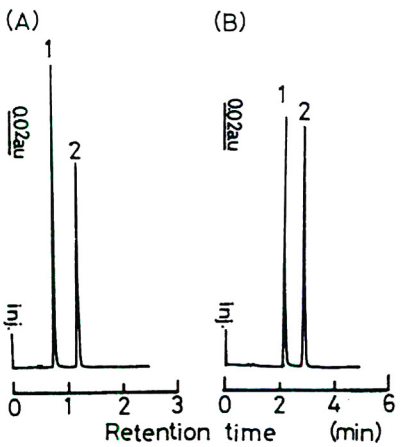

Fig. 2. Elution profiles of pyridine on RP columns. Column, (A) TSKgel Super-ODS (50 mm × 4.6 mm I.D.) and (B) TSKgel ODS-80Ts (150 mm × 4.6 mm I.D.); mobile phase, (A) acetonitrile–water (30:70) and (B) acetonitrile–water (50:50); detection, UV at 254 nm (ν = 50 ms); flow-rate, 1 ml/min; temperature, ambient. Peaks: 1 = pyridine; 2 = phenol.

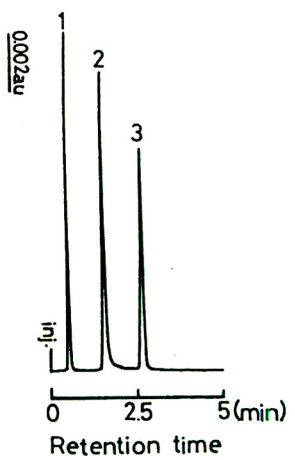

Fig. 3. Chromatogram of chelating reagent on Super-ODS. Column, TSKgel Super-ODS (50 mm × 4.6 mm I.D.); mobile phase, 20 m*M* Na_2HPO_4 (pH 6.8, adjusted with concentrated H_3PO_4)–acetonitrile (70:30); detection, UV at 245 nm; other conditions as in Fig. 2. Peaks: 1 = uracil; 2 = 8-quinolinol; 3 = methyl benzoate.

Table 5
Comparison of planar recognition ability on ODS columns

Column	o-Terphenyl		Triphenylene		Separation factor, α(OT/TR)	Resolution factor, R_s(OT/TR)
	k'	TP	k'	TP		
TSKgel Super-ODS	2.19	9596	3.84	6059	1.98	13.53
TSKgel ODS-80Ts	6.65	14163	8.00	14571	1.27	5.53

Mobile phase, methanol–water (80:20) for Super-ODS and (85:15) for ODS-80Ts; detection, UV at 254 nm; sample, o-terphenyl (OT)–triphenylene (TR). The void volume of each column, v_0, was estimated from the elution volume of Uracil.

Table 6
Effect of void volumes in connecting tube on column efficiency of Super-ODS

(A) Injector–column			(B) Column–detector		
Tube length (cm)	Void volume (μl)	TP/column	Tube length (cm)	Void volume (μl)	TP/column
10	0.79	10741	10	0.79	10741
15	1.19	10635	15	1.19	10631
30	2.36	9569	30	2.36	10540
50	3.93	9076	50	3.93	9340
70	5.50	8496	70	5.50	9021

Stainless-steel tubes of 0.1 mm I.D. were used. In (A) the connecting tube length between the column and the detector was 10 cm and in (B) the tube length between the injector and the column was 10 cm. Other conditions as in Table 3.

connecting tubes, flow cell and sample volume injected. Table 6 shows the effect of the void volume in the connecting tubes on the number of theoretical plates. To prevent a decrease in column efficiency, the void volumes in the connecting tubes between the injector and column and the column and detector should be less than 2 μl.

The effect of the cell volume on column

Table 7
Effect of cell volume on column efficiency

Cell volume (μl)	TP/column	Decrease in column efficiency (%)
2	10767	0
10	10150	6
10[a]	3104	71

Detection, UV at 254 nm. Other conditions as in Table 3.
[a] The 10-μl flow cell was equipped with a heat sink coil of 1000 mm × 0.25 mm I.D.

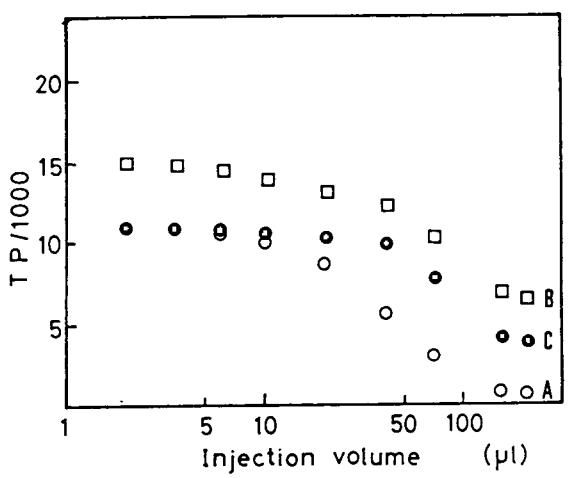

Fig. 4. Relationship between column efficiency and sample volume. Column, (A, C) TSKgel Super-ODS (50 mm × 4.6 mm I.D.) and (B) TSKgel ODS-80Ts (150 mm × 4.6 mm I.D.); mobile phase, (A, B, C) methanol–water (70:30); sample, naphthalene dissolved in (A, B) methanol–water (70:30) and (C) methanol–water (40:60); sample concentration, 0.1 mg/ml; other conditions as in Fig. 2.

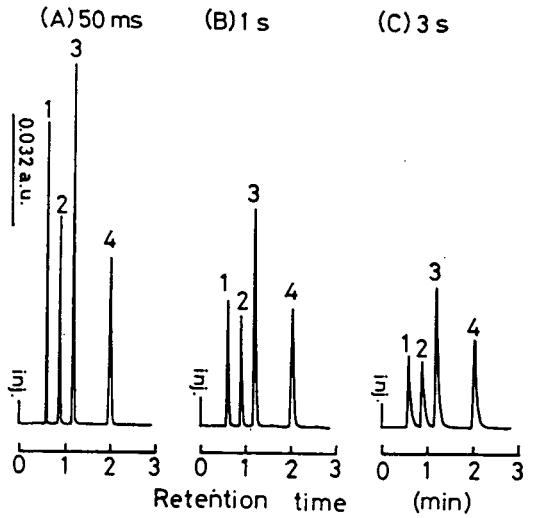

Fig. 5. Effect of time constant on peak shapes on Super-ODS. Mobile phase, acetonitrile–water (50:50); detection, UV at 254 nm [ν = (A) 50 ms, (B) 1 s and (C) 3 s]; other conditions as in Fig. 2. Peaks: 1 = uracil; 2 = benzene; 3 = toluene; 4 = naphthalene.

efficiency is summarized in Table 7. The use of a small cell volume is necessary to obtain high column efficiencies.

Fig. 4 shows the relationship between sample volume injected and column efficiency. The number of theoretical plates on Super-ODS decreased steeply with injection volumes over 10 μl (curve A). On the other hand, high column efficiencies on ODS-80Ts were maintained up to

Table 8
Effect of time constant on column efficiency

Time constant (ν)	TP/column	Resolution factor, *Rs* (TOL/NAP)
50 ms	10 529	13.37
1 s	6996	10.37
3 s	3420	6.87

injections of 50 μl (curve B). This is attributable to the difference in the surface areas of the packing materials. Although Giesche et al. [2] suggested that the sample volume must be 0.6 μl in their LC system, it is obvious that the surface area of their non-porous gel was too small to retain solutes adequately. With the injection of a sample solution that contains smaller amount of an organic solvent than that in the mobile phase, much larger sample volumes could be applied to the Super-ODS column without a decrease in column efficiency (curve C).

The time constant of the detector is another important factor, as reported by Giesche et al. [2]. The numbers of theoretical plates for the drugs on Super-ODS measured with different time constants are listed in Table 8. The TP measured with ν = 3 s decreased drastically. Fig. 5 illustrates the chromatograms of the drugs with different time constants (ν = 50 ms, 1 s and 3 s).

Fig. 6 shows the relationship between HETP and linear velocity, u (cm/min), using (A)

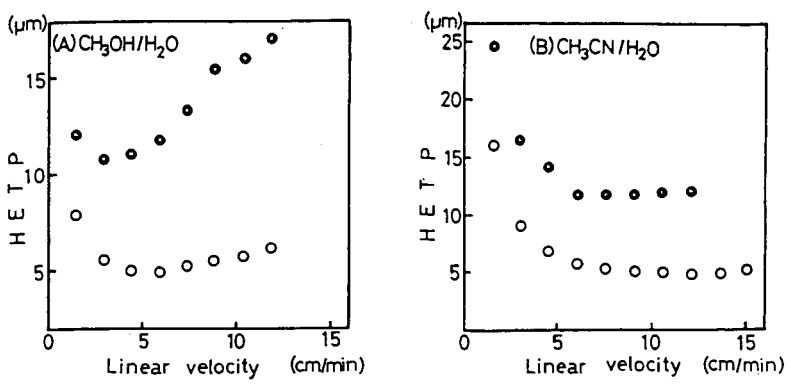

Fig. 6. H versus u curves on Super-ODS and ODS-80Ts with different mobile phases. Column, ○ = TSKgel Super-ODS; ● = ODS-80Ts; mobile phase, (A) methanol–water (70:30); (B) acetonitrile–water (50:50); sample, fluorene; flow-rate, 0.25–2.5 ml/min; other conditions as in Fig. 2.

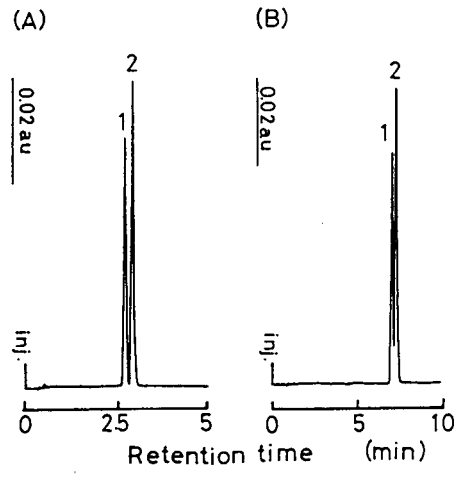

Fig. 7. Comparison of resolution between vitamin D_2 and D_3 on Super-ODS and ODS-80Ts. Mobile phase, methanol; other conditions as in Fig. 2. Peaks: 1 = vitamin D_2; 2 = vitamin D_3.

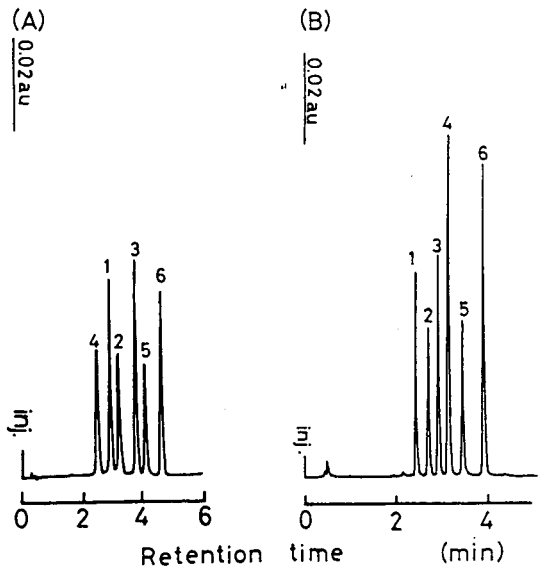

Fig. 8. Comparison of the separation of peptides on Super-ODS and Octadecyl-NRP. Column, (A) TSKgel Octadecyl-NPR (35 mm × 4.6 mm I.D.) and (B) TSKgel Super-ODS (50 mm × 4.6 mm I.D.); mobile phase, 13 m*M* perchloric acid–acetonitrile, with linear gradients of acetonitrile from 0% (for NPR) and 10% (for Super-ODS) to 50% in 10 min; detection, UV at 220 nm (ν = 50 ms); amounts of each solute injected, 0.1–0.2 μg; flow-rate, 1.5 ml/min on Octadecyl-NPR and 2 ml/min on Super-ODS; other conditions as in Fig. 2. Peaks: 1 = oxytosin; 2 = α-endorphin; 3 = bombesin; 4 = leu-enkephalin; 5 = γ-endorphin; 6 = somatostatin.

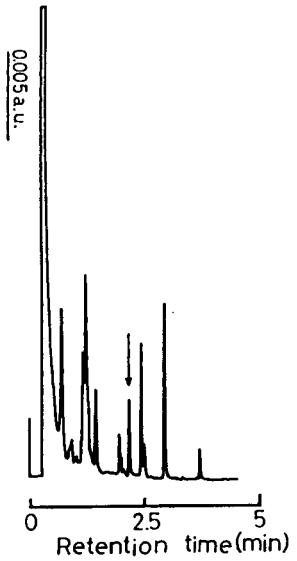

Fig. 9. Chromatogram of pork extract on TSKgel Super-ODS. Column, TSKgel Super-ODS (50 mm × 4.6 mm I.D.); mobile phase, 0.1% H_3PO_4–acetonitrile, with a 5-min linear gradient of acetonitrile from 10% to 40%; flow-rate, 2 ml/min; amount of sample injected, 10 μl of extract solution; detection, UV at 260 nm. The arrowed peak was investigated with the photodiode-array detector.

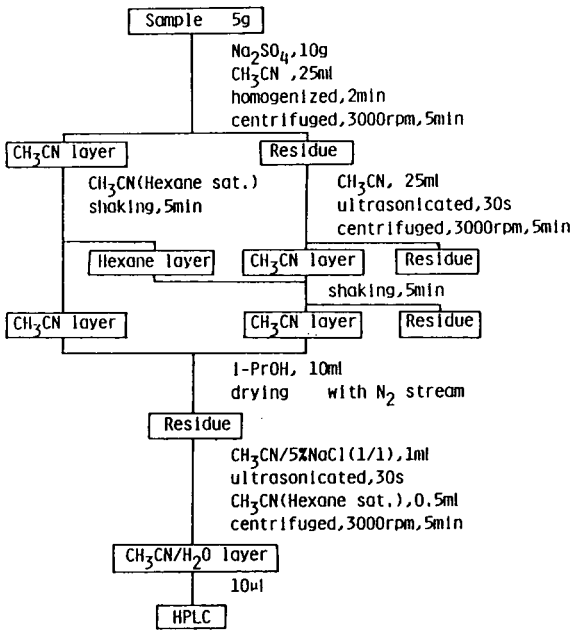

Fig. 10. Procedure for extraction of antibacterials in pork.

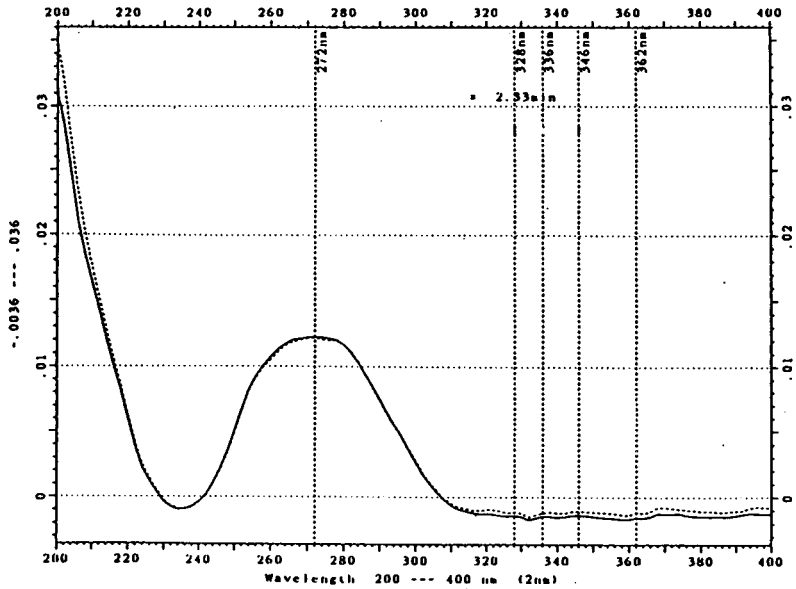

Fig. 11. Spectra of the arrowed peak in Fig. 9 (dashed line) and standard sulfadimethoxine (solid line). Detection with multi-channel photodiode-array detector. The similarity index was 960/1000. The *y*-axis represents absorbance units.

methanol–water and (B) acetonitrile–water systems. The smallest HETPs with methanol–water were obtained at 3 cm/min on ODS-80Ts and 6 cm/min on Super-ODS. Whereas the HETPs on each column increased with increase in linear velocity using methanol–water, slight changes in the HETPs on both columns were observed at more than 6 cm/min with acetonitrile–water. This is due to the difference in the viscosities of the mobile phases. Consequently, the use of the acetonitrile–water as the mobile phase would be convenient in fast LC.

Fig. 7 shows a comparison of the separation of vitamin D_2 and D_3 on Super-ODS and ODS-80Ts. The $\alpha(D_2/D_3)$ values were 1.10 on Super-ODS and 1.03 on ODS-80Ts. Evidently Super-ODS gives a fast and excellent resolution.

Fig. 8 compares peptide separation on Super-ODS and Octadecyl-NPR, which is an RP column based on a non-porous resin for separating biological macromolecules [17]. Under the optimum conditions, the peptide mixture was successfully separated on Super-ODS within 5 min and also on the non-porous column.

Fig. 9 shows the chromatogram for an extract from pork meat obtained as described in Fig. 10. By measurement of the arrowed peak on the chromatogram using the multi-channel photodiode-array detector, the presence of an antibacterial chemical (sulfadimethoxine) in the pork was recognized (Fig. 11).

4. Conclusions

The reversed-phase material, TSKgel Super-ODS, based on 2-μm porous microspherical silica gel, possesses a polymeric ODS layer on high-purity silica gel. This column showed less ionic and metal interactions than other columns. The use of the small particle size gives higher column efficiencies than other RP columns for many compounds. Therefore, fast separations and better resolutions can be achieved on Super-ODS. A few factors must be considered, however, when using this column: the retention ability is lower than that of other conventional ODS columns so that the content of organic modifier in the mobile phase should be lowered,

and the void volumes in the operating system must be minimized as much as possible.

References

[1] K.K. Unger, G. Jilge, R. Jansen and J.N. Kinkel, *Chromatographia*, 22 (1986) 379.

[2] H. Giesche, K.K. Unger, U. Esser, U. Trüdinger and J.N. Kinkel, *J. Chromatogr.*, 465 (1989) 39.

[3] K. Kalghatgi and Cs. Horvath, *J. Chromatogr.*, 443 (1988) 343.

[4] Y. Kato, T. Kitamura, A. Mitsui and T. Hashimoto, *J. Chromatogr.*, 398 (1987) 327.

[5] J. Keith, Duncan, A.J. Chen and C.J. Sieber, *J. Chromatogr.*, 397 (1987) 3.

[6] Y. Kato, T. Kitamura, S. Nakatani and T. Hashimoto, *J. Chromatogr.*, 483 (1989) 401.

[7] Y. Kato, T. Kitamura, A. Mitsui, Y. Yamasaki, T. Hashimoto, T. Murotsu, S. Fukushige and K. Matsubara, *J. Chromatogr.*, 481 (1988) 212.

[8] N.D. Danielson and J.J. Kirkland, *Anal. Chem.*, 59 (1987) 2501.

[9] N. Tanaka, H. Kinoshita, M. Arai and T. Tsuda, *J. Chromatogr.*, 332 (1985) 57.

[10] J. Köhler, D.B. Chase, R.D. Farlee, A.J. Vega and J.J. Kirkland, *J. Chromatogr.*, 352 (1986) 275.

[11] P.C. Sadek and C.J. Koester, *J. Chromatogr. Sci.*, 25 (1987) 489.

[12] M. Ohtsu, Y. Shiojima, J. Kayama, K. Nakamura, O. Nakata, K. Kimata and N. Tanaka, *J. Chromatogr.*, 481 (1989) 147.

[13] S.M. Cremer, B. Nathanael and Cs. Horvath, *J. Chromatogr.*, 295 (1984) 405.

[14] H. Moriyama, K. Komiya, T. Yamato and M. Aoki, *J. Liq. Chromatogr.*, 295 (1992) 411.

[15] K. Jinno and K. Kawasaki, *Chromatographia*, 17 (1983) 445.

[16] A.M. Krstulovic and P.R. Brown, *Reversed-Phase High Performance Liquid Chromatography*, Wiley, New York, 1982, pp. 21–26.

[17] Y. Yamasaki, T. Kitamura, S. Nakatani and Y. Kato, *J. Chromatogr.*, 481 (1989) 391.

ELSEVIER

Journal of Chromatography A, 691 (1995) 91–99

JOURNAL OF CHROMATOGRAPHY A

Nano-scale design of novel stationary phases to enhance selectivity for molecular shape and size in liquid chromatography

Kiyokatsu Jinno[a,*], Kazuyo Nakagawa[a], Yoshihiro Saito[a], Hatsuichi Ohta[a], Hideo Nagashima[a], Kenji Itoh[a], Jim Archer[b], Yung-Lin Chen[b]

[a]*School of Materials Science, Toyohashi University of Technology, Toyohashi 441, Japan*

[b]*J&W Scientific, Folsom, CA 95630-4714, USA*

Abstract

The design of novel stationary phases in liquid chromatography (LC) which offer enhanced selectivity or better resolution of fullerenes is described. Fullerene molecules have been chosen due to their recent popularity and importance in both chemistry and the materials science fields. From the previous studies on octadecyl modified silica (ODS) stationary phases in LC an important structural requirement for stationary phases that can effectively separate fullerenes has been identified. The distance between each bonded functional group on the silica surface that is best-fit to the fullerene diameter (e.g. C_{60} has ca. 7 Å diameter and inter-ligand distance 7.1 Å of ODS phase is the best-fit size) is the key to improve the separation performance. A phenyl ligand contribution to fullerenes retention has also been found to be important. The size and shape of the cavity-like multilegged phenyl bonded phases is the dominant parameter for the structural recognition of fullerenes. By utilizing these factors a novel stationary phase structure is proposed.

1. Introduction

The design of novel stationary phases which can offer enhanced selectivity for structural isomer separations in liquid chromatography (LC) is one of the most important tasks for separation chemists. The huge demands for such stationary phases to solve practical separation problems are needed in pharmaceutical, medicinal, biochemical and materials science fields. In order to establish such scheme and concept, we have to know the nano-scale molecular–molecular interactions between bonded phases and solute molecules. We have selected a very special class of carbon compounds—fullerenes as our sample probe for this investigation [1–5].

In this study, three tactics are targeted to propose a novel stationary phase which can offer good resolution and selectivity for fullerene separations. First, we have evaluated commercially available octadecylsilica (ODS) stationary phases in fullerene separations; the results provide us the basic understanding and knowledge for designing novel stationary phases. Second is the design and synthesis of novel phases using the knowledge obtained by ODS evaluation. We can then confirm that these novel stationary phases are applicable to enhance fullerene selectivity or not. Finally, we compare the performance of these novel phases to several newly

* Corresponding author.

0021-9673/95/$09.50
SSDI 0021-9673(94)00998-8

developed multilegged bonded phases in the same application.

2. Experimental

Two LC systems were used in this study. For the basic evaluation of bonded phases, a micro-LC system consisted of a Microfeeder MF-2 (Azuma Electric, Tokyo, Japan) and an Uvidec-100 UV detector (Jasco, Tokyo, Japan) with a Rheodyne 7520 injector (0.2 μl, CA, USA). The stationary phases were packed into the fused-silica capillaries of 150 mm × 0.53 mm I.D. length and the mobile phase flow-rate was 2 μl/min. For the conventional column evaluation, a Jasco 880-PU pump coupled with a Jasco MD-915 photodiode array detector (200–900 nm detectable range) using a Rheodyne 7125 injector. The column size was 250 mm × 4.6 mm I.D. length and the mobile phase flow-rate was 1 ml/min.

Most of the stationary phases were synthesized by the methods reported previously [6,7]. The diphenylalkyl bonded phases were monomerically synthesized by using alkyldiphenylchlorosilanes such as butyl, octyl and octadecylsilanes as the starting materials in the usual way. The alternative alkyl bonded phases were also synthesized by using alkylmonochlorosilanes as the starting material. The synthesized materials had been evaluated in their quality by elemental analysis and solid-state NMR spectroscopy. Multilegged phases were also synthesized by a similar method reported in our previous publications [8–10]. The basic difference between these phases and other conventional phases is the structure on the silica surface. The multilegged phases have a unique structure which covers the silica surface horizontally, whereas typical phenyl and ODS phases are attached vertically to the silica surface by siloxane bonding. As the bidentate or tridentate reagents synthesized in the laboratory can form two or three bonds to the silica surface for each molecule of silane, these multi-bonds produce a multi-membered ring with the silica structure (i.e., they can produce cavity-like structure on the surface). Develosil ODS phases were obtained from Nomura Chemicals (Seto, Japan) as gifts.

The mobile phase solvents and other chemicals were all commercially available except for the fullerenes samples. The mixture of fullerenes and pure C_{60} were obtained by the carbon soot which was produced at Science Core in Toyohashi (Japan). Solvent extraction and column chromatography were used to pre-purify those samples.

3. Results and discussion

3.1. ODS study

Polymeric and monomeric ODS phases

Two different types of ODS phases were evaluated in this study. The first are the monomeric ODS phases which were synthesized using monochlorosilane as a starting material. The second are polymeric ODS phases which were produced from trichlorosilane. These two types of phases differ in their molecular shape and size recognition capability, especially for polycyclic aromatic hydrocarbons (PAHs) [11–15]. This difference can be found in fullerene separations as well [16–18]. In our previous work [16,18], the separation of fullerenes with monomeric and polymeric ODS phases using *n*-hexane or toluene–acetonitrile as the mobile phase has been discussed. Fullerene retention with the monomeric ODS is greater than that with the polymeric phase and the resolution for higher fullerenes with the monomeric is better than the polymeric phase. The elution order of higher fullerenes is also different between these two phases. For example, using a toluene–acetonitrile mobile phase with the monomeric ODS, the elution is C_{76}, $C_{78\text{-}C2v'}$, $C_{78\text{-}C2v}$ and D_3 together, and then C_{82} and C_{84}. However, the elution order of the fullerenes with the polymeric ODS phase is $C_{78\text{-}C2v'}$, C_{76}, $C_{78\text{-}C2v}$, D_3, C_{84} and C_{82}. Since the polymeric ODS phase has better capabilities of recognizing molecular shape and size than the monomeric ODS phase, the fullerene elution order with the polymeric phase is strongly dependent on the shape difference of the

fullerene molecules. More experiments have been performed using the monomeric ODS phases in fullerene separations to elucidate the retention mechanism.

Influence of physical parameters

A number of physical parameters can change the retention characteristics of fullerenes within monomeric ODS phases, such as pore diameter, surface area, surface coverage and the distance between the adjacent C_{18} functional groups, etc. Using the same silica gel, these parameters can be minimized. In our recent work [18], three monomeric ODS phases were carefully studied. The results of this work are summarized in Table 1. Three ODS phases having varying surface coverages made from the same silica gel are compared in the separation performance of C_{60} and C_{70}. The retention data show that the higher surface coverage ODS phases provided longer retention and separation power for C_{60} and C_{70}. A temperature dependence study of C_{60} and C_{70} retention on these three different phases also showed that the higher coverage ODS is better than its low coverage counterparts at higher temperature. It has been clearly demonstrated that a maximum retention existed at a given temperature for each phase. The high coverage phase gave the longest retention around −20°C, medium coverage was about −30°C and the low coverage phase was about −50°C. The highest coverage ODS gave the highest maximum retention temperature for C_{60} and C_{70} which contradicts the general rule of retention of PAHs in reversed-phase LC where the lower the temperature is the longer the retention time will be.

A mixture of PAHs and C_{60} were chosen a test probes with these three monomeric ODS phases in order to determine the uniqueness of the separation mechanism needed to resolve C_{60}. For PAHs, decreasing temperature resulted in increasing their retentions. However, when the test temperature is below −20°C, the retention of the C_{60} would not increase even with decreasing temperature. It is apparent that the recognition mechanism of the monomeric ODS phase with the fullerene molecule is different from that applied to PAHs. It has also been found from a plot of the separation factors of C_{60} and C_{70} against temperature that the separation factors for C_{60} and C_{70} are monotonically increasing with decreasing temperature with a lower surface coverage ODS phases, when the temperature is lower than −20°C the separation factors are almost constant while the retentions of both C_{60} and C_{70} are decreasing with decreasing temperature. The separation factors with the highest carbon load Develosil ODS-5 at temperatures less than −20°C showed similar values to those of the polymeric ODS phase. This means the physical property of the high surface coverage monomeric ODS phase is very similar to the polymeric phase at very low temperatures.

The results can be easily explained by the drawings shown in Fig. 1, using the concept of different inter-ligand distance among the bonded C_{18} functional groups. At ambient and/or higher temperature, the C_{18} functional groups are easily relaxed and movable so they can interact with the solute C_{60} without any restriction. With a high surface coverage phase, the distance between each C_{18} group is about 7.1 Å which is

Table 1
Retention data of C_{60} and C_{70}

Stationary phase	C (%)	Surface coverage (μmol/m^2)	Capacity factor (k')		Separation factor C_{70}/C_{60}
			C_{60}	C_{70}	
Develosil ODS-5	20	3.31	0.87	1.61	1.85
Develosil ODS N-5	16	2.47	0.81	1.32	1.63
Develosil ODS P-5	11	1.57	0.44	0.64	1.45

Mobile phase: *n*-hexane at room temperature.

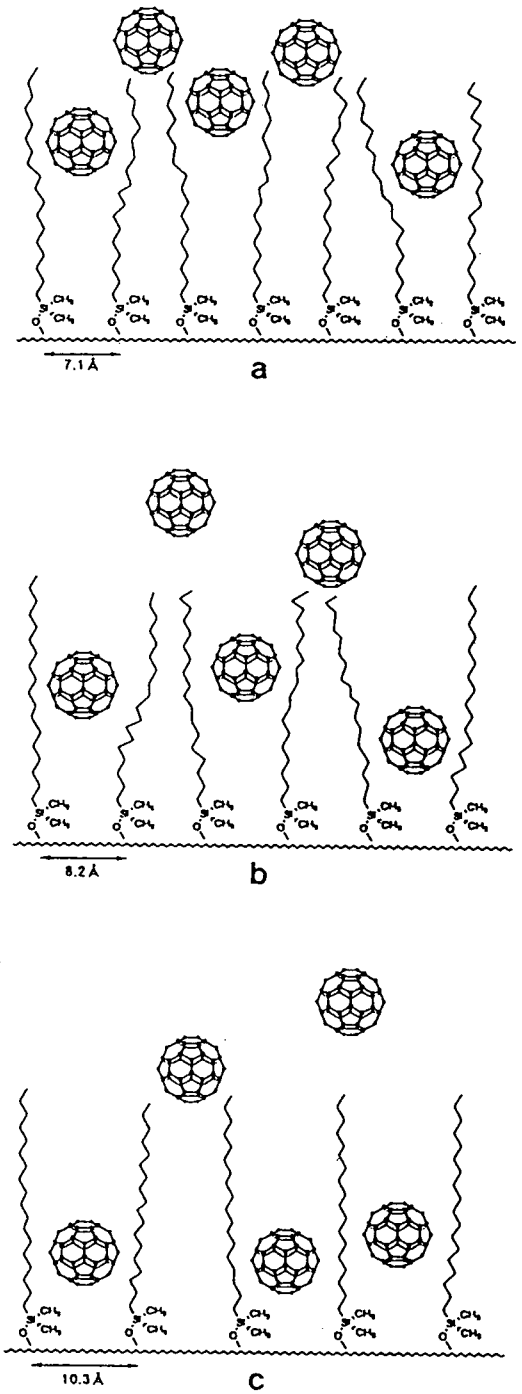

Fig. 1. Schematic diagram of the ODS bonded phase on a silica surface when interaction occurs between the C_{18} phase and C_{60}. (a) Develosil ODS-5; (b) Develosil ODS N-5; (c) Develosil ODS P-5.

very similar to the diameter of the C_{60} molecule which results in very efficient interactions. However, decreasing the surface coverage of ODS results in increasing the distance between C_{18} functional groups which results in less interaction with the C_{60} molecule. At high temperatures, all the C_{18} ligands of the three bonded phases have freedom to move and there is not much difference in C_{60} recognition among these phases caused by difference in distance, but the possibility that interaction occurs is dominant. The C_{18} ligands become more rigid and ordered at lower temperatures and the ligand distance becomes very crucial enabling them to interact with the C_{60} molecule. Any mismatch of ligand distance and diameter of the C_{60} molecule results in a weak interaction and similar retentions. As a conclusion, the ODS ligand distance between each adjacent pair is the most important aspect in obtaining a better selectivity for fullerenes in reversed-phase LC.

3.2. Newly synthesized stationary phases study

There are other important factors at the surface of the bonded phases, such as the length of alkyl chain in conjunction with other functional groups. When phenyl groups were present, they expected to form strong $\pi-\pi$ interactions with fullerenes. Therefore several novel phases have been synthesized, these are depicted in Fig. 2. The phases consist of a monoalkyl chain such as ODS, octyl (C_8) and butyl (C_4) phases with two phenyl or two methyl groups.

Retention data obtained from these phases are summarized in Table 2. The data for phases A, B, C, D, E and F reveal the contribution of the alkyl chain length and phenyl groups versus their dimethyl counterparts. Since A, B and C have the same surface coverage, the distance between the functional groups are almost identical. Any discrimination of fullerene selectivities results from the different alkyl chain lengths. When comparing phases A, B and C to their dimethyl D, E and F counterparts, it is clearly demonstrated that the diphenyl phases exhibit much better separation than those of dimethyl phases. It also appeared that the phenyl group contribu-

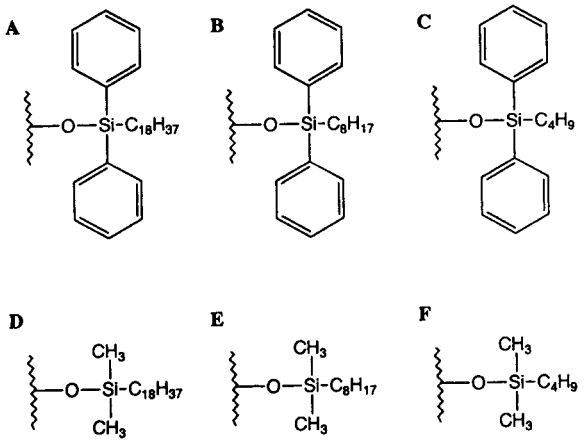

Fig. 2. Novel stationary phases investigated in this work. (A) C_{18}Diph; (B) C_8Diph; (C) C_4Diph; (D) C_{18}; (E) C_8; (F) C_4.

tion to the fullerene separations is larger than the ligand distance contribution if one compares the data for phases C and F which have a similar ligand distance.

3.3. Multilegged stationary phases study

Basic concept of multilegged phases

Another conclusion that can be drawn from the examinations described above is that the phenyl group is a key ingredient for fullerene separations in addition to shorter inter-ligand distance and longer alkyl chain length. All the stationary phases we evaluated so far are vertical types of stationary phases. The typical example of the vertical type of chemically bonded phase is shown in the upper part of Fig. 3. We can design the phase from a different approach such that the bonded phase is situated in the horizontal position relative to the silica surface. This example is shown in the right part of Fig. 3. As described above the phenyl groups at the bottom part of the ODS bonded phase are contributing to the retention of fullerenes. It seems to be a requirement to insert phenyl groups in the bonded phase to enhance the retention and the selectivity for fullerene separations. To investigate this, we have designed new phases as shown in Fig. 4. These phases are called multilegged bonded phases. Each phenyl moiety is situated in a parallel way in the cavity-like structure on the silica surface. The walls of the cavity can be made by several methyl groups attached to two or three silicon atoms which are bonded to the silica surface and to phenyl groups such as phenyl, biphenyl, benzyl and anthracene groups. BP, BMB and BBB were made to investigate the contribution to the retention of the biphenyl group, methylene groups and the varying size of the cavity. An anthracene moiety was also made to investigate a different geometrical contribution to the retention.

For the separation of C_{60} and C_{70} TP has been tried first, because it has been shown in our work that TP was very effective for the separation of planar and non-planar small PAHs [8]. The size of its cavity is the most suitable for the retention of non-planar small PAHs. Compared to ODS phases, TP has been found to have a reversed-elution order in *o*-terphenyl and triphenylene. Such retention behaviour is reasonably explained by the molecular modelling interpretation.

Table 2
Basic characteristics of bonded phases and retention data for C_{60} and C_{70} with these phases. Mobile phase; n-hexane at 30°C

Bonded phase		Pore size (Å)	C (%)	Surface coverage (μmol/m^2)	Ligand interval (Å)	k'		Separation factor
						C_{60}	C_{70}	
A	C_{18}Diph	120	8.48	1.54	10.4	1.02	1.67	1.64
B	C_8Diph	120	5.89	1.56	10.3	0.42	0.57	1.36
C	C_4Diph	120	4.15	1.35	11.1	0.41	0.56	1.37
D	C_{18}	120	9.08	2.52	8.1	0.52	0.84	1.63
E	C_8	120	5.08	2.68	7.9	0.086	0.124	1.44
F	C_4	120	1.73	1.50	10.5	0.061	0.087	1.43

Table 3
Surface coverages of multilegged bonded phases

Stationary phase	C (%)	Surface coverage (μmol/m^2)
BBB	14.2	3.11
BMB	13.4	2.88
BMA	11.6	2.16

phase produces a different situation. The cavity size of the BP phase is about 9–10 Å and the size of C_{60} is 7 Å, and C_{70} is 7×9 Å. Therefore, the size of C_{70} makes it a better fit to the cavity of the BP phase. The retention of C_{70} should be larger than C_{60} and the separation should be improved.

Retention behaviours of fullerenes with multilegged phases

Based on this concept other multilegged phases were also evaluated and the results have indicated that this mechanism works very well for fullerene separations. Table 3 shows the basic properties of several multilegged stationary phases such as BBB, BMB and BMA. The big difference of the basic properties of those phases are surface coverage. BMA has the smallest coverage. And this induces the lowest retention for C_{60} and C_{70} even though it has a large selectivity.

The retention data are summarized in Table 4. BBB and BMB phases retain C_{60} and C_{70} more than either BP or ODS phases. The BMB phase shows the largest retention and good selectivity for C_{60} and C_{70}. The difference between BBB and BMB is the location of the methylene groups in their structures. BMB has a diphenyl group in its structure and this group can easily interact with fullerenes because the movement of the diphenyl group is allowed due to two methylene groups between the diphenyl and the silicon atom which can work as a buffer for such movement. Such movement can interact with fullerenes through $\pi-\pi$ interaction. The benzyl group of the BBB phase does not have the ability to move freely because one edge is bonded to a silicon atom. The BP phase also does not have such freedom of movement found in the BMB phase. Therefore BMB is the most suitable stationary phase for fullerene separations. The BMA phase also has freedom of movement because the anthracene moiety is not connected to the silicon atom and the phase showed very high selectivity. However, its low surface coverage does not give a large retention because of difficulty of bonding chemistry.

Using BMB another practical possibility has been evaluated. As fullerenes have low solubilities in most organic solvents the mobile phase for preparative scale separations can be selected from only a very few solvents (e.g. toluene). However, pure toluene will not make a good separation, therefore we need to use the mobile phase with toluene used only as a modifier. In

Table 4
Retention data for C_{60} and C_{70} with various stationary phases

Stationary phase	Capacity factor, k'		Separation factor
	C_{60}	C_{70}	C_{70}/C_{60}
BP	0.75	1.22	1.63
BBB	2.36	4.26	1.80
BMB	5.36	12.0	2.23
BMA	0.24	0.96	2.21
Develosil ODS-5	0.59	0.96	1.65

Mobile phase: *n*-hexane.

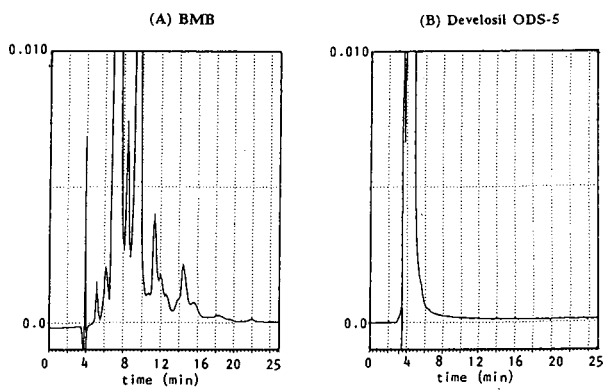

Fig. 5. Chromatograms for the separation of a fullerenes mixture with BMB (A) and Develosil ODS-5 (B). Mobile phase; *n*-hexane–toluene (70:30), flow-rate; 1 ml/min.

Table 3
Surface coverages of multilegged bonded phases

Stationary phase	C (%)	Surface coverage (μmol/m^2)
BBB	14.2	3.11
BMB	13.4	2.88
BMA	11.6	2.16

phase produces a different situation. The cavity size of the BP phase is about 9–10 Å and the size of C_{60} is 7 Å, and C_{70} is 7×9 Å. Therefore, the size of C_{70} makes it a better fit to the cavity of the BP phase. The retention of C_{70} should be larger than C_{60} and the separation should be improved.

Retention behaviours of fullerenes with multilegged phases

Based on this concept other multilegged phases were also evaluated and the results have indicated that this mechanism works very well for fullerene separations. Table 3 shows the basic properties of several multilegged stationary phases such as BBB, BMB and BMA. The big difference of the basic properties of those phases are surface coverage. BMA has the smallest coverage. And this induces the lowest retention for C_{60} and C_{70} even though it has a large selectivity.

The retention data are summarized in Table 4. BBB and BMB phases retain C_{60} and C_{70} more than either BP or ODS phases. The BMB phase shows the largest retention and good selectivity for C_{60} and C_{70}. The difference between BBB and BMB is the location of the methylene groups in their structures. BMB has a diphenyl group in its structure and this group can easily interact with fullerenes because the movement of the diphenyl group is allowed due to two methylene groups between the diphenyl and the silicon atom which can work as a buffer for such movement. Such movement can interact with fullerenes through $\pi-\pi$ interaction. The benzyl group of the BBB phase does not have the ability to move freely because one edge is bonded to a silicon atom. The BP phase also does not have such freedom of movement found in the BMB phase. Therefore BMB is the most suitable stationary phase for fullerene separations. The BMA phase also has freedom of movement because the anthracene moiety is not connected to the silicon atom and the phase showed very high selectivity. However, its low surface coverage does not give a large retention because of difficulty of bonding chemistry.

Using BMB another practical possibility has been evaluated. As fullerenes have low solubilities in most organic solvents the mobile phase for preparative scale separations can be selected from only a very few solvents (e.g. toluene). However, pure toluene will not make a good separation, therefore we need to use the mobile phase with toluene used only as a modifier. In

Table 4
Retention data for C_{60} and C_{70} with various stationary phases

Stationary phase	Capacity factor, k'		Separation factor
	C_{60}	C_{70}	C_{70}/C_{60}
BP	0.75	1.22	1.63
BBB	2.36	4.26	1.80
BMB	5.36	12.0	2.23
BMA	0.24	0.96	2.21
Develosil ODS-5	0.59	0.96	1.65

Mobile phase: *n*-hexane.

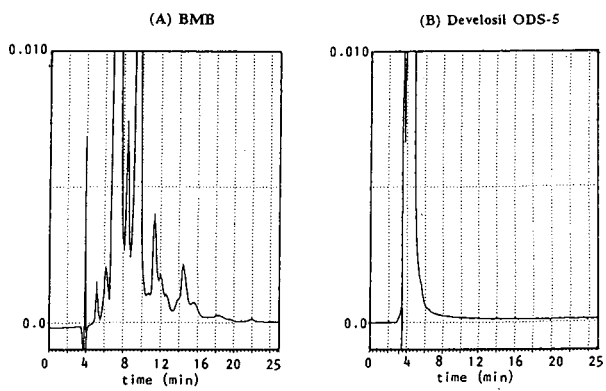

Fig. 5. Chromatograms for the separation of a fullerenes mixture with BMB (A) and Develosil ODS-5 (B). Mobile phase; *n*-hexane–toluene (70:30), flow-rate; 1 ml/min.

order to know the practicality of using BMB as the stationary phase we have tried to use a toluene–*n*-hexane mixture as the mobile phase. As a result two chromatograms were obtained as shown in Fig. 5. *n*-Hexane–toluene (70:30) BMB can give a good separation and selectivity for higher fullerenes but monomeric ODS can only give one peak for all of the fullerenes. So BMB can be useful for preparative scale separations.

3.4. Proposing novel stationary phase

As a conclusion, in order to design a novel stationary phase for enhancing selectivity for fullerenes the following items are required. (i) If the bonded phase is a non-aromatic moiety longer alkyl chains are preferable and the distance between the bonded moieties is crucial to enhancing selectivity (vertical situation). (ii) If the separation mechanism based on size-fit and

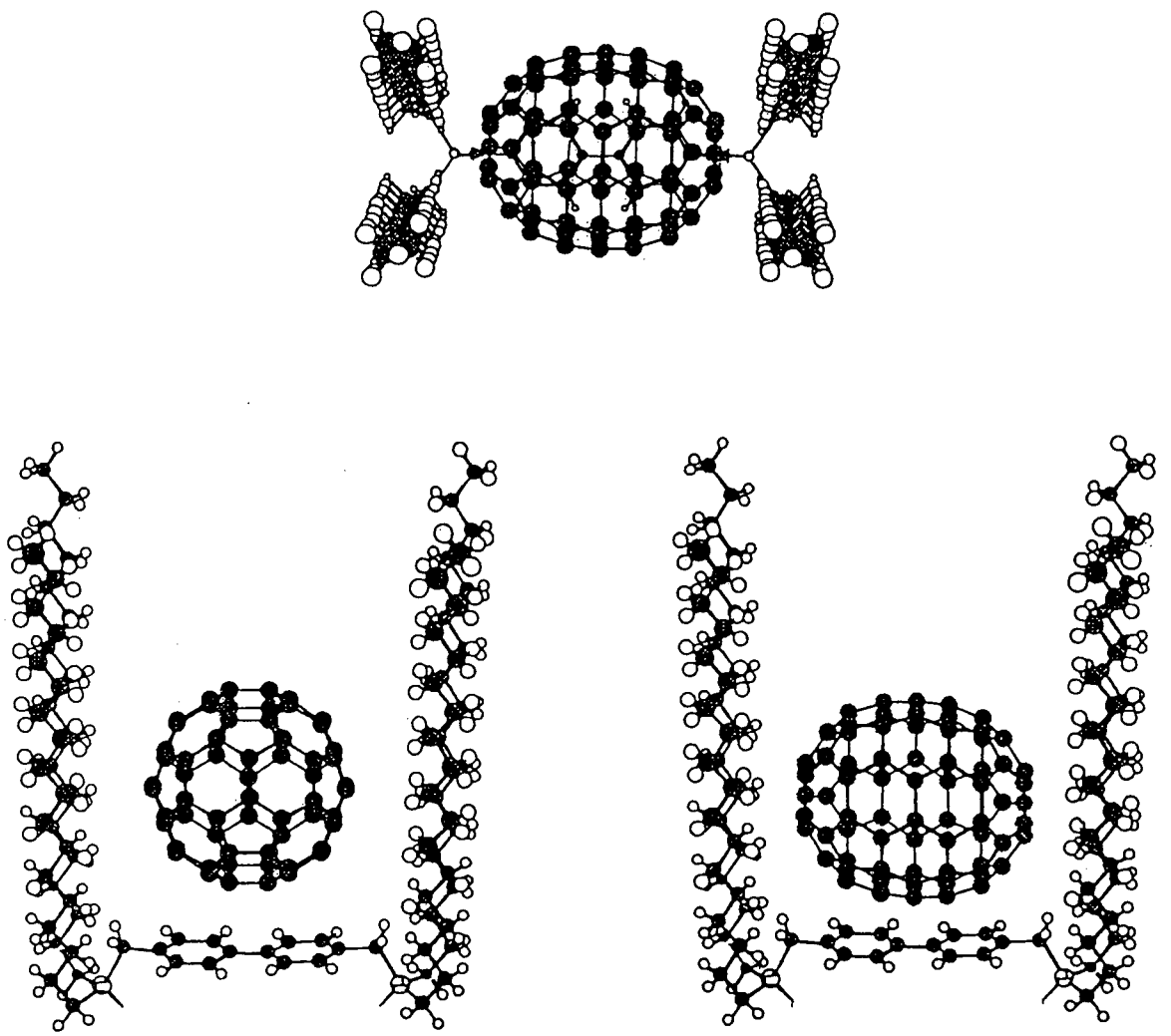

Fig. 6. A novel stationary phase proposed by this investigation. The phase should be made by a silane compound called 4,4′-bis(dioctadecylchlorosilylmethyl)biphenyl.

shape-fit is expected, multilegged phases are the most preferred phases because they can produce a cavity-like structure on the silica surface. The diphenyl group should be included in the structure (horizontal situation). (iii) Combining (i) and (ii) will produce the most desirable novel phase which has long alkyl chains and diphenyl groups at the bottom part of the cavity-like structure. Utilizing these assets a novel phase can be designed as in Fig. 6, where the schematic picture of the most desirable phase is shown. A long alkyl chain (C_{18}) can catch fullerenes and can also form the cavity walls. Biphenyl group at the bottom part can catch fullerenes by $\pi-\pi$ interaction when the solutes enter the cavity. The biphenyl group and methylene group also work to control the distance among each alkyl chain. This novel phase will be synthesized and evaluated in our laboratory in the near future. The discussion in this communication is only focusing on fullerene separations but this concept can be useful for designing new stationary phases to solve other separation problems which require enhanced selectivity.

Acknowledgements

The authors would like to acknowledge many useful discussions with Drs. John C. Fetzer and Wilt. R. Biggs of Chevron Research and Technology Company (Richmond, CA, USA), and Professor Joseph J. Pesek of San Jose State University (San Jose, CA, USA). We also thank to Mr. Norikadzu Nagae of Nomura Chemicals (Seto, Japan) for his kind donation of Develosil ODS phases used in this study. This work is financially supported by a Grant-in-Aid Scientific Research (Grant No. 05233108) from the Ministry of Education and Culture, Japan.

References

[1] H.W. Kroto, J.R. Heath, S.C. O'Brien, R.F. Curl and R.E. Smalley, *Nature*, 318 (1985) 162.
[2] J.R. Heath, S.C. O'Brien, Q. Zhang, Y. Liu, R.F. Curl, H.W. Kroto, F.K. Tittel and R.E. Smalley, *J. Am. Chem. Soc.*, 107 (1985) 7779.
[3] R. Taylor, J.P. Hare, A.K. Abdul-Sada and H.W. Kroto, *J. Chem. Soc. Chem. Commun.*, (1990) 1423.
[4] R.D. Johnson, G. Meijer and D.S. Bethune, *J. Am. Chem. Soc.*, 112 (1990) 8983.
[5] R.D. Johnson, G. Meijer, J.R. Salem and D.S. Bethune, *J. Am. Chem. Soc.*, 113 (1991) 3619.
[6] K. Jinno, Y. Saito, Y-L. Chen, G. Luehr, J. Archer, J.C. Fetzer and W.R. Biggs, *J. Microcolumn Sep.*, 5 (1993) 135.
[7] K. Jinno, H. Ohta, Y. Saito, T. Uemura, H. Nagashima, K. Itoh, Y-L. Chen, G. Luehr, J. Archer, J.C. Fetzer and W.R. Biggs, *J. Chromatogr.*, 648 (1993) 71.
[8] K. Jinno, K. Yamamoto, H. Nagashima, T. Ueda and K. Itoh, *J. Chromatogr.*, 517 (1990) 193.
[9] K. Jinno, K. Yamamoto, T. Kuwamoto, H. Nagashima, T. Ueda, S. Tajima, E. Kimura, K. Itoh, J.C. Fetzer and W.R. Biggs, *Chromatographia*, 34 (1992) 381.
[10] K. Jinno, K. Yamamoto, T. Ueda, H. Nagashima, K. Itoh, J.C. Fetzer and W.R. Biggs, *J. Chromatogr.*, 594 (1992) 205.
[11] L.C. Sander and S.A. Wise, *Anal. Chem.*, 59 (1987) 2309.
[12] L.C. Sander and S.A. Wise, *Anal. Chem.*, 61 (1989) 1749.
[13] K. Jinno, T. Ibuki, N. Tanaka, M. Okamoto, J.C. Fetzer, W.R. Biggs, P.R. Griffiths and J.M. Olinger, *J. Chromatogr.*, 461 (1989) 209.
[14] K. Jinno, Y. Saito, R. Malhan nee Chopra, J.J. Pesek, J.C. Fetzer and W.R. Biggs, *J. Chromatogr.*, 557 (1991) 459.
[15] K. Jinno, J. Wu, M. Ichikawa and I. Takata, *Chromatographia*, 37 (1993) 627.
[16] K. Jinno, T. Uemura, H. Ohta, H. Nagashima and K. Itoh, *Anal. Chem.*, 65 (1993) 2650.
[17] K. Jinno, T. Uemura, H. Ohta, H. Nagashima and K. Itoh, *Chem. Oggi*, in press.
[18] H. Ohta, Y. Saito, K. Jinno, H. Nagashima and K. Itoh, *Chromatographia*, submitted for publication.

ELSEVIER

Journal of Chromatography A, 691 (1995) 101–112

JOURNAL OF CHROMATOGRAPHY A

Displacement chromatography in biotechnological downstream processing

Ruth Freitag*, Jürgen Breier

Institut für Technische Chemie, University of Hannover, Callinstrasse 3, 30167 Hannover, Germany

Abstract

Displacement chromatography was used for the isolation and purification of recombinant antithrombin III (rh-AT III), an anticoagulant of high pharmaceutical interest, which is usually isolated from human blood plasma. A fully automated system was developed, where the preparative chromatographic unit is continuously monitored by fast analytical HPLC. High purities and high concentrations were achieved in a single step. Macroporous hydroxyapatite (HA, diameter 2 μm, pore size 1000 Å) was used to pack the displacement column. Adsorption isotherms were recorded for various proteins. The influence of the column length, the mobile phase composition and the conditioning of the adsorptive surface on the separation by displacement of both basic and acidic proteins was investigated. Much attention was paid to the design of a suitable protein displacer. Cytochrome *c* and the polycation PEI (polyethyleneimine) were used for the displacement of basic proteins. Better results were achieved for the cytochrome *c*. A number of polyacids, proteins and Ca^{2+} complexing agents were investigated as putative displacers of acidic proteins from HA. While the polyacids, PA (polyacrylic acid, M_r 6000) and PGA (polyglutaminic acid, M_r 12 000), were unsuited to the task, the carboxylate cluster-carrying protein β-casein was more successful. The best results were obtained with complexing agents such as the commercially available EGTA [ethylene glycol bis(β-aminoethyl ether)-N,N,N′,N′-tetraacetic acid, M_r 380.4] and IDA–PEG (polyethylene glycol carrying iminodiacetic acid end-groups, $M_{r\,PEG}$ 1000), synthesized for the purpose of protein displacement. Short reversed-phase columns packed with non-porous beads were used for the fast monitoring of the effluent of the displacement column. By working at 60°C the mobile phase flow-rate could be increased to an extent where the time required for a single analysis was reduced to 20 s. Including column regeneration, an analytical frequency of 2 min^{-1} could be maintained. As the flow-rates in the preparative column were chosen such (usually 100 μl/min), that a displacement including column regeneration required ca. 1 h, this analytical frequency is high enough to allow adequate monitoring and documentation of the purification and to permit automatic collection of the product-containing fractions.

1. Introduction

The importance of chromatographic separations for the isolation and purification of the more valuable products of modern biotechnology is unsurpassed [1–3]. At present, non-linear elution chromatography dominates the field, although neither the stationary nor the mobile phase are used efficiently in such processes and the superiority of displacement chromatography in terms of throughput, recovery, final product concentration and waste production has been recognized [4–10]. Other than in, e.g., affinity chromatography, several substances can be iso-

* Corresponding author.

SSDI 0021-9673(94)01000-5

lated simultaneously in displacement chromatography and concomitantly concentrated.

In displacement chromatography, the substance mixture to be separated is loaded on to the preparative column until saturation. Subsequently the displacer, a substance with an exceptionally high affinity for the stationary phase, is introduced at high concentration. Owing to the competition for the adsorptive sites ensuing between the various substances and the displacer, the so-called "displacement train" is formed. Consecutive zones of the pure substance move through the column at the speed of the displacer front. When suitable conditions are chosen, the final substance concentration in the respective zones will be considerably higher than that in the feed. While the theory of displacement chromatography is more involved than that of elution chromatography, it is now possible to predict the effect of column length, sample volume and concentration and also the displacer concentration on mass transport and separation efficiency [11–14].

Displacement chromatography is rarely used in biotechnological or pharmaceutical downstream processing. The lack of suitable protein displacers is one of the reasons for this [6,15–20]; the lack of adequate means for the automatic monitoring of the progress of a separation may also contribute. As the purified proteins appear consecutively in highly concentrated zones, at the column outlet, monitoring of the composition of the column effluent by means other than simple UV detection becomes necessary. Usually this is being done by laboriously collecting and analysing fractions. Besides some model separations using reversed-phase chromatography (RPC), hydrophobic interaction chromatography (HIC) and most often ion-exchange chromatography (IEC), only a few applications of displacement chromatography have been reported [6,8,21]. The antibiotic Cephalosporin C has been isolated from culture supernatants [6] and the enzyme alkaline phosphatase has been recovered from the periplasm of *Escherichia coli* [22]. Polyclonal IgG has been isolated from serum [23] and monoclonal IgG from ascites [7]. The number of protein displacers described in the literature is limited. Since 1979, Torres and Peterson have used carboxymethyldextranes to separate proteins in ion-exchange displacement chromatography [7,22,24,25]. The anionic carbohydrate chondroitin sulfate [17], carboxymethyl starch [15], Nacolyte [18] and the polycation polyethyleneimine (PEI) [6] have also been used. Good results were obtained for polyvinylsulfonic acid [20] and dextran sulfates [26], and also with portentous protein displacers [19].

Hydroxyapatite [$Ca_{10}(PO_4)_6(OH)_2$, HA], a ceramic substance, is an interesting support for the chromatographic purification of high-molecular-mass biological substances [27–31]. Well defined biological macromolecules (proteins, DNA, etc.) are retained on HA, whereas low-molecular-mass substances and denatured proteins are less well retained and are thus easily removed. As HA stabilized the proteins during recovery, the yields of active product tend to be high. The exact mechanism of protein retention on HA is still under discussion, but conditions for adsorption and elution depend on the net charge of the protein in question. Acidic proteins such as bovine serum albumin (BSA), commonly added to most cell culture media, do not interfere with the isolation of a more basic product and vice versa. Several interactions may contribute to protein retention of HA, depending on whether the phosphate or the calcium sites at the HA surface are involved. Often a phosphate buffer is used as mobile phase, which causes the adsorption of more phosphate groups on the HA surface and concomitantly a negative net charge. At near neutral pH, basic proteins will be retained by unspecific electrostatic interaction of their positive net charge with the negative net charge of the HA surface. Such proteins may consequently be eluted by the addition of anions to the mobile phase or by cations with a high affinity for phosphate such as Ca^{2+}. Acidic proteins, on the other hand, interact by complexing the calcium sites with their carboxylate groups. At the same time they are repelled by the negative net charge of the HA surface. Desorption may be achieved by ions that form insoluble calcium salts such as F^- and PO_4^{2-}. Neutral proteins are also adsorbed on HA and

they can be eluted with PO_4^{2-}, Mg^{2+} and F^- but not Ca^{2+}.

2. Experimental

2.1. Materials

Proteins and fine chemicals were obtained from Sigma (Deisenhofen, Germany) and bulk chemicals for buffer and eluent purification from Fluka (Neu-Ulm, Germany). AT III derived from human blood (Kybernin) was donated by the Behring Werke (Margburg, Germany). AT III-containing cell culture supernatants of CHO (Chinese hamster ovary) cells were donated by the Cell Culture Technology Group (Dr. G. Kretzmer) of our Institute. Polymeric displacers and precursors thereof were from Polyscience (Warrington, PA, USA). The HA stationary phases were obtained from Asahi Optical (Tokyo, Japan). The particles were of 2- and 10-μm diameter with average pore size of 1000 Å. Non-porous 2-μm Micropell C_{18} beads (Glycotech, Hamden, CT, USA) were used to pack the analytical RPC columns.

2.2. MALDI-MS

Matrix-assisted laser desorption/ionization mass spectrometric (MALDI-MS) measurements were kindly carried out by Dr. U. Bahr (Institut für Medizinische Physik und Biophysik, University of Münster, Münster, Germany) using a Vision 2000 laser time-of-flight mass spectrometer (Finnigan MAT, Bremen, Germany). Samples were dissolved in water at a concentration of 5 g/l. The matrix was a 10 g/l solution of 2,5-dihydroxybenzoic acid in water–ethanol (9:1). Volumes of 0.5 μl of sample and 2 μl of matrix solution were applied to a silver target and allowed to dry. A post-acceleration voltage of 10 kV was used during the measurements.

2.3. Preparative chromatography

The preparative chromatographic system was assembled from a Gyncotech (Germering, Germany) Model 300 CS pump, a Shodex pulse damper (Showa Denko, Tokyo, Japan) and a Valco (Houston, TX, USA) ten-port valve. A 1-ml sample loop was used for sample injection, while the displacer was introduced from a preparative sample loop (Knauer, Berlin, Germany), that could hold up to 11 ml. Preparative columns were packed at 200 bar. Unless indicated otherwise, the column dimensions were 100 mm × 4.6 mm I.D. A flow-rate of 100 μl/min was used in the displacements. The effluent from the displacement column was analysed twice per minute by analytical RPC or 50-μl fractions were collected and analysed likewise by analytical RPC. For column regeneration, 400 m*M* phosphate buffer (pH 6.8) was used. In the case of protein displacements by Ca^{2+} chelating agents, 100 m*M* $CaCl_2$ solution was used instead for column regeneration.

2.4. Analytical chromatography

The high-pressure gradient system for the analytical HPLC was assembled from two IRICA S 871 pumps (ERC, Alteglofsheim, Germany) controlled by an Autochrom gradient controller (ERC) and a 250-ml dynamic mixing chamber (Knauer, Berlin, Germany). An SF 757 UV detector (ABI, Applied Biosystems, Foster City, CA, USA) equipped with a 0.5-ml/1-mm micro flow cell (0.1-s filter time) with the detection wavelength set at 214 nm was used. For sample injection (5 μl), either an electrically driven EC6W valve (Valco) or a pressure-driven Model 7010 valve (Rheodyne, Cotati, CA, USA) was used. The electrically driven valve caused a high-pressure pulse during injection. The column dimensions were 30 mm × 4.6 mm I.D. Buffer A consisted of deionized water with 0.1% (v/v) of trifluoroacetic acid (TFA) added, and buffer B of acetonitrile with 0.08% (v/v) of TFA added. The gradient was run from 30% to 70% B. By using a flow-rate of 4 ml/min and an operating temperature of 60°C, an analysis was completed within 20 s. Data collection and interpretation were carried out with a Spectra-Physics (now Thermo-Separation Products) (Darmstadt, Germany) SP4270 integrator or a PC using the

CAFCA (computer-assisted flow control and analysis) software developed by Dr. B. Hitzmann and co-workers. (Institut für Technische Chemie, University of Hannover, Hannover, Germany).

2.5. Isotherm measurements

The isotherms were determined as described in Ref. 32. A mobile phase flow-rate of 100 μl/min was used in all instances. The column dimensions were 50 mm × 2 mm I.D. and the detection wavelength was 280 nm. For the basic proteins, 10-μm HA particles (pore size 1000 Å) and 10 m*M* phosphate buffer (pH 6.8) were used. For the acidic proteins, 5 m*M* phosphate buffer (pH 6.8) containing 0.4 m*M* $CaCl_2$ was used as the mobile phase and 2-μm HA particles (pore size 1000 Å) were used to pack the 50 mm × 2 mm I.D. column. For comparison, the basic protein lysozyme (p*I* 10.5) was included in both groups of isotherm measurements.

3. Results and discussion

Many of the highly valuable products of modern biotechnology are produced by mammalian cells. The natural and environmental requirements of such cells are complex. Many culture media contain, e.g., significant amounts of foetal calf serum (FCS). The product is therefore contaminated by a large number of proteins, peptides and other substances, many of which have never been isolated and characterized. BSA (bovine serum albumin, p*I* 4.9), b-IgG (bovine immunoglobulin G, p*I* 7.3) and b-transferrin (p*I* 5.5) must be expected as major product contaminants [33]. The so-called serum-free media usually contain some BSA and b-transferrin. As explained above, depending on its net charge, a protein interacts preferably with the phosphate or the calcium sites on the HA surface. Consequently, acidic proteins such as BSA do not interfere with the isolation of a more basic product, and vice versa. The separation, e.g., of immunoglobulins (p*I* 7.2–7.5) from other more acidic serum proteins therefore poses no problem. Most proteins [34] and consequently most biotechnological products belong, however, to the group of acidic proteins. In such cases the removal of BSA and b-transferrin, but not b-IgG, is necessary and HA displacement chromatography will be most valuable.

For some time now, the aim of our group has been the development of chromatographic separations in the displacement mode for the isolation of pharmaceutically applicable substances (e.g. recombinant h-AT III, monoclonal antibodies) from mammalian cell culture supernatants. The monitoring of the progress of a separation tends to be a problem in displacement chromatography. Usually volume fractions of the displacement train are collected at the column outlet and analysed. Consequently, the time required for documentation may be considerably longer than that necessary for the separation proper. This handicaps process development and prevents the formulation of an on-line process algorithm. We developed a fully automated system instead, where the preparative unit is quasi-continuously monitored by an extremely fast analytical HPLC system (Fig. 1).

3.1. Monitoring of the displacement

The achievement of short analysis times necessitates high mobile phase flow-rates. Following a suggestion of Kalghati and Horvath [35], the viscosity of the mobile phase was lowered by raising the temperature, thus making high flow-rates comparable to a still sustainable pressure drop. A number of macroporous and non-porous RPC stationary phases and macroporous IEC resins were evaluated with regard to their suitability for providing such fast analytical columns. The best results in terms of resolution and long-term stability at high flow-rates were achieved with columns packed with non-porous 2-μm Micropell C_{18} resin.

By using a temperature of 60°C and a flow-rate of 4 ml/min, the composition of the effluent of the displacement column could be analysed within 20 s. Including column regeneration, an analytical frequency of 2 min^{-1} could be maintained. This frequency allowed the quasi-on-line monitoring and documentation of the purification and made accurate control of the fractiona-

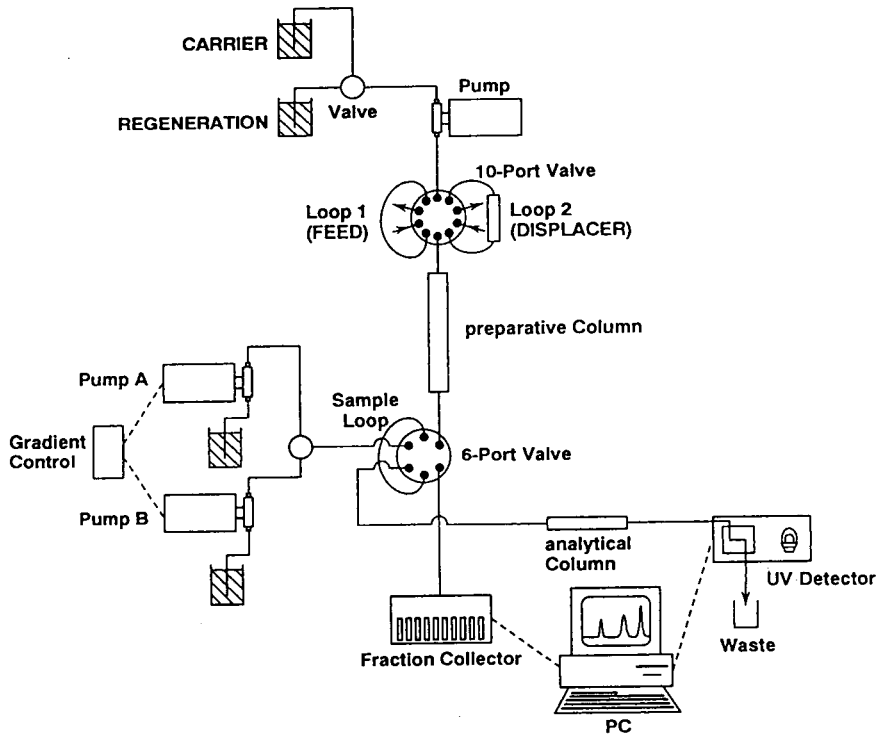

Fig. 1. Schematic diagram of the chromatographic system. The preparative unit is continuously monitored by fast analytical HPLC.

tion possible. The increase in temperature had the beneficial side-effect of improving the resolution at a given flow-rate, perhaps owing to an improvement in the diffusional mass transport at that temperature. In Fig. 2, examples are given of analytical runs performed on the feed and at two points during the displacement of basic (lysozyme, myoglobin; displacer, cytochrome *c*) and acidic (AT III, BSA, b-transferrin; displacer, polyglutaminic acid) proteins. The sample volume was 5 μl in the standard assay but might be decreased to 1 μl by using a microinjection loop; little product was therefore lost in the analysis.

3.2. Displacement of basic proteins

In Fig. 3, the adsorption isotherms of several basic proteins on HA are shown; 10-μm HA particles and 10 m*M* phosphate buffer (pH 6.8) were used. The availability of a suitable displacer is most important in displacement chromatography. In Fig. 4a, the polycation PEI (polyethyleneimine) is used to displace lysozyme (p*I* 10.5) and cytochrome *c* (p*I* 11.2). In Fig. 4b, cytochrome *c* serves as displacer of lysozyme and myoglobin (p*I* 7.4). Not only is the separation better in the latter instance, but also the concentration in the "product" is zones higher. Less contamination of these zones by the displacer is found in the case of protein displacement by cytochrome *c*. Moreover, the removal of cytochrome *c* from the displacement column posed no problem, as flushing with 400 m*M* phosphate buffer sufficed, whereas the removal of the PEI was extremely difficult and time consuming.

In Fig. 5, the influence of the column length on the displacement of lysozyme and myoglobin by cytochrome *c* is demonstrated. The separation quality is clearly improved when a 100- rather than a 50-mm column is used. A further increase in the column length, e.g., 250 mm did not

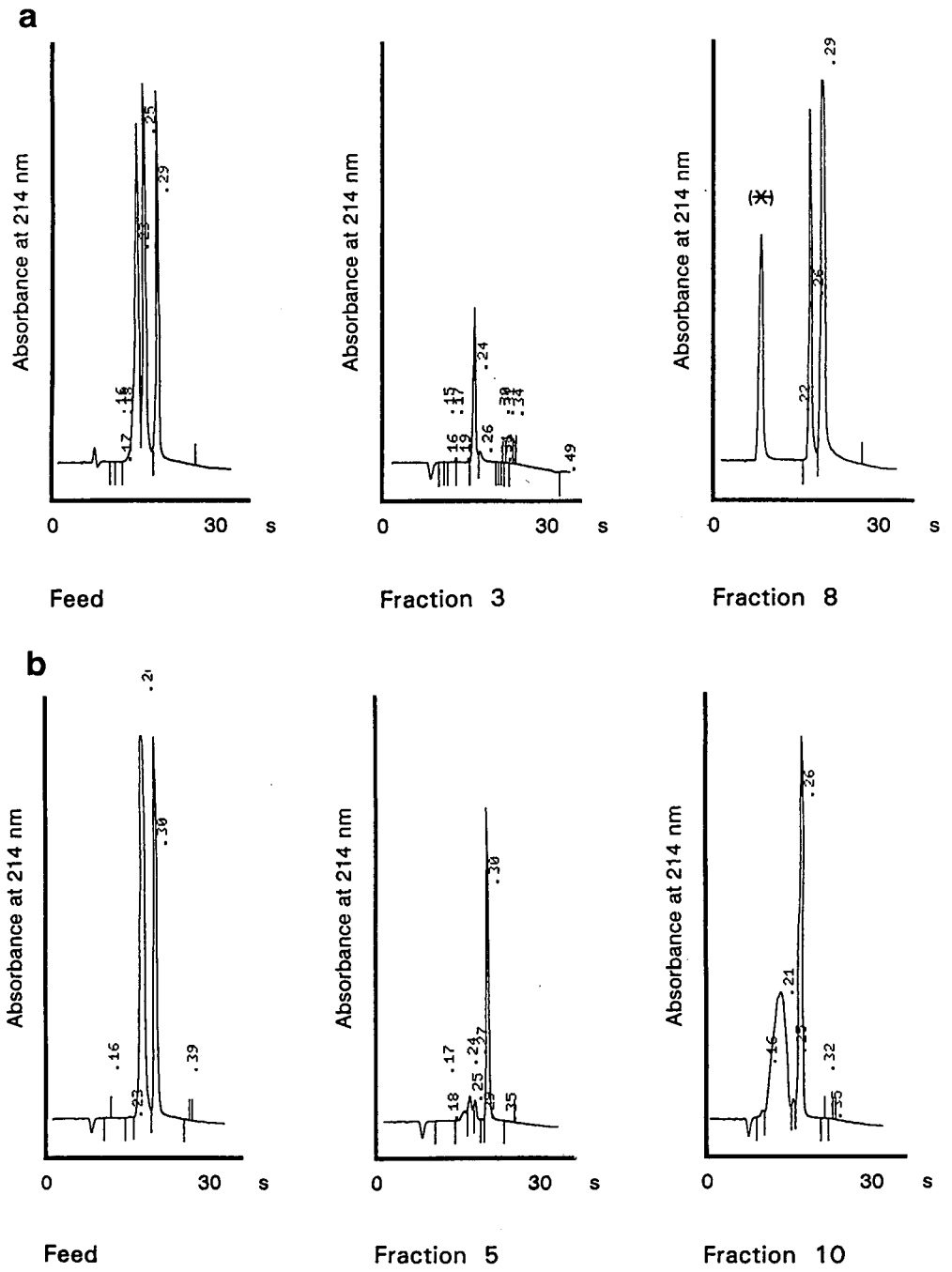

Fig. 2. (a) RPC analysis of the feed and at two points during the separation of the acidic proteins b-transferrin (retention time 0.24 min, p*I* 5.5), BSA (retention time 0.26 min, p*I* 4.9) and AT III (retention time 0.29 min, p*I* 4.6–5.1) by displacement chromatography, using polyglutaminic acid (*) as displacer. (b) RPC analysis of the feed and at two points during the separation of the two basic proteins lysozyme (retention time 0.26 min, p*I* 10.5) and myoglobin (retention time 0.30 min, p*I* 7.4) by displacement chromatography using cytochrome *c* (retention time 0.21 min) as displacer.

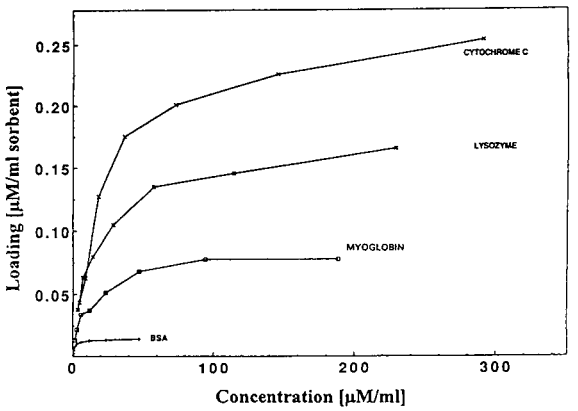

Fig. 3. Selected adsorption isotherms of basic proteins on HA.

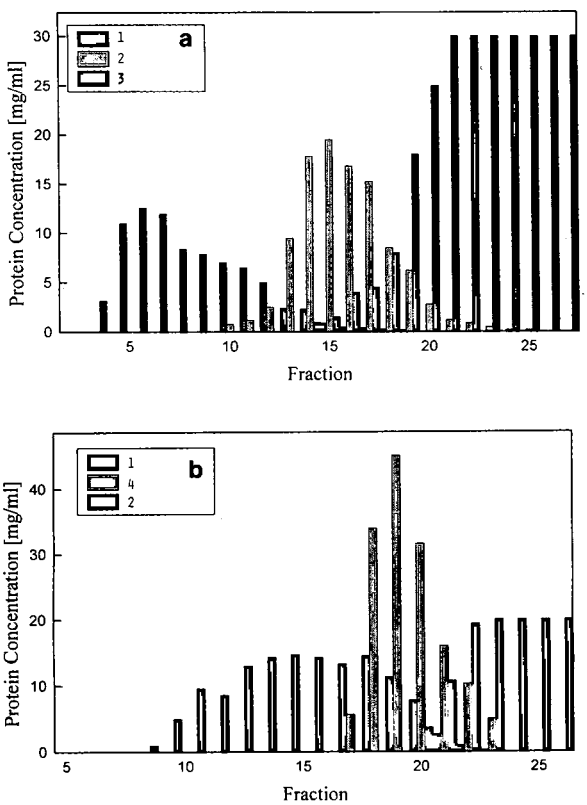

Fig. 4. (a) Displacement of lysozyme and cytochrome *c* (both 10 mg/ml) by PEI (30 mg/ml, M_r 60 000). (b) Displacement of myoglobin and lysozyme (both 10 mg/ml) by cytochrome *c* (30 mg/ml). 1 = Lysozyme; 2 = cytochrome *c*; 3 = PEI; 4 = myoglobin.

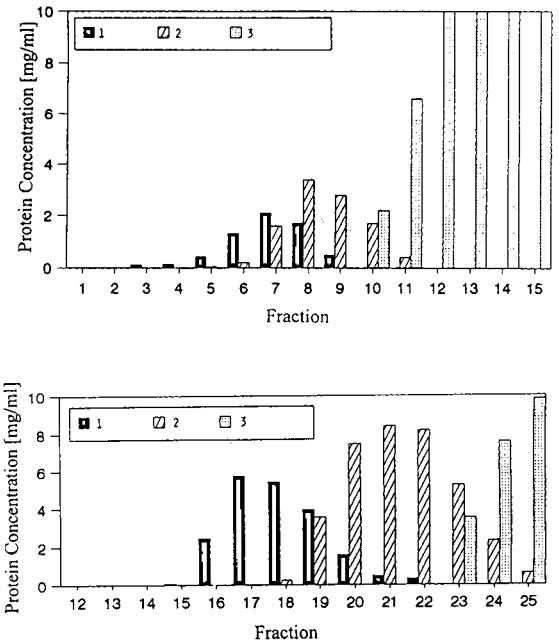

Fig. 5. Influence of the column length on a displacement of myoglobin (1.1 mg/ml) and lysozyme (1.7 mg/ml) by cytochrome *c* (10 mg/ml). Column dimensions: (top) 50 mm × 4 mm I.D.; (bottom) 100 mm × 4.6 mm I.D. 1 = Myoglobin; 2 = lysozyme; 3 = cytochrome *c*.

improve the separation any further, however, while necessarily increasing the time required for the experiment. Thus, when 10 m*M* phosphate buffer (pH 6.8) is used, myoglobin and lysozyme can be well separated when displaced by cytochrome *c*. Presumably, however, the conditioning of the HA surface by the phosphate ions of the buffer is necessary, as a displacement carried out in Tris buffer of similar pH and concentration (10 m*M*, pH 7.0) yielded less satisfactory results (Fig. 6). When 1 m*M* $CaCl_2$ were added to the Tris buffer (Fig. 6), lysozyme, but not myoglobin, was hardly retained, even though this protein showed a higher affinity to HA than myoglobin in most other instances.

3.3. Displacement of acidic proteins

To improve protein retention and capacity by decreasing the repelling effect of the surface and increasing the number of adsorptive sites, HA

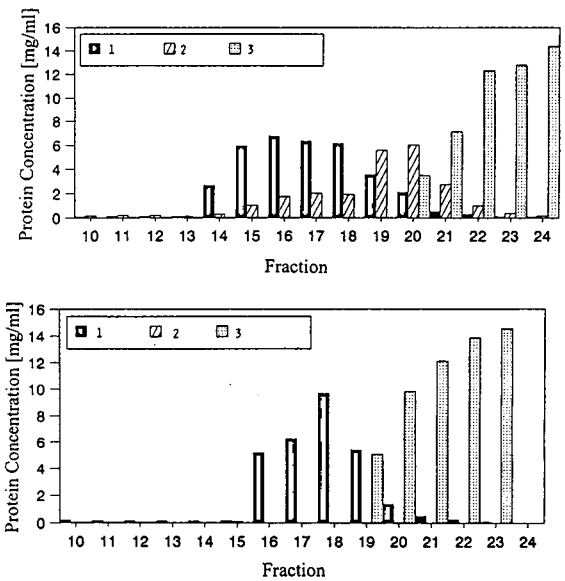

Fig. 6. Displacement of myglobin (1.1 mg/ml) and lysozyme (1.7 mg/ml) by cytochrome *c* (10 mg/ml) using as mobile phase (top) 10 m*M* Tris buffer (pH 7.0) and (bottom) 10 m*M* Tris buffer (pH 7.0) with 1 m*M* $CaCl_2$. 1 = Myoglobin; 2 = lysozyme; 3 = cytochrome *c*.

columns were conditioned by a wash with 2 ml of 200 m*M* $CaCl_2$ solution (in Tris buffer) prior to any displacement of acidic proteins. In addition, Tris rather than phosphate buffers were used as mobile phases in the displacement experiments. In Fig. 7, the adsorption isotherms of acidic proteins are shown. For comparison, the adsorption isotherm of the basic lysozyme as obtained under these conditions is also included. Even under conditions favourable to the adsorption of acidic proteins, the HA material shows a higher capacity for the basic protein than for any of the acidic proteins. Whereas with basic proteins the elution order usually corresponds to the saturation capacities, this is not necessarily so for the acidic proteins.

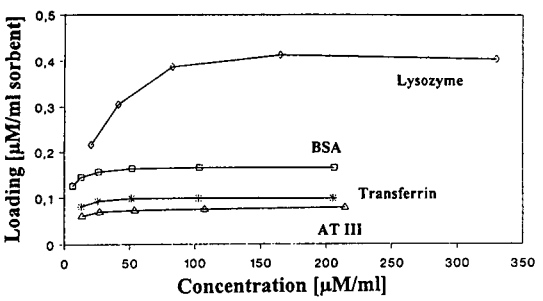

Fig. 7. Selected adsorption isotherms of basic proteins on HA. The isotherm of lysozyme is included for comparison.

Acidic proteins are assumed to interact with the Ca^{2+} sites of HA via their deprotonated carboxylate groups. Therefore, the displacement of acidic proteins such as BSA (p*I* 4.9), AT III (p*I* 4.6–5.1) and b-transferrin (p*I* 5.5) was initially attempted with certain polyacids such as polyacrylic acid (PAA, M_r 6000) and polyglutaminic acid (PGA, M_r 12 000) (Fig. 8a–8c). Neither displacer substance gave satisfactory results. Hardly any protein separation took place, regardless of column length, mobile phase composition or type and average molecular mass of the displacer. Significant amounts of polymeric displacer were found in the protein zones.

Carboxylate cluster-carrying proteins are known for their exceptional HA affinity. In some instances basic carboxylate cluster-carrying proteins have been observed to behave similarly to acidic proteins in their adsorption and elution behaviour, e.g., in their resistance to elution by Ca^{2+}. Here one of these proteins, namely β-casein, was investigated as a protein displacer (Fig. 9). Even though neither the column length nor the buffer composition was ideal for the displacement of acidic proteins, the results achieved with the β-casein displacer are distinctly superior to those obtained with the polyacids. Apparently, not only the number but also the arrangement of the carboxylate groups is of consequence.

As the arrangement of the carboxylate groups appears to be of importance, it is not surprising that the best results were found when a Ca^{2+}-chelating agent was used to displace acidic proteins. Here EGTA [ethyleneglycol bis(β-aminoethyl ether)-N,N,N′,N′-tetraacetic acid, M_r 380.4], a high-molecular-mass analogue of EDTA, was used (Fig. 10). However, when EGTA was used to purify AT III in the presence of both BSA and b-transferrin, hardly any separation between AT III and BSA took place. This is a general problem in the isolation of AT III

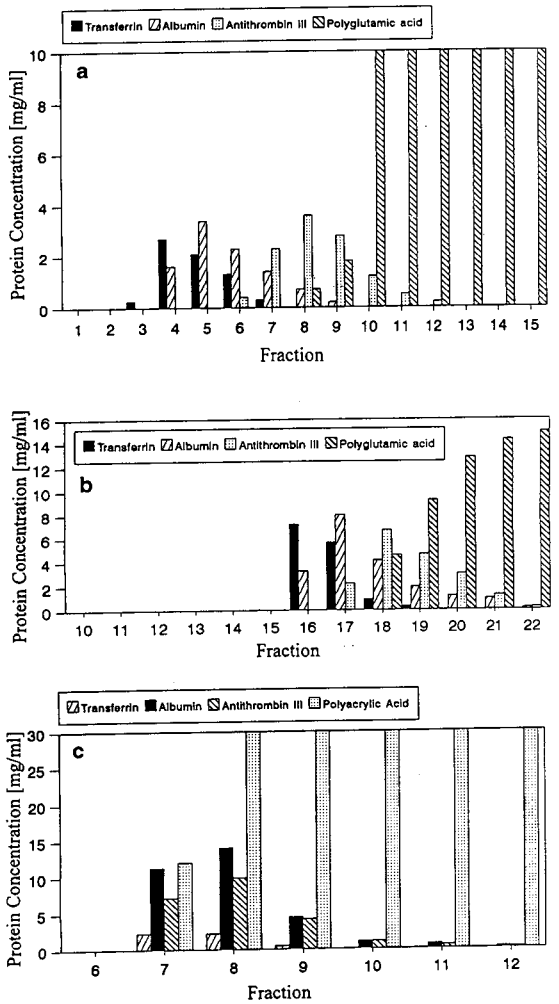

Fig. 8. (a) Displacement of transferrin (0.7 mg/ml), BSA (0.8 mg/ml) and AT III (0.9 mg/ml) by PGA (15 mg/ml, M_r 12 000). Mobile phase, 5 mM phosphate (pH 6.8) with 0.3 mM $CaCl_2$; column, 50 mm × 4 mm I.D. (b) Displacement of transferrin (0.8 mg/ml), BSA (1.8 mg/ml) and AT III (1.2 mg/ml) by PGA (15 mg/ml, M_r 12 000). Mobile phase, 2 mM phosphate (pH 6.8) with 1 mM $CaCl_2$; column, 100 mm × 46 mm I.D. (c) Displacement of transferrin (0.8 mg/ml), BSA (01.4 mg/ml) and AT III (1.0 mg/ml) by PAA (30 mg/ml, M_r 6000). Mobile phase, 10 mM Tris (pH 7.5) with 0.3 mM $CaCl_2$; column, 100 mm × 4.6 mm I.D.

from cell culture supernatants [33], since BSA is part of almost any cell culture medium recipe. The physiological function of BSA as a transport protein requires close adherence to the various blood factors, including, unfortunately, AT III.

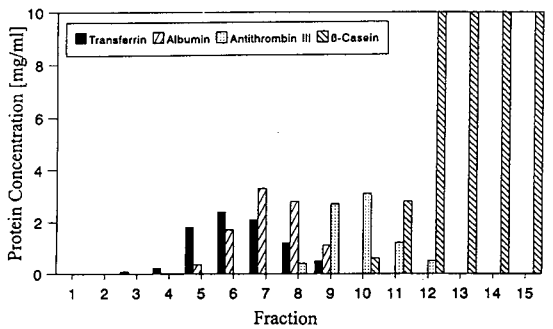

Fig. 9. Displacement of transferrin (0.8 mg/ml), BSA (0.8 mg/ml) and AT III (0.6 mg/ml) by β-casein (15 mg/ml). Mobile phase, 5 mM phosphate (pH 6.8) with 0.3 mM $CaCl_2$; column, 50 mm × 4 mm I.D.

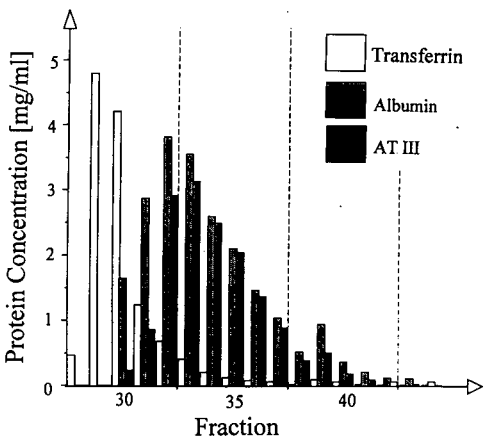

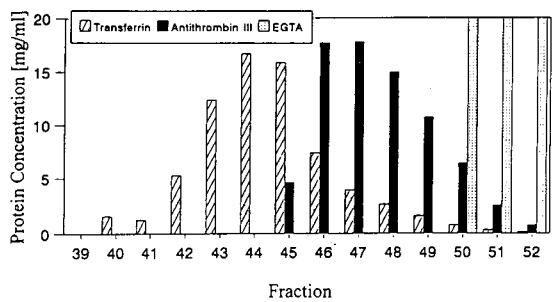

Fig. 10. Top: displacement of transferrin (4.2 mg/ml), BSA (2.8 mg/ml) and AT III (3.1 mg/ml) by EGTA (20 mg/ml, M_r 380.4. Mobile phase, 20 mM Tris (pH 9.0). Bottom: displacement of transferrin (4.2 mg/ml) and AT III (3.1 mg/ml) by EGTA (20 mg/ml, M_r 380.4). Mobile phase, 20 mM Tris (pH 9.0).

If the BSA is removed at the earliest possible moment, e.g., by Cibacron Blue affinity chromatography [33], a much improved separation is found (Fig. 10, bottom).

Polymeric displacers usually show a broad molecular mass distribution and also tend to vary in structure. As a consequence, the affinity for the stationary phase tends to be inhomogeneous and often less well retained displacer molecules contaminate the preceding protein zones. With EGTA, on the other hand, a sharp displacer front is observed, as all displacer molecules are alike in mass and structure. The final AT III concentration in the displacement fractions is several times higher than that in the original feed. The yields were generally better than 98%. With a time requirement of 30 min, displacement chromatography is fast compared with the multistage chromatographic systems used before [33]. When the biological activity of the recovered AT III was tested using a heparin co-factor activity assay (Boehringer, Mannheim, Germany) [36], displacement chromatography was found to be not only a fast but also a mild means for protein purification.

3.4. Synthesis and application of a polymeric displacer of acidic proteins

Starting from a highly homogeneous (molecular mass standard) PEG (polyethylene glycol, M_r 1000), a novel protein displacer was synthesized (Fig. 11), by adapting procedures given in Refs. [37] and [38]. The displacer carries IDA (iminodiacetic acid) groups at both ends, which are assumed to form strong chelates with the calcium sites of the HA. When the PEG educt and the final displacer were investigated by MALDI-MS, the expected shift in molecular mass was clearly seen (Fig. 12). The resulting polymer was used in a displacement experiment (Fig. 13) and appeared to be an excellent displacer of acidic proteins from HA. High protein concentrations are found. A sharp displacer front is again observed. Moreover, other than in the case of the PEI used for the displacement of basic

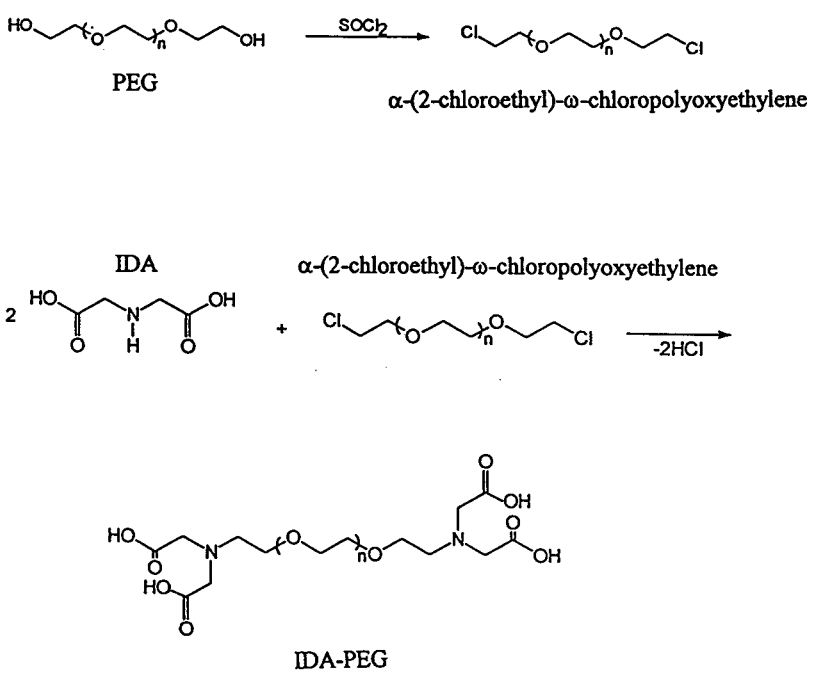

Fig. 11. Synthesis of a polymeric protein displacer according to Refs. [37] and [38].

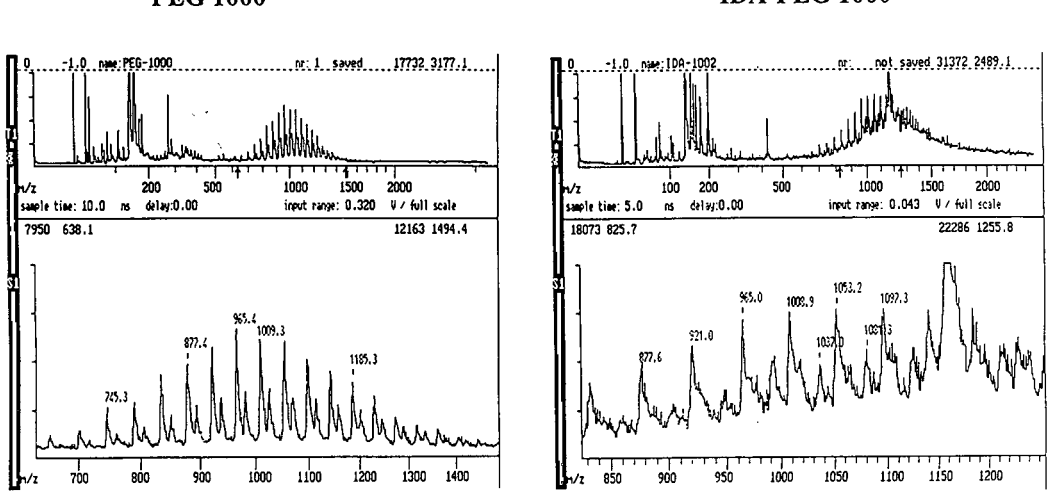

Fig. 12. MALDI-MS measurements of the PEG 1000 molecular mass marker and the synthesized IDA–PEG.

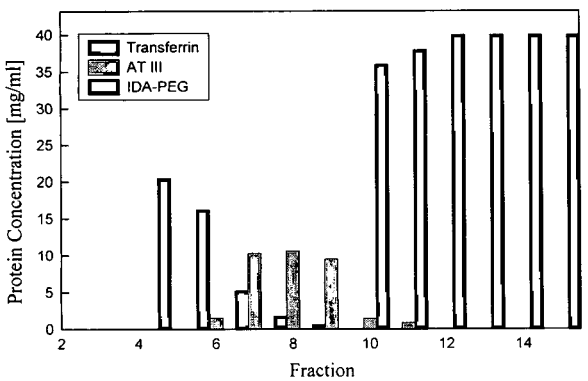

Fig. 13. Displacement of transferrin (2.4 mg/ml) and AT III (2.1 mg/ml) by IDA–PEG (40 mg/ml). Mobile phase, 20 m*M* Tris (pH 9.0).

proteins, the IDA–PEG displacer could easily be removed from the HA column, e.g., by washing with 100 m*M* $CaCl_2$ solution in Tris buffer.

Acknowledgement

Dr. Ute Bahr is thanked for the MALDI-MS measurements.

References

[1] J. Bonnerjea, S. Oh, M. Hoare and P. Dunnill, *Bio/Technology*, 4 (1986) 954.
[2] M.A. Taipa, M.R. Aires-Barros and J.M.S. Cabral, *J. Biotechnol.*, 26 (1992) 111.
[3] T. Burnoff, *Bioseparation*, 1 (1991) 383.
[4] S.M. Cramer and G. Subramanian, *Sep. Purif. Methods*, 19 (1990) 31.
[5] J.L. Dwyer, *AIChE Symp. Ser.*, 80 (1984) 120.
[6] J. Frenz and C. Horváth, in C. Horváth (Editor), *High-Performance Liquid Chromatography–Advances and Perspectives*, Vol. 8. Academic Press, New York, 1988.
[7] A.R. Torres and E.A. Peterson, *J. Chromatogr.*, 499 (1990) 47.
[8] G. Subramanian, M.W. Phillips and S.M. Cramer, *J. Chromatogr.*, 439 (1988) 341.
[9] F. Antia and Cs. Horváth, *Ber. Bunsenges. Phys. Chem.*, 93 (1989) 962.
[10] A.M. Katti, E.V. Dose and G. Guiochon, *J. Chromatogr.*, 540 (1991) 1.
[11] A.W. Liao, Z. El Rassi, D. LeMaster and Cs. Horváth, *Chromatographia*, 24 (1987) 881.
[12] G. Guichon and S. Ghodbane, *J. Phys. Chem.*, 92 (1988) 3682.
[13] A.M. Katti and G. Guichon, *J. Chromatogr.*, 449 (1988) 25.
[14] A. Felinger and G. Guichon, *J. Chromatogr.*, 609 (1992) 35.
[15] S. Ghose and B. Mattiasson, *J. Chromatogr.*, 547 (1991) 145.
[16] A.R. Torres and E.A. Peterson, *J. Biochem. Biophys. Methods*, 1 (1979) 349.

[17] A.L. Lee, A.W. Liao and Cs. Horváth, *J. Chromatogr.*, 443 (1988) 31.
[18] G. Subramanian, M.W. Phillips, G. Jayaraman and S.M. Cramer, *J. Chromatogr.*, 484 (1989) 225.
[19] J.A. Gerstner and S.M. Cramer, *BioPharm*, 5 (1992) 42.
[20] S.C.D. Jen and N.G. Pinto, *J. Chromatogr.*, 519 (1990) 87.
[21] B.E. Dunn, S.E. Edberg and A.R. Torres, *Anal. Biochem.* 168 (1988) 25.
[22] A.R. Torres, G.G. Krnger and E.A. Peterson, *Anal. Biochem.*, 144 (1985) 469.
[23] S. Ghose and B. Mattiasson, *J. Chromatogr.*, 547 (1991) 145.
[24] E.A. Peterson, *Anal. Biochem.*, 90 (1987) 767.
[25] A.R. Torres and E.A. Peterson, *J. Biochem. Biophys. Methods*, 1 (1979) 349.
[26] G. Jayaraman, S.D. Gadam and S.M. Cramer, *J. Chromatogr.*, 630 (1993) 53.
[27] G. Bernadi, M.G. Giro and C. Gaillard, *Biochim. Biophys. Acta*, 278 (1972) 409.
[28] M.J. Gorbunoff, *Anal. Biochem.*, 136 (1984) 425.
[29] M.J. Gorbunoff, *Anal. Biochem.*, 136 (1984) 433.
[30] M.J. Gorbunoff and S.N. Timasheff, *Anal. Biochem.*, 136 (1984) 440.
[31] T. Sato, T. Okuyama and M. Ebihara, *Bunseki Kagaku*, 38 (1989) 34.
[32] J. Jacobson, J. Frenz and Cs. Horváth, *J. Chromatogr.*, 316 (1984) 53.
[33] O.-W. Reif and R. Freitag, *Bioseparation*, submitted for publication.
[34] E. Gianazza and P.G. Righetti, *J. Chromatogr.*, 193 (1980) 1.
[35] K. Kalghati and Cs. Horváth, *J. Chromatogr.*, 398 (1987) 335.
[36] U. Abildgard, M. Lie and O.R. Odegard, *Thromb. Res.*, 11 (1977) 549.
[37] G. Birkenmeier, M.A. Vijayalakshmi, T. Stigbrand and G. Kopperschläger, *J. Chromatogr.*, 539 (1991) 267.
[38] A.F. Bückmann, M. Morr and M.R. Kula, *Biotechnol. Appl. Biochem.*, 9 (1987) 258.

ELSEVIER

Journal of Chromatography A, 691 (1995) 113–122

JOURNAL OF CHROMATOGRAPHY A

Preparation and use of immunoglobulin-binding affinity supports on Emphaze beads

Greg T. Hermanson*, Gloria R. Mattson, Randall I. Krohn

Pierce Chemical Co., P.O. Box 117, Rockford, IL 61105, USA

Abstract

The Emphaze support couples to nucleophiles with a leak-resistant linkage resulting from the reaction with intrinsic azlactone functionalities. Protein A, protein G, and protein A/G were coupled to the Emphaze support and to an agarose matrix at various concentrations of ligand. Mannan Binding Protein was similarly coupled to the Emphaze matrix and agarose. These supports were investigated as to their binding characteristics toward immunoglobulins, both in a gravity separation format and using a medium pressure chromatography system under high linear flow. In addition, the lectin jacalin was coupled both to Emphaze and agarose and compared for total binding capacity toward human IgA. There were significant differences in the binding characteristics of human IgG for the Emphaze and agarose supports. Mouse monoclonal IgG1 showed a binding optimum at pH 5 on Emphaze protein A, A/G and G as compared to an optimum of pH 8 for the agarose supports. Similar binding pH optimums were observed for human IgG. Slightly higher capacities were observed for the Emphaze IgG binding than for the corresponding agarose supports. Emphaze Mannan Binding Protein had an almost identical binding capacity for mouse IgM as did a similarly loaded agarose support.

1. Introduction

Affinity chromatography is a powerful technique based on the specific attraction of a ligand for its target molecule(s). The ligand typically is covalently attached to an insoluble matrix and is subsequently used to purify its target from a complex mixture. The matrix composition and the ligand coupling chemistry are very important parameters for the specific binding of target molecules. The ideal chromatography support has several characteristics critical to its performance. The matrix should be a beaded, spherical, porous support with narrow particle size distribution and good chromatographic qualities. The non-specific binding character of the matrix should be low. In addition, the potential for using high linear flow rates with the support is advantageous, because it allows the chromatographic operation to be done in shorter periods. Finally, the support must be easily derivatized with the affinity ligand, resulting in a stable linkage.

Activated agarose is often used for the immobilization of ligands for affinity purification. There are several activation schemes commonly used: CNBr, reductive amination, N,N′-carbonyldiimidazole (CDI) coupling and NHS-ester coupling (for review, see Hermanson et al. [1]). A new support material, the 3M Emphaze Biosupport Medium AB 1, has recently been used in the preparation of a number of immobil-

* Corresponding author.

0021-9673/95/$09.50
SSDI 0021-9673(94)01029-3

ized proteins useful for the purification of immunoglobulins. The polymeric Emphaze matrix is well suited for affinity chromatography operations, having large pores (1000 Å) and an exclusion limit in excess of 2 000 000 relative molecular mass. The rigid nature of the beads (average particle size 50–80 μm) allows linear flow-rates up to 3000 cm/h, permitting use of the support in automated chromatography systems.

The Emphaze support is prepared by the copolymerization of vinyldimethylazlactone and the cross-linking monomer, methylenebisacrylamide [2]. Due to the presence of the azlactone monomer incorporated during the manufacturing process, the support contains amine-reactive groups. The Emphaze matrix is supplied dry to prevent hydrolysis of the azlactone groups during storage. The hydrated volume of the support is approximately 8–10 ml/g of dried beads.

An azlactone can react with an amine-containing ligand in a ring-opening reaction to form a leak-resistant amide-bond linkage (Fig. 1). This process creates an indigenous 5-atom spacer arm terminating in an amide bond with the ligand. After coupling, the resulting gel surface environment is completely hydrophilic, displaying very low non-specific binding character.

Amine-containing molecules can be immobilized onto the beads simply by dissolving the ligand in a suitable coupling buffer and adding the dry support to the solution with mixing. Coupling is usually complete in 1 h. The remaining active sites are quenched with ethanolamine.

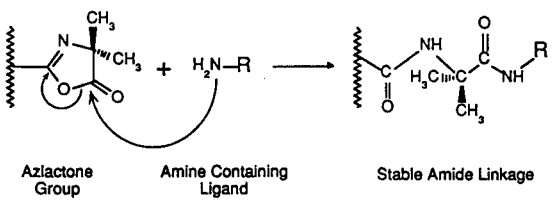

Fig. 1. The reaction of an amine-containing ligand with the azlactone groups on the surface of the Emphaze beads proceeds by nucleophilic attack on the electron-deficient carbonyl. The ring-opening process results in the creation of a stable amide-bond linkage with the ligand and the formation of an indigenous 5-atom spacer arm.

One idiosyncrasy of the coupling of proteins to the Emphaze support is the necessity for the presence of a high molar concentration of a lyotropic salt in the coupling buffer [3]. A protein with its charged outer surface has difficulty getting near enough to the azlactone polymer to react. The lyotropic salt drives the protein close enough to the bead to couple efficiently.

Previous studies investigated the immobilization of protein A or antibodies on the Emphaze support with special emphasis on obtaining high binding capacity or activity [4,5]. In this study, the immobilization and performance of five different immunoglobulin-binding proteins is investigated: native protein A, recombinant protein G, recombinant protein A/G, jacalin and rabbit-serum mannan binding protein (MBP). The use of protein A and protein G immobilized on agarose and other support materials for immunoglobulin purification is well documented in the literature [6–13]. Protein A/G is a recombinant fusion protein which combines the binding characteristics of protein A with the binding properties of protein G [14,15]. Jacalin is a lectin that can be used to purify human IgA1 from human serum [16]. MBP has binding specificity for mouse IgM and can be used to purify monoclonal IgM antibodies from ascites [17]. A comparison of the coupling yields for immobilizing these proteins on Emphaze is investigated versus a typical reductive amination coupling procedure using periodate-oxidized agarose (CNBr coupling for MBP). In addition, the use of some of these affinity supports for subsequent purification of immunoglobulins from various sources is discussed and compared to their agarose counterparts.

2. Experimental

2.1. Reagents

3M Emphaze Biosupport Medium AB 1, buffer salts, BCA protein assay reagent, native protein A, recombinant protein A/G, recombi-

nant protein G, jacalin and AminoLink coupling gel were obtained from Pierce (Rockford, IL, USA). Rabbit serum was obtained from Pel-Freeze (Rogers, AK, USA). Mouse IgG1 (clone MOPC-21) and human IgA were obtained from Sigma (St. Louis, MO, USA).

The supports that were prepared on Emphaze beads and the prepacked columns that were used can be obtained from Pierce.

2.2. Chromatographic equipment

Waters 650E protein purification system with Waters 996 PDA detector was used for all automated chromatography separations. The fraction collector was a Retriever II from ISCO. The spectrophotometer used was a Hitachi U-2000.

2.3. Preparation and analysis of immobilized protein A, protein A/G and protein G

Native protein A, recombinant protein A/G and recombinant protein G were coupled to 3M Emphaze Biosupport Medium AB 1. Two coupling buffers were compared for coupling efficiency: 0.1 *M* sodium phosphate, 0.6 *M* sodium citrate, pH 7.5 and 0.1 *M* sodium carbonate, 0.6 *M* sodium citrate, pH 9. For the preparation of each ml of Emphaze affinity support, either 3, 6 or 9 mg of protein A, protein A/G, or protein G were dissolved in 2 ml of the appropriate coupling buffer and added to 0.125 g of dry Emphaze beads. The solution was fully mixed and reacted for 1 h at room temperature. Excess protein solution was drained, and the gel was washed with water and 1 *M* NaCl to completely remove uncoupled protein. Next, 2 ml of 3 *M* ethanolamine, pH 9 were added to quench unreacted azlactone sites. The reaction was continued for 2 h at room temperature. The resulting affinity support was washed thoroughly with water, 1 *M* sodium chloride and another water wash. The gel was stored in 0.02% sodium azide at 4°C until used.

Coupling efficiency was determined by comparing the amount of protein in the reaction prior to coupling with the amount of protein left in the solution after coupling. It is necessary to use a protein assay system such as BCA instead of absorbance at 280 nm because of the interference of a small amount of Triton X-100 remaining from the manufacture of the beads. The detergent is added to allow sufficient hydration of the support without introducing bubbles.

Native protein A, recombinant protein A/G and recombinant protein G were coupled using AminoLink coupling gel according to the manufacturer's protocol. AminoLink is periodate oxidized agarose which couples amines using reductive amination. The support was charged with both 3 and 6 mg of the appropriate immunoglobulin binding protein.

2.4. Capacity of human IgG under gravity flow conditions

To determine human IgG binding capacities for each of the prepared supports, 2 ml columns of Emphaze immobilized protein A, protein A/G and protein G and the corresponding agarose supports were prepared. Emphaze and agarose immobilized protein A and protein A/G were equilibrated in binding buffer 1 (0.1 *M* potassium phosphate, 0.15 *M* NaCl, pH 8.0). An overload binding capacity analysis was performed on each support by applying 100 mg of human IgG in binding buffer 1 to each column and washing with binding buffer 1 until the absorbance at 280 nm reached baseline. Elution was performed by applying 2-ml aliquots of 0.1 *M* glycine, pH 2.8, collecting fractions and monitoring absorbance at 280 nm.

Columns (2 ml) of Emphaze and agarose immobilized protein G were equilibrated in binding buffer 2 (100 m*M* sodium acetate, pH 5.0). Overload total binding capacity analysis was performed for each column by applying 100 mg of human IgG in binding buffer 2 to each 2-ml column. The columns were washed with binding buffer 2 until the absorbance at 280 nm reached baseline. Elution was performed by applying 2-ml aliquots of 0.1 *M* glycine, pH 2.8,

collecting fractions and monitoring the absorbance at 280 nm.

2.5. Investigation of binding conditions for IgG binding supports

Studies were performed to determine the effect of varying buffer pH conditions on the binding of human IgG to the Emphaze and agarose protein A, A/G and G columns. The binding buffers used were: 0.1 *M* acetic acid, pH 4.0; 0.1 *M* citric acid, pH 4.5; 0.1 *M* sodium acetate, 0.15 *M* sodium chloride, 0.05% sodium azide, pH 5.0; 0.1 *M* 2-(N-morpholino)-ethanesulfonic acid (MES), 0.15 *M* sodium chloride, 0.05% sodium azide, pH 6.0; 0.1 *M* sodium phosphate, 0.15 *M* sodium chloride, 0.05% sodium azide, pH 7.2; 0.1 *M* 4-(2-hydroxyethyl)-1-piperazineethanesulfonic acid (HEPES), 0.15 *M* sodium chloride, 0.05% sodium azide, pH 8.0; 0.1 *M* sodium carbonate, 0.15 *M* sodium chloride, 0.05% sodium azide, pH 9.0; 0.1 *M* 3-cyclohexylamino-1-propanesulfonic acid (CAPS), 0.15 *M* sodium chloride, 0.05% sodium azide, pH 10.0. The elution buffer used was 0.1 *M* glycine, pH 2.8.

The supports were packed into 50 mm × 3.0 mm columns (0.353 ml R-PAC (rapid protein affinity chromatography) columns (Pierce) for automated chromatography. The columns were equilibrated in the appropriate binding buffer for 10 min at a flow-rate of 1 ml/min. Human IgG was dissolved at a concentration of 20 mg/ml in deionized water. The human IgG solution was diluted 1:1 in the corresponding binding buffer. At time = 0 min, 2.0 ml of the diluted human IgG sample were injected onto the column using a flow-rate of 1 ml/min of binding buffer. At time = 6 min, 100% elution buffer was introduced and at time = 14 min, the buffer was changed to 0.02% sodium azide in water. The absorbance was monitored at 280 nm.

The binding of mouse IgG1 (clone MOPC-21) to Emphaze immunoglobulin binding supports was also investigated using the same protocol above, except that an injection of 0.2 ml of 20 mg mouse IgG1/ml of gel was used.

2.6. Preparation and analysis of immobilized jacalin

Emphaze immobilized jacalin was prepared by coupling 3 mg of purified jacalin per ml of gel in carbonate/citrate buffer, pH 9.0 as described above. Agarose-jacalin was prepared using AminoLink coupling gel according to manufacturer's instructions and charged with 4.5 mg of jacalin per ml of gel. The prepared supports were tested for binding capacity of human IgA. A 1-ml column of each support was equilibrated in 0.1 *M* sodium phosphate, 0.15 *M* sodium chloride, pH 7.2 (PBS) under gravity flow. Human IgA (1 mg/ml) was prepared in PBS. Approximately 6 ml of sample were applied to a 1-ml column of both Emphaze immobilized jacalin and agarose jacalin. The columns were washed until the absorbance at 280 nm reached baseline. Elution was performed by adding 0.1 *M* melibiose in PBS to each column. Fractions (1 ml) were collected and monitored by absorbance at 280 nm.

2.7. Preparation and analysis of immobilized mannan binding protein

The preparation of immobilized mannan and its subsequent use for the isolation of MBP from rabbit serum is based on a method described by Kozutsumi et al. [18] and modified as by Nevens et al. [17]. The immobilization of MBP on agarose is as described by Nevens et al. [17].

Coupling of mannan binding protein to Emphaze was performed according to the immunoglobulin binding protocol described above except a carbonate–citrate buffer of pH 8.5 instead of 9.0 was used. The coupling reaction was carried out overnight for convenience.

2.8. Purification of IgM on immobilized MBP

A 1-ml column of the Emphaze MBP was packed and equilibrated with 10 m*M* Tris, 1.25 *M* sodium chloride, 20 m*M* calcium chloride, pH 7.4 (binding buffer). The equilibration and binding steps were performed at 4°C. Purified mouse IgM solution (4 ml) was applied to the column

and 2 ml fractions were collected. The columns were washed with binding buffer until baseline was reached. After warming the columns to room temperature, bound IgM was eluted with 10 m*M* Tris, 1.25 *M* sodium chloride, 2 m*M* EDTA, pH 7.4 (elution buffer). Fractions were collected and A_{280} was measured.

3. Results and discussion

3.1. Coupling efficiencies of Emphaze protein A, protein A/G and protein G

The coupling efficiency of amine-containing ligands to the Emphaze support is affected by the pH of the reaction buffer. As in many nucleophilic coupling mechanisms, increasing the pH from physiological to more alkaline values results in higher reaction rates. Since potential increases in the hydrolysis rate at elevated pH may overshadow any reaction rate enhancements, it is instructive to determine the coupling characteristics of the azlactone functionality as the pH is increased. Table 1 shows the results of coupling the immunoglobulin-binding proteins, protein A, protein G and protein A/G, at two different pH conditions. Both buffer compositions contained the same amount of lyotropic salt (0.6 *M* sodium citrate) to eliminate any potential variation in coupling yield due to that component. The results indicate that coupling of protein A to the Emphaze support was the only one not dramatically influenced by pH. The immobilization of protein A/G and protein G was more efficient at pH 9 than pH 7. This finding correlates to the results obtained coupling other proteins (such as avidin and streptavidin) to the Emphaze support. In general, to obtain the maximum degree of coupling with proteins that are stable under such conditions, performing the Emphaze immobilization reaction in an elevated pH environment will result in better yields than coupling at physiological pH.

3.2. Binding capacities of immobilized protein A, protein A/G, and protein G

The capacities of the three IgG-binding supports were determined for purifying human IgG under gravity conditions. The results of this study are found in Table 2. All capacities are expressed as mg human IgG bound per ml of gel.

Using overload analysis, the capacities of the IgG binding supports for human IgG prepared on the 3M Emphaze Biosupport Medium were equal to or greater than those prepared under similar conditions on an agarose support. Since the same amount of each protein was charged to the immobilization reactions in both the Emphaze and agarose preparations, the increases in capacity for the Emphaze supports may be due to better coupling yields in the azlactone reaction. Possibly the immobilized protein remains in a more active state on Emphaze than when

Table 1
Coupling efficiency of various proteins to the Emphaze matrix at two different pH values

Ligand	Coupling efficiency (%)					
	Phosphate, pH 7.5			Carbonate, pH 9.0		
	Loading 3 mg/ml	Loading 6 mg/ml	Loading 9 mg/ml	Loading 3 mg/ml	Loading 6 mg/ml	Loading 9 mg/ml
Protein A	88	89.6	94	88	89	96
Protein G	58.8	76	74.7	93	95	92.6
Protein A/G	86	90.8	87.4	94.6	96.6	97.3
Avidin	81.3	81	80	90	89	92
Streptavidin	43	70.4	97.8	91	97.8	98

Table 2
IgG binding capacities for protein A, protein G, and protein A/G immobilized on Emphaze Biosupport Medium or an agarose matrix

	IgG Binding capacity (mg IgG bound per ml gel)					
	Protein A		Protein G		Protein A/G	
	Ligand loading 3 mg/ml	Ligand loading 6 mg/ml	Ligand loading 3 mg/ml	Ligand loading 6 mg/ml	Ligand loading 3 mg/ml	Ligand loading 6 mg/ml
Capacity on Emphaze	24	37	22	31	20	35
Capacity on agarose	17	35	10	18	14	26

coupled to agarose under reductive amination conditions. In addition, since the binding studies for protein A and protein A/G were done at the pH optimum determined for the two proteins when coupled to agarose supports (pH 8.0), the Emphaze matrices would show an even greater differential of binding capacity if the separations were done at pH 5.0 (see the results of the pH study, below).

3.3. Binding of human IgG on prepacked columns of Emphaze and agarose protein A, A/G and G using various binding buffer pH values

Note: In this study, the prepacked columns of agarose required that considerable caution be used to prevent collapse of the support when used on automated chromatography systems. To condition the columns, the flow-rate was brought up very slowly to 1 ml/min. The agarose could not withstand the high flow-rates achievable with the Emphaze support, therefore all comparative studies were done at a flow-rate compatible with the agarose matrix.

Purification of human IgG using various pH binding buffers under medium pressure conditions yielded some surprising results. Optimal binding for protein A is typically observed at approximately pH 8 [8]. By contrast, Emphaze protein A displayed a maximum binding point at pH 5. Even the binding at pH 4 and 4.5 for the Emphaze protein A was higher than that observed at pH 8. Agarose protein A displays minimal binding at pH 4.5; significant binding at pH 5, 6 and 7.2, and a maximum binding point at pH 8. The human IgG applied to the columns was a purified, lyophilized preparation of IgG and was highly soluble in all binding buffer conditions. To determine if the support was merely non-specifically binding protein at the lower pH values, bovine serum albumin was applied to the column. There was no detectable binding of the albumin to the column under the conditions described in the Experimental section. Figs. 2 and 3 illustrate the results of this comparison.

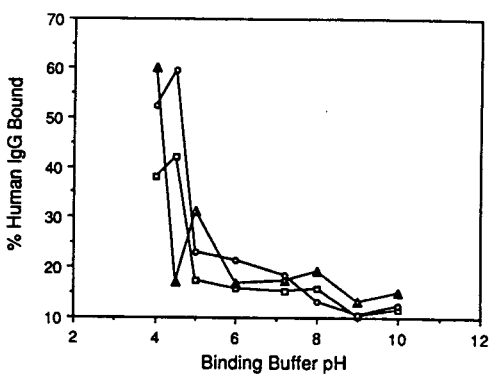

Fig. 2. Binding capacity for human IgG as a function of binding buffer pH using Emphaze protein A (▲), G (○) and A/G (□).

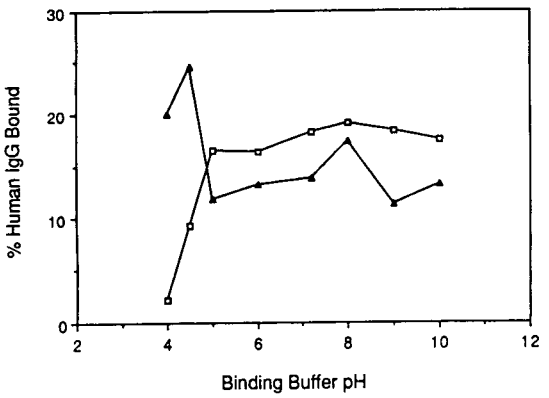

Fig. 3. Binding capacity for human IgG as a function of binding buffer pH using agarose protein A (□) and protein A/G (▲).

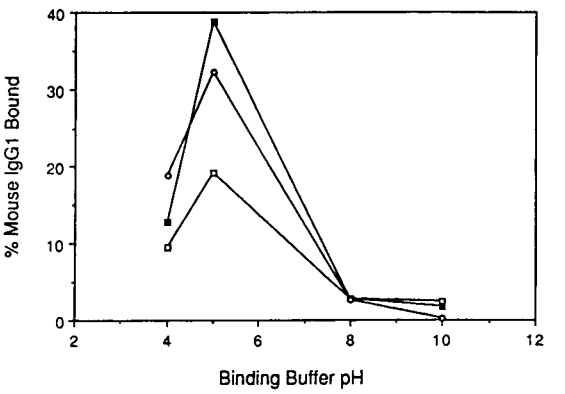

Fig. 4. Binding capacity for mouse monoclonal IgG1 as a function of binding buffer pH using Emphaze protein A (□), G (○) and A/G (■).

Emphaze protein A/G demonstrated a similar binding pattern as Emphaze protein A with an optimal percent human IgG bound at pH 4.5. Binding of human IgG was efficient on protein A/G from pH 4–8. The percent binding of human IgG dropped significantly at pH 9. Protein A/G immobilized on agarose also showed a binding optimum for human IgG at pH 4.5. The binding dropped significantly at pH 5, 6 and 7.2 and showed an increase at pH 8. Albumin was again applied to determine if there was non-specific binding occurring, but no binding was observed.

Protein G displayed significantly higher binding for human IgG at pH 4 and 4.5. Typically, the optimal pH for binding IgGs to protein G is described as pH 5 [11]. A large decrease in the binding of human IgG at pH 5 and another decrease at pH 7.2 was observed.

Prepacked columns of Emphaze protein A showed very surprising pH binding characteristics for the mouse monoclonal tested (IgG1 clone MOPC-21) (Fig. 4). Optimal binding was observed at pH 5. Binding was also enhanced at pH 4. Significantly, binding was very inefficient at pH 8 and 10. Prepacked columns of Emphaze protein A/G and protein G had optimal binding for this monoclonal at pH 5. There was also excellent binding at pH 4 and minimal binding at pH 8 and 10. The monoclonal studies were not duplicated on the agarose prepared supports.

3.4. Binding of human IgA to immobilized jacalin

Emphaze jacalin was charged with 3 mg of jacalin, while agarose jacalin was charged with 4.5 mg of the lectin. Nevertheless, Emphaze jacalin had a binding capacity for human IgA of 2.6 mg/ml gel versus 1.5 mg/ml gel for agarose jacalin.

3.5. Binding of mouse IgM from ascites on MBP immobilized on agarose and emphaze beads

Nevens et al. [17] showed that mouse monoclonal IgM can be purified in a single step using rabbit MBP immobilized on agarose. Although the IgM obtained was greater than 95% pure based on gel filtration analysis, the speed of the gravity separation was limiting. The necessity for equilibration and binding at 4°C, extensive washing steps, and subsequent warming of the column to room temperature for elution of the bound fraction resulted in an 8–10-h chromatography procedure.

Because the Emphaze support can withstand higher linear flow-rates than the agarose matrix, the Emphaze MBP gel was investigated for use in a rapid protein affinity chromatography (R-PAC) format to decrease the time of IgM purification. Instead of doing the separation in a cold

room for the binding step, the binding buffer was merely kept on ice and the sample chilled until needed. The elution buffer was maintained at room temperature to facilitate the rapid elution conditions required under increased linear flow. It was determined that the Emphaze MBP support could separate IgM from mouse ascites in minutes instead of hours. Typical separation times of 2–15 min were obtained, depending on the instrument used and the void volume of buffer in the lines. A representative separation is shown in Fig. 5. Attempts to use the agarose MBP support under similar high-flow conditions failed due to collapse of the matrix and increases in back-pressure that essentially shut down the instrument.

The bound and not-bound peaks from the separation on Emphaze MBP were collected to analyze the composition of the fractions. HPLC gel filtration separations were done using a program that identifies the major components of ascites fluid based upon standards. The results of these separations are shown in Figs. 6 and 7. Analysis of the not-bound fraction indicates that a slight amount of IgM was not completely removed by the Emphaze MBP column under the sample size and flow conditions used. Also present in the not-bound fraction were a minor amount of mouse IgG and albumin. For the bound fraction, the only significant peak present in the gel filtration analysis was IgM. Analysis by area percent indicates a relative IgM purity of about 98% in the Emphaze MBP bound peak.

To investigate whether Emphaze MBP could be used to purify IgM from serum samples, similar affinity separations were done with serum samples from a number of different animals, and the bound and not-bound peaks analyzed by gel filtration. In all the serum samples tested, significant binding of a 150 000 molecular mass component and several low-molecular-mass species completely masked any capacity for binding pentameric IgM (data not shown). While dialysis of the samples effectively eliminated the low-molecular-mass contaminants from binding, the

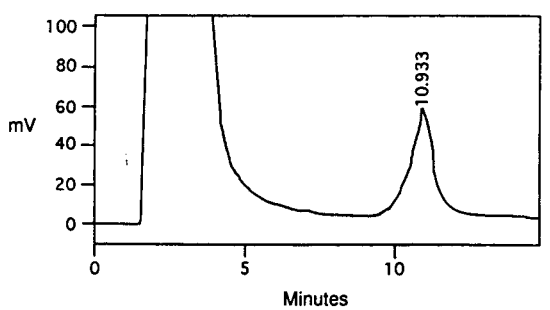

Fig. 5. Purification of mouse monoclonal IgM from ascites fluid using Emphaze MBP according to the Experimental section.

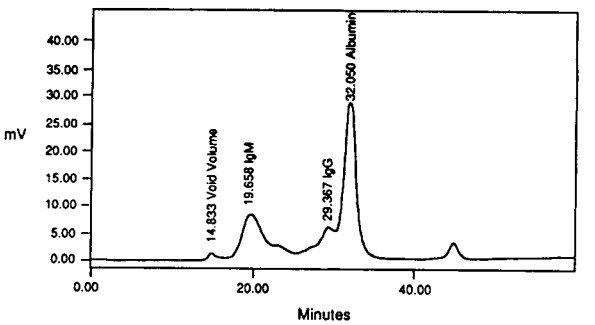

Fig. 6. Gel filtration profile of the not-bound fractions from the purification of mouse monoclonal IgM (from ascites) on Emphaze MBP. The ascites fluid normally contains IgG and albumin components. The peaks were identified by the retention time of standards applied to the column.

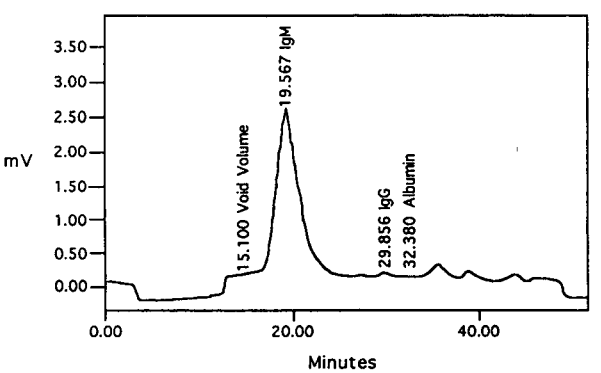

Fig. 7. Gel filtration profile of the bound fractions from the purification of mouse monoclonal IgM (from ascites) on Emphaze MBP. Note the removal of contaminating IgG and albumin normally present in the ascites fluid.

150 000 molecular mass component could not be so easily removed. The 150 000 molecular mass component co-elutes with typical IgG. There are two possible explanations for this. It is possible that the 150 000 molecular mass component is a monomeric form of IgM. However, the most plausible explanation is that in species other than mouse and human, IgG binding occurs. Further studies need to be done to determine the identity of this component. Since MBP is a calcium-dependent lectin, it most probably binds carbohydrate residues on antibody molecules. In ascites fluid containing IgM monoclonals, the predominate contaminating protein is albumin, not IgG. In serum samples, however, many polysaccharide-containing molecules are present in larger quantities than IgM, some of which have sugar residues that may be able to compete for binding sites on the affinity support. For this reason, the utility of MBP affinity supports appears to be limited to IgM purification from ascites and cell culture supernatant.

When purified IgM was applied to the Emphaze MBP column, a 97% recovery of protein was observed. The column had a capacity of 1.03 mg/ml of gel for purified mouse IgM. Agarose MBP had a nearly identical capacity. Emphaze MBP offers significant time savings; minutes vs. 8–10 h. The same prepacked column of Emphaze MBP was used for all purifications. Over 20 purifications were done on the same support material with no loss of binding capabilities.

4. Conclusions

The 3M Emphaze Biosupport Medium is a novel chromatographic material that comes preactivated with azlactone groups, making it suitable for coupling amine-containing ligands. The ease of immobilization and lack of hazardous materials necessary for performing the chemistry make it an attractive alternative to more traditional coupling methods.

The immobilization of immunoglobulin binding proteins to the Emphaze matrix resulted in affinity supports which displayed high binding characteristics. There were, however, discrepancies between binding capacities at various pH values of the Emphaze IgG-binding supports versus the agarose IgG-binding supports. Especially interesting was the binding characteristics of the supports using lower pH binding buffers. Emphaze protein A had maximum binding capacity for human IgG at pH 5 versus a pH optimum of 8 for agarose protein A. Chromatography of mouse IgG1 showed significant binding to Emphaze protein A at pH 5 and 4. Mouse IgG1 does not normally display such strong binding characteristics to protein A supports, especially in the absence of high-salt binding buffers. These data suggest that perhaps a binding optimization for each monoclonal could validate the use of Emphaze protein A for the purification of mouse IgG1 monoclonals with greater efficiency than when using other protein A matrices. Particularly, higher yields of mouse IgG1 may be achieved by using lower pH binding environments. Emphaze protein G and A/G, which also bound this monoclonal optimally at pH 5 could also be considered for purification. The large fluctuation in binding due to binding buffer pH, regardless of the support being employed, should be carefully considered in each purification strategy, especially in large-scale optimizations.

In the case of coupling jacalin to the Emphaze and agarose supports, the polymeric matrix again displayed increased binding capacities. Although less lectin was charged to the Emphaze matrix compared to agarose, the Emphaze support showed higher total binding of human IgA1. Again, it may be that the azlactone coupling chemistry is more efficient than reductive amination or that the immobilization results in a superior binding support.

The time savings that can be realized using the Emphaze support was most dramatically illustrated in the purification of IgM. Agarose MBP separation takes 8–10 h to yield >95% pure IgM. The same purification on Emphaze MBP in an automated medium pressure system was accomplished in 2–15 min with remarkable recovery and purity. The durability of the support was also demonstrated in that there was no loss of binding capability even after 20 uses.

In summary, the 3M Emphaze support shows several distinct advantages over agarose: the Emphaze support can be used in small columns for analytical methods development on an automated medium pressure or HPLC system, allowing rapid optimization of affinity chromatography conditions under high linear flow. Since the support has a particle size of approximately 60 μm, the separation can then be scaled up directly to large process columns utilizing the information developed on the automated system. With regard to antibody purification, the Emphaze support yielded better binding characteristics than an agarose matrix, especially under low pH conditions. The potential for increased yields for the purification of mouse monoclonal IgG1 antibodies makes the support deserving of consideration for process separations.

References

[1] G.T. Hermanson, A.K. Mallia and P.K. Smith, *Immobilized Affinity Ligand Techniques*, Academic Press, San Diego, CA, 1992.
[2] J.K. Rasmussen, J.I. Hembre, N.I. Koski and D.S. Milbrath, *Makromol. Chem., Macromol. Symp.*, 54/55 (1992) 535–550.
[3] P.L. Coleman, M.M. Walker, C.L. Reese and D.S. Milbrath, *FASEB J.*, (1991) A805.
[4] P.L. Coleman, M.M. Walker, D.S. Milbrath and D.S. Stauffer, *J. Chromatogr.*, 512 (1990) 345–363.
[5] M.A.J. Godfrey, P. Kwasowski, R. Clift and V. Marks, *J. Immunol. Methods*, 160 (1993) 97–105.
[6] J.W. Goding, *J. Immunol. Methods*, 20 (1978) 241–253.
[7] R. Lindmark, K. Thoren-Tolling and J. Sjoquist, *J. Immunol. Methods*, 62 (1983) 1–13.
[8] P.L. Ey, S.J. Prowse and C.R. Jenkin, *Immunochemistry*, 15 (1978) 429–436.
[9] J.J. Langone, *Adv. Immunol.*, 32 (1982) 157–252.
[10] A. Forsgren and J. Sjoquist, *J. Immunol.*, 97 (1966) 822–827.
[11] B. Akerstrom and L. Bjorck, *J. Biol. Chem.*, 261 (1986) 10 240–10 247.
[12] B. Akerstrom, T. Brodin, K.J. Reis and L. Bjorck, *J. Immunol.*, 135 (1985) 2589–2592.
[13] L. Bjork and G. Kronvall, *J. Immunol.*, 133 (1984) 969–974.
[14] M. Eliasson, R. Andersson, A. Olsson, H. Wigzell and M. Uhlen, *J. Immunol.*, 142 (1989) 575–581.
[15] M. Eliasson, A. Olsson, E. Palmcrantz, D. Wiberg, M. Inganas, B. Guss, M. Lindberg and M. Uhlen, *J. Biol. Chem.*, 263 (1988) 4323–4327.
[16] H. Kondoh, K. Kobayashi, K. Hagiwara and T. Kajii, *J. Immunol. Methods*, 88 (1986) 171–173.
[17] J.R. Nevens, A.K. Mallia, M.W. Wendt and P.K. Smith, *J. Chromatogr.*, 597 (1992) 247–256.
[18] Y. Kozutsumi, T. Kawasaki and I. Yamashina, *Biochem. Biophys. Res. Commun.*, 95 (1980) 658.

ELSEVIER

Journal of Chromatography A, 691 (1995) 123–131

JOURNAL OF CHROMATOGRAPHY A

Effect of resin sulfonation on the retention of polar organic compounds in solid-phase extraction

Philip J. Dumont*, James S. Fritz

Ames Laboratory, US Department of Energy and Department of Chemistry, Iowa State University, Ames, IA 50011, USA

Abstract

The hydrophobic nature of polymeric resins used in solid-phase extraction (SPE) often limits their efficiency by preventing intimate surface contact with aqueous samples. A polymeric resin modified by a series of chemical derivatizations with sulfuric acid was found to display excellent surface hydrophilicity and improved extraction efficiencies. The degree of sulfonation was found to play a vital role in determining the SPE efficiency of such resins. By measuring the capacity factor of several polar organic solutes in pure water, an optimum sulfonation capacity of 0.6 mequiv./g was determined. Loose sulfonated resin and Empore membranes embedded with sulfonated resin were used for SPE. Average recoveries were greater than 95% for both types of sulfonated resin for a wide variety of organic compounds including phenols, alcohols, nitro compounds, aldehydes, esters and halogenated alkanes. Breakthrough curves for *p*-cresol, ethyl acetoacetate, isophorone and nitrobenzene were used to compare Empore membranes embedded with sulfonated and unsulfonated resin. The sulfonated membrane yielded sharper and more efficient breakthrough for all compounds tested.

1. Introduction

Sample preparation has been identified as often the slowest and therefore the most expensive step in the analytical process [1]. Solid-phase extraction (SPE) has become the preferred technique for sample preconcentration. Being a multi-stage method it is more efficient than simple liquid–liquid extraction. Analytes undergo multiple equilibrations with the resin and are therefore more strongly retained than in simple liquid extraction where only a single equilibration occurs. It is also more easily automated and much less polluting than liquid extraction techniques that often use relatively large volumes of organic solvents [2]. An early comprehensive paper investigated thoroughly the technique, scope, and limitations of SPE with porous polymeric resins (Rohm & Haas, XAD) [3]. Several reviews on SPE have been published [4,5]. Bonded-phase silica particles (mostly C_{18}- or C_8-) dominate the field, although porous polystyrene resins are finding increasing use because of their efficiency, ruggedness, and broader pH range.

One problem with extraction materials now used is the inability of aqueous solutions to adequately wet their surface, which is usually hydrophobic. This is true for both C_{18}-modified resin and underivatized polystyrene–divinylbenzene (PS–DVB). Pretreatment of the resin column or cartridge with methanol is usually necessary to obtain better surface contact with the aqueous solution [6,7].

* Corresponding author.

0021-9673/95/$09.50
SSDI 0021-9673(94)00766-7

Recently it has been shown that introduction of polar groups into a PS–DVB resin greatly increases the retention of polar organic compounds. Sun and Fritz [6] modified PS–DVB with alcohol and acetyl functional groups. These modified resins exhibited excellent hydrophilicity and a lesser dependence on wetting prior to extraction. They also yielded higher recoveries compared to their unmodified analogue. This was attributed to an increase in surface polarity allowing the aqueous sample to make better contact with the resin surface. Schmidt and Fritz [8] used a sulfonated PS–DVB resin for the simultaneous extraction of bases and neutrals. Bases bind via ion exchange and neutrals by hydrophobic interactions. A two-step elution was then used to elute the bases and neutrals sequentially. Excellent recovery of both bases and neutrals was obtained. Mills et al. [9] recently compared sulfonated and unsulfonated C_{18}-modified resins for the extraction of triazine compounds. Once again, higher recoveries were obtained with the sulfonated resin. This was not attributed to the increased resin hydrophilicity but to hydrogen bonding between the amine functionality of the analytes and the sulfonic acid group on the resin. They also determined distribution coefficients (K_D) for the atrazine compounds on both resins, and found much high values for the sulfonated resins.

It is now shown that porous PS–DVB resins modified with surface sulfonic acid groups are superior to the unmodified PS–DVB for SPE of organic solutes from aqueous samples. However, the extent of the sulfonation is critical in determining extraction efficiency of such resins. The modified resins can be used for SPE in either of two modes: resin packed into mini columns or disks of resin-loaded membranes.

2. Experimental

2.1. Reagents and chemicals

Chemicals used for the sulfonation reactions were of reagent grade. All analytes studied were >99% pure and used as obtained from Aldrich and Fischer. Distilled water was further purified with a Barnstead Nanopure II System (Sybron Barnstead, Boston, MA, USA).

Several sulfonated resins were prepared from 8-μm PS–DVB obtained from Sarasep (Santa Clara, CA, USA). General reaction conditions are shown in Table 1. Specifically, 2 g of resin were mixed with 5 ml glacial acetic acid to form a slurry. Concentrated sulfuric acid was added with stirring. After a given reaction time, the mixture was quickly added to ice water to quench the sulfonation reaction. The resin was then filtered through a medium glass frit, and rinsed with deionized (DI) water, methanol, 2-propanol and finally acetone. After drying, the cation-exchange capacity was determined. A 1-ml volume of 1 *M* HCl was passed through a known amount of resin to ensure all exchange sites were protonated. After rinsing with DI water to remove excess HCl, 5 ml of a standardized NaOH solution were slowly passed through the column and collected into a flask containing 10 ml of a standard HCl solution. Following another DI water rinse, this was titrated with NaOH to the phenolphthalein endpoint. Capacities were calculated as milliequivalents SO_3^- per gram of resin.

2.2. Determination of k'

A small (20 × 2.1 mm I.D.) guard column (Supelco, Bellefonte, PA, USA) was filled with

Table 1
General reaction conditions for resin sulfonation

Capacity (mequiv./g)	H_2SO_4 (ml)	Reaction time (min)	Temperature
0.0			
0.1	5	0.5	Ice
0.4	50	2	Ice
0.6	50	4	Ice
1.0	50	10	Room temp.
1.2	50	20	Room temp.
1.5	50	90	Room temp
2.1	50	90	50°C
2.7	50	90	85°C

approximately 20 mg of resin. This guard column was contained within a guard column holder and connected to the HPLC system via two injection loops; a 10-μl loop from the injector (Rheodyne, Berkeley, CA, USA) and a 50-μl loop to the detector. The HPLC system consisted of a Gilson (Middleton, WI, USA) Model 302B HPLC pump equipped with a Model 802B Gilson manometric module and Scientific Systems (State College, PA, USA) Model LP-21 pulse dampener and a Kratos 783 UV–Vis detector (Applied Biosystems, Ramsey, NJ, USA). Retention times were measured with a Hitachi D-2000 Chromato-Integrator (EM Science, Cherry Hill, NJ, USA).

Samples (50 ppm, w/w) were prepared by diluting stock solutions in DI water. Depending on the absorbance of the analyte, 10–50 μl were injected. Phenols were detected at 270 nm and the carbonyl compounds at 205 nm. DI water at 0.5 ml/min was used as the eluent. The column dead time, t_0 was determined using the retention time of bromide (sodium bromide). This value included the travel time through the tubing (60 μl total volume); therefore 0.12 min was subtracted from the measured time to calculate the true t_0. This value was also subtracted from all analyte retention times.

Capacity factors were determined for the unwetted and methanol wetted resin. Wetting was accomplished by injecting two successive portions of methanol from a 500-μl loop, followed by a 4-ml rinse with DI water. During the water rinse the 500-μl injection loop was replaced with the smaller loop for sample injection.

2.3. Procedure for SPE

The apparatus for SPE consisted of a 30-ml glass syringe barrel fitted with a luer tip. A 1.5-ml polypropylene SPE column (P.J. Corbert Assoc., St. Louis, MO, USA) was connected to the glass reservoir via a universal adapter. Loose 8-μm sulfonated resin and Empore (3M Co., St. Paul, MN, USA) membranes embedded with sulfonated resin were used as the SPE adsorbents. This was placed between two 20-μm polyethylene frits (P.J. Corbert Assoc.) in the column. The bed height measured approximately 1 cm. Positive pressure was used to force liquids through the adsorbents. Prior to use, about 1 ml methanol and 2 ml water were used to rinse the column.

Samples were prepared by adding a 100-μl aliquot of a 150-ppm methanol solution containing 5–10 analytes to 15 ml of DI water. The final concentration of each compound in the sample was about 1 ppm. Air pressure was adjusted to provide a flow of 1–2 ml/min (30–60 p.s.i.; 1 p.s.i. = 6894.76 Pa). After loading, the glass reservoir was rinsed with 3–5 ml water and air was blown through the column to remove any remaining water. A 1-ml volume of ethyl acetate or methanol was used to elute the compounds into a GC vial. An internal standard (100 μl of a 150-ppm toluene solution in methanol) was added to the vial, which was then analyzed by gas chromatography. A Shimadzu (Kyoto, Japan) GC 14A equipped with an AOC-14 autoinjector, flame ionization detector and a C-R4A Chromatopac data analysis system was used to separate and quantitate the analytes. The GC column was a 15-m SPB-5 (Supelco) column. Recoveries were calculated as an average of three trials by comparing the relative peak areas with standards that were not subjected to SPE.

2.4. Breakthrough curve procedure

Breakthrough curves on a 46-mg sulfonated Empore membrane and a 44-mg unsulfonated Empore membrane were determined by passing a dilute solution (5–10 ppm) of analyte continually through the SPE column. Fractions of 5 or 10 ml were collected in volumetric flasks. In order to concentrate the analyte, the collected sample was passed through another sulfonated Empore membrane, which was eluted with 1 ml of methanol into a GC vial. After addition of the internal standard, the analyte concentration was determined by GC. Fractions were collected until the concentration of analyte remained constant.

3. Results and discussion

3.1. Sulfonation of resins

Our goal was to make the resin surface more hydrophilic while keeping the interior surface hydrophobic enough to allow extraction of organic solutes. A fairly rapid sulfonation with sulfuric acid seemed appropriate to accomplish this because sulfonation of resins is known to proceed from the outside into the resin. Reacting for a short time will therefore only modify the surface of the resin bead. In order to achieve more even wetting of the resin with viscous conc. sulfuric acid, the resin was first slurried with a little glacial acetic acid. Acetic acid has both a hydrophobic ($-CH_3$) and hydrophilic (–COOH) portion. This aids in contacting the polar acid and non-polar resin. Without the acetic acid the resin sits on surface of the sulfuric acid and does not react well.

Porous PS–DVB resin beads (average 8 μm) were sulfonated under a variety of conditions to produce sulfonated resins ranging in capacity from 0.1 to 2.7 mequiv./g. The sulfonation conditions and capacities are given in Table 1.

3.2. Measurement of k'

The efficiency of resins used for SPE is most commonly determined by measuring the percentage recovery of test solutes. However, this process depends on the efficiency of elution of the analytes from the SPE column as well as the efficiency of the initial extraction step. Laconto [5] has pointed out that for 90% recovery the K_D for the extraction step may be anywhere between 10 and 100. A better way to compare the behavior of different resins is to measure the capacity factor of the extraction step. Several methods have been used to measure k' in aqueous solutions. One common method for measuring capacity factors consists of measuring k' vs. φ, the percentage of organic solvent in the eluent. After obtaining several points, an extrapolation to 0% organic solvent is possible. Although this is a common procedure [10], it may not be the most accurate for SPE where aqueous samples are used. Surface modifications are undoubtedly taking place due to adsorption of some of the organic portion of the eluent onto the resin surface. It is better to determine k' in the same sample matrix that is common for SPE samples: 100% water. However, this can be difficult when k' is very large. Mills et al. [9] equilibrated a spiked aqueous sample with resin for 24 h. The analyte concentration remaining in the aqueous solution was used to calculate the equilibrium constant.

In the present work the k' values of various analytes were determined by elution from a very small resin column using pure water as the eluent. The method is quick and convenient and requires no extrapolation since no organic modifier is used in the eluent. The capacity factor is determined from the recorded elution curve using the well-known relationship: $k' = (t_R - t_0)/t_0$. In order for this method to be feasible, the column must be small; otherwise, many hours may be required for elution with water as the eluent. The values of k' are also dependent on the measured t_0, although an error in t_0 will still give relative values of k' that can be compared for different resins. Details of this method are given in the Experimental section.

Even with a small column non-polar compounds such as benzene would be retained for several hours and give flat elution "peaks". For this reason more polar, water-soluble compounds were chosen as test materials: phenol, catechol, 2,3-butanedione and ethyl pyruvate. These compounds are polar enough to elute in a reasonable time and are easily detected by a UV–Vis detector.

The k' values of these four test compounds are given in Table 2 and are plotted against the sulfonic acid capacity of the resins in Figs. 1 and 2. In each case the k' increases with increasing sulfonation capacity, reaching a maximum at about 0.6 mequiv./g. Further increases in sulfonic acid capacity are marked by a rapid decrease in k'.

The increasing k' values up to 0.6 mequiv./g can be attributed to the fact that a surface-sulfonated resin is more hydrophilic and therefore more easily wettable. The ability of water to

Table 2
Effect of sulfonation capacity on the retention of polar organic solutes in 100% water

Sulfonation capacity (mequiv./g)	Capacity factor							
	Phenol		Catechol		Ethyl pyruvate		2,3-Butanedione	
0.0	**49**	21	**10**	1	**0**	0	**1**	1
0.1	**124**	40	**32**	1	**4**	0	**2**	0
0.4	**350**	272	**45**	34	**49**	40	**4**	3
0.6	**457**	436	**90**	74	**79**	60	**14**	12
1.0	**381**	315	**70**	59	**55**	54	**8**	8
1.2	**324**	290	**78**	56	**57**	38	**7**	7
1.5	**209**	183	**45**	38	**34**	26	**6**	6
2.1	**127**	80	**25**	16	**16**	9	**4**	3
2.7	**55**	47	**12**	10	**6**	5	**2**	2

Values are averages of two trials. Bold numbers refer to methanol-wetted resins.

come into intimate contact with the resin surface facilitates the transfer of analyte from the aqueous sample to the resin surface. The wettability of a resin may be quickly checked by adding a few milligrams of dry resin to water. Hydrophobic resins will remain on the surface of the water even if stirred. Hydrophilic resins will be dispersed throughout the solution because of the ability of polar surface to reduce the surface tension of the water, thus allowing water to closely approach the resin surface. In terms of capacity, 0.6 mequiv./g is the minimum sulfona-

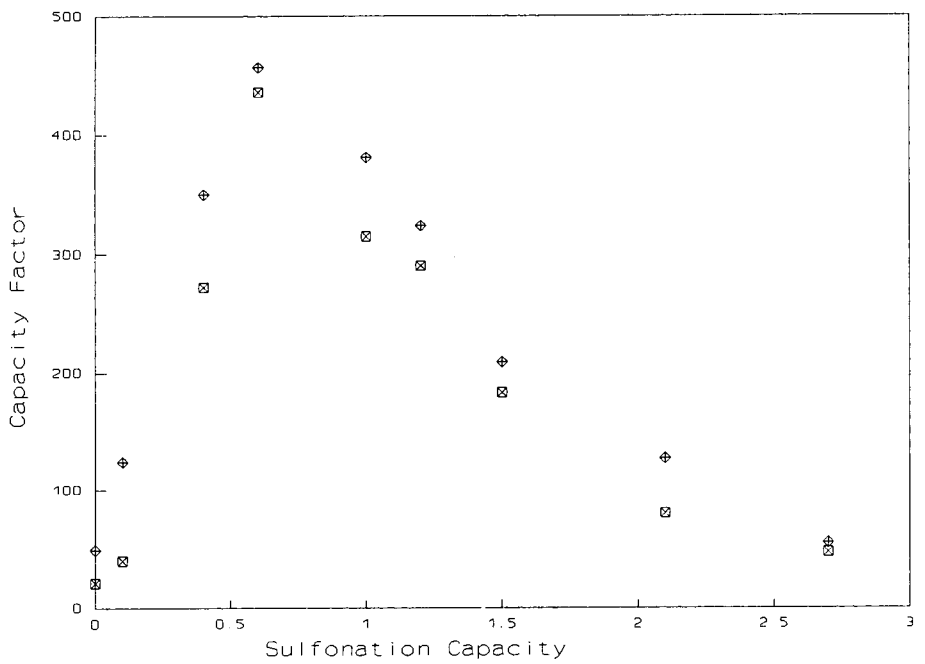

Fig. 1. Effect of PS–DVB sulfonation capacity (in mequiv./g) on retention of phenol in pure water for methanol wetted (◇) and unwetted (□) resins.

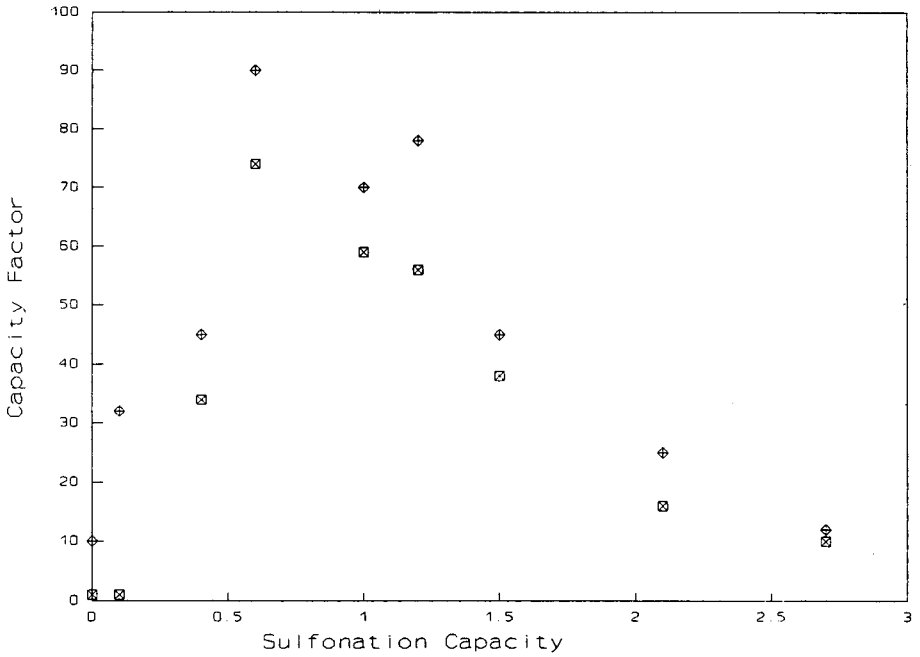

Fig. 2. Effect of PS–DVB sulfonation capacity (in mequiv./g) on retention of catechol in pure water for methanol wetted (◇) and unwetted (□) resins.

Table 3
Comparison between sulfonated (0.4 mequiv./g) and unsulfonated resins

Compound	Recovery (%)			
	Sulfonated		Unsulfonated	
	Not wetted	Wetted	Not wetted	Wetted
Anisole	94	93	83	89
Benzaldehyde	90	89	87	96
Nitrobenzene	96	95	88	96
Hexyl acetate	94	94	84	82
Benzylalcohol	90	98	78	81
Phenol	98	95	77	89
Catechol	59	34	ND	ND
m-Nitrophenol	98	99	89	95
Mesityl oxide	98	97	93	99
tert.-2-Hexenyl acetate	93	90	79	89
Average ± R.S.D. (%)[a]	95 ± 3.2%	94 ± 3.4%	84 ± 5.5%	91 ± 6.3%

Values are averages of three trials. Wetting solvent is methanol. ND = Not detected.
[a] Catechol not included.

tion necessary to produce a hydrophilic resin surface. Underivatized PS–DVB and slightly sulfonated (up to 0.6 mequiv./g) are not wetted by water, while resins with a capacity of 0.6 mequiv./g or greater are wetted.

The lower k' values above 0.6 mequiv./g may be attributed to lower overall hydrophobicity of the resin at higher concentrations of sulfonic acid groups. The hydrophobic resin matrix may become increasingly shielded by the bulky, polar sulfonic acid groups. Wetting with methanol had a greater effect on the lightly sulfonated resins compared to those of higher capacity. The purpose of methanol pretreatment is to increase surface hydrophilicity, but this does not make a large difference with the higher capacity resins. All of the compounds used in this experiment were quite polar, but a similar trend would be expected for more non-polar analytes, although the change may not be as dramatic. Obtaining curves for hydrophobic analytes would be difficult and time consuming. The retention time for phenol, the most non-polar compound used for this study, was about 65 min. Judging by the peak shape, a maximum retention time of about 2 h may still yield a detectable peak, which leads to an upper k' limit for this technique of 1000.

3.3. SPE with sulfonated resins

The ability of sulfonated and unsulfonated resins to extract various organic test compounds from aqueous samples was compared using identical small columns packed with the resins. After the extraction step, the test compounds were eluted with 1.0 ml of ethyl acetate or methanol and determined by GC. The percentage recoveries are given in Table 3. The small resin size (8 μm) allows even the hydrophobic underivatized resin to extract the compounds, but the sulfonated resin, with a more polar surface, is even more efficient for extracting these analytes. Note the sulfonation capacity for this table is 0.4 mequiv./g which is close to the optimum capacity of 0.6 mequiv./g. The effect of wetting the resin with methanol is also shown. As expected, this has a major effect on the underivatized resin, but is not as important with

Table 4
Recoveries of organic solutes (1 ppm) with a sulfonated Empore membrane (0.6 mequiv./g)

Compound	Recovery (%)
Phenol	98
p-Cresol	102
2,5-Dimethylphenol	98
p-Chlorophenol	97
o-Chlorophenol	95
m-Nitrophenol	97
4-*sec.*-butylphenol	98
4-*tert.*-butylphenol	100
4-Hexylresorcinol	101
2-Methylresorcinol	91
p-Isopropylphenol	96
Dodecyl alcohol	94
1-Hexanol	94
Cyclohexanol	93
2-Ethyl-1-hexanol	97
Benzyl alcohol	94
1-Octanol	96
Phenethyl alcohol	96
3-Phenyl-1-propanol	98
Benzonitrile	99
Nitrobenzene	100
3-Nitroacetophenone	98
Benzothiazole	97
o-Nitrotoluene	97
Isophorone	100
Benzophenone	96
Acetophenone	102
Hexyl aldehyde	95
Octyl aldehyde	96
Nonyl aldehyde	93
9-Anthraldehyde	98
Salicylaldehyde	100
Benzaldehyde	104
Anisole	96
Phenetole	91
Ethyl acetoacetate	97
Methyl benzoate	96
Ethyl cinnamate	95
Hexyl acetate	93
tert.-2-Hexenyl acetate	91
Isopentyl benzoate	92
1-Iodoheptane	98
1-Bromododecane	92
1-Chlorododecane	90
Average ± R.S.D. (%)	96 ± 3.1

the sulfonated resin. The surface of the sulfonated resin is hydrophilic enough that methanol does not significantly modify it.

3.4. SPE with resin-loaded membranes

Empore membranes embedded with sulfonated resin of approximately 0.6 mequiv./g were also used for SPE. These membranes embedded with other materials have been used and described previously [11–13]. They offer several advantages over loose resin including lower back pressure necessary to load samples, decreased channeling, and improved mass transfer [14,15]. In this study, sulfonated membranes were used to extract neutral organic compounds from water. Averaged triplicate recoveries of 45 analytes are shown in Table 4. Many classes of compounds are represented including phenols, alcohols, aldehydes, ketones and esters. Polar analytes, like the phenols, and non-polar analytes such as the halogenated alkanes are all efficiently recovered. Recoveries are over 90% for all compounds with relative standard deviations commonly near 3%. These recoveries compare very favorably with data reported previously for alcohol and acetyl derivatized PS–DVB resins and membranes [6,13].

3.5. Analysis of breakthrough curves

The adsorption capacity for several organic compounds was determined by passing a 5- or 10-ppm aqueous solution of the analyte through a resin-loaded membrane until breakthrough occurred. Since breakthrough is closely related to k' [4], the breakthrough volume (V_B) or retention volume (V_R) for a particular analyte is a good indication of the extraction ability of the resin. For this study V_B is defined as the volume after extrapolating the middle portion of the curve to the x-axis, and V_R as the volume at $C/C_0 = 0.5$. C/C_0 is the ratio of analyte effluent concentration to influent concentration. The resin load capacity may also be determined from a breakthrough curve. This is the total number of moles of analyte adsorbed by a resin, and is calculated by multiplying V_R by the influent concentration [16].

Breakthrough curves of several compounds were compared for two Empore membranes —one embedded with underivatized PS–DVB

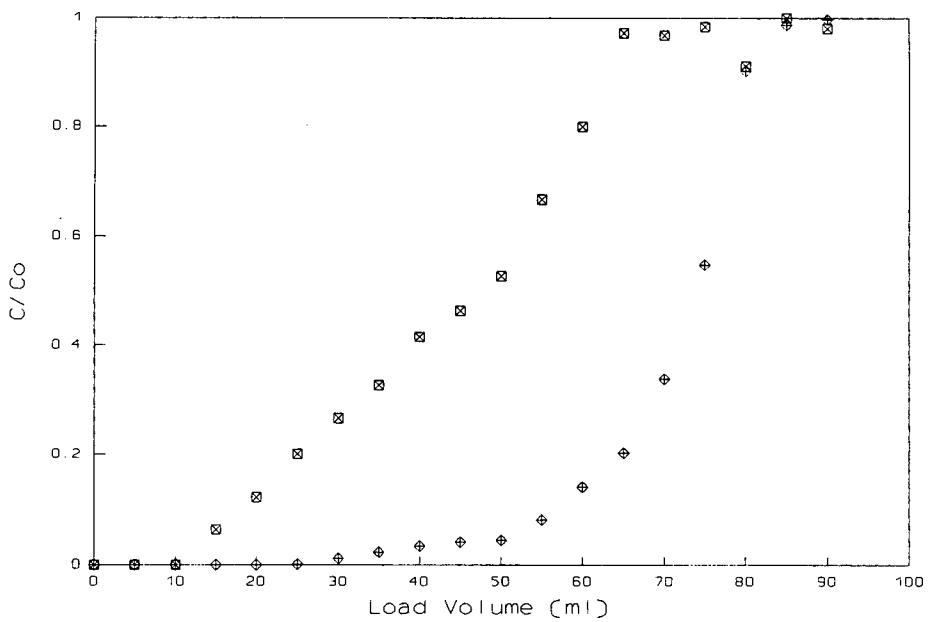

Fig. 3. Breakthrough curves for p-cresol on a sulfonated (◇) and unsulfonated (□) Empore membrane.

Table 5
Comparison of breakthrough data for Empore membranes embedded with unsulfonated PS–DVB and sulfonated (0.6 mequiv./g) PS–DVB

Compound	Load capacity (10^{-6} mol/g)		V_R (ml)		V_B (ml)	
	Sulfonated	Unsulfonated	Sulfonated	Unsulfonated	Sulfonated	Unsulfonated
p-Cresol	74.2	47.4	74	46	34	12
Ethyl acetoacetate	39.3	13.1	46	15	38	0
Nitrobenzene	223	241	126	132	76	28
Isophorone	173	185	109	114	45	27

and the other with sulfonated PS–DVB (0.6 mequiv./g capacity). Breakthrough curves for *p*-cresol are shown in Fig. 3. The sulfonated resin membrane, being more hydrophilic, produces a much sharper breakthrough than the underivatized membrane, which allows breakthrough almost immediately.

The parameters calculated from the breakthrough curves of four compounds are shown in Table 5. Extraction efficiency of the more polar compounds, *p*-cresol and ethyl acetoacetate, is dramatically increased with the sulfonated membrane. Load capacity, V_R, and V_B, are all much larger on this membrane. It may be expected that less polar compounds would be more easily extracted with an underivatized resin, but this is not necessarily the case. The less polar compounds, nitrobenzene and isophorone, do have slightly higher load capacities and V_R on the underivatized membrane, but V_B is still much lower. This is caused by the poor curve shape and early breakthrough on the underivatized membrane. V_B is the parameter of most concern for SPE because dilute samples are usually used and the load capacity of a resin is seldom approached. A sulfonated membrane would therefore be the better adsorbent to use for SPE of these types of compounds.

Acknowledgements

We would like to thank Doug Gjerde of Sarasep for the 8-μm resins used for all sulfonation reactions. This research was supported by a grant from the 3M Co., St. Paul, MN, USA. The work was performed in the Ames Laboratory at Iowa State University. Ames Laboratory is operated for the US Department of Energy under contract No. W-7405-Eng-82.

References

[1] R. Stevenson, *Am. Lab.*, June (1993) 24H.
[2] J. Snyder, *Pollution Eng.*, 11 (1992) 40–43.
[3] G.A. Junk, J.J. Richard, M.D. Griesa, D. Witiak, J.L. Witiak, M.D. Arguello, R. Vick, H.J. Svec, J.S. Fritz and C.V. Calder, *J. Chromatogr.*, 99 (1974) 745–762.
[4] I. Liska, J. Krupcik and P.A. Leclercq, *J. High Resolut. Chromatogr.*, 12 (1989) 577–590.
[5] P. Laconto, *LC·GC*, 9 (1991) 752–760.
[6] J.J. Sun and J.S. Fritz, *J. Chromatogr.*, 590 (1992) 197–202.
[7] N. Simpson, *Am. Lab.*, August (1992) 37–43.
[8] L. Schmidt and J.S. Fritz, *J. Chromatogr.*, 640 (1993) 145–149.
[9] M.S. Mills, E.M. Thurman and M.J. Pedersen, *J. Chromatogr.*, 629 (1993) 57–67.
[10] S. Bitteur and R. Rosset, *J. Chromatogr.*, 394 (1987) 279–293.
[11] D.F. Hagen, C.G. Markell and G.A. Schmidt, *Anal. Chim. Acta*, 236 (1990) 157–164.
[12] D.F. Hagen, C.G. Markell and V.A. Bunnelle, *LC·GC*, 9 (1991) 332–337.
[13] L. Schmidt, J.J. Sun, J.S. Fritz, D.F. Hagen, C.G. Markell and E.E. Wisted, *J. Chromatogr.*, 641 (1993) 57–67.
[14] B. Bryan, *Today's Chemist*, 2 (1994) 39–43.
[15] D.D. Blevins and S.K. Schultheis, *LC·GC*, 12 (1994) 12–14.
[16] C.M. Josefson, J.B. Johnston and R. Trubeg, *Anal. Chem.*, 56 (1984) 764–768.

ELSEVIER

Journal of Chromatography A, 691 (1995) 133–140

JOURNAL OF CHROMATOGRAPHY A

Methods and materials for solid-phase extraction

James S. Fritz*, Philip J. Dumont, Luther W. Schmidt

Ames Laboratory, US Department of Energy and Department of Chemistry, Iowa State University, Ames, IA 50011, USA

Abstract

Solid-phase extraction (SPE) with porous solid particles goes back to the early 1970s. However, SPE has become more popular recently due to the availability of more efficient particles and the need to replace liquid extraction procedures that require the use of large quantities of organic solvents. Chemical introduction of acetyl or hydroxymethyl groups into polymeric resins improves the efficiency of SPE by providing better surface contact with aqueous samples.

Lightly sulfonated resins display excellent hydrophilicity and improved extraction efficiencies of polar organic compounds over underivatized resins. It is shown that the degree of sulfonation has a major effect on retention of such compounds. Sulfonated resins can also be used for group separation of neutral and basic organic compounds. The advantages of performing SPE with resin-loaded membranes is discussed.

1. Introduction

Sample preparation is often the most time-consuming step in a chemical analysis. One survey found that sample preparation accounted for 61% of the time typically required to perform analytical tasks [1]. Considerable attention is now being paid to solid-phase extraction (SPE) as a way to isolate and concentrate desired components from a sample matrix. In addition to being fast, efficient and easily automated, SPE is a clean analytical procedure. It is rapidly replacing liquid-extraction procedures that require the use of large quantities of polluting organic solvents [2,3].

In liquid–liquid extraction a temporary emulsion is formed by agitating two immiscible liquids, such as water and an organic solvent. Mass transfer of the solute takes place rapidly because of the large interfacial area of the emulsion. In SPE the extractant is a porous, particulate solid which has a large surface area available for interaction with the liquid sample solution. The porous solid particles are usually packed into a small tube and the aqueous sample passed through. The principles and applications of SPE have been reviewed [4].

The use of porous, polymeric resins for SPE goes back to the early 1970s. Columns filled with Rohm and Haas XAD resins were used for concentration, identification and quantitative measurement of trace organic pollutants in drinking water. Excellent recoveries were obtained for 85 different organic compounds in one paper [5], which was recently identified as one of the twenty most-cited papers published in the *Journal of Chromatography* [6]. However, practical use of this method was undoubtedly hindered by the necessity of grinding, sizing and purifying the early XAD resins. Now, with the ready availability of pure bonded-phase silica particles and, more recently, of pure polymeric

* Corresponding author.

0021-9673/95/$09.50
SSDI 0021-9673(94)00756-X

resins of appropriate particle size, SPE is becoming the preferred method for isolation of organic components from predominately aqueous samples. In this paper, we review some of our most recent research in methods and techniques for SPE.

2. Experimental

2.1. SPE with chemically modified resins

Amberchrome 161 resins (Supelco, Bellefonte, PA, USA) with an average size of ca. 40 μm were derivatized as described previously [7]. For SPE small columns were packed with ca. 100 mg of resin. The C_{18} silica SPE column was obtained from Alltech (Deerfield, IL, USA). This column was 55 × 6 mm I.D., packed to a bed height of 8–10 mm with resin of 40 μm particle size. Derivatized and underivatized Amberchrome 161 resins were packed dry to a bed height of 12 mm into empty 55 × 6 mm I.D. plastic columns obtained from P.J. Cobert Assoc. (St. Louis, MO, USA). Each column contained polyethylene frits to support and cover the resins. Each SPE column was connected to a laboratory-made reservoir by an adaptor (P.J. Cobert Assoc.). The flow-rate of the sample solution from the reservoir was controlled by air pressure applied to the top of the reservoir.

The organic compounds eluted from SPE column with ethyl acetate were collected and then analyzed using an HP 5880A gas chromatograph with a flame ionization detector, an HP 5880A Series Level 4 integrator and an HP 7673A automatic sampler (Hewlett-Packard, Avondale, PA, USA). The gas chromatographic columns used were J & W fused-silica capillary megabore DB-5 and minibore DB-1 (Alltech) and Supelco fused-silica capillary columns.

Approximately 1 ml of methanol was added to the SPE column to serve as an "activating" solvent. Aqueous samples (ca. 20 ml) containing about 5 ppm (w/w) of each test compound were passed through the column at a flow-rate of about 5 ml/min. After washing with 1 ml of pure water, the SPE column was disconnected from the reservoir and the adsorbed analytes eluted with 1 ml of ethyl acetate. A measured amount of internal standard was added to the effluent and the individual analytes determined by gas chromatography (GC) [7].

2.2. SPE with lightly sulfonated resins

Sulfonation of resins

Sulfonated resins were prepared from 8 μm polystyrene–divinylbenzene (PS–DVB) resins obtained from Sarasep (Santa Clara, CA, USA). For sulfonation, 2 g of resin was mixed with 5 ml of glacial acetic acid and 50 ml of sulfuric acid were added with stirring. Reaction times ranged from 0.5 to 90 min at temperatures ranging from ice temperature to 90°C [8]. After a given reaction time, the mixture was quickly added to ice water to quench the sulfonation reaction. The resin was then filtered through a medium glass frit, and rinsed with deionized (DI) water, methanol, 2-propanol and finally acetone. After drying, the cation-exchange capacity was determined by acid–base titration.

Procedure for k determination

A small (20 × 2.1 mm I.D.) guard column (Supelco) was filled with approximately 20 mg of resin. This guard column was contained within a guard column holder and connected to the HPLC system via two injection loops; a 10-μl loop from the injector (Rheodyne, Berkeley, CA, USA) and a 50-μl loop to the detector. The HPLC system consisted of a Gilson Model 302B HPLC pump equipped with a Model 802B Gilson manometric module (Gilson, Middleton, WI, USA) and Model LP-21 Scientific Systems pulse dampener (Scientific Systems, State College, PA, USA) and a Kratos 783 UV–Vis detector (Applied Biosystems, Ramsey, NJ, USA). Retention times were measured with a Hitachi D-2000 Chromato-Integrator (EM Science, Cherry Hill, NJ, USA).

Samples (50 ppm) were prepared by diluting stock solutions in DI water. Depending on the absorbance of the analyte, 10–50 μl were injected. Phenols were detected at 270 nm and the carbonyl compounds at 205 nm. DI water at 0.5

ml/min was used as the eluent. The column dead time, t_0 was determined using the retention time of bromide (sodium bromide). This value included the travel time through the tubing (60 μl total volume) therefore 0.12 min were subtracted from the measured time to calculate the true t_0. This value was also subtracted from all analyte retention times.

Procedure for SPE

The apparatus for SPE consisted of a 30-ml glass syringe barrel fitted with a luer tip. A 1.5-ml polypropylene SPE column (P.J. Cobert Assoc.) was connected to the glass reservoir via a universal adapter. Loose 8-μm sulfonated resin and Empore membranes embedded with sulfonated resin were used as the SPE adsorbents. This was placed between two 20-μm polyethylene frits (P.J. Corbert Assoc.) in the column. The bed height measured approximately 1 cm. Positive pressure was used to force liquids through the adsorbents. Prior to use, the column was rinsed with 1 ml methanol and then with water.

Samples were prepared by adding a dilute methanol solution of several organic compounds to 15 ml of DI water. The final concentration of each compound in the sample was about 1 ppm. Air pressure was adjusted to provide a flow of 1–2 ml/min (30–60 p.s.i.; 1 p.s.i. = 6894.76 Pa). After loading, the glass reservoir was rinsed with 3–5 ml water and air was blown through the column to remove any remaining water. A 1-ml volume of ethyl acetate or methanol was used to elute the compounds into a GC vial. An internal standard was added to the vial, which was then analyzed by GC [8].

2.3. Group separation of neutral and acidic compounds

Preparation of anion-exchange resin

Amberchrome 161, ca. 40 μm was converted to a quaternary ammonium resin by the following procedure: 1 g of resin was wetted with 1 ml of glacial acetic acid and then reacted with 25 ml of a 2.2 *M* solution of paraformaldehyde in concentrated hydrochloric acid for 24 h at 70°C. After filtering and rinsing with water and methanol, the resin was aminated by adding 25 ml of 25% trimethylamine in ethanol and stirring at room temperature for 24 h. The resin was then rinsed with methanol, water and acetone. The exchange capacity of the resin was determined by acid–base titration to be 0.9 mequiv./g.

Procedure for SPE and group separation

Approximately 100 mg of resin was packed into a column similar to that used for the previous SPE procedures. Prior to initial use, the anion-exchange column was cleaned with 1 ml each of acetonitrile and methanol. Then 5 ml of 0.1 *M* NaOH was added to ensure the resin was in the basic form. Aqueous samples containing ca. 0.5 to 5.0 ppm of each test compound were treated with dilute NaOH to raise the pH to approximately 11. The sample was then put into the reservoir and passed through the column at ca. 1 ml/min. The column and reservoir were then rinsed with ca. 5 ml of water.

The neutral fraction was eluted from the column with 1 ml of methylene chloride. This fraction was collected in a GC vial and spiked with 0.1 ml of an quinoxaline or toluene internal standard solution. The vial was capped, mixed with an orbital stirrer, and analyzed by GC. A 1-μl sample was injected with a split ratio of 1:40. Helium carrier gas was used at a flow-rate of 1 ml/min. The oven temperature was held initially at 50°C for 2 min, then ramped at 15°C/min to a final temperature of 225°C. A flame ionization detector was used. The acid fraction was then eluted with 1 ml of 0.1 *M* HCl in methanol. When the acid fraction contained phenols, the analysis was performed by GC as described for the neutral fraction. Recoveries were calculated by comparison of relative peak area to that of samples prepared and not subjected to SPE.

Samples containing carboxylic acids were eluted with 1 ml of 2 *M* HCl in methanol and analyzed by HPLC. A 5-μl aliquot of the sample was injected onto a 5-cm laboratory-prepared column of 1 mequiv./g sulfonated 5-μm PS–DVB resin. Separations were performed using an aqueous eluent of 10% acetonitrile, 1 to 2% butanol and 1 m*M* H_2SO_4. Quantitation was

achieved by comparison of peak areas to known standards.

3. Results and discussion

3.1. Chemical modification of resins

For analytical purposes, SPE is usually performed using a small column containing an appropriate solid packing, or with a membrane loaded with an appropriate solid material [9–11]. Following uptake of extractable solutes from a predominately aqueous sample, the adsorbed materials are eluted from the resin with a small volume of an organic solvent. The individual analytes are then determined quantitatively, usually by gas or liquid chromatography.

Chemically bonded silica, usually with a C_{18} or C_8 organic group, is by far the most commonly used material for SPE. However, cross-linked polystyrene and other porous polymeric resins are finding increasing use. Such polymers are more rugged and pH stable than silica materials. Our research has consistently shown that the percentage recoveries for many types of analytes are significantly higher with polymeric resins than with silica materials [12].

Chemically bonded silica and porous polystyrene resins have several shortcomings for use in SPE [13]. While silica itself is hydrophilic, the hydrocarbon chains make the surface hydrophobic. The consequence is poor surface contact with predominantly aqueous solutions. Porous polystyrene resins also have a hydrophobic surface [14]. Pretreatment of the SPE materials with an activating solvent (such as methanol, acetone or acetonitrile) must be used to obtain better surface contact with the aqueous solution being extracted. However, the activating solvent can be gradually leached out of the resin, thereby causing the extraction to become ineffective. This is particularly true if the SPE column inadvertently becomes dry, causing air to be sucked into the column [5].

A better strategy is to make the surface of a solid-phase extractant permanently hydrophilic through a chemical reaction. Sun and Fritz [7,15] introduced an acetyl, hydroxymethyl, or cyanomethyl group into cross-linked polystyrene resins at a capacity of approximately 1 mmol/g. The modified resins were easily wetted by water alone and gave significantly higher recoveries for many of the organic analytes tested (Table 1). Each of the resin columns in this table was pretreated with 1 ml of methanol to aid in wetting the resin surface. When this step was omitted the average recoveries were as follows: silica C_{18} 26%, Amberchrome 35%, Amberchrome–CH_2OH 88%, Amberchrome–$COCH_3$ 93%.

Sulfonation of resins also increases their hydrophilicity and makes them wettable with water alone [16]. The degree of sulfonation was found to be very important [8,17]. The best performance for SPE was found to be with resins with about 0.6 mequiv./g of sulfonate groups.

The effect of sulfonate capacity of the resin on SPE was studied by measuring the capacity factor (k) of several solutes using a very small column packed with a sulfonated resin. A small volume of analyte solution (10–50 μl) was added to the top of the resin column and deionized water was passed through the column until an elution peak for the solute was obtained. The capacity factor was calculated from the well-known relationship

$$k = \frac{t_R - t_0}{t_0}$$

where t_R is the retention time of the peak and t_0 is the dead time. The value of t_0 was determined from the elution time of a non-sorbed solute (bromide) and a correction was applied for this solute to pass through the connecting tube.

A plot of k for phenol as a function of resin sulfonate capacity is given in Fig. 1. Curves of very similar shape were obtained for catechol, ethyl pyruvate and 2,3-butanedione, although the capacity factors of these are lower than for phenol. The following points are significant for the four solutes tested:

(1) In each case the plot has a maximum at approximately 0.6 mmol sulfonate/g resin. This value coincides with the onset of wetting of the dry resin by water without any pretreatment.

Table 1
SPE recoveries of phenolic and aromatic compounds with different sorbents

Compound	Recovery (%)			
	SiC_{18}	Amberchrome	Amberchrome–CH_2OH	Amberchrome–$COCH_3$
Phenol	6.3	90.7	94.0	99.7
p-Cresol	16.2	91.1	98.1	100.9
p-Ethylphenol	65.9	96.0	98.5	101.2
2-Nitrophenol	44.7	92.9	94.9	96.0
3-Nitrophenol	<5	81.0	84.9	92.5
4-Nitrophenol	<5	87.0	85.7	86.6
2,4-Dimethylphenol	70.8	94.7	97.3	100.2
4-*tert.*-Butylphenol	82.9	88.2	95.5	99.5
Anisol	77.9	90.6	94.1	98.1
Aniline	9.1	94.0	96.1	99.5
Benzylalcchol	10.2	91.5	98.2	99.2
Nitrobenzene	53.6	92.4	96.3	99.9
2,4-Dinitroflourobenzene	43.9	83.0	96.0	98.4
o-Hydroxyacetophenone	88.1	84.9	94.7	96.0
Isopentylbenzoate	83.8	71.8	89.2	95.2
Diethylphthalate	90.2	87.2	95.5	100.1
Average	47.1	88.6	94.3	97.6

(2) Increasing degrees of sulfonation cause a marked decrease in k.

(3) Unsulfonated resin and sulfonated resin 2.17 mmol/g were mixed in a proportion to give an average capacity of 0.6 mmol/g. However, the k for this mixture was low (ca. 50), indicating that the actual degree of sulfonation, rather than the average degree of sulfonation, is the critical factor.

SPE with sulfonated resin of the optimum capacity was found to be excellent with recoveries of typical analytes averaging higher than unsulfonated. Table 2 compares recoveries (average of three trials) of several analytes on sulfonated and unsulfonated SPE resin columns. The data indicate that it is not necessary to pretreat the column with methanol when the sulfonated resin is used. Recoveries with the unsulfonated resin average somewhat higher when the methanol pretreatment is included. However, the small particle size of the resins used still permits pretty good recoveries with unsulfonated resin and no pretreatment.

3.2. Use of resin-loaded membranes

For best efficiency a SPE column should be very short (a few millimeters) and should be packed with resins of quite small particle size (5–10 μm). However, some problems are often encountered. Smaller particles require a higher pressure to force the sample through the column. Incomplete retention of sample solutes can occur because of channeling through very short columns.

These difficulties can be largely avoided by using resin-loaded membranes of the type produced by the 3M Co. The sample solutes make intimate contact with the immobilized resins within the membrane, yet a high flow-rate is possible with only modest applied pressure [9–11]. These membranes can be used much like a piece of filter paper in a Buchner funnel. However, we elected to cut small disks from a larger membrane so that the disks would fit snugly into a 5 mm I.D. plastic tube. Tests with a red dye showed that the dye is adsorbed evenly over the

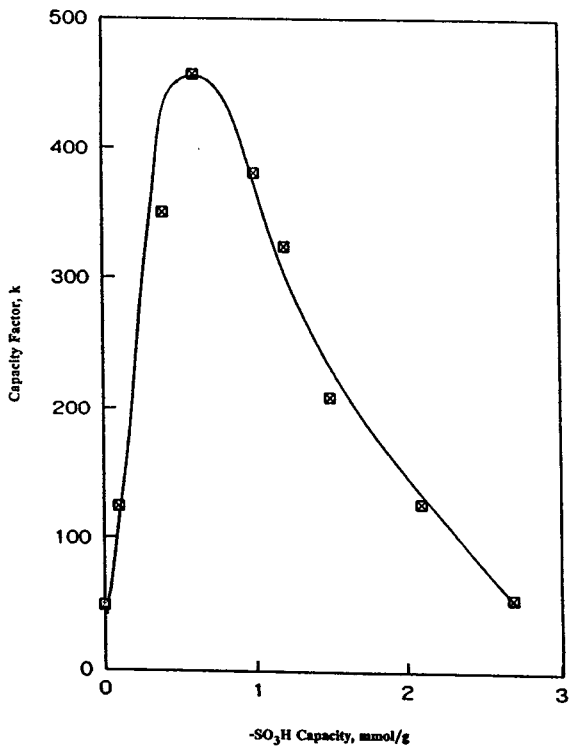

Fig. 1. Capacity factors of phenol on sulfonated resins (aqueous solution).

top area of the circle with no apparent channeling. These properties make it possible to use a very short SPE column with consequent elution of the adsorbed analytes by a very small volume of eluting solvent.

An extensive survey was made of SPE of 44 different analytes (1 ppm each) using sulfonated resin (0.6 mmol/g) incorporated in an Empore membrane [8]. The analytes included several compounds containing each of the following functional groups: alcohol, phenol, aldehyde, ketone, ether, ester, haloalkane, nitrile and nitro. The average recovery was 96% with a relative standard deviation of ca. 3%.

3.3. Simultaneous SPE and group separation of organic solutes

With samples containing many different organic compounds it is often desirable to simplify the analysis by a preliminary separation into neutral, basic and acidic groups. Sulfonation of a polymeric resin converts it into a cation exchanger. If the sulfonation is performed quickly under very mild conditions, the resulting resin retains organic solutes by two different mechanisms. Neutral compounds are retained by sim-

Table 2
Comparison between sulfonated (0.4 mequiv./g) and unsulfonated resins

Compound	Recovery (%)			
	Sulfonated		Unsulfonated	
	Not wetted	Wetted	Not wetted	Wetted
Anisole	94	93	83	89
Benzaldehyde	90	89	87	96
Nitrobenzene	96	95	88	96
Hexylacetate	94	94	84	82
Benzylalcohol	90	98	78	81
Phenol	98	95	77	89
Catechol	59	34	ND	ND
m-Nitrophenol	98	99	89	95
Mesityl oxide	98	97	93	99
tert.-2-Hexenyl acetate	93	90	79	89
Average ± R.S.D. (%)	95 ± 3.2%	94 ± 3.4%	84 ± 5.5%	91 ± 6.3%

Wetting solvent is methanol. Average of three runs. ND = Not detected.

ple adsorption, while protonated bases are retained by an ion-exchange mechanism. Simultaneous concentration of organic compounds thus becomes possible from aqueous samples, followed by selective elution of neutral and basic compounds.

The scheme for separating neutral and basic organic solutes into groups is as follows:

(1) The organic solutes are retained by passing an aqueous sample (adjusted to pH 2.0) through a small column packed with a macroporous resin particles with a sulfonate capacity of approximately 1.0 mmol/g.

(2) Neutral compounds are eluted with methylene chloride and the individual compounds determined by GC.

(3) Basic compounds are eluted by 2 *M* methylamine in methanol and the individual solutes separated and determined by GC.

(4) A solution of 2 *M* HCl in methanol is passed through to regenerate the resin. Full experimental details are given in a recent paper [16].

The purpose of the methylamine in the final elution step is to neutralize the protonated organic base cations so that the free base is formed, which is readily eluted by the methanol. The relatively low exchange capacity of the sulfonated resin, as well as the small amount of resin used (ca. 100 mg), permits neutralization of all of the resin protons with a small volume of $MeNH_2$ in methanol.

Initially, 2 *M* ammonia in methanol was used instead of 2 *M* methylamine. The ammonia–methanol eluent gave good recoveries of weak bases, such as pyridine and aniline, but the elution of stronger bases, such as alkylamines, was essentially zero. Methylamine is a much stronger base than ammonia and is able to deprotonate alkylammonium cations. The volatility of methylamine is also advantageous, causing the excess methylamine to elute well before the analyte bases in the GC analysis.

Excellent resolution of a number of test compounds into neutral and basic fractions was obtained using this procedure. The recoveries of test compounds were mostly 90–100%.

A similar procedure can be used to concentrate and separate neutral and acidic organic compounds into groups. In this case a macroporous anion-exchange resin of fairly low exchange capacity is used. The resin column is

Table 3
Average recoveries of neutral and acidic organic compounds concentrated from dilute aqueous solution by anion-exchange resin

Neutral compound	Recovery (%)	Acidic compound	Recovery (%)
Ethyl butyrate	101	*p*-Hydroxybenzoic acid	99
Chlorobenzene	87	Benzoic acid	96
Cyclohexanol	100	*p*-Nitrobenzoic acid	99
1-Bromohexane	90	1,2,4-Benzenetricarboxylic acid	105
Salicylaldehyde	99	Salicylhydroxamic acid	102
1-Octanol	100	2,4-Dihydroxybenzoic acid	99
Nonylaldehyde	100	Isophthalic acid	100
Triethyl orthopropionate	84	Phenol	87
1-Decanol	96	2-Chlorophenol	95
Benzyl alcohol	93	4-Chlorophenol	99
Octylaldehyde	92	2-Nitrophenol	99
Nitrobenzene	103	3-Nitrophenol	100
Toluene	93	*p*-Cresol	98
Anisole	96	2,5-Dimethylphenol	94
		4-Isopropylphenol	100

Neutral compounds were eluted with methylene chloride and acidic compounds were subsequently eluted with 1 *M* HCl in methanol.

treated with dilute sodium hydroxide to convert it to the OH^- form. The aqueous sample is also made basic to convert the acidic organic solutes to the anionic form. After passing an aqueous sample through the resin column, neutral solutes are eluted with 1 ml of methylene chloride and measured by GC. Then the acidic substances are eluted by 1 *M* HCl in acetonitrile or methanol. Excellent group separations of neutral/acidic compounds were obtained and the overall recovery of test compounds was also very high (Table 3).

Acknowledgements

The authors wish to thank Sarasep (Santa Clara, CA, USA) for gifts of some of the resins used in this work. We also thank Don Hagen and Craig Markell of 3M for preparing the resin-loaded membranes used in this research.

This research was supported by a grant from the 3M Co. (St. Paul, MN, USA). The work was performed in the Ames Laboratory at Iowa State University. Ames Laboratory is operated for the US Department of Energy under contract No. W-7405-Eng-82.

References

[1] R. Stevenson, *Am. Lab.*, June (1993) 24H.
[2] J. Snyder, *Pollut. Eng.*, 11 (1992) 40–43.
[3] J.L. Snyder, R.L. Grob, M.E. McNally and T.S. Oostdyk, *LC·GC*, 12 (1994) 230.
[4] I. Liška, J. Krupik and P.A. Leclerq, *J. High Resolut. Chromatogr.*, 12 (1989) 577–590.
[5] G.A. Junk, J.J. Richard, M.D. Grieser, D. Witiak, J.L. Witiak, M.D. Arguello, R. Vick, H.J. Svec, J.S. Fritz and G.V. Calder, *J. Chromatogr.*, 99 (1974) 745–762.
[6] J.S. Fritz and G.A. Junk, *J. Chromatogr.*, 625 (1992) 87–90.
[7] J.J. Sun and J.S. Fritz, *J. Chromatogr.*, 522 (1990) 95–105.
[8] P.J. Dumont and J.S. Fritz, *J. Chromatogr. A*, 691 (1995) 123.
[9] D.F. Hagen, C.G. Markell and G.A. Schmitt, *Anal. Chim. Acta*, 236 (1990) 157–164.
[10] C.G. Markell, D.F. Hagen and V.A. Bunnelle, *LC·GC*, 9 (1991) 332–337.
[11] L. Schmidt, J.J. Sun, J.S. Fritz, D.F. Hagen, C.G. Markell and E.E. Wisted, *J. Chromatogr.*, 641 (1993) 57.
[12] J.J. Sun and J.S. Fritz, *J. Chromatogr.*, 590 (1992) 197.
[13] C.H. Marvin, I.D. Brindle, C.D. Hall and M. Chiba, *Anal. Chem.*, 62 (1990) 1495.
[14] G.A. Junk and J.J. Richard, *Anal. Chem.*, 60 (1988) 451.
[15] J.J. Sun and J.S. Fritz, *US Pat.*, 5 071 565, (10 Dec. 1991).
[16] L. Schmidt and J.S. Fritz, *J. Chromatogr.*, 640 (1993) 145–149.
[17] P.J. Dumont, J.S. Fritz, D.F. Hagen, C. Markell and L.W. Schmidt, *US Pat. Appl.*, May 1994.

ELSEVIER

Journal of Chromatography A, 691 (1995) 141–150

JOURNAL OF CHROMATOGRAPHY A

Characteristics and applications of a new high-performance liquid chromatography guard column

Mark Capparella, Walter Foster III, Mark Larrousse, Dorothy J. Phillips*, Arthur Pomfret, Yuri Tuvim

Waters Corporation, 34 Maple Street, Milford, MA 01757, USA

Abstract

A new HPLC guard column has been developed that significantly increases chromatographic efficiencies when placed in series with an analytical column. When compared with other commercially available guard columns, only the Sentry guard column was found to result in increased plates. All other guard columns evaluated resulted in a 10–60% loss of chromatographic efficiency.

By stressing the Sentry guard columns with injections of crude mouse serum it was shown that analytical column lifetimes could be extended. The Sentry guard columns have also been shown to have higher capacity for contaminants than most competitive guard cartridges. Over 8000 injections of a standard mixture have been made on the Symmetry C_8 analytical columns protected by Sentry guard columns with no significant change in the analytical columns' performances.

1. Introduction

Guard cartridge columns are widely used as a cost-effective means of prolonging analytical HPLC column lifetime [1–4]. They protect the analytical column from particles, sub-particles and molecular contaminants. These contaminants originate from the sample matrix, the mobile phase and/or the HPLC instrumentation (e.g., seals). The ideal guard column is designed to protect the analytical column from any or all three failure modes which are (1) a sample irreversibly adsorbing onto the stationary phase, (2) particulate in the sample plugging the inlet frit and (3) particulate in the sample passing through the frit and plugging the packed bed.

The first protection a guard column provides is a highly porous frit made of either stainless steel or an inert material that filters particles larger than its pore size. Particulate debris builds up on the guard column, resulting in an increase in backpressure. This problem is corrected on an unprotected analytical column by cleaning or changing the inlet filter, providing that the column design permits this operation. The analytical column can also be cleaned by reversing the flow direction in order to force the particulate out of the column [1].

The sub-particulate debris can pass through the column frit. The HPLC column can act as a depth filter for this sub-particulate debris, trapping these particles at the head of the column. This can result in a change in hydrodynamic flow at the column entrance which may have unfavorable effects on column performance (peak tailing and/or splitting). One common example of sub-

* Corresponding author.

0021-9673/95/$09.50
SSDI 0021-9673(94)01002-1

particulates that can affect column performance are proteins. Injection of an aqueous protein sample on to a reversed-phase column may result in precipitation of the protein on the top of the column bed because of both filtration and adsorption. In an unprotected column this type of contamination would lead to an irreparable failure. The guard column protects the analytical column from this sub-particulate debris; this type of contamination leads to an increase in backpressure for the guard column.

Adsorption of significant amounts of molecular contaminants may mask the chromatographic surface and result in deviations in absorption behavior. Such molecular adsorption can cause changes in retention (reduction in k'), distorted peak shapes and a decrease in column performance. In this case the unprotected column would have to be washed with a strong solvent to recover performance.

The designs of most guard cartridges allow particulate and chemical contaminants to be removed; however, typical guard columns are usually poorly packed to keep costs low. This results in a significant reduction in the performance of the analytical column. Some guard cartridges cause as much as a 60% decrease in efficiency.

This report discusses a new guard column that not only has high capacity for mechanical and chemical filtration but also increases the efficiency of the analytical column. The efficiency and capacity of the Sentry guard column were compared to those of other commercial guard columns. Lifetime studies were done with Nova-Pak and Symmetry reversed-phase columns to show how the Sentry guard column extends column lifetime.

2. Experimental

2.1. Materials and reagents

Sulfanilamide, sulfadiazine, sulfathiazole, sulfamerazine, sulfamethazine and succinylsulfathiazole were from Sigma (St. Louis, MO, USA). Carbamazepine, carbamazepine-10,11-epoxide, 2-ethyl-2-phenylmalonamide, primidone, phenytoin and phenobarbital were from Alltech (Deerfield, IL, USA). Mouse serum came from BioProducts for Science (Indianapolis, IN, USA). Acetonitrile, acetone, methanol, trifluoroacetic acid, acenaphthene and potassium phosphate, dibasic were from J.T. Baker (Phillipsburg, NJ, USA). Glacial acetic acid and potassium phosphate, monobasic were from EM Science (Cherry Hill, NJ, USA).

Sentry guard columns, Nova-Pak C_{18} and Symmetry C_8 columns were from Waters (Milford, MA, USA). Direct-Connect guard columns with Econosil (10 μm C_{18}) and with Adsorbosphere (5 μm C_{18}) (10 mm × 4.6 mm) were from Alltech. Upchurch ODS cartridge (10 mm × 4.3 mm) was from Upchurch Scientific (Oak Harbor, WA, USA). Zorbax Reliance Rx-C_8 (12.5 mm × 4.0 mm) was from MAC-MOD Analytical (Chadds Ford, PA, USA). Brownlee MPLC NewGuard cartridge (RP-18) and holder came from Applied Biosystems (Foster City, CA, USA).

The 0.45-μm Millex HV filter unit was from Millipore. The Eppendorf micro centrifuge Model 5415C was supplied by Brinkmann Instruments (Westbury, NY, USA). The Mistral column thermostat was from Euramark (Euro-American Marketing Groups, Mount Prospect, IL, USA). The Rheodyne injector is manufactured by Rheodyne (Cotati, CA, USA).

2.2. HPLC systems

The efficiency measurements on the guard columns alone and with the analytical column were performed using a low-dispersion or microbore HPLC system. The microbore system included the Waters 625 LC System, the Waters 484 tunable absorbance detector fitted with a microbore cell, and a Model 7520 Rheodyne injector equipped with a 0.5-μl polyether ether ketone (PEEK) rotor. This system had a bandspread of 30 μl at 0.2 ml/min flow-rate.

The lifetime studies with crude and spiked mouse serum were done on a Waters 625 LC System, a Waters 484 tunable absorbance detector or the Model 490 multiwavelength detector

and either a Waters Model 715 autoinjector or the WISP Model 712. The lifetime study with sulfa drugs used the Waters 590 programmable solvent-delivery module, Waters Model 440 absorbance detector and the WISP Model 712.

All data were acquired and analyzed using the Waters 845 Station with System Suitability Software Package and ExpertEase version 3.0.

2.3. Efficiency measurements

The plate count sample was prepared by dissolving 200 mg acenaphthene in 50 ml acetonitrile and then adding two 10-ml portions of water, shaking after each addition. As a void volume marker, 2.4 ml of acetone were added to the plate count sample. The injection volume was 0.5 ml.

The flow-rates for the efficiency measurements were 0.5 and 0.7 ml/min, respectively, for the 3.9 mm and 4.6 mm I.D. columns. The mobile phase was acetonitrile–water (50:50, v/v).

The efficiencies of the guard columns were measured on the microbore HPLC system, as well as the efficiencies of the analytical columns alone and in series with the guard columns. The guard columns and analytical columns that were connected in series were matched by the packing chemistry and the column inner diameter.

2.4. Extra-column band broadening

When a guard column is placed in series with an analytical column, the efficiency expected for the column alone ($N_{c,calc}$) can be calculated. The guard column contribution to peak broadening is subtracted out.

$$N_{c,calc} = \frac{25(t_{c+g} - t_g)^2}{w^2_{c+g4.4} - w^2_{g4.4}}$$

where t_{c+g} is the retention time of the analyte with the guard column in line, t_g is the retention time of the analyte for the guard column alone, $w_{c+g4.4}$ is the width of the peak at 4.4% of peak height with the guard column in line and $w_{g4.4}$ is the width of the peak at 4.4% of peak height for the guard column alone.

2.5. Lifetime studies

Crude mouse serum

The mouse serum was filtered using a 0.45-μm Millex HV filter unit. The plate count of the Nova-Pak C_{18} column (150 mm × 3.9 mm) in series with a Sentry guard column was measured. Afterward five injections of filtered mouse serum were made. These series of injections (plate count analysis followed by five mouse serum injections) were repeated until the efficiency decreased 50%.

A gradient analysis was done for the mouse serum chromatography. The mobile phases were 0.1% aqueous trifluoroacetic acid (TFA) as solvent A and acetonitrile with 0.1% TFA as solvent B. The gradient was 0 to 100% solvent B in 10 min at 1 ml/min. The wavelength used to monitor absorbance was 254 nm.

Spiked mouse serum

The proteins were removed from the mouse serum by adding two parts acetonitrile to one part serum. After mixing, the sample was centrifuged at 1500 *g* for 5 min and the supernatant decanted and collected. The deproteinated mouse serum was then spiked with the antiepileptic drugs and their metabolites. The final serum sample contained 25 μg/ml of each drug which included carbamazepine, carbamazepine-10,11-epoxide, 2-ethyl-2-phenylmalonamide, primidone, phenytoin and phenobarbital.

The Nova-Pak C_{18} column was tested with and without the Sentry guard column. The mobile phase was 10 m*M* potassium phosphate, pH 7.0–acetonitrile–methanol (110:50:30, v/v/v). The flow-rate was 0.5 ml/min with temperature controlled at 40°C using the Mistral column thermostat. The absorbance was monitored at 214 nm.

The injections of spiked mouse serum were continued until there was a significant change in backpressure, efficiency, retention time or relative retention.

Sulfa drugs

The lifetime studies with the sulfa drugs were on Sentry guard columns in series with the

Symmetry C_8 column (150 mm × 3.9 mm). The mobile phase was water–methanol–glacial acetic acid (79:20:1, v/v/v). The mobile phase was recycled and changed approximately every 1000th injection. The chromatography was monitored at 254 nm and used a flow-rate of 1 ml/min and a run time of 11 min. The temperature was controlled at 25°C using a the Mistral column thermostat. The sample contained 10 μg/ml of sulfanilamide, 25 μg/ml of sulfadiazine and sulfathiazole, 29 μg/ml of sulfamerazine, and 39 μg/ml of sulfamethazine and succinylsulfathiazole. The injection volume of this sample was 10 μl.

Guard columns were changed either when the backpressure increased (30%) or exceeded 3000 p.s.i. (1 p.s.i. = 6894.76 Pa), or when the performance changed (30% decrease in efficiency or relative retention). The retention time and retention factor as well as peak asymmetry were also monitored.

3. Results and discussion

3.1. Guard column efficiency

Table 1 summarizes the results for the plate count tests for the Waters Sentry guard column and other commercial guard cartridges. The efficiency of the Sentry guard column approached analytical values (1000 plates/cm). The Alltech Direct-Connect Econosil and the Upchurch ODS cartridges have the next highest efficiencies, 480 and 450 plates/cm, respectively. The results for the Brownlee NewGuard, Zorbax Reliance and Direct-Connect Adsorbosphere guard cartridges are not close to analytical column values.

The geometry of the hardware and the packing process have an impact on the efficiency of the guard cartridge. In order to achieve efficiencies similar to those of analytical columns the guard columns should be filled by a high-performance packing technique. Dry filling or low-pressure packing probably contributed to the lower efficiencies observed for the guard cartridges. A high-pressure packing process using a slurry was developed for the Sentry guard columns to give both high efficiency and a stable bed.

3.2. Effect of guard column on HPLC column efficiency

A typical 5-μm Symmetry C_8 column (150 mm × 3.9 mm) had 12 400 plates. The 3.9 mm and 4.6 mm Nova-Pak C_{18} columns (150 mm length) averaged 13 200 and 14 000 plates, respectively. The 4-μm Nova-Pak columns were used with all commercial cartridges except the Zorbax Reliance cartridge. The Zorbax Rx-C_8 (150 mm × 4.6 mm) which had 11 500 plates was used with the Zorbax Reliance guard cartridge.

The diameters of the analytical columns and those of the guard columns were matched as closely as possible. The 4.6 mm Nova-Pak C_{18}

Table 1
Efficiencies of commercial guard columns

Guard Column	Dimensions	No. of plates
Waters Sentry Nova-Pak C_{18} (4 μm)	20 mm × 3.9 mm	2000
Alltech Direct-Connect	10 mm × 4.6 mm	
Econosil C_{18} (10 μm)		480
Adsorbosphere C_{18} (5 μm)		280
Brownlee MPLC NewGuard RP-18 (7 μm)	15 mm × 3.2 mm	90
Upchurch ODS Cartridge (5 μm)	10 mm × 4.6 mm	450
Zorbax Reliance Rx-C_8 (5 μm)	12.5 mm × 4.0 mm	60

The guard columns were analyzed on a microbore HPLC system. The mobile phase was acetonitrile–water (50:50, v/v). The sample contained acenaphthene (2.9 mg/ml) and acetone (34 μl/ml). The flow-rate was adjusted on the basis of the guard column inner diameter in order for all analysies to be at the same linear velocity (0.5 ml/min for 3.9 mm I.D. column). All analyses were at 254 nm.

column was used with the Alltech and Upchurch guard cartridges (4.6 mm I.D.) whereas the 3.9 mm column was used with the Brownlee cartridge (3.2 mm). Fig. 1 shows the effects of the guard cartridges on the analytical columns' efficiencies. The plate counts for the Nova-Pak C_{18} and Symmetry C_8 columns (150 mm × 3.9 mm) were enhanced when they were in series with the corresponding Sentry guard columns. The Direct-Connect Adsorbosphere cartridge caused only a slight decrease (2% lower) in the efficiency of the Nova-Pak C_{18} column. Greater decreases in the efficiency of the analytical columns were noted when placed in series with the other cartridges. A 60% decrease in plates was observed for the Zorbax Rx-C_8 column when the Zorbax Reliance Rx-C_8 cartridge was put in line.

A decrease in efficiency is expected when the diameter of the guard column is greater than that of the analytical column or when there is a large difference in particle size [2,5]. The deterioration in performance due to the guard column having the larger diameter has been well documented by users of the Waters Guard-Pak cartridges (5 mm I.D.) with the 3.9 mm I.D. HPLC columns. We observed a 30% decrease in plate count of the Nova-Pak column when in series with a Guard-Pak cartridge. No effects from inner diameter should have been apparent in this study since the guard and analytical columns were matched. In addition, particle size did not vary significantly in most cases. The only exception was the Direct-Connect Econosil cartridge that contains 10-μm particles and was used with the 4-μm Nova-Pak column. Therefore, the fact that the Direct-Connect Econosil cartridge caused the greatest decrease in efficiency for the Nova-Pak column

Table 2
Extra-column effects from guard column: plate counts for Nova-Pak columns

	No. of plates	
	Column length 50 mm	Column length 150 mm
Measured (column alone)	3900	13 200
Calculated (minus Sentry guard column contribution)	3500	12 800
Change (%)	−10	−3

Plate counts were measured for the Nova-Pak C_{18} columns (150 mm and 50 mm × 3.9 mm I.D.) alone and in series with the Sentry guard column. The sample contained acenaphthene (2.9 mg/ml) and acetone (34 μl/ml). The data are for the acenaphthene peak at 254 nm. Mobile phase was acetonitrile–water (50:50, v/v) at a flow-rate of 0.5 ml/min. See Experimental section for equation for calculations.

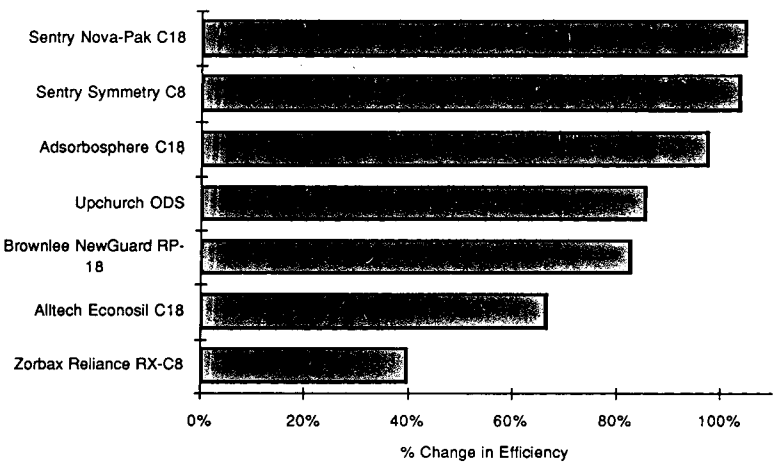

Fig. 1. Effect of guard columns on HPLC columns' efficiencies. Analytical column, Nova-Pak C_{18} (150 mm × 3.9 mm or 4.6 mm) except Zorbax Rx-C_8 (150 mm × 4.6 mm) with Zorbax Reliance cartridge. See Table 1 for dimensions of guard columns. Mobile phase, acetonitrile–water (50:50, v/v); flow-rate 0.5 ml/min for 3.9 mm I.D. and 0.7 ml/min for 4.6 mm I.D column; detection, 254 nm. The sample was 0.5 μl injection of acenaphthene (2.9 mg/ml) and acetone (34 μl/ml) in acetonitrile–water (70:30, v/v).

could be partially related to differences in particle size.

Extra-column volume was minimized by using low-dead-volume compression fittings and a minimal length of narrow-bore tubing (≤ 0.01 in. I.D., 1 in. = 2.54 cm)) to connect the guard cartridge to the analytical column [2,4]. The depression in analytical column efficiency is probably related to the efficiency of the guard cartridge itself. Most of the guard columns were not packed efficiently as noted in Table 1.

Since the Sentry guard column enhanced the analytical column efficiency, it was assumed that this guard column did not contribute to band broadening. When a guard column is placed in series with an analytical column the efficiency expected for the column alone can be calculated [4]. The guard column contribution to peak broadening is subtracted out. Using the formula given in the Experimental section, the plate count for the analytical column alone was calculated ($N_{c,calc}$) and compared to the measured value. The data are in Table 2. The % change in Table 2 is a qualitative measure of the contribution to peak broadening not merely due to volume increase by the guard column. The Sentry guard column showed little additional peak broadening, therefore, acting as an extension of the HPLC column length. These results support the enhancement of efficiency by this guard column.

In summary, the Sentry guard column causes an increase in efficiency when added to an analytical column. The design of the Sentry

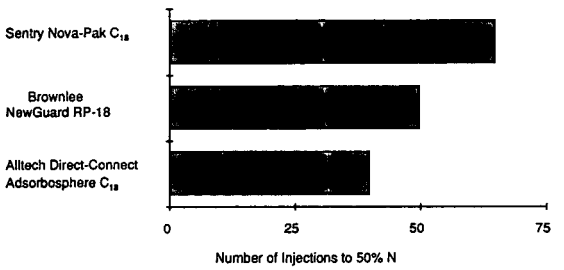

Fig. 3. Number of injections of crude mouse serum before a 50% decrease in plate count. Plate count measured following each set of five mouse serum injections. Figs. 1 and 2 give methods for plate count measurement and mouse serum injections, respectively.

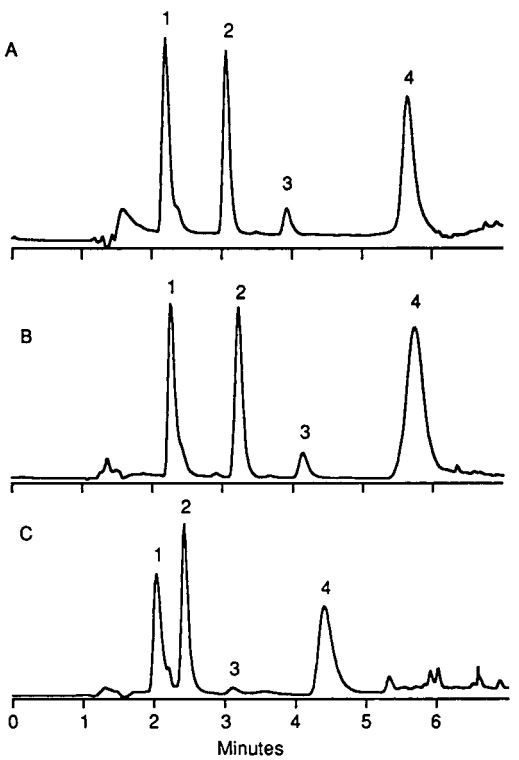

Fig. 2. Crude mouse serum capacity test with and without Sentry guard column. Analytical column, Nova-Pak C_{18} (150 mm × 3.9 mm) with and without Nova-Pak C_{18} Sentry guard column. Mobile phase A, 0.1% aqueous trifluoroacetic acid (TFA); mobile phase B acetonitrile with 0.1% TFA; gradient, 0 to 100% B in 10 min; flow-rate, 1 ml/min; detection, 254 nm. The sample was 10 μl filtered mouse serum. (A), (B) First and 55th injections, respectively, of mouse serum on column with Sentry guard column; (C) 55th injection on unprotected column. (The peaks were not identified; they are general serum proteins.)

Table 3
Change from 1st to 200th injection of spiked mouse serum

	Change (%)			
	Column alone		Column with Sentry	
	Peak 4	Peak 6	Peak 4	Peak 6
Retention time	−3.2	−4.5	2.6	2.8
Plates	−17	−10	2.3	−3.7

Experimental conditions same as in Fig. 4. Peaks 4 and 6 (from Fig. 4) = carbamazepine-10,11-epoxide and carbamazepine, respectively.

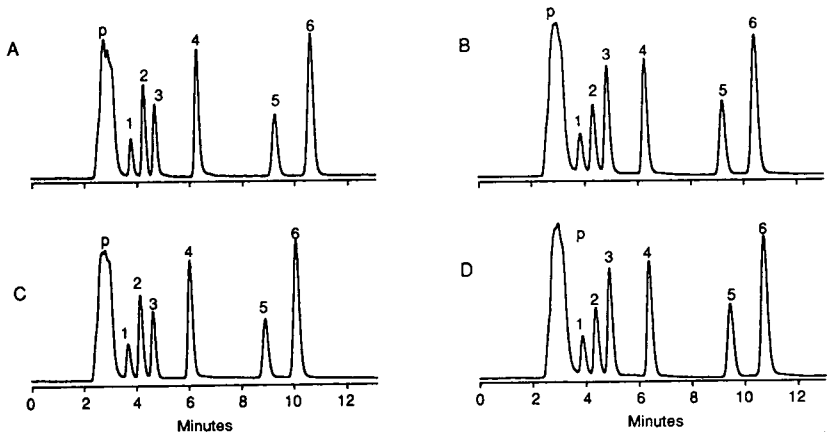

Fig. 4. Effect of guard column on column lifetime with spiked mouse serum sample. Analytical column, Nova-Pak C_{18} (150 mm × 4.6 mm); mobile phase, 10 m*M* potassium phosphate, pH 7.0–acetonitrile–methanol (110:50:30, v/v/v); flow-rate, 0.5 ml/min; temperature, 40°C; detection, 214 nm; injection volume, 5 μl of sample with 25 μg/ml of each component in mouse serum. Peaks: p = serum matrix; 1 = phenylethyl malonamide; 2 = primidone; 3 = phenobarbital; 4 = carbamazepine-10,11-epoxide; 5 = phenytoin; 6 = carbamazepine (see Fig. 5 for chemical structures). (A), (B) First injection on analytical column without and with matching Sentry guard column, respectively; (C), (D) 200th injection on analytical column without and with matching Sentry guard column, respectively.

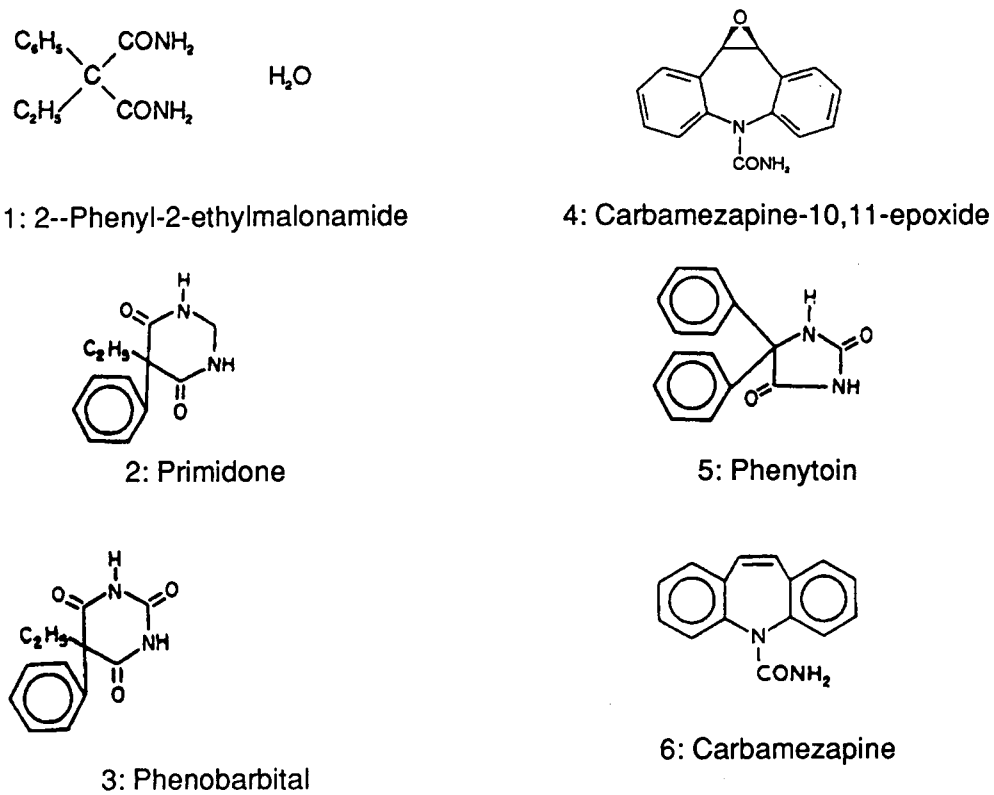

Fig. 5. Structures of antiepileptic drugs and metabolites in Fig. 4.

guard column and the high quality of the packed bed are the reasons for this increase in efficiency. The Sentry guard column length (2 cm) increases the total packed bed length which should theoretically increase plate count. The Sentry guard column does not cause extra-column band-spreading because its diameter is the same or less than that of the analytical columns. Therefore, the expected increase in efficiency due to length is observed. The combination of the Sentry guard column with the analytical column has a higher plate count than the analytical column alone.

3.3. Crude mouse serum capacity test

An important benefit of the guard column is to protect the analytical column from debris. The guard column should be used anytime a sample contains anything that can be irreversibly bound to the analytical column. Mouse serum contains proteins that are not completely removed with each gradient run. Therefore, an accumulation of particulate debris and molecular contaminants on the guard columns was expected with this sample. The chromatography for the mouse serum injections on Nova-Pak C_{18} columns (150 mm × 3.9 mm) with and without the Sentry guard column are given in Fig. 2. The chromatography in Fig. 2C shows a major change after 55 injections on an unguarded Nova-Pak column; molecular contaminants resulted in a change in chromatographic performance. This column went high pressure after 59 injections probably due to the inlet frit being plugged. The addition of the Sentry guard column extended the lifetime of the column to more than 70 injections with no apparent changes in performance.

The data in Fig. 3 show the number of injections of mouse serum before the original plate count decreased 50%. The numbers are the average values for three different guard columns each in series with a Nova-Pak C_{18} column. The Sentry guard column withstood over 70 injections whereas the Brownlee NewGuard RP-18 cartridge and the Alltech Direct-Connect Adsorbosphere cartridge failed after less than 50 injections. The greater volume of the Sentry guard column (0.24 ml) than the Brownlee (0.12 ml) or the Upchurch (0.17 ml) cartridges probably contributed to its increased capacity for mouse serum. The efficiency of the guard column may also play a role in its ability to distribute the debris over the bed prior to failure. A poorly packed bed is more likely to result in poorer hydrodynamics that are most affected by subparticulate (such as protein) accumulation.

3.4. Spiked mouse serum capacity test

The pre-clinical and clinical studies for the approval of a new drug require analysis of the parent drug and its metabolites. The desire is to have HPLC columns that are used for this application be able to withstand several hundred

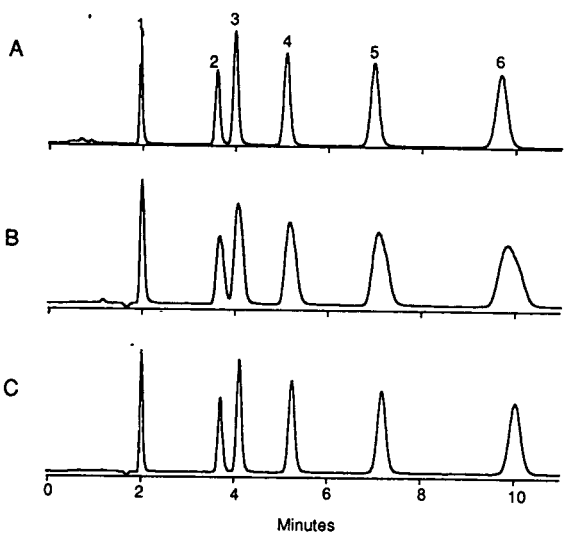

Fig. 6. Extension of column lifetime with guard column using a mixture of sulfa drugs as the sample. Analytical column, Symmetry C_8 (150 mm × 3.9 mm) with matching Sentry guard column; mobile phase, water–methanol–glacial acetic acid (79:20:1, v/v/v); flow-rate, 1 ml/min; temperature, 25°C; detection, 254 nm; injection volume, 10 μl of sulfa drug mixture (10 to 39 μg/ml of each drug). Peaks: 1 = sulfanilamide; 2 = sulfadiazine; 3 = sulfathiazole; 4 = sulfamerazine; 5 = sulfamethazine; 6 = succinylsulfathiazole (see Fig. 7 for chemical structures). (A) Initial injection on Symmetry C_8 Sentry guard column, (B) after 550 injections on same Sentry guard column, (C) new Sentry guard column for injection 551 on analytical column.

injections before chemical or mechanical failure. The guard column is a valuable tool for preserving column lifetime for these analyses. The Sentry guard column was effective in extending the lifetime of the Nova-Pak C_{18} column that was subjected to repeated injections of spiked mouse serum. The initial chromatography with and without the guard column in Figs. 4A and 4B for the antiepileptic drugs (primidone, carbamazepine and phenytoin) and their metabolites were very similar. After 200 injections a noticeable change was observed in the chromatography for the column alone in Fig. 4C. Table 3 quantitates the difference in the protected and unprotected column after 200 injections. On the unprotected Nova-Pak column the peaks for carbamazepine and its metabolite, carbamazepine-10,11-epoxide, had shifted in retention times as much as 4.5% and decreased in efficiency up to 17%. In contrast, the Nova-Pak column in series with the Sentry guard column continued to perform well with an improvement in the plate count for carbamazepine-10,11-epoxide. The unprotected column showed a change in retention time and peak shape probably from molecular contaminants (small molecules in deproteinated serum).

3.5. Lifetime study with standards

The Sentry guard columns with the Symmetry C_8 packing has prolonged the life of the Symmetry C_8 columns (150 mm × 3.9 mm). The Sentry guard column has been changed every time the pressure increased approximately 500 p.s.i. which was the predominant failure mode during the study. The guard column was also changed when performance deteriorated as noted by decreased resolution and plate count. Fig. 6 gives an example of the ability of the guard column to extend column lifetime. Fig. 6A shows the chromatography for the first sulfa drug injection on a new guard column; all peaks are sharp and there is baseline resolution between peaks 2 and 3. After 550 injections on this Sentry guard column the peaks became very broad leading to a loss of the baseline resolution between peaks 2 and 3 as shown in Fig. 6B.

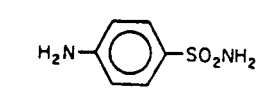

1: Sulfanilamide

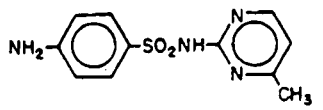

4: Sulfamerazine

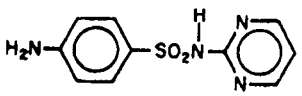

2: Sulfadiazine

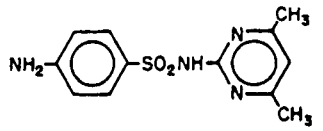

5: Sulfamethazine

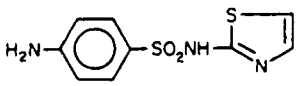

3: Sulfathiazole

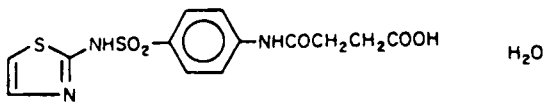

6: Succinylsulfathiazole

Fig. 7. Structures of sulfa drugs in Fig. 6.

When a new guard column was put in line the chromatography returned to that observed originally as noted in Fig. 6C. The analytical column was not damaged and its use was continued for many more injections; over 8000 injections were obtained on these Symmetry C_8 columns. The average number of injections per guard column was approximately 800. By changing the guard column at regular intervals the life of the analytical column can be increased. The guard column is considered the disposable part of the HPLC system and used to maintain the analytical column [3].

4. Conclusions

The Sentry guard column connected in series with an analytical column enhances the performance of the HPLC column. Guard cartridges that are less efficiently packed result in decreased chromatographic performance.

All guard columns tested extended the lifetime of the analytical column. The Sentry guard column was the most effective of the commercial guard cartridges tested in prolonging column lifetime. The lifetime studies stress the importance of changing the guard column regularly for maximum protection of the analytical column.

In summary, the Sentry guard column has been designed to protect the HPLC analytical column from deleterious contaminants without compromising chromatographic performance.

References

[1] D.R. Gere, *LC·GC*, 11 (1993) 708.
[2] H. McNair, *LC·GC*, 10 (1992).
[3] J. Dolan, *LC·GC*, 11 (1993) 790
[4] J.J. Kirkland, W.W. Yau, H.J. Stoklosa, and C.H. Dilks, Jr., *J. Chromatogr. Sci.*, 15 (1977) 303.
[5] U. Neue, personal communication.

ELSEVIER

Journal of Chromatography A, 691 (1995) 151–162

JOURNAL OF CHROMATOGRAPHY A

Reversed-phase high-performance liquid chromatography using enhanced-fluidity mobile phases

Yi Cui, Susan V. Olesik*

Department of Chemistry, The Ohio State University, 120 West 18th Avenue, Columbus, OH 43210, USA

Abstract

The use of enhanced-fluidity liquids in reversed-phase HPLC separations is characterized. Enhanced fluidi liquids are commonly used liquids with high proportions of low viscosity fluids, such as carbon dioxide, added. When carbon dioxide is added to the methanol–water mobile phase, substantially lower plate heights and time of analysis are achieved without losing mobile phase solvent strength. The results indicate that these improvements are caused by the combination of the increased diffusivity of the enhanced-fluidity solvents and the ability of carbon dioxide to readily break hydrogen bonds in the methanol–water mixtures.

1. Introduction

High-performance liquid chromatography (HPLC) is often used to separate non-volatile compounds. However, HPLC does have limitations. HPLC typically has longer analysis times and lower efficiencies than supercritical fluid chromatography (SFC). The primary cause of these deficiencies is the low rate of diffusion in liquids compared to that in supercritical fluids. Liquids have diffusion coefficients on the order of 10^{-5} cm^2/s compared to $10^{-4} - 10^{-3}$ cm^2/s for supercritical fluids. Yet, SFC is incapable of separating highly polar compounds.

We previously showed that liquid mobile phases with enhanced fluidity could provide HPLC some of the advantages of SFC, such as decreased time of analysis without losing a significant advantage of liquids which is high solvent strength [1]. To produce these enhanced-fluidity solvents, large proportions of low viscosity liquids are dissolved in common eluents used for HPLC. The previous work was a demonstration of the advantage of using methanol–CO_2 mixtures as the eluent in porous glassy carbon HPLC.

In this paper, we describe the use of enhanced-fluidity solvents in reversed-phase HPLC. The most common eluents used in HPLC are mixtures of water with methanol or acetonitrile. There are substantial drawbacks to the use of methanol–water mixtures as eluents. The methanol–water mixture viscosity is larger than that of the components. For example, at 50% (w/w) methanol (or 0.56 mole ratio methanol–water), the mixture viscosity is approximately twice the viscosity of water [2]. In addition, high viscosities will lower efficiencies and increase the time of analysis. This paper describes the use of methanol–water–carbon dioxide mixtures as eluents for reversed-phase HPLC. We hypothesized that the addition of substantial portions of carbon dioxide to the mixture would decrease

* Corresponding author.

0021-9673/95/$09.50
SSDI 0021-9673(94)00878-7

the mixture viscosity without affecting the solvent strength substantially.

2. Theory

The theory involved in the use of enhanced-fluidity solvents in HPLC was described in detail previously [1]. The details pertinent to reversed-phase separations are reviewed herein. In reversed-phase liquid chromatography the predominant contribution to band dispersion is commonly diffusion in the stagnant mobile phase inside the porous packing. Using the Knox equation [3], the C term, that describes the non-equilibrium between the mobile phase and the stationary phase, is a function of capacity factor, k', and an inverse function of D_m, the diffusion coefficient of the analyte in the mobile phase and $u_{min} \propto D_m/[f(k')]^{1/2}$. If by lowering the viscosity, the diffusion coefficients of the solutes can be increased without a substantial increase in k', then the time of analysis should decrease and efficiency should increase in reversed-phase separations by addition of carbon dioxide to the mobile phase.

The mobile phase system chosen for analysis includes a constant methanol–water mole ratio of 2.3 with carbon dioxide added to it in proportions that varies from 0 to 0.5 mole fraction. This methanol–water mixture is commonly used as an eluent in isocratic HPLC separations and its viscosity is approximately 1.5 times that of water [2]. Three polynuclear aromatic hydrocarbons (PAHs), naphthalene, phenanthrene and pyrene were used as test analytes.

2.1. Analyte diffusion coefficients

Two models were used to predict the binary diffusion coefficients of the analytes in these enhanced fluidity mixtures, the modified Wilke–Chang [4] (Eqs. 1 and 2) and Perkins–Geankoplis [5] (Eq. 3). Both theories have been successful in predicting diffusion coefficients in mixed liquids.

$$D_{Am} = 7.4 \cdot 10^{-8} \cdot \frac{(\phi M)^{1/2} T}{\eta_m V_A^{0.6}} \quad (1)$$

$$\phi M = \sum (x_i \phi_i M_i) \quad (2)$$

where D_{Am} is the diffusion coefficient of solute A in mixture m, η_m is the mixture viscosity, V_A is the molar volume of solute A at its normal boiling temperature, T is temperature, x_i is mole fraction, ϕ_i is the Wilke–Chang association constant of solvent component i and M_i is molecular mass of solvent component i.

$$D_{Am}\eta_m^{0.8} = \sum x_i D_{Ai} \eta_i^{0.8} \quad (3)$$

where x_i is mole fraction of i in the mixture; η_i is the viscosity of pure i and D_{Ai} is the diffusion coefficient of A in pure component i. The viscosities of the methanol–water–CO_2 mixtures (Fig. 1) were calculated using the Teja–Rice method [6–8]. The viscosities of methanol and water were corrected for operating pressures using the estimation technique of Lucas [9]. Literatures values of the viscosity of CO_2 at various pressures were used [10]. The accuracy of the viscosity predictions using the pressure-modified Teja–Rice method was estimated by comparison with experimentally measured viscosities of methanol–CO_2 mixtures [1]. The

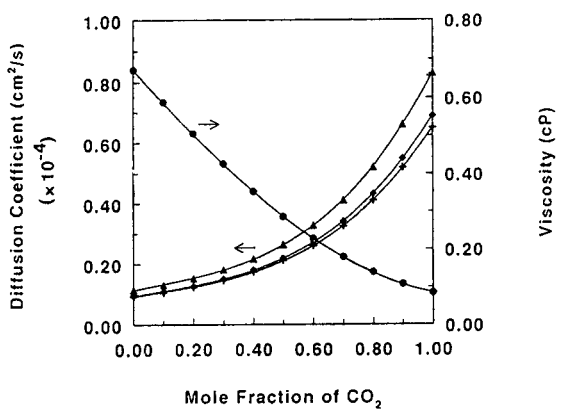

Fig. 1. Calculated diffusion coefficients of naphthalene (▲), phenanthrene (◆), pyrene (+), and viscosities (○) of methanol–water–CO_2 mixtures at 25°C and 204 atm with methanol–water mole ratio held at 2.3.

viscosity predictions were within 5% of the experimental values.

To evaluate the accuracy of each model for predicting the diffusion coefficients of solutes in enhanced-fluidity liquids, experimental diffusion coefficients of methanol–CO_2 mixtures [11] were compared to the predictions. The predicted diffusion coefficients were within 5% of the experimental values. Fig. 1 shows the predicted average diffusion coefficients for the analytes as a function of solvent composition calculated using Eqs. 1–3. The calculated diffusion coefficient of naphthalene varied from $1.2 \cdot 10^{-5}$ to $2.7 \cdot 10^{-5}$ cm^2/s when the mole fraction of CO_2 varied from 0 to 0.5.

3. Experimental

3.1. Column preparation

A packed capillary column containing Adsorbosphere octadecyl polysiloxane-coated 5-μm silica particles with 80 Å pore size (Alltech, Deerfield, IL, USA) was used in this study. The column was prepared by slurry packing the particles in acetonitrile with 1% Triton X-100 surfactant (Aldrich, Milwaukee, WI, USA) [12]. The ODS particles were held in the fused-silica column with a microbore end-fitting (U-434, Upchurch Scientific, Oak Harbor, WA, USA) that contained a 2-μm frit (C407 ×, Upchurch Scientific). The ODS slurry was placed in a 15 cm × 5 mm I.D. stainless-steel tube (used as a reservoir) and then pushed into a 30 cm × 320 μm I.D. fused-silica tube (Polymicro Technologies, Phoenix, AZ, USA). The pressure was increased gradually up to approximately 300 atm (1 atm = 101 325 Pa), then maintained at that pressure for at least 2 h. The column was depressurized overnight by turning off the pump and allowing the whole system to gradually approach atmospheric pressure.

3.2. Chromatographic system

The chromatographic system used in this study was similar to that used in the previous study of enhanced-fluidity HPLC [1]. The instrumentation included an ISCO (Lincoln, NE, USA) LC-2600 syringe pump, a Valco (Houston, TX, USA) W-series high-pressure injection valve with an internal injection volume of 60 nl, and a Spectroflow 757 UV–Vis absorbance detector (Kratos, Ramsey, NJ, USA). The detector wavelength was 254 nm. The end of the chromatographic column was connected with a zero-dead-volume fitting to a piece of 100-μm I.D. fused-silica tubing. The polyimide coating was removed from a 5-mm length of this tubing to create the detection cell. A 5- or 10-μm I.D. fused-silica restricting tube was placed after the detector to control the linear velocity in the column. As in SFC, the flow restrictor is a necessary part of the chromatographic system. Additionally, in enhanced-fluidity HPLC, the column pressure must be maintained above a minimum pressure to avoid having the mobile phase mixture separate into two phases (liquid–gas). For example, for 0 and 0.5 mole fractions of CO_2 the necessary column outlet pressures were 61 and 82 atm, respectively [13]. The column inlet pressure was maintained at 204 atm throughout the study. Sodium nitrite, methylene chloride and acetone were considered as possible non-retained markers. The retention times of all three compounds were the same across the whole mixture composition range. Acetone was used as the non-retained marker because the concentration needed to provide an observed response was least.

3.3. Materials

The analyte test mixture was a methanol solution containing 0.4 mg/ml naphthalene and 0.5 mg/ml each of phenanthrene and pyrene. All solvents and analytes were obtained from Aldrich with purity levels of $\geq 98\%$. Supercritical fluid-grade CO_2 was obtained from Scott Specialty Gases (Plumsteadville, PA, USA). Methanol–water–CO_2 mixtures were prepared by using two syringe pumps. A 2.3 mole ratio mixture of methanol and water of a given volume was placed in a syringe pump. The liquid CO_2 was maintained at 272 atm and room

temperature in another syringe pump. From the known density of CO_2 under these conditions, the requisite volume of CO_2 was added to the methanol–water mixture in the other syringe pump to make a given solution composition. The final solution was pressurized to 204 atm, and equilibrated at 25°C for at least 12 h.

3.4. Data collection and analysis

An IBM-AT-compatible computer was used for all data collection and analysis. The chromatograms were collected at a sampling rate of 10 points/s using a DT2821 12-bit, 50 kHz analog-to-digital converter (Data Translations, Marlboro, MA, USA). Data analysis was accomplished by using original programs written in the ASYST programming environment (Keithley Data Acquisition Div., Taunton, MA, USA). Post-run analysis included calculation of the zeroth, first and second statistical moments of a given chromatographic band. The second statistical moment was used to determine the experimental plate heights. A Gaussian peak of known variance was overlayed onto the experimental chromatographic band to allow visual confirmation of the second statistical moment.

4. Results and discussion

4.1. Evaluation of column bed quality

Before the properties of reversed-phase separations using enhanced-fluidity mobile phases were determined, the integrity of the column bed was evaluated. The flow resistance parameter, φ, is often used to evaluate the quality of the packing structure in the chromatographic column. The flow resistance parameter is defined as:

$$\varphi = \frac{\Delta P t_0 d_p^2}{\eta L_c^2} \quad (4)$$

where ΔP is the pressure drop along the column, t_0 is the dead time of the column, d_p is the packing particle diameter, η is the eluent viscosity and L_c is the column length. A well-packed column of spherical particles should have a φ value between 500 and 1000 [14]. Higher values of the flow resistance parameter are indicative of crushed packing or the presence of too many fines in the column packing. The slurry-packed ODS column with the 2.3 mole ratio mixture of methanol and water as mobile phase had a flow resistance parameter of 775 which is well within the acceptable range for a well-packed column. Fig. 2 shows the variation of the flow resistance parameter with mobile phase composition. The flow resistance parameter decreased with increased percent CO_2 in the mobile phase.

Another characteristic which is commonly used to evaluate columns is the total porosity, ϵ_T, which is defined as the following equation:

$$\epsilon_T = \frac{F_v t_0}{r_c^2 L_c \pi} \quad (5)$$

where F_v is the volumetric flow-rate and r_c is the column radius. With a mixture of water and methanol, the slurry-packed ODS column had a total porosity, $\epsilon_T = 0.723$. The total porosity is the sum of the column interparticle porosity, ϵ_u, and intraparticle porosity, ϵ_i. Estimates of ϵ_u and ϵ_i can be determined by non-chromatographic methods, e.g. mercury porosimetry. However, porosities measured with Hg may not accurately represent the pore structure observed by the

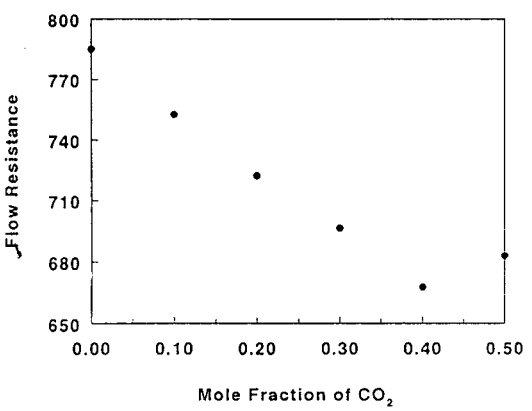

Fig. 2. Dependence of the flow resistance on mole fraction of CO_2 in the mobile phase with methanol–water mole ratio held at 2.3.

analytes in the column. The column interparticle porosities were determined with the modified Kozeny–Carman equation [15]:

$$\varphi = 180\psi^2 \cdot \frac{(1-\epsilon_u)^2\epsilon_T}{\epsilon_u^3} \quad (6)$$

where ψ^2 is a structural factor which is equal to 1 for spherical packing [15]. The intraparticle porosity was then determined by difference, $\epsilon_T - \epsilon_u$. Both experimental values of interparticle porosity, $\epsilon_u = 0.394$, and intraparticle porosity, $\epsilon_i = 0.329$ correspond well with those reported by other groups for similar well-packed ODS columns [15–17].

4.2. Retention

The expected gains in chromatographic efficiency and lowering of the analysis time is predicated on the assumption that the capacity factor will not increase significantly with added carbon dioxide. Fig. 3 shows the change in the capacity factors (k') versus the mole fraction of added CO_2 in the mobile phase. For all three analytes, the retention decreased with added CO_2. From 0–0.3 mole fraction CO_2 in the mobile phase, capacity factors decreased 38, 51 and 54% for naphthalene, phenanthrene and pyrene, respectively. However, over the range of 0.3–0.50 mole fraction CO_2, the analyte retention remained fairly constant.

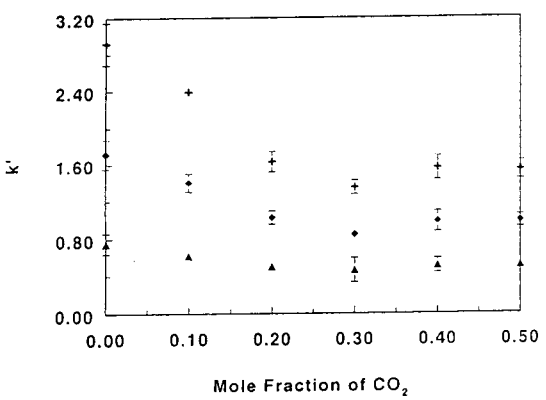

Fig. 3. Variation of capacity factors with mole fraction of CO_2 in the mobile phase when the methanol–water mole ratio is held at 2.3. ▲ = Naphthalene; ◆ = phenanthrene; + = pyrene.

4.3. Solvent strength measurement

To better understand the eluent strength of the methanol–water–CO_2 mixtures a study of solvent strength variation with added CO_2 was undertaken. Kamlet–Taft solvatochromic parameters, π^*, α and β were measured for the mixed methanol–water–CO_2 eluent (Fig. 4). The specific details of the solvatochromic measurements were described in a previous work [1]. These methods are also similar to those used by Kamlet et al. [18] and Cheong and Carr [19]. Both π^* and α decrease slowly when the percentage of CO_2 in the mobile phase increased, while β increased with added CO_2.

In a previous publication [1], we measured the solvent strength variation that occurred when 0 to 100% carbon dioxide was added to methanol. The addition of carbon dioxide had negligible effect on the measured α and β values until more than 60% carbon dioxide was added and for CO_2 concentrations higher than 60%, the observed decrease in the α and β parameters was similar. The minimal change in the hydrogen-bond acidity or basicity was believed to be caused by carbon dioxide functioning as a struc-

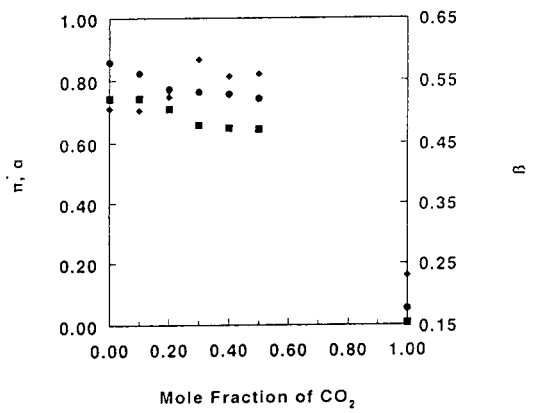

Fig. 4. Variation of experimentally measured Kamlet–Taft parameters with mole fraction of CO_2 in the mobile phase when the methanol–water mole ratio is held at 2.3. The standard error for π^* (□), α (○) and β (◆) are ± 0.02, ± 0.06 and ± 0.04, respectively.

ture breaker, lowering the extent of self-association in methanol and therefore maintaining the hydrogen-bond acidity and basicity of the mixture. In the same methanol–CO_2 mixture, the π^* value decreased by approximately 50% over the 0–60% CO_2 composition range. The solvent strength variation in the methanol–water–CO_2 system is much different with added CO_2 than the methanol–CO_2 system. α and π^* decrease by approximately 10% over the range of 0–0.5 mole fraction CO_2 and the β value increases with added CO_2. Also a marked increase in H-bond basicity is observed between 0.2 and 0.40 mole fraction of added CO_2. Liquid CO_2 has solvent strength parameters of $\alpha = 0.05$, $\pi^* = 0.07$ and $\beta = 0.23$ at 170 atm and 25°C (Fig. 4). Again the CO_2 is decreasing the hydrogen-bond association in the solvent. Otherwise the solvent strength would decrease montonically with added CO_2. Methanol ($\beta = 0.62$) is a much stronger H-bond base than CO_2 or water ($\beta = 0.18$). Therefore monomeric methanol is probably being released from hydrogen-bond self-association or methanol–water hydrogen-bond association to cause the observed increase in H-bond basicity.

Sadek et al. [20] first showed that solute hydrogen-bond basicity and to a lesser extent solute dipolarity were important in establishing retention behavior in reversed-phase separations using ODS. Increases in the hydrogen-bond basicity and dipolarity of solutes lead to decreased retention. Solute hydrogen-bond acidity variation did not seem to impact the measured retention. Accordingly, changing to mobile phases with decreased acidity should also cause decrease solute retention because of expected increased affinity of the solutes for the mobile phase.

The observed decrease in α over the same eluent composition region where the substantial decrease in retention occurs may mean that solvent hydrogen-bond acidity is important in controlling the retention in this reversed-phase ODS system similar to what Sadek et al. [20] described in their system. However, solvent polarity is not the only factor typically involved in the retention of PAH compounds on reversed-phase stationary phases. The shape or structure of the stationary phase also affects the retention of PAH molecules [21,22]. We show later in this paper that the ordering of the stationary phase or mobile phase is also substantially affected by the addition of CO_2 to the eluent.

4.4. Chromatographic efficiency

The separation of naphthalene, phenanthrene and pyrene was complete for all of the mobile phase compositions studied. The column efficiency was measured using an eluent composition that varied from 0 to 0.5 mole fraction CO_2 with the mole ratio of methanol–water maintained at 2.3. The inlet pressure was maintained at 204 atm, and temperature was maintained at 25°C throughout these measurements. The maximum mobile phase velocity was limited by the minimum pressure necessary to keep the eluent mixture one phase at the end of the column. As described in the Experimental section, with increasing proportions of CO_2 in the mobile phase, higher post-column pressure was necessary. Therefore, the maximum possible linear velocity decreased with added CO_2. As Fig. 5 shows, linear velocities higher than typically used in HPLC were readily achieved with the chosen experimental conditions. If higher linear velocities than those in Fig. 5 are desired, this can be readily achieved by increasing the column inlet pressure. We chose however to standardize the study by maintaining the column inlet pressure at 204 atm.

Fig. 5 illustrates the variation in the reduced plate height versus reduced velocity for the three analytes under different mobile phase compositions. Each data point is an average of 2–3 values to ensure the precision of the results. Using Eq. 7, these values were also corrected for the band dispersion contribution caused by the connecting tubing which included the detector volume (see Experimental section).

$$\sigma_T^2 = \frac{\pi^2 r_T^6 L_T u_T}{24 D_m} \quad (7)$$

σ_T^2 is the connecting tube volumetric variance, r_T is the tube radius, L_T is the tube length, u_T is the linear velocity within the tube, and D_m is the

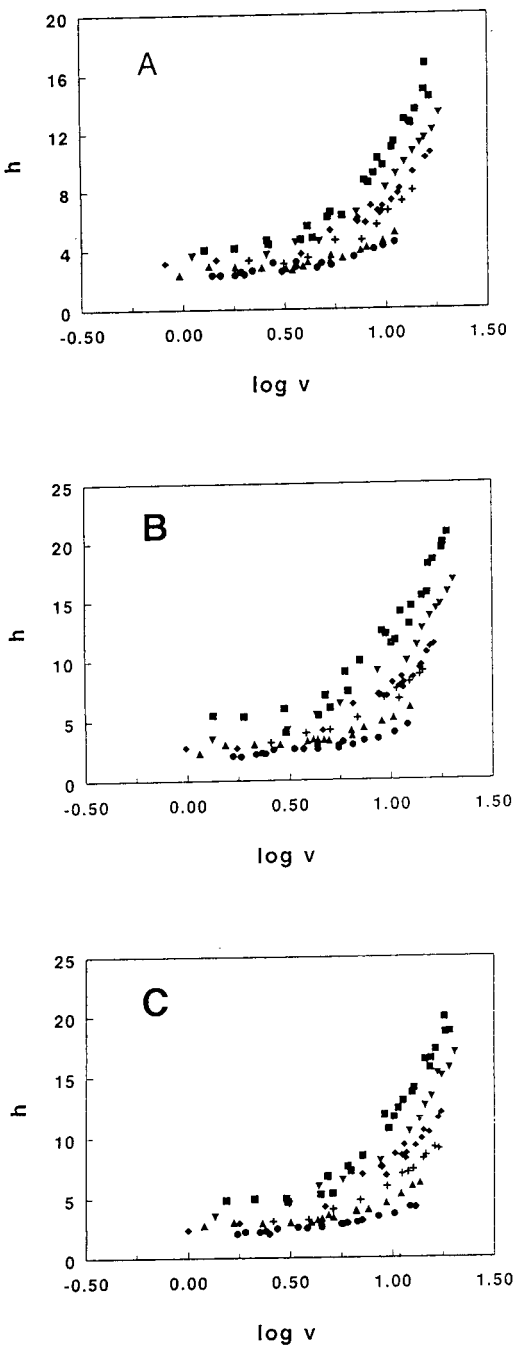

Fig. 5. Reduced plate height (h) of (A) naphthalene, (B) phenanthrene and (C) pyrene vs. reduced linear velocity (ν). □ = methanol–water; ▼ = 0.1 CO_2 mole fraction; ◆ = 0.2 CO_2 mole fraction; + = 0.3 CO_2 mole fraction; ▲ = 0.4 CO_2 mole fraction; ○ = 0.5 CO_2 mole fraction in the methanol–water–CO_2 mobile phase when the methanol–water mole ratio is held at 2.3.

solute binary diffusion coefficient. The contribution to band dispersion caused by the interconnecting tubing caused 2% error in the band dispersion at the lowest linear velocities and 5% error at the highest velocity studied. Other extracolumn sources of error contributed $<1\%$. No effort was taken to correct the measured peak widths for such small errors. The curves for all three analytes are very similar. With increasing CO_2 in the eluent, the reduced plate height decreased across the entire velocity range studied. However, the decrease in plate height was marked at high velocities. For example, at a reduced velocity of 2, the reduced plate height for naphthalene changed from 4 (or $H = 0.02$ mm) to 2 (or $H = 0.01$ mm) for a change in eluent composition of 0 to 0.5 mole fraction CO_2; however for a reduced velocity of 10, the reduced plate height for naphthalene decreased from 11 to 4 for the same eluent composition change.

To better understand the chromatographic band dispersion process involved in this system the data in Fig. 5 were fit to the Knox equation [3]. The Knox equation is defined as:

$$h = A\nu^{1/3} + B/\nu + C\nu \tag{8}$$

where h is the reduced plate height and ν is the reduced linear velocity. $A\nu^{1/3}$ describes the band dispersion from flow anisotropy in the mobile phase and $C\nu$ describes the band dispersion caused by mass transfer between the mobile and stationary phases. B/ν describes the dispersion caused by axial molecular diffusion, and it contributes to the total band dispersion only when ν is smaller than 2. When the B term was included in the fitting equation, it was found to be statistically insignificant because the low-velocity region was not sampled in this study. Therefore the final equation used to fit the experimental data included only the flow anisotropy and mass transfer terms at $\nu > 2$. All the fitted equations had coefficients of correlation for the fits, $r \geq 0.95$. Fig. 6 shows the change in coefficients A and C with added CO_2 in the mobile phase.

Typical values of the constant A for a well packed column are approximately 1. A values greater than 2 or 3 indicate a poorly packed

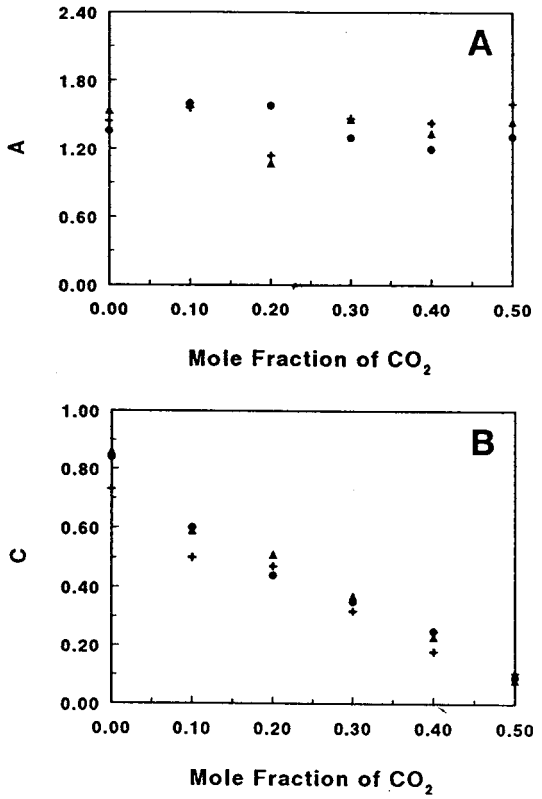

Fig. 6. Variation of (A) flow anisotropy, A term and (B) mass transfer resistant, C term with mole fraction of CO_2 in the mobile phase when methanol–water mole ratio is held at 2.3. The average standard errors for the A and C terms are ± 0.1 and ± 0.04, respectively.

column [3,23]. For all three analytes, the constant A varied from 1–1.5 with no trend with composition change observed. The last constant in the Knox equation is the C term, the sum of resistance to mass transfer and the kinetics of analyte desorption from the stationary phase. In Fig. 6B, the C terms of all three analytes are plotted versus the mole fraction CO_2 in the mobile phase. With no added CO_2, the C values are approximately 0.75–0.85. Karlsson and Novotny [24] recently reported a C value of 0.37 for a 265-μm I.D. capillary column packed with 5-μm ODS coated silica particles. They also showed that the value of the measured C term increased with the internal diameter of the microcolumn. The internal diameter of the column used in this study was larger, 320 μm. However, it is highly doubtful that this small difference in column internal diameter would cause the C value to double. A more logical cause of the differences in the measured C values is the different mobile phases used in each study. Karlsson and Novotny used acetonitrile–water and we used methanol–water. The viscosity difference between the mixture and the pure components is much larger for the methanol–water mobile phase than in the acetonitrile–water mobile phase. In addition, as more CO_2 was added to the methanol–water system, the C terms for all the analytes decreased dramatically to values as low as $C = 0.08$ for naphthalene with 0.5 mole fraction CO_2. The C terms also did not vary significantly among the analytes studied which indicates that the trend in C term was not caused by capacity factor variation.

The most likely causes of the large C coefficient with the methanol–water mobile phase include: unaccounted extra-column band broadening such as injection profile, column quality, or slow kinetics associated with the reversible binding of the PAH compounds by the stationary phase. We believe the primary cause of the large C coefficient is slow kinetics. Using the theoretical model of Karger et al. [25], the band dispersion caused by the injection profile was calculated to be less than 1% of the total measured variance and was therefore considered negligible. The quality of the column was documented early in this paper and other results that are described later will further substantiate its integrity.

Eq. 9 is the relationship derived by Horváth and Lin [26,27] which describes the dispersion in the stagnant mobile phase inside the pores of the particles (C_{stag}) and the kinetics of desorption at the stationary phase (C_{kin}).

$$C = C_{stag} + C_{kin} = \frac{\theta(k_0 + k' + k_0k')^2}{30k_0(1 + k_0)^2(1 + k')^2} + \frac{2k'D_m}{(1 + k_0)(1 + k')^2d_p^2k_d} \cdot \nu \quad (9)$$

D_m is the diffusion coefficient of the analyte in a

given solvent, θ is the tortuosity factor for the porous packing and k_0 is the ratio of the intraparticulate void volume to the interstitial void space in the column (which can be experimentally determined from the intraparticular and interstitial porosities), k_d is the desorption rate constant and d_p is particle diameter of the column packing. Using our experimental data and Eq. 9 the band broadening caused by diffusion in the stagnant mobile phase of the pores was predicted. Then this value was subtracted from the total C value to provide an estimate of the proportion of the band broadening caused by slow desorption kinetics, C_{kin}. The estimated diffusion coefficients described previously were then substituted into the expression for C_{kin} to allow the calculation of an approximate k_d. This calculation was used to show the order of magnitude changes in the rate constant. Table 1 shows the variation of the desorption rate constant as a function of added CO_2 to the mobile phase. The rate constant increased significantly with added CO_2.

The plate height contribution caused by slow desorption kinetics is inversely related to the desorption rate constant and the particle size. Horváth and Lin [27] predicted significant band dispersion contributions from kinetic resistance for ODS particle sizes less than 6 μm. Others have also reported the significance of kinetic resistance in reversed-phase HPLC [28]. However, the cause of the low desorption rate was not discussed. When methanol–water mobile phases are used, the evidence below indicates the major cause of slow desorption kinetics is the formation of a polar hydrogen-bonded layer of water or water–methanol on the stationary phase surface. When increasing quantities of CO_2 are added to the methanol–water eluent, structure breaking of the hydrogen-bonded layer occurs and the desorption rate constant increases.

Fig. 7 shows data that supports this hypothesis. β-Naphthol and naphthalene have similar capacity factors across the entire eluent composition range. For example, for the eluent with methanol–water mole ratio of 2.3, the capacity factors of naphthalene and β-naphthol were 0.75 and 0.28, respectively. However, the reduced plate height of each chromatographic band was different as shown in Fig. 7. The slope of the β-naphthol curve, which mainly represents the effect of the C term contributions, is smaller than that of naphthalene. The hydroxyl on β-naphthol may allow ready movement of naphthol

Table 1
Calculation of rate constants of the desorption kinetics

Analyte	Mole fraction of CO_2	Calculated C_{stag}	Observed C (i.e., $C_{stag} + C_{kin}$)	Calculated k_d (s^{-1})
Naphthalene	0.00	0.091	0.73	19
	0.10	0.084	0.50	32
	0.20	0.077	0.47	37
	0.30	0.075	0.31	70
	0.40	0.078	0.17	209
Phenanthrene	0.00	0.12	0.86	13
	0.10	0.11	0.59	24
	0.20	0.10	0.51	34
	0.30	0.095	0.37	59
	0.40	0.10	0.23	152
Pyrene	0.00	0.14	0.84	11
	0.10	0.13	0.60	21
	0.20	0.12	0.44	40
	0.30	0.11	0.35	65
	0.40	0.11	0.25	137

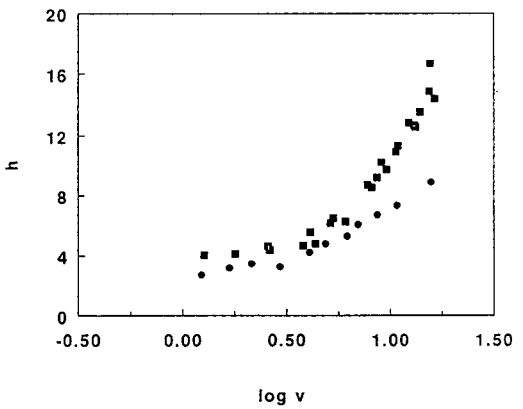

Fig. 7. Plots of reduced plate height (h) of naphthalene (□) and naphthol (○) vs. reduced linear velocity (v) when methanol–water mixture was used as mobile phase.

through the structured layer above the ODS phase; while naphthalene has more difficulty.

Our hypothesis of the existence of the hydrogen-bonded surface layer that is broken by increasing proportions of carbon dioxide is also compatible with the predominance of other published information in stationary phase composition, structure and polarity. Yonker et al. [29] proposed a ternary component model of the stationary phase that was composed of a combination of silica substrate, bonded organic moiety and solvated layer consisting of mobile phase components. For the methanol–water composition used in our study, Yonker et al. [29] proposed a "brush"-like solvated stationary phase structure in which the C_{18} chains become erect and minimal intermolecular interactions between individual chains occurs. Also at this composition, the individual C_{18} chains were believed to be highly solvated by the methanol in the system which resulted in liquid-like motion of the C_{18} chains and partitioning into the chain structure as part of the retention mechanism. However, more recent NMR studies of ODS motion in methanol–water solutions comparable to those used herein shows that the ODS chain motion under these conditions is highly hindered. Gangoda and Gilpin [30] showed that the ^{13}C NMR spectrum of ODS solvated with a methanol–water (60:40, v/v) mixture (0.67 mole ratio), was very similar to that of unsolvated ODS. This was contrasted to the NMR spectrum of ODS solvated with pure methanol which had line shapes that were liquid-like. If a highly order hydrogen-bonded surface layer of water and methanol were sheathing the ODS, then the observed hindered chain motion could be rationalized.

This proposed structure is also compatible with the present understanding of the microstructure of the methanol–water solvent. For solutions of methanol–water where the methanol concentration is significantly higher than that of water, such as the mixture used in this study, two different statistical mechanical simulations [31,32] predicted that hydrophobic solvation of the methanol molecules cause ca. sixteen self-associated water molecules to form a cage around the methyl portion of the alcohol; whiie the hydroxyl portion of the alcohol forms hydrogen bonds with only ca. 2.6 water molecules. Similar engagement of the C_{18} phase by associated water or a water–methanol sheath may be causing the observed low desorption rate constant for naphthalene and the interaction with ODS when solvated in the 2.3 methanol–water mole ratio eluent.

4.5. Time of analysis

In the previous section, improvements in efficiency were demonstrated. However, instead of simply improving efficiency of a separation, a more practical goal is to increase resolution per unit time and therefore decrease the time of analysis. If the time of analysis, t, is defined as the retention time of the last eluting peak, then Eq. 10 shows the relationship between experimentally controlled chromatographic variables and t for the separation of two analytes.

$$t = 16R_s^2 \cdot \left(\frac{\alpha}{\alpha - 1}\right)^2 \cdot \left(\frac{(1+k')^3}{k^2}\right) \cdot \left(\frac{H}{u}\right) \qquad (10)$$

where t is time of analysis, R_s is resolution, α is separation factor, k' is capacity factor of the peak, H is the plate height and u is the mobile

phase linear velocity. Once the chromatographic system is chosen (stationary phase, solvent, solute, etc.), capacity factors and the separation factor are constants. Therefore, when R_s is fixed for a required separation, the ratio of H to u must be minimized to decrease time of analysis not H itself.

Fig. 8 shows the variation of H/u versus u for the methanol–water mixture and for the methanol–water mixture with 0.5 mole fraction CO_2 added for naphthalene. When methanol–water was the eluent, the H/u ratio reached a minimum value for a linear velocity of 0.15 cm/s or reduced linear velocity of ca. 5. The H/u ratio for the eluent with 0.5 mole fraction CO_2 does not reach a minimum until linear velocities of 0.4–0.5 cm/s are reached. Also, the mobile phase with 0.5 mole fraction CO_2 shorten the analysis time by factors of 2.5 and 8 at linear velocity of 0.15 ($\nu = 5$) and 0.35 ($\nu = 17$) cm/s, respectively. If a specific analysis time is required, the low H/u value at high velocity for the eluent with added CO_2 will allow longer column lengths to be used without losing resolution. Because the permeability of the column is much higher when CO_2 is added to the mobile phase, very long packed capillary columns should be possible at workable inlet pressures for the separation of highly complicated samples.

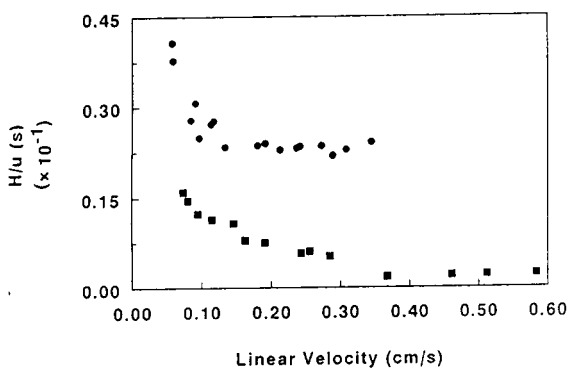

Fig. 8. Variation of the ratio of plate height to linear velocity with mole fraction of CO_2 in the mobile phase for naphthalene. ■ = 0.5 Mole fraction of CO_2 in the methanol–water–CO_2 mobile phase with the methanol–water mole ratio held at 2.3; ● = methanol–water mixture as mobile phase.

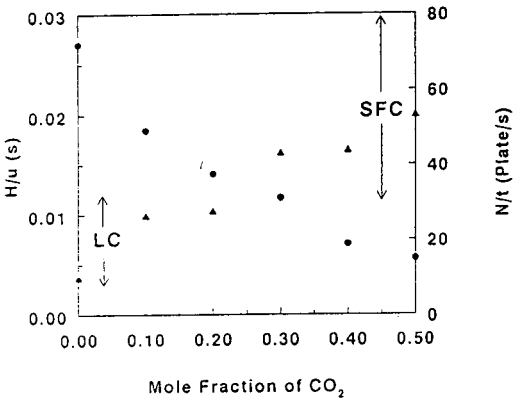

Fig. 9. Variation of observed number of plates per unit time, N/s (▲) and the ratio of plate height to the mobile phase linear velocity, H/u (●) with mole fraction of CO_2 in the mobile phase when the methanol–water mole ratio was maintained at 2.3. Vertical lines show typical N/s values in HPLC and SFC.

Finally, Fig. 9 shows the variation in the H/u and N/t (number of theoretical plates per unit time) ratios as a function of added CO_2 for naphthalene at a reduced linear velocity of 5. The range of N/t for standard packed HPLC and packed SFC with 5-μm particles is also marked [33]. Clearly, as expected the use of enhanced-fluidity mobile phases moves the measured N/t into a range larger than found in standard HPLC and common for SFC.

Acknowledgement

We gratefully acknowledge financial support for this work by the National Science Foundation under Grant CHE-9118913.

References

[1] Y. Cui and S.V. Olesik, *Anal. Chem.*, 63 (1991) 1812.
[2] J. Timmermans, *The Physico-Chemical Constants of Binary Systems in Concentrated Solutions*, Vol. 4, Interscience, New York, 1960, p.162.
[3] J.H. Knox, *J. Chromatogr. Sci.* 15 (1977) 352.
[4] C.R. Wilke and P. Chang, *AIChE J.*, 1 (1955) 264.
[5] L.R. Perkins and C.J. Geankoplis, *Chem. Eng. Sci.*, 24 (1969) 1035.

[6] A.S. Teja and P. Rice, *Chem. Eng. Sci.*, 36 (1981) 7.
[7] A.S. Teja and P. Rice, *Ind. Eng. Chem. Fundam.*, 20 (1981) 77.
[8] P.C. Reid, J.M. Prausnitz and B.E. Poling, *The Properties of Gases and Liquids*, McGraw-Hill, New York, 4th ed., 1987, p. 480.
[9] K. Lucas, *Chem. Ing. Tech.*, 53 (1981) 959.
[10] K. Stephan and K. Lucas, *Viscosity of Dense Fluids*, Plenum Press, New York, 1979, p. 75.
[11] P.R. Sassiat, P. Mourier, M.H. Caude and R.H. Rosset, *Anal. Chem.*, 59 (1987) 1164.
[12] R.T. Kennedy and J.W. Jorgenson, *Anal. Chem.*, 61 (1989) 1128.
[13] T. Chang and R.W. Rousseau, *Fluid Phase Equilib.*, 23 (1985) 243.
[14] J.H. Knox, *J. Chromatogr. Sci.*, 18 (1980) 453.
[15] C.A. Cramers, J.A. Rijks and C.P.M. Schutjes, *Chromatographia*, 14 (1981) 439.
[16] C. Borra, M.H. Soon and M. Novotny, *J. Chromatogr.*, 385 (1987) 75.
[17] R. Ohmacht and I. Halász, *Chromatographia*, 14 (1981) 155.
[18] M.J. Kamlet, J.L.M. Abboud and R.W. Taft, *Prog. Phys. Org. Chem.*, 13 (1983) 485.
[19] W.J. Cheong and P.W. Carr, *Anal. Chem.*, 60 (1988) 820.
[20] P.C. Sadek, P.W. Carr, R.M. Doherty, M.J. Kamlet, R.W. Taft and M.H. Abraham, *Anal. Chem.*, 57 (1985) 2971.
[21] S.A. Wise and L.C. Sander, *J. High Resolut. Chromatogr. Chromatogr. Commun.*, 8 (1985) 248.
[22] K. Jinno and M. Okamoto, *Chromatographia*, 18 (1984) 495.
[23] L.R. Snyder and J.J. Kirkland, *Introduction to Modern Liquid Chromatography*, Wiley, New York, 2nd ed., 1979, p. 836.
[24] K.-E. Karlsson and M. Novotny, *Anal. Chem.*, 60 (1988) 1662.
[25] B.L. Karger, M. Martin and G. Guiochon, *Anal. Chem.*, 46 (1974) 1640.
[26] Cs. Horváth and H.-J. Lin, *J. Chromatogr.*, 126 (1976) 401.
[27] Cs. Horváth and H.-J. Lin, *J. Chromatogr.*, 149 (1978) 43.
[28] R.P.W. Scott and P. Kucera, *J. Chromatogr.*, 169 (1979) 51.
[29] C.R. Yonker, T.A. Zwier and M.F. Burke, *J. Chromatogr.*, 241 (1982) 257.
[30] M.E. Gangoda and R.K. Gilpin, *Langmuir*, 6 (1990) 941.
[31] W.L. Jorgensen and J.D. Madura, *J. Am. Chem. Soc.*, 105 (1983) 1407.
[32] M. Ferrario, M. Haughney, I.R. McDonald and M.L. Klein, *J. Chem. Phys.*, 93 (1990) 5156.
[33] M.L. Lee and K.E. Markides (Editors), *Analytical Supercritical Fluid Chromatography and Extraction*, Chromatography Conferences, Provo, UT, 1990, p. 27.

ELSEVIER

Journal of Chromatography A, 691 (1995) 163–170

JOURNAL OF CHROMATOGRAPHY A

Short communication

Modification of a conventional high-performance liquid chromatography autoinjector for use with capillary liquid chromatography

Richard C. Simpson

Department of Drug Metabolism and Pharmacokinetics, SmithKline Beecham Pharmaceuticals, P.O. Box 1539, King of Prussia, PA 19406, USA

Abstract

This paper will discuss the conversion of a conventional HPLC autoinjector to a format which is suitable for use with capillary HPLC. In addition to the actual modification procedure, the paper will also present data which characterize the performance of the modified injector. These data include items such as precision (approximately 1%), optimal valve loop loading volume (approximately 35–40 μl), and absence of sample carryover between injections.

1. Introduction

Capillary HPLC has several characteristics which make its use attractive in a variety of applications. These attractive features include significantly reduced solvent consumption, enhanced sensitivity when dealing with limited sample volume [1,2], and easy direct interfacing with a mass spectrometer [3–5]. However for any technique to realize its full potential, it must be capable of unattended automated operation. At the present time few autoinjectors are commercially available for use specifically with capillary HPLC, thus slowing its acceptance as a viable and practical technique. Alternatively, individuals performing an initial evaluation of the use of capillary HPLC as related to their specific application may not be willing or able to justify the expense of purchasing a dedicated capillary system autoinjector. This paper will describe the conversion of a conventional HPLC autoinjector to a configuration which is compatible with capillary HPLC, as well as the characterization of the modified autoinjector's performance based upon various experimental parameters.

2. Experimental

2.1. Equipment and supplies

The conventional HPLC autoinjector modified in this procedure was a Model 506 unit (Beckman Instruments, Palo Alto, CA, USA). The microinjector valve (with 0.5- or 1-μl loop volume) was a Model 7526 pneumatically activated unit (Rheodyne, Cotati, CA, USA) connected to a Model 7163 12 V double three-way solenoid valve (Rheodyne). The solenoid valves were activated by the chromatographic system hardware with contact closures directed through a

0021-9673/95/$09.50
SSDI 0021-9673(94)01053-6

Model 201A 12 V d.c. solenoid interface (Autochrom, Milford, MA, USA) operated in the step-input mode. Manual injections were performed with a Model 7520 valve with a 0.5-μl loop volume (Rheodyne). The capillary HPLC columns (150 × 0.32 mm 3-μm C_{18} and 300 × 0.32 mm 5-μm C_{18}) and guard cartridges were purchased from LC Packings (San Francisco, CA, USA). Ultraviolet detection was at 254 nm and was performed using a Model 783 detector (Applied Biosystems, Ramsey, NJ, USA) fitted with a capillary flow cell (LC Packings). The mobile phase was delivered to the system by a L6200A/L6000 binary solvent-delivery system (Hitachi Instruments, Danbury, CT, USA) through an AccuRate flow splitter (LC Packings). For all studies, the mobile phase was delivered to the column at a flow-rate of 4 μl/min. The mobile phase consisted of water–CH_3CN (35:65) for precision and peak height studies and water–CH_3CN (50:50) for column efficiency studies. The mobile phase used for comparison of isocratic and gradient elution consisted of water and CH_3CN (80% CH_3CN for isocratic elution and a linear ramp of 80–90% CH_3CN over a 10-min period for the gradient elution mode). The test probe for peak height and precision studies consisted of acetophenone in water at a concentration of 10 μg/ml with an injection volume of 1 μl. Column efficiency studies were conducted using a commercially available reversed-phase test mixture (Supelco, Bellefonte, PA, USA) diluted 1:1 with water and using a 0.5-μl injection sample loop. The comparison of isocratic and gradient elution modes was performed using a commercially available reversed-phase test mixture in methanol (Hitachi) containing (in elution order) naphthalene (80 μg/ml), anthracene (2.5 μg/ml) and chrysene (3 μg/ml), diluted 1:4 with water and using a 1-μl injection sample loop. Polyether ether ketone (PEEK) tubing and Fingertight fittings were supplied by Upchurch Scientific (Oak Harbor, WA, USA). Chromatographic data were collected and processed using Access*Chrom software (PE/Nelson, Cupertino, CA, USA).

2.2. Autoinjector modification

The actual modification of the standard autoinjector is a relatively straightforward procedure. The standard injection valve is disconnected from the system. The microvalve itself is attached directly to the top of the autoinjector housing. The liquid flow from the pumps is directed into the microvalve by a short length (15–20 cm) of 50 μm I.D. fused-silica capillary tubing between the flow splitter and liquid inlet port on the microvalve. The tubing from the autoinjector syringe is disconnected from the standard valve and connected instead to the waste port of the microvalve. Connection of the microvalve sample inlet (needle) port to the autoinjector needle tower assembly requires removal of the needle port tube assembly from the valve. In its place is inserted a short (approximately 10 cm) length of 0.010 in. I.D. × 1/16 in. O.D. PEEK tubing (1 in. = 2.54 cm), with a Rheodyne ferrule pre-swaged onto the tubing. The PEEK tubing is retained in the microvalve sample inlet port by means of the reduced-diameter compression screw/spring assembly previously used to hold the needle port tube assembly in position. The remaining end of the PEEK tubing is connected to the autoinjector needle tower assembly using a PEEK 1/4·28 Fingertight fitting.

Operation of the system is controlled primarily by contact closure signals from the autoinjector. The valve is initially configured in the "LOAD" position. Upon completion of the sample loading into the sample loop, the autoinjector provides two simultaneous contact closure signals to initiate the chromatographic run. One signal goes to the 12 V solenoid interface which in turn activates the solenoid valves for rotation of the microvalve from the "LOAD" position to the "INJECT" position, thus introducing sample onto the head of the column. The second contact closure signal is directed to the data system to initiate acquisition of chromatographic data. Due to the presence of only two contact closure terminals on the autoinjector, the remaining signals must be generated by the data system and

solvent-delivery system. Immediately upon initiation of data acquisition the data system provides a contact closure signal to start the solvent delivery system timer cycle. At the end of the chromatographic analysis (if the assay used isocratic elution) or column re-equilibration period (if the assay used gradient elution) the solvent delivery system transmits a contact closure signal to the 12 V solenoid interface to return the microvalve to the "LOAD" position and wait for initiation of the next injection.

3. Results and discussion

Initial attempts to use the autoinjector in its standard configuration proved to be unsuccessful. Upon injection of 1 μl of the acetophenone test probe, extreme peak tailing was observed, presumably due to unacceptably large dead volume within the standard valve. Even use of a small volume (5 μl) sample loop did not significantly improve the peak shape to an acceptable degree. An example of the peak obtained with the conventional valve is shown in Fig. 1. The column performance was independently evaluated using the same conditions, but using a manual microvalve, and found not to be the source of the extremely poor peak shape. Thus it became apparent that modification of the autoinjector would be necessary in order to obtain satisfactory performance.

As described above, a simple exchange of the conventional injection valve with the microvalve was not performed. Although such an approach would have been easier it was not possible due to the different angles of travel for the two valves (45° for the microvalve and 60° for the standard valve). However as assembled the modified system retains the same flow path design as in the original system. During sample loop loading, the valve is in the "LOAD" position and the needle is inserted into the sample vial. The syringe withdraws the specified volume from the vial, pulling the sample through the needle, PEEK transfer line, and sample loop. Thus the injector may be described as operating in a "PULL" mode for sample loading. Upon injection (i.e. rotation of the microvalve to the "INJECT" position) the microvalve, PEEK transfer line, and needle are automatically rinsed by the autoinjector wash solvent, just as in the standard autoinjector configuration, thus decreasing or eliminating sample carryover between injections.

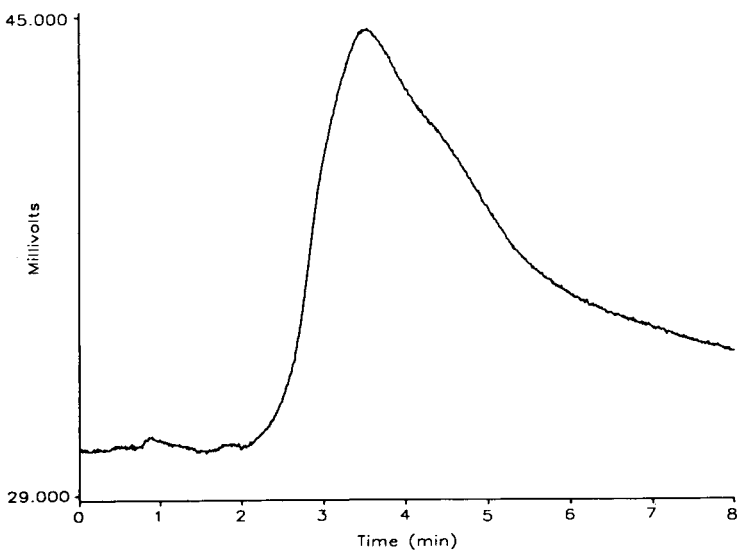

Fig. 1. Chromatographic peak obtained for the acetophenone test probe using the conventional valve on the autoinjector. Mobile phase: water–CH_3CN (35:65) at 4 μl/min. Column: 150 × 0.32 mm 3-μm C_{18} with guard.

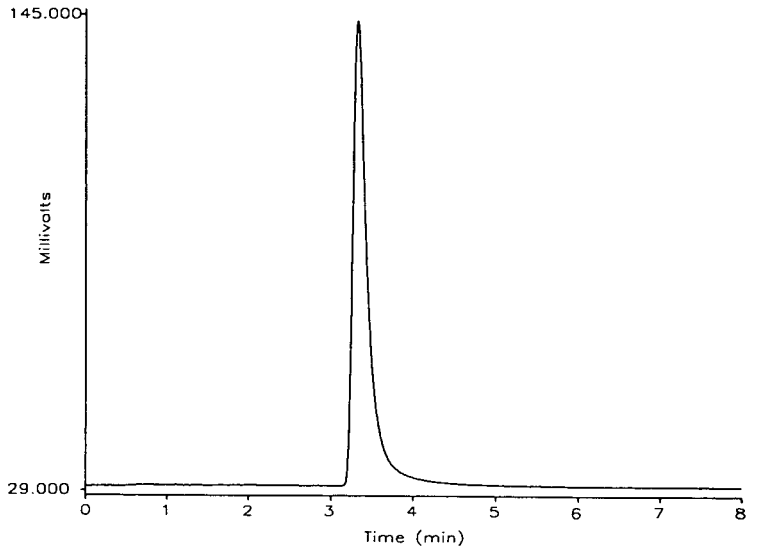

Fig. 2. Chromatographic peak obtained for the acetophenone test probe using the modified autoinjector with the microvalve. Mobile phase: water–CH_3CN (35:65) at 4 μl/min. Column: 150 × 0.32 mm 3-μm C_{18} with guard.

As previously stated, the valve is not returned from the "INJECT" position to the "LOAD" position until just prior to the initiation of a sample injection sequence. This was done specifically to accommodate gradient elution operation. This timing sequence enables use of gradient elution without trapping strong elution solvents in the sample loop which could interfere with the separation of the following sample. Since this event occurs at the end of any column re-equilibration period, use of the HPLC pump system to provide the required contact closure as a timed event is the easiest approach to ensure the valve switch occurs at the very end of any re-equilibration step.

Although only the two initial contact closure signals to initiate sample injection and data acquisition are from the autoinjector, such an arrangement is dictated by the fact that there are only two contact closure switches on the output terminal of the autoinjector used in this study. If more contact closure outputs were available on the autoinjector, it could provide all signals required for operation of the system. Following the above modifications, the acetophenone test probe was again injected onto the system, but

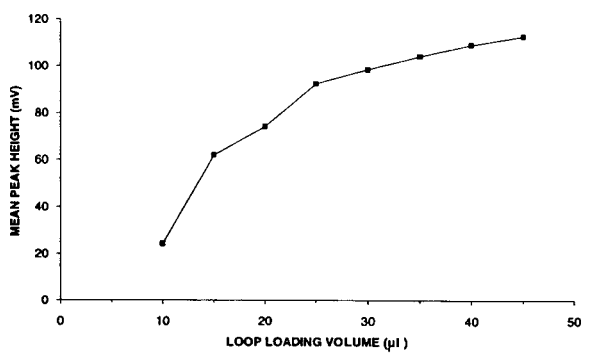

Fig. 3. Average peak height as a function of loop loading volume.

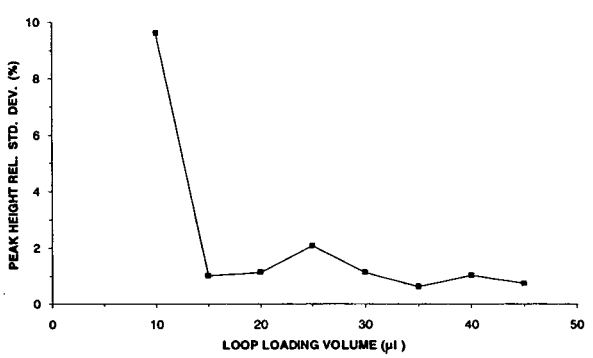

Fig. 4. Peak height relative standard deviation (%) as a function of loop loading volume.

using the modified autoinjector. The peak obtained for a 1-μl injection of the acetophenone probe is shown in Fig. 2. Upon comparison with the results obtained with the standard valve (Fig. 1), the improvement in performance is easily noted.

In order to characterize the performance of the modified autoinjector, a variety of experiments were performed. The first study was designed to determine the optimal loop loading volume (i.e. sample volume withdrawn by the syringe) to fill a 1-μl loop. The study involved making 10 injections at each of a series of loop loading volumes ranging from 10 to 45 μl and monitoring the peak heights obtained. The test analyte used in this study was acetophenone in water (10 μg/ml). The mean peak heights obtained at each loop loading volume are plotted in Fig. 3. As seen in the plot, the response increases dramatically up to loop loading volumes

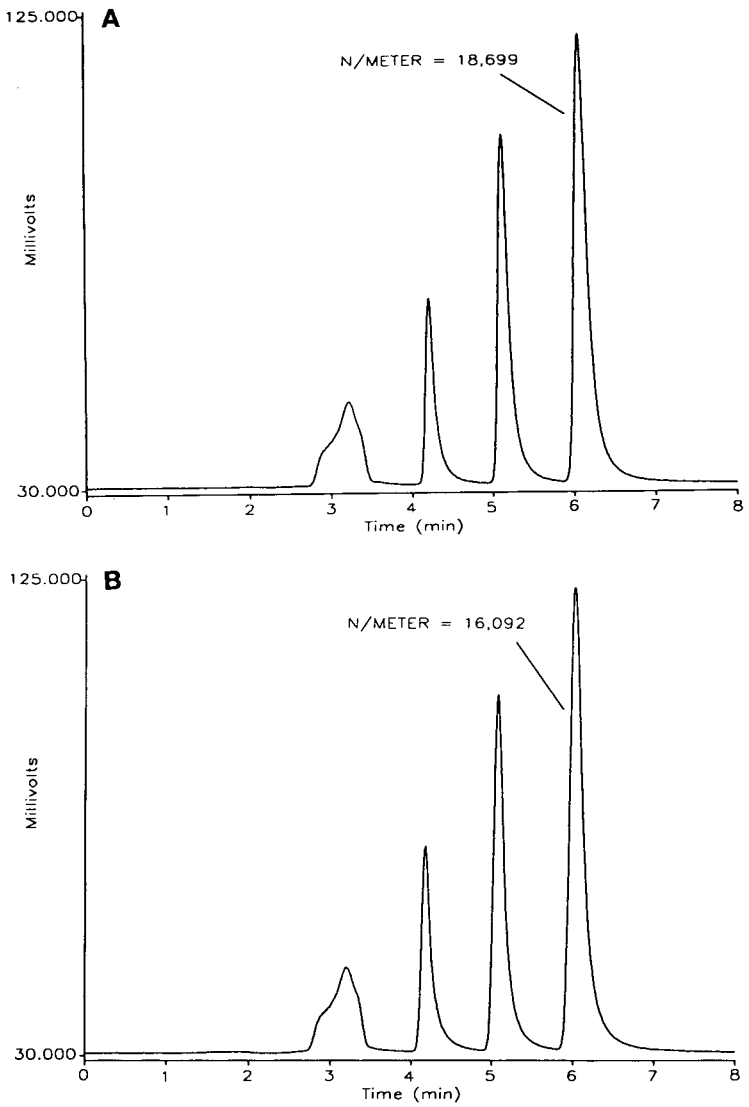

Fig. 5. Chromatographic system efficiency obtained using (A) modified autoinjector and (B) manual microvalve. Mobile phase: water–CH_3CN (50:50) at 4 μl/min. Column: 150 × 0.32 mm 3-μm C_{18} with guard.

of 30–35 μl, with only modest gains beyond that. With a measured needle and PEEK transfer line dead volume of 13 μl (i.e. dead volume between sample vial and sample loop), these data indicate that an approximately 3-fold flush volume of sample is sufficient to give acceptable on-column sample loading.

Not only is sample loading an issue, but so is reproducibility. Fig. 4 presents a plot of the relative standard deviation (R.S.D.) of the peak heights obtained in the loop loading study above. As illustrated in the figure, the variability drops to a fairly constant level in the range of 0.5 to 1% at loop loading volumes of 15 μl or greater. These data in conjunction with those from the loop loading volume study indicate that a loop loading volume of 35–40 μl should provide acceptable performance in terms of adequate sample loading and reproducibility.

Another important issue to consider is whether use of the modified autoinjector will have any adverse effect on column efficiency. Fig. 5 presents two chromatograms of a commercially available reversed-phase test mixture injected using the modified autoinjector and also by a manually operated microvalve. Although the chromatographic conditions used for the separation are not necessarily optimal for the capillary column used, the efficiency data generated indicate that use of the modified autoinjector results in system efficiency equivalent to that obtained with a manual micro-injection system.

The issue of sample carryover was also examined. As stated earlier, the modifications described permit the normal wash cycle of the standard autoinjector to be employed in the modified version. Fig. 6 shows the chromatogram of a blank injection of mobile phase following an injection of the reversed-phase test mixture. As is readily apparent, there is no evidence of any significant sample carryover in the chromatogram. Thus the modified autoinjector exhibits behavior comparable to the normal configuration.

Finally, the use of the modified autoinjector in gradient separations was examined. Fig. 7 shows a comparison of the separation of a three-component test mixture using both isocratic and gradient elution modes following a 1-μl injection by the modified autoinjector. As can be seen in the figure, the modified autoinjector performs well in either mode, thus allowing the automated capillary system to be operated with the same

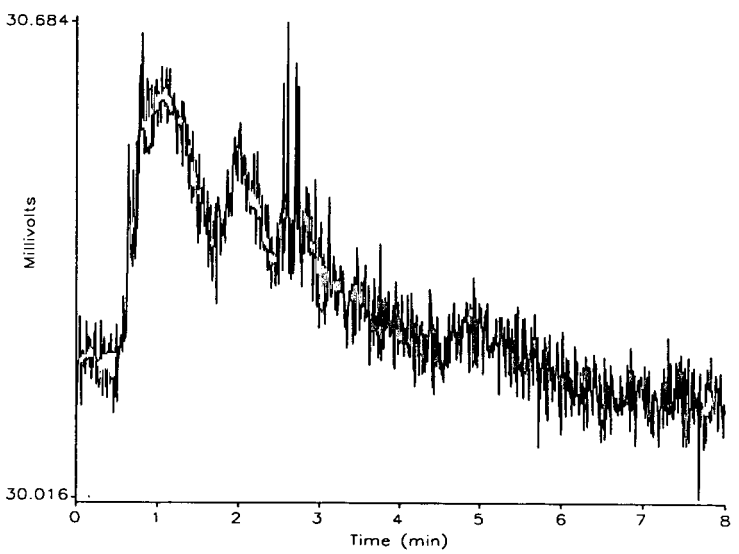

Fig. 6. Blank mobile phase injection following injection of reversed-phase test mixture. No significant sample carryover is observed. Mobile phase: water–CH_3CN (35:65) at 4 μl/min. Column: 150 × 0.32 mm 3-μm C_{18} with guard.

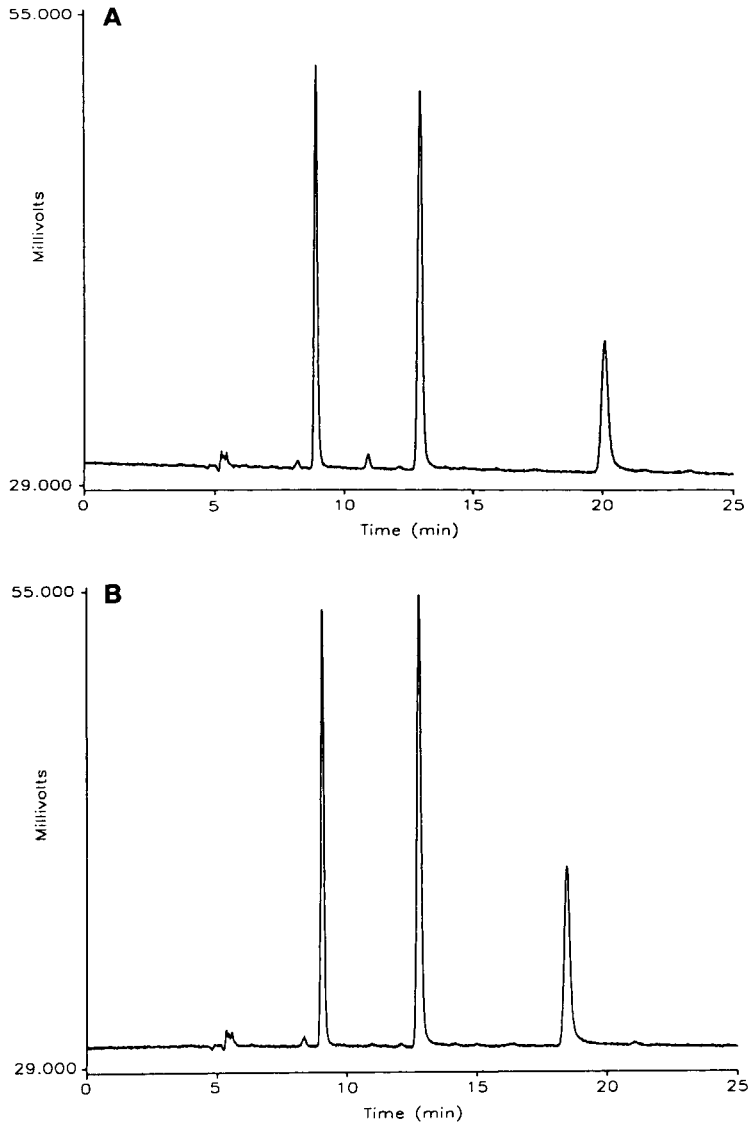

Fig. 7. Comparison of (A) isocratic and (B) gradient separations of a three-component test mixture following injection with the modified autoinjector. Mobile phase solvents: A = water, B = CH_3CN; flow-rate: 4 μl/min. Column: 300 × 0.32 mm 5-μm C_{18} with guard. Isocratic conditions: A–B (20:80). Gradient conditions: 80–90% B linearly over 10 min.

degree of flexibility as can be expected when using an automated conventional HPLC system.

4. Conclusions

This paper has described a straightforward procedure for the modification of a conventional autoinjector to a format acceptable for use with capillary HPLC. Various experimental parameters were investigated to characterize and demonstrate the suitability of the modified system for use in capillary HPLC applications. Although the modifications were applied to a specific model of autoinjector in the current paper, the basic approach should also be generically applic-

able to autoinjectors supplied by different vendors.

References

[1] O. Shirota, D. Rice and M. Novotny, *Anal. Biochem.*, 205 (1992) 189.
[2] M.T. Davis and T.D. Lee, *Protein Sci.*, 1 (1992) 935.
[3] A. Capiello and F. Bruner, *Anal. Chem.*, 65 (1993) 1281.
[4] J.E. Evans, A. Ghosh, B.A. Evans and M.R. Natowicz, *Biol. Mass Spectrom.*, 22 (1993) 331.
[5] J. Liu, K.J. Volk, E.H. Kerns, S.E. Klohr, M.S. Lee and I.E. Rosenberg, *J. Chromatogr.*, 632 (1993) 45.

ELSEVIER

Journal of Chromatography A, 691 (1995) 171–185

JOURNAL OF CHROMATOGRAPHY A

Solvent modulation in liquid chromatography: extension to serially coupled columns

Patrick H. Lukulay, Victoria L. McGuffin*

Department of Chemistry, Michigan State University, East Lansing, MI 48824-1322, USA

Abstract

The concept and theory of solvent modulation are extended to serially coupled columns in liquid chromatography. Because the mobile phases are maintained in separate zones and the stationary phases in separate columns, solute retention is a simple, time-weighted average of the individual environments to which the solute is exposed. Thus, optimization of complex multidimensional chromatographic separations is more accurate and predictable. This approach is demonstrated by application to the separation of isomeric polynuclear aromatic hydrocarbons using octadecylsilica and β-cyclodextrin silica stationary phases with aqueous methanol and acetonitrile mobile phases.

1. Introduction

Liquid chromatography has gained acceptance as the method of choice for the separation of complex mixtures of non-volatile solutes. Solute retention and selectivity are controlled by the physical and chemical properties of both the stationary and mobile phases. In general, optimization is performed in two successive stages: a coarse adjustment is achieved by selection of the appropriate stationary phase(s) and a fine adjustment by means of the mobile phase(s), whose composition can be more readily varied [1,2].

A variety of methods has been developed to optimize the strength and selectivity of the mobile phase. In most of these methods, a preliminary series of experiments is performed to measure solute retention in mobile phases of known composition. From these measurements, the optimum composition for isocratic or gradient elution is predicted by using a predefined mathematical function [3–8]. On the basis of thermodynamic considerations, solute retention is generally considered to be a linear or quadratic function of the composition of the mobile phase [7–9]. This presumption implies that the solute interacts independently with each solvent component of the mobile phase. Unfortunately, molecular interactions are not completely independent of one another in water and many polar organic solvents [10]. This non-ideal behavior limits the accuracy and precision with which solute retention may be predicted using linear or quadratic models [7,11].

To enable the solute to interact independently with each solvent component, several workers have investigated the introduction of the mobile phase as separate zones onto the chromatographic column. Berry [12] has developed a method in which one or more zones of a weak eluent, typically water, are strategically timed to arrive at a pair of unresolved solutes and facilitate their

* Corresponding author.

0021-9673/95/$09.50
SSDI 0021-9673(94)01184-2

separation. Berry et al. [13,14], Gluckman et al. [15], and Little et al. [16] have demonstrated that several zones with different elution properties, such as pH, ion pairing, and hydrophobic interactions, may be used to resolve strong and weak acids and bases as well as neutral solutes. More recently, Wahl et al. [17–19] have generalized this concept and theory for multiple solvent zones that are applied to the column in a random or repeating sequence. Because the solvent zones are spatially and temporally separated, solute retention is controlled independently within each zone. Therefore, the overall retention is a simple time-weighted average of the solute capacity factors in the individual solvent zones. This technique, known as solvent modulation by Wahl et al. [17–19], appears to provide a versatile alternative to premixed mobile phases for the rapid and accurate optimization of separations.

In addition to optimization strategies for the mobile phase, stationary phase optimization has also been implemented to resolve complex mixture of solutes. When a single stationary phase is not sufficient, mixed or multimodal stationary phases have been used to combine dissimilar but compatible retention mechanisms. Mixed phases that have been successfully used include reversed-phase with size exclusion [20–23], cation or anion exchange with size exclusion [23], reversed-phase with cation or anion exchange [24–28], and cation with anion exchange [27,29]. These stationary phases may be combined in several ways: by incorporating or chemically bonding the stationary phases on the same particles (chemically mixed support), by incorporating the phases on different particles that are mixed within a single column (physically mixed support), or by incorporating the phases on different particles that are contained in separate columns connected in series [28]. Isaaq et al. [22] observed that solute retention on chemically or physically mixed supports may not be predictable as a linear function of the stationary phase composition. This non-linear additivity of solute retention may arise as a consequence of interactions between the different stationary phases. On the other hand, retention on serially coupled columns is generally additive and predictable because the stationary phases are physically separated.

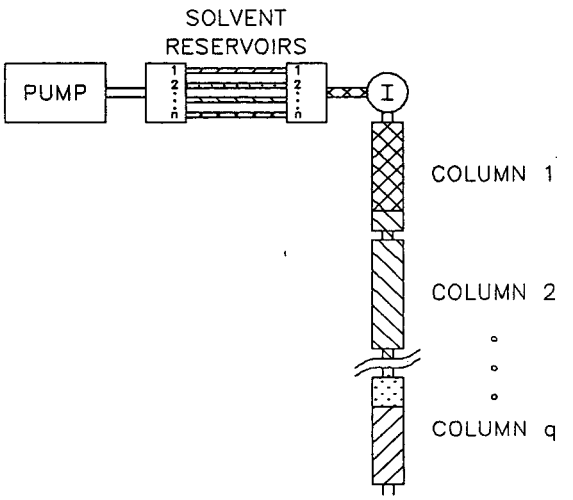

Fig. 1. Schematic illustration of n solvent zones in q serially coupled columns.

In this work, the use of serially coupled columns and solvent modulation is investigated as a viable strategy for the optimization of both stationary and mobile phases. By maintaining the stationary phases in separate columns and the mobile phases as separate zones, the solute will interact independently in each environment (Fig. 1). Thus, overall solute retention will be a simple, predictable function of the capacity factor weighted by the time that the solute is exposed to each stationary and mobile phase. This approach should allow accurate prediction of solute retention and, hence, allow optimization of multidimensional separations with a minimum number of preliminary experiments.

2. Theory

2.1. Theory of solute retention

In order to optimize separations on serially coupled columns under the conditions of solvent modulation, the theoretical basis of retention must be established. The inherent assumption underlying this theory is that solute retention is controlled independently within each solvent zone. In addition, it is assumed that the column is able to achieve steady-state conditions rapidly

after each change of solvent. This latter requirement may restrict the selection of both mobile and stationary phases. The validity of these assumptions has been demonstrated previously for a single column [17,18], and is extended here for serially coupled columns.

The capacity factor (k_{ijp}), which is the thermodynamic measure of solute retention, may be expressed as follows:

$$k_{ijp} = \frac{t_{ijp}}{t_{ojp}} - 1 \tag{1}$$

where t_{ijp} and t_{ojp} are the elution time of a retained and a non-retained solute, respectively, in solvent j and on column p. It may be readily shown [17,30] that the residence time of a solute in a solvent zone of length x_j is given by:

$$t_{ijp} = \frac{x_j}{u_p}\left(\frac{1 + k_{ijp}}{k_{ijp}}\right) \tag{2}$$

where u_p is the mobile phase linear velocity on column p. The total retention time (T_i) of the solute is the summation of residence times in each solvent and on each column

$$T_i = \sum_{p=1}^{q}\sum_{j=0}^{n} t_{ijp} = \sum_{p=1}^{q}\sum_{j=0}^{n} \frac{x_j}{u_p}\left(\frac{1 + k_{ijp}}{k_{ijp}}\right) \tag{3}$$

Because the volumetric flow-rate (F) of the mobile phase remains constant within the chromatographic system, the linear velocity on each column is related by

$$F = \pi r_p^2 \varepsilon_p u_p \tag{4}$$

where r_p is the radius and ε_p is the total porosity of column p. By rearrangement of Eq. 4 and substitution into Eq. 3, the total retention time may be expressed in terms of the known column parameters

$$T_i = \sum_{p=1}^{q}\sum_{j=0}^{n} \frac{\pi r_p^2 \varepsilon_p x_j}{F} \cdot \left(\frac{1 + k_{ijp}}{k_{ijp}}\right) \tag{5}$$

The limit of the summation index (n), which represents the total number of solvent zones required to elute the solute from a column of length l_p, is determined by evaluating the expression

$$\sum_{j=0}^{n} \frac{x_j}{k_{ijp}} = l_p \tag{6}$$

If the limit has a non-integer value for the first column ($p = 1$), the summation in Eq. 5 is performed in the normal manner for the integer solvent zones 0 to n, and the fraction is treated as a multiplier for the last solvent zone. This solvent zone subsequently enters the second column, where the remainder is used as a multiplier for the first solvent zone ($n = 0$) on the second column ($p = 2$). The computation is performed in an analogous manner for all subsequent columns.

2.2. Theory of solute band broadening

In order to optimize the separation of solutes on serially coupled columns, the variance of the solute peak must be determined at the exit of the last column. If the broadening arises primarily from the packed bed and is relatively independent of solute and solvent, the variance in length units $(\sigma_{ijp})_l^2$ can be expressed as:

$$(\sigma_{ijp})_l^2 = h_p d_p l_p \tag{7}$$

where h_p is the reduced plate height, d_p is the particle diameter, and l_p is the length of column p. Since variances are only independent and additive in the time domain [31,32], the length variance within each solvent zone on each column must be converted to the corresponding temporal variance $(\sigma_{ijp})_t^2$

$$(\sigma_{ijp})_t^2 = \frac{(\sigma_{ijp})_l^2}{u_p^2} \cdot \left(\frac{t_{ijp}}{t_{ojp}}\right)^2 \tag{8}$$

where the elution time of a retained solute is given by Eq. 2 and the elution time of a non-retained solute (t_{ojp}) is given by

$$t_{ojp} = \frac{l_p}{u_p} \tag{9}$$

By substitution of these expressions into Eq. 8, the total temporal variance can be expressed as a summation of the contributions within all solvent zones and all columns

$$(\sigma_i)_t^2 = \sum_{p=1}^{q}\sum_{j=0}^{n}(\sigma_{ijp})_t^2 = \sum_{p=1}^{q}\frac{h_p d_p}{l_p} \cdot \left[\sum_{j=0}^{n}\frac{\pi r_p^2 \varepsilon_p x_j}{F}\cdot\left(\frac{1+k_{ijp}}{k_{ijp}}\right)\right]^2 \quad (10)$$

Finally, the effective number of theoretical plates (N) for the coupled column system under the conditions of solvent modulation is given by

$$N = \frac{T_i^2}{(\sigma_i)_t^2} \quad (11)$$

where the total retention time and temporal variance are evaluated from Eqs. 5 and 10, respectively.

2.3. Theory of solvent zone broadening

In order to ensure that solute retention is controlled independently within each solvent zone, it is necessary that the zones exhibit minimal mixing at the boundaries. Such mixing will adversely influence the accuracy of predicting solute retention from the theoretical models. Moreover, distortion and even splitting of solute peaks may occur if they elute at or near the solvent zone boundary.

The zone purity can be expressed as the ratio of the lengths of the unmixed fraction of the final solvent zone to that of the original zone

$$\frac{x_j - \xi x_j}{x_j} = 1 - \xi \quad (12)$$

When defined in this manner, the zone purity approaches unity when no intermixing occurs and approaches zero when the solvent zone is completely mixed by column broadening processes.

Determination of the zone purity by means of Eq. 12 requires an estimation of the mixed fraction (ξ) of the solvent zone. This mixed fraction may be estimated by assuming that the initial solvent zone has an ideal rectangular profile of width x_j and that column broadening processes are adequately described by a Gaussian profile with variance given by Eq. 7, as illustrated schematically in Fig. 2. The mixed fraction is then calculated, with a statistical accuracy of 95%, by presuming that mixing extends $2(\sigma_o)_l$ at each boundary of the solvent zone, so that the total mixed region is $4(\sigma_o)_l$. The mixed fraction is, thus, given by

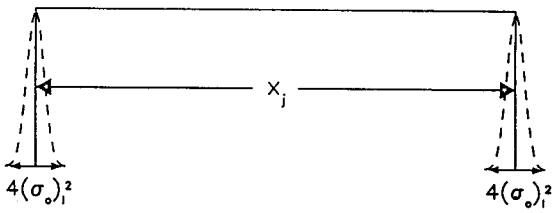

Fig. 2. Schematic illustration of solvent zone broadening ($1 - \xi = 0.95$).

$$\xi = \frac{4(\sigma_o)_l}{x_j} \quad (13)$$

where the total variance for a non-retained solvent zone $(\sigma_o)_l^2$ in length units is

$$(\sigma_o)_l^2 = \frac{\left(\sum_{p=1}^{q} l_p\right)^2\left(\sum_{p=1}^{q} h_p d_p l_p r_p^4 \varepsilon_p^2\right)}{\left(\sum_{p=1}^{q} l_p r_p^2 \varepsilon_p\right)^2} \quad (14)$$

The effect of solvent zone length on the calculated zone purity is shown in Fig. 3. It is apparent that the reduction of particle diameter and column length is important to maintain the integrity of the solvent zone. If the minimum acceptable value for the zone purity is arbitrarily defined to be 95%, as illustrated in Fig. 2, the requisite solvent zone length may be determined from Eq. 13 as follows

$$x_j = 80(\sigma_o)_l \quad (15)$$

For example, a solvent zone length greater than 12.7 cm would be required to maintain 95% purity for a column with 5 μm particle diameter and 25 cm length. The limiting zone length given by Eq. 15 is the minimum value that may be used with confidence under the conditions of solvent modulation in order to ensure adherence to the assumptions of the theoretical models.

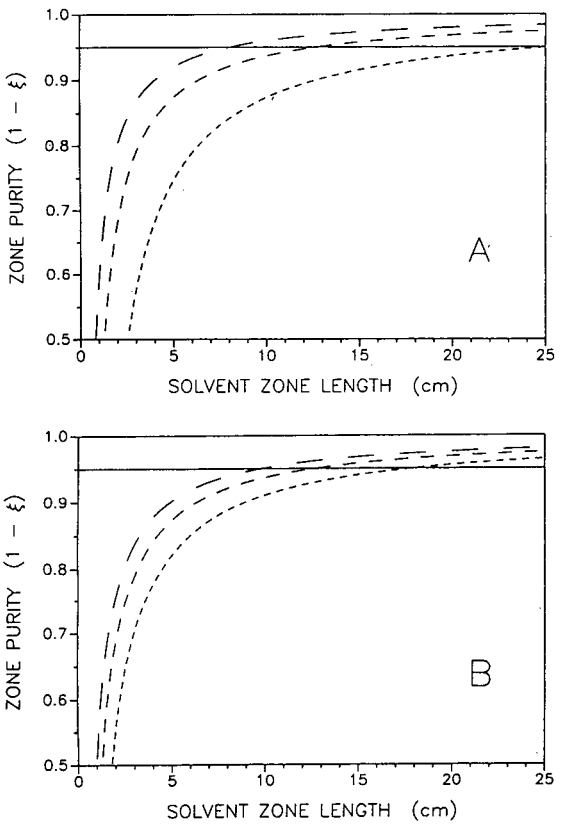

Fig. 3. Effect of solvent zone length on zone purity according to Eqs. 12–14. (A) Constant particle diameter (5 μm) with varying column lengths of 10 cm (——), 25 cm (– –), and 100 cm (---). (B) Constant column length (25 cm) and varying particle diameters of 3 μm (——), 5 μm (– –), and 10 μm (---).

2.4. Optimization strategy

The strategy for optimizing separations requires preliminary measurement of the solute capacity factors in each solvent system on each column to be employed. From these measurements, the retention time and variance can then be predicted by using Eqs. 5 and 10, respectively, for any given solvent zone length and column length in any sequence. After the retention time and variance are calculated for each solute, the extent of separation between adjacent solutes is given by the resolution ($R_{i,i+1}$)

$$R_{i,i+1} = \frac{(T_{i+1} - T_i)}{2[(\sigma_{i+1})_t + (\sigma_i)_t]} \tag{16}$$

The quality of the overall separation is then assessed using a modified form of the multivariate function developed by Schlabach and Excoffier [33], known as the chromatographic resolution statistic (CRS)

$$\mathrm{CRS} = \left[\sum_{i=1}^{m-1} \left(\frac{R_{i,i+1} - R_{\mathrm{opt}}}{R_{i,i+1} - R_{\mathrm{min}}}\right)^2 \cdot \frac{1}{R_{i,i+1}} + \sum_{i=1}^{m-1} \frac{(R_{i,i+1})^2}{(m-1)R_{\mathrm{avg}}^2}\right] \cdot \frac{T_{\mathrm{f}}}{m} \tag{17}$$

where m is the total number of solutes, T_{f} is the elution time of the final solute, R_{opt} is the optimum or desired resolution, R_{min} is the minimum acceptable resolution, and R_{avg} is the average resolution which is given by

$$R_{\mathrm{avg}} = \frac{1}{m} \cdot \sum_{i=1}^{m} R_{i,i+1} \tag{18}$$

The first term of the CRS function is a measure of the extent of separation between each pair of adjacent solute peaks in the chromatogram. This term approaches zero when the individual resolution elements approach the optimum value, and approaches infinity when the individual resolution elements approach the minimum value. The second term of the CRS function reflects the uniformity of spacing between solute peaks, and approaches a minimum value of unity when the sum of the individual resolution elements is equal to the average value. The final term of the CRS function is intended to minimize the analysis time, and may be neglected if this is not a primary goal of the optimization.

In the original expression defined by Schlabach and Excoffier [33], $(R_{i,i+1} - R_{\mathrm{opt}})^2$ passes through a minimum and $1/(R_{i,i+1} - R_{\mathrm{min}})^2$ passes through a maximum as $R_{i,i+1}$ increases. As a result, whenever any individual value of $R_{i,i+1}$ approaches R_{min}, the CRS value becomes extremely high and may no longer be representative of the overall separation quality. More importantly, however, values of $R_{i,i+1}$ that are equidistant from R_{min}, whether higher or lower

in magnitude, are ranked equally. The detrimental consequence is that deceptively low CRS values may be assigned when an individual resolution element approaches zero [34]. This problem may be addressed by altering the form of the CRS function such that, if $R_{i,i+1}$ is less than or equal to $R_{min} + 0.01$, the first term in Eq. 17 is replaced by the constant term

$$\left(\frac{R_{opt} - R_{min}}{0.01}\right)^2 \cdot \frac{1}{R_{min}} \quad (19)$$

In order to optimize the separation, the experimental conditions that yield the minimum value of the CRS function must be determined. The optimum conditions may be determined in two ways: (i) by varying the sequence and length of the solvent zones and columns in a systematic manner to construct a complete CRS response surface, from which the optimum is identified by visual inspection, or (ii) by using an iterative search routine such as the simplex method [19,35].

3. Experimental

3.1. Reagents

Reagent-grade polynuclear aromatic hydrocarbons (PAHs) are obtained from Sigma (St. Louis, MO, USA). Standard solutions are prepared at 10^{-4} *M* by dissolution of the PAHs in spectroscopic-grade methanol. Organic solvents are high purity distilled-in-glass grade (Baxter Healthcare, Burdick and Jackson Division, Muskegon, MI, USA); water is deionized and doubly distilled in glass (Model MP-3A, Corning Glass Works, Corning, NY, USA).

3.2. Experimental system

The chromatographic system consists of a dual syringe pump (Model 140, Applied Biosystems, San Jose, CA, USA), which is programmed to deliver solvent zones for a specified time period at a nominal flow-rate of 1 μl/min. Sample introduction is achieved by using a 1.0-μl injection valve (Model ECI4W1, Valco Instruments, Houston, TX, USA), after which the effluent stream is split (75:1) and applied to the chromatographic column. The microcolumns are prepared from fused-silica capillary tubing (200 μm I.D., Polymicro Technologies, Phoenix, AZ, USA), whose length can be readily adjusted, which is terminated with a quartz wool frit. The microcolumns are packed with octadecylsilica and β-cyclodextrin silica materials (5 μm diameter, Advanced Separation Technologies, Whippany, NJ, USA) according to the slurry packing procedure described previously [36]. The octadecylsilica and β-cyclodextrin silica columns, respectively, have total porosity (ε_p) of 0.81 and 0.80, separation impedance (ϕ_p) of 890 and 720, and reduced plate height (h_p) of 3.2 and 12.9 using pyrene as a model solute under standard test conditions [36].

The PAH solutes are detected using both laser-induced fluorescence and UV-absorbance in a 75 μm I.D. fused-silica capillary flow cell. In the fluorescence detection system [37,38], a helium–cadmium laser (325 nm, 25 mW, Model 3074-40M, Omnichrome, Chino, CA, USA) is reflected by a dielectric mirror and is focussed on the capillary with a quartz lens. The fluorescence emission is collected perpendicular and coplanar to the excitation beam with another quartz lens, spectrally isolated with a bandpass interference filter (420 nm, S10-420-F, Corion, Holliston, MA, USA), and focussed onto a photomultiplier tube (Model Centronic Q4249B, Bailey Instruments, Saddle Brook, NJ, USA). The photocurrent is amplified and converted to voltage by a picoammeter (Model 480, Keithley Instruments, Cleveland, OH, USA). A variable-wavelength UV-absorbance detector (Model Uvidec 100-V, Japan Spectroscopic Co., Tokyo, Japan), operated at 254 nm, is placed in series after the fluorescence detector. Data are acquired simultaneously from both detectors using an analog-to-digital converter (Model DT2805-5716, Data Translation, Marlborough, MA, USA) together with a personal computer (Model ZMF-248-40, Zenith Data Systems, St. Joseph, MI, USA). The data acquisition programs are written in the Forth-based programming language ASYST

(Version 2.1, Keithley Asyst, Rochester, NY, USA).

3.3. Computer optimization program

The computer optimization program is written in the FORTRAN 77 language to be executed on a VAXstation 3200 computer (Digital Equipment, Maynard, MA, USA). This program generates a complete CRS response surface by using a systematic mapping procedure. The lengths of each column and solvent zone are varied independently within prescribed limits; column lengths are varied from 0 to 75 cm and solvent zones are varied from the minimum length that maintains 95% purity (Eq. 15) to the maximum length required to elute all solutes. For each combination of column and solvent lengths, the total retention time and variance of each solute peak are calculated by means of Eqs. 5 and 10, respectively. The resolution between each pair of adjacent solute peaks is calculated by using Eq.

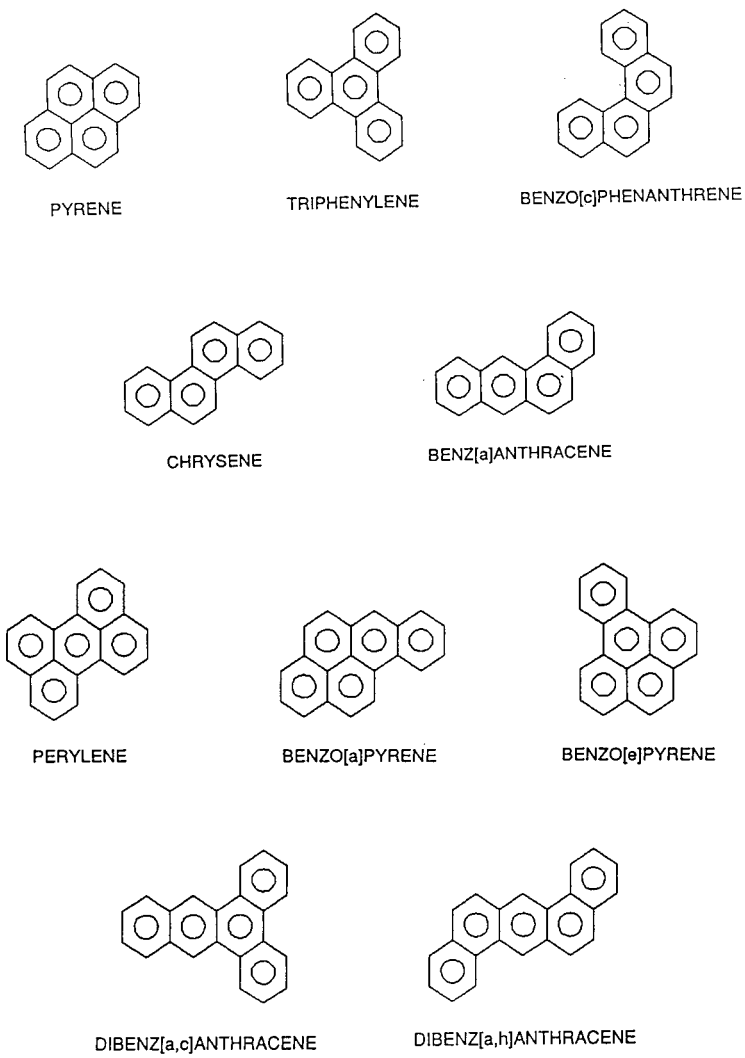

Fig. 4. Structures of isomeric four- and five-ring polynuclear aromatic hydrocarbons.

16. Finally, the overall quality of the separation is assessed by means of the modified CRS function (Eqs. 17 and 19), using selected values for the optimum and minimum acceptable resolution of 1.5 and 0.3, respectively. By graphing the CRS value as a function of the column and solvent zone lengths, a complete multidimensional response surface may be constructed. The minimum CRS value is then identified by visual inspection of the response surface. To assist in identifying the minimum CRS value, the five best conditions are continuously updated and stored in a file by the computer program.

4. Results and discussion

The goal of these preliminary studies is to demonstrate the conceptual basis and to test the theoretical models of solvent modulation using serially coupled columns. To facilitate these goals, the stationary phases were selected for their dissimilar retention mechanisms but compatible mobile phase requirements. Octadecylsilica retains solutes predominantly by a partition mechanism, whereas β-cyclodextrin silica forms inclusion complexes based on the size and shape of the solute. Although both of these phases interact with solutes by Van der Waals forces, monomeric octadecylsilica is dominated by enthalpic effects while β-cyclodextrin silica has a significant entropic contribution. This difference in retention mechanisms may be advantageous for the separation of isomeric four- and five-ring PAHs, whose structures are shown in Fig. 4.

The capacity factors for each PAH were measured on the octadecylsilica and β-cyclodextrin silica stationary phases using mobile phases with compositions of 80% and 90% aqueous methanol as well as 50% and 70% aqueous acetonitrile. On the octadecylsilica phase (Table 1), many of the isomeric four- and five-ring compounds are well separated. However, there are several critical pairs that are difficult to resolve in all mobile phases, most notably chrysene and benz[*a*]anthracene, as well as benzo[*e*]pyrene and perylene.

Table 1
Capacity factors (k_{ijp}) for PAHs on octadecylsilica stationary phase using aqueous methanol and acetonitrile mobile phases

PAH	Capacity factor (k_{ijp})			
	Methanol		Acetonitrile	
	80%	90%	50%	70%
Pyrene	4.65	1.93	14.5	4.12
Triphenylene	5.90	2.39	18.7	5.01
Benzo[*c*]phenanthrene	6.23	2.69	20.9	5.37
Chrysene	6.91	2.61	22.6	5.52
Benz[*a*]anthracene	7.00	2.61	23.0	5.64
Benzo[*e*]pyrene	10.5	3.78	31.8	8.16
Perylene	10.8	3.74	32.0	8.18
Benzo[*a*]pyrene	13.0	4.01	39.3	9.45
Dibenz[*a*,*c*]anthracene	15.0	4.64	49.0	10.6
Dibenz[*a*,*h*]anthracene	17.6	5.45	56.4	11.7

Although PAHs are reported to form inclusion complexes with β-cyclodextrin silica [22,39–42], the capacity factors are very small under all experimental conditions examined herein (Table 2). Only by using the weakest mobile phases is the PAH retention measurable and the resolution partially achieved. Although methanol mobile phases show no selectivity based on either solute size or shape, the acetonitrile mobile

Table 2
Capacity factors (k_{ijp}) for PAHs on β-cyclodextrin silica stationary phase using aqueous methanol and acetonitrile mobile phases

PAH	Capacity factor (k_{ijp})			
	Methanol		Acetonitrile	
	80%	90%	50%	70%
Pyrene	0.09	0.06	0.18	0.08
Triphenylene	0.11	0.06	0.16	0.08
Benzo[*c*]phenanthrene	0.13	0.06	0.18	0.07
Chrysene	0.15	0.07	0.17	0.08
Benz[*a*]anthracene	0.15	0.06	0.19	0.09
Benzo[*e*]pyrene	0.12	0.06	0.25	0.14
Perylene	0.18	0.14	0.36	0.17
Benzo[*a*]pyrene	0.15	0.07	0.26	0.15
Dibenz[*a*,*c*]anthracene	0.16	0.08	0.35	0.16
Dibenz[*a*,*h*]anthracene	0.18	0.08	0.37	0.17

phases appear to be able to discriminate between the four- and five-ring classes. The most noteworthy and useful result is that perylene may be readily separated from both benzopyrene isomers on the β-cyclodextrin silica phase.

Based on these results, it seems reasonable to expect that resolution of the PAHs can be achieved by serial coupling of the octadecylsilica and β-cyclodextrin silica columns. However, there are 64 possible permutations for the columns and solvents examined in this study: 8 one-column/one-solvent systems, 24 one-column/two-solvent systems, 8 two-column/one-solvent systems, and 24 two-column/two-solvent systems. It would clearly be impossible to examine all of these possibilities by time-consuming, trial-and-error experimental measurements. However, the computer program described previously provides a rapid and effective means to identify the most promising permutation. The individual capacity factors (k_{ijp}) for the PAH solutes shown in Tables 1 and 2 are used to calculate the retention time and variance according to Eqs. 5 and 10, respectively. The resolution of each adjacent pair of solutes is calculated from Eq. 16, and the overall quality of the separation is assessed by the CRS function in Eq. 17. For each possible combination and sequence of columns and solvents, the minimum CRS values are stored in a file and are used to identify the most promising permutation for further study. The results of these preliminary simulations are summarized in Table 3 for the permutations of a two-column/two-solvent chromatographic system. If the minimum CRS value is used as the criterion for evaluation, then the best column sequence is predicted to be octadecylsilica followed by β-cyclodextrin silica, and the best solvent sequence is 80% methanol followed by 50% acetonitrile. These conditions should provide a minimum resolution of 0.97 with a total analysis time of 113 min.

If resolution and not analysis time is considered to be the primary goal, the final term may be neglected in evaluation of the CRS function in Eq. 17. Under these conditions, the results for the permutations of a two-column/two-solvent chromatographic system are summarized in Table 4. In some cases, the optimum separation is virtually identical to that identified in Table 3; in other cases, a significant increase in resolution is achieved, usually at the expense of an increase in analysis time. Again, the most promising choice for column sequence is octadecylsilica followed by β-cyclodextrin silica, and the most promising solvent sequence is 80% methanol

Table 3
Evaluation of the permutations of a two-column/two-solvent chromatographic system for the separation of PAHs

Column 1	Column 2	Solvent 1	Solvent 2	T_t (min)	$(R_{i,i+1})_{min}$	CRS_{min}
ODS	β-CD	80% CH_3OH	90% CH_3OH	326	0.61	520
ODS	β-CD	90% CH_3OH	80% CH_3OH	373	0.61	590
ODS	β-CD	50% CH_3CN	70% CH_3CN	349	0.71	250
ODS	β-CD	70% CH_3CN	50% CH_3CN	344	0.72	250
ODS	β-CD	80% CH_3OH	50% CH_3CN	113	0.97	33
ODS	β-CD	50% CH_3CN	80% CH_3OH	159	0.99	43
ODS	β-CD	80% CH_3OH	70% CH_3CN	326	0.85	160
ODS	β-CD	70% CH_3CN	80% CH_3OH	318	0.87	160
ODS	β-CD	90% CH_3OH	50% CH_3CN	282	0.59	530
ODS	β-CD	50% CH_3CN	90% CH_3OH	259	0.59	480
ODS	β-CD	90% CH_3OH	70% CH_3CN	241	0.46	3,100
ODS	β-CD	70% CH_3CN	90% CH_3OH	209	0.48	2,500

The columns are octadecylsilica (ODS) and β-cyclodextrin silica (β-CD); the solvents are aqueous mixtures of methanol (CH_3OH) and acetonitrile (CH_3CN) as given in Tables 1 and 2. The analysis time (T_t), minimum resolution [$(R_{i,i+1})_{min}$] and minimum chromatographic resolution statistic (CRS_{min}) function corresponding to the optimum conditions are given.

Table 4
Evaluation of the permutations of a two-column/two-solvent chromatographic system for the separation of PAHs

Column 1	Column 2	Solvent 1	Solvent 2	T_f (min)	$(R_{i,i+1})_{min}$	CRS_{min}
ODS	β-CD	80% CH_3OH	90% CH_3OH	374	0.61	16
ODS	β-CD	90% CH_3OH	80% CH_3OH	373	0.61	16
ODS	β-CD	50% CH_3CN	70% CH_3CN	349	0.71	7.3
ODS	β-CD	70% CH_3CN	50% CH_3CN	344	0.72	7.2
ODS	β-CD	80% CH_3OH	50% CH_3CN	666	1.39	1.9
ODS	β-CD	50% CH_3CN	80% CH_3OH	586	1.37	2.0
ODS	β-CD	80% CH_3OH	70% CH_3CN	326	0.85	5.0
ODS	β-CD	70% CH_3CN	80% CH_3OH	322	0.87	5.0
ODS	β-CD	90% CH_3OH	50% CH_3CN	427	0.70	15
ODS	β-CD	50% CH_3CN	90% CH_3OH	386	0.70	15
ODS	β-CD	90% CH_3OH	70% CH_3CN	241	0.46	130
ODS	β-CD	70% CH_3CN	90% CH_3OH	209	0.48	120

The columns are octadecylsilica (ODS) and β-cyclodextrin silica (β-CD); the solvents are aqueous mixtures of methanol (CH_3OH) and acetonitrile (CH_3CN) as given in Tables 1 and 2. The analysis time (T_f), minimum resolution $[(R_{i,i+1})_{min}]$ and minimum chromatographic resolution statistic (CRS_{min}) function corresponding to the optimum conditions are given, when analysis time is not considered to be a goal of the optimization.

followed by 50% acetonitrile. This permutation will be evaluated in further detail below.

In order to identify the most favorable experimental conditions, the computer program is used first to determine the optimum lengths of the octadecylsilica and β-cyclodextrin silica columns. The topographic and contour maps of the CRS response surface are shown in Fig. 5 as a function of the column length. It is apparent that the overall quality of the separation improves dramatically with increasing length of the octadecylsilica column. Although the extent of the

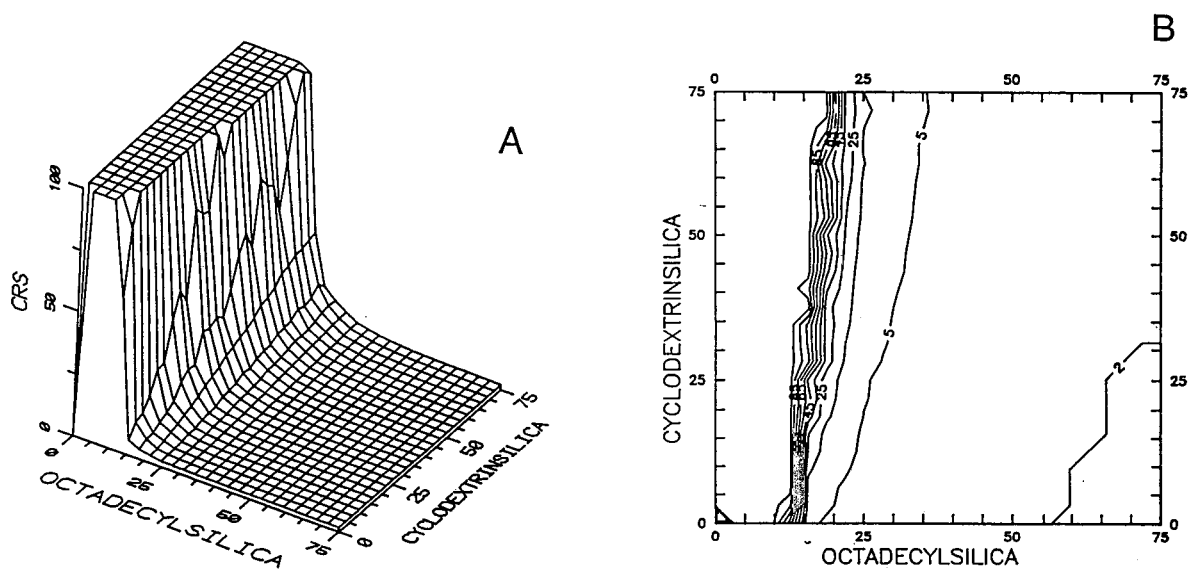

Fig. 5. Topographic (A) and contour (B) maps of the CRS response surface as a function of the column length (cm) for octadecylsilica and β-cyclodextrin silica.

improvement after 25 cm is relatively small, the minimum CRS value is achieved for a column length of 75 cm. In contrast, the β-cyclodextrin silica column has no beneficial effect upon the separation and, thus, has an optimal column length of 0 cm.

The computer program is used next to determine the optimum lengths of the 80% methanol and 50% acetonitrile solvent zones. The topographic and contour maps of the CRS response surface are shown in Fig. 6 as a function of the solvent zone length. There are several regions that yield low values for the CRS function; the overall minimum value is observed for solvent lengths of 167 cm of 80% methanol and 318 cm of 50% acetonitrile.

The predicted separation of the isomeric four- and five-ring PAHs with a 75-cm octadecylsilica column is shown in Fig. 7. The optimal solvent modulation sequence of 80% methanol and 50% acetonitrile in zones of 167 and 318 cm length, respectively, provides a good overall separation (CRS = 1.9) with an analysis time of 666 min. Under these conditions, the critical solute pair is chrysene and benz[*a*]anthracene ($R_{i,i+1} = 1.39$). All other solute pairs have resolution greater than the optimum value (1.5), which is desirable for accurate qualitative and quantitative analysis.

Although this optimized separation initially appears to be very promising, a more detailed examination of the CRS response surfaces is warranted. In the immediate vicinity of the optimum conditions shown in Fig. 6, the CRS function is found to vary in a significant and abrupt manner. For example, as the solvent zone length of 80% methanol changes by ±5 cm, the

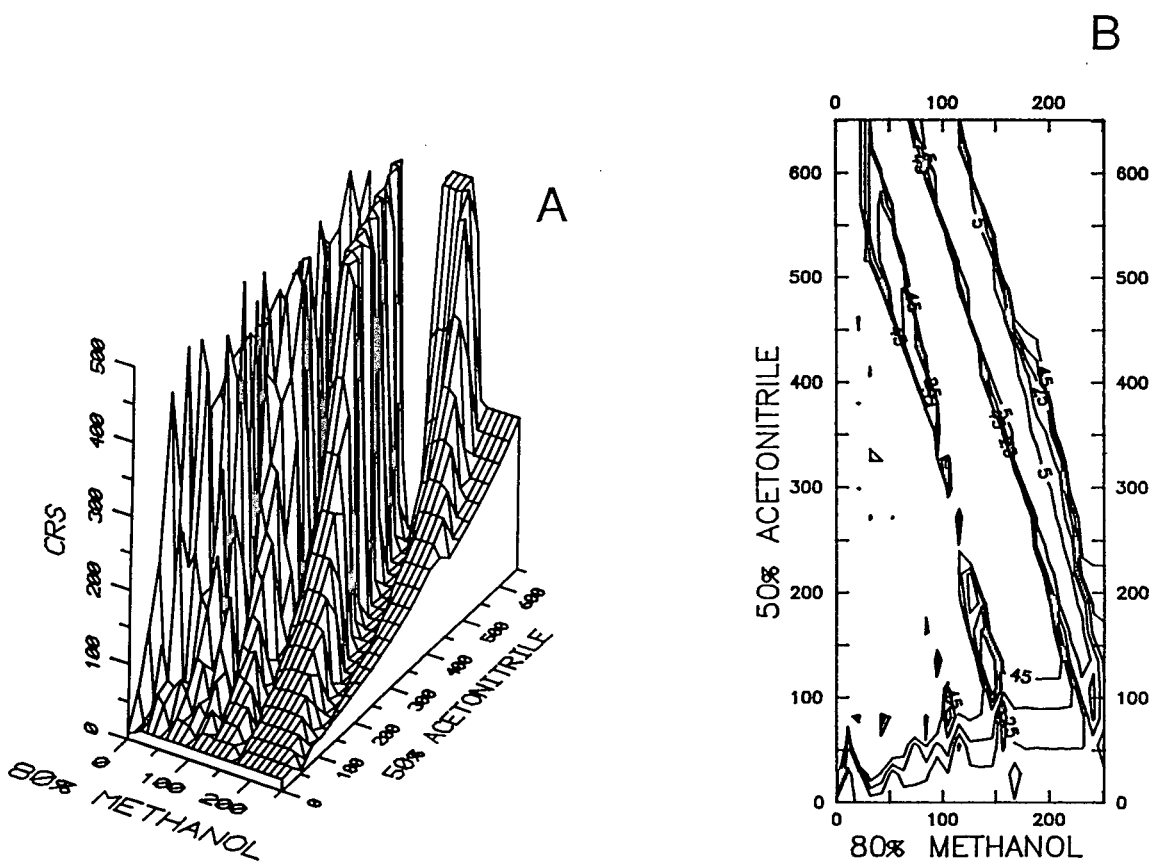

Fig. 6. Topographic (A) and contour (B) maps of the CRS response surface as a function of the solvent zone length (cm) for 80% methanol and 50% acetonitrile.

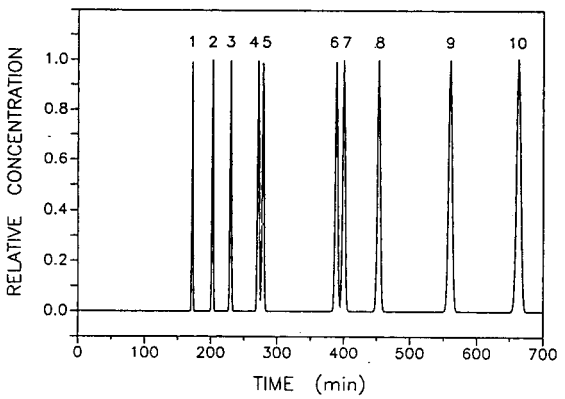

Fig. 7. Predicted chromatogram for the isomeric PAHs with a 75-cm octadecylsilica column using the optimal solvent modulation sequence of 80% methanol and 50% acetonitrile in zones of 167 and 318 cm length, respectively. Solutes: 1 = pyrene; 2 = triphenylene; 3 = benzo[*c*]phenanthrene, 4 = chrysene; 5 = benz[*a*]anthracene; 6 = benzo[*e*]pyrene; 7 = perylene; 8 = benzo[*a*]pyrene; 9 = dibenz[*a*,*c*]anthracene; 10 = dibenz[*a*,*h*]anthracene.

CRS value increases by approximately two orders of magnitude. Thus, small variations in the experimental conditions may have a highly detrimental effect upon the quality of the separation. The next most favorable permutation identified from Table 4, in which the column sequence is octadecylsilica followed by β-cyclodextrin silica and the solvent sequence is 70% acetonitrile followed by 80% methanol, does not suffer from this limitation. This permutation will be evaluated in further detail below.

The topographic and contour maps of the CRS response surface are shown in Fig. 8 as a function of the column length. The overall quality of the separation improves continuously with increasing length of the octadecylsilica column, up to the limit of 75 cm. As noted for the previous case, β-cyclodextrin silica is relatively ineffectual and, thus, has an optimal length of 0 cm.

The topographic and contour maps of the CRS response surface are shown in Fig. 9 as a function of the solvent zone length. There is a broad region of the surface having relatively low values for the CRS function; the minimum value is achieved for solvent lengths of 203 cm of 70% acetonitrile and 634 cm of 80% methanol.

The predicted separation of the isomeric four- and five-ring PAHs with a 75-cm octadecylsilica column is shown in Fig. 10. The optimal solvent modulation sequence of 70% acetonitrile and 80% methanol in zones of 203 and 634 cm length, respectively, provides an excellent sepa-

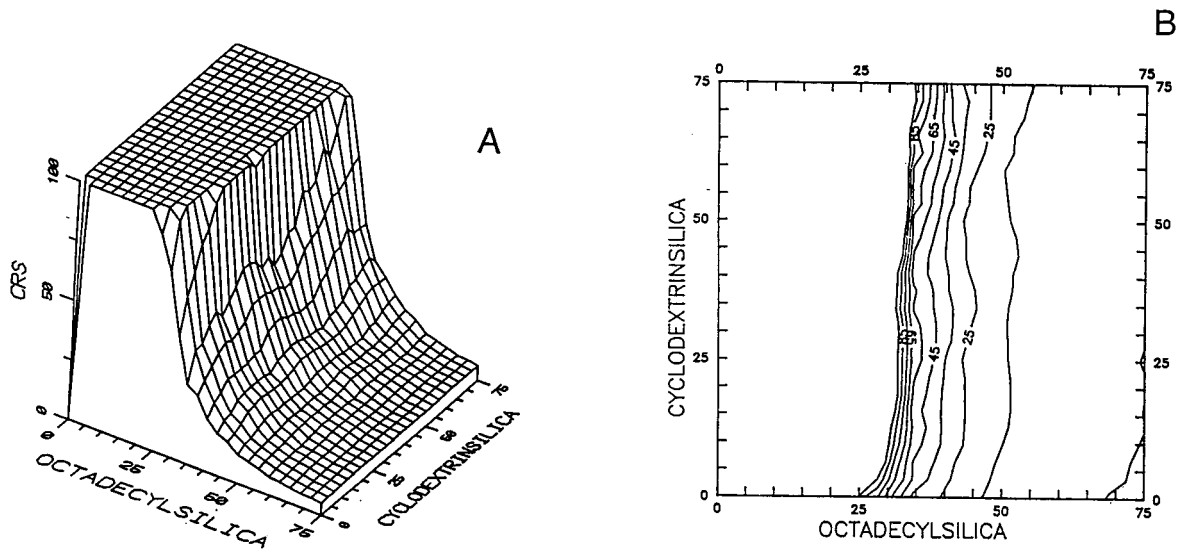

Fig. 8. Topographic (A) and contour (B) maps of the CRS response surface as a function of the column length (cm) for octadecylsilica and β-cyclodextrin silica.

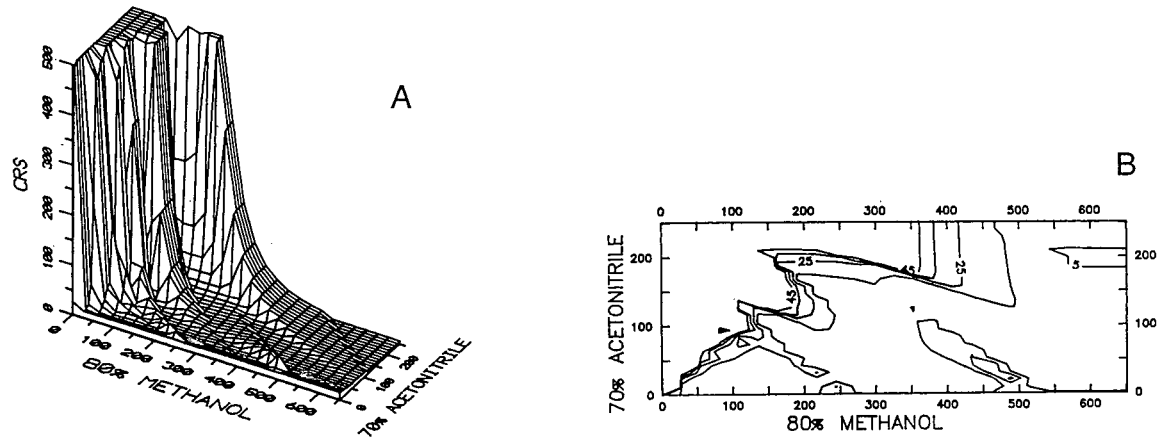

Fig. 9. Topographic (A) and contour (B) maps of the CRS response surface as a function of the solvent zone length (cm) for 70% acetonitrile and 80% methanol.

ration (CRS = 5.0) with an analysis time of 320 min. All solute pairs have resolution greater than the minimum acceptable value (0.3), whereas two pairs have resolution less than the optimum value (1.5). These critical solute pairs are chrysene and benz[*a*]anthracene ($R_{i,i+1} = 0.88$), as well as benzo[*e*]pyrene and perylene ($R_{i,i+1} = 0.88$). Because the CRS response surfaces shown in Figs. 8 and 9 are relatively flat in the vicinity of the optimum, small discrepancies in column length and solvent zone length should have little effect upon the quality of the separation. Thus, the analytical method should be relatively reproducible and rugged.

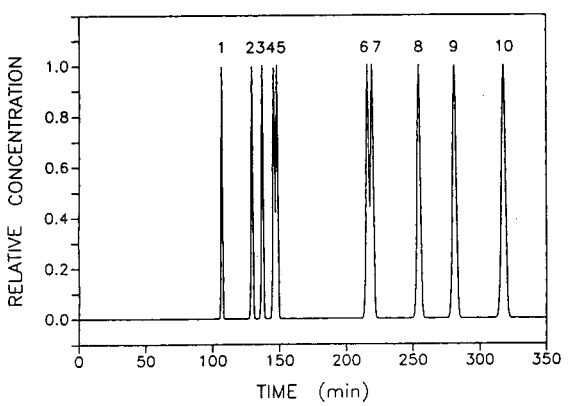

Fig. 10. Predicted chromatogram for the isomeric PAHs with a 75-cm octadecylsilica column using the optimal solvent modulation sequence of 70% acetonitrile and 80% methanol in zones of 203 and 634 cm length, respectively. Solutes as given in Fig. 7.

In order to demonstrate the practical application of this method, the separation of the isomeric four- and five-ring PAHs was performed under the predicted optimum conditions. The experimental chromatogram (Fig. 11) shows excellent separation of all PAH standards with resolution comparable to that in the predicted chromatogram (Fig. 10). The experimental retention time and peak width for each PAH standard agree well with the theoretically predicted values from Eqs. 5 and 10, respectively, as summarized in Table 5. The average relative error is ±3.5% for retention time and ±21% for peak width. Thus, the theoretical models developed herein can accurately predict the experimental results for solvent modulation in serially coupled columns.

5. Conclusions

The complete optimization of separations in multimodal or multidimensional liquid chromatography is a non-trivial task due, in part, to the large number of variable parameters and, in part, to deviations from ideal retention behavior. The use of serially coupled columns with solvent

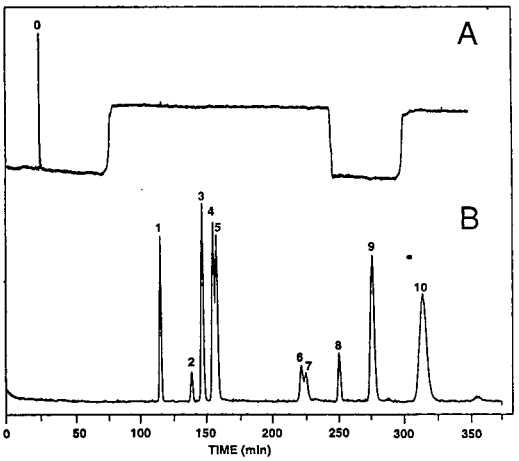

Fig. 11. Experimental chromatogram obtained under the predicted optimum conditions. Column: 75 cm × 200 μm I.D. fused-silica capillary, packed with 5 μm octadecyl silica. Mobile phase: solvent modulation sequence of 70% acetonitrile and 80% methanol in zones of 203 and 634 cm length, respectively, 0.95 μl/min. Detectors: (A) UV–visible absorbance at 254 nm to indicate solvent modulation sequence, (B) Laser-induced fluorescence with excitation at 325 nm and emission at 420 nm to indicate solute retention. Solutes: 0 = injection solvent; 1 = pyrene; 2 = triphenylene; 3 = benzo[*c*]phenanthrene; 4 = chrysene; 5 = benz[*a*]anthracene; 6 = benzo[*e*]pyrene; 7 = perylene; 8 = benzo[*a*]pyrene; 9 = dibenz[*a*,*c*]anthracene; 10 = dibenz[*a*,*h*]anthracene.

modulation appears to be a promising approach to this problem. Because the individual stationary and mobile phases are spatially separated from one another, solute retention is a simple, time-weighted average of each environment to which the solute is exposed. For a system comprised of q columns and n solvents, only $q \times n$ measurements of the solute capacity factor are necessary. From these measurements, retention may be accurately predicted for any sequence and length of the stationary and mobile phases. This approach was demonstrated for the separation of isomeric polynuclear aromatic hydrocarbons using octadecylsilica and β-cyclodextrin silica stationary phases with aqueous methanol and acetonitrile mobile phases. Based on these results, this approach appears to be a viable strategy for the simultaneous optimization of stationary and mobile phase environments.

Acknowledgements

The authors are grateful to Thomas E. Beesley (Advanced Separation Technologies) for providing the octadecylsilica and β-cyclodextrin silica

Table 5
Comparison of experimental (Expt) and theoretical (Theory) retention time and peak width under the predicted optimum conditions illustrated in Figs. 10 and 11

PAH	Retention time (min)			Width (min)		
	Expt	Theory[a]	Error (%)[b]	Expt	Theory[c]	Error (%)[b]
Pyrene	112	107	4.7	2.3	2.0	15
Triphenylene	136	129	5.4	2.8	2.4	17
Benzo[*c*]phenanthrene	143	137	4.4	3.0	2.5	20
Chrysene	151	146	3.4	3.1	2.7	15
Benz[*a*]anthracene	154	148	4.1	3.1	2.7	15
Benzo[*e*]pyrene	218	217	0.5	3.2	4.0	−20
Perylene	221	220	0.5	3.2	4.1	−22
Benzo[*a*]pyrene	247	257	−3.9	4.1	4.8	−15
Dibenz[*a*,*c*]anthracene	271	284	−4.6	5.1	5.2	−6.0
Dibenz[*a*,*h*]anthracene	310	320	−3.1	9.9	5.9	68
Average			±3.5			±21

[a] Calculated from Eq. 5.
[b] Error (%) = 100 (Expt − Theory)/Theory.
[c] Calculated from Eq. 10, assuming a peak width of $4(\sigma_i)_t$.

stationary phases, and to Matthew Bosma (Baxter Healthcare) for providing high-purity solvents. This research was supported by the US Department of Energy, Office of Basic Energy Sciences, Division of Chemical Sciences, under contract number DE-FG02-89ER14056.

References

[1] Cs. Horváth, W. Melander and I. Molnár, *J. Chromatogr.*, 125 (1976) 129.
[2] P. Jandera, H. Colin and G. Guiochon, *Anal. Chem.*, 54 (1982) 435.
[3] S.T. Balke, *Quantitative Column Liquid Chromatography: A Survey of Chemometric Methods* (*Journal of Chromatogr. Library*, Vol. 29), Elsevier, Amsterdam, 1984.
[4] J.C. Berridge, *Techniques for the Automated Optimization of HPLC Separations*, Wiley, New York, 1985.
[5] P.J. Schoenmakers, *Optimization of Chromatographic Selectivity* (*Journal of Chromatogr. Library*, Vol. 35), Elsevier, Amsterdam, 1986.
[6] J.L. Glajch and L.R. Snyder, *Computer-Assisted Method Development for High-Performance Liquid Chromatography*, Elsevier, Amsterdam, 1990.
[7] J.L. Glajch, J.J. Kirkland, K.M. Squire and J.M. Minor, *J. Chromatogr.*, 199 (1980) 57.
[8] J.W. Dolan, L.R. Snyder and M.A. Quarry, *Chromatographia*, 24 (1987) 261.
[9] S.J. Costanzo, *J. Chromatogr. Sci.*, 24 (1986) 89.
[10] G.J. Janz and R.P.T. Tomkins, *Nonaqueous Electrolyte Handbook*, Volume 1, Academic Press, New York, 1972.
[11] H. Colin, G. Guiochon and P. Jandera, *Anal. Chem.*, 55 (1988) 442.
[12] V.V. Berry, *J. Chromatogr.*, 321 (1985) 33.
[13] V.V. Berry and R.W. Shansky, *J. Chromatogr.*, 284 (1984) 303.
[14] V.V. Berry, *J. Chromatogr.*, 290 (1984) 143.
[15] J.C. Gluckman, K. Slais, U.A.T. Brinkman and R.W. Frei, *Anal. Chem.*, 59 (1987) 79.
[16] E.L. Little, M.S. Jeansonne and J.P. Foley, *Anal. Chem.*, 63 (1991) 33.
[17] J.H. Wahl, C.G. Enke and V.L. McGuffin, *Anal. Chem.*, 62 (1990) 1416.
[18] J.H. Wahl, C.G. Enke and V.L. McGuffin, *Anal. Chem.*, 63 (1991) 1118.
[19] J.H. Wahl and V.L. McGuffin, *J. Chromatogr.*, 485 (1989) 541.
[20] I.H. Hagestam and T.C. Pinkerton, *Anal. Chem.*, 57 (1985) 1757.
[21] C.P. Desilets, M.A. Rounds and F.E. Regnier, *J. Chromatogr.*, 544 (1991) 25.
[22] H.J. Issaq, D.W. Mellini and T.E. Beesley, *J. Liq. Chromatogr.*, 11 (1988) 333.
[23] B. Feibush and C.T. Santasania, *J. Chromatogr.*, 544 (1991) 41.
[24] J.B. Crowther and R.A. Hartwick, *Chromatographia*, 16 (1982) 349.
[25] R. Bischoff and L.W. McLaughlin, *J. Chromatogr.*, 270 (1983) 117.
[26] L.A. Kennedy, W. Kopaciewicz and F.E. Regnier, *J. Chromatogr.*, 359 (1986) 73.
[27] Z. El Rassi and Cs. Horváth, *J. Chromatogr.*, 359 (1986) 255.
[28] H.J. Issaq and J. Gutierrez, *J. Liq. Chromatogr.*, 11 (1988) 2851.
[29] D.J. Pietrzyk, S.M. Senne and D.M. Brown, *J. Chromatogr.*, 546 (1991) 101.
[30] J.H. Wahl, *Ph.D. dissertation*, Michigan State University, East Lansing, MI, 1991.
[31] J.C. Giddings, *Dynamics of Chromatography*, Marcel Dekker, New York, 1965.
[32] J.C. Sternberg, *Adv. Chromatogr.*, 2 (1966) 205.
[33] T.D. Schlabach and J.L. Excoffier, *J. Chromatogr.*, 439 (1988) 173.
[34] M.F.M. Tavares and V.L. McGuffin, *Anal. Chem.*, in press.
[35] S.N. Deming and S.L. Morgan, *Anal. Chem.*, 45 (1973) 278A.
[36] J.C. Gluckman, A. Hirose, V.L. McGuffin and M. Novotny, *Chromatographia*, 17 (1983) 303.
[37] V.L. McGuffin and R.N. Zare, *Appl. Spectrosc.*, 39 (1985) 847.
[38] M.A. Heindorf and V.L. McGuffin, *J. Chromatogr.*, 464 (1989) 186.
[39] D.W. Armstrong, W. DeMond, A. Alak, W.L. Hinze, T.E. Riehl and K.H. Bui, *Anal. Chem.*, 57 (1985) 234.
[40] D.W. Armstrong, A. Alak, W. DeMond, W.L. Hinze and T.E. Riehl, *J. Liq. Chromatogr.*, 8 (1985) 261.
[41] M. Olsson, L.C. Sander and S.A. Wise, *J. Chromatogr.*, 477 (1989) 277.
[42] P.R. Fielden and A.J. Packham, *J. Chromatogr.*, 516 (1990) 355.

ELSEVIER

Journal of Chromatography A, 691 (1995) 187–193

JOURNAL OF CHROMATOGRAPHY A

Chiral separation retention mechanisms in high-performance liquid chromatography using bare silica stationary phase and β-cyclodextrin as a mobile phase additive

Robert H. Pullen[a,b], John J. Brennan[b], Gabor Patonay[a,*]

[a]*Department of Chemistry, Georgia State University, University Plaza, Atlanta, GA 30303, USA*

[b]*Solvay Pharmaceuticals, Inc., 901 Sawyer Road, Marietta, GA 30062, USA*

Abstract

This report describes a novel approach to direct chiral separations using bare silica stationary phase with an aqueous mobile phase containing sodium phosphate, β-cyclodextrin (β-CD), and 2-methyl-2-propanol. Two racemic cycloheptaindole derivatives were used as model compounds for the study. Both enantiomer pairs were resolved in a single chromatographic run. Analyte retention mechanisms were consistent with ion-exchange, β-CD inclusion, and hydrophobic modes of interaction. Adding triethylamine to the mobile phase improved peak symmetry and reduced retention. Consistent separations were obtained with different lots of β-CD and different analytical columns. The technique has a number of attractive features that may broaden the use of chiral mobile phase additives for direct enantioseparations.

1. Introduction

Chiral separations are a topic of great interest because of their importance in several fields, including biomedical research. High-performance liquid chromatography (HPLC) is the primary chiral separation technique used for pharmaceutical applications. Three approaches are generally used to achieve chiral separations by HPLC: indirect separations using chiral reagents to form permanent diastereomers, direct separations using a chiral stationary phase (CSP), and direct separations using chiral mobile phase additives [1]. Several reports demonstrate the utility of β-cyclodextrin (β-CD) as a chiral mobile phase additive (CMPA) for the direct separation of enantiomers using reversed-phase HPLC [2,3].

β-CD is a cyclic oligosaccharide composed of seven D-(+)-glucopyranose units joined by α-1–4 linkages. CDs are capable of forming inclusion complexes with other molecules. Enantiomers may show different inclusion complex stabilities based on differences in hydrophobic and hydrogen bonding interactions with the β-CD molecule.

Silica has been largely overlooked as a potential stationary phase for CMPA HPLC separations with β-CD. Gazdag et al. [4] noted the advantage of employing a cyanopropylsilica bonded phase for the enantioseparation of some model compounds with CD CMPA because of the low organic solvent concentration required to achieve reasonable retention times. Solubility of β-CD diminishes rapidly as the organic solvent

* Corresponding author.

0021-9673/95/$09.50
SSDI 0021-9673(94)00822-1

concentration is increased. Gazdag et al. [5] suggested using silica stationary phase for non-polar molecules but no data were presented. Walhagen and Edholm [6] later used this approach to separate chlorthalidone and oxazepam enantiomers with a mobile phase of β-CD in ammonium acetate buffer.

The goal of our research was to investigate the chromatographic behavior of a system comprised of β-CD CMPA and bare silica stationary phase. A racemic, serotonin receptor agonist (DU 124884), and its potential N-desmethyl metabolite (KC 9048) were used as model compounds for the study. Both molecules contain one chiral center. Retention and enantioselectivity were characterized as a function of mobile phase conditions and column type.

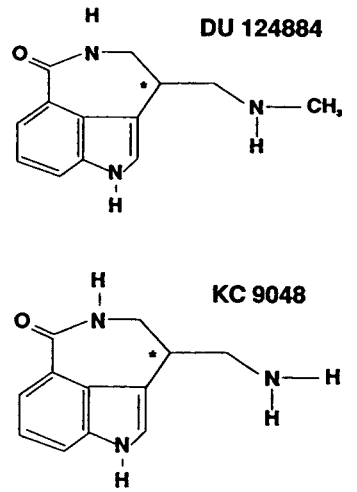

Fig. 1. Structures of model chiral amines DU 124884 (free base) and KC 9048.

2. Experimental

2.1. Materials

DU 124884, 99.9% purity, {(±)-3-methylaminomethyl - 3,4,5,6 - tetrahydro - 6 - oxo - 1H-azepino[5,4,3-*cd*]indole hydrochloride} and KC 9048, 95% purity, {(±)-3-aminomethyl-3,4,5,6-tetrahydro-6-oxo-1H-azepino[5,4,3-*cd*]indole} were synthesized by Solvay Pharma Deutschland Research Labs. (Hannover, Germany). Fig. 1 shows the structures of these compounds. β-CD, reagent and high-purity grades, was purchased from TCI Americas (Portland, OR, USA). The following high purity (≥99%) reagents were purchased from Aldrich (Milwaukee, WI, USA): 2-methyl-2-propanol, triethylamine, monobasic and dibasic sodium phosphate. Phosphoric acid, 85%, was also obtained from Aldrich. Deionized water was obtained by reverse osmosis using the Nanopure filtration system (Barnstead, Dubuque, IA, USA).

2.2. Standard solutions

Aqueous standard solutions of DU 124884 and KC 9048 used for chromatographic studies were prepared by serial dilution from a 1 mg/ml stock solution of racemic free base in water. Analytical standard concentrations were 100 and 10 μg/ml. The stock standard was stable for at least a month when stored at 4°C. Analytical standard solutions were prepared fresh weekly.

2.3. Chromatographic instrumentation and conditions

The HPLC apparatus consisted of a Rheodyne (Cotati, CA, USA) Model 7130 six-port injection valve with a 20-μl sample loop, a 232D pump, and a UV-100 variable-wavelength detector with deuterium source lamp (SSI, State College, PA, USA). A second system used for some studies was identical with the exception of an SSI Model UV 106 fixed-wavelength detector with a mercury source lamp. The separation was performed using a silica NewGuard cartridge guard column, 15 × 3.2 mm I.D., 7 μm particle size (Applied Biosystems, Foster City, CA, USA) and a Supelcosil LC-Si 250 × 4.6 mm I.D., 5 μm particle size silica analytical column (Supelco, Bellefonte, PA, USA). A Spherisorb silica 250 × 4.6 mm I.D., 5 μm particle size analytical column (MetaChem Technologies, Torrance, CA, USA) and a Zorbax Rx-SIL 150 × 4.6 mm I.D., 5 μm particle size silica

analytical column (MAC-MOD Analytical, Chadds Ford, PA, USA) were used in a manufacturer comparison study. A column water jacket and temperature-controlled circulating water bath were used to study temperature effects. Detector output was collected and analyzed using a personal computer equipped with VIS4 chromatography software (SSI).

The mobile phase composition is described in the figure legends and text of the Results and discussion section. All mobile phases were filtered through a 0.45-μm nylon 66 membrane filter before use. A flow-rate of 1.00 ml/min was used in all experiments. Unless indicated otherwise, work was conducted at an ambient temperature of approximately 21°C. The column was equilibrated with a minimum of 15–20 column volumes of mobile phase between composition changes. Absorbance was monitored at 231 nm with the variable-wavelength detector or 254 nm with the fixed-wavelength detector. The system void volume was calculated using the column porosity factor provided by the manufacturer. The accuracy of this estimate was confirmed by measuring the time to the first deflection in the baseline upon injecting water. Data represent the average of two or more injections where retention times agreed within 2%.

3. Results and discussion

3.1. Inclusion complex equilibria

According to Walhagen and Edholm [6], retention in systems containing β-CD as a CMPA can be described by the following relationship:

$$\frac{1}{k} = \frac{1}{k_0} + \frac{[CD]K_f}{k_0}$$

Thus, a plot of $1/k$ versus the cyclodextrin concentration will be a straight line through the origin, assuming that no other retention mechanism exists. The plot yields a slope of K_f/k_0, where K_f is the apparent formation constant for the inclusion complex and k_0 is the retention factor in the absence of CD. This treatment assumes that CD and complexed analyte are not retained by the stationary phase.

Studies to evaluate the influence of β-CD on retention were conducted using a mobile phase composition of 10 mM sodium phosphate buffer, pH 7, and 1% (w/v) 2-methyl-2-propanol (t-BuOH). Fig. 2 shows the effect of β-CD on retention and separation factor. The linear regression correlation coefficient for a plot of $1/k$ versus β-CD exceeded 0.993 for all four enantiomers. The following values for K_f (M^{-1}) were calculated from the plot: (−)-KC 9048 = 26, (+)-KC 9048 = 17, (−)-DU 124884 = 32, and (+)-DU 124884 = 21. Accordingly, the separation factor also varied as a function of β-CD concentration. The enantiomer pairs were unresolved at 0, 1 and 2 mM β-CD, but separation

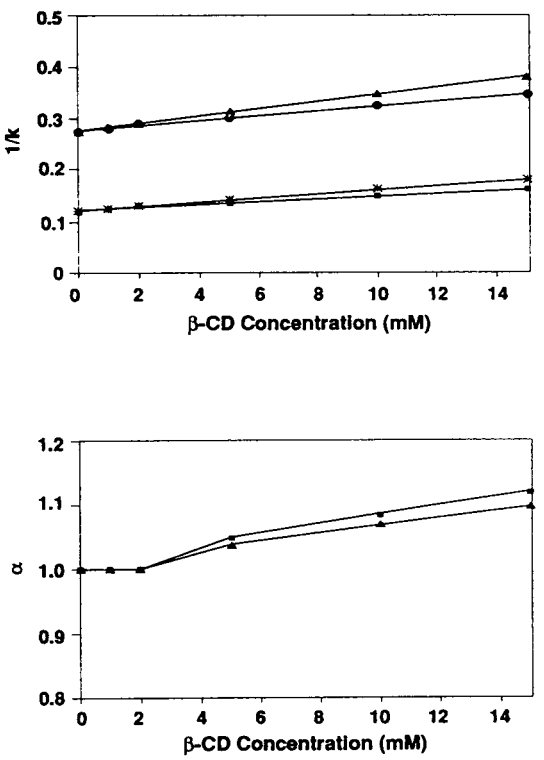

Fig. 2. Retention and separation as a function of β-CD concentration. Mobile phase: 10 mM sodium phosphate/1% t-BuOH, pH 7. Top: ▲ = (−)-KC 9048; ○ = (+)-KC 9048; * = (−)-DU 124884; □ = (+)-DU 124884. Bottom: ▲ = KC 9048; □ = DU 124884.

factors increased as the β-CD concentration increased from 5 to 15 m*M* β-CD.

3.2. Ion-exchange equilibria

Retention of basic compounds on silica under "reversed-phase" conditions is a complex function of the pH, and the organic solvent and buffer concentrations [7]. Retention mechanisms are a combination of ion-exchange interactions with ionized silanol groups and hydrophobic interactions with siloxane groups on the silica surface [8].

Sodium ion concentration effects

The effect of buffer concentration on k and α for the two enantiomer pairs was evaluated from 16 to 160 m*M* sodium. The pH, β-CD concentration, and % t-BuOH were held constant at 7, 15 m*M* and 1%, respectively. The reciprocal retention factor increased non-linearly as a function of the sodium ion concentration. The separation factor was unaffected by sodium ion concentration.

pH effects

The silica surface has a pK_a of about 6.5 [8]. Thus, at pH 7 the surface is ionized and capable of cation-exchange retention. The effects of pH were studied from pH 3 to 7. The ionic strength was held constant ($\mu = 0.06$) while the pH was altered by the appropriate combination of three phosphate buffer solutions: H_3PO_4, NaH_2PO_4 and Na_2HPO_4. Fig. 3 shows the retention factor increased non-linearly as the pH was increased. The separation factors for DU 124884 remained unchanged as a function of pH. KC 9048 separation was optimal at pH 7 due to insufficient retention ($k < 2$) under more acidic conditions.

3.3. Alcohol modifier and hydrophobic retention

The elution order of DU 124884 and its N-desmethyl metabolite was consistent with the elution order expected for reversed-phase separations using alkyl bonded-phase columns. The alcohol modifier was necessary for inclusion

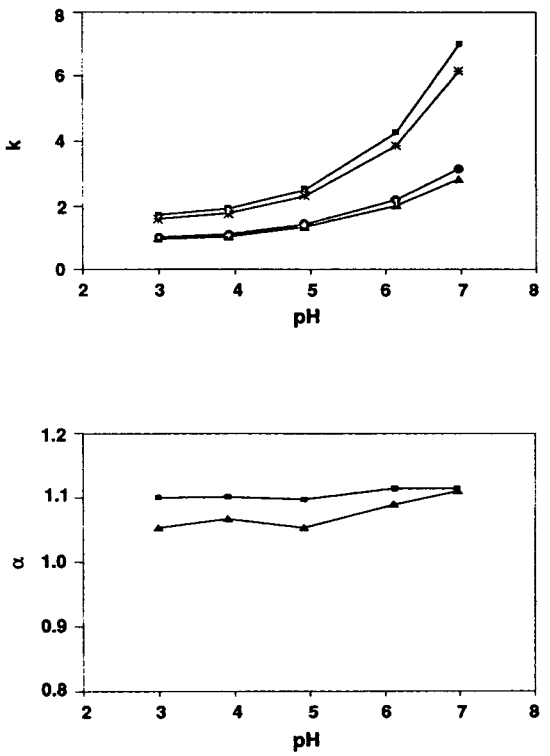

Fig. 3. Retention and separation as a function of mobile phase pH. Mobile phase: 10 m*M* sodium phosphate buffer/15 m*M* β-CD/1% t-BuOH. Symbols as in Fig. 2.

complex formation. Other workers have noted the ability of t-BuOH to stabilize analyte–β-CD complexes [3]. In the absence of t-BuOH, mobile phases of 10 m*M* sodium phosphate buffer (pH 7), and 10 m*M* sodium phosphate buffer (pH 7)/15 m*M* β-CD produced identical analyte retention factors.

Fig. 4 shows the influence of the organic modifier concentration on retention. The mobile phase composition was 10 m*M* sodium phosphate buffer, pH 7/15 m*M* β-CD. The reciprocal retention factor increased non-linearly as a function of the percentage t-BuOH from 0.5 to 2.5%. Peak splitting of KC 9048 occurred at 2.5% t-BuOH and retention factors were not calculable as a result of the distortion. The reason for the peak splitting is not clear. Separation factors did not change between 0.5 and 2.5% because t-BuOH was present in large

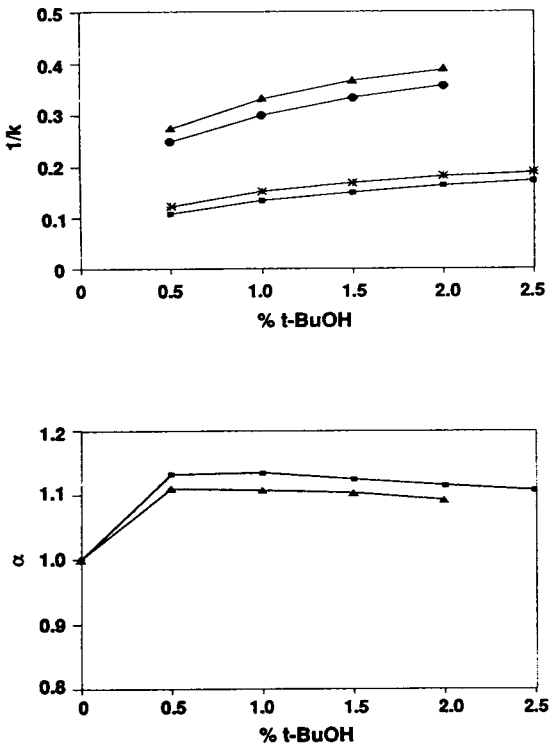

Fig. 4. Retention and separation as a function of percentage t-BuOH. Mobile phase: 10 m*M* sodium phosphate buffer/15 m*M* β-CD, pH 7. Symbols as in Fig. 2.

molar excess at all concentrations (0.5% = 67 m*M*).

3.4. Influence of amine modifier

Analyte peaks displayed poor symmetry with the three-component mobile phase. Organic amine modifiers are commonly used in reversed-phase separations of non-chiral amines to improve peak symmetry through hydrogen bonding, ionic interaction, or adsorption to the silica surface [8]. Fig. 5 shows the improvement in peak shape upon addition of 2 m*M* triethylamine (TEA) to the mobile phase. The retention factors diminished from 0.5 to 2 m*M* TEA, but were unchanged between 2 and 3 m*M* TEA. Separation factors were constant over the TEA concentration range studied.

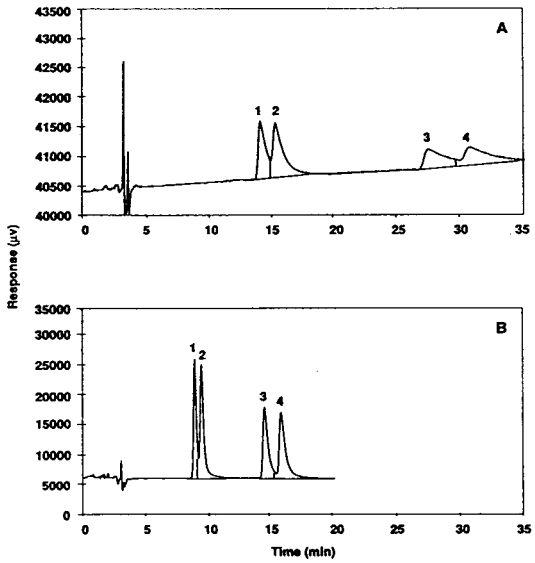

Fig. 5. Influence of triethylamine on the separation. (A) 10 m*M* sodium phosphate buffer/15 m*M* β-CD/1% t-BuOH, pH 7. (B) 10 m*M* sodium phosphate buffer/15 m*M* β-CD/1% t-BuOH/2 m*M* TEA, pH 7. Peaks: 1 = (−)-KC 9048; 2 = (+)-KC 9048; 3 = (−)-DU 124884; 4 = (+)-DU 124884.

3.5. Influence of the separation temperature

Fig. 6 shows a Van 't Hoff plot of log *k* versus $1/T$ using a mobile phase of 10 m*M* sodium phosphate buffer, pH 7/7.5 m*M* β-CD/1% t-

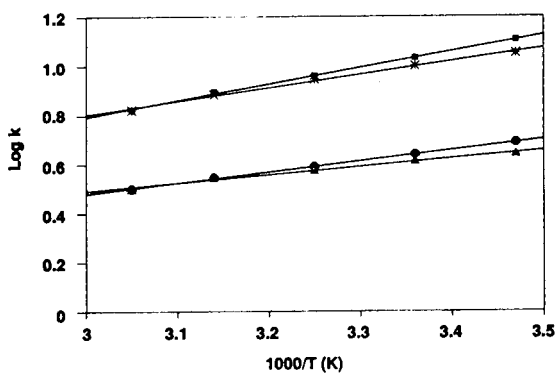

Fig. 6. Van 't Hoff plot of log *k* vs. $1000/T$ (K) using a mobile phase of 10 m*M* sodium phosphate, pH 7/7.5 m*M* β-CD/1% t-BuOH. ▲ = (−)-KC 9048; ○ = (+)-KC 9048; ∗ = (−)-DU 124884; □ = (+)-DU 124884.

BuOH. The log-transformed data displayed excellent linearity ($r \geq 0.993$). Separation factors at 15°C using 7.5 mM β-CD were comparable to those obtained with 15 mM β-CD at ambient temperature (21°C). However, retention factors were greater at 15 vs. 21°C, and β-CD shows limited aqueous solubility at lower temperatures (11 mM at 15°C) [9]. Therefore, it is doubtful that any advantage would be gained by operating at subambient temperatures with β-CD CMPA.

3.6. System ruggedness

The ruggedness of the separation was evaluated by studying the influence of different lots and grades of β-CD on the separation. There was no change in retention or separation between lots or between grades of β-CD material. A comparison of different columns showed that retention factors differed but chiral resolution remained constant from column to column. Fig. 7 shows the results of a comparison of silica columns from different manufacturers. Once again, retention factors differed, but chiral separation remained constant. Retention factors can be easily optimized by changing the buffer concentration without deleterious effects on α. All columns provided adequate direct separations for both enantiomer pairs in less than 24 min. The column used for the retention mechanism studies was subjected to 500 injections over a 12-month period without an appreciable change in chromatographic performance.

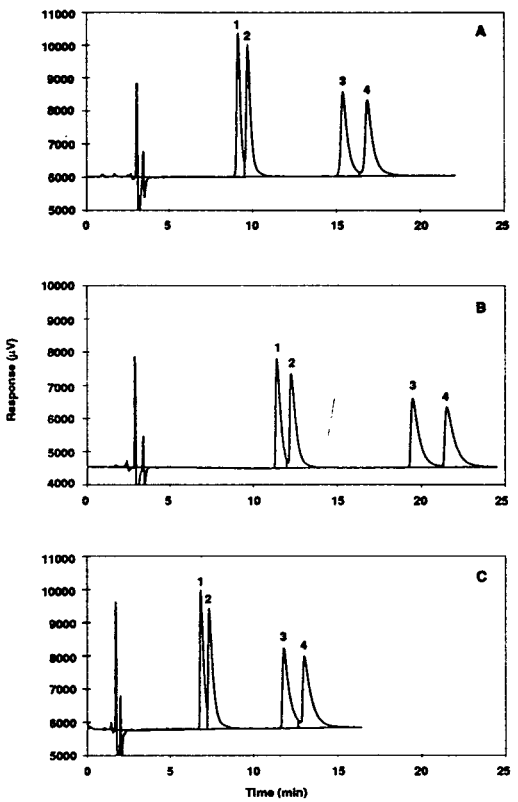

Fig. 7. Comparison of different manufacturers silica columns. (A) Supelcosil LC-Si, 250 × 4.6 mm; (B) Spherisorb SIL, 250 × 4.6 mm; (C) Zorbax Rx-SIL, 150 × 4.6 mm. Peaks: 1 = (−)-KC 9048; 2 = (+)-KC 9048; 3 = (−)-DU 124884; 4 = (+)-DU 124884.

4. Conclusions

This study demonstrates the utility of bare silica stationary phase with an aqueous–organic mobile phase containing β-CD for the enantioseparation of a pair of model pharmaceutical amines. The consistency of the separation between columns and between column manufacturers affords the chromatographer a great deal of flexibility and assurance that the method will not collapse with the next column purchase. An upcoming report will describe the application of this separation technique to the determination of DU 124884 in rat plasma.

Acknowledgements

The test compounds were kind gifts of Dr. Warner Benson of Solvay Pharma Deutschland and Dr. Ton Hulkenberg of Solvay Duphar B.V. The authors gratefully acknowledge Dr. Alkis Sophianopolus of Georgia State University, Dr. Aqeel A. Fatmi of Solvay Pharmaceuticals, Inc. and Dr. Maikel Raghoebar of Solvay Duphar B.V. for their helpful comments, and the technical assistance of Ms. Yan Lin, Ms. Vanessa Owen and Ms. Allyson McFry.

References

[1] A.M. Dyas, *J. Pharm. Biomed. Anal.*, 10 (1992) 383.
[2] K. Cabrera and G. Schwinn, *Am. Lab.*, 8 (1990) 22.
[3] N. Husain and I.M. Warner, *Am. Lab.*, 11 (1993) 80.
[4] M. Gazdag, G. Szepesi and L. Huszar, *J. Chromatogr.*, 371 (1986) 227.
[5] M. Gazdag, G. Szepesi and L. Huszar, *J. Chromatogr.*, 436 (1988) 31.
[6] A. Walhagen and L.E. Edholm, *Chromatographia*, 32 (1991) 215.
[7] G.B. Cox and R.W. Stout, *J. Chromatogr.*, 384 (1987) 315.
[8] B.A. Bidlingmeyer, J.K. Del Rios and J. Korpl, *Anal. Chem.*, 54 (1982) 442.
[9] J. Szejtli, *Cyclodextrins and their Inclusion Complexes*, Akademiai Kiado, Budapest, 1982, Ch. 1, p. 33.

ELSEVIER

Journal of Chromatography A, 691 (1995) 195–204

JOURNAL OF CHROMATOGRAPHY A

Laser-based dynamic surface tension detection for liquid chromatography by probing a repeating drop radius

Lawrence R. Lima III, Robert. E. Synovec*

Department of Chemistry, BG-10, University of Washington, Seattle, WA 98195, USA

Abstract

Modifications to the design of the time-based dynamic surface tension detection (DSTD) system are reported. Both a theoretical and experimental evaluation of the modifications are presented to demonstrate a reduction in flow-rate fluctuation derived systematic noise. The instrument-based limit of detection in relative surface tension change for the improved volume-based DSTD is determined to be 0.15% (3 × root-mean-square noise) as compared to the 0.45% level achieved and previously reported for the time-based method. The radius-based limit of detection for the drop is determined to be 0.5 μm, and may be limited by the vibrational stability of the drop. Detector selectivity is shown to remain unchanged after the modifications as only the observed noise levels are affected. Limits of detection for a variety of commercially available surfactant solutions are presented, along with those for a number of common organic and ionic chromatographic mobile phase modifiers, in order to demonstrate the enhanced selectivity of the DSTD for surface active species. The utility of the volume-based DSTD is demonstrated for the detection of trace intermediate to high molecular mass impurities in a high concentration low molecular mass surface active polymer matrix by comparing the response of refractive index and volume-based dynamic surface tension detection of a Carbowax sample analyzed using size-exclusion chromatography.

1. Introduction

The selective detection of surface active species is of interest for many analytical applications, such as the synthesis of polymeric surfactants, the monitoring of waste effluent streams, and in a wide array of manufacturing processes. Physical interactions of the polar and non-polar functionalities that comprise and characterize surface active species with the bulk solvent result in the preferential migration of these analytes to the surface, where due to energetic and entropic considerations, concentrated surface layers are formed. The concentration of surfactants at an air–liquid interface can be 10^5 times greater than in the bulk solution [1], and can result in a dramatic change in the surface tension of the solution. It is this physical property of surfactants that has made them useful as emulsifiers, flow improvers, and solution stabilizers [2–5] in the production of pesticides, cosmetics, soaps and detergents, food products, and vast collection of other commercially available products [6–8].

Surface tension is traditionally measured by one of a number of classical physical chemistry methods, such as by drop weight [9–13] or by use of the Wilhelmy plate [14–16], under static conditions [17–25]. These static methods require time for equilibrium conditions to be met and

* Corresponding author.

0021-9673/95/$09.50
SSDI 0021-9673(94)00538-K

are impractical for use in a real-time laboratory or process analyzer. The novel time-based dynamic surface tension detection (DSTD) apparatus developed by Cronan [26] and characterized by Lima III et al. [27] shows promise in this regard. Based upon relating changes in the rate of detachment of drops suspended from a capillary tip to changes in the surface tension of a solution, the time-based DSTD allows for selective and sensitive detection of surface active species in real time. Use of the time-based DSTD apparatus under analytical conditions has promise for the analysis of weight-to-weight part-per-million (ppm) levels of surfactant species in solution, but use of the current detector configuration can be problematic due to the sensitivity of the time-based DSTD apparatus to flow-rate fluctuations. Presently, flow-rate fluctuations manifest themselves as changes in system surface tension and are the major source of systematic noise. The instrument limit of detection (LOD) for the time-based DSTD has been reported as being 0.45%, which is the LOD of the relative surface tension change [27].

An improvement in detector design will be reported in this manuscript. A laser beam with dimensions much smaller than that of the drop radius is used to probe the physical dimensions of the drop surface. Rather than infer drop volume changes from the rate of drop detachment, changes in the radius of the growing drop are measured. As such, we present the volume-based dynamic surface tension detector. A treatment of the signal response of the detector is presented in relation to previously reported theory in order to provide a means to quantitatively compare the two detector configurations. It will be shown that because drop volume is being measured directly, rather than inferred from drop rate, that the sensitivity to flow-rate fluctuations has been reduced for the volume-based DSTD apparatus. With this improvement the instrument detection limit for volume-based DSTD will be shown to be 0.15% and analyte limits of detection on the order of 1 ppm are observed for commercial products such as Carbowax 1450 (1450 g/mol nominal molecular mass). With a more complete evaluation of the calibration curve presented in our previous report [27] a factor of four improvement in LOD over the time-based method is reported. A preliminary analysis of two commercial soaps is presented, as well as the LODs for a number of species that are not surface active, including some common organic and ionic chromatographic mobile phase modifiers. Because the fundamental basis for detection has not changed by measuring the physical dimensions of the drop, as will be shown in the direct relationship between the theoretical basis for the signal response of the two methods, the volume-based DSTD apparatus is shown to retain the selectivity benefit of the original time-based configuration. Insensitivity to common mobile phase additives suggests that the volume-based DSTD apparatus holds promise for use with high-performance liquid chromatography (HPLC) or flow injection analysis (FIA). Lastly, Carbowax 200 (200 g/mol, nominal molecular mass) is examined by size-exclusion chromatography (SEC) with the volume-based DSTD apparatus in series and following a refractive index (RI) detector, to demonstrate the utility of the volume-based DSTD apparatus for the detection of trace intermediate molecular mass impurities in a concentrated low molecular mass matrix. It will be shown that volume-based DSTD offers a dramatically different view of Carbowax 200 than does RI detection. The combination of high selectivity for surface active components and high sensitivity makes the volume-based DSTD ideal for use as a quality control detector for the production of surface active polymers.

2. Theory

For the sake of clarity, we distinguish a description of the bulk solvent with a subscript of 1, the analyte with a subscript of 2, and a mixture with the subscript 1,2. From a fundamental point of view, changes in surface tension, $\Delta\gamma_{1,2}$, relative to some baseline surface tension, as caused by the presence of a surface active species are related to changes in drop

volume, $\Delta V_{1,2}$, relative to some baseline drop volume as shown by

$$\frac{\Delta\gamma_{1,2}}{\gamma_1} = \frac{\Delta V_{1,2}}{V_1} \quad (1)$$

From a combination of the treatment of surface tension of a two-phase system as reported by Connors and Wright [1] and a the classical drop weight method of surface tension determination presented by Adamson [10], the response of the time-based DSTD, $S(t)$, as described in our previous report [27] is defined as an indirect measure of relative changes in drop volume and given by

$$S(t) = \frac{\Delta V_{1,2}}{V_1}(t) = \frac{\Delta t_{1,2}}{t_1}(t) = C_2\left(\frac{t_1}{t_{eq}}\right)\frac{M_1}{10^6 M_2}\beta K_2\left(\frac{\gamma_2}{\gamma_1} - 1\right) \quad (2)$$

where t_1 is the baseline drop interval for the solvent, C_2 is the concentration of the analyte near the surface as observed at the detector, t_{eq} is defined as the time required for the solution to reach equilibrium under static conditions, M_1 and M_2 are the molecular masses of the solvent and analyte, respectively, β describes the relative geometry of the analyte, K_2 is the surface binding constant for the analyte, and γ_1 and γ_2 are the coefficients of surface tension for the solvent and analyte, respectively. Thus, the detector signal is defined as a combination of three contributions, relative change in surface tension, relative degree of surface activity, and transport of the surface active species to the air–liquid interface [27].

Similar to RI detection, the volume-based DSTD requires an absolute change in the probed physical property. The term $(\gamma_2/\gamma_1) - 1$ describes this absolute change in surface tension and is the basis for detection. However, the selectivity and enhanced sensitivity for surfactants depends upon the degree of surface activity of the analyte. Species that are surface active tend to form surface layers at which the concentration of the surfactant can be 10^5 greater than in the bulk solution [1]. From Connors and Wright [1], the term βK_2 combines the ability and tendency of a species to form and maintain a concentrated surface layer to describe the relative surface activity of an analyte. Thus, βK_2 describes the selectivity of dynamic surface tension detection. The final consideration in the basis for a signal response is the transport of the analyte to the surface by means of both convection and diffusion. From our previous report [27], the concentration of the analyte at the surface can be described by

$$\frac{ADC_2 t_1}{V_{SL}\delta} = C_2(t) \quad (3)$$

where A is the surface area of the interface, D is the effective translational diffusion coefficient of the analyte, V_{SL} is the volume of the surface layer, and δ is a diffusion distance characterized by the various transport mechanisms. Because a dynamic process is being examined, and because C_2 is fundamentally determined as the concentration of the analyte at the surface under equilibrium conditions, a relationship between the time scales of the two methods, dynamic and static, is needed. $C_2(t)$ is defined as unbound relative to the adsorption phenomena that occur at the surface, where $C_2(t) < C_2$. The equilibrium signal is defined when t_1 equals t_{eq} and $C_2(t)$ equals C_2, and the linear approximation is

$$C_2(t) = \frac{t_1}{t_{eq}} C_2 \quad (4)$$

where t_1 in practice with the DSTD is generally less than t_{eq}. Thus, the term $C_2(t_1/t_{eq})$ describes the transport of the analyte to the surface and relates the determination of surface tension by static and dynamic methods.

Let us consider Eq. 1 in more detail, to discover how to minimize the noise in the DSTD function. Time-based DSTD assumes a constant flow-rate, F, and since $V = Ft$, then the change in drop time, $\Delta t_{1,2}$, relative to a baseline drop time can infer the relative change in drop volume, as given by

$$\frac{\Delta V_{1,2}}{V_1} = \frac{F\Delta t_{1,2}}{Ft_1} = \frac{\Delta t_{1,2}}{t_1} \quad \text{(constant } F\text{)} \quad (5)$$

However, even with a high-quality pump with a

pulse dampener there are short term fluctuations in flow-rate that introduce noise to the system as these fluctuations manifest themselves as drop volume changes. While keeping t_1 constant, Eq. 5 is rewritten

$$\frac{\Delta V_{1,2}}{V_1} = \frac{\Delta F t_1}{F t_1} = \frac{\Delta F}{F} \quad (\text{constant } t_1) \tag{6}$$

and it is observed that changes in F are detected as apparent changes in t_1. It will be shown that flow-rate fluctuations directly affect the measured signal as noise. Flow-rate fluctuations do not greatly affect t_1 in terms of the transport of the analyte to the surface, as described by Eq. 3, but are a major source of baseline noise. The instrument LOD for the time-based DSTD apparatus, as defined as 3 times the root-mean-square noise, has been reported as 0.45%, and can be attributed to fluctuations in flow-rate. Furthermore, while flow-rate may drift a few percent per hour with a poor pump, one might anticipate severe baseline drift with the time-based DSTD method, whereas measuring $(\Delta V_{1,2})/(V_1)$ directly should perform substantially better.

Volume-based dynamic surface tension detection is based upon probing a length dimension of the drop and making a direct relation of changes in drop volume to changes in surface tension. If the geometry of the drop is assumed to be spherical, for the sake of simplicity, then the volume of the drop can be described by $V_1 = (4\pi/3)\, r_1^3$, where r_1 is the radius of the drop when only the solvent is present. The spherical assumption need not be entirely valid to achieve an acceptable model for the volume measurement. If we let $\Delta V_{1,2} = V_1 - V_{1,2}$ so that $V_{1,2} = V_1 - \Delta V_{1,2}$, then following Eq. 2

$$S(t) = \frac{V_{1,2}}{V_1} = \left(\frac{r_{1,2}}{r_1}\right)^3 \tag{7}$$

If $\Delta r_{1,2} = r_1 - r_{1,2}$ then

$$\frac{V_{1,2}}{V_1} = \left(\frac{r_1 - \Delta r_{1,2}}{r_1}\right)^3 = \left(1 - \frac{\Delta r_{1,2}}{r_1}\right)^3 \tag{8}$$

Since $(1+x)^n$ can be approximated by $1+nx$ for small x, then we can approximate that

$$1 - \frac{\Delta V_{1,2}}{V_1} = 1 - \frac{3\Delta r_{1,2}}{r_1} \tag{9}$$

and thus,

$$S(t) = \frac{\Delta V_{1,2}}{V_1} = 3\left(\frac{\Delta r_{1,2}}{r_1}\right) \tag{10}$$

The term $3(\Delta r_{1,2}/r_1)$ therefore describes the instrument-based LOD when $\Delta r_{1,2}$ is determined from measuring the radius of successive drops, and when $\Delta r_{1,2}$ is three times the standard deviation of the drop dimension. In general $3(\Delta r_{1,2}/r_1)$ is the relative volume change, and thus the signal for the DSTD can be described by combining Eqs. 2 and 10 as

$$S(t) = \frac{\Delta t_{1,2}}{t_1}(t) = \frac{3\Delta r_{1,2}}{r_1}(t) = C_2\left(\frac{t_1}{t_{eq}}\right)\frac{M_1}{10^6 M_2}\beta K_2\left(\frac{\gamma_2}{\gamma_1} - 1\right) \tag{11}$$

The direct relationship between the time- and volume-based detection methods allows for a quantitative comparison of the instrument-based detection limits. Selectivity and sensitivity of the two methods should be equal, but the improvements in noise levels gained from volume-based detection allow for greater detectability and detector reliability.

3. Experimental

3.1. High-performance liquid chromatography (HPLC)

The experimental apparatus is shown in Fig. 1. 100% HPLC-grade water was used as the base mobile phase for all chromatographic and FIA analyses. Analytes consisted of sodium dodecylsulfate (SDS), a series of poly(ethylene glycol) molecular mass standards with molecular masses from 200 to 22 000 g/mol, samples of Dawn dishwasher detergent and Dial hand soap purchased from a local supermarket, HPLC-grade methanol and acetonitrile, phosphoric acid, sodium hydroxide, and a series of Carbowax samples (nominal molecular mass range

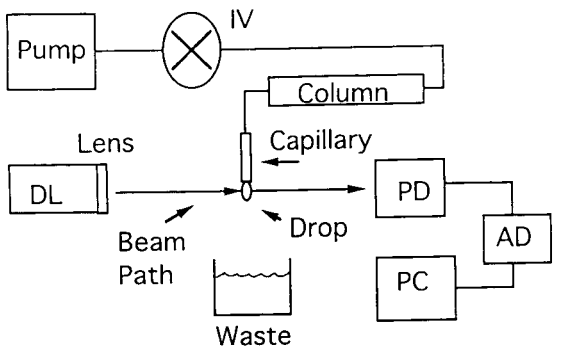

Fig. 1. Schematic of the volume-based dynamic surface tension detection (DSTD) apparatus: DL = diode laser with attached focusing lens; PD = photodiode; AD = data acquisition board; PC = personal computer; Pump = syringe pump; IV = injection valve; Column = size-exclusion column and pulse dampener. A pinhole type mask, not shown for clarity, is positioned between the suspended drop and the photodiode and used to block light that is not relevant to the detection.

of 200 to 8000 g/mol) (Union Carbide, Danbury, CT, USA). All solutions were sonicated thoroughly prior to introduction to the analyzing system. Analytes were introduced to the system using an injection valve (Rheodyne, 7520, Cotati, CA, USA) fitted with either a 10-μl (for FIA) or 100-μl (for HPLC) injection loop. The injection valve was connected to a RI detector (BioRad, Model 1670450, Hercules, CA, USA) using a short length of 1/16 in. O.D. $\times$ 0.005 in. I.D. (1 in. = 2.54 cm) poly(ether etherketone) (PEEK) tubing. For experiments involving a chromatographic separation a 2 mm $\times$ 250 mm column with 9-μm Asahipak (Keystone Scientific, Asahipak, Bellefonte, PA, USA) packing was inserted in place of this tubing length. Another short piece of PEEK tubing was used to contain the flow output from the RI detector. Into the open end of this piece of tubing a 0.33 mm O.D. $\times$ 0.20 mm I.D. glass capillary was inserted and secured using an epoxy. Drops from this capillary tip have a radius of roughly 1000 μm and a volume of approximately 6 μl. The tubing–capillary assembly was mounted using a clamp on a vertical post and connected to a X-Y-Z stage micrometer (Newport, 460 X-Y-Z, Fountain Valley, CA, USA).

3.2. Detector

A 670-nm diode laser (Lasermax, Rochester, NY, USA) was positioned 6 cm from the output of the capillary tip. The output from the laser was focused by means of a lens incorporated into the laser down to a 400 μm high by 200 μm rectangle such that the smaller beam dimension was placed in the horizontal growth axis of the drop. A pinhole type mask with a 0.5 cm radius hole was positioned 9 cm from the capillary tip and was used to block light not relevant to the detection mechanism. A photodiode array was positioned 4 cm behind the mask, and covered to block out any sources of stray light. A diagram of the relation between the drop, probe beam, and mask from the point of view of the laser is shown in Fig. 2, although not drawn to relative scale. The photodiode was interfaced to an amplifier/voltage offset box and then to a personal computer (Delphi, 80486-33, Seattle, WA, USA) via a data acquisition board, and to a chart recorder. Raw data was collected at 3000 points/s, and was smoothed by a 300 collected point/data point running average. The processed data consisted of a measure of the final radius growth of the drop, represented as an intensity voltage,

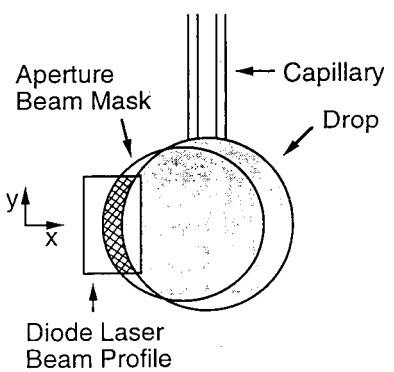

Fig. 2. Close-up schematic of the relationship between the focused laser profile, shown as the rectangle, the drop (shaded) and the pinhole mask, shown as the open circle. Light relevant to detection is shown with cross-hatching. Calibration of the intensity–drop radius relationship is performed by moving the drop along the x-axis, shown, into the beam profile until the beam is completely blocked. The beam width, not drawn to scale, is actually about 15% of the drop radius.

which was converted to $S(t)$ using Eq. 11 and the detector calibration data, as will be described. Additionally, the drop rate (time method) was simultaneously performed as in our previous report [27]. Using the translational stage, the drop was moved into the path of the beam so that a calibration curve relating drop radius to intensity voltage could be determined. All analyses were performed in the linear portion of the radius–intensity calibration curve. The detector system was optimized for the detection of small changes in relative drop radius, with a range on the order of 150 μm, or about 15% of the drop radius as the dynamic range. Since the drop dimension was substantially larger than the probe beam dimension, to a good approximation the detector simply measures changes in drop radius along the x-axis in Fig. 2. For the examination of flow-rate fluctuations, measurements of both baseline and analytical behavior were made with and without the chromatographic column in the flow line.

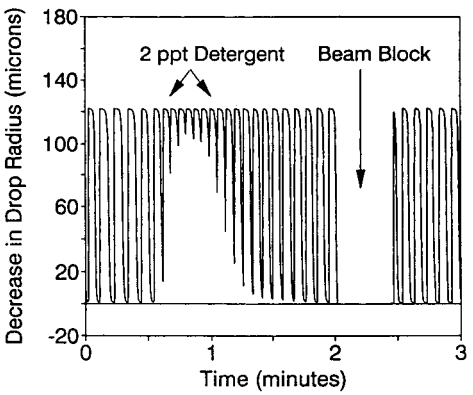

Fig. 3. Raw data collected at 4 points/s for the FIA analysis of a solution of 2 ppt Dawn liquid dishwasher detergent in water as observed by the volume-based DSTD method. The signal for complete beam blockage represents the position for the maximum baseline growth of the drop, labeled as 0 μm in the decrease of the drop radius. Analyte detection is observed as a decrease in the final radius of the drop, resulting in an increase in observed light intensity. The 2 ppt Dawn solution in water is shown to cause a 120 μm decrease in the radius of drop growth, from an initial radius of about 1000 μm for water.

4. Results and discussion

The volume-based DSTD apparatus works by monitoring the radial dimension of the repeating drop and measuring the changes in the intensity of the light that is blocked by the drop surface. Raw data, collected at 4 points/s, that demonstrates the basic principles of detection is presented as Fig. 3. Under baseline operating conditions, the repeating drop grows to a radius of about 1000 μm. As the drop grows, light that is normally transmitted to the photodiode detector is partially blocked, resulting in a loss in intensity observed at the detector. The intensity observed at the maximum radius of the drop was calibrated as a function of the linear position of the drop within the beam, and then the drop was positioned so that the beam would be almost completely blocked at full growth. At this position, the detector is optimized for radius changes on the order of 100 μm. From Fig. 3 it is observed that the intensity of the beam observed at the detector changes over the last 120 μm of the growth of the drop, and at full drop growth nearly all the light is blocked by the surface of the drop as is observed by the intensity observed when the beam is completely blocked by a solid mask. Due to the influence of a surface active species, in this case 2 ppt of Dawn liquid detergent in water, the surface tension of the system decreases. This surface tension decrease manifests as a change in final drop volume, and therefore a decrease in the radius of the drop. Since the drop now grows to a smaller final volume, the intensity of the light that is no longer obstructed by the drop surface increases. For the experimental conditions used, 10 to 50 drops typically define a surface active component peak, and the raw data peak for Dawn liquid detergent clearly shows a change in the surface tension of the drop system. For most experimental conditions, the raw data is processed during the data collection and only the maximum radius of drop growth is collected. The raw data is processed during collection using a program written in-house that collects the raw data at 3000 points/s and runs a 300 point/processed

point average over the raw data to determine the final maximum radius of drop growth.

Concurrently with the intensity data, the interval between repeating drops is recorded, so data for both the time-based and volume-based methods are collected simultaneously. This allows for a direct comparison of the two detection methods as explained in Eq. 11. Presented in Fig. 4 are the DSTD signals, following Eq. 11, for a FIA examination of a solution of 15.6 ppm Carbowax 1450 in water using a flow-rate dampener to minimize flow-rate fluctuations. Both data sets were smoothed by a 5-point running box car average and offset from zero for clarity. Detector signal was converted first from intensity voltage to drop radius in microns using a calibration curve what relates observed intensity to the position of the drop, as mentioned previously. From Eq. 9, radius changes can be converted to volume changes by dividing the radius signal, $\Delta r_{1,2}$, by the baseline radius of the drop, r_1, and multiplying the resulting value by 3. The instrument LOD of $S(t)$ for the time-based method of 0.45% from our previous report was determined from 3 times the root-mean-square noise of $\Delta t_{1,2}/t_1$ data. The instrument LOD of $S(t)$ for the volume-based method was determined by converting the radius data to the relative volume change equivalent as described in Eqs. 10 and 11. The standard deviation of $\Delta r_{1,2}$ was determined to be 0.16 μm for a radius change LOD of 0.5 μm with a baseline drop radius of 1000 μm. Thus, the instrument LOD of $S(t)$ for the volume-based method is determined to be 0.15%, representing a factor of 3 improvement in the amount of noise as compared to the time-based method. The smallest detectable radius change is limited by the vibrational stability of the drop. After removing the pulse dampener, the standard deviation in $S(t)$ for the noise levels for the volume- and time-based methods were once again determined, and are presented in Table 1. The instrument LOD for the time-based method increased by 60% as a result of the increase in flow-rate fluctuations caused by the removal of the pulse dampener, while the instrument LOD for the volume-based method remained unchanged. The enhancement of the volume-based method is even greater, as the time-based method is sensitive to not only flow-rate fluctuations, but also flow-rate drift as observed somewhat in Fig. 4. The volume-based DSTD is insensitive to gradual flow-rate drift, and demonstrates a net factor of four improvement in analyte detection. The limits of detection for a variety of species, including surfactants, organic and ionic chromatographic mobile phase modifiers, and non-surface active species is presented in Table 2. Note that a 1 ppm LOD is now observed for

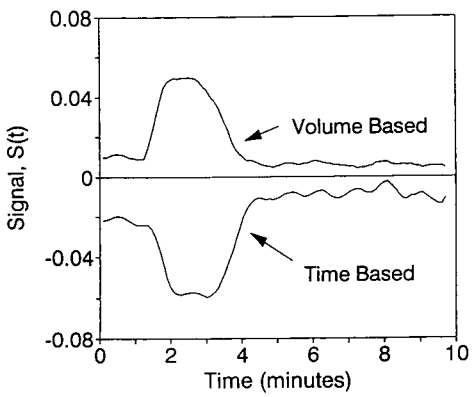

Fig. 4. Simultaneous collection of the DSTD data by volume- and time-based methods for a solution of 15.6 ppm Carbowax 1450 in water for comparison of signal response and relative noise levels. The volume-based (upper data set) data represents a decrease in the final radius of the drop while the time-based (lower data set) data represents a decrease in the time interval between successive drops. Both data sets are smoothed by a 5-point boxcar average, and are offset by a value of 0.01 from their respective baselines at a signal value, $S(t)$, of 0. Noise levels for the volume-based data are a factor of 3 less than for the time-based data. The sensitivity of both methods is equivalent as represented by the equal signal heights.

Table 1
LOD of $S(t)$ from noise levels determined for time- and volume-based DSTD methods with and without pulse dampener, in signal units

	With dampener	Without dampener
Volume-based DSTD	0.0015	0.0015
Time-based DSTD	0.0045	0.0072

Table 2
LODs for a variety of surfactants, non-surfactants, and common chromatographic mobile phase additives, as observed in water

	LOD (ppm)
Surfactants	
Poly(ethylene glycol) 1450	1
Poly(ethylene glycol) 7100	2
Sodium dodecylsulfate	1
Dawn liquid detergent	8
Dial liquid hand soap	8
Non-surfactants	
Poly(ethylene glycol) 200	1000
Ethylene glycol	10 000
Mobile phase modifiers	
Methanol	500
Acetonitrile	500
1 m*M* NaOH	–[a]
1 m*M* H_3PO_4	–[a]
Water (blank injection)	–[a]

[a] Not detectable.

PEG 1450, as compared to the 4 ppm LOD determined for PEG 1470 in our previous report [27]. Improvement in the sensitivity of volume-based DSTD is observed for sodium dodecylsulfate (SDS) as compared to our previous report. Ionic surfactants can be used to titrate non-ionic surfactants resulting in decreased surface activity in the pairing, and we believe the presence of PEG in solution led to the determination of an artificially high LOD for SDS in our previous report. Insensitivity of the volume-based DSTD to common organic and ionic mobile phase modifiers, as well as for non-surface active species, demonstrates that the selectivity of the detector has not been affected by the modifications to the experimental design. In addition, these results suggest that the volume-based DSTD apparatus would be well suited for use with HPLC and FIA.

To demonstrate this utility, an application of the volume-based DSTD apparatus in an industrial product evaluation and using SEC is presented. The ability to detect intermediate to high molecular mass impurities in high concentration low molecular mass matrices is a concern in the synthesis of surface active polymers. Using an RI detector and volume-based DSTD apparatus in series we performed a SEC analysis of a commercial sample of Carbowax 200, composed of poly(ethylene glycol) (PEG) with a nominal molecular mass of 200 g/mol. From previous reports, we have determined the sensitivity of the PEG series as a function of molecular mass and have shown that PEG 200 is not highly surface active [27]. Fig. 5A shows the RI response for a 1% solution of Carbowax 200 in water collected at 2 points/s and after smoothing by a 30-point boxcar average. One peak appears, and according to our calibration of the SEC as presented in a previous report the molecular mass of that peak corresponds roughly to PEG 200 [28]. The retention volume positions for PEGs of increasing molecular mass are shown. Fig. 5B shows the response for the volume-based DSTD apparatus in conjunction with that for the RI detector. From the volume-based DSTD apparatus, two peaks appear with severe overlapping of the second and smaller peak by the first. From the retention volume data in Fig. 5A, the second peak in Fig. 5B corresponds to the detection of PEG 200, however the first, and more sensitively detected peak possesses no refractive index counterpart. Subsequent analysis of a series of PEG molecular mass standards and comparison to the retention calibration curve in Fig. 5A for the size-exclusion column suggests that the peak corresponds to that expected for PEG 1250. While the sensitivity of the two species using RI detection is nearly equivalent, PEG 1250 is approximately 200 times more sensitive than PEG 200 using the DSTD. From the calibration series determined for PEG 1450, a similar species, the concentration of PEG 1250 detected is on the order of 200 ppm in the original sample and 20 ppm at the detector. The use of the volume-based DSTD apparatus has substantially improved the diagnostic capability in this analysis.

The performance of the new volume-based DSTD apparatus is shown to possess a factor of four enhancement over that of the time-based DSTD apparatus design. Detection limits of the order of 1 ppm are observed for surface active species, while the selectivity of the detection remains enhanced for surface active species.

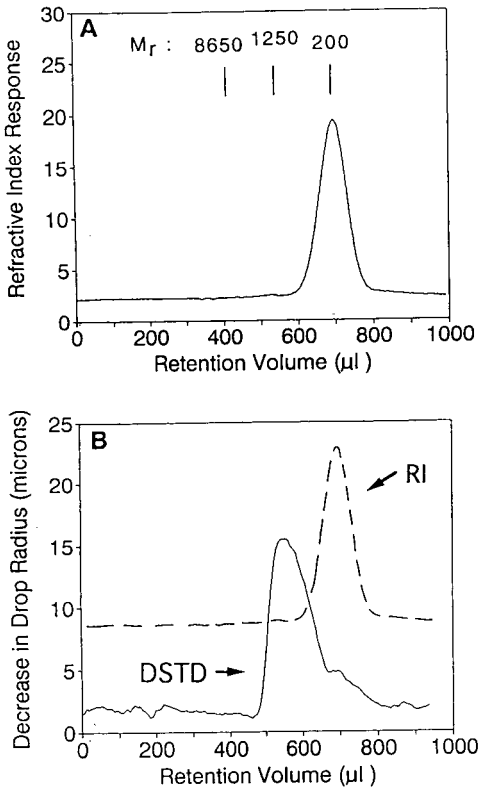

Fig. 5. (A) RI detection of a 1% solution of Carbowax 200 as analyzed using size-exclusion chromatography. The retention volume positions, as determined from a calibration of the column by higher molecular mass (M_r) PEG species is indicated, yet only the peak for PEG 200 is observed. (B) Overlay of the sequentially and simultaneously collected RI and volume-based DSTD detector responses. A small peak representing the minimally surface active PEG 200 is observed, but is severely overlapped by a peak for an analyte that is tentatively identified as the surface active species, PEG 1250. RI detector sensitivity for the two species is equivalent, but substantial enhancement for the detection of the surface active higher molecular mass species is observed using volume-based DSTD. From calibration curves for a similar species, PEG 1470, the concentration of the PEG 1250 peak is approximately 20 ppm at the detector which is consistent with not observing the impurity in the RI chromatogram.

Insensitivity of the volume-based DSTD apparatus to organic and ionic mobile phase modifiers suggests that the detector is promising for use with HPLC or FIA. Analysis of two commercially available soaps is performed to show the utility of the detector for analysis of complex mixtures. Lastly, the combination of selectivity for surfactants and sensitivity is demonstrated for the detection of intermediate molecular mass surface active species in more concentrated low molecular mass, non-surface active matrices with implication towards use for the synthesis of surface active polymers.

Acknowledgement

We thank the Royalty Research Fund from the University of Washington for financial assistance.

References

[1] K. Connors and J. Wright, *Anal. Chem.*, 61 (1989) 194–198.
[2] A. Getmanets, S. Kramerev, V. Balabaiko and P. Dul'nev, *Khim. Sel'sk. Khoz.*, 7 (1991) 100–102.
[3] A. Syldath, K. Schmid and P. Kischkel, *GER. OFFEN. DE*, 4 105 851 (1992).
[4] C. Yamazaki, *Jpn. Kokai Tokkyo Koho*, JP 04 134 023 (92 134 023) (1992)
[5] M. Sanchez, *Rev. Quim. Text.*, 104 (1991) 57–59.
[6] Z. Wang and B. Brooks, *Polym. Int.*, 28 (1992) 239–244.
[7] C. Eberlein, M. Guttieri and W. Schaffers, *Weed Technol.*, 6 (1992) 85–90.
[8] A. Reviejo, J. Pingarron and L. Polo, *Talanta*, 39 (1992) 899–906.
[9] G. Parsons, G. Buckton and S. Chatham, *Int. J. Pharm.*, 82 (1992) 145–150.
[10] A. Adamson, *Physical Chemistry of Surfaces*, Wiley, New York, 1982, pp. 20–22.
[11] J. Beck, A. Lefebvre and T. Koblish, *J. Propul. Power.*, 7 (1991) 207–212.
[12] C. Sun and Q. Deng, *Huaxue Tongbao*, 9 (1992) 50–52.
[13] H. Ewart and E. Kenneth, *J. Chem. Ed.*, 69 (1992) 814–815.
[14] D. Bergink-Martens, C. Bisperik, H. Bos, A. Prins and A. Zuidberg, *Colloids Surf.*, 65 (1992) 191–199.
[15] H. Zhou, *Xheijing Daxue Xuebao Ziran Kevueban*, 26 (1992) 139–146.
[16] G. Kigle-Boeckler, *Surf. Phenom. Addit. Water-Based Coat. Print. Technol. 1990, Proc. Int. Symp.*, 269–282.
[17] I. Hundt and P. Neuberg, *Tagunsber. Akad. Landwirtschaftswiss.*, 294 (1990) 311–316.
[18] J. Comyn, *Int. J. Adhes. Adhes.*, 12 (1992) 145–149.
[19] P. Kharlashin, *Zavod. Lab.*, 58 (1992) 34–37.
[20] M. Chaudhury and G. Whitesides, *Science*, 256 (1992) 39–41.
[21] R. Cade, *J. Electrostat.*, 26 (1991) 275–289.

[22] V. Cauwenberg, C. Messemaekers, P. Von Pompay and M. Slater, *Process Metall.*, 7B (1992) 1265–1270.
[23] A. Avaranas and N. Papadopolous, *Langmuir*, 8 (1992) 2804–2809.
[24] T. Baumberger, F. Perrot and D. Beysens, *Europhys. Lett.*, 20 (1992) 577.
[25] A. Abramson, N. Makagonova, Y. Desten and T. Cherpalova, *Kolloidn. Zh.*, 54 (1992) 197–199.
[26] C. Cronan, *US Pat.*, 4 646 562 (1987).
[27] L. Lima III, D. Dunphy and R. Synovec, *Anal. Chem.*, 66 (1994) 1209–1216.
[28] L. Lima III and R. Synovec, *Anal. Chem.*, 65 (1993) 128–134.

ELSEVIER

Journal of Chromatography A, 691 (1995) 205–212

JOURNAL OF CHROMATOGRAPHY A

Chemometric characterization of Lewis base-modified zirconia for normal phase chromatography

David A. Whitman, Thomas P. Weber[1], John A. Blackwell*[,2]

Analytical Research and Development, 3M Pharmaceuticals, 3M Center, Building 270-4S-02, St. Paul, MN 55144-1000, USA

Abstract

Microporous zirconia was evaluated for its chromatographic properties as a normal phase support. Since previous studies in aqueous media had indicated a strong effect of eluent Lewis base on chromatographic properties, a number of Lewis base pretreatments of the support were evaluated as to their effect on normal phase selectivities. The retention characteristics of over thirty well characterized probe solutes were determined on eight different "acid"- or "base"-washed zirconia supports. These results were compared with those obtained for a silica column. Chemometric methodology was used to characterize the similarities and differences between the "acid"- and "base"-washed supports. The lack of chromatographic reproducibility previously observed under normal-phase conditions on zirconia appears to be a result of the lack of specific descriptions regarding the "acid" or "base" pretreatment.

1. Introduction

Early in the development of porous microparticulate zirconium oxide as a stationary phase for high-performance liquid chromatography, Rigney et al. [1,2] showed that this material demonstrates remarkable chemical stability. Zirconia does not dissolve to any significant extent in very basic or acidic solutions, thus allowing a wide variety of pH values to be used for separations. In addition, columns which have been used for bioseparations may be chemically sterilized by treatment with hot caustic without degradation of the support material.

Subsequent experiments have shown that the adsorptive properties of this material may be significantly altered by dynamically treating the support with Lewis bases [3–10]. Lewis bases show varying degrees of interaction with the Lewis acid sites present on the zirconia surface depending upon structure, charge, etc. Hence, they show varying degrees of eluotropic strength towards other solute Lewis bases which compete for the same Lewis acid sites [6,7,9]. Although some interactions may be quite strong, washing the support with 0.1 *M* sodium hydroxide brings back to the original adsorptive properties of the material [3,9]. This recycling can be carried out numerous times with the main limitation being the stability of the stainless steel column and pumping hardware in caustic. Since the adsorptive properties of this material are readily man-

* Corresponding author. Present address: Chemical Process R&D, Du Pont Merck Pharmaceutical Company, PRF-1, Chambers Works, Deepwater, NJ 08023, USA.

[1] Present address: CIMA Labs. Inc., 7325 Aspen Lane, Minneapolis, MN 55428, USA.

[2] Present address: Chemical Process R + D, Dupont Merck Pharmaceutical Company, PRF-1, Chambers Works, Deepwater, NJ 08023, USA.

0021-9673/95/$09.50
SSDI 0021-9673(94)01098-6

ipulated and regeneration is rapid and reproducible, the support is an ideal candidate for use as a "custom" adsorbent for normal-phase chromatography.

Selectivity in normal-phase chromatography is presently dominated by the composition of the mobile phase [11]. The adsorption strength of silica or alumina is usually modified by addition of water or other polar additives. Retention is then optimized by adjusting the eluotropic strength of the eluent. The shape selectivity, which is the dominant advantage in normal-phase chromatography, is more or less constant for a given adsorbent. Some differences are observed between acidic, neutral and basic alumina, but these differences are not well characterized [11].

The object of this investigation is the development of novel adsorptive phases using zirconium oxide as an underlying support. Adsorption of various Lewis bases should affect the net adsorptive interactions towards solutes through the masking of Lewis acid sites and production of secondary interactions between adsorbed Lewis bases and the solutes. These customized phases could be used for various separations requiring unique selectivities. After the separations are performed, the support could be stripped of the Lewis base modifier and the zirconia, modified with a different Lewis base, used for another separation. This would give the separation scientist a spectrum of selectivities with only one column. To facilitate the rational characterization of a number of Lewis base-modified phases, a combination of solvatochromic theory and principal component analysis was used for cluster analysis. Principal components analysis allows effective data reduction and visualization of results.

2. Experimental

2.1. Chemicals

All solutes used in this study were reagent grade or better and were obtained from commercial sources. Sodium fluoride, ammonium hydroxide (30% solution), sodium hydroxide (50% solution), phosphoric, sulfuric, boric, hydrochloric and formic acids were analytical-reagent grade reagents obtained from Mallinckrodt (Paris, KY, USA). Isopropanol, dichloromethane and hexane were ChromAR-grade solvents also from Mallinckrodt. HPLC-grade water was obtained from Baxter Scientific (McGraw Park, IL, USA).

2.2. Chromatographic systems

Chromatography was performed on two separate systems. Retention studies were performed on a Hewlett-Packard (Avondale, PA, USA) Model 1090M liquid chromatograph with a DR5 ternary solvent-delivery system and a diode array detector. Data were processed using a Hewlett-Packard 9000/Series 300 computer outfitted with ChemStation software. Corrosive solutions were pumped using a Dionex (Sunnyvale, CA, USA) Model 300 liquid chromatograph.

2.3. Chromatographic supports

The porous microparticulate zirconium oxide particles used in this study were obtained from the Ceramic Technology Center at 3M and were described in detail earlier [1–3,9]. The particles had a nominal diameter of 5.3 μm ± 1.3 μm, an average pore diameter of 308 Å by mercury porosimetry and an average BET surface area of 32.5 m^2/g. The particles were initially pretreated in order to remove as many of the manufacturing impurities as possible and provide a consistent starting point, as described in detail earlier [3,9].

Columns were prepared in 50 mm × 4.6 mm column blanks fitted with 1/4-in. Parker end fittings (1 in. = 2.54 cm). Titanium screens with 2 μm mesh were used instead of frits to minimize any potential metal ion contamination from the frits. Columns were packed by the upward slurry technique using isopropanol as the solvent. Packing pressure was 4500 p.s.i. (1 p.s.i. = 6894.76 Pa). Following the packing procedure, all columns were flushed with water to displace all the packing solvent prior to further treatment. The silica column was packed with 5 μm Spherisorb silica (50 mm × 4.6 mm) and was obtained from Phenomenex (Torrance, CA, USA).

Lewis base modification was accomplished by flushing 50 ml of 0.1 *M* sodium hydroxide through the columns at 1.0 ml/min (25°C). For each of the different phases, this was followed by 50 ml of 0.1 *M* ammonium hydroxide, 0.1 *M* hydrochloric acid, 0.1 *M* sulfuric acid, 0.1 *M* phosphoric acid, 0.1 *M* sodium fluoride with 0.05 *M* hydrochloric acid, 0.1 *M* boric acid or 0.1 *M* formic acid. This was immediately followed by a flush with 50 ml HPLC-grade isopropanol.

2.4. Stability studies

The stability of each of the Lewis base-modified supports was assessed by monitoring the retention of benzyl alcohol at 45°C. The eluent [1% (v/v) isopropanol in hexane] was pumped at 0.75 ml/min at 45°C and 10-μl volumes of 1000 ppm (w/w) benzyl alcohol in dichloromethane were made each hour following a 1000 column equilibration period. Stability was then assessed for a period of 4000 column volumes. A commercially prepared silica column was also tested for comparison. The capacity factors were calculated based on peak maxima.

2.5. Retention studies

The retention characteristics of the Lewis base-modified phases were probed using a wide variety of solutes. Injections of 10 μl of each solute (1000 ppm in dichloromethane) were made and elution monitored at 254 nm.

2.6. Multivariate data analysis

The inherent similarity of the Lewis base-modified zirconia phases and solutes was investigated using principal components analysis. The use of principal components analysis for exploratory data analysis is well known [12]. The data were analyzed using the singular value decomposition (SVD) approach to principal components analysis [13]. All data transformations and calculations were made using built-in routines of MATLAB 4.0 (MathWorks, Natick, MA, USA, 1993). The principal component axes that define the variance in both the Lewis base pretreatment (chemical modification) and the variance in the probe solutes were calculated using log transformed k' data.

3. Results and discussion

3.1. Column stability

Benzyl alcohol was chosen as a probe of stationary phase stability since its retention is sensitive to changes in hydrogen bonding. Loss of adsorbed water or chemisorbed Lewis base would affect the amount and strength of hydrogen bonding sites, thus affecting the resulting capacity factor. The results of these stability studies are given in Table 1.

A commercially available silica column was

Table 1
Stability of Lewis base-modified phases

Treatment	*n*	k'		h	
		Average	R.S.D. (%)	Average	R.S.D. (%)
NaOH	53	2.67	1.3	25.5	4.0
NH_4OH	53	5.18	1.3	12.7	18.8
HCl	53	1.85	1.9	9.2	9.2
H_2SO_4	52	1.02	4.9	6.0	5.4
H_3PO_4	51	1.05	4.0	13.0	5.5
H_3BO_3	52	7.50	3.2	176.9	12.7
HCOOH	51	6.19	1.6	87.9	3.2
NaF/HCl	51	1.88	2.4	12.3	1.5
Silica	53	1.20	4.4	3.0	2.7

used, as received from the vendor, as a reference system. The equilibration of silica columns in normal-phase chromatography is known to be quite slow [11]. Therefore, to compare stability rather than equilibration periods, the columns were pre-equilibrated with 1000 column volumes of eluent. Stability was then assessed with the assumption that most of the equilibration had been completed.

The Lewis base-modified zirconia phases showed a reasonable degree of stability compared to the silica phase. A slow change in capacity factor was evident in the data, but may be attributed to the last stages of water content equilibrium. Despite this effect, the standard deviations for the modified zirconia phases showed remarkable stability.

3.2. Retention of test solutes

A wide variety of solutes was used to further assess the changes incurred by pretreatment of the zirconia particles. Table 2 lists the solutes and their solvatochromic parameters which will be useful in rationalizing the changes in retention between the phases [15,16]. The terms are described as: π^* = solute dipolarity/polarizability, α = hydrogen bond acidity and β = hydrogen bond basicity.

The capacity factors for the test solutes in a hexane eluent containing 1% (v/v) chloroform are shown in Table 3. In general, the Lewis base-modified zirconia phases show similar selectivity to silica. However, a number of solutes deviate markedly from this generalization.

Weakly retained solutes, on silica and modified zirconia, tend to have low π^*, α and β values. These include aromatic solutes with aliphatic and halogen substituents. Little selectivity or retention is shown for any of these solutes despite the relatively weak eluent.

On silica, solutes with larger solvatochromic parameters (α and β) tend to have higher capacity factors. This trend is also observed among the modified zirconia supports, although the different phases show quite different selectivities towards these solutes.

It is evident from the data of Tables 2 and 3 that most solutes with large α and β values are not eluted under these mild elution conditions. Of the solutes which do elute, significant differences in selectivity are observed. For example, sodium hydroxide-washed zirconia shows small capacity factors for benzaldehyde, nitromethane and pyridine while the other phases show very large capacity factors under identical conditions. Even ammonium hydroxide-washed zirconia shows significantly different retention patterns despite both being "base-washed" zirconia (Fig. 1). Other less dramatic differences in retention are observed for benzyl cyanide.

In order to better understand the inherent differences and similarities between the probe solutes and Lewis base modified zirconia phases

Table 2
Solvatochromic parameters for probe solutes

Solute	Number	π^*	α	β
Acetone	26	0.38	0.01	0.50
Acetophenone	16	0.90	0.00	0.51
Aniline	12	0.73	0.26	0.38
Anisole	13	0.73	0.00	0.26
Benzaldehyde	19	0.92	0.00	0.42
Benzene	32	0.59	0.00	0.14
Benzonitrile	2,33	0.90	0.00	0.42
Benzyl alcohol	15	0.99	0.39	0.42
Benzyl cyanide	6	0.75	0.00	0.48
Bromobenzene	18	0.79	0.00	0.06
2-Butanone	29	0.39	0.00	0.48
n-Butylbenzene	17	0.49	0.00	0.12
tert.-Butylbenzene	7	0.42	0.00	0.12
Chlorobenzene	4	0.71	0.00	0.07
m-Cresol	20	0.68	0.58	0.24
o-Dichlorobenzene	3	0.80	0.00	0.03
p-Dichlorobenzene	5	0.70	0.00	0.03
Ethylbenzene	8	0.53	0.00	0.15
Iodobenzene	21	0.81	0.00	0.05
Methyl benzoate	28	0.76	0.00	0.39
Nitrobenzene	22	1.01	0.00	0.30
Nitromethane	27	0.85	0.12	0.25
o-Nitrotoluene	10	0.90	0.00	0.25
Phenol	25	0.72	0.60	0.22
n-Propylbenzene	9	0.51	0.00	0.12
Pyridine	31	0.87	0.00	0.62
Styrene	24	0.55	0.00	0.18
Toluene	23	0.55	0.00	0.14
m-Xylene	30	0.51	0.00	0.17
o-Xylene	14	0.51	0.00	0.17
p-Xylene	11	0.51	0.00	0.17

Table 3
k' for 1% (v/v) chloroform in hexane

Solute	Silica	NaOH	HCl	NH_4OH	H_3PO_4	H_2SO_4	NaF	H_3BO_3	HCOOH
Acetone	0.85	0.15	0.19	0.10	0.15	0.34	0.39	0.03	0.05
Acetophenone	0.30	0.04	0.15	0.08	0.08	0.12	0.12	0.01	0.03
Aniline	0.48	0.37	4.79	0.75	>30	>30	5.05	1.01	1.56
Anisole	0.04	0.03	0.07	0.06	0.03	0.04	0.01	0.00	0.01
Benzaldehyde	0.19	0.12	0.18	0.20	0.09	0.18	0.15	0.07	0.11
Benzene	0.01	0.07	0.09	0.10	0.05	0.05	0.01	0.00	0.01
Benzonitrile	0.13	0.07	0.09	0.09	0.05	0.09	0.10	0.01	0.02
Benzyl alcohol	1.10	3.00	1.92	5.27	0.99	1.27	1.95	8.15	6.99
Benzyl cyanide	0.17	0.09	0.10	0.08	0.05	0.13	0.14	3.05	0.02
Bromobenzene	0.00	0.04	0.08	0.08	0.03	0.05	0.01	0.00	0.01
2-Butanone	0.53	0.12	0.17	0.11	0.11	0.16	3.13	0.02	0.03
n-Butylbenzene	0.00	0.04	0.06	0.09	0.03	0.05	0.01	0.00	0.01
tert.-Butylbenzene	0.00	0.04	0.07	0.08	0.02	0.05	0.00	0.00	0.00
Chlorobenzene	0.00	0.05	0.05	0.06	0.04	0.08	0.01	0.01	0.01
m-Cresol	0.64	>30	7.94	>30	0.51	0.50	1.86	>30	>30
o-Dichlorobenzene	0.00	0.04	0.07	0.07	0.04	0.06	0.01	0.00	0.01
p-Dichlorobenzene	0.00	0.04	0.07	0.10	0.03	0.07	0.01	0.00	0.01
Ethyl benzene	0.00	0.04	0.06	0.07	0.02	0.05	0.01	0.00	0.00
Iodobenzene	0.00	0.05	0.07	0.08	0.03	0.05	0.01	0.00	0.01
Methyl benzoate	0.17	0.08	0.10	0.07	0.06	0.05	0.08	0.00	0.02
Nitrobenzene	0.02	0.06	0.08	0.11	0.04	0.09	0.00	0.00	0.00
Nitromethane	0.12	>30	0.09	>30	0.06	0.07	0.14	>30	>30
o-Nitrotoluene	3.01	0.04	0.08	0.09	0.03	0.08	2.91	0.00	0.00
Phenol	0.69	>30	8.85	>30	0.56	0.50	2.27	>30	>30
n-Propylbenzene	0.00	0.05	0.08	0.09	0.03	0.05	0.00	0.00	0.00
Pyridine	6.70	0.62	23.33	1.79	>30	>30	5.57	2.88	4.82
Styrene	0.00	0.04	0.07	0.12	0.04	0.04	0.00	0.00	0.00
Toluene	0.00	0.06	0.08	0.06	0.04	0.04	0.01	0.00	0.01
m-Xylene	0.00	0.05	0.07	0.11	0.03	0.04	0.01	0.00	0.01
o-Xylene	0.00	0.05	0.08	0.07	0.02	0.04	0.01	0.00	0.01
p-Xylene	0.00	0.04	0.08	0.08	0.03	0.06	0.01	0.00	0.00

with respect to silica, a multivariate approach to data analysis was taken.

3.3. Principal components analysis

The data from Table 3 were evaluated by principal component analysis (PCA) using the singular value decomposition method. The singular value decomposition allows simultaneous principal component analysis of both the solute (column) space and the chemical modification (row) space.

In PCA of a matrix $\boldsymbol{R}$ (n samples $\times$ m responses), the eigenvectors of the variance–covariance matrix ($\boldsymbol{R}\boldsymbol{R}^{\mathrm{T}}$) are computed. The eigenvectors or principal components axes define the weight each response contributes to account for the maximum variance between the samples.

The singular value decomposition states that any matrix $\boldsymbol{R}$ can be decomposed into three matrices $\boldsymbol{U}$, $\boldsymbol{S}$ and $\boldsymbol{V}$ (Eq. 1):

$$\boldsymbol{R} = \boldsymbol{U}\boldsymbol{S}\boldsymbol{V}^{\mathrm{T}} \quad (1)$$

where the columns of $\boldsymbol{U}$ are the eigenvectors of $\boldsymbol{R}\boldsymbol{R}^{\mathrm{T}}$, that is the principal component axes describing the variance in the solute (column) space for these data. The columns of $\boldsymbol{V}$ are the eigenvectors of $\boldsymbol{R}^{\mathrm{T}}\boldsymbol{R}$. In other words, the columns of $\boldsymbol{V}$ define the principal component axes of $\boldsymbol{R}^{\mathrm{T}}$ which describe the variance in the chemical modification (row) space of these data. The main diagonal elements of $\boldsymbol{S}$ are the square roots of the eigenvalues of both $\boldsymbol{R}\boldsymbol{R}^{\mathrm{T}}$ and $\boldsymbol{R}^{\mathrm{T}}\boldsymbol{R}$.

It is known from solvatochromic theory that there is an approximate linear relationship between ln k' and the solvatochromic parameters π^*, α and β. This intrinsic linear relationship to

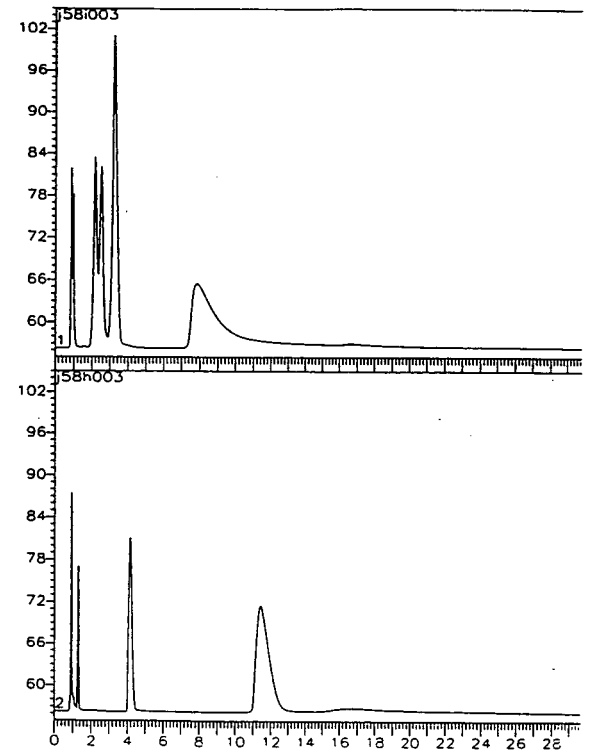

Fig. 1. Chromatograms show the difference between "base"-washed zirconias. (Top) Sodium hydroxide-washed zirconia; (bottom) ammonium hydroxide-washed zirconia. x-axis: Time in min; y-axis: absorbance at xxx nm.

the ln k' data is supported when the eigenvalues are compared for the k' and ln k' matrices. The first eigenvector describes 72% of the variance when the k' data is analyzed using PCA, whereas, the first eigenvector of the log transformed data describes 92% of the variance in the data. In addition, the ln k' data show better resolution between the both solutes and the chemical modifications so a more meaningful interpretation of the data is possible. For these reasons the remainder of the discussion and all conclusions will be based on the PCA of the ln k' data.

It is possible to do a form of cluster analysis using the principal component axes and coordinants (scores) to investigate the inherent similarities between solutes and chemical modifications. The same plots can be used to visually determine which solutes are important in defining differences between the chemical modifications and conversely which chemical modifications are useful in resolving the solutes.

Two principal component axes were used for characterization of these data. The reasons for using only two eigenvectors stem from the precision of the data analyzed. Over 97% of the variance is described in the first two eigenvectors of the log transformed data. From Table 1, the precision of these retention data is good to about 3–4%. Given the small incremental contribution to the description of variance by additional eigenvectors, and the precision of the measurements, it is reasonable to expect that most chemical information should be evident in the first two principal components.

3.4. Solute role in chemical modification variance

The contributions of the solutes to describe differences between the chemical modifications will be shown. The easiest manner to display these data is to plot the solutes scores in the chemical modification space. The solutes scores are plotted in the space defined by the chemical modification principal component axes 1 and 2 (Fig. 2). The number labels in the graph correspond to the solute number in Table 2 (solute 1 is the system blank). Solutes with positive scores are positively correlated to the variance defined by the principal component and those with negative scores are negatively correlated. It is important to note that both positive and negative scores are equally important in the description of the variance.

Many observations can be made from Fig. 2. Immediately, one can see a cluster of solutes that are only weakly retained on all the chemically modified zirconia phases. This tightly grouped cluster contains about half of all the solutes. It is noteworthy that these solutes have π^* values that are representative of the range covered by all solutes, however, every point in the cluster has low α and β parameters. The second cluster is not quite as tight as the first but is well defined. These solutes uniformly have high β

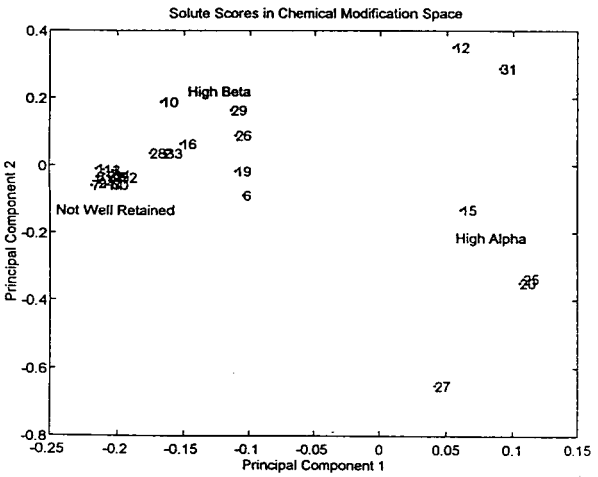

Fig. 2. Solutes plotted in Lewis base modification principal component space (principal component 1 versus 2). PCA performed on ln k' data from Lewis base-modified zirconia only. Clusters are evident for those solutes which are not well retained, those with high β values and those with high α values.

parameters with the exception of *o*-nitrotoluene (solute 10). The third cluster is composed of all solutes that have high α parameters. Each of these analytes has a positive score in principal component 1, whereas all other solutes have negative scores. The one anomaly in this cluster is pyridine (solute 31) which has a very high β parameter but a low α. Pyridine is well known as a very good Lewis base. Parameters that define Lewis basicity (e.g. β and π^*) for some Lewis bases may be different for pyridine. These observations point to the current lack of a Lewis basicity scale, but also to the possibility of establishing such a scale. These observation show that the differences between the Lewis base-modified zirconia are best displayed by test solutes with high α or β parameters. These are solutes with high Lewis base character.

Solutes 2 and 33 both represent benzonitrile. This solute was run first and last as a check of reproducibility of the chromatographic phases. Fig. 2 shows that the scores for the replicates are almost identical which supports the claim of stability and reproducibility.

3.5. Chemical modification role in solute variance

To characterize the inherent similarities and differences between the Lewis base-modified zirconia and bare silica, the chemical modification scores were plotted on the solute space principal component axes. In this section, the (PCA) will compare and contrast the selectivities of the Lewis base-modified zirconia for the probe solutes. The data for silica are included in this analysis to be used as a comparator. The chemically modified zirconia and silica scores are shown for solute space principal component 1 versus 2 in Fig. 3. The chemically modified zirconia points are labeled with both a number and the identity of the Lewis base modification. There are four clusters that can be seen in the plot of principal component 1 versus 2. These clusters can be categorized as strong bases, strong acids, weak acids (with high Lewis basicity), and silica.

Interestingly, the sodium fluoride-modified zirconia is very similar to bare silica. There is almost no difference in the scores of these materials on principal component 1 which ac-

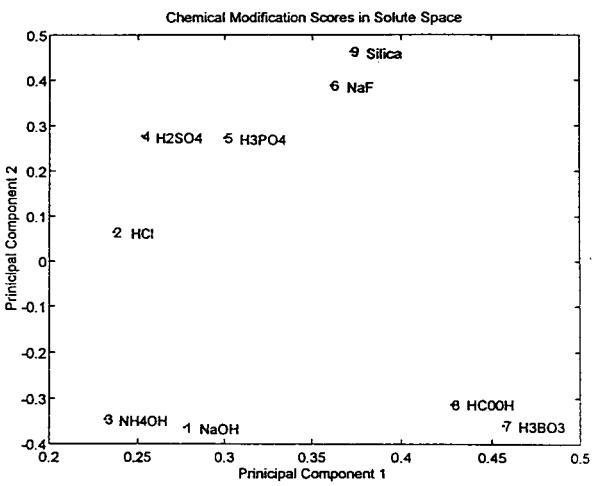

Fig. 3. Lewis base-modified zirconia phases and bare silica phase plotted in solute principal component space (principal component 1 versus 2). The differences between "acid" or "base" treatments are illustrated.

counts for over 90% of the variance in the data. In addition, these phases are very close in the principal component 2 space. The practical implication of this is that from a first-order approximation, there is little difference in the selectivity of silica and NaF-pretreated zirconia.

The "strong base" and "weak acid"-modified zirconia (sodium hydroxide, ammonium hydroxide, formic acid and boric acid) show solute retention characteristics which are opposite to silica in principal component 2. The important observation between these two phases is that there is a significant difference between "strong base"-modified zirconias. Caution must be taken by the analyst to specifically state which base wash is required.

The distribution of the acids on this plot is even more pronounced than for the bases. There is a large and clear separation between the strong and weak acids. The significant difference between sulfuric and phosphoric acids on principal component axis 1 and hydrochloric and sulfuric acid on principal component axis 2 emphasizes that the nature of the "acid" wash must be clearly defined or perceived reproducibility problems will arise.

4. Conclusions

Care should be taken when preparing "acid"- or "base"-washed zirconia for normal-phase applications. Changes in selectivity and efficiency result from interactions between Lewis bases in the wash solution and the zirconia Lewis acid sites. Any pretreatment of an adsorbent, prior to use under normal-phase conditions, should be explained and reproduced in detail.

Once modified, however, the zirconia supports prove to be quite stable and useful for obtaining a variety of selectivities with only one column. Hydrogen bonding interactions are quite pronounced for the Lewis base-modified zirconia, the extent of which differs greatly among the various Lewis bases used to modify the zirconia. Dipolarity/polarizability appears to be a much weaker interaction under the conditions employed in these studies. Similar results can be expected for alumina adsorbents as well, since the Lewis acid properties of alumina are comparable to that of zirconia [10].

PCA was shown to be a powerful tool for the characterization of diverse chromatographic phases. Qualitative PCA, in combination with solvatochromic theory, suggests that a quantitative Lewis basicity scale may be able to be established.

References

[1] M.P. Rigney, *Ph.D. Thesis*, University of Minnesota, Minneapolis, MN, 1988.
[2] M.P. Rigney, E.F. Funkenbusch and P.W. Carr, *J. Chromatogr.*, 499 (1990) 291.
[3] J.A. Blackwell and P.W. Carr, *J. Chromatogr.*, 547 (1991) 43.
[4] J.A. Blackwell and P.W. Carr, *J. Chromatogr.*, 547 (1991) 59.
[5] J.A. Blackwell and P.W. Carr, *J. Liq. Chromatogr.*, 14 (1991) 2875.
[6] J.A. Blackwell and P.W. Carr, *Anal. Chem.*, 64 (1992) 853.
[7] J.A. Blackwell and P.W. Carr, *Anal. Chem.*, 64 (1992) 863.
[8] J.A. Blackwell and P.W. Carr, *J. Chromatogr.*, 596 (1992) 27.
[9] *J.A. Blackwell, Ph.D. Thesis*, University of Minnesota, Minneapolis, MN, 1991.
[10] J.A. Blackwell, *Chromatographia*, 35 (1993) 133.
[11] J.J. Kirkland, *Introduction to Modern Liquid Chromatography*, Wiley, New York, 2nd ed., 1979.
[12] M.A. Sharaf, D.L. Illman and B.R. Kowalski, *Chemometrics*, Wiley, New York, 1986.
[13] T. Naes and H. Martens, *Commun. Statistics Simula. Computa.*, 14 (1984) 735.
[14] J. Li, Y. Zhang, A.J. Dallas and P.W. Carr, *J. Chromatogr.*, 550 (1991) 101.
[15] J.H. Park and P.W. Carr, *J. Chromatogr.*, 465 (1989) 123.
[16] M. Andersson, E. Arvidsson, S. Jansson and E. Johansson, presented at the *16th International Symposium on Column Liquid Chromatography, Baltimore, MD, June 1992.*

ELSEVIER

Journal of Chromatography A, 691 (1995) 213–216

JOURNAL OF CHROMATOGRAPHY A

High-performance chiral displacement chromatographic separations in the normal-phase mode III. Separation of the enantiomers of 5-vinylpyrrolidin-2-one using the Chiralcel-OD stationary phase

Pearle L. Camacho-Torralba[1], Gy. Vigh*

Chemistry Department, Texas A&M University, College Station, TX 77843, USA

Abstract

A normal-phase displacement chromatographic method has been developed for the preparative-scale separation of the enantiomers of 5-vinylpyrrolidin-2-one using Chiralcel OD as chiral stationary phase, a solvent mixture of isopropanol–*n*-hexane (10:90, v/v) as carrier solution and 2-pyrrolidinone as displacer. Sample loads as high as 28 mg could be applied onto the 4.6 mm I.D. columns. Effluent fractions of 100 μl were collected during the displacement chromatographic runs and analyzed for enantiomeric purity in order to calculate the percent recoveries and the production rates.

1. Introduction

Earlier, we demonstrated [1] that successful normal-phase displacement chromatographic separations of enantiomers could be achieved using a family of 3,5-dinitrobenzoyl ester derivatives as displacers [2] on the N-(2)-naphthylalaninate silica π-electron donor chiral stationary phase (CSP) developed by Pirkle et al. [3–7]. This paper describes the first successful use of the chiral stationary phase Chiralcel OD, a silica-based material physically coated with cellulose tris(3,5-dimethylphenyl carbamate), in the normal-phase displacement chromatographic mode of preparative separation.

Both enantiomers of the potent GABA-T inhibitor, 4-amino-5-hexenoic acid, have been prepared by the potassium hydroxide hydrolysis [8] of the corresponding enantiomer of 5-vinylpyrrolidin-2-one (VP) [9,10]. A preparative separation method was sought to augment the enantioselective synthetic efforts to produce laboratory-scale quantities of enantiomerically pure *S*-VP. The enantiomers could be well separated on the Chiralcel OD column on the analytical scale, with the interesting *S*-enantiomer eluting last [11]. Therefore, VP was selected to demonstrate that effective displacement chromatographic separations can be developed on the Chiralcel OD stationary phase when operated in the normal-phase mode.

2. Experimental

Three 4.6 mm I.D. × 250 mm Chiralcel OD

* Corresponding author.

[1] Present address: Fujisawa USA, Melrose Park, IL 60160, USA.

0021-9673/95/$09.50
SSDI 0021-9673(94)01103-6

columns, containing cellulose tris(3,5-dimethylphenyl carbamate) physically coated onto silica, were obtained from Chiral Technologies (Exton, PA, USA). One of the columns was used for the linear elution mode retention studies and the fraction analysis work. The other two columns, connected in series, were used for the displacement chromatographic separations. The columns were thermostatted at 30°C by a water jacket and a Model UF-3 recirculating water bath (Science/Electronics, Dayton, OH, USA).

The displacement chromatographic separations were carried out with a displacement chromatograph, built in our laboratory, as described in Ref. [1]. The system consisted of two Type 2020 pumps, a Type 2050 variable-wavelength UV detector (set at 210 nm) and a Type RI-3 differential refractive index detector (all from Varian, Walnut Creek, CA, USA). The samples were injected by a pneumatically activated, computer-controlled Type 7125 injection valve, equipped with a 1-ml sample loop (Rheodyne, Cotati, CA, USA). The carrier and displacer solutions, delivered by the two Type 2020 pumps, were switched by a Type 7010 switching valve (Rheodyne). System control, data collection and analysis was achieved with the aid of a Model 4270 integrator (Varian), connected to a NEC Powermate I AT-compatible computer (Computer Access, College Station, TX, USA), and the Chrom1 program developed in our laboratory [12]. Both the UV detector signals and the RI detector signals were recorded simultaneously. During the displacement chromatographic separations, 100 μl effluent fractions were collected with a Cygnet fraction collector (ISCO, Lincoln, NE, USA) as soon as the detector signals began to rise. Both data and fraction collection were halted when the RI detector signal reached its upper plateau. After the displacement chromatographic run, the displacer was removed from the columns by pumping an isopropanol–*n*-hexane (10:90, v/v) solvent mixture through them until the absorbance of the column effluent matched that of the fresh wash solvent.

A liquid chromatograph consisting of a Type 2020 pump, a Type 2050 variable-wavelength UV detector (Varian), a pneumatically activated, computer-controlled Type 7125 injection valve (Rheodyne) equipped with a 10-μl sample loop, and a Maxima 820 Chromatographic Work Station (Millipore, Bedford, MA, USA), was used to complete the elution mode retention studies and the fraction analysis work.

The carrier solution, used at a flow-rate of 1 ml/min, was an isopropanol–n-hexane (10:90, v/v) solvent mixture prepared from HPLC grade solvents (Baxter, Muskegon, MI, USA). The displacer, reagent grade 2-pyrrolidinone (PD), was obtained from Aldrich (Milwaukee, WI, USA). The sample, VP, was obtained from Dow Chemical (Midland, MI, USA), and used without further purification. Both the sample and the displacer were dissolved in the carrier solution.

For fraction analysis, the solvent was evaporated from each collected 100 μl fraction, the residues were redissolved in 500 μl volumes of the eluent [isopropanol–*n*-hexane (10:90, v/v) solvent mixture] that contained 2-phenylethanol (Aldrich) as achiral internal standard, and analyzed for chiral purity using peak areas and individual calibration curves. The reconstructed displacement chromatograms were obtained from these data and used to calculate product purities, recoveries and production rates.

3. Results and discussion

The chromatogram of a dilute VP sample, obtained with the isopropanol–*n*-hexane (10:90, v/v) solvent mixture as eluent, is shown in Fig. 1. The capacity factors for the less retained and the more retained enantiomers are 1.38 and 1.85, and the separation selectivity, α, is 1.34. Because VP is lightly retained on the Chiralcel OD column, it was expected that its starting material, PD, which is somewhat more polar than VP itself, could act as a displacer candidate. Indeed, when analyzed at infinite dilution, the capacity factor of PD was found to be higher (2.66) than that of VP; its adsorption isotherm proved to be sufficiently competitive and there

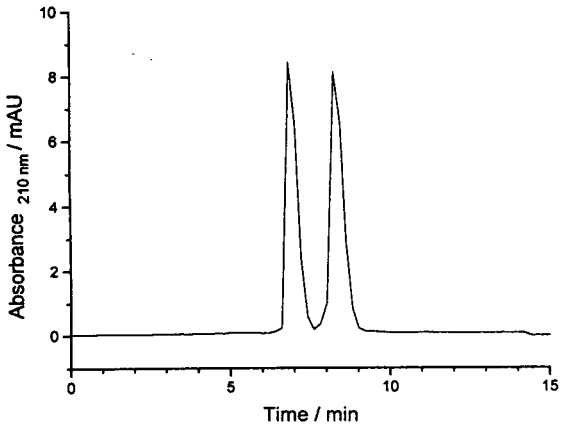

Fig. 1. Recorded elution mode chromatogram of a dilute sample of VP on a 4.6 mm I.D. × 250 mm Chiralcel OD column. Eluent: isopropanol–*n*-hexane (10:90, v/v) solvent mixture. Flow-rate: 1 ml/min. Temperature: 30°C.

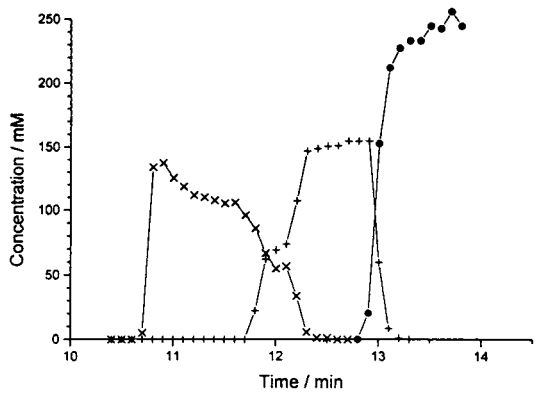

Fig. 3. Reconstructed displacement chromatogram of a 28-mg sample of VP. Conditions as in Fig. 2.

were no solubility or column stability problems up to a displacer concentration of 250 m*M* [13]. Thus, 2-pyrrolidinone, was deemed a suitable displacer for the preparative experiments.

A displacement chromatographic separation of a 28-mg VP sample, obtained with a 250-m*M* PD displacer solution is shown in Fig. 2. Analysis of the collected fractions (100 μl each) and the plotting of the results in the reconstructed displacement chromatogram (Fig. 3) revealed that at this load the displacement train is not quite developed yet (a portion of the less retained enantiomer leaves the column by elution), and that there is a small mixed zone between the two pure enantiomers. However, the more retained *S*-enantiomer and the displacer are separated by a well-defined, sharp zone.

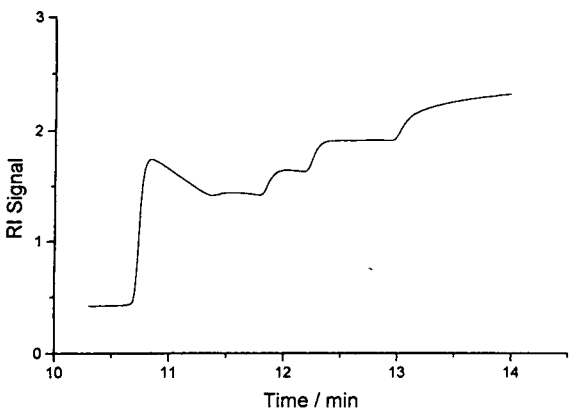

Fig. 2. Recorded displacement chromatogram of a 28-mg sample of VP obtained on two 4.6 mm I.D. × 250 mm Chiralcel OD columns connected in series. Displacer solution: 250 m*M* PD dissolved in a solvent mixture of isopropanol–*n*-hexane (10:90, v/v) used as carrier solution. Flow-rate: 1 ml/min.

The enantiomeric purities of the pooled fractions were calculated from the reconstructed displacement chromatogram and are shown in Fig. 4 as a function of the recovered amount (bottom axis) and the production rate (top axis). Forward pooling was used for the less retained *R*-enantiomer, backward pooling for the more retained *S*-enantiomer. It can be seen that about 11 mg of the *R*-enantiomer and 7 mg of the *S*-enantiomer can be collected at an enantiomeric purity of better than 99.9%. When the purity requirement is relaxed to 95%, almost identical amounts (12.5 mg vs. 12.6 mg) can be collected for both enantiomers.

Production rates (shown on the top axis) were calculated from the actual separation times, with no allowance for column regeneration. When 100% enantiomeric purity is required, about 820 μg/min can be produced of the *R*-enantiomer. For the *S*-enantiomer, the production rate at the

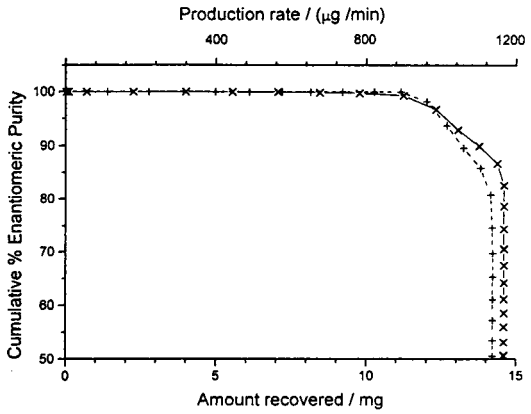

Fig. 4. Plot of cumulative % enantiomeric purity vs. amount of enantiomer recovered (bottom axis) and production rate (top axis) plots for the displacement chromatographic separation shown in Fig. 3. Symbols × = *R*-VP; + = *S*-VP.

100% purity level is lower, about 520 μg/min. Lowering the target purity to 95% boosts the production rates for both enantiomers to the same, higher level: 920 and 930 μg/min, respectively.

The recovery values for both enantiomers are very encouraging: about 78% of the *R*- and 48% of the *S*-enantiomer loaded onto the column can be recovered at 100% enantiomeric purity. For a lower, 95% target enantiomeric purity, 88% of the *R* and 87% of the *S*-enantiomer can be recovered.

4. Conclusions

It has been found that the enantiomers of VP, a pharmaceutical intermediate, could be separated on a cellulose-based Chiralcel OD stationary phase with a modest selectivity coefficient of 1.34, and moderate retention (capacity factor of the more retained enantiomer is 1.85). PD, the starting material used in the synthesis of VP, is more retained than VP itself, has a competitive, non-linear adsorption behavior, and can be readily used as a displacer for the separation. Under the selected conditions, up to 28 mg of racemic VP could be loaded onto the two 4.6 mm I.D. analytical columns connected in series. The good enantiomeric purity and high yield of the separated fractions demonstrates that though the Chiralcel OD column contains a physically coated chiral stationary phase, it can be used in the normal-phase mode to achieve preparative displacement chromatographic separations of pharmaceutically interesting enantiomers.

Acknowledgements

Partial financial support by the National Science Foundation (CH-8919151), the Texas Coordinating Board of Higher Education TATR Program (Grant Number 3376) and the Dow Chemical Company (Midland, MI, USA) is gratefully acknowledged. The authors are indebted to Dr. Nishimura of Chiral Technologies for the donation of the Chiralcel OD columns used in this study, and L. Nicholson of Dow Chemicals for valuable discussions.

References

[1] P.L. Camacho-Torralba, M.D. Beeson, Gy. Vigh and D.H. Thompson, *J. Chromatogr.*, 646 (1993) 259.
[2] P.L. Camacho, Gy. Vigh and D.H. Thompson, *J. Chromatogr.*, 641 (1993) 31.
[3] W.H. Pirkle, J.M. Finn, J. L Schreiner and B.C. Hamper, *J. Am. Chem. Soc.*, 103 (1981) 3964.
[4] W.H. Pirkle and T.C. Pochapsky, *J. Org. Chem.*, 51 (1986) 102.
[5] W.H. Pirkle and T.C. Pochapsky, *J. Am. Chem. Soc.*, 108 (1986) 352.
[6] W.H. Pirkle and T.C. Pochapsky, *J. Am. Chem. Soc.*, 108 (1986) 5267.
[7] W.H. Pirkle, T.C. Pochapsky, G.S. Mahler, D.E. Corey, D.S. Reno and D.M. Alessi, *J. Org. Chem.*, 51 (1986) 102.
[8] C.T. Goralski, J.F. Hoops and K.A. Ramanarayanan, *Eur. Pat.*, 0 427 197 B1, April 27, 1994.
[9] Z.Y. Wei and E.E. Knauss, *Syn. Lett.*, (1993) 295.
[10] Z.Y. Wei and E.E. Knauss, *Tetrahedron*, 50 (1994) 5569.
[11] L. Nicholson, Dow Chemical Company, private communication.
[12] Gy. Vigh, G. Quintero and Gy. Farkas, *J. Chromatogr.*, 484 (1989) 251.
[13] P.L. Camacho, *Dissertation*, Texas A&M University, College Station, TX, 1991.

ELSEVIER

Journal of Chromatography A, 691 (1995) 217–224

JOURNAL OF CHROMATOGRAPHY A

Comparison of the retention of organic acids on alkyl and alkylamide chemically bonded phases

T. Czajkowska[a], I. Hrabovsky[a], B. Buszewski[b,1], R.K. Gilpin[b], M. Jaroniec[b,*]

[a]*Agricultural Research Division, American Cyanamid Company, Princeton, NJ 08543, USA*

[b]*Department of Chemistry, Kent State University, Kent, OH 44242, USA*

Abstract

Retention of pyridine and indole carboxylic acids was studied on alkylamide bonded phases under reversed-phase conditions at 35°C. The alkylamide phases were synthesized by a two-step process, in which an initial amino phase was prepared under environmentally isolated conditions and subsequently reacted with alkanoyl chlorides. The retention measurements were carried out using acetonitrile–water eluent at different volume compositions and different pH values. For the comparative purposes analogous retention data were collected for conventional octyl phases bonded to various silicas. A comparison of the retention data measured on alkyl and alkylamide packings have demonstrated that the later, polymeric or monomeric, are better for separating pyridine and indole carboxylic acids. The comparative analysis of the chromatographic systems studied suggests that retention of these acidic solutes on alkylamide phases is governed by a mixed partition–displacement and ion-exchange mechanism.

1. Introduction

Chromatographic analysis of multifunctional compounds with acidic and/or basic groups is of great importance for many laboratories, especially those involved in agricultural and pharmaceutical research. Many of these compounds can be analyzed by high-performance liquid chromatography under reversed-phase conditions (RPLC) using alkyl-bonded phases, which currently are most popular because of their hydrophobic character and very good chemical, thermal and mechanical stabilities [1–4]. However, the performance of chromatographic columns packed with alkyl-bonded phases becomes worse for the compounds of complex stereochemistry and functionality. Several authors [5–7] reported that these factors affect significantly the column efficiency and peak asymmetry. For instance, McCalley [5] studied the retention of pyridine and some alkyl-substituted derivatives under reversed-phase conditions using an octadecyl-bonded phase with 14% carbon loading and demonstrated that the solute stereochemistry in close vicinity of the basic group influences strongly the peak shape. According to his studies, alkyl groups in close proximity of the basic site had the most pronounced effect, apparently hindering interactions in the stationary phase. Vervoort et al. [6] and Ascah and Feibush [7] found the peak asymmetry increased with increasing pK_a of the analyte. Also, they studied the effect of the solute stereochemistry in close vicinity to the basic nitrogen atom on the peak

* Corresponding author.

[1] Permanent address: Department of Environmental Chemistry, Copernicus University, 87100 Torun, Poland.

0021-9673/95/$09.50
SSDI 0021-9673(94)01034-X

shape. The same authors considered possible interactions between the protonated nitrogen atom of the solute molecule and residual surface silanols.

The molecular mechanism of retention becomes more complex when acidic groups are present in vicinity of the basic nitrogen atom, e.g., pyridine and indole carboxylic acids. These compounds, especially those with the carboxylic group in close proximity to the ring nitrogen atom, are known as the substances difficult to analyze on the currently available reversed-phase columns. The hydrogen bond, which could be formed between the ring nitrogen atom and the carboxylic group proton, facilitates ionization of the molecule and promotes interactions with the residual surface silanols. This leads to the deterioration of elution bands or to irreversible adsorption. When these acidic compounds are accompanied by analytes of another charge type or different relative hydrophobicity, addition of ion-pairing reagents is necessary in order to achieve a proper peak shape and satisfactory separation of all components of interest.

Another alternative for improving chromatographic separation of the above-mentioned analytes is application of the chemically bonded phases of specific stereochemistry and functionality. Alkylamide phases, which contain terminal alkyl chains attached to the surface via an alkylamide group, possess specific chromatographic properties. These phases have been recently studied by us [8–10] and appeared to have interesting physicochemical properties. A detailed study of alkylamide packings under reversed-phase conditions has shown that the specific interaction site, i.e., amide group, located in the hydrophobic ligand has a significant influence on the solute retention and selectivity. In addition, improved peak symmetry was observed for polar solutes such as amines which makes these phases attractive for carrying separation of base-type compounds.

In the current work we have explored the possibility of using alkylamide phase for separating complex compounds, which possess acidic groups located in close proximity to the ring nitrogen atom. Retention behavior of a series of pyridine and indole carboxylic acids was studied on selected alkylamide phases under reversed-phase conditions using acetonitrile–water mixture as the eluent. For the comparative purposes, additional retention data were collected for these solutes on various octyl bonded phases. The retention data were measured at different compositions and pH of the mobile phase in order to get more information about retention mechanism of multifunctional acidic compounds on alkylamide phases. A long-term aim of the work is elaboration of chromatographic conditions for analyzing these compounds.

2. Experimental

2.1. Introductory remarks

Retention measurements were carried out on two types of alkylamide phases with an acetonitrile–water mobile phase at different pH values and different concentrations of the organic solvent. For comparative purposes, organic compounds which do not form internal hydrogen bonding, e.g., benzoic acid and 5-methylpyridinedicarboxylic acid dimethyl ester, were also studied. In addition, analogous retention measurements were performed on conventional octyl phases bonded to various silicas.

2.2. Reagents and materials

Two types of spherical silica used to prepare alkylamide-bonded phases were 10-μm LiChrosorb Si-60 (EM Science, Cherry Hill, NJ, USA) and 5-μm Inertsil (MetaChem Technologies, Torrance, CA, USA). The BET specific surface areas of these materials were 500 and 320 m^2/g, respectively.

The surface modification reagents, 3-aminopropyltriethoxysilane and suitable alkanoyl chlorides were purchased from Aldrich (Milwaukee, WI, USA). The remaining surface modification reagents, octyldimethylchlorosilane and 3-aminopropyldimethylmethoxysilane were purchased,

respectively, from Huls America (Bristol, PA, USA) and Pertrarch Systems (Levittown, PA, USA). The other chemicals used in chromatographic measurements and synthesis of the bonded phases, such as methanol, acetonitrile, 2-propanol, toluene, etc. were purchased from Aldrich. The chromatographic solutes (see Fig. 1) were purchased from Aldrich. The deionized water was purified in the laboratory using a Millipore (El Paso, TX, USA) Model Milli-Q water system.

2.3. Alkylamide-bonded phases

Mono- and polymeric alkylamide phases, i.e., AA-12 (with attached C_{12} ligand) and AA-8 (with attached octyl ligand), were prepared at Kent State University by a two-step process, in which an initial aminopropyl phase was synthesized and subsequently reacted with suitable alkanoyl chloride. The synthesis procedure was described previously [8–11]. The monomeric AA-12 phase was synthesized by modifying initially the silica surface with 3-aminopropyldimethylmethoxysilane, however 3-aminopropyltriethoxysilane was used for preparing the polymeric AA-8 phase. The AA-12 packing was obtained using a 5-μm Inertsil support and the AA-8 phase was synthesized using a 10-μm LiChrosorb silica gel. The elemental analysis data for the AA-12 and AA-8 phases are as follows: (i) polymeric phase: 4.66% of C and 1.06% of N in the initial aminopropyl phase, and 14.32% of C and 1.09% of N in the final AA-8 phase, and (ii) monomeric phase: 3.37% of C and 0.39% of N in the initial aminopropyl phase, and 8.89% of C and 0.39% of N in the final AA-12 phase.

Both bonded phases were packed into 150 mm × 4.6 mm I.D. stainless-steel column blanks which were purchased from Supelco (Bellefonte, PA, USA). Prior to packing a slurry was prepared using 35 ml of 2-propanol and sonicated the mixture for 5 min. Subsequently, the columns were packed using a Haskel (Burbank, CA, USA) Model DST-52 pump at a pressure of 50 MPa and methanol as the carrier solvent.

2.4. Octyl-bonded phases

The commercial 150 mm 5-μm RP C_8 columns Eka Nobel Kromasil, Metachem Inertsil, Waters NovaPak, and Supelco Supelcosil DB along with a C_8 column prepared at Kent State University and packed with a octyl phase bonded to 5-μm Inertsil silica (coverage density 4.25 μmol/m^2, carbon loading 13.27%), were used for comparative purposes.

2.5. Chromatographic equipment

The modular liquid chromatograph, consisted of a Spectra-Physics SP8800 pump, a LKB Model 2125 column oven, a variable-wavelength UV detector (ABI 785A), and a Hewlett-Packard 1050 autosampler was used to measure the retention volumes as a function of the mobile phase composition and pH. The retention data were acquired and processed using a Hewlett-Packard 3350 laboratory data system.

2.6. Chromatographic measurements

The retention data of a series of alkyl- and amino-substituted pyridine and indole carboxylic acids were measured at different acetonitrile concentrations and pH values of the mobile phase. Chromatographic measurements were collected at the pH range of 2–5.5 (50 m*M* sodium phosphate buffer) and the acetonitrile concentration range from 0 to 20%. The influence of pH on the solute retention was examined for the mobile phases containing 5% of acetonitrile. However, the mobile phase composition effects were studied at pH 2.0 or 2.3. All experiments for alkylamide phases were carried out at 35°C and 1 ml/min flow-rate.

3. Results and discussion

A comparative study of the alkyl- and alkylamide-bonded phases under reversed-phase conditions showed that the intercalation (competitive sorption) of solvent molecules into the stationary phase depends strongly on the specific

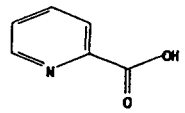

Picolinic Acid

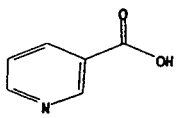

Nicotinic Acid

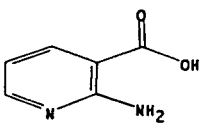

2-Amino Nicotinic Acid

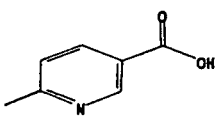

6-Methyl Nicotinic Acid

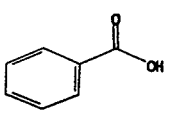

Benzoic Acid

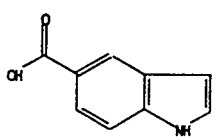

Indole-5-Carboxylic Acid (5-Indole COOH)

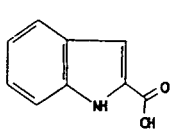

Indole-2-Carboxylic Acid (2-Indole COOH)

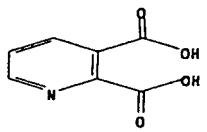

2,3-Pyridine Dicarboxylic Acid (2,3-PDC)

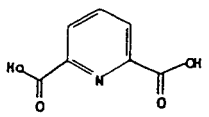

2,6-Pyridine Dicarboxylic Acid (2,6-PDC)

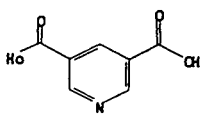

3,5-Pyridine Dicarboxylic Acid (3,5-PDC)

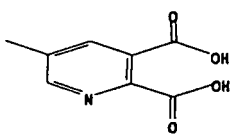

5-Methyl-Pyridine Dicarboxylic Acid (MPDC)

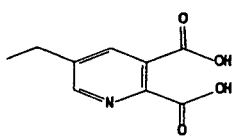

5-Ethyl-Pyridine Dicarboxylic Acid (EPDC)

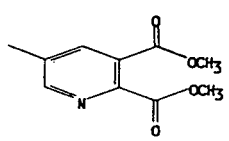

5-Methyl Pyridine Dicarboxylic Acid Dimethyl Ester (MPDC.DME)

Fig. 1. Chemical structures of the pyridine- and indolecarboxylic acids studied.

interaction groups localized in hydrophobic ligands [8]. These specific groups, e.g., amide group in the alkylamide phases, decrease hydrophobic character of the bonded phase. This effect is stronger for the alkylamide phases with shorter terminal alkyl chains. Thus, for the alkylamide phases, especially those with short terminal alkyl chains, the preferential sorption of organic solvent into the stationary phase is smaller in comparison to the corresponding alkyl-bonded phases. While the residual surface silanols are the only polar groups in the monomeric alkyl-bonded phases, the alkylamide-bonded phases in addition to the specific alkylamide ligands contain also the residual silanols and aminopropyl groups. All specific groups present in the alkylamide phases are able to form a special structure of the stationary phase, the physicochemical properties of which differ significantly from that for a conventional alkyl phase [8,9]. This structure plays an essential role in separating multifunctional solutes under reversed-phase conditions.

Shown in Fig. 2 are the experimental dependencies of the capacity ratio k' on pH for EPDC on all columns studied. Analysis of these dependencies indicates that in the case of alkylamide phases the ionic type of interactions plays a substantial role in the retention mechanism. For all alkyl columns the retention of EPDC decreases with the degree of acid ionization, while on both alkylamide columns the acidic solutes are retained longer at the higher pH values. The obtained pH-dependent plots are analogous to those observed in ion chromatography [12]. However, the retention of EPDC dimethyl ester, which does not form ionic species, remains independent of pH. Similar behavior is observed for all other acids studied as shown in Figs. 3–5. To explain the difference in retention on the AA-8 and AA-12 phases one should consider the following factors:

(i) Structural difference between two phases: AA-8 is a polymeric phase with C_8 terminal chain, whereas AA-12 is a monomeric phase with C_{12} terminal chain.

(ii) Different nature of silicas used in the synthesis of both phases: AA-8 was prepared on LiChrosorb, whereas AA-12 was synthesized on Inertsil.

(iii) Different concentrations of surface ligands: for the AA-8 phase the coverage density of alkylamide ligands and residual amino groups

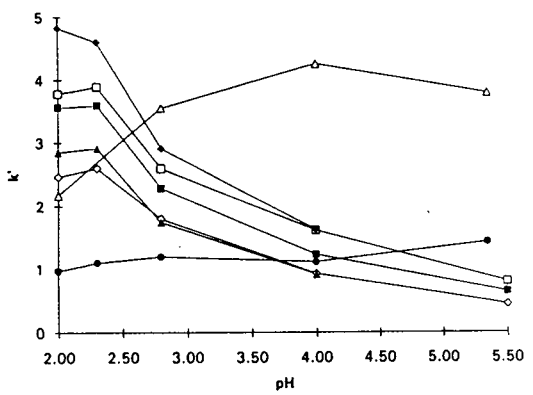

Fig. 2. A comparison of the k' vs. pH dependencies for 5-ethylpyridinedicarboxylic acid (EPDC) on the alkyl- (45°C) and alkylamide- (35°C) bonded phases. The hydro–organic mobile phase contained 5% of acetonitrile. Columns: ■ = Kent Inertsil C_8; □ = MetaChem Inertsil; ◆ = Kromasil C_8; ◇ = Supelcosil C_8-DB; ▲ = NovaPak C_8; △ = Kent AA-8; ● = Kent AA-12.

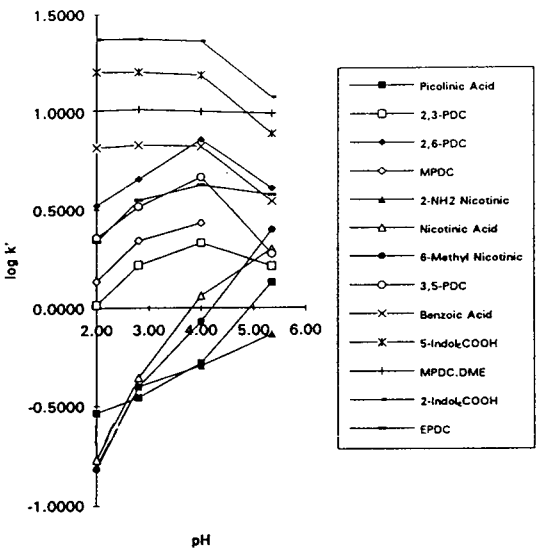

Fig. 3. A comparison of the log k' vs. pH dependencies for all solutes listed in Fig. 1 on the polymeric AA-8 phase. Chromatographic conditions as in Fig. 2.

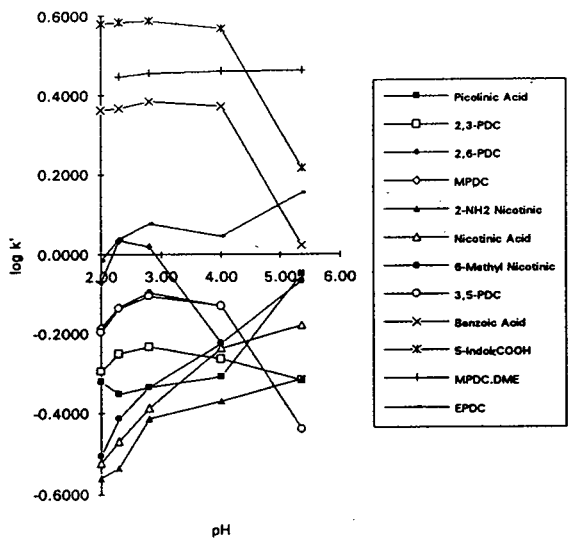

Fig. 4. A comparison of the log k' vs. pH dependencies for all solutes listed in Fig. 1 on the monomeric AA-12 phase. Chromatographic conditions as in Fig. 2.

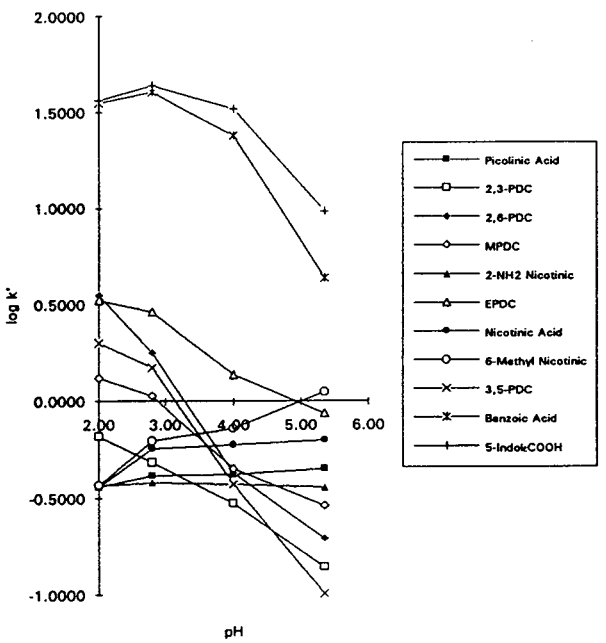

Fig. 5. A comparison of the log k' vs. pH dependencies for all solutes listed in Fig. 1 on the Kent monomeric C_8 phase. Chromatographic conditions as in Fig. 2.

are 1.36 and 0.4 μmol/m^2, respectively; however, for the AA-12 phase these concentrations are 1.4 and 0.4 μmol/m^2.

The basic properties of the nitrogen atom in the amide group are very week. So, when the amide group accepts a proton, it does through the oxygen atom. In comparison to the amide nitrogen the basicity of the nitrogen atom in the amine group is much stronger. Therefore, the aminoalkyl phases retain much longer organic acids than the corresponding alkylamide phases. Since both, monomeric and polymeric, alkylamide phases contain ligands with terminal amino groups (residual amino groups) and internal amide groups, the overall retention is strongly affected by the concentration of the unreacted amino groups. Although the coverage densities of the AA-8 and AA-12 packings studied were similar, residual amino groups and silanols were screened more effectively for the later material. In addition, an internal masking of the amino groups by the residual surface silanols is also possible. Thus, the AA-8 phase adsorbs more water than the AA-12 phase and its structure and physicochemical properties depend much more on pH of the mobile phase. Due to the possibility of mutual interactions between residual silanols and amino groups the amide groups seem to play an important role in the retention mechanism on the AA phases. Additional spectroscopic studies are in progress in order to identify molecular interactions that control retention on the AA phases.

As shown in Figs. 6–9 the acetonitrile concentration influences differently the retention of multifunctional acids on the alkyl- and alkylamide-bonded phases. For the conventional C_8 column (Figs. 6 and 7) the retention volumes of all acids decrease in a similar manner as the concentration of acetonitrile increases from 0 to 20%. In this case the experimental dependencies of k' versus the acetonitrile concentration for acids are similar to that for diester on the AA-8 and AA-12 columns (Figs. 8 and 9). For the later columns, the retention volumes of the acids studied decrease much more slowly with increasing acetonitrile concentrations than for the corresponding RP C_8 columns. The dependencies of

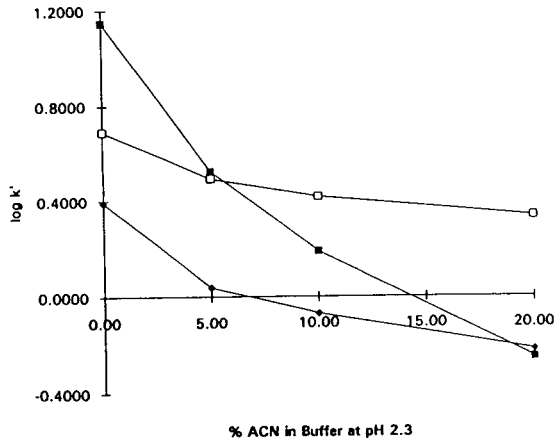

Fig. 6. A comparison of the log k' vs. % acetonitrile (ACN) dependencies for 5-ethylpyridinedicarboxylic acid (EPDC) on the Kent monomeric C_8 (■), polymeric AA-8 (□) and monomeric AA-12 (◆) packings at 35°C and pH 2.3.

log k' on the acetonitrile concentration in the mobile phase are almost flat in the range between 10 and 20% due to the lower methylene selectivities on the AA phases. It was shown in

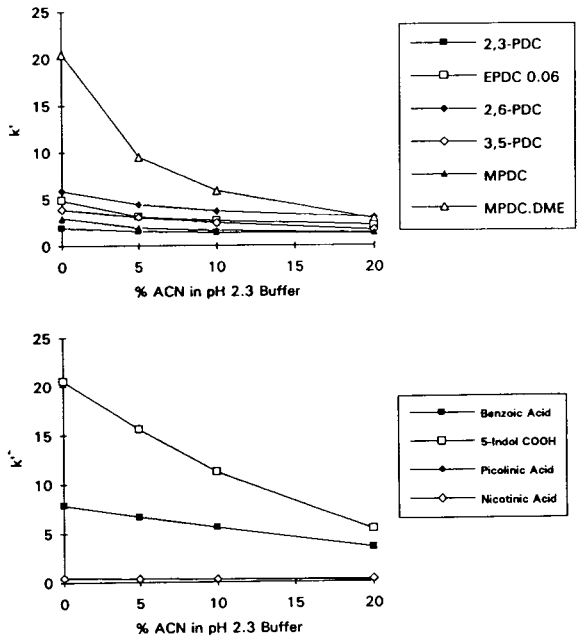

Fig. 8. A comparison of the k' vs. % ACN dependencies for diacids (top panel) and monoacids (bottom panel) on the polymeric AA-8 packing at 35°C and pH 2.3.

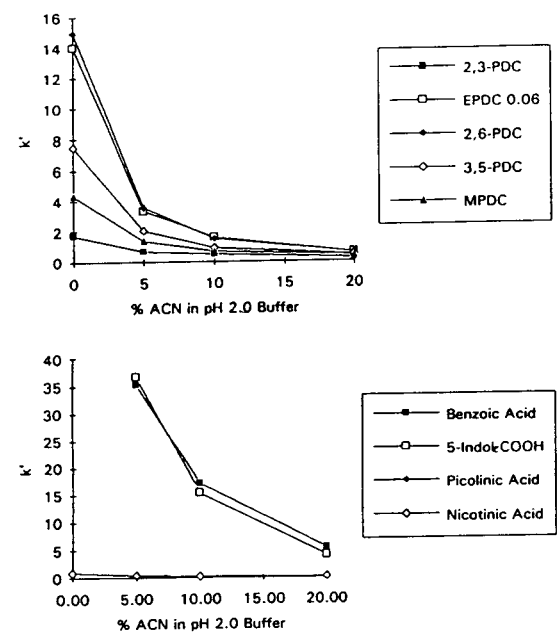

Fig. 7. A comparison of the k' vs. % ACN dependencies for diacids (top panel) and monoacids (bottom panel) on the Kent monomeric C_8 packing at 35°C and pH 2.0.

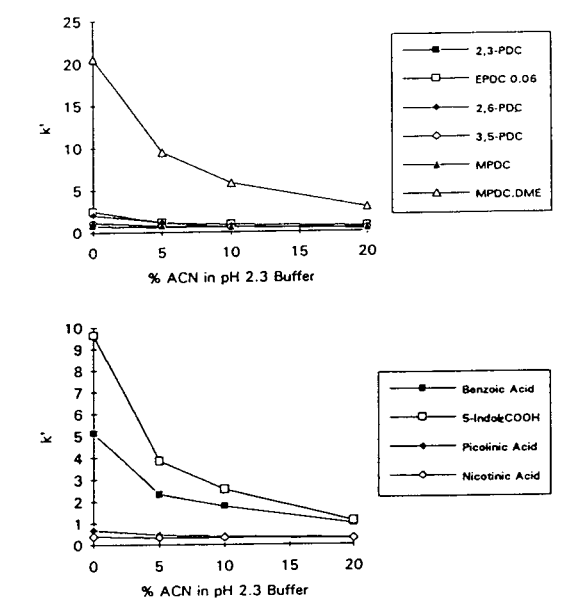

Fig. 9. A comparison of the k' vs. % ACN dependencies for diacids (top panel) and monoacids (bottom panel) on the monomeric AA-12 packing at 35°C and pH 2.3.

the previous work [8] that the methylene selectivities on the AA phases can be about 25–50% lower in comparison to those on the corresponding alkyl phases. For instance, at 20% of acetonitrile in the mobile phase ester elutes before 2,6-pyridinedicarboxylic acid. A comparison of all types of the columns studied is shown in Fig. 6. Similarly, as in the case of pH-dependent retention studies, the concentration effects are more pronounced for the polymeric AA-8 phase. As shown in Fig. 8 the concentration-dependent plots for acidic solutes are quite well separated. However, for the AA-12 packing these plots overlap. This means that the AA-8 phase is better for separating the acidic solutes studied.

The dependencies of log k' on pH or acetonitrile concentration for mono- and diacids falls into two different categories. Experimental points for monoacids seem to fit a linear pH dependence of retention, while points for diacids seem to lie on a parabolic curve. This different behavior can be probably attributed to the greater charge effects of the latter compounds as well as to their ability to form intermolecular hydrogen bonding.

4. Conclusions

The current work suggest that the retention mechanism of multifunctional organic acids on the conventional alkyl phases, including those with high coverage density (e.g., Kent C_8) occurs according to the partition–displacement mechanism, which is characteristic for typical RPLC systems [13]. However, the retention mechanism of these solutes on alkylamide phases is governed by a mixed ion-exchange and partition–displacement mechanism. It has been shown that the contribution of ion-type interaction to the overall retention is greater for polymeric alkylamide phases than for monomeric ones.

A comparison of the retention measurements for alkyl and alkylamide phases have demonstrated that the later phases, polymeric or monomeric, are better for separating the pyridine and indole carboxylic acids than conventional alkyl packings. They allow separation of these acidic solutes from hydrophobic compounds over a wide range of the mobile phase compositions (including highly aqueous conditions) without adding ion-pair reagents and/or applying the mobile phase gradient. Currently chromatographic and spectrometric studies are in progress in order to characterize further the structural features of the alkylamide bonded phases and to enrich our understanding about the molecular mechanism of the solute retention on these packing materials.

Acknowledgement

M.J. thanks the Agricultural Research Center of American Cyanamid Co. (Princeton, NJ, USA) for supporting his participation at the *18th International Symposium on Column Liquid Chromatography, Minneapolis, MN, 1994.*

References

[1] L.C. Sander and S.A. Wise, *CRC Crit. Rev. Anal. Chem.*, 18 (1987) 299.
[2] C.F. Poole and S.K. Poole, *Chromatography Today*, Elsevier, Amsterdam, 1991.
[3] B. Buszewski, *Sc.D. Thesis*, Slovak Technical University, Bratislava, 1992 (in Slovak).
[4] J.G. Dorsey, J.P. Foley, W.T. Cooper, R.A. Barford and H.G. Barth, *Anal. Chem.*, 64 (1992) 324A.
[5] D.V. McCalley, *J. Chromatogr. A*, 664 (1994) 139.
[6] R.J. Vervoort, F.A. Maris and H. Hindriks, *J. Chromatogr.*, 623 (1992) 207.
[7] T.L. Ascah and B. Feibush, *J. Chromatogr.*, 506 (1990) 357.
[8] B. Buszewski, M. Jaroniec and R.K. Gilpin, *J. Chromatogr. A*, 668 (1994) 293.
[9] B. Buszewski, M. Jaroniec and R.K. Gilpin, *J. Chromatogr. A*, 673 (1994) 11.
[10] P. Kasturi, B. Buszewski, M. Jaroniec and R.K. Gilpin, *J. Chromatogr. A*, 659 (1994) 261.
[11] B. Buszewski, J. Schmid, K. Albert and E. Bayer, *J. Chromatogr.*, 552 (1991) 415.
[12] M.C. Gennaro, C. Abrigo and E. Marengo, *J. Liq. Chromatogr.*, 17 (1994) 1231.
[13] M. Jaroniec, *J. Chromatogr. A*, 656 (1993) 37.

ELSEVIER

Journal of Chromatography A, 691 (1995) 225–229

JOURNAL OF CHROMATOGRAPHY A

Use of secondary chemical equilibria in liquid chromatography to determine dissociation constants of leukotriene B_4 and prostaglandin B_2

J.E. Hardcastle*, Ming He, Basharat Begum, Rachal Vermillion-Salsbury

Department of Chemistry and Physics, Texas Woman's University, Denton, TX 76204-1973, USA

Abstract

The secondary chemical equilibrium of a monoprotic acid in reversed-phase high-performance liquid chromatography (RP-HPLC) is controlled both by the pH of aqueous component and the ratio of organic solvent to water in the mobile phase. The pH dependence of capacity factors of a monoprotonic acid follows the titration curve of the acid. The midpoint of the sigmoidal curve corresponds to the pK_a value of the acid. Therefore, the pK_a of the acid can be determined by RP-HPLC. Capacity factors of prostaglandin B_2 and leukotriene B_4 were measured at several mobile phase pH values, and acetonitrile mobile phase compositions. pK_a values determined at various ratios of acetonitrile to water were plotted against percent acetonitrile. The straight line that resulted was extrapolated to 100% aqueous solution. The thermodynamic pK_a values of prostaglandin B_2 and leukotriene B_4 were determined to be 5.07 and 5.17, respectively.

1. Introduction

Leukotrienes and prostaglandins are two groups of biologically active compounds derived from arachidonic acid in normal biological processes such as the maintenance of blood pressure and body temperature, and in anaphylaxis [1].

The systematic name for leukotriene B_4 (LTB_4) is 5(*S*),12(*R*)-dihydroxy-6*Z*,8*E*,10*E*, 14*Z*-eicosatetraenoic acid. That for prostaglandin B_2 (PGB_2) is 7-[2-(3-hydroxy-1-octenyl)-5-oxocyclopent-1-enyl]-5-heptenoic acid. These two compounds are carboxylic acids, and a knowledge of the acid–base dissociation constants of these metabolites can lead to a better understanding of their solution biochemistry. This information can help to improve the analytical methodology for the separation of these metabolites from their biological environment, and for preparation for further analysis.

The dissociation constants of benzoic acid and phenylacetic acid were determined by this technique in order to have pK_a values to compare with literature values for well studied compounds.

2. Theory

The dissociation of weak acids in HPLC is considered to be a secondary chemical equilibrium because the primary equilibrium is the distribution of the solute between the mobile phase and the stationary phase [2]. For a mono-

* Corresponding author.

0021-9673/95/$09.50
SSDI 0021-9673(94)00768-3

protic weak acid equilibrium, $HA \rightleftharpoons H^+ + A^-$, the observed chromatographic retention of the analyte in RP-HPLC will be the mol-fraction weighted average of the retention of the dissociated and undissociated forms. In terms of mol fractions (X) and capacity factors (k'), this can be expressed as

$$k'_{obs} = X_{HA}k'_{HA} + (1 - X_{HA})k'_A \quad (1)$$

Since the equilibrium can be shifted without changing the retention behavior of the two forms of the weak acid, the equilibrium constant and the limiting capacity factors for the two forms can be obtained from multiple values of the average retention behavior. From the equilibrium constant expression, $K_a = [H^+][A^-]/[HA]$, and Eq. 1, the expression

$$k'_{obs} = \frac{k'_{HA}[H^+] + k'_A K_a}{[H^+] + K_a} \quad (2)$$

can be derived. Eq. 2 predicts that a plot of k'_{obs} versus pH will be sigmoidal with a midpoint pH value which corresponds to the pK_a of the weak acid. Simply, the pH dependence of the capacity factor follows the dissociation curve [3]. This concept is reviewed and other pertinent literature is referenced in two papers by Foley and May [4,5], and one by Van de Venne et al. [6].

3. Experimental

3.1. Chromatographic system

A Waters (Ventura, CA, USA) HPLC system consisting of two Model 510 pumps, U6K injector, Model 484 tunable UV detector, and Model 510 refractive index detector were used. The Waters Baseline 810 workstation and computer software (version 3.30) were used to control the system and to collect the data. The column used was a Phenomenex (Torrance, CA, USA) Spherex ODS, 5 μm, 250 × 4.6 mm. Isocratic elution was performed using a mobile phase flow-rate of 1.0 ml/min. The UV detector was set at 254 nm for benzoic acid and phenylacetic acid, and at 280 nm for LTB_4 and PGB_2. All work was performed at ambient temperature which was 22 ± 1°C.

3.2. Reagents

The mobile phase was prepared by mixing HPLC-grade acetonitrile with the appropriate aqueous buffer to obtain mixtures in the range of 40–70% (v/v) acetonitrile. The mobile phase buffer was prepared from sodium acetate for pH below 6, and from monobasic sodium phosphate for pH above 6. Buffers were prepared at a strength of 0.01 M. Sodium perchlorate (0.02 M) was used to maintain constant ionic strength independent of pH. The mobile phase solution was degassed and filtered through a 0.45-μm nylon 66 membrane filter disc prior to use.

The samples of LTB_4 and PGB_2 were dissolved in acetonitrile at a concentration of approximately 10 μg/ml, and 10 μl of these solutions were injected. Benzoic acid and phenylacetic acid were injected at 0.01 M concentration in acetonitrile. Sodium nitrate (0.01 M) was used to determine void volume. Retention times were determined with three replicate injections for each sample at each pH and percent acetonitrile.

A Corning Model 215 pH meter was used to determine pH to within ± 0.01 pH units. The apparent pH of the bulk mobile phase was measured, and any adjustments were made, before the mobile phase was used. Also, samples for pH determination were collected during solute elution. It was found that the apparent pH did not change by passing through the chromatographic system.

3.3. Data analysis

The experimental data were fitted to Eq. 2 using the non-linear least square program MINSQ (version 3.12) from MicroMath Scientific Software, Salt Lake City, UT, USA.

4. Results and discussion

Observed capacity factors were determined for each compound at each pH and percent acetonitrile. Computer-generated plots of k' versus pH

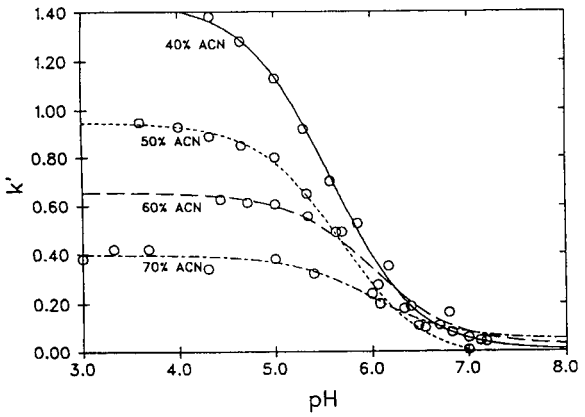

Fig. 1. Observed capacity factor (k') versus pH for benzoic acid in acetonitrile (ACN)–buffer mixture.

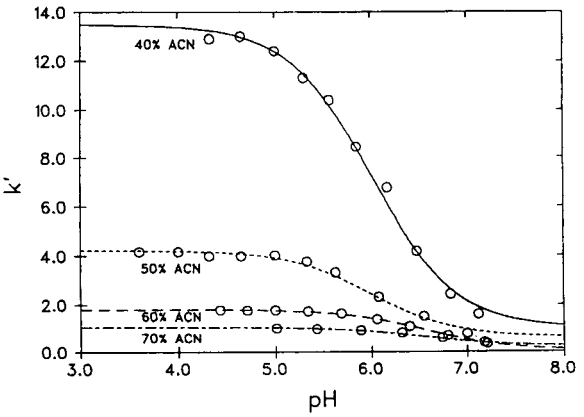

Fig. 3. Observed capacity factor (k') versus pH for LTB_4 in acetonitrile (ACN)–buffer mixture.

are shown in Figs. 1–4. The retention of the analyte decreased with increase in pH, and the sigmoidal relationship between k' and pH is very similar to a typical weak acid titration curve. The inflection point in a curve of this type, as determined by least square regression analysis, can be used to determine the acid dissociation constant.

The calculated pK_a values for the organic acids at different percent acetonitrile are given in Table 1. Plots of pK_a versus percent acetonitrile are linear, and linear regression analysis produced the following equations:

for benzoic acid

$y = 4.63 + 0.0221x$, $R^2 = 0.935$ and $R = 0.97$;

for phenylacetic acid

$y = 4.81 + 0.0220x$, $R^2 = 0.981$ and $R = 0.99$;

for LTB_4

$y = 5.01 + 0.0255x$, $R^2 = 0.939$ and $R = 0.97$;

for PGB_2

$y = 5.11 + 0.0259x$, $R^2 = 0.901$ and $R = 0.99$.

The intercept with the y-axis, in this case the pK_a-axis, gives the aqueous pK_a value. From the

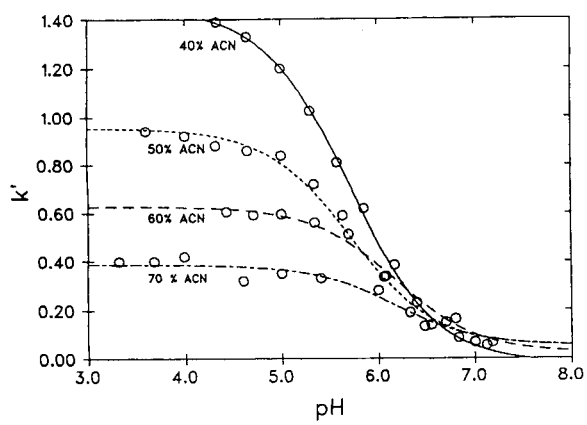

Fig. 2. Observed capacity factor (k') versus pH for phenylacetic acid in acetonitrile (ACN)–buffer mixture.

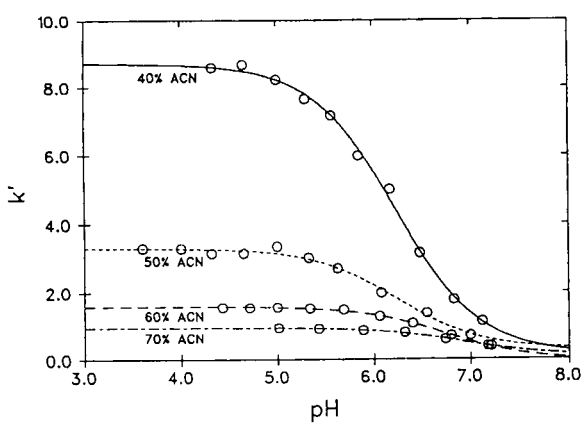

Fig. 4. Observed capacity factor (k') versus pH for PGB_2 in acetonitrile (ACN)–buffer mixture.

Table 1
pK_a values determined in different percentages of acetonitrile

Acetonitrile (%)	Benzoic acid		Phenylacetic acid		LTB_4		PGB_2	
	pK_a	S.D.	pK_a	S.D.	pK_a	S.D.	pK_a	S.D.
40	5.57	0.03	5.71	0.03	6.11	0.03	6.23	0.04
50	6,63	0.03	5.86	0.02	6.17	0.05	6.25	0.08
60	6.01	0.04	6.17	0.02	6.56	0.02	6.74	0.02
70	6.18	0.03	6.34	0.03	6.83	0.01	6.93	0.02

S.D. = Standard deviation.

above equations, these values are 4.63 for benzoic acid, 4.81 for phenylacetic acid, 5.01 for LTB_4 and 5.11 for PGB_2. Since the aqueous pK_a values determined here are influenced by salt effects, the Davies [7] modification of the Debye–Hückel equation was used to calculate thermodynamic pK_a values. The thermodynamic pK_a values are benzoic acid, 4.69; phenylacetic acid, 4.87; LTB_4, 5.07; and PGB_2, 5.17.

The pK_a values determined for benzoic acid and phenylacetic acid in this research effort are much higher than values reported in the literature. The major source of this discrepancy is the media effect. The extrapolation of the data from acetonitrile–water solutions to 100% water suffers from lack of data in the range of 0–40% acetonitrile. It could be possible to supplement this data for benzoic acid and phenylacetic acid in the 0–40% acetonitrile range. However, the eicosanoids (PGB_2 and LTB_4) are strongly retained by the octadecyl-silica (ODS) column. At acetonitrile concentration below 40%, PGB_2 and LTB_4 could not be eluted from the C_{18} column. The pK_a values determined for LTB_4 and PGB_2 are of a magnitude to be expected for compounds of this type of structure. Because of their similar structures, other monoprotic eicosanoids and most of the prostaglandins would be expected to have very similar pK_a values to those determined for LTB_4 and PGB_2.

The advantage of HPLC can be exploited for such physico-chemical measurements when a chromatographic system with an eluent, which is a proper medium for the equilibrium constant to be evaluated, and yields conveniently measurable retention ratios, is available, and very low analyte concentrations in the effluent can be monitored by a sensitive detector.

Unlike all other methods, the use of HPLC affords measurements with impure samples without further purification because with properly chosen efficient chromatographic systems impurities are separated from the analyte. In our experiments, commercially available substances were employed without further purification and in all cases peaks representing impurities were present on the chromatogram.

This method is applicable for the measurement of dissociation constants only in those cases when the rate of equilibration in the mobile phase is rapid on the time scale of the chromatographic run. Otherwise poor peak shape and peak splitting render the evaluation of retention factors difficult without the computer.

Because of the low solute concentration in the eluent, the solubility does not impose constraints on determining dissociation constants by HPLC, whereas poor sample solubility often limits the employment of conventional techniques. Submicrogram quantities of a substance may be adequate to measure equilibrium constants by HPLC, whereas conventional methods require larger quantities of the substance being analyzed.

Acknowledgement

This research was supported by a grant to the Department of Chemistry and Physics from the Robert A. Welch Foundation.

References

[1] J. Ninneman, *Prostaglandins, Leukotrienes, and the Immune Response*, Cambridge Univ. Press, New York, 1988.
[2] B.L. Karger, J.N. LePage and N. Tanaka, in Cs. Horváth (Editor), *High-Performance Liquid Chromatography —Advances and Perspectives*, Vol. 1, Academic Press, New York, 1980, p. 113.
[3] Cs. Horváth, W. Melander and I. Molnár, *Anal. Chem.*, 49 (1977) 142.
[4] J.P. Foley and W.E. May, *Anal. Chem.*, 59 (1987) 102.
[5] J.P. Foley and W.E. May, *Anal. Chem.*, 59 (1987) 110.
[6] J.L.M. van de Venne, J.L.H.M. Hendrikx and R.S. Deelder, *J. Chromatogr.*, 167 (1978) 1.
[7] C.W. Davies, *J. Chem. Soc.*, (1938) 2093.

ELSEVIER

Journal of Chromatography A, 691 (1995) 231–237

JOURNAL OF CHROMATOGRAPHY A

Simultaneous sorption and analytical derivatization on a polystyrene–divinylbenzene polymer Preparation of chromophoric and fluorophoric derivatives of the prostaglandins

Jack M. Rosenfeld*, Xingchun Fang

Department of Pathology, McMaster University, Hamilton, Ontario L8N 3Z5, Canada

Abstract

A solid phase consisting of a macroreticular styrene–divinylbenzene polymer was used as a support for the sorption and derivatization of the prostaglandins to form chromophoric and fluorophoric esters. These highly potent physiological mediators are a group of 20 carbon, oxygenated carboxylic acids which at neutral pH are highly water soluble. In addition to functioning as a support for the simultaneous isolation and derivatization, the solid phase also retained the derivatized analytes while a substantial amount of excess reagent was selectively eluted. The final clean-up was by semi-preparative chromatography.

1. Introduction

Analytical derivatization is an essential requirement for the analysis of compounds such as the prostaglandins (PGs) which possess no inherent electrophore, chromophore or fluorophore. Because of the high sensitivities required, PGs are typically determined by gas chromatography (GC) with mass spectrometric (MS) detection. The GC–MS techniques are well established and have been the basis for numerous investigations in physiology and pharmacology [1–3]. The multi-functional nature of the PGs, however, necessitates a complex sample preparation technique for the determination by GC–MS. Derivatization is a major aspect of these techniques [1–3] and includes: oximation of carbonyls; esterification of the carboxyl group; silylation of hydroxyl groups. All of these steps require anhydrous conditions which can be hard to maintain.

Since the PGs are polar molecules, high-performance liquid chromatography (HPLC) would be a preferred technique. Analysis of PGs by HPLC still requires analytical derivatization but only to provide a group that could be detected by ultraviolet absorption or fluorescence. The additional derivatizations to stabilize the E, D or 6-keto series to increase volatility are not required. Determination of PGs by HPLC as opposed to GC is, therefore, attractive and preparation of chromophoric and fluorophoric

* Corresponding author.

0021-9673/95/$09.50
SSDI 0021-9673(94)01025-0

derivatives of these analytes has been reported [4,5]. These methods, however, are all post-extraction techniques and require both evaporation of the extract to dryness and subsequent reaction in solution. Such sample preparation procedures are relatively difficult to automate. Reactions on solid supports preparatory to instrumental analysis have been studied and described by several groups and are believed to be a very useful approach to automating sample preparations where analytical derivatization is a requirement.

Krull and co-workers [6,7] incorporated reactive groups covalently linked to the surface of a polystyrene–divinylbenzene (PS–DVB) resin. Reactions occur simultaneously with the sorption and only a stoichiometric amount of reagent is used. This technique is used to determine amines which react rapidly with the functional groups on the surface.

Our group at McMaster also utilized a PS–DVB resin but with reagent that had been sorbed onto the surface. In this technique, unmodified, commercially available resin could be used and reagents could be altered at will. For example, to derivatize organic acids preparatory to GC–electron-capture detection (ECD), the analytes were converted to their pentafluorobenzyl (PFB) derivatives by shaking the aqueous sample with XAD-2 that was loaded with PFB bromide (PFBBr) [8,9]. Carbonyls were oximated under the same conditions if the resin was loaded with O-benzylhydroxylamine or O-pentafluorobenzylhydroxylamine [10]. Reactions conditions were completely compatible with aqueous matrix and occurred simultaneously with sorption of the analyte. Evaporation was used to separate excess PFBBr from the non-volatile PFB esters or ethers. Excess oximating reagents were eluted with acid buffer prior to recovery of the oximes.

The technique of using reagents sorbed onto XAD-2 has now been extended to include formation of chromophoric or electrophoric derivatives for HPLC determination of PGs in order to further simplify sample preparation procedures for the study of this important class of compounds.

2. Experimental

2.1. Chemicals

The chromophoric reagent, *p*-bromophenacyl bromide (pBrPhBr) was supplied by Aldrich (St. Louis, MO, USA). The fluorophore, [*p*-(9-anthroyloxy)]phenacyl bromide (PANBr), native PGs and carbon-14 radiolabelled PGs were obtained from Sigma (St. Louis, MO, USA). PFBBr was purchased from Caledon Labs. (Georgetown, Canada). Diisopropylethylamine (DiIPEA) and the solid phase XAD-2 were obtained from BDH (Toronto, Canada) and prepared according to methods previously published.

2.2. Preparation of standards

The ester derivatives which were used as standards were prepared by established procedures [4,5]. The analyte was dissolved in a solution of the esterifying agent (i.e. pBrPhBr, PANBr or PFBBr) and DiIPEA in acetonitrile. This solution was maintained at ambient temperature for 1 h followed by standard work-up [4]. Standards were then further purified by semi-preparative chromatography. The product which was homogenous, as determined by HPLC, was weighed and served as a standard.

2.3. Instrumentation

The pBrPh or the PAN esters were determined on a Waters NovaPak ODS reversed-phase column chromatography with solutions of acetonitrile in water as mobile phases. A Waters M510 pump was used to control flow of the mobile phase and detection was by ultraviolet absorption at 254 nm. The PFB ester of $PGF_{2\alpha}$ was determined on a Hewlett-Packard (HP) 5790 gas chromatograph equipped with J & W telescopic on-column injector, a J & W fused-silica capillary column DB-1, 30 m × 0.321 mm with film thickness of 0.25 μm and a pulse-linearized electron-capture detector.

2.4. Sample preparation

Preparation of a the reaction mixture for derivatization with pBrPhBr

A 1-ml volume of buffer containing PGs or 1 ml biological incubate was added to 4 ml of phosphate buffer at pH 7.4. The resulting 5 ml of analytical sample was added to 300 mg XAD-2 which had been was pre-wetted with 300 μl acetonitrile. A 150-μl volume of a solution containing the esterifying reagent was then added to this heterogenous mixture to commence the reaction.

Preparation of the reaction mixture for derivatization with PANBr.

The reagent was dissolved in acetonitrile at a concentration of 1 mg/ml. A 1-ml volume of this solution was added to 300 mg of XAD-2 followed by 150 μl of trichloroethylene (TCE) and the reaction mixture was shaken for 5 min. A 5-ml volume of water was then slowly added to precipitate the reagent onto the surface of the resin. The liquid phase was discarded. A 5-ml volume of 0.1 *M* phosphate buffer at pH 7.4 and containing the PGs were then added to the resin that had been impregnated with the reagent.

Reaction conditions common to use of both reagents

In one procedure the reaction mixture was shaken at 40°C for 2 h. The resin was isolated by aspiration washed with distilled water. A 10-ml volume of hexane was then added, the mixture was shaken for 10 min and the hexane was removed. The procedure was repeated. The derivatized analyte was eluted with 10% ethylene chloride in diethyl ether which was evaporated to dryness. The residue was taken up in acetonitrile and injected onto the HPLC column. Alternatively the residue was purified by semi-preparative column chromatography (see below).

In the second procedure the shaking was carried out at ambient temperature and the resin was isolated and washed with water as before. Prior to any elution of analyte or excess reagent, the resin was dried under a stream of nitrogen at 40°C. The dried resin was shaken with 10 ml of hexane and the procedure was repeated. Derivatized analytes were eluted and analyzed as described above or were purified by semi-preparative chromatography (see below).

2.5. Determination of yield

By HPLC

A calibration curve was determined by from the responses obtained by injection of known amounts of pure derivative. The recoveries calculated by comparison of the response from injection of an aliquot of the sample.

By recovery of radiolabel

Radiolabelled PGE_2 or $PGF_{2\alpha}$ was added to the reaction mixture and the components of the reaction mixture were separated by semi-preparative chromatography (see below). This procedure had been shown to remove PGs underivatized at the carboxyl group from the esterified products [10]. The yield was then determined from the recovery of radiolabel.

2.6. Semi-preparative chromatography

The residue was taken up in 300 μl dichloromethane and transferred to a 20 × 16 mm Florisil column. The column was washed successively with 20 ml each of hexane, 50% diethyl ether in hexane, diethyl ether and 10% methanol in diethyl ether. Esterified $PGF_{2\alpha}$ was recovered in the last fraction which was concentrated as before. The residue was taken up in a volume of acetonitrile for injection onto the HPLC.

2.7. Measurement of prostaglandins from fibroblast culture

The culture medium contained fibroblasts and 2% fetal calf serum. Three types of samples were run. The first was a blank consisting only of the culture medium. The second sample was a positive control and contained fibroblasts that had been stimulated with interleukin 1 but in the presence of indomethacin to suppress PG production. The third was the experimental sample

Table 1
Effect of mass of XAD-2, structure of reagent and mass of reagent on yield for derivatization of $PGF_{2\alpha}$ from buffer at 40°C for 2 h

	200 mg XAD-2			300 mg XAD-2,
	0.065 mmol (17 mg) PFBBr	0.0036 mmol (1 mg) pBrPhBr	0.0054 mmol (1.5 mg) pBrPhBr	
Yield (%)[a]	90 ± 9	60 ± 13	93 ± 5	96 ± 6

[a] Average ± relative standard deviation ($n = 5$).

which contained fibroblasts stimulated by interleukin 1 to produce PGs.

3. Results and discussion

Solid-phase reaction of PGs with pBrPhBr produced derivatives suitable for HPLC determination but required considerably less reagent than the corresponding reaction with PFBBr (Table 1). Quantitative isolation and pentafluorobenzylation of $PGF_{2\alpha}$ from buffer onto XAD-2 required 0.065 m*M* (17 mg) of PFBBr, a reaction time of 2 h and a temperature of 40°C. Under similar conditions 0.0036 m*M* (1 mg) of pBrPhBr was required to affect similar yield. The fact that less reagent could be used was important because unlike PFBBr, pBrPhBr is involatile and cannot be removed by evaporation. This results in interferences to the determination of these analytes (Fig. 1) and it is evident that a substantial increase in the chromophoric reagent used would produce prohibitive interferences.

One approach to reducing interferences would be to reduce the amount of reagent used in the reaction. This approach was considered because in solution reactions the phenacyl bromides are 1000 times more reactive that the benzyl bromides [11]. With 200 mg of XAD-2, however, reducing the amount of pBrPhBr to 1 mg reduced the yield to 60%. If, however, the mass of XAD-2 was increased to 300 mg then 1 mg of reagent was sufficient to produce quantitative yield. Further reduction in the mass of reagent by increasing the mass of XAD-2 beyond 300 mg

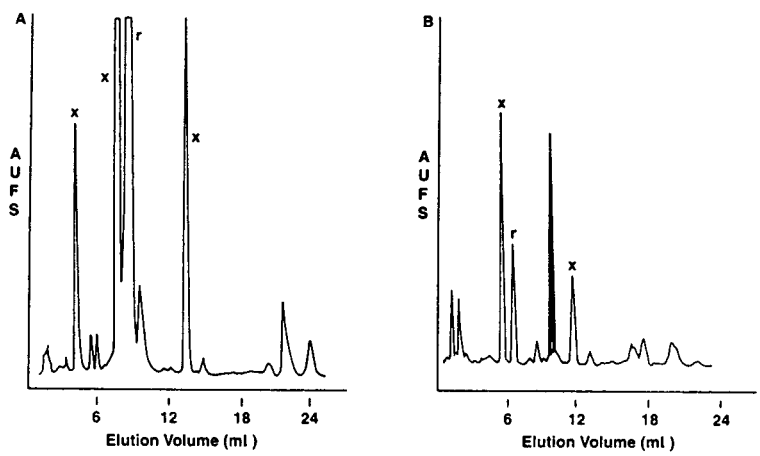

Fig. 1. HPLC traces of the isolates from the derivatization of 5 μg $PGF_{2\alpha}$ with pBrPhBr. (A) Hexane, (B) 10% methanol in diethyl ether. r = Reagent peak; × = peaks from XAD-2.

was not feasible due to difficulty in obtaining efficient mixing in a 100 × 16 mm tube.

These results are consistent with a reaction occurring on the surface of the XAD-2. An increase in surface area would either increase sorption of the analyte or increase the amount of reactive sites. If this is the case then further reduction in the amount of reagent could be obtained by increasing the amount of surface area available in the reaction mixture.

Preparation of the PAN derivative required a modification of the technique for adding the reagent to the reaction mixture. Adding reagent in 150 μl TCE to 300 mg of resin had been previously shown to increase the yield [8] by dispersing the reagent over the total pore volume of the resin bed. PANBr, however, cannot be dissolved at a concentration of 1 mg/150 μl TCE. In consequence, PANBr was co-precipitated with TCE solution onto the resin by the addition of water to a mixture of 300 mg XAD-2 and 1 ml of an acetonitrile solution containing 1 mg reagent and 150 μl TCE. The limited solubility reduced the molar loading of reagent on the surface and as a result the yield of the PAN esters was reduced to 54%.

In order to further reduce the interferences a preliminary clean-up was attempted based on selective elution of the reagent from the XAD-2 with hexane. The reactor bed was treated with hexane immediately after shaking and removed more than 80% of the excess reagent from the XAD-2. In addition, because excess reagent was rapidly removed the reaction was quenched. The derivatized analytes could be subsequently eluted with 10% methanol in diethyl ether (Fig. 1). The removal of excess PANBr was also successfully carried out in this manner (Fig. 2) although there were other interferences in the ultraviolet detection trace possibly arising from the XAD-2.

In an attempt to further improve efficiency for eluting the excess reagent, a variation in the procedure was investigated and this led to an alternative derivatization technique. It was considered that more reagent could be removed by increasing the contact between the XAD-2 surface and the eluting solvent. To this end the

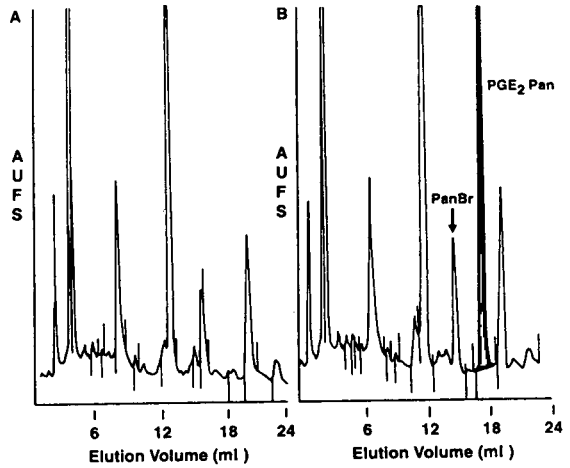

Fig. 2. HPLC traces of the 10% methanol in diethyl ether eluates from XAD-2 for derivatization of 5 μg PGE_2 with PANBr. (A) Blank, (B) sample.

reactor bed was dried in order to remove the water which is a considered necessary for effective contact between lipophilic solvent and the resin.

Under these conditions, it was found that high yield was obtained with reaction times as low as 20 min *and* at room temperature (Table 2). This unexpected finding was attributed to reaction during the drying phase and the sorption of 70% of the native analyte (Table 2). The latter result was surprising. The pH was 7.4 which ensured ionization of the carboxyl group and moreover $PGF_{2\alpha}$ has three hydroxyl groups which would further enhance the water solubility. As a result methods for isolation of PGs that use solid-phase sorption usually require acidification [3]. It appears, however, that there remains sufficient lipophilic character in the PGs to allow substantial sorption onto XAD-2.

Normal-phase semi-preparative column chromatography was used to separate the final amount of excess reagent. After transfer to a Florisil column the interferences were eluted with a solvents or solvent mixtures with low to moderate eluotropic power. The pBrPh ester of $PGF_{2\alpha}$ was eluted with 10% methanol in diethyl ether. This procedure allowed recovery of the derivatives in a clean fraction (Fig. 3).

Table 2
Recoveries of the pBrPhenacyl ester of $PGF_{2\alpha}$ after reaction at ambient temperature using 300 mg of XAD-2

mmol (mg) pBrPhBr	Recovery (%)[a]		
	HPLC		Radiolabel
	Shaking time 20 min	Shaking time 60 min	Shaking time 20 min
0.0036 (1)	79 ± 5	83 ± 6	80 ± 7
0.009 (2.5)	80 ± 6	81 ± 4	80 ± 5
0.036 (10)	100 ± 5	n.d.[b]	n.d.[b]
0	0	0	70 ± 7

[a] Average ± relative standard deviation ($n = 3$).
[b] n.d. = Not done.

Determination of PGs from plasma provides a worst-case scenario of matrix effects. Plasma exerts major effect of yield that can be overcome to some extent by an increase in the amount of reagent used or an increase in reaction time (Table 3). The mechanism of the inhibition is not due to a decrease in sorption since again 70% of the $PGF_{2\alpha}$ is sorbed onto the surface of the resin.

For in vitro studies the simple clean up and reaction at room temperature may prove to be quite sufficient. As shown in Fig. 4 both PGE_2 and $PGF_{2\alpha}$ were formed in the experimental sample where fibroblasts were stimulated with interleukin 1. The two peaks do not appear in the blank or in the control sample where the formation of PG was inhibited by indomethacin.

One major advantage of solid-phase sample preparation is that the technique is more readily amenable to automation. This work demonstrates that a combination of sorption and reaction on solid phase followed by chromatographic purification can be used to prepare PGs for determination by HPLC using either fluorophoric or chromophoric detection. In addition, sorption of PGs is high even at neutral pH and allows reaction without the requirement of agitation. This would further facilitate the application of this technique to automation. Such a development would also facilitate the purification of the

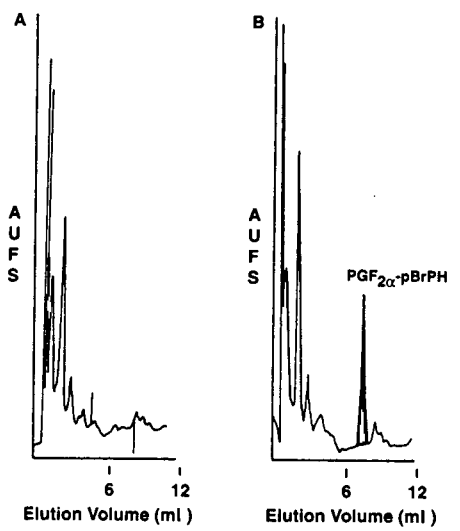

Fig. 3. HPLC traces of the isolate from derivatization of 1 μg $PGF_{2\alpha}$ with pBrPhBr following purification by selective elution and Florisil chromatography. (A) Blank, (B) sample.

Table 3
Recoveries of the pBrPhenacyl ester of $PGF_{2\alpha}$ from plasma as a function of reaction time and reagent

Mass of pBrPhBr (mg)	Recovery (%)[a]	
	Shaking time 20 min	Shaking time 60 min
0.0036 (1)	n.d.[b]	30 ± 8
0.009(2.5)	49 ± 4	50 ± 7

[a] Average ± relative standard deviation ($n = 3$).
[b] n.d. = Not done.

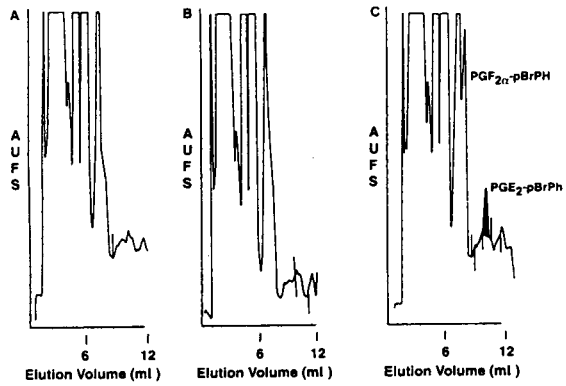

Fig. 4. Extracts of a fibroblast culture. (A) Buffer blank, (B) fibroblasts stimulated with interleukin 1 in the presence of indomethacin, (C) fibroblasts stimulated with interleukin 1.

derivatized analytes which could be done more effectively with automated column switching rather than the manual technique currently in use.

References

[1] K.A. Waddell, I.A. Blair and J. Welby, *Biomed. Environ. Mass Spectrom.*, 10 (1983) 83–87.
[2] N. Shindo, T. Saito and K. Muriyama, *Biomed. Environ. Mass Spectrom.*, 15 (1988) 25–32.
[3] H.A. Leaver, A. Howie and N.H. Wilson, *Prost. Leukotri. Essent. Fatty Acids*, 42 (1991) 217–224.
[4] D.R. Knapp, *Analytical Derivatization Reactions*, Wiley, New York, 1980, p. 537.
[5] W.D. Watkins and M.B. Peterson, *Anal. Biochem.*, 125 (1982) 30–40.
[6] A.J. Bourque, I.S. Krull and B. Feldbush, *Anal. Chem.*, 65 (1993) 2983–2989.
[7] A.J. Bourque and I.S. Krull, *J. Chromatogr.*, 537 (1991) 123–152.
[8] J.M. Rosenfeld, M. Mureika-Russell and S. Yeroushalmi, *J. Chromatogr.*, 358 (1986) 137–146.
[9] J.M. Rosenfeld, M. Mureika-Russell and M. Love, *J. Chromatogr.*, 489 (1989) 263–272.
[10] J.M. Rosenfeld, Y. Moharir and R. Hill, *Anal. Chem.*, 63 (1991) 1365–1370.
[11] J. Hine, *Physical Organic Chemistry*, McGraw-Hill, New York, 1956, p. 158.

ELSEVIER

Journal of Chromatography A, 691 (1995) 239–246

JOURNAL OF CHROMATOGRAPHY A

Use of particle-loaded membranes to extract steroids for high-performance liquid chromatographic analyses Improved analyte stability and detection

Gary L. Lensmeyer*, Carol Onsager, Ian H. Carlson, Donald A. Wiebe

Clinical Toxicology/Special Chemistry Laboratories and Departments of Pathology and Laboratory Medicine, University of Wisconsin Hospital and Clinics, Madison, WI 53792, USA

Abstract

Cortisol, cortisone, corticosterone, prednisone and prednisolone are extracted from serum using the novel particle-loaded octyl (C_8)-bonded silica in PTFE membrane. Extracts are directly injected, without further concentration, onto a narrow (2.0 mm) *or* conventional (4.6 mm) bore octyldecyl (C_{18}) HPLC column. Method performance data demonstrate linearity from 0.4 μg/dl (low limit of detection) up to at least 60 μg/dl. Extraction recoveries exceeded 85% and precision (between-run) R.S.D.s averaged $<5\%$. Interferences were minimal and selectivity was improved over conventional immunochemical steroid assays. When compared to large particle sorbents packed in columns or to traditional liquid–liquid extractions, the membrane extracted steroids in less time, used less reagent, and had smaller elution volumes, thereby obviating steroid instability/adsorption problems associated with traditional concentrating techniques required to improve analytical sensitivity.

1. Introduction

Commercial immunochemical assays offer a technically simple and expedient way to measure steroids in blood. However, analytically these assays are often inaccurate due to interferences from sample matrix and cross-reactivity with chemically similar steroids [1,2]. With cortisol assays, commercial antisera are non-specific and unable to differentiate between cortisol, some of its metabolites and some therapeutically administered steroids. Inaccuracy problems associated with immmunochemical assays for steroids are not always obvious or appreciated by physicans or other users of these test systems. Previously we reported descrepancies for cortisol results in a patient sample comparison study [2]; others describe similar results [3]. Sera collected from patients in a major medical center were tested both by immunoassay and HPLC with solid-phase packed-column extraction. Regression data (with $n = 134$, and $y =$ immunoassay, $x =$ HPLC) demonstrated $y = 0.851x + 7.21$, $r = 0.956$, $Sy/x = 3.8$ μg/dl. The two methods did not compare well. For several serum specimens, the immunoassay reported cortisol concentrations when none was detected by HPLC. The presence of prednisolone in serum always grossly elevated the "apparent cortisol" value. The interference problem is not limited to cross-reactivites from administered steroid drugs. Patients with a disrupted hypothalamic-pituitary-

* Corresponding author.

0021-9673/95/$09.50
SSDI 0021-9673(94)00659-8

adrenal axis often generate abnormal steroids that cross-react with the antisera [4] and give falsely high cortisol values. Ironically, immunoassays seem to perform best on serum specimens from healthy individuals [5,6].

Fortunately, improved analytical selectivity is available with the somewhat more complex chromatographic procedures [2–4,7,8] for steroids. Most often though, time-consuming extractions are necessary with these assays. Simplification of extraction processes is one way by which chromatography would be a cost-effective, practical, accurate and more clinically relevant alternative to immunoassays.

Advances in solid-phase extraction (SPE) technology have recently extended the benefits of this sorbent technique over traditional liquid–liquid extractions. Second generation SPE materials in the form of thin membranes or disks loaded with small particle sorbents have been introduced [9] and demonstrated advantages over large particle sorbents loosely packed in columns. Application reports of assays for environmental pollutants [9] and drugs [10–12] attest to the benefits of the membrane extraction.

Here we demonstrate the effectiveness of the thin PTFE (SPE) membrane —loaded with small-particle C_8-bonded silica— in the extraction and companion HPLC analysis of the endogenous steroids cortisol, cortisone, corticosterone and the therapeutically administered steroids prednisone, and prednisolone in patients' serum specimens. To measure overall performance, we evaluated linearity, recovery, precision and lowest limit of quantitation. Method optimization charts for each step of the process are presented. A comparative study with conventional large-particle C_8 sorbent packed in columns demonstrates the advantages of the membrane format for extraction of steroids.

2. Experimental

2.1. Chemicals and reagents

Pure prednisone, cortisone, prednisolone, corticosterone, fludrocortisone and methylprednisolone were purchased from Sigma (St. Louis, MO, USA). Cortisol was from the the National Bureau of Standards (Washington, DC, USA). Hydrochloric acid and all solvents (HPLC grade), including acetonitrile, methanol, ethanol and tetrahydrofuran (THF) were from J.T. Baker, Phillipsburg, NJ, USA. Sodium borate (reagent grade) was from Fisher Scientific, Fair Lawn, NJ, USA. Distilled deionized water was prepared with the Milli-Q water-purification system (Millipore, Bedford, MA, USA). Other solutions include hydrochloric acid, 0.8 *M*, methanol–water (18:82, v/v), and saturated sodium borate solution.

2.2. SPE membrane

Empore extraction disk cartridges (4 mm diameter, 500 μm thick secured in 1-ml polypropylene columns) containing octyl (C_8)-bonded silica (8 μm average particle size) enmeshed in PTFE fibrils were supplied by 3M Co., St. Paul, MN, USA (Fig.1).

2.3. Instrument and mobile phase

The HPLC system consisted of a Model 126 solvent-delivery unit and Model 167 detector

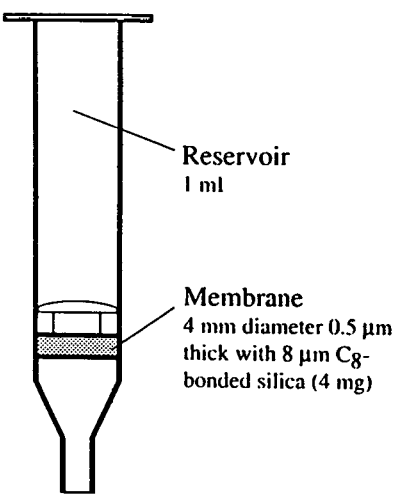

Fig. 1. Diagram of the solid-phase extraction disk cartridge.

module set at 254 nm with attenuation at 0.015 AU full scale (all from Beckman Instruments, Berkeley, CA, USA). A Model HP1050 auto-injector and Model HP3395 integrator were from Hewlett-Packard, Rolling Meadows, IL, USA. An Omniscribe strip-chart recorder (Houston Instruments) was used also. A dry-packed mobile phase silica saturating column (150 × 4.6 mm) containing 37–53-μm particle diameter silica gel (Whatman, Clifton, NJ, USA) was connected between the pump and the injector. Use of a saturator column is extremely important. Otherwise, chromatographic separation will deteriorate and the performance of the analytical column will be significantly decreased. A guard column (20 × 2 mm; Upchurch Scientific, Oak Harbor, WA, USA) was packed with 30-μm diameter particles of Permaphase ETH (DuPont Instruments, Wilmington, DE, USA) and connected to precede the Ultrasphere C_{18} (250 × 2.0 mm *or* 250 × 4.6 mm) analytical column (Beckman Instruments, Fullerton, CA, USA). All columns (silica saturating, guard and analytical) are located in an oven (Eldex column heater, San Carlos, CA, USA) maintained at 55°C. The mobile phase was water–THF (80:20, v/v). Flow-rates were 0.18 ml/min *or* 0.8 ml/min for the 2.0 mm or 4.6 mm internal diameter columns, respectively.

2.4. Standard solutions

Individual stock standards of cortisol (20 mg/100 ml), cortisone (10 mg/100 ml), corticosterone (10 mg/100 ml) and prednisolone (20 mg/100 ml) were prepared in methanol. Prednisone standard (10 mg/100 ml) was prepared in ethanol. A stock mixture solution was prepared by combining aliquots of the individual stock solutions and diluting the mixture to 500 ml with methanol. Final concentrations of this secondary stock mixture are 40 μg/dl each for cortisol, prednisone, prednisolone and 20 μg/dl each for cortisone and corticosterone. To obtain working concentrations encompassing the calibration curve (6.0, 12.0, 24.0, 36.0, 48.0 and 60.0 μg/dl for cortisol, prednisone and prednisolone; 2.25, 4.5, 9.0, 13.5, 18.0 and 22.5 μg/dl for cortisone and corticosterone) portions of the mixed stock are placed in polypropylene tubes, the solvent removed using vacuum (Speed Vac concentrator, Savant Instruments, Farmingdale NY, USA), and the steroids reconstituted with steroid-free serum. The steroid-free serum was prepared in our laboratory by sorbent adsorption of endogenous steroids with minimal disruption of native serum matrix.

2.5. Internal standards (I.S.) solution

Stock solutions of fludrocortisone (20 mg/100 ml) and methylprednisolone (30 mg/100 ml) were prepared in methanol. Portions (0.5 ml) of each stock were combined and the mixture diluted to 100 ml with water to get final concentrations of fludrocortisone 100 μg/100 ml and methylprednisolone 150 μg/100 ml. Equal parts of this mixture and of hydrochloric acid (0.8 *M*) are combined to prepare a working I.S. solution. Working solution is prepared daily. The second I.S., methyprednisolone, is used in the event of an interference with fludrocortisone, the primary I.S.

2.6. Extraction procedure

Combine 300 μl serum (or standard calibrators) and 150 μl of the working I.S. solution [0.4 *M* HCl containing fludrocortisone (50 μg/100 ml) and methylprednisolone (75 μg/100 ml)] in a polypropylene microfuge test tube (1.7-ml size). Incubate sample at room temperature for 10 min to release steroids bound to proteins. Add 800 μl saturated sodium borate solution, mix. If necessary, centrifuge (12 400 *g*) the sample mixture for 3 min to settle particulate that could plug the extraction membrane. Pour sample into the reservoir of a primed Empore C_8 extraction disk unit. To prime the membrane. place about 0.5 ml methanol in the reservoir, and force through three drops of liquid using a syringe with adapter; discard the remaining liquid. Next fill the reservoir with water and force three drops through; pour off the remaining water. The sample mixture is forced through the membrane by either (a) centrifuging (swinging

bucket) the unit at 100–120 *g* for 5 min, (b) manually applying pressure with a syringe or (c) pulling with a vacuum. We prefer centrifugation; constant flow-rates can be maintained and many samples can be processed simultaneously. After sample passes, wash membrane to remove proteins and interference. Manually force through 200 μl of water followed by 500 μl methanol–water (18:82, v/v). To elute the retained steroids, suspend unit in a 5-ml polypropylene test tube. Add 50 μl acetonitrile to reservoir and gently push liquid through; follow with 150 μl water; mix eluates. Inject 20 μl onto the narrow-bore C_{18} HPLC column (*or* 50–100 μl onto a 4.6-mm HPLC column). Relative retention time and relative peak height techniques are used for identification and quantitation, respectively. Fludrocortisone is the primary I.S. used in these calculations, except when an interference occurs; then methylprednisolone is used.

3. Results

Typical chromatograms from extracted standard calibrator, steroid-free serum, and patients' serum specimens are presented in Fig. 2. Method performance data (precision, recovery and linearity) are listed in Table 1. Extraction recovery was determined by comparing analytical reponse of steroid extracted from serum to response of unextracted steroid in acetonitrile–water (25:75, v/v). To be assured of accurate results, the assay is always calibrated with steroid standards in serum extracted in same manner as patient specimens. Linearity was determined by extracting standards in the concentration range listed in the *Standard solutions* section. The lowest limit of quantitation —described as two times baseline noise— was 0.4 μg/dl for all steroids. Studies demonstrated freedom from interference of other steroids. Table 2 lists those

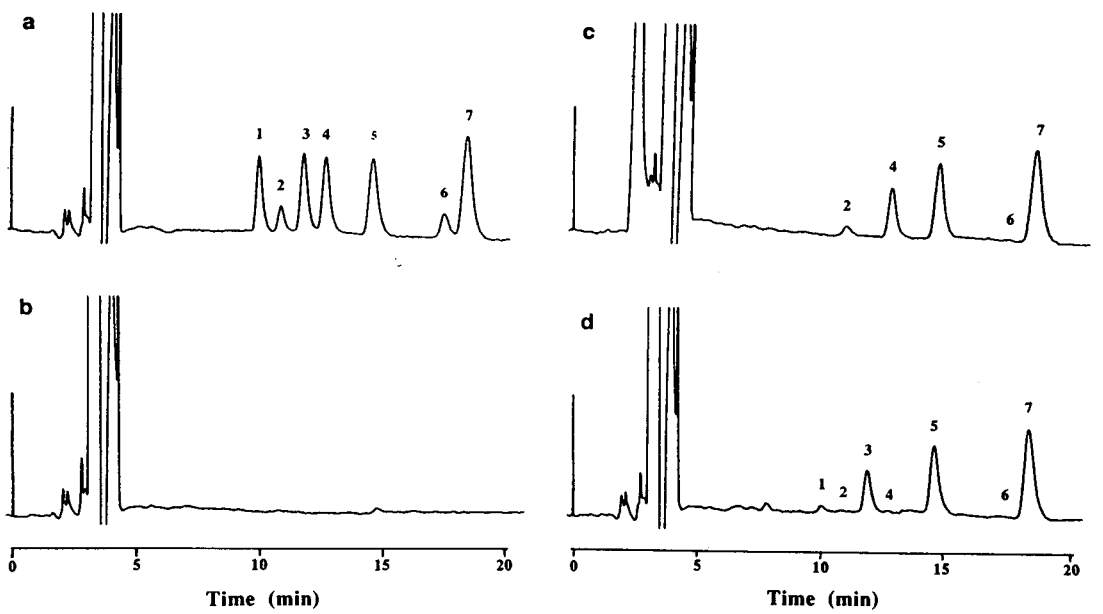

Fig. 2. Typical chromatograms of extracts from: (a) steroid-free serum supplemented with steroid standards (peaks: 1 = prednisone, 20 μg/dl; 2 = cortisone, 7.5 μg/dl; 3 = prednisolone, 20 μg/dl; 4 = cortisol, 20 μg/dl; 5 = fludrocortisone, I.S.1; 6 = corticosterone, 7.5 μg/dl; 7 = methylprednisolone, I.S.2); (b) steroid-free serum; (c) serum from healthy individual (peaks: 2 = cortisone, 2.7 μg/dl; 4 = cortisol, 13.6 μg/dl; 5 = I.S.1; 6 = corticosterone, < 0.4 μg/dl); 7 = I.S.2; and (d) serum from patient who received therapy with prednisone (peaks: 1 = prednisone, 2.3 μg/dl; 2 = cortisone, < 0.4 μg/dl; 3 = prednisolone, 12.3 μg/dl; 4 = cortisol, < 0.4 μg/dl; 5 = I.S.1; 6 = corticosterone, < 0.4 μg/dl); 7 = I.S.2. (Note: prednisone is metabolized to prednisolone.)

Table 1
Method performance data

	Precision (between-run, $n = 14$)			Recovery (%)	Linearity ($n = 6$)			
	Mean (μg/dl)	S.D. (μg/dl)	R.S.D. (%)		Slope	y-Intercept	r	Sy/x
Prednisone	5.03	0.180	3.6	87–99	0.0572	−0.0215	1.00	0.0161
	19.72	0.677	3.4	89–93				
	40.8	1.27	3.1	86–91				
Cortisone	1.98	0.056	2.8	89–92	0.0511	−0.0153	1.00	0.0206
	7.46	0.502	6.7	91–94				
	14.9	0.770	5.1	86–88				
Prednisolone	5.02	0.111	2.2	85–90	0.0565	−0.0383	1.00	0.0390
	19.75	0.603	3.1	88–93				
	40.5	1.26	3.1	86–89				
Cortisol	5.03	0.125	2.5	92–94	0.0549	−0.0551	1.00	0.0697
	19.82	0.668	3.4	86–93				
	40.3	1.41	3.5	86–89				
Corticosterone	2.08	0.168	8.0	87–93	0.0434	0.0126	1.00	0.0091
	7.53	0.344	4.6	86–91				
	14.9	0.713	4.8	87–91				

S.D. = Standard deviation; R.S.D. = relative standard deviation; r = correlation coefficient; Sy/x = S.D. of regression line at mean concentration.

compounds tested and respective retention time. Optimization data and performance characteristics are in Fiq. 3 and include the influence of: HCl concentration on recovery; acetonitrile content of wash solution on recovery; and relationship of serum sample volume size to analytical response.

4. Discussion

We discovered, as have other investigators, that pretreatment of serum samples before extraction with sorbents is necessary to improve analytical recovery of some steroids. Sorbent extractions are prone to give low recoveries because of competition between serum proteins and sorbent ligand for the steroid. Pretreatment frees those steroids bound to proteins [13] by either denaturating the protein or displacing the bound steroid with another compound. Heat [7] and steroid-displacing agents, such as 8-anilino-1-naphthalenesulfonic acid [13], have been used by others to pretreat serum and increase recovery. Using the membrane extraction with *no* serum pretreatment we observed recoveries of only 82, 75 and 73% for cortisol, prednisolone and corticosterone, respectively. Similar results have been reported with the packed-column sorbent format [3,7]. We discovered that HCl (0.4 M) mixed with serum in a ratio of 1:2 (v/v) effectively denatures the steroid-binding proteins and increases extraction recovery. Most important, the accuracy of the membrane extraction depends on calibration with steroid standards in serum processed in the same manner as patients' specimens.

The performance of the membrane disk and conventional SPE column format were compared. The steroid extraction was duplicated on SPE columns containing loosely packed large particle (40 μm) C_8 sorbent. Both membrane

Table 2
Interference study: relative retention times of 20 steroids chromatographed in the HPLC system

Steroid	Relative retention time[a]
Aldosterone	0.38
Triamincinolone	0.46
Metyrapone	0.49
Prednisone	0.68
Cortisone	0.74
Prednisolone	0.80
Cortisol	0.86
Fludrocortisone	1.00
Corticosterone	1.20
Methylprednisolone	1.35
11-Deoxycortisol	1.70
Dexamethasone	1.71
21-Deoxycortisone	1.82
Androsteindione	2.33
Beclomethasone	2.44
11-Deoxycorticosterone	2.83
Testosterone	3.34
17-Hydroxyprogesterone	>3.50
Progesterone	>3.50
Pregnenolone	>3.50

[a] Relative to fludrocortisone.

and column contained C_8 sorbent from the same manufacturer (Varian Sample Preparation Products, Harbor City, CA, USA). The most remarkable dissimilarity between the disk and packed column was the volume of solvent required to completely elute all retained steroids. Elution profiles (analyte recovery versus fractional volume of eluting solvent) were established to better illustrate this difference (Fig. 4). Experimentally, we passed 35-μl portions of acetonitrile, followed by 150 μl of water through a sorbent with retained steroids. An aliquot of the eluate mixture was chromatographed. The elution process was repeated until all retained steroids were completely removed from a sorbent. Recovery of steroids was calculated for each fraction. With this study, a total of 50 μl of acetonitrile was needed for complete elution off the membrane; 310 μl were required with the packed column. Overall, the membrane afforded an extract that was five to six times more concentrated than the extract from the column.

The extract from the membrane disk could be injected directly into the HPLC system without sacrificing analytical sensitivity. The extract from the column needed to be evaporated/concentrated/reconstituted to achieve comparable analytical sensitivity. In our hands, the evaporation process sometimes led to lower recoveries, depending on the type of glass test tube used to hold the sample. Deactivation of the glass surface did not solve the problem.

The improved efficiency of the membrane over the packed column is due to the smaller particle size (8 versus 40 μm) and smaller sorbent mass (4 versus 100 mg) of the membrane. Both characteristics afford greater capacity per mg of sorbent and allow for smaller volume of solvent for elution resulting in a more concentrated solution of steroids and increased analytical sensitivity. Our studies demonstrate that the capacity of the 4-mm diameter C_8 membrane is more than adequate for the described steroid analysis of clinical serum specimens. However, with much larger sample volumes or when greater capacity is required, larger-diameter (7 or 10 mm) membranes should be used. When making a switch from the 4-mm diameter disk to a larger-size disk, the volume sizes of wash and eluting solutions must be reoptimized.

5. Conclusions

The C_8 particle-loaded membrane efficiently extracts cortisol, cortisone, corticosterone, prednisone and prednisolone from serum specimens at concentrations seen clinically in patients. Most notable is the improvement in specificity when this extraction–HPLC analysis is compared to immunochemical assays prone to interferences. Method performance data demonstrates overall between-run precison R.S.D.s of 3.79% ± 1.4%, extraction recoveries that average 90% ± 3.3%, and linearity from 0.4 μg/dl (low limit of detection) to at least 60 μg/dl. When necessary, increased capacity can be achieved by choosing a larger-size diameter membrane.

In some respects both the SPE membrane and traditional large-particle packed columns per-

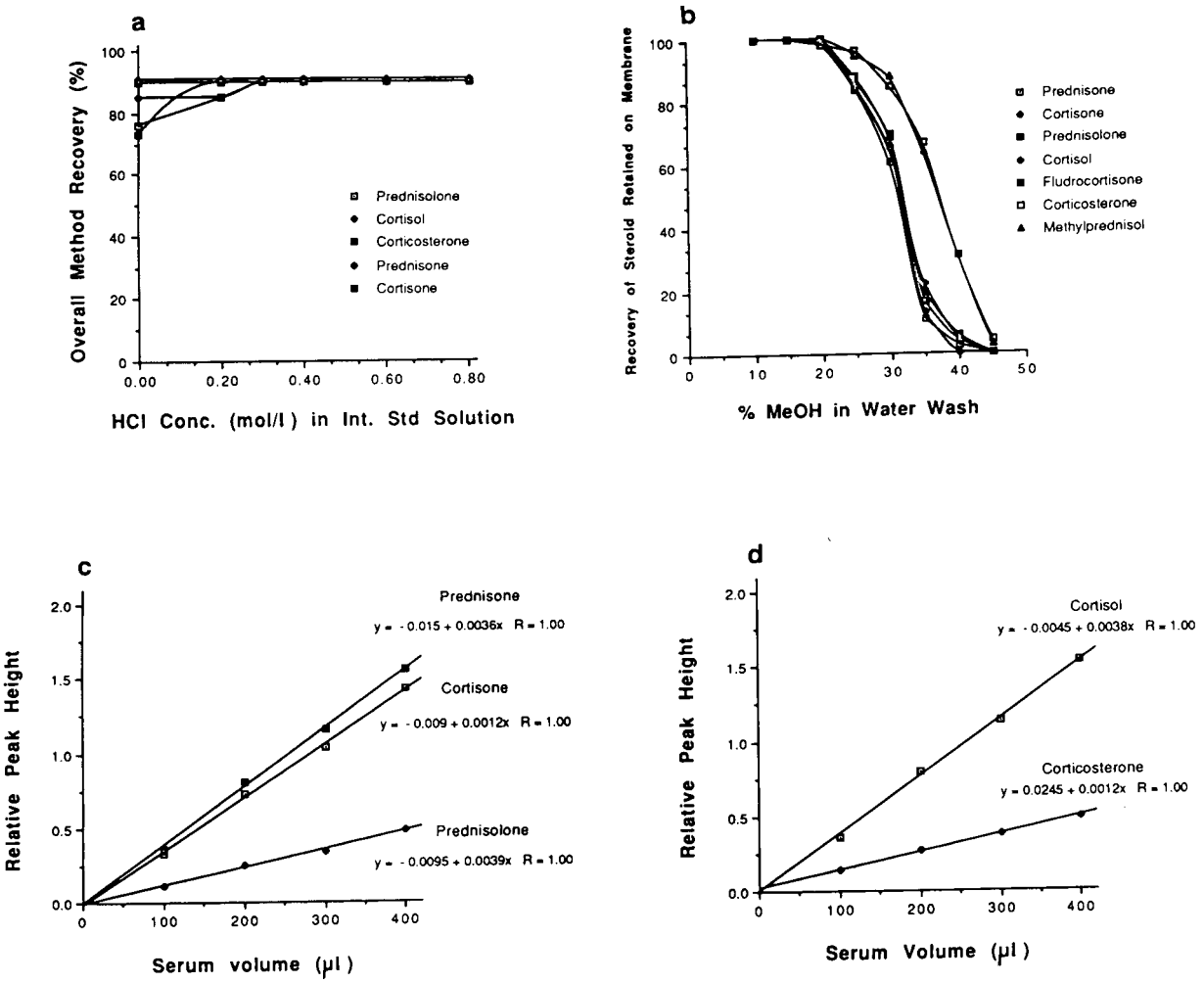

Fig. 3. Optimization charts showing influence of (a) HCl concentration in internal standard (Int. Std) solution on recovery, (b) methanol content of wash solution on recovery and (c, d) relationship of serum volume size to analytical response. Steroid concentrations tested were the same as contained in mid-range sample used in precision study.

formed similarly, however we observed distinct advantages with the membrane. Remarkably, the steroids could be eluted off the membrane in a small volume and the eluate directly injected onto the HPLC system without additional concentration or loss of sensitivity. Extracts from the SPE column required an additional solvent evaporation/concentration/reconstitution step. Overall, when compared to the SPE column, the membrane gave smaller elution volumes, afforded five times greater analytical sensitivity, circumvented instability problems associated with conventional concentrating processes, and simplified extraction to give a faster analysis.

The improved concentrating ability of the membrane can be attributed to the robust configuration of the sorbent within an inert support. The small 8-μm diameter particle size particles tightly held within PTFE gives greater surface area and increased capacity per mg of sorbent than conventional 40-μm particle sorbents packed in columns. Most important though, this

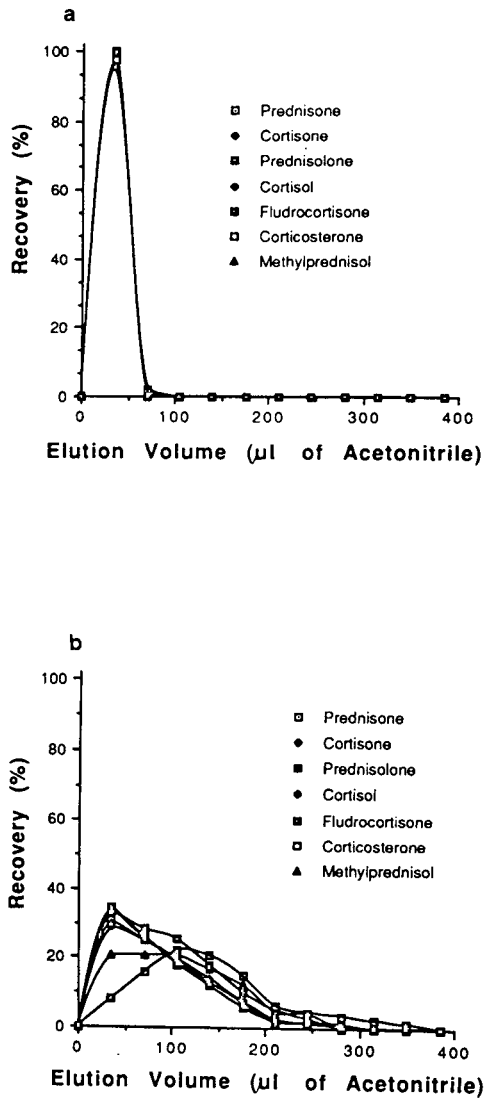

Fig. 4. Comparison of elution volume required to completely recover steroids retained on (a) SPE C_8 disk membrane (4 mm) and (b) SPE C_8 packed column (100 mg).

second generation form of solid-phase material is a new tool capable of decreasing the complexity of highly selective chromatographic procedures to offer accurate and clinically relevant steroid results.

Acknowledgement

We thank the 3M Company for supplies and support in this work.

References

[1] J.J. Miller and R. Valdes, *Clin. Chem.*, 37 (1991) 144.
[2] G.L. Lensmeyer, I.H. Carlson, D.A. Wiebe and D. deVos, *Clin. Chem.*, 38 (1992) 945.
[3] D.C. Turnell, J.D. Cooper, B. Green, G. Hughes and D.J. Wright, *Clin. Chem.*, 34 (1988) 1816.
[4] T. Wong, C.H.L. Shackleton, T.R. Covey and G. Ellis, *Clin. Chem.*, 38 (1992) 1830.
[5] J.Q. Wei, X. Zhou and J.L. Wei, *Clin. Chem.*, 33 (1987) 1354.
[6] E. Canalis, A. Caldarella and G. Reardon, *Clin. Chem.*, 25 (1979) 1700.
[7] M. Hariharan, S. Naga, T. VaanNoord and E. Kindt, *Clin. Chem.*, 38 (1992) 346.
[8] J.H. McBride, D.O. Rodgerson, S.S. Park and A.F. Reyes, *Clin. Chem.*, 37 (1991) 643.
[9] D.F. Hagen, C.G. Markell and G.A. Schmitt, *Anal. Chim. Acta*, 236 (1990) 157.
[10] G.L. Lensmeyer, D.A. Wiebe and T. Doran, *Therap. Drug Monit.*, 13 (1991) 244.
[11] G.L. Lensmeyer, D.A. Wiebe and B.A. Darcey, *J. Chromatogr. Sci.*, 29 (1991) 444.
[12] K. Ensing, J.P. Franke, A. Temmink, X. Chen and R.A. de Zeeuw, *J. Forensic Sci.*, 37 (1992) 460.
[13] A. Moore, R. Aitken, C. Burke, S. Gaskell, G. Groom, G. Holder, C. Selby and P. Wood, *Ann. Clin. Biochem.*, 22 (1985) 435.

ELSEVIER

Journal of Chromatography A, 691 (1995) 247–254

JOURNAL OF CHROMATOGRAPHY A

High-performance liquid chromatographic analysis of human erythrocyte oxysterols as Δ^4-3-ketone derivatives

Jon Ie Teng*, Leland L. Smith

Department of Human Biological Chemistry and Genetics, University of Texas Medical Branch, Galveston, TX 77555, USA

Abstract

Following oxidation by cholesterol oxidase human erythrocyte oxysterols were analyzed as the corresponding hydroxy-Δ^4-3-ketones by HPLC with effluent monitoring at 235 nm. Variable amounts of epimeric cholest-5-ene-3β,7-diols, 3β-hydroxycholest-5-en-7-one, cholest-5-ene-3β,19-diol, cholest-5-ene-3β,20-diol, cholest-5-ene-3β,25-diol and cholest-5-ene-3β,26-diol were detected in erythrocyte membranes of patients with sickle cell anemia or sickle cell trait. Only 3β-hydroxycholest-5-en-7-one was detected in erythrocyte membranes of healthy donors.

1. Introduction

Proper analysis of tissue oxysterols, simple sterol oxidation products, requires resolution of up to ten or so components by thin-layer (TLC), gas or high-performance liquid (HPLC) chromatography. Of the most frequently encountered oxysterols, the B-ring oxidized sterols cholest-5-ene-3β,7α-diol (**1**), cholest-5-ene-3β,7β-diol (**2**), 3β-hydroxycholest-5-en-7-one (**3**) constitute one set, the isomeric 5,6-epoxides 5,6α-epoxy-5α-cholestan-3β-ol (**4**) and 5,6β-epoxy-5β-cholestan-3β-ol (**5**) and their common hydration product 5α-cholestane-3β,5,6β-triol (**6**) another, and the cholesterol metabolites oxidized in the side-chain (20*S*)-cholest-5-ene-3β,20-diol (**7**), (24*S*)-cholest-5-ene-3β,24-diol (**8**), cholest-5-ene-3β,25-diol (**9**), and (25*R*)-cholest-5-ene-3β,26-diol (**10**) yet another.

Each oxysterol set has individual analysis requirements, and despite the many analysis schemes devised analysis of all ten oxysterols yet poses problems of resolution, detection and estimation. Recovery of individual oxysterols for characterization and other work is best served by HPLC, and the Δ^5-oxysterols **1–3** and **7–10** have been resolved in a variety of HPLC procedures that generally rely on effluent monitoring at 205–215 nm [1,2]. The presence of confounding non-sterol tissue components limits these means to relatively pure tissue sterol samples.

In seeking to devise improved yet simplified means of resolution and recovery of common tissue oxysterols in complex tissue matrices we explored analysis of oxysterols **1**, **2** and **7–10** that are substrates for microbial cholesterol oxidases (cholesterol: O_2 oxidoreductase, EC 1.1.3.6) [3–7]. The 7-ketone **3** is not a substrate [7,8], but as a hydroxy-α,β-unsaturated ketone the 7-ketone **3** and the enzyme product hydroxy-Δ^4-3-ketones from **1** and **2**, and **7**, **9** and **10** are resolved by HPLC and detected at 235–240 nm together as a set. The longer monitoring wavelength eliminates interferences from non-sterol tissue components, and the enzymic alteration of oxysterol samples prior to HPLC ensures that only

* Corresponding author.

0021-9673/95/$09.50
SSDI 0021-9673(94)00986-4

genuine oxysterol Δ^5-3β-alcohols will be observed at the improved sensitivity.

Application of this approach to analysis of Δ^5-sterols and oxysterols has been previously described [9–14], and we record here exploration of the oxysterol composition of human erythrocyte membranes by these means.

2. Experimental

2.1. Materials

Oxysterols **1–10** are from our extensive sterol collection and from Steraloids (Wilton, NH, USA). Cholest-5-3β,19-diol (**11**) and cholesterol oxidase from *Nocardia erythropolis* were obtained from Sigma (St. Louis, MO, USA). Reference samples of oxysterol Δ^4-3-ketones were prepared by incubation of parent oxysterols **1**, **2**, **7** and **9–11** with cholesterol oxidase, with isolation of the product by TLC. Solvents for HPLC are from Burdick & Jackson Labs. (Muskegon, MI, USA).

2.2. Erythrocyte sample preparation

Erythrocytes from fresh blood samples obtained from hospitalized patients with sickle cell trait or sickle cell anemia (1.0–2.0 ml) and from healthy volunteers (4.0–6.0 ml) were washed three times with two volumes each of 0.001 *M* phosphate–saline pH 7.5 buffer and centrifuged at 1500 *g* for 15 min at 4°C. The erythrocytes were then lysed with three volumes of 0.01 *M* pH 8.6 phosphate buffer, centrifuged at 4000 *g* for 15 min, and transferred to a 100 × 13 mm glass tube. Lysed erythrocyte membranes were mixed with an equal volume of methanol (alternatively 2-propanol) on a vortex shaker to avoid aggregation, and total lipids were extracted by mixing in a vortex shaker with two volumes chloroform (1.5 volumes if 2-propanol used). Following centrifugation the chloroform phase was removed and the extraction process repeated twice with premixed chloroform–methanol (2:1, v/v) or chloroform–2-propanol (11:7, v/v). The chloroform–methanol extraction gave a yellow-colored extract whereas the chloroform–2-propanol solvent gave a colorless extract but with slightly less cholesterol and phospholipids recovered. Chloroform–methanol was the preferred extraction solvent.

Pooled chloroform extracts were evaporated under nitrogen, redissolved in 0.5–1.0 ml chloroform, and applied as a zone no more than 10 cm long to 20 × 20 cm Uniplate HLF silica gel chromatoplates 0.25 mm thick (Analtech, Newark, DE, USA), together with reference oxysterols 3β,7α-diol **1** and 3β,20-diol **7** well away from the applied test sample. The applied material was concentrated into a compact, thin zone by ascending irrigation with chloroform–methanol (2:1, v/v), and then irrigated with hexane–diethyl ether–acetic acid (65:35:1, v/v/v) in ascending fashion to a height of 15 cm two times. The sample region was covered with a 20 × 10 cm glass plate and the chromatogram exposed to iodine vapors to visualize the reference oxysterols **1** and **7** as guides for recovery of the oxysterols in the test sample. The test sample zone limited by oxysterols **1** and **7** was excised, packed into a 2-ml ASTM Pyrex filter funnel, and eluted with three 2.0-ml portions of chloroform–methanol (3:1, v/v). The combined oxysterols eluates were evaporated under nitrogen.

2.3. Cholesterol oxidase incubations

Incubation procedures of Goh et al. [9] were modified. To the total oxysterols dissolved in 50 μl 2-propanol in a 75 × 12 mm culture tube were added 250 μl saline, the mixture mixed by vortex shaker briefly, and 500 μl 20 m*M* pH 7.5 phosphate buffer containing 0.1% sodium cholate and 0.3% (w/v) Tween 20 were added. After gentle mixing by vortex shaker a clear dispersion was obtained. Samples of cholesterol (200 μg) so treated may be cloudy at this point.

To the clear dispersion was added 100 μl 0.1 *M* pH 7.8 Tris buffer containing 60 units catal-

ase, and oxidation was initiated at 37°C by adding 100 μl of the same buffer containing 0.4 unit cholesterol oxidase. After 60 min 300 μl methanol were added to stop the reaction, after which products were extracted with three 2-ml portions of light petroleum (b.p. 35–60°C).

2.4. Chromatography

TLC was conducted with 20 × 20 cm chromatoplates 0.25 mm thick irrigated twice in ascending fashion with hexane–diethyl ether (2:3, v/v). Steroid Δ^4-3-ketones were detected by their 254 nm light absorption; Δ^5-sterols were detected with iodine vapors.

HPLC was conducted using Beckman Instruments equipment consisting of system controller Model 421A, solvent-delivery module Model 114M, and organizer Model 340 with universal sample injection valve Model 210 with 20-μl sample loop, variable-wavelength detector Model 165 with 5-mm micro flow cell (2.2 ml illuminated volume, set at 0.01 AUFS), all connected to two Waters Model 740 data modules (attenuation setting 16).

Samples (0.005–5.0 μg in 10 μl chloroform) were injected through a Perisorb A precolumn onto the analysis column: system A, 250 mm × 4.6 mm Ultrasphere SIL 5 μm particle size (Beckman Instruments), or system B, 300 × 3.9 mm μPorasil · 10 μm particle size (Waters), irrigated with hexane–2-propanol (50:1, v/v) at 1 ml/min flow-rate. Effluent was monitored at 210 nm for oxysterols and at 235 nm for the corresponding Δ^4-3-ketosteroids.

3. Results

Oxysterols **1**, **2**, **7** and **9–11** were smoothly transformed by cholesterol oxidase to the corresponding hydroxy-Δ^4-3-ketones. Resolution of oxysterols **1–3**, **7** and **9–11** and of the corresponding hydroxy-Δ^4-3-ketones and hydroxy-Δ^5-7-ketone **3** by TLC and by HPLC is accomplished with our systems (Table 1, Fig. 1) (with the exception of the 3β,25-diol **9** and 7α-hydroxy-Δ^4-3-ketone pair), thus according means of analysis of oxysterol and oxidized oxysterol mixtures.

Comparison of detection sensitivity of the Δ^4-3-ketones (235 nm) versus their parent Δ^5-3β-alcohols (210 nm) (Table 2) shows improved sensitivity ranging from 3.1–24-fold by peak height, 1.8–20-fold by peak area. Linear relationships between steroid mass and absorbance (peak height) were obtained over the range 0.1–5.0 μg for the oxysterols, but linear responses were had for the Δ^4-3-ketones at lower levels: 0.04–1.0 μg (100 pmol–2.5 nmol) for the 7α-, 20-, 25- and 26-hydroxy-Δ^4-3-ketones; 0.04–2.0 μg (100 pmol–5 nmol) for the 19-hydroxy-Δ^4-3-ketone; and 0.16–4.0 μg (400 pmol–10 nmol) for the 7β-hydroxy-Δ^4-3-ketone. Absorbance responses (AU/μg steroid) were very similar for the 7α-hydroxy- (0.025), 19-hydroxy- (0.026), 20-hydroxy- (0.026), 25-hydroxy- (0.024) and 26-hydroxy- (0.025) Δ^4-3-ketones but less for the 7β-hydroxy-Δ^4-3-ketone (0.011). A detection limit of 0.005–0.05 μg (12–125 pmol) is suggested, somewhat greater than 10 pmol suggested in other work [9,10].

Recoveries of 100-μg samples of the hydroxy-Δ^4-3-ketone derivatives taken through the full procedure of TLC, elution, concentration, and HPLC averaged 90 ± 5% for the 20-, 25- and 26-hydroxyketones, 92 ± 5% for the 7α- and 19-hydroxyketones, and 88 ± 5% for the 7β-hydroxyketone.

Human blood samples from four healthy subjects, from four sickle cell trait patients, and from nine patients with sickle cell anemia or sickle cell trait (uncertain which) were analyzed by our procedure. In those cases where blood sample size permitted analysis of both oxysterol and hydroxy-Δ^4-3-ketone mixtures, there was agreement between the analyses with regard to the number and identity of oxysterols detected.

Oxysterols detected in erythrocyte membranes of ill patients as the corresponding Δ^4-3-ketones included the epimeric 3β,7-diols **1** and **2**, 3β,19-

Table 1
Chromatographic properties of oxysterols and their Δ^4-3-ketones

	Relative mobility[a]		
	TLC	HPLC system A	HPLC system B
Cholesterol	1.98	0.16	–
Cholest-4-en-3-one	2.31	0.10	0.11
Cholest-5-ene-3β,7α-diol (**1**)	1.02	2.70	–
7α-Hydroxycholest-4-en-3-one	1.19	0.53	0.51
Cholest-5-ene-3β,7β-diol (**2**)	1.08	2.55	–
7β-Hydroxycholest-4-en-3-one	1.05	1.35	1.00
3β-Hydroxycholest-5-en-7-one (**3**)	1.00	1.00	1.00
Cholest-5-ene-3β,19-diol (**11**)	0.64	2.07	–
19-Hydroxycholest-4-en-3-one	0.93	0.93	0.93
(20*S*)-Cholest-5-ene-3β,20-diol (**7**)	1.66	0.26	–
20-Hydroxy-(20*S*)-cholest-4-en-3-one	1.83	0.39	0.15
Cholest-5-ene-3β,23-diol	–	0.41	–
23-Hydroxycholest-4-en-3-one	–	0.43	–
(24*S*)-Cholest-5-ene-3β,24-diol (**8**)	–	0.35	–
24-Hydroxy-(24*S*)-cholest-4-en-3-one	–	–	–
Cholest-5-ene-3β,25-diol (**9**)	1.24	0.54	–
25-Hydroxycholest-4-en-3-one	1.37	0.46	0.27
(25*R*)-Cholest-5-ene-3β,26-diol (**10**)	1.20	0.76	–
26-Hydroxy-(25*R*)-cholest-4-en-3-one	1.37	0.57	0.39

[a] Mobility data are calculated with 3β-hydroxycholest-5-en-7-one (**3**) (unaltered by cholesterol oxidase) as unit mobility, with R_F 0.40 in TLC system hexane–diethyl ether (2:3, v/v), retention time 50 min in HPLC system A: Ultrasphere SIL, hexane–2-propanol (50:1, v/v), and retention time 58 min in HPLC system B: μPorasil, hexane–2-propanol (50:1, v/v).

diol **11**, 3β,20-diol **7**, 3β,25-diol **9**, 3β,26-diol **10**, the 7-ketone **3** and an unidentified component. Moreover, oxysterols were not detected in erythrocyte membranes from four healthy donors; only a low level (30 ng/ml) of **3** was detected in one sample (Table 3).

In membrane extracts where cholesterol was not excluded by prior TLC low levels of 20-hydroxycholest-4-en-3-one and 25-hydroxycholest-4-en-3-one were detected following cholesterol oxidase incubations where the corresponding oxysterol 3β,20-diol **7** and 3β,25-diol **9** had not been detected in unoxidized samples. Repeated incubations of 200 μg cholesterol with 0.4 units cholesterol oxidase even in the presence of 60 units catalase established that both 20- and 25-hydroxy-Δ^4-3-ketone products were regularly formed. Also, some cholesterol autoxidation products 3β,7α-diol **1** and 3β,7β-diol **2** (detected as the corresponding 7α- and 7β-hydroxy-Δ^4-3-ketones) and 7-ketone **3** were detected following cholesterol oxidase treatment.

4. Discussion

The indicated increased sensitivity, linear responses, good analyte recoveries and resolution of the hydroxy-Δ^4-3-ketosteroids of interest provides an improved means of their analysis in complex mixtures. The procedure applied to analysis of these oxysterols in human erythrocytes also gives additional insight into the enzymic oxidation of cholesterol by cholesterol oxidase and into the nature of erythrocyte membrane oxysterols of patients suffering from sickle cell anemia and sickle cell trait.

The adventitious autoxidation of cholesterol to

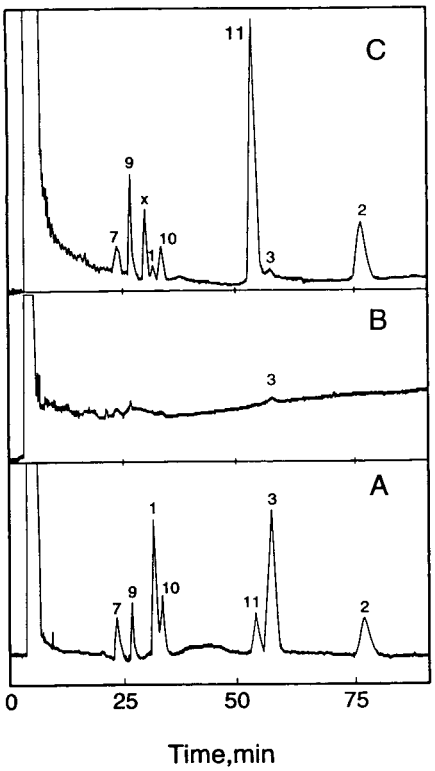

Fig. 1. HPLC elution profiles of oxysterol α,β-unsaturated ketones in system A [Ultrasphere SIL with hexane–2-propanol (50:1, v/v) monitored at 235 nm for absorbance]. The ordinate scale is 0.01 absorbance unit for the initial pen excursion from start to solvent peak height. Components: (A) reference Δ^5-7-ketone **3** and Δ^4-3-ketone derivatives of oxysterols **1**, **2**, **7**, **9**–**11**; (B) absorbing components obtained following cholesterol oxidase treatment of total oxysterols from erythrocyte membranes of a healthy donor; only Δ^5-7-ketone **3** is evident; (C) Δ^5-7-ketone **3** and Δ^4-3-ketones of oxysterols **1**, **2**, **7**, **9**–**11** formed by cholesterol oxidase treatment of total oxysterols from erythrocyte membranes of a sickle cell trait patient; peak x is an unidentified absorbing component.

3β,7α-diol **1**, 3β,7β-diol **2** and 7-ketone **3** during cholesterol oxidase incubations represents yet another example of this insidious process. However, the additional oxidation of cholesterol at the tertiary C-20 and C-25 carbon atoms yielding 20- and 25-hydroxy-Δ^4-3-ketones poses new concern about the nature of the enzymic oxidation. The oxidation of cholesterol at the C-20 and C-25 sites by cholesterol oxidase of *Pseudomonas fluorescens* has previously been observed [15]. This complication necessarily affects the analysis of tissue oxysterols, and both autoxidation and C-20 and C-25 oxidations must be avoided rigorously. Accordingly, only the more polar erythrocyte membrane oxysterols are taken for analysis, and the bulk membrane cholesterol is excluded carefully in our procedure.

Whereas the oxysterol composition of selected human tissues, plasma and serum has been extensively examined, analysis of human erythrocyte oxysterols has received very limited attention. Our early gas chromatography study [16] of human erythrocyte sterols suggested the presence of low levels of a cholest-5-ene-3β,26-diol, and later TLC examination of human erythrocytes sterols by others failed to detect oxysterols [17–19]. More recently the epimeric 3β,7-diols **1** and **2**, 7-ketone **3**, 5α,6α-epoxide **4**, 3β,5α,6β-triol **6**, 3β,20-diol **7** and 3β,25-diol **9**, but also the 3β,19-diol **11** have been detected as oxysterol components of human sickle cell erythrocyte membranes [20].

Our present study confirms some of these results but differs in other aspects. Compounds **1**, **2**, **3**, **11**, **7** and **9** were found in both studies, and we also detect the 3β,26-diol **10** but not the 5α,6α-epoxide **4** and 3β,5α,6β-triol **6** that are undetectable by our methods. Although the 5,6-epoxides **4** and **5** may be poor substrates [11], their oxidized products are not Δ^4-3-ketones, and the 3β,5α,6β-triol **6** is not a substrate [7].

The individual oxysterol patterns and levels (Table 3) vary from case to case. Although **3** is present in all samples and **1**, **2**, **7** and **9** in most, **11** and **10** were found in but a few instances. Moreover, oxysterol levels range from undetected to traces to high levels (**1**, 19.2 μg/dl; **2**, 18.2 μg/dl; **3**, 75.0 μg/dl; **7**, 20.2 μg/dl; **9**, 25.2 μg/dl; **10**, 9.0 μg/dl; **11**, 30.6 μg/dl) comparable to levels previously reported for sickle cell erythrocytes and for human plasma and serum. For the ubiquitous 7-ketone **3** we estimate 1.0–75.0 μg/dl whole blood, Küçük et al. [20] report 900 ng/ml erythrocytes, and human plasma and serum levels of 0.4–373 ng/ml occur [21].

The B-ring oxysterols **1**–**6** are generally regarded as arising from in vivo interception by

Table 2
Increased sensitivity of detection of Δ^4-3-ketosteroids in comparison with parent Δ^5-3β-hydroxysterols

Parent Oxysterol	Peak height (cm)			Peak area (cm^2)		
	Δ^5-3β-Alcohol	Δ^4-3-Ketone	Ratio	Δ^5-3β-Alcohol	Δ^4-3-Ketone	Ratio
3β,7α-Diol **1**	0.2	4.8	24.0	0.025	0.500	20.0
3β,7β-Diol **2**	0.4	1.9	4.8	0.200	0.475	2.4
3β,19-Diol **11**	0.3	4.1	13.6	0.125	0.820	6.6
3β,20-Diol **7**	1.0	3.1	3.1	0.100	0.310	3.1
3β,25-Diol **9**	1.5	5.5	3.7	0.220	0.600	2.7
3β,26-Diol **10**	1.7	6.3	3.7	0.340	0.620	1.8

Data are from elution charts obtained with 0.2 μg parent oxysterol or Δ^4-3-ketone derivative in 10 μl chloroform injected on column, eluate measured at 210 nm for Δ^5-3β-hydroxysteroids, at 235 nm for Δ^4-3-ketosteroids.

cholesterol of reactive oxygen species, whereas the side-chain hydroxylated sterols **7–10** (and 3β,7α-diol **1**) are cholesterol metabolites [21]. The 3β,19-diol **11** has not previously been recognized as a component of human tissues, although the oxysterol **11** is suggested present in meat

Table 3
Oxysterol levels in sickle cell erythrocytes

Patient[a]	Oxysterols found (μg/dl)[b]						
	3β,7α-Diol **1**	3β,7β-Diol **2**	7-Ketone **3**	3β,20-Diol **7**	3β,25-Diol **9**	3β,26-Diol **10**	3β,19-Diol **11**
Sickle cell trait							
No. 1	19.2	18.2	5.4	9.0	25.2	9.0	2.4
	–	–	35.8	12.0	–	–	–
No. 2	1.2	7.2	4.2	2.4	12.6	3.6	1.2
	1.6	0.8	1.2	2.4	4.8	2.4	–
	2.5	tr	1.0	tr	tr	–	30.6
No. 3	1.2	tr	1.0	tr	tr	–	3.8
No. 4	tr	–	4.0	–	tr	–	–
Sickle cell anemia and/or sickle cell trait							
No. 5	7.8	–	36.8	16.8	–	–	–
No. 6	tr	–	13.8	16.8	–	–	–
No. 7	4.8	–	75.0	19.8	tr	–	–
No. 8	8.0	tr	4.0	11.0	tr	–	–
No. 9	8.0	tr	2.0	2.0	3.0	–	tr
No. 10	–	–	2.5	5.0	–	–	–
No. 11	–	–	1.0	–	11.0	–	–
	4.0	tr	1.0	tr	20.0	–	–
No. 12	–	–	6.0	20.2	–	–	–
No. 13	6.0	–	60.0	2.4	tr	tr	–

[a] Patients: No. 1 = male pediatric; No. 2 = female pediatric; No. 3 = male adult; No. 4 = female adult, with diagnosed sickle cell trait. Diagnoses and personal data for patients Nos. 5–13 not available.
[b] Calculated for whole blood. Where there is no entry, the component was not detected; unmeasured trace amounts abbreviated tr.

products [22] and is implicated in sterol metabolism of the sponge *Axinella polypoides* [23].

Thus, the two oxysterol sets **7**, **9**, **10** and **1–4**, **6** found indicate that sickle cell and sickle cell trait erythrocytes accumulate cholesterol metabolites, perhaps from plasma, and also products of cholesterol oxidation by reactive oxygen species formed via in vivo oxygen metabolism. As sickle cell erythrocytes appear to generate substantial amounts of superoxide, peroxide, and hydroxyl radical [24], the B-ring oxidized sterols **1–4** and **6** may be formed within the cell as well as accumulated from the plasma. In any event, these items suggest that increased oxidative stress be a component of the disease.

Blood samples for two pediatric sickle cell trait patients, Nos. 1 and 2 (Table 3) were analyzed at different times. Considerable variations appear among data for patient No. 1, with high levels of 3β,7-diols **1** and **2** and 3β,25-diol **9** at one time but lacking in a sample two months later, at which time increased level of 7-ketone **3** is evident. For patient No. 2 a high level of 3β,19-diol **11** occurs three months after an analysis in which the oxysterol was undetected. Data for adult patients Nos. 3 and 4 suggest similar variable erythrocyte membrane composition.

Data for patients Nos. 5–13 for whom diagnoses and personal data are unavailable exhibit similar variability but with greater absence of 3β,7β-diol **2**, 3β,19-diol **11** and 3β,26-diol **10**. Two samples from patient No. 11 demonstrate variation from time to time in the same patient.

In view of the limited diagnosis and personal data it is not possible to conclude whether patient age or sex are factors, and whether sickle cell anemic or sickle cell trait affect results. However, the variations in data do not appear to represent experimental error. Rather, the variable presence and levels of oxysterols may reflect the periodic crisis nature of the disease in which variable non-enzymic oxidation processes occur.

However, other factors (liver function, bile acid biosynthesis) influence fluctuations in plasma levels of oxysterols and may also affect erythrocyte membrane levels. The presence in human plasma of 3β,7α-diol **1** and its oxidation product 7α-hydroxycholest-4-en-3-one (3–40 ng/ml [25,26]) may arise in part from hepatic biosynthesis of bile acids subject to various health states.

Acknowledgement

The financial support of the M.D. Anderson Foundation, Houston, TX, USA for acquisition of HPLC instrumentation is gratefully acknowledged.

References

[1] L.L. Smith, *J. Liq. Chromatogr.*, 16 (1993) 1731.
[2] E.J. Parish, in W.D. Nes and E.J. Parish (Editors), *Analysis of Sterols and Other Biologically Significant Steroids*, Academic Press, New York, 1989, pp. 133–149.
[3] A.G. Smith and C.J.W. Brooks, *J. Chromatogr.*, 101 (1974) 373.
[4] C.J.W. Brooks and A.G. Smith, *J. Chromatogr.*, 112 (1975) 499.
[5] A.G. Smith and C.J.W. Brooks, *Biochem. Soc. Trans.*, 3 (1975) 675.
[6] A.G. Smith and C.J.W. Brooks, *J. Steroid Biochem.*, 7 (1976) 705.
[7] L. Ögren, I. Csiky, L. Risinger, L.G. Nilsson and G. Johansson, *Anal. Chim. Acta*, 117 (1980) 71.
[8] J.P. Slotte, *J. Steroid Biochem. Molec. Biol.*, 42 (1992) 521.
[9] E.H. Goh, S.M. Colles and K.D. Otte, *Lipids*, 24 (1989) 652.
[10] B. Petrack and B.J. Latario, *J. Lipid Res.*, 34 (1993) 643.
[11] C.J.W. Brooks, W.J. Cole, T.D.V. Lawrie, J. MacLachlan, J.H. Borthwick and G.M. Barrett, *J. Steroid Biochem.*, 19 (1983) 189.
[12] T. Ogishima and K. Okuda, *Anal. Biochem.*, 158 (1986) 228.
[13] W. Song, W.M. Pierce, R.A. Prough and R.N. Redinger, *Biochem. Pharmacol.*, 41 (1991) 1439.
[14] P.B. Hylemon, E.J. Studer, W.M. Pandak, D.M. Heuman, Z.R. Vlahcevic and J.Y.L. Chiang, *Anal. Biochem.*, 182 (1989) 212.
[15] K. Liu, B. Ramjiawan, M.J.B. Kutryk and G.N. Pierce, *Molec. Cell. Biochem.*, 108 (1991) 49.
[16] J. Ie Teng and L.L. Smith, unpublished results.
[17] F.P.M. de Goeij and J. van Steveninck, *Clin. Chim. Acta*, 68 (1976) 115.
[18] J.P. Thomas, R.D. Hall and A.W. Girotti, *Cancer Lett.*, 35 (1987) 295.

[19] B. Kalyanaraman, J.B. Feix, F. Sieber, J.P. Thomas and A.W. Girotti, *Proc. Natl. Acad. Sci. U.S.A.*, 84 (1987) 2999.
[20] Ö. Küçük, L.J. Lis, T. Dey, R. Mata, M.P. Westerman, S. Yachnin, R. Szostek, D. Tracy, J.W. Kauffman, D.A. Gage and C.C. Sweeley, *Biochim. Biophys. Acta*, 1103 (1992) 296.
[21] L.L. Smith, *Free Radical Biol. Med.*, 11 (1991) 47.
[22] N.A. Higley, S.L. Taylor, A.M. Herian and K. Lee, *Meat Sci.*, 16 (1986) 175.
[23] M.H. Rabinowitz and C. Djerassi, *J. Am. Chem. Soc.*, 114 (1992) 304.
[24] R.P. Hebbel, J.W. Eaton, M. Balasingham and M.H. Steinberg, *J. Clin. Invest.*, 70 (1982) 1253.
[25] M. Axelson, M. Aly and J. Sjövall, *FEBS Lett.*, 239 (1988) 324.
[26] M. Axelson and J. Sjövall, *J. Steroid Biochem.*, 36 (1990) 631.

ELSEVIER

Journal of Chromatography A, 691 (1995) 255–261

JOURNAL OF CHROMATOGRAPHY A

High-performance liquid chromatographic determination of sulfated peptides in human hemofiltrate using a radioactivity monitor

Andreas G. Schepky*, Peter Schulz-Knappe, Wolf-Georg Forssmann

Niedersächsisches Institut für Peptid-Forschung GmbH, Feodor-Lynen-Strasse 31, 30625 Hannover, Germany

Abstract

Specific labeling of tyrosine sulfate-containing peptides was achieved using a differential iodination approach. In a complex peptide mixture from human hemofiltrate, cold iodination to saturate free iodine binding sites was followed by mild acidic desulfation of tyrosine sulfate and subsequent radioiodination using iodine-125. Reaction steps were controlled by amino acid analysis using *o*-phthaldialdehyde precolumn derivatization and by spiking with a sulfated cholecystokinin fragment (CCK4-S). Separation of the peptide mixture with RP-HPLC on a C_{18} column coupled to a radioactivity monitor led to the sensitive (≤ 5 p*M*) and specific determination of tyrosine sulfate-containing peptides.

1. Introduction

Most known peptides containing tyrosine sulfate are constitutive and regulatory peptides like cholecystokinin (CCK), gastrin, secretogranin I and II and leu-enkephalin [1–4]. The specific labeling of tyrosine sulfate-containing peptides will enable the monitoring of metabolic activity and may yield in the quantification of regulatory processes.

A large variety of sulfated peptides is found in plasma. Animal cells also contain a high number of sulfated peptides and proteins as shown by sodium dodecyl sulfate–polyacrylamide gel electrophoresis after incorporation of $^{32}SO_4$. Most of these proteins are not characterized [3]. Alkaline hydrolysis in combination with amino acid analysis has been used to determine sulfation of tyrosine in proteins and peptides in the picomolar range [5–7]. Similarly, a shift of peptide retention time resulting from desulfation by mild acid hydrolysis serves to verify the sulfation of a peptide [8]. The latter method can only be applied for known molecules with known retention times or relatively purified mixtures with only several peptides.

The method presented here is a new approach to facilitate the detection and subsequent quantification of sulfated peptides in crude biological mixtures. In this paper the new method is used for the first time in a plasma-like crude mixture.

Human hemofiltrate (HF) from patients with end-stage renal disease contains plasma-like concentrations of biologically active peptide hormones [cardiodilatin/atrial natriuretic peptide (CDD/ANP), guanylin, parathormone (PTH)] [9,15]. After peptide extraction using preparative anion-exchange chromatography, a concentrated

* Corresponding author.

0021-9673/95/$09.50
SSDI 0021-9673(94)00683-0

mixture of peptides was obtained. Using this mixture, the determination of tyrosine sulfate was performed as shown by amino acid analysis with *o*-phthaldialdehyde (OPA) precolumn derivatization [10].

First amino acid analysis of tyrosine sulfate [5–8] was modified and led to quantitative determination of tyrosine sulfate in peptides. This was controlled by quantitative desulfation to tyrosine.

The chloramine-T method [11] was used to evaluate the specific labeling of sulfated tyrosine without hydrolysis of the peptides as described by Schepky et al. [12]. In brief, tyrosine residues and other possible iodine binding sites were saturated with cold iodine, then tyrosine sulfate was desulfated and subsequently labeled with radioiodine. The goal is to radiolabel only tyrosine residues which were previously sulfated. The difference in electron donor capacity of the aromatic ring enables the differentiation between tyrosine and tyrosine sulfate. This difference results in distinct changes in chemical reactivity. The presence of a sulfate group instead of the hydroxyl group reduces the reactivity, especially in the presence of reactants for electrophilic substitution. Electrophilic substitution in *ortho* position is strongly favored for tyrosine compared to tyrosine sulfate [13]. Iodination takes place via this electrophilic substitution in the iodination procedure using the chloramine-T method.

After 30 s iodination of free tyrosine was performed with high efficiency. Biiodination was completed after 240 s. Sequential radioiodination for 120 s showed incorporation of less than 7% of iodine-125 after 120 s. Free tyrosine sulfate was also iodinated using the chloramine-T method. Sequential radioiodination showed incorporation of iodine-125 of less than 5% at 120 s reaction time for both iodination steps.

The susceptibility of the amino acids arginine, cysteine, histidine, lysine, methionine, phenylalanine, serine and tryptophan for iodination and/or degradation by the chloramine-T method was evaluated at different incubation times. Tryptophan and methionine were degraded after 30 and 60 s, respectively. Final reaction products were not determined. Only basic amino acids showed a low amount of iodine incorporation (arginine 3%, histidine 5%), whereas the other amino acids were almost inert after 240 s total reaction time [12].

Detection of radiolabeled peptides from HF was performed using RP-HPLC coupled to a radioactivity monitor.

2. Experimental

2.1. Materials

$Na^{125}I$ was obtained from Amersham (Braunschweig, Germany). OPA and 0.133 *M* borate buffer were obtained from Hewlett-Packard (Waldbronn, Germany). All other chemicals were purchased from Merck (Darmstadt, Germany).

Sulfated cholecystokinin$_{26-29}$ (Asp–Tyr-[SO_3H]–Met–Gly–NH_2, CCK4-S) was from Saxon Biochemicals (Hannover, Germany).

2.2. Extraction of peptides from human hemofiltrate

A 2000-l volume of human hemofiltrate were extracted by preparative anion-exchange chromatography. After batchwise elution an ultrafiltration step with a molecular cutoff of M_r 20 000 was carried out for quantitative elimination of high-molecular-mass compounds. The ultrafiltrate was processed via anion-exchange liquid chromatography and eluted with increasing ammonium acetate concentrations. Fractions obtained were lyophilized and samples of 10–25 μg were used for determination of tyrosine sulfate.

2.3. Synthesis of tyrosine sulfate, sodium salt

Tyrosine sulfate was synthesized according to Penke and Nyerges [14] and yielded 73.4% of pure tyrosine sulfate. The purity of the product was controlled using capillary zone electropho-

resis, mass spectrometry and amino acid analysis.

2.4. Alkaline hydrolysis

Since tyrosine sulfate is degraded to tyrosine and sulfate using a conventional acid hydrolysis procedure (e.g. 6 *M* HCl, gas-phase hydrolysis for 2 h), alkaline hydrolysis was performed to preserve tyrosine sulfate.

Lyophilized fractions were subjected to alkaline hydrolysis with 0.2 *M* $Ba(OH)_2$ for 22 h at 110°C. Barium was eliminated by precipitation with 2 *M* H_2SO_4 at room temperature. The supernatant was neutralized with 1 *M* NaOH and lyophilized.

2.5. Dowex extraction

Samples were dissolved in 200 μl 0.1 *M* formic acid and applied to a pipette tip filled with 200 μl Dowex 50W-X2 cation exchanger (Serva, Heidelberg, Germany) previously washed with 3 volumes of 0.1 *M* formic acid. Unbound free tyrosine sulfate was recovered with 750 μl 0.1 *M* formic acid. The collected sample was adjusted to pH 5.5 with 1 *M* NaOH, lyophilized and dissolved in 25 μl of 0.4 *M* borate buffer pH 7.2. Finally tyrosine sulfate was measured using amino acid analysis as described below.

2.6. Amino acid analysis

Amino acid analysis was carried out on an amino acid analyzer (AminoQuant 1090, Series II, Hewlett-Packard). The samples (1 μl) were subjected to precolumn derivatization with OPA as described in the Hewlett-Packard instruction manual. Separation of amino acids was performed on an AminoQuant RP C_{18} column 200 × 2.1 mm (particle size 5 μm, Hewlett-Packard) with a gradient from 100% buffer A (20 m*M* sodium acetate, 0.018% triethylamine, pH 7.2, 0.3% tetrahydrofuran) to 60% buffer B (20 m*M* sodium acetate; pH 7.2, 40% acetonitrile, 40% methanol) in 17 min at 0.45 ml/min. Data were collected with the HP 9000 Series 300 data system.

2.7. RP-HPLC on a C_{18} column coupled to a radioactivity monitor

Separation of radioiodinated samples was performed on a Kontron 322 HPLC system with a HPLC 360 autosampler and a HPLC detector 742 (Kontron, Neufahrn, Germany) connected to a radioactivity monitor LB 506 C-1 with a γ-measuring cell J-1000 (volume: 100 μl; Berthold, Wildbad, Germany). Data acquisition was controlled by the LB 506 C-1 HPLC data system. Separation of analytes was performed on a 250 mm × 4 mm I.D. RP C_{18} column (particle size 5 μm, pore size 300 Å; Biotek, Östringen, Germany) at a flow-rate of 0.75 ml/min. The gradient was developed using 0.1% trifluoroacetic acid in water (A) and 0.1% trifluoroacetic acid in acetonitrile–water (80:20) (B): 0–50% B in 50 min; 50–100% B in 10 min; 100% B for 5 min; 100–0% B in 5 min. A 50-μl volume of each radioactive sample was loaded onto the column.

2.8. Saturation of tyrosine with iodine-127 (cold)

A 450-μl volume of 0.5 *M* sodium phosphate buffer (pH 7.5), 100 μl $Na^{127}I$ (285 mg/ml in phosphate buffer), 250 μl chloramine-T (10 mg/ml in phosphate buffer) and the samples dissolved in 100 μl phosphate buffer, all in an Eppendorf vial, were incubated at room temperature. After 120 s the reaction was stopped with 100 μl $Na_2S_2O_5$ (315 mg/ml in phosphate buffer).

2.9. Extraction with Sep-Pak cartridges

Sep-Pak C_{18} cartridges (Waters-Millipore, Eschborn, Germany) were preconditioned with 10 ml methanol followed by 20 ml of 10 m*M* HCl. After application of the sample iodinated with iodine-127 the cartridge was rinsed with 10 ml of 10 m*M* HCl to remove unbound material. Elution was carried out in two steps using 1 ml 30% isopropanol in 0.01 *M* HCl followed by 1 ml 50% isopropanol in 0.01 *M* HCl. The eluate was neutralized with 1 *M* NaOH and lyophilized.

2.10. Desulfation

In the desulfation process, lyophilized samples were dissolved in 20 μl 1 *M* HCl in a glass vial and incubated for 3 min in boiling water. The samples were then lyophilized.

2.11. Radioiodination

Samples were dissolved in 45 μl 0.5 *M* sodium phosphate buffer (pH 7.5) and added to an Eppendorf vial containing 10 μl 0.5 *M* sodium phosphate buffer (pH 7.5) with $2.7 \cdot 10^6$ cpm iodine-125, 25 μl chloramine-T (10 mg/ml in phosphate buffer). After incubation for 120 s, reaction was stopped by the addition of 10 μl $Na_2S_2O_5$ (315 mg/ml in phosphate buffer). Total assay volume was 90 μl. A 50-μl volume of the mixture was directly applied to the RP-HPLC system.

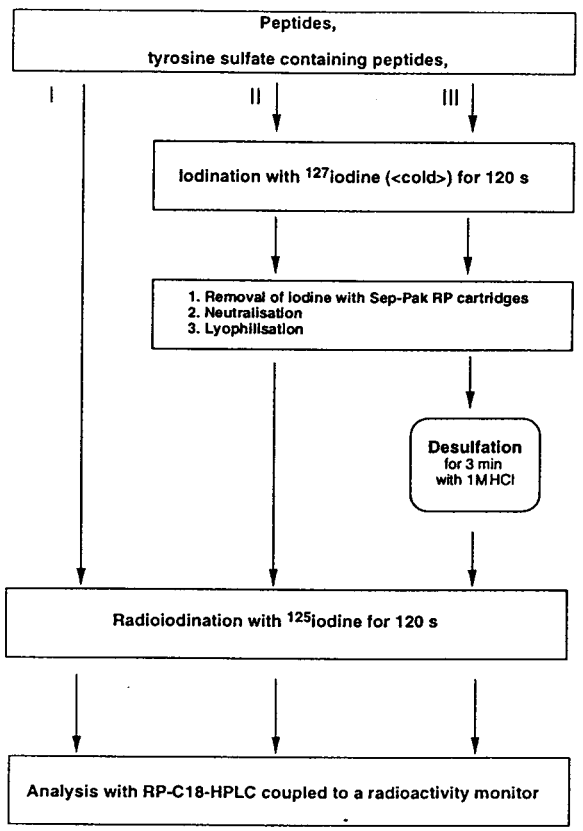

Fig. 1. Reaction scheme of differential iodination for determination of tyrosine sulfate.

2.12. Sequence for determination of sulfated peptides

The complete reaction sequence for determination of sulfated peptides is shown in the flow sheet (Fig. 1). The procedure can be divided into three main steps.

Step I. Sample is radioiodinated for 120 s.

Step II. Sample is first iodinated with iodine-127 for 120 s, followed by Sep-Pak extraction and a second radioiodination for 120 s.

Step III. Sample is desulfated with 1 *M* HCl after the first iodination, followed by Sep-Pak extraction and a subsequent second radioiodination for 120 s.

After radioiodination, samples are directly analyzed by RP-HPLC.

3. Results and discussion

In previous work we have shown that incorporation of radioactive iodine in synthetic peptides containing tyrosine sulfate was achieved [12]. Here we report the identification of tyrosine sulfate-containing peptides from a complex biological source.

3.1. Desulfation and amino acid analysis determination of tyrosine sulfate

Tyrosine sulfate (11 p*M*) and 1.5 p*M* tyrosine were mixed and subjected to amino acid analysis (Fig. 2). A clear separation of the two amino acids was achieved. After desulfation with 1 *M* HCl, no tyrosine sulfate but 12 p*M* tyrosine were detected (Fig. 2) (recovery 96%; $n = 5$). Desulfation was quantitative and lead to the generation of tyrosine readily detected with amino acid analysis. The generation of tyrosine proved the presence of tyrosine sulfate in the respective peak in amino acid analysis.

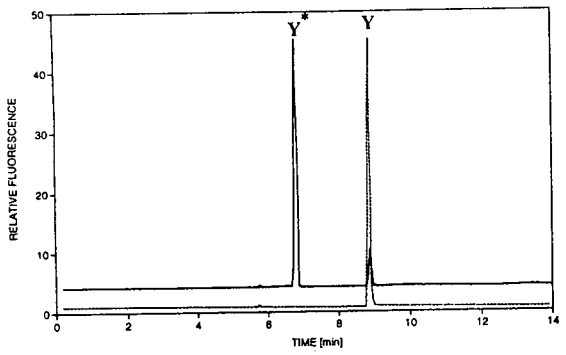

Fig. 2. Amino acid analysis with OPA precolumn derivatization. Solid line: 11 p*M* tyrosine sulfate and 1.5 p*M* tyrosine coinjected onto the column; Y* = tyrosine sulfate; Y = tyrosine. Broken line: 11 p*M* tyrosine sulfate and 1.5 p*M* tyrosine after desulfation; Y* = tyrosine sulfate; Y = tyrosine. Chromatographic conditions are described in the text.

3.2. Determination of tyrosine sulfate by amino acid analysis in complex peptide mixtures

To determine tyrosine sulfate in peptides, alkaline hydrolysis of samples followed by Dowex cation exchange was performed as described. Peptides from human HF were fractionated by anion exchange and aliquots of 10–25 μg were tested by amino acid analysis. In one fraction 5.9 p*M* tyrosine sulfate and 1.2 p*M* tyrosine could be determined (Fig. 3A). After desulfation of this sample a peak was detected eluting at the position of tyrosine sulfate (Fig. 3B). "Tyrosine sulfate" (1.19 p*M*) and 5.8 p*M* tyrosine could be detected. Either incomplete desulfation in this complex mixture or the occurrence of an additional substance coeluting with tyrosine sulfate could be the reason for this phenomenon. The real concentration of tyrosine sulfate may be calculated as the amount of tyrosine generated by desulfation. This additional approach is applicable in most cases, where tyrosine levels are kept low following Dowex extraction. The increase in tyrosine from 1.2 to 5.8 p*M* shows the conversion of the majority of tyrosine sulfate to tyrosine, thus proving the presence of tyrosine sulfate in this hemofiltrate peptide extract. In several hemofiltrate fractions no tyrosine sulfate could be detected. After desulfation procedure of these fractions no increased amount of tyrosine could be measured. Desulfation of tyrosine sulfate was shown to be complete when synthetic mixtures of tyrosine sulfate and tyrosine were used [12].

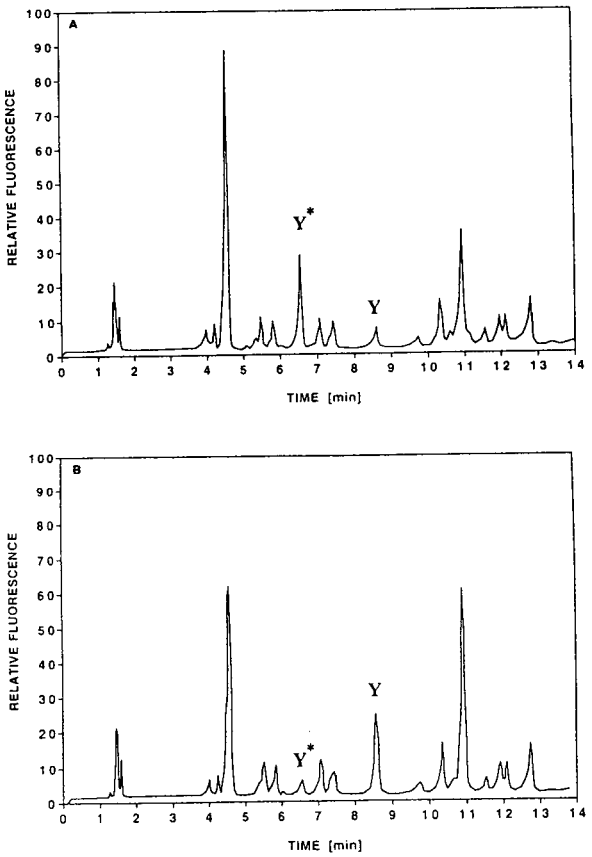

Fig. 3. Amino acid analysis with OPA precolumn derivatization. (A) A hemofiltrate fraction is injected onto the column after alkaline hydrolysis and Dowex cation-exchange extraction; Y* = tyrosine sulfate; Y = tyrosine. (B) The hemofiltrate fraction is treated as in (A) and then subjected to acidic desulfation; Y* = tyrosine sulfate; Y = tyrosine. Sample preparation and chromatographic conditions are described in the text.

3.3. Determination of endogenous sulfated peptides with differential iodination

The chloramine-T method [11] was used to evaluate the specific labeling of sulfated tyrosine without hydrolysis of the peptides as described by Schepky et al. [12]. In a first step (step I), an

aliquot of the sample was directly radioiodinated and separated using RP-HPLC on a C_{18} (data not shown). Incorporation of radioiodine results in a whole series of peaks as detected by radioactivity monitoring. This test is a good way of controlling the general labeling of our sample. Fig. 4A shows the chromatogram of the sample after first iodination with iodine-127 for 120 s, followed by Sep-Pak extraction and a second radioiodination for 120 s (step II). Two distinct peaks (Y and Z) can be seen eluting at high solvent concentrations and two minor peaks are found (X). Cold iodination does not seem to be quantitative since radioiodine is incorporated. Desulfation prior to radioiodination (step III) results in the appearance of an additional major peak at position X, whereas Y is practically unchanged and Z is increased. From Fig. 4A and B we conclude that X represents one or a few peptides containing tyrosine sulfate. After desulfation the strong increase in radioactivity suggests the presence of tyrosine sulfate converted to tyrosine by the desulfation procedure. The incorporated radioactivity is increased by a factor of 10. Peak Y shows no additional incorporation of radioiodine after desulfation and is therefore judged to contain little or no tyrosine sulfate. Peak Z also incorporates additional radioiodine after desulfation also suggesting the presence of tyrosine sulfate. At least two peaks were distinguishable in the chromatogram by increased incorporation of radioiodine after desulfation compared to the control HPLC.

These results show the necessity to perform two assays with the samples tested. First the degree of radioiodination without previous desulfation must be determined to obtain control values and then the sequence of cold iodination, desulfation and radioiodination has to be applied. The data acquired may then be submitted to subtractive analysis thus reducing the background of radioiodination due to incomplete saturation of iodine binding sites.

3.4. Spiking of the same fraction with CCK4-S

For internal control of our reaction sequence (quantification and recovery), the fraction was spiked with 4 p*M* CCK4-S (2.2 μg/ml). Fig. 4C shows the sample plus CCK4-S after "cold" iodination, Sep-Pak extraction, desulfation with

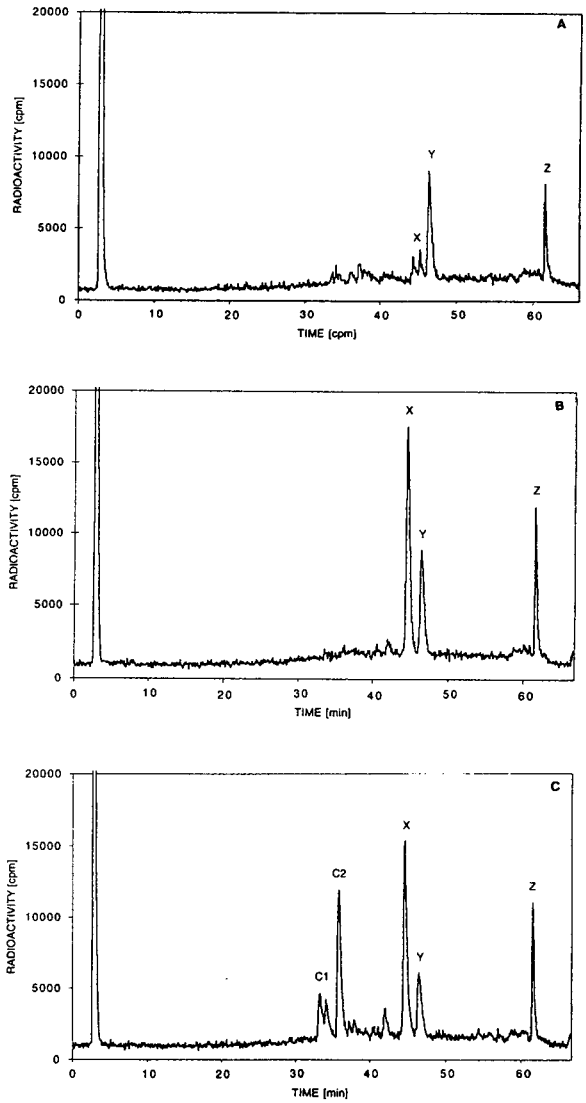

Fig. 4. RP-HPLC radiomonitored chromatograms of radioiodinated samples from a hemofiltrate fraction. (A) Radioiodination after first "cold" iodination and Sep-Pak extraction (X, Y, Z = detected peaks). (B) Radioiodination after first "cold" iodination, Sep-Pak extraction and desulfation for 3 min (X, Y, Z = detected peaks). (C) Radioiodination of the sample plus 4 p*M* CCK4-S (spiking of sample) first "cold" iodination, Sep-Pak extraction and desulfation (C1 = monoiodinated CCK4; C2 = biiodinated CCK4; X, Y, Z = detected peaks).

1 *M* HCl and radioiodination. Two further peaks appear in the chromatogram. Peak C1 is monoiodinated CCK4 (desulfated), peak C2 is biiodinated CCK4 (desulfated). Retention times and concentration are determined by standardization with different concentrations of CCK4-S using step III (data not shown). In the range 1–1000 p*M* a linear relationship with sufficient signal-to-noise ratio is achieved. Recovery of radioiodinated CCK4 in the crude hemofiltrate fraction is >95%. Without desulfation no peaks eluting at the positions C1 and C2 were found in radioactive measurement, which is consistent with the absence of tyrosine in CCK4-S and the absence of other iodine binding sites (data not shown). This spiking experiment shows that quantitation of known sulfated peptides added to crude peptide fractions is possible using this method.

One observation from Fig. 4C has to be discussed in detail. The spiking of the crude peptide fraction with one sulfated peptide results in the generation of two radioactive products after completion of the entire reaction sequence. In earlier experiments the identity of C1 and C2 was shown to represent CCK4 (monoiodinated, C1 and biiodinated, C2). Again, complete biiodination is not consistently achieved within 120 s incubation time. The difference in retention time for small peptides (≤5 amino acids) is explained by the increased hydrophobicity in biiodinated products. Peptides with more amino acid residues show no significant difference in retention time for their mono- or biiodinated products. This problem with small peptides can be solved using cation- or anion-exchange chromatography. The hydrophobic iodines play no significant role in this case. Results can be obtained in the same quality (data not shown). In general, all chromatographic media are suitable.

4. Conclusions

The HPLC method of differential iodination is a helpful tool for the labeling and detection of sulfated peptides in biological samples. Even complex mixtures containing a high number of non-sulfated peptides can be screened for the presence of small amounts (low picomolar range) of tyrosine sulfate-containing peptides. In combination with amino acid analysis for control and quantification, the method of differential iodination using RP-HPLC coupled to a radioactivity monitor is fast and selective within the limits of 1–1000 p*M*. Our method allows the monitoring of metabolic processes involving sulfation and desulfation of peptides and proteins from biological sources.

Acknowledgements

The authors wish to thank I. Uhrlandt and J. Barras-Akhnoukh for their expert technical assistance.

References

[1] W.B. Huttner, *Nature*, 299 (1982) 273.
[2] P.A. Baeuerle and W.B. Huttner, *J. Cell Biol.*, 105 (1987) 2655.
[3] W.B. Huttner, *Ann. Rev. Physiol.*, 50 (1988) 363.
[4] G.L. Rosenquist and H.B. Nicholas, Jr., *Prot. Science*, 2 (1993) 215.
[5] D.W. McCourt, J.F. Leykam and B.D. Schwartz, *J. Chromatogr.*, 327 (1985) 9.
[6] D.L. Christie, R.M. Hill, K. Isakow and P.M. Barling, *Anal. Biochem.*, 154 (1986) 92.
[7] H. Blode, T. Heinrich and H. Diringer, *Biol. Chem. Hoppe-Seyler*, 371 (1990) 45.
[8] J. Lucas and A. Henschen, *J. Chromatogr.*, 369 (1986) 357.
[9] A.G. Schepky, K.W. Bensch, P. Schulz-Knappe and W.G. Forssmann, *Biomed. Chromatogr.*, 8 (1994) 90.
[10] B.N. Jones, in J.E. Shively (Editor), *Methods of Protein Microcharacterisation*, Humana Press, Clifton, NJ, 1986, p. 121.
[11] W.M. Hunter and F.C. Greenwood, *Nature*, 194 (1962) 495.
[12] A.G. Schepky, A.M. Schmidt, T. Schmidt, P. Schulz-Knappe and W.G. Forssmann, *Biol. Chem. Hoppe-Seyler*, 375 (1994) 201.
[13] G.E. Means, in G.E. Means and R.E. Feeney (Editors), *Chemical Modification of Proteins*, Holden Day, San Francisco, CA, 2nd ed., 1985, p. 175.
[14] B. Penke and L. Nyerges, *Peptides Res.*, 4 (1991) 289.
[15] W.G. Forssmann, P. Schulz-Knappe, M. Meyer, K. Adermann, K. Forssmann, D. Hock and A. Aoki, in N. Yanaihara (Editor), *Peptide Chemistry 1992 (Proceedings on the 2nd Japan Symposium on Peptide Chemistry)*, Escom, Leiden, 1993, p. 553.

ELSEVIER

Journal of Chromatography A, 691 (1995) 263–271

JOURNAL OF CHROMATOGRAPHY A

High-performance liquid chromatography of amino acids, peptides and proteins CXXXVIII[☆]. Adsorption of horse heart cytochrome *c* onto a tentacle-type cation exchanger

Jianrong Xie, Marie-Isabel Aguilar, Milton T.W. Hearn*

Centre for Bioprocess Technology and Department of Biochemistry, Monash University, Clayton, Victoria 3168, Australia

Abstract

Determination of the change in the Gibb's free energy from the adsorption isotherm associated with the interaction between a biomolecule and an ion-exchange resin is often achieved by assuming that a Langmuirean model prevails. However, the adsorption of horse heart cytochrome *c* onto the tentacle-type cation exchanger LiChrospher 1000 SO_3^- at pH 4.00 showed an isotherm of rectangular form. In this case the Langmuirean model is not applicable. In this paper, we propose an alternative way to deal with this situation, whereby the adsorption capacity of the adsorbent with a defined protein sample is studied as a function of displacing-ion concentration. The experimental conditions over defined ranges are then selected in order to relate this function to the change in the Gibb's free energy for the interaction between the protein and the ion exchanger. Additional comments about the general utility of the on-line adsorption vessel system employed to determine the adsorption isotherms are also made.

1. Introduction

Adsorption isotherms are widely used to study the thermodynamics of the interaction between a biomolecule and an ion exchanger. Interpretation of the molecular basis of these isotherms represents a key requirement in developing a detailed understanding of the adsorption/desorption processes which occur in high-performance ion-exchange chromatography (HPIEC) of proteins and peptides [1–5]. In liquid–solid systems of a non-competitive type, the shape of the isotherm is often assumed to conform to the Langmuir type equation [1]:

$$q^* = \frac{q_m C^*}{K_d + C^*} \quad (1)$$

where q_m is the maximum adsorption capacity of the biomolecule on the ion-exchanger particles (which in most cases does not increase continuously but comes to a limiting value manifested in the plateau), K_d represents the dissociation constant of adsorption equilibrium, and q^* is the adsorption capacity at equilibrium of the biomolecular sample at a concentration C^*. A double reciprocal plot of $1/q^*$ against $1/C^*$ permits q_m and K_d to be evaluated. Moreover, the related thermodynamic parameters, ΔG_{assoc} and ΔH_{assoc} can be obtained by applying the well-known Van 't Hoff equation. In the same

* Corresponding author.

☆ For Part CXXXVII, see Ref. [24].

0021-9673/95/$09.50
SSDI 0021-9673(94)00632-6

manner, a quantitative interpretation of the protein–ion-exchange ligand binding can then be achieved in terms of the chromatographic retention parameters (capacity factors) [6,7]. From these procedures information can then be derived on the nature of the protein surface, protein conformation and related interactive processes with ion-exchange ligands [8].

Recently, a novel type of tentacle-type silica-based ion exchanger has been developed by Muller [9], and claimed to provide a better performance and maintenance of biological activity than conventional types of ion exchangers [10,11]. A previous study on the adsorption properties of these so-called tentacular adsorbents has already demonstrated their very high affinity for various proteins [12] with the chromatographic behaviour of biomolecules described mainly in terms of an on–off mechanism. This behaviour means that under certain conditions the adsorption of the biomolecule is independent of sample concentration but depends mainly on the concentration of the displacing ions. The sample components are desorbed and eluted without further interaction if the concentration of the displacing ions exceeds a specific value. Moreover, the isotherm for such an interaction can be predicted to assume a rectangular form in the absence of displacing ions. In this case, the Langmuir model cannot be applied. A critical adsorbate concentration (C_r) for the sample protein must exist in order for this adsorption isotherm to be generated, with no additional adsorption taking place above this critical concentration. However, below this critical concentration the dissociation constant is very small and the assumption of reversible interaction implicit to the Van 't Hoff equation is no longer applicable.

We propose here an alternative way to study this type of more complex adsorption behaviour through variation of the displacing-ion concentration and evaluation of the change in the Gibb's free energy. At low displacing-ion concentrations, e.g. in the range of 0–0.1 *M*, the adsorption capacity of the target biomolecule onto the ion exchanger is expected to be inversely proportional to the concentration of the displacing ion. This proportionality is directly related to the available binding sites on the ion-exchange ligand(s) and also to the conformational status of the sample protein in solution. Consequently, the study of the change in Gibb's free energy through variation of the displacing-ion concentration represents one approach to study biomolecule conformation and its interaction with the ion-exchange ligand under these circumstances. In this paper, we present an adsorption study of horse heart cytochrome *c* onto a tentacle-type cation exchanger (LiChrospher 1000 SO_3^-) over the temperature range 2–44°C with NaCl as the displacing salt. The results confirm that the change in Gibb's free energy can be derived in this manner for rectangular isotherms such as found with cytochrome *c* and this cation exchanger.

2. Experimental

2.1. Materials and chemicals

Horse heart cytochrome *c* was purchased from Sigma (St. Louis, MO, USA). The tentacle-type cation exchanger LiChrospher 1000 SO_3^- (particle size, 5 μm) was provided by E. Merck (Darmstadt, Germany). Further information about the physical characteristics of the LiChrospher series of ion exchangers can be found in Ref. [13]. The cation-exchanger particles were dried under vacuum before use. Sodium chloride was obtained from Ajax Chemicals (analytical reagent; Australia). Glacial acetic acid ($d = 1.05$ mg/ml at 20°C) was obtained from May & Baker (a Division of Rhone-Poulenc Australia).

An Orion pH meter (Model SA520) calibrated against a standard buffer solution of pH 4.00 was employed to prepare the buffer solutions. A UV–visible spectrophotometer (type 4050, LKB/Biochrom, UK) was used to determine the concentration of cytochrome *c* in solution. The adsorption measurements were carried out as static experiments in a temperature-controlled

incubator (Thermline, Australia) which covers all the experimental temperatures (± 0.1°C).

2.2. Preparation of buffer solution

The experimental buffer solution was freshly prepared each time. Glacial acetic acid (1.50 ml) was added to distilled water (500 ml) to make a solution concentration [HAc] = 0.05 *M*. The pH value of this solution was then adjusted with a 10 *M* NaOH solution to 4.00. The concentration of sodium ions in this final buffer solution was calculated to be 0.0076 *M* which was taken into account as part of the displacing-ion concentration in the experiments.

2.3. Determination of cytochrome c concentration in solution

The cytochrome *c* concentration was determined by the UV–visible detector at wavelength 215 nm. All measurements were carried out at room temperature. The concentration calibration and determination were achieved by comparing the optical absorbance of the sample solution with the initial buffer solution as a blank reference. The linear range of absorbance versus cytochrome *c* concentration in solution was found experimentally to encompass the range 0–0.08 mg/ml. The calibration factor was 15.09 ± 0.24 AU · ml/mg obtained following extensive measurements.

2.4. Adsorption isotherm and adsorption capacity

The adsorption isotherms were obtained with the on-line adsorption vessel system reported previously [1]. In the present study, about 50 mg LiChrospher 1000 SO_3^- ion-exchange particles and 30 ml of the appropriate buffer solution were introduced into the vessel. The porosity of the sintered glass filter used in the vessel was between 1.0–1.7 μm. The cytochrome *c* concentration in the vessel was determined by recycling the supernatant solution directly through the UV–visible detector cell. This solution was then returned to the adsorption vessel by a reciprocal pulse pump. The equilibrium time needed for each addition of cytochrome *c* and its concentration sampling was between 1.5–2.0 h which was found to be sufficient for this high-affinity adsorption process.

The adsorption capacity required for the free energy calculation was measured by a static method. Based on the experimental results, the displacing-salt concentration was kept below 0.1 *M*. Experimental data corresponding to 4–6 concentration points were taken within this range. The concentration of the displacing ion was estimated on the basis of the sum of the added quantity of sodium chloride and the initial concentration of sodium ion in the buffer solution. A precisely known mass of about 10 mg LiChrospher 1000 SO_3^- particles was weighed in a plastic centrifuge tube. The desired amount of sodium chloride in solid form was then introduced into the tube. The cytochrome *c* in the appropriate buffer solution was directly prepared at a concentration of 0.2 mg/ml. According to the adsorption capacity and mass of the adsorbent particles in the tube, an estimated volume (ranged from 8–10 ml in the experiments) of this cytochrome *c* solution was put into each tube. This estimation was made in order to obtain a final supernatant solution after the adsorption, whereby the cytochrome *c* concentration was larger than the critical concentration C_r, but within the linear range of the concentration calibration. After all components were added into the tubes, the tubes were rapidly put into the incubator at the desired temperature. Continuous gentle agitation was started 1 h later for at least 15 h to ensure that the adsorption process took place under the desired temperature conditions. Centrifugation under the same temperature conditions was used to separate the particles from the supernatant. The cytochrome *c* concentration in the supernatant was determined as described above. The adsorbed quantity of cytochrome *c* on the particles was deduced from the total amount of cytochrome *c* added to the tube.

3. Results and discussion

3.1. Theory to evaluate the change in Gibb's free energy

In the case under study, the components in solution can be considered to form a dilute aqueous electrolyte mixture. At equilibrium, the ion-exchange interaction may thus be regarded as a ternary mixture consisting of the biomolecule sample (p), the displacing ions (i) and water (w) associated with the ion-exchange adsorbent. As the relative composition of the ion exchanger changes upon adsorption or desorption of the protein, displacing ions or water content, the variation in the Gibb's free energy will then be given by [14,15] :

$$dG = RT \ln \alpha_p dn_p + RT \ln \alpha_i dn_i + RT \ln \alpha_w dn_w \quad (2)$$

where α is the adsorbate activity on the ion exchanger, dn is the differential quantity of the adsorbate involved in the process, T is the temperature in K and R is the gas constant. For a system where the adsorption of the biomolecule sample is thermodynamically favoured and the ion-exchange adsorbent becomes saturated (which means the biomolecule sample concentration in the solution is greater than the critical concentration C_r in the case of a rectangular adsorption isotherm), the variation in the Gibb's free energy can be rewritten in the following form if only the change in the concentration of the displacing ion is considered, i.e. the change in the concentration of water is assumed to be very small, approaching zero:

$$dG = -(RT \ln \alpha_p dn_p + RT \ln \alpha_i dn_i) \quad (3)$$

If it is assumed that the activity coefficients involved are independent of the displacing-ion concentration and if the quantity of displacing ion adsorbed by the ion exchanger is proportional to its concentration in the solution (these are assumptions expected to approximate the condition of a loading buffer with a low displacing-ion concentration), the free energy change brought about by the change in the displacing-ion concentration can be evaluated from the following equation, obtained by integration of Eq. 3 with regard to the ionic concentration:

$$-\Delta G^0 = RT \ln [A - q_m] - RT \ln C_i = RT \ln [(A - q_m)/C_i] \quad (4)$$

where A is the adsorption capacity in the absence of the displacing ion, and q_m is the maximum adsorption capacity with a displacing-ion concentration C_i. The combined term $(A - q_m)/C_i$ represents the slope of the plot of maximum adsorption capacity q_m against displacing-ion concentration C_i and can be evaluated under defined experimental conditions according to:

$$q_m = A - BC_i \quad (5)$$

where the slope B is $(A - q_m)/C_i$. The change in the Gibb's free energy at a particular temperature for the protein–ion-exchange interaction can thus be determined for the specific system from the experimental data utilising Eqs. 4 and 5. It can be seen from these equations that the success of the experimental approach depends on the extent of linearity between the adsorption capacity and the displacing-ion concentration.

In order to obtain the relevant thermodynamic parameters, the relationship between the experimentally derived critical concentration and the displacing-salt concentration was determined from the adsorption isotherms. As explained above, under conditions where the adsorption is independent of target protein concentration in the solution, linearity between the adsorption capacity and the displacing-ion concentration was anticipated.

3.2. Adsorption isotherms

The adsorption isotherms for the horse heart cytochrome c and LiChrospher 1000 SO_3^- system, presented in Fig. 1, were obtained with the on-line adsorption vessel system. One of the advantages of this method is that a large number

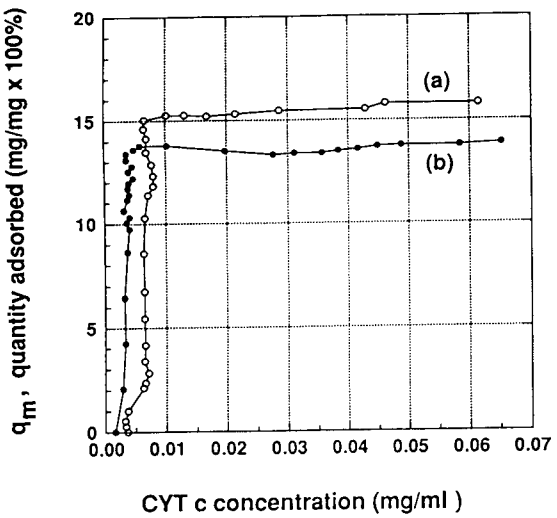

Fig. 1. Adsorption isotherms obtained with horse heart cytochrome *c* (CYT c) and the LiChrospher 1000 SO_3^- tentacle-type cation exchanger in 0.05 *M* acetic acid at pH 4.00, 25°C. (a) No added displacing salt; (b) displacing salt NaCl added at a concentration of 0.1 *M*.

of data points can be obtained continuously within a relatively short time, offering a very flexible experimental approach to the measurement of isotherms and the acquisition of detailed information about the adsorption process. However, in the case of the adsorption of horse heart cytochrome *c* to the LiChrospher 1000 SO_3^- particles, the experiment lasted several days for the determination of a single complete isotherm, resulting in some minor variation occurring in the day-to-day experimental measurements due to the evaporation of water when an open recycling unit was used. As a result, some of the experimental data points do not coincide with the theoretical profile expected for an "irreversible" adsorption. This problem can be circumvented through the use of a closed recycling system.

The differences between the isotherms shown in Fig. 1 and the conventional Langmuir model are very evident. The experimental isotherms clearly show a saturated plateau of protein adsorption and its critical concentration (C_r). The uptake of the protein is higher in the absence of displacing salt (isotherm a) and is consistent with a higher adsorption capacity. In addition, the critical sample concentration was found to be higher when no displacing salt was present. The estimated critical concentrations of cytochrome *c* are about $C_r = 0.003$ mg/ml and 0.006 mg/ml in the presence and absence of 0.1 *M* NaCl, respectively.

As the isoelectric point (p*I*) of horse heart cytochrome *c* is about 10, the protein will be positively charged under the chosen experimental conditions. The displacing salt here plays a dual role in solution, i.e. the sodium ions act as the displacing ions and the chloride ion as the counter-ion for the protein molecules. Compared to the case where the displacing salt NaCl is absent, the microenvironment of the tentacle chains within the ion-exchange particles will manifest a smaller negative electrical potential in the presence of 0.1 *M* NaCl due to ion suppression by the adsorbed Na^+ ions. On the other hand, the molecular surface of the horse heart cytochrome *c* molecule will become slightly more negative in the presence of 0.1 *M* NaCl, compared to when the displacing salt is absent, because of the preferential adsorption by the protein of the Cl^- counter-ions. The consequence of these ion–protein and ion–adsorbent interactions will be reflected as a lower critical concentration of the protein when the displacing salt is present.

The adsorption isotherm with a displacing-salt concentration of 0.4 *M* is presented in Fig. 2. Two regions of the isotherm are discernable. A steep change in q_m versus cytochrome *c* concentration is evident up to the protein concentration of 0.005 mg/ml, followed by an asymptotic shape reminiscent of the Langmuir-type isotherm. Despite the high concentration of displacing salt, the normally strong electrostatic interaction associated with this cation exchanger [16] may primarily dominate the first part of the adsorption. When the protein concentration increases and the electrostatic binding sites become gradually occupied, the "multilayer dissolution" mechanism proposed for the tentacle-type ion exchanger [12] may become more dominant, making the second part of the adsorption process of relatively lower affinity.

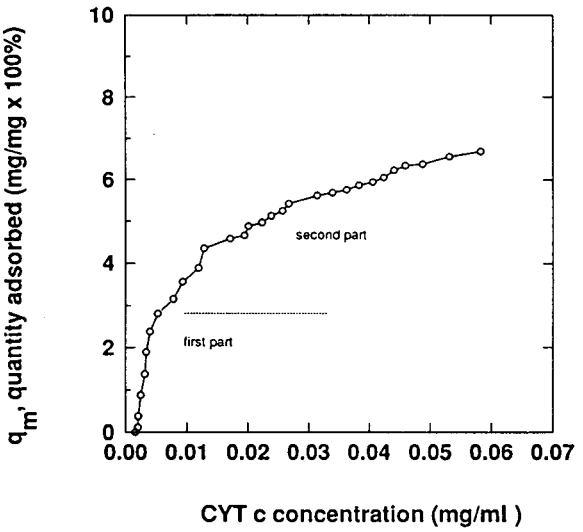

Fig. 2. Adsorption isotherm obtained with horse heart cytochrome *c* (CYT c) and the LiChrospher 1000 SO_3^- tentacle-type cation exchanger in 0.05 *M* acetic acid at pH 4.00, 25°C. The displacing-salt (NaCl) concentration was 0.4 *M*.

It can be noted that the isotherms presented in Fig. 1, where the displacing-salt concentrations were significantly lower, did not show the same curve pattern as evident in Fig. 2 over the same protein concentration range. It is known [17,18] that one of the major effects of salts on the electrostatic interactions between polyelectrolytes such as proteins and charged surfaces is the ability of salts to influence the structure of the polymer backbone through ion–dipole interactions. Under conditions of low ionic strength it is thus unlikely that the "multilayer dissolution" mechanism will make a significant contribution to the adsorption/desorption process due to the large number of protein molecules already bound on-site. Under these low-ionic-strength conditions with few positive charged small ions, like Na^+ present, the tentacle chains probably will curve around the globular-shaped cytochrome *c* molecules, giving little possibility for the protein to be adsorbed by a "multilayer dissolution" mechanism.

With buffers of low ionic strength, the sulphonic acid-modified tentacular ligands will most probably exist as self-repelling extended chain entities due to their high charge density. When a positively charged biopolymer such as horse heart cytochrome *c* is present, charge complementarity between the ligand and the adsorbate could result in these extended tentacular ligands collapsing around the biopolymer. Similarly, with buffers of higher ionic strength, the intrinsic molarity of the displacing ion (in this case Na^+) could reach significant levels, possibly above 4 *M*, within the Donnan double layer due to the repetitive nature of the sulphonic acid group linked to each monomer unit of the graft linear polymer within the tentacular adsorbent. Depending on the extent of molecular entrapment of the protein by the tentacular ligands, adsorption capacities exceeding monolayer coverage could occur with an affinity distribution in binding sites. As the ionic strength increases, the adsorption capacities for the protein will decrease dramatically, with narrowing of the affinity distribution. The differences between the isotherms, in the absence of NaCl, and when 0.1 and 0.4 *M* NaCl are present, could thus have their origin in such a phenomenon. Similar conclusions have been reached for the adsorption of bovine serum albumin to the N-trimethylammoniummethyl (TMAE)-LiChrospher 1000 anion exchanger [12], an anion exchanger with similar isothermal behaviour.

3.3. Thermodynamic parameters

As shown by the data presented above, the adsorption isotherms for horse heart cytochrome *c* with the LiChrospher 1000 SO_3^- consist of a plateau uptake with a clearly defined critical concentration when the displacing-salt concentration is below 0.1 *M*. This adsorption process does not occur in the same way when the displacing-salt concentration is increased to 0.4 *M*. Consequently, in order to determine the thermodynamic parameters, the concentration of the displacing salt in our static experiments was limited to ionic strength values below 0.1 *M* NaCl. The experiments were designed so that the cytochrome *c* concentration in the supernatant solution was higher than 0.006 mg/ml after equilibrium adsorption was reached.

The dependence of the adsorption capacity on the displacing-ion concentration for the adsorption of horse heart cytochrome *c* onto the LiChrospher 1000 SO_3^- sorbent between 2 and 45°C is shown in Fig. 3. The initial concentration of sodium ions (0.0076 *M*) in the buffer solution has been included within the total [Na^+] value. The deduced slopes per mol unit and the coefficients determined from linear regression analysis of the plots, as well as the calculated change in Gibb's free energy are listed in Table 1. It can be seen that good linearity was obtained over the entire temperature range. Janzen et al. [12] have studied the adsorption capacity of bovine serum albumin (BSA) with tentacle-type anion exchangers at different displacing-salt concentrations. Their results also showed that the adsorption capacity decreased linearly over the low range of displacing-salt concentrations (approximately up to 0.15 *M*) and reached zero at a concentration of displacing salt of 0.4 *M*.

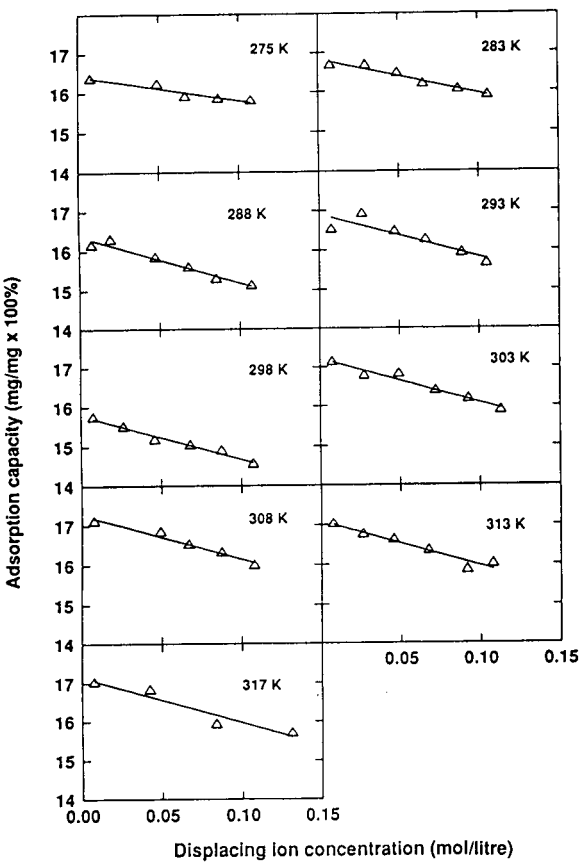

Fig. 3. Plot of the adsorption capacity (mg/mg × 100%) against the displacing-ion concentration (*M*) for horse heart cytochrome *c* adsorption onto the LiChrospher 1000 SO_3^- tentacle-type cation exchanger over the temperature range 275–317 K.

Table 1
Experimentally obtained slope of the plots of adsorption capacity versus the displacing-ion concentration, and the derived change in Gibb's free energy for the adsorption of horse heart cytochrome *c* onto the LiChrospher 1000 SO_3^- tentacle-type cation exchanger

Temperature (K)	Slope *B* (mol^{-1})	Regression coefficient	$-\Delta G^0$ (kJ/mol)
275	6.36	0.95	4.23
283	8.89	0.98	5.13
288	12.11	0.96	5.97
293	10.79	0.89	5.80
298	11.21	0.99	5.99
303	11.34	0.98	6.12
308	11.23	0.98	6.19
313	11.28	0.97	6.31
317	11.75	0.96	6.48

The ΔG^0 values for the interaction between cytochrome *c* and the adsorbent were determined from the experimental data according to Eqs. 4 and 5. The plot of ΔG^0 against temperature (Fig. 4) shows that there are two regions, denoting two different patterns of binding between the horse heart cytochrome *c* and the cation exchange ligands. Overall, the ΔG^0 values generally increased with increasing temperature. Two sets of related thermodynamic parameters (ΔH^0_{assoc} and ΔS^0_{assoc}) could be deduced from these plots over the temperature ranges from 2 to 20°C and from 20 to 44°C and the results are listed in Table 2. These results reveal that the relative contribution of the apparent entropy and enthalpy to the overall change in the Gibb's free energy for the cytochrome *c* adsorption to the LiChrospher 1000 SO_3^- adsorbent varies with the operating temperature. Roush et al. [19] derived thermodynamic parameters for the adsorption of cytochrome b_5 onto an anion exchanger which were of similar magnitude range as those found in the present investigations for the adsorption of cytochrome *c* onto the LiChrospher 1000 SO_3^-.

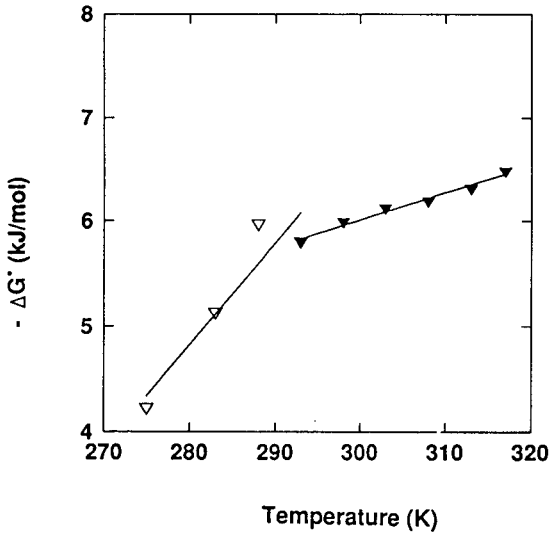

Fig. 4. Plot of the change in Gibb's free energy, ΔG^0 against temperature over the range 275–317 K.

Moreover, these investigators demonstrated that the stoichiometric displacement parameter Z, which can be directly related to $\Delta G^0_{\text{adsorption}}$, depends on temperature and showed an increase in Z value with increasing temperature. Their findings are thus in a good agreement with the results presented here.

Studies on the effect of temperature on the three-dimensional structure of horse heart cytochrome c have demonstrated [20–22] that the protein changes conformation at low pH and low temperature. The two different patterns of interaction between horse heart cytochrome c and the tentacle-type cation-exchange ligand may arise either from conformational changes of the protein molecule or from changes in the orientation and folding pattern of the tentacle chains of the ion exchanger itself. The relative contribution of these two processes in the interaction can be revealed from Hill plots of the experimental data when single step, hyperbolic isotherm of well defined saturation value are obtained at different temperature, provided the heat of adsorption does not vary with the extent of adsorbate coverage [23]. These observations warrant further examination by other independent methods such as microcalorimetry.

Table 2
Experimentally obtained thermodynamic parameters for the interaction between horse heart cytochrome c and the LiChrospher 1000 SO_3^- tentacle-type cation exchanger

Temperature range (K)	$\Delta G^0 = \Delta H^0 - T\Delta S^0$
275–293	$\Delta H^0 = 22.2$ kJ/mol $\Delta S^0 = -96$ J/mol·K
293–317	$\Delta H^0 = 1.79$ kJ/mol $\Delta S^0 = -26$ J/mol·K

4. Conclusions

The measurement of the change in Gibb's free energy associated with the adsorption of a biopolymer to an adsorbent as proposed here has provided an alternative way to study biomolecule interactions with tentacle-type ion exchangers, and other HPIEC adsorbents generating rectangular isotherms. The success of the method relies on the linearity between the adsorption capacity and the displacing-ion concentration, which can normally be observed experimentally over a narrow range of low concentrations for high-affinity ion exchangers. Employing the on-line adsorption vessel system to acquire data on the isotherm allows a large number of data points to be taken continuously, and the experimental information on the nature of the isotherm and the adsorption process directly to be obtained.

This study on the adsorption of horse heart cytochrome c with the tentacle-type cation exchanger, LiChrospher 1000 SO_3^-, has shown that over a temperature range from 2 to 44°C two different adsorption processes were involved depending on the ionic strength of the buffer. The experimentally derived values of the thermodynamic parameters were found to be of similar magnitude to the findings reported by other researchers for other types of protein–anion exchanger interactions.

Acknowledgements

This investigation was supported by the Australian Research Council and from funds provided by the Buckland Foundation.

References

[1] F.B. Anspach, A. Johnston, H.J. Wirth, K.K. Unger and M.T.W. Hearn, *J. Chromatogr.*, 476 (1989) 205.
[2] F.B. Anspach, A. Johnston, H.J. Wirth, K.K. Unger and M.T.W. Hearn, *J. Chromatogr.*, 499 (1990) 103.
[3] H.J. Wirth, K.K. Unger and M.T.W. Hearn, *Anal. Biochem.*, 208 (1993) 16.
[4] A. Johnston and M.T.W. Hearn, *J. Chromatogr.*, 557 (1991) 335.
[5] Q.M. Mao, A. Johnston, I.G. Prince and M.T.W. Hearn, *J. Chromatogr.*, 548 (1991) 147.
[6] W. Kopaciewicz, M.A. Rounds, J. Fausnaugh and F.E. Regnier, *J. Chromatogr.*, 266 (1983) 3.
[7] R.D. Whitley, R. Wachter, F. Liu and N.-H.L. Wang, *J. Chromatogr.*, 465 (1989) 137.
[8] M.I. Aguilar, A.N. Hodder and M.T.W. Hearn, in M.T.W. Hearn (Editor), *HPLC of Proteins, Peptides and Polynucleotides*, VCH, New York, 1991, p. 199.
[9] W. Muller, *Eur. J. Biochem.*, 155 (1986) 203.
[10] W. Muller, presented at the *8th International Symposium on HPLC of Proteins, Peptides and Polynucleotides, Copenhagen, 31 October–2 November 1988*, paper 121.
[11] K.K. Unger, K.D. Lork and H.J. Wirth, in M.T.W. Hearn (Editor), *HPLC of Proteins, Peptides and Polynucleotides*, VCH, New York, 1991, p. 72.
[12] R. Janzen, K.K. Unger, W. Muller and M.T.W. Hearn, *J. Chromatogr.*, 522 (1990) 77.
[13] G. Jilge, K.K. Unger, U. Esser, H.J. Schafer, G. Rathgeber and W. Muller, *J. Chromatogr.*, 476 (1989) 37.
[14] G.E. Myers and G.E. Boyd, *J. Phys. Chem.*, 60 (1956) 521.
[15] H.F. Walton, in E. Heftmann (Editor), *Chromatography (Chemistry Textbook Series)*, Reinhold, New York, 2nd ed., 1967, Ch. 12.
[16] G. Malmquist and N. Lundell, *J. Chromatogr.*, 627 (1992) 107.
[17] C.T. Shibata and A.M. Lenhoff, *J. Colloid Interface Sci.*, 148 (1992) 469.
[18] C.T. Shibata and A.M. Lenhoff, *J. Colloid Interface Sci.*, 148 (1992) 485.
[19] D.J. Roush, D.S. Gill and R.C. Willson, *J. Chromatogr. A*, 653 (1993) 207.
[20] M. Ohgushi and A. Wada, *FEBS Lett.*, 164 (1983) 21.
[21] S. Potekhin and W. Pfeil, *Biophys. Chem.*, 34 (1989) 55.
[22] Y. Kuroda, S. Kidokoro and A. Wada, *J. Mol. Biol.*, 223 (1991) 1139.
[23] S.J. Gregg and K.S.W. Sing, *Adsorption, Surface Area and Porosity*, Academic Press, London, 2nd ed., 1982, p. 199.
[24] M.I. Aguilar and M.T.W. Hearn, *Methods Enzymol.*, (1994) in press.

ELSEVIER

Journal of Chromatography A, 691 (1995) 273–283

JOURNAL OF CHROMATOGRAPHY A

High-performance liquid chromatography of amino acids, peptides and proteins CXXXIX☆. Impact of operating parameters in large-scale chromatography of proteins

Qi-Ming Mao, Ian G. Prince, Milton T.W. Hearn*

Centre for Bioprocess Technology, Monash University, Clayton, Victoria 3168, Australia

Abstract

Large-scale chromatography has been playing an important role in downstream treatment processing in biotechnology. In order to improve the productivity, the throughput of the chromatographic equipment was often increased by increasing the flow-rate and/or by increasing the column sample loading. This paper reports the results of a study on the impact of these and other operating parameters in affinity and ion-exchange chromatographic columns when used for protein purification. A sectional model was developed to predict protein adsorption processes in a packed column. The formulations of this mathematical model are presented in the Appendix. The present study was carried out with computer simulation based on this model and using data obtained from laboratory-scale columns. This model can simulate both the adsorption and washing stages of the protein purification process for both porous and non-porous particles. The effects of changing operating parameters were simulated and contour plots were generated for the easy identification of these effects. It was shown that both flow-rate and column loading can have a considerable impact on the processing rate and the yield of the column. As for the column capacity utilization, the impact of changing flow-rate is not significant at column loading of less than 80% in the test case. It was suggest that the present investigation provides a systematic predictive strategy which will greatly reduce the need for expensive, labour-intensive and time-consuming experimental work during process scale-up.

1. Introduction

The importance of using chromatographic methods for the large-scale purification of high value proteins has been extensively realized over the past decade [1–3]. Competitive commercial pressures involved in product development now mean that improved approaches to process scale-up and optimization are required [4–9]. As a consequence, the synergy between process simulation with mathematical models and directed experimental design to achieve essential data for the estimation of optimum parameters has become increasingly evident, particularly when iterative approaches based on physically relevant models are employed. The present investigations address a practical procedure developed in this Centre for the selection of operating parameters in ion-exchange or affinity chromatographic beds

* Corresponding author.

☆ For Part CXXXVIII, see Ref. [21].

0021-9673/95/$09.50
SSDI 0021-9673(94)00876-0

as part of a large-scale protein purification process. Computer simulations, generated from the analysis of the concentration–time profiles and derived from batch and packed-bed adsorption and washing stage experiments with different adsorbents and mixtures of proteins, form part of the selection procedure for the appropriate choice of fluid velocity, sample loading volume and concentration and column length and diameter. The primary objective of these investigations was to maintain maximum production rates for these stages with packed-bed systems during scale-up, whilst ensuring that the basic requirements of product yield and purity at predetermined levels were achieved. Increasing the mobile phase flow-rate and increasing the column loading are the main avenues to achieve high production rates. As such, the study of the effect of these two parameters formed a major part of the current investigation.

As part of this interactive scale-up procedure involving experimental measurements of protein adsorption behaviour and simulation of this behaviour under a defined set of conditions, a mathematical model developed in this Centre was used to fit the experimental breakthrough curves to extract the surface interaction rate constants. This model is capable of independently addressing both the external mass transfer and surface interaction, yet retains the simplicity of analytical solution. The adsorption and washing behaviour of the column under various operating conditions were simulated and compared with the experimental behaviour. The product yield, column capacity utilization and production rate were then calculated.

These data can then be meshed with the specific process economics to yield an overall optimum outcome. The region of optimum large-scale operation can then be established on the basis of limited small-scale experimentation.

2. Experimental

Experimental data from a number of protein–sorbent systems studied in this Centre were used in the current study. Specific details on the materials, methods, equipment set-up and operating procedures have been published elsewhere [10–13]. Preliminary results on the simulation of the adsorption of lysozyme to Cibacron Blue F3GA biomimetic affinity systems have been presented previously for both non-porous [8,14] and porous [9] particles. Experimental results for two additional systems are reported in this paper. In one of the systems studied the matrix used was an iminodiacetic acid–copper(II) [IDA–Cu(II)]-modified 1.5-μm diameter non-porous silica adsorbent. The adsorbates used were concanavalin A and hen egg-white lysozyme. The column used was 19 mm $\times$ 4 mm I.D. The detailed procedure for the preparation of the IDA adsorbent and other experimental details can be found elsewhere [11,12]. The data for the human serum albumin (HSA)–DEAE-Trisacryl M ion-exchange system were measured [13] in a 5-mm I.D. column (Pharmacia 5/5 HR). HSA was supplied as a 21% solution from Commonwealth Serum Laboratories (CSL) (Melbourne, Australia). DEAE-Trisacryl M ion-exchange resin (particle size 40–80 μm) was purchased from Australia Chemical Co. (Melbourne, Australia). The computer programs (BEDSTP and BEDSTS) using the sectional model described in the Theoretical considerations section and the Appendix were written in FORTRAN. The computation was carried out using an IBM PC compatible machine linked to a VAX 8700 mainframe computer. The figures were drawn with a Macintosh computer.

3. Results and discussion

3.1. Theoretical considerations

Owing to the complexity of the protein–sorbent systems which occurs in large-scale chromatography, it is not possible to identify ideal optimum operating conditions from a single analytical chromatographic experiment. This investigation thus aimed at defining an optimum region of a set of parameters within which the predetermined production criteria can be

achieved. A large number of simulations will be required, hence a simple yet rigorous mathematical model is essential. For example, the model should still be able to take into account the effects of all major rate-limiting factors and also accommodate the influence of different adsorption isotherms.

A sectional model of a chromatographic column developed in this Centre was used in the optimization study reported in this paper. In this model, the column is divided into a series of sections. Each section is then treated as a well mixed tank, with the equations used in the batch adsorption model developed earlier [15] forming the key algorithm of the model. This model is similar to the discrete cell model or the discrete stage model available in the literature [16,17]. In this type of model, the flow conceptually is treated as non-continuous parameter. According to this model, in each section of the column the fluid containing the solute protein (adsorbate) of interest is brought into contact with the adsorbent and interaction is allowed to occur for a period of time, Δt. At the end of each time increment, the content of the liquid (mobile) phase in each section is transferred to the next section. The time increment Δt is calculated as $\Delta t = L/U^*n$ where L is the column length, U the superficial velocity (linear flow-rate) of the fluid and n the number of the sections.

For adsorption with fresh or regenerated adsorbent particles, the initial adsorbate concentration in the solid (stationary) phase is zero for all the sections at the beginning of the process, and the column is assumed to be saturated with buffer solution. For the adsorption stage, the initial adsorbate concentration in the liquid phase is equal to C_0, the inlet concentration. For washing and elution stages, $C_0 = 0$.

The basic assumptions for rate limiting steps in the adsorption process are the same as those used in our non-porous particle adsorption model for a finite bath [15]. This treatment also permits other types of isothermal behaviour, e.g., Freundlich or multi-component Langmuirean isotherms to be accommodated. However, for the purpose of the present discussion only a single-component non-linear Langmuirean isotherm will be discussed. In this simple case, the assumptions are: (a) the transport of adsorbate from the bulk fluid to the surface of the particle can be described by a film resistance mechanism and (b) the interaction between the adsorbate and the adsorption site at the particle surface can be described by a Langmuir-type process. In addition, as each section is assumed to be well mixed, the concentration of the adsorbate in the liquid phase is assumed to be uniform throughout that section.

For the case with porous particles, a linear driving force approximation was used to describe the mass transfer of the adsorbate in the liquid phase from the entrance of the pores at the external surface to the particle internal surface. With this approximation, the pore fluid can be treated as a mass transfer medium rather than a separate phase, thus enabling it to be combined with the bulk fluid in the overall mass balance. At the end of each time increment, the pore fluid was assumed to remain stagnant, and only the bulk fluid was transferred to the next section.

With the above assumptions and initial conditions, the concentrations of the adsorbate in both the liquid and solid phases can be calculated. The liquid-phase concentration in the last section, C_n, is the outlet concentration. The concentration–time plot, i.e., the breakthrough curve, can then be constructed. As the concentrations in each section were stored for each complete time cycle during the calculation, the axial concentration profiles can also be produced for any particular time. Detailed formulation and derivation of the model and its solution are presented in the Appendix.

One of the key variables in the sectional model is the number of the sections, n. It was found that when n was larger than 16 in the test case, the effect of "numerical dispersion" was negligible and the breakthrough curves produced by the sectional model and the analytical solution of a packed bed [14] were synonymous and overlapped. The advantage of this model is thus its versatility. The adsorption stage may be terminated at any time without causing any difficulty in the calculation of the time–concentration curves in the washing stage. Another

important feature is that non-linear Langmuir adsorption isotherms were assumed.

3.2. Comparison of experimental and simulated data

The comparison of calculated and the experimental breakthrough curves is a favoured method by many researchers and has often been used in the validation of mathematical models of protein adsorption–desorption behaviour with chromatographic adsorbents and in extracting system parameters for further simulation [14,18–20]. The same approach was used in this study. Fig. 1 shows the result for the concanavalin A–IDA–Cu(II) adsorption system. Three concentrations of concanavalin A were used, i.e., $C_0 = 0.092$, 0.053 and 0.011 mg/ml. Other parameters were $q_m = 2.9$ mg/ml solid, $K_d = 0.0366$ mg/ml and $U = 0.66$ mm/s [12]. A reasonable fit was obtained between the predicted and experimental breakthrough curves for all three protein concentrations. The breakthrough curves calculated for this non-porous particle system by the sectional model were indistinguishable with the curves generated with the non-porous particle adsorption model (NPPAM) published previously [14]. As the model simulation for a non-porous particle system using the NPPAM model under different operating conditions has been presented previously, this paper will concentrate on the model simulation using the sectional model for a porous particle system.

Fig. 2 shows a typical curve fit of our model prediction to the experimental breakthrough curve for the albumin (HSA) adsorption to DEAE-Trisacryl M, which is a porous ion-exchange resin. The parameters used were column length = 13 mm, $C_0 = 1.5$ mg/ml, $q_m = 44$ mg/ml bed, $K_d = 0.0179$ mg/ml and $U = 0.42$ mm/s [13]. Although the model predictions fit experimental data reasonably well in these two figures, the agreement between the predicted and experimental breakthrough curves for some other situations studied was not as complete. For example, as discussed previously [14,15], complicated mass transfer and surface interaction processes, e.g., aggregation, multilayer formation and surface reorientation at high protein concentrations in the microenvironment of the adsorbent, may be the cause of divergences between the predicted and experimental breakthrough curves, since these phenomena have not been incorporated in the present model.

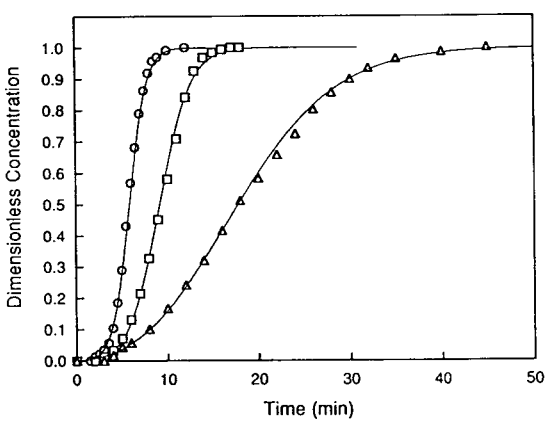

Fig. 1. Predicted (lines) and experimental (points) breakthrough curves for the adsorption of concanavalin A on an IDA–Cu(II)-modified 1.5-μm diameter non-porous silica adsorbent for three concentrations of concanavalin A, i.e., C_0 = (○) 0.092, (□) 0.053 and (△) 0.011 mg/ml. The column used was 19 mm × 4 mm I.D. Other parameters: $q_m = 2.9$ mg/ml solid; $K_d = 0.0366$ mg/ml; $U = 0.066$ cm/s.

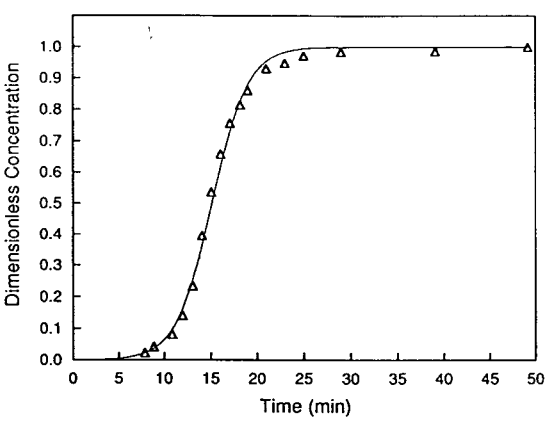

Fig. 2. Predicted (line) and experimental (points) breakthrough curves for the adsorption of human serum albumin (HSA) on DEAE-Trisacryl M ion-exchange sorbent. Column, 13 mm × 5 mm I.D.; $C_0 = 1.5$ mg/ml; $q_m = 44$ mg/ml bed; $K_d = 0.0179$ mg/ml; $U = 0.042$ cm/s.

3.3. Simulations of the effects of operating parameters

For most simulations, a column length of 100 mm was used. For the results shown in Figs. 4–11, a constant washing volume of ten column void volumes at a constant liquid velocity of 0.5 mm/s was employed. The washing stage was included to provide a more realistic simulation and a detailed discussion on this consideration has been presented previously [9]. The number of sections, n, was set as 20. Other parameters used are the same as for Fig. 2.

Although the study of breakthrough curves (frontal analysis) will provide detailed information about the behaviour of the chromatographic system in question, the availability of experimental breakthrough curves is often restricted to the laboratory-scale columns. Experimental results with process-scale chromatographic beds are often not reported in the literature because of issues of commercial sensitivity or simply because most industrial practitioners still underutilize the total capacity, preferring zonal elution. In a practical protein purification column, only a finite sample volume will be applied to the column and the breakthrough may not occur before the loading (adsorption) stage terminates. Therefore, the adsorption behaviour of large-scale columns has historically been studied largely from model simulation based on data acquired with small-scale, laboratory columns. The current study has concentrated on the sample loading volume and flow-rate as the main operating parameters owing to their practical importance.

It was well known that an increase in the flow-rate causes the spreading of the breakthrough curves due to the dispersion of adsorbates within the solid (stationary) phase [14,18]. With the assistance of the sectional model, this phenomenon can be simulated. Fig. 3 shows the effect of flow-rate on the axial concentration profiles in the solid phase of the bed when the same sample volume was loaded. At a very low flow-rate (5 ml/min), the concentration front in the solid phase is sharp. More than half of the column has been saturated but there is no adsorbate in the last 20% of the column. When

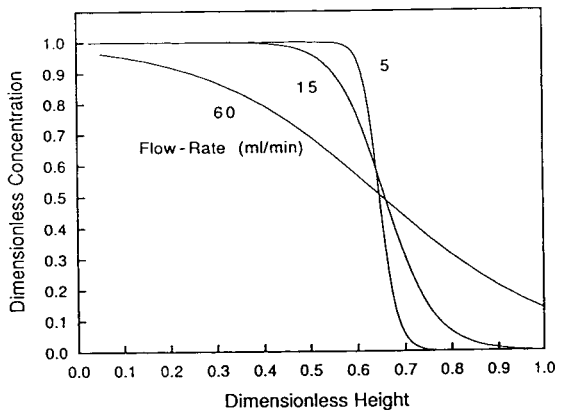

Fig. 3. Concentration profiles in the solid phase at different flow-rates for the same column sample loading for the HSA–DEAE-Trisacryl M ion-exchange system.

the flow-rate was increased to 15 ml/min, the saturated section reduced and the adsorbate migrated throughout almost the whole length of the column. For these two cases, no breakthrough was detected. For 60 ml/min, the breakthrough occurs before any part of the column becomes saturated.

The effects of flow-rate and column height on the maximum loading volume are shown in Fig. 4. The column was loaded to the point just

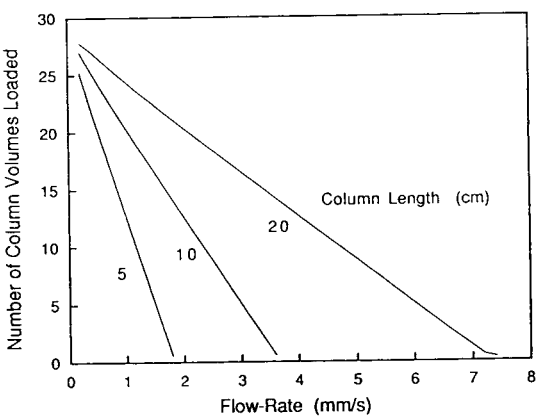

Fig. 4. Maximum column sample loading versus superficial liquid velocity for different column lengths at a fixed effluent concentration (0.1% of inlet concentration) for the HSA–DEAE-Trisacryl M ion-exchange system.

before breakthrough occurs ($C/C_0 = 0.001$). Under this condition (constant effluent concentration), the maximum loading volume, as shown, increases with increasing column length and is a linear function of the flow-rate. The effects on processing rate are shown in Fig. 5. The processing rate can be defined as the amount of protein retained after washing per unit volume of resin per unit processing time. Similarly to the results of earlier investigations reported from this Centre [8,9] and elsewhere [3,18], there exists an optimum flow-rate at which a maximum processing rate can be achieved. This optimum flow-rate is higher for the longer column but the value of maximum processing rate is higher for the shorter column [9,18].

The effects of column loading on processing rate are shown in Fig. 6. The column loading value used was defined as the percentage of the attainable column adsorption capacity. For the range where column loading is less than 100%, the processing rate increases with the increase of column loading and flow-rate. The yield, which is defined as the percentage of total protein applied to the column retained after washing, decreases with the increase of both flow rate and column loading, as shown in Fig. 7.

The operating range and the limitations of the two main operating parameters can be shown more clearly in the derived contour plots. From Fig. 8, it can be seen that high processing rates occur only at the top-right hand corner where both the flow-rate and the column loading are high. The high yield, however, is restricted to the low flow-rate and relatively low loading region, as shown in Fig. 9. Owing to the asymptotic nature in the calculation of the yield values by the sectional model, a value of 99.999% yield was chosen to be an approximation of 100%

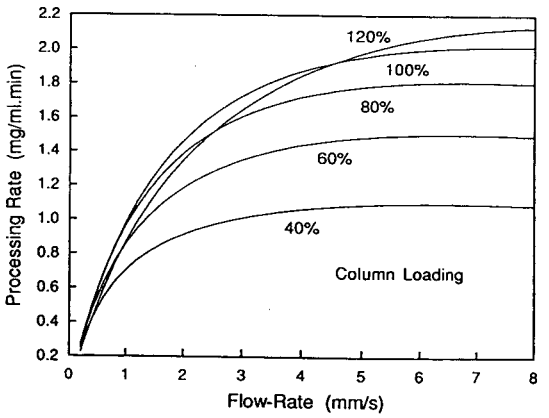

Fig. 6. Processing rate versus superficial liquid velocity at different column loadings (as percentages of the attainable column adsorption capacity) for the HSA–DEAE-Trisacryl M ion-exchange system.

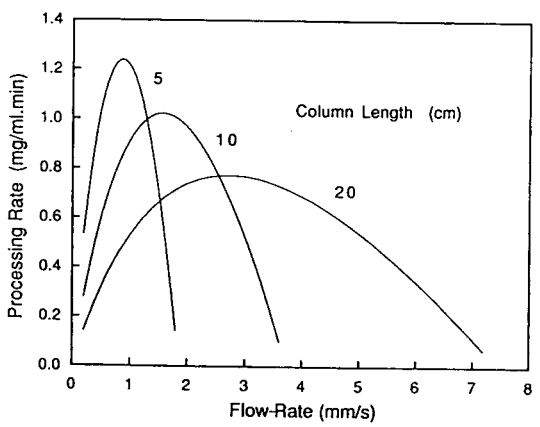

Fig. 5. Processing rate versus superficial liquid velocity for different column lengths at a fixed effluent concentration (0.1% of inlet concentration) for the HSA–DEAE-Trisacryl M ion-exchange system.

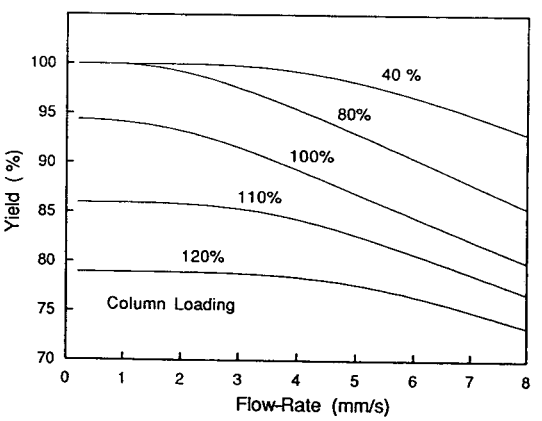

Fig. 7. Product yield versus superficial liquid velocity at different column loadings (as percentages of the attainable column adsorption capacity) for the HSA–DEAE-Trisacryl M ion-exchange system.

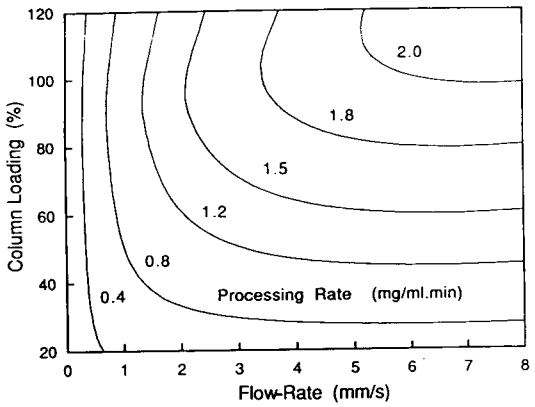

Fig. 8. Effects of liquid velocity and column sample loading on the processing rate (mg/ml · min) of an HSA–DEAE-Trisacryl M ion-exchange chromatographic column.

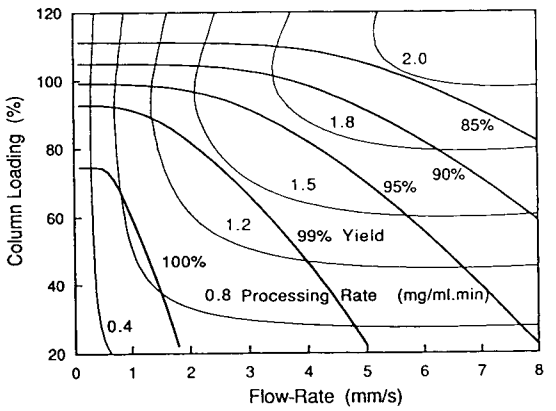

Fig. 10. Operating regions based on the product yield and processing rate for an HSA–DEAE-Trisacryl M ion-exchange chromatographic column.

yield. It can be seen that in order to improve the yield from 99% to 100%, the flow-rate has to be reduced to less than half and the column loading may also have to be reduced. This interdependence becomes more evident when these two sets of curves are plotted together, as shown in Fig. 10. When the yield was allowed to drop from 100% to 99%, this 1% decrease resulted in a 60–70% increase in the processing rate. Depending on the actual yield requirement of the production, the expected processing rates and the operating range of the flow-rate and column loading can thus be easily estimated from these plots.

Another production criterion worth mentioning is the column capacity utilization, which can be defined as the percentage of the attainable column capacity used in the adsorption–washing cycle [9]. This criterion is important as it directly affects the column life and the equipment cost. High column capacity utilization is generally preferred. As shown in Fig. 11, changes in the flow-rate have little effect on the capacity utilization when the column loading is low. When the

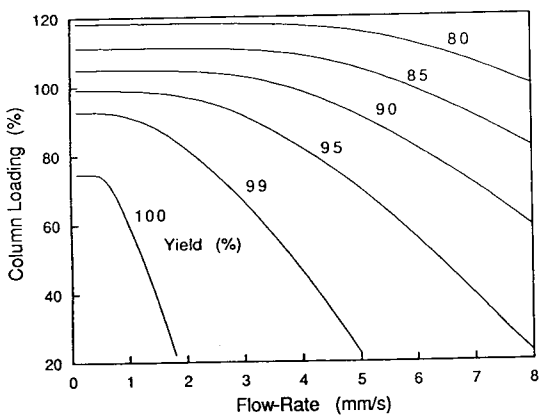

Fig. 9. Effects of liquid velocity and column sample loading on the product yield of an HSA–DEAE-Trisacryl M ion-exchange chromatographic column.

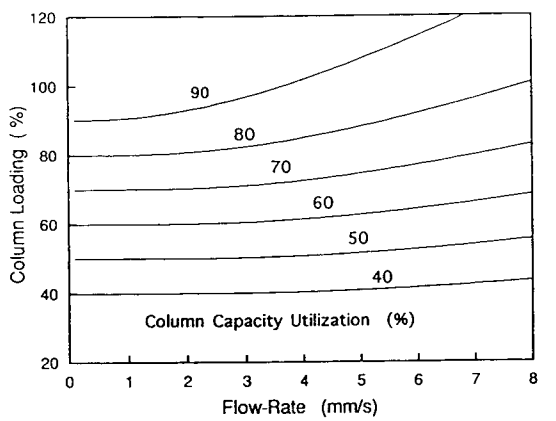

Fig. 11. Effects of liquid velocity and column sample loading on the column capacity utilization level of an HSA–DEAE-Trisacryl M ion-exchange chromatographic column.

column loading is higher than 80% in this particular example, however, the increase in flow-rate will result in a decrease in the column capacity utilization.

4. Conclusions

The results of this study clearly demonstrate that the operating parameters involved in the chromatography of proteins, such as flow-rate and column sample loading, can have a significant impact on the outcome of the process. Whilst higher flow-rates will result in a higher processing rate, the yield drops with increase in flow-rate. In large-scale processes, the production rate will be a primary determinant, but the requirement for high yield and column capacity utilization must also not be overlooked. The final balance of these factors will depend on the process economics. Selection of optimum operating parameters thus represents a critical compromise between several variables. The procedures currently under development in this Centre can offer assistance in these aspects. The present investigation provides a systematic predictive strategy which greatly reduces the need for expensive, labour-intensive and time-consuming experimental work during process scale-up.

Symbols

a	external surface area per unit volume of adsorbent particles
A	parameter defined by Eq. A10
B	parameter defined by Eq. A12
C_i	adsorbate concentration in the liquid phase in section i
$C_{i,0}$	initial adsorbate concentration in the liquid phase in section i
$C_{p,i}$	adsorbate concentration in the pore fluid in section i
$C_{T,i}$	equivalent adsorbate concentration when total amount of the adsorbate in the system was assumed in the liquid phase in section i
C_i^*	intermediate adsorbate concentration in the liquid phase at (1) external surface of the particles in section i for the case with non-porous particles and (2) internal surface of the particles in section i for the case with porous particles
C_n	adsorbate concentration in the liquid phase in the last section, which represents the outlet adsorbate concentration
C_0	inlet concentration of adsorbate in the liquid phase
k_1	forward surface interaction rate constant
K_d	adsorption equilibrium constant
K_e	overall effective liquid-phase mass transfer coefficient
K_f	liquid-side film mass transfer coefficient
L	column length
M	parameter defined by Eq. A9
n	number of the sections in the sectional model (Eq. A1)
q_i	adsorbate concentration on the solid phase in section i
q_m	maximum solid adsorption capacity
$q_{i,0}$	initial adsorbate concentration on the solid phase in section i
R_0	particle radius
R_v	volume ratio of solid phase to liquid phase
Δt	time increment which is the residence time of bulk fluid in any one section
U	superficial velocity (linear flow-rate) of the fluid
x_1	positive root of quadratic Eq. A11
x_2	the other root of Eq. A11
ε	volume fraction of liquid phase in the column
ε_p	particle void fraction

Acknowledgements

These investigations were supported by the Australian Research Council and a research grant provided by CSL as part of the Industry Research and Development (IRD) board funding programme of the Department of Industry, Trade and Regional Development. The assistance of Dr. H.-J. Wirth in the acquisition of the

adsorption data with the non-porous adsorbents is greatly appreciated.

Appendix: the sectional model

In this model the chromatographic column is assumed to be divided into a series of sections. Each section is then treated as a well mixed tank. In each section the fluid containing the solute protein (adsorbate) of interest is brought into contact with the adsorbent and interaction is allowed to occur for a period of time Δt. At the end of each time increment, the content of the liquid phase in each section is transferred to the next section. The time increment Δt is calculated as

$$\Delta t = \frac{L}{Un} \tag{A1}$$

where L is the column length, U the superficial velocity of the fluid and n the number of the sections. The interaction between the adsorbate and the adsorption site at the particle surface is assumed in the treatment described below to be governed by a Langmuir-type isothermal model, but other isothermal models can be also employed. As each section is assumed to be well mixed, the concentration of the adsorbate in the liquid phase is uniform throughout the section.

Adsorption with non-porous particles

The overall mass balance for the adsorption with non-porous particles in a section i is

$$\varepsilon C_i + (1-\varepsilon)q_i = \varepsilon C_{T,i} \tag{A2}$$

where C_i is the adsorbate concentration in the bulk of the liquid phase, q_i is the adsorbate concentration on the solid phase, ε is the volume fraction of liquid phase in the column, which is assumed a constant throughout the column and the variable $C_{T,i}$ is the equivalent total adsorbate concentration when the total amount of the adsorbate in that section is assumed only in the liquid phase. $C_{T,i}$ can be calculated from

$$C_{T,i} = C_{i,0} + R_v q_{i,0} \tag{A3}$$

where $C_{i,0}$ is the adsorbate concentration in the liquid phase at the beginning of the time increment, $q_{i,0}$ is the adsorbate concentration in the solid phase at the beginning of the time increment and R_v is the volume ratio of the solid phase to the liquid phase, i.e. the phase ratio (often represented as Φ):

$$R_v = \frac{1-\varepsilon}{\varepsilon} \tag{A4}$$

The differential form of Eq. A2 then can be expressed as

$$\frac{dC_i}{dt} + R_v \cdot \frac{dq_i}{dt} = 0 \tag{A5}$$

As in the case with the non-porous particle adsorption model [14,15], the transport of adsorbate from the bulk fluid to the surface of the particle is described by a film resistance mechanism:

$$\frac{dq_i}{dt} = aK_f(C_i - C_i^*) \tag{A6}$$

where a $(=3/R_0)$ is the interfacial area per unit volume of the adsorbent particles, R_0 is the radius of the particle, K_f is the liquid field mass transfer coefficient and C_i^* is the intermediate concentration of the adsorbate in the liquid phase at the surface of the particles.

The interaction between the adsorbate and the immobilized ligand at the particle surface is described by the second-order reversible equation

$$\frac{dq_i}{dt} = k_1[(q_m - q_i)C_i^* - K_d q_i] \tag{A7}$$

where k_1 is the forward interaction rate constant, q_m is the maximum adsorption capacity of the immobilized ligand and K_d is the adsorption equilibrium constant. At equilibrium, Eq. A7 becomes the Langmuir isotherm equation.

Eliminating C_i^*, q_i and its derivative from Eqs. A3, A5, A6 and A7, the rate of change of C_i with time can be written as follows:

$$-\left(\frac{1}{M} + \frac{1}{k_1}\right)\frac{dC_i}{dt} = (C_i - x_1)(C_i - x_2) \tag{A8}$$

where

$$M = \frac{A}{R_v q_m - C_{T,i} + C_i} \tag{A9}$$

and

$$A = aK_f R_v \tag{A10}$$

x_1 and x_2 are the roots of the quadratic equation

$$C_i^2 - BC_i - K_d C_{T,i} = 0 \tag{A11}$$

where

$$B = C_{T,i} - R_v q_m - K_d \tag{A12}$$

and

$$x_1 = \frac{1}{2}[B + \sqrt{B^2 + 4K_d C_{T,i}}] \tag{A13}$$

$$x_2 = \frac{1}{2}[B - \sqrt{B^2 + 4K_d C_{T,i}}] \tag{A14}$$

Eq. A8 can be directly integrated to yield

$$\left(C_{T,i} - R_v q_m - \frac{A}{k_1}\right) \ln\left(\frac{C_i - x_1}{C_i - x_2}\frac{C_{i,0} - x_2}{C_{i,0} - x_1}\right) - x_1 \ln\left(\frac{C_i - x_1}{C_{i,0} - x_1}\right) + x_2 \ln\left(\frac{C_i - x_2}{C_{i,0} - x_2}\right) = A(x_1 - x_2)\,\Delta t \tag{A15}$$

Eq. A15 can be used to calculate the liquid-phase concentration at the end of each time increment Δt for section i. In this equation and also in Eq. A8 both the film mass transfer and surface interaction rates are considered finite.

Adsorption with porous adsorbent particles

Two additional assumptions were used for the porous particle case in the sectional model. One assumption is that a linear driving force approximation can be used to describe the mass transfer of the adsorbate in the liquid from the entrance of the pores at the external surface to the particle internal surface [15]. The second assumption is that the pore fluid can be assumed to be stagnant, and therefore only the bulk fluid was transferred to the next section at the end of each time increment.

The overall mass balance in section i is

$$\varepsilon C_i + (1-\varepsilon)\varepsilon_p C_{p,i} + (1-\varepsilon)(1-\varepsilon_p) q_i = [\varepsilon + (1-\varepsilon)\varepsilon_p] C_{T,i} \tag{A16}$$

where $C_{p,i}$ is the adsorbate concentration in the pore fluid and ε_p is the particle void fraction. Other symbols are the same as defined in Eq. A2. The unit of q_i is taken as the mass per unit volume of solid. With the linear driving force approximation the pore fluid can be treated as a mass transfer medium rather than a separate phase, thus enabling it to be combined with the bulk fluid in the overall mass balance [15]. Therefore, the pore fluid was lumped with the bulk fluid, i.e., $C_{p,i} = C_i$. Eq. A16 then becomes

$$[\varepsilon + (1-\varepsilon)\varepsilon_p] C_i + (1-\varepsilon)(1-\varepsilon_p) q_i = [\varepsilon + (1-\varepsilon)\varepsilon_p] C_{T,i} \tag{A17}$$

In this case, the value of $C_{T,i}$ can be calculated by Eq. A3, with the volume ratio of the solid phase to the liquid phase, R_v, becoming

$$R_v = \frac{1 - [\varepsilon + (1-\varepsilon)\varepsilon_p]}{\varepsilon + (1-\varepsilon)\varepsilon_p} \tag{A18}$$

and the value of $C_{i,0}$ is calculated as

$$C_{i,0} = \frac{\varepsilon}{\varepsilon + (1-\varepsilon)\varepsilon_p} \cdot C_{i-1} + \frac{(1-\varepsilon)\varepsilon_p}{\varepsilon + (1-\varepsilon)\varepsilon_p} \cdot C_i \tag{A19}$$

Eq. A19 indicates that at the end of each time increment, the pore fluid remained in the section, and only the bulk fluid in section $i-1$ was transferred to section i.

The differential form of Eq. A17 is then identical in form with Eq. A5. The solution for the case with porous particles can then be obtained with the same approach in Eqs. A5–A14. The differences are that an effective overall liquid-phase mass transfer coefficient, K_e, replaces K_f in Eqs. A6 and A10, and in Eqs. A6 and A7 C_i^* is redefined as the intermediate concentration of the adsorbate in the liquid phase at the internal surface of the particles. A more detailed discussion on these points has been presented previously [15].

Two simplified cases

As discussed in the case of a finite bath [15], two simplified cases for chromatographic packed beds may be considered. First, if the surface interaction rate constant k_1 is assumed to be infinite, the mass transfer becomes the rate-controlling step. As a result, when the forward rate constant for adsorption is very large Eq. A15 can be simplified to

$$(C_{T,i} - R_v q_m) \ln\left(\frac{C_i - x_1}{C_i - x_2}\frac{C_{i,0} - x_2}{C_{i,0} - x_1}\right) - x_1 \ln\left(\frac{C_i - x_1}{C_{i,0} - x_1}\right) + x_2 \ln\left(\frac{C_i - x_2}{C_{i,0} - x_2}\right) = A(x_1 - x_2)\,\Delta t \quad \text{(A20)}$$

This equation implies that equilibrium exists between the adsorbate and the adsorbate–ligand complex at each point on the particle surface and is referred to as the equilibrium case.

Second, if the mass transfer rate is very high, then the surface interaction (second-order kinetics) is considered as the rate-controlling step. As a result, Eq. A8 becomes

$$-\frac{1}{k_1}\cdot\frac{dC_1}{dt} = (C_i - x_1)(C_i - x_2) \quad \text{(A21)}$$

and the integrated form is

$$-\frac{1}{k_1}\ln\left(\frac{C_i - x_1}{C_i - x_2}\cdot\frac{C_{i,0} - x_2}{C_{i,0} - x_1}\right) = (x_1 - x_2)\,\Delta t \quad \text{(A22)}$$

This case can be referred to as the kinetic controlling case. In this case, the concentration of the adsorbate in the liquid phase as a function of time then can be expressed as

$$C_i = \frac{x_1(C_{i,0} - x_2) - x_2(C_{i,0} - x_1)\,e^{(x_2 - x_1)k_1\,\Delta t}}{(C_{i,0} - x_2) - (C_{i,0} - x_1)\,e^{(x_2 - x_1)k_1\,\Delta t}} \quad \text{(A23)}$$

which can be used directly to calculate the concentration in the liquid phase at time Δt. In the cases where the value of the liquid mass transfer coefficients are finite, i.e., Eqs. A15 or A20 is required, a bisectional method can be adopted to calculate the concentrations.

References

[1] M.T.W. Hearn, *Aust. J. Biotechnol.*, 3 (1989) 183.
[2] Y.D. Clonis, in J.A. Asenjo (Editor), *Separation Processes in Biotechnology*, Marcel Dekker, New York, 1990, p. 401.
[3] A. Jungbauer, *J. Chromatogr.*, 639 (1993) 3.
[4] J.-C. Janson and P. Hedman, *Biotechnol. Prog.*, 3 (1987) 9.
[5] G.H. Cowan, I.S. Gosling and W.P. Sweetenham, *J. Chromatogr.*, 484 (1989) 187.
[6] P. Dantigny, Y. Wang, J. Hubble and J.A. Howell, *J. Chromatogr.*, 545 (1991) 27.
[7] P.R. Levison, S.E. Badger, D.W. Toome, M.L. Koscielny, L. Lane and E.T. Butts, *J. Chromatogr.*, 590 (1992) 49.
[8] Q.M. Mao, I.G. Prince and M.T.W. Hearn, in I.G. Prince (Editor), *Proceedings of the 10th Australian Biotechnology Conference, Melbourne 4–7 February, 1992*, Australian Biotechnology Association, Melbourne, 1992, pp. 308–311.
[9] Q.M. Mao, I.G. Prince and M.T.W. Hearn, *J. Chromatogr.*, 646 (1993) 81.
[10] F.B. Anspach, A. Johnston, H.-J. Wirth, K.K. Unger and M.T.W. Hearn, *J. Chromatogr.*, 499 (1990) 103.
[11] H.-J. Wirth, K.K. Unger and M.T.W. Hearn, *Anal. Biochem.* 208 (1993) 16.
[12] H.-J. Wirth, *Ph.D. Dissertation*, Joh.-Gutenberg University, Mainz, 1990.
[13] A. Johnston, Q.M. Mao and M.T.W. Hearn, *J. Chromatogr.*, 548 (1991) 127.
[14] Q.M. Mao, A. Johnston, I.G. Prince and M.T.W. Hearn, *J. Chromatogr.*, 548 (1991) 147.
[15] Q.M. Mao, R. Stockmann, I.G. Prince and M.T.W. Hearn, *J. Chromatogr.*, 646 (1993) 67.
[16] D.D. Do, *AIChE J.*, 31 (1985) 1329.
[17] J. Hubble, *Biotechnol. Tech.* 3., (1989) 113.
[18] S. Yamamoto and Y. Sano, *J. Chromatogr.*, 597 (1992) 173.
[19] A.I. Liapis, B. Anspach, M.E. Findley, J. Davies, M.T.W. Hearn and K.K. Unger, *Biotechnol. Bioeng.*, 34 (1989) 467.
[20] B.J. Horstmann and H.A. Chase, *Chem. Eng. Res. Des.*, 67 (1989) 243.
[21] J. Xie, M.I. Aguilar and M.T.W. Hearn, *J. Chromatogr. A*, 691 (1995) 263.

ELSEVIER

Journal of Chromatography A, 691 (1995) 285–299

JOURNAL OF CHROMATOGRAPHY A

Compositional analysis of the phenylthiocarbamyl amino acids by liquid chromatography–atmospheric pressure ionization mass spectrometry with particular attention to the cyst(e)ine derivatives

Karl Schmeer[a], Mohamed Khalifa[b], János Császár[c], Gyula Farkas[d], Ernst Bayer[a], Ibolya Molnár-Perl[b,*]

[a]*Institute of Organic Chemistry, Tübingen University, Auf der Morgenstelle 18, D-7400 Tübingen 1, Germany*
[b]*Institute of Inorganic and Analytical Chemistry, L. Eötvös University, P.O. Box 32, H-1518 Budapest 112, Hungary*
[c]*Institute of Organic Chemistry, L. Eötvös University, P.O. Box 32, H-1518 Budapest 112, Hungary*
[d]*Chinoin Pharmaceutical Works, P.O. Box 110, H-1325 Budapest, Hungary*

Abstract

An approach presented recently for the high-performance liquid chromatographic determination of DL- and L-cystines and cysteines as phenylthiocarbamyl (PTC) derivatives has been completed (i) with the determination of D-cystine/cysteine, (ii) by a study relating to the spectral characteristics of the PTC cystine/cysteine derivatives performed with diode-array detection and (iii) by the fragment analysis of the PTC-cyst(e)ine derivatives, applying the extremely soft conditions of the liquid chromatography–atmosphere pressure ionization mass spectrometry (LC–API-MS). In accordance with earlier experiences it has been repeatedly demonstrated that cystines and cysteines can be determined on the basis of two or four derivatives, with the same retention times and molar responses, without any special pretreatment, furnishing a simple possibility for the determination of the total cystine/cyteine in protein hydrolysates. The UV spectra of all four PTC derivatives provided by diode-array-detected purity parameters (PuP) showed that the corresponding PTC derivatives of DL-L- and D-cystine and -cysteine are identical and homogeneous, and do not show any characteristic differences. On the basis of the fragmentation patterns of seventeen PTC-amino acids and those of six PTC-cyst(e)ines, obtained under the very soft conditions of the LC-API-MS procedure, it can be stated that two characteristic PTC derivatives are formed: (i) the main product ("a" and "b" diastereoisomers, >80% of the total), shown to be the fragment of $m/z = 255$, a monomeric cysteine derivative, and (ii) the other characteristic constituent ("c" and "d" stereoisomers, <20% of the total), consisting of a fragments of $m/z = 255$ and its oxidised form of $m/z = 287$.

1. Introduction

The unusual behaviour of the D-, L- and DL-cysteines/cystines (monomers/dimers) in their interactions with phenyl isothiocyanate (PITC) has been reported recently [1–7]. It has been shown that independently of their original condition, i.e. from the monomeric cysteines and dimeric cystines equally, the same phenylthiocarbamyl (PTC) derivatives are formed. On the basis both of our experiences [1] and of literature data [2–4], we assumed that under the deri-

* Corresponding author.

0021-9673/95/$09.50
SSDI 0021-9673(94)00741-1

vatization conditions oxidative scission of the dimeric cystine disulphide bond takes place, resulting in two monomeric PTC-cysteine derivatives. The oxidative cleavage of the disulphide bond has been reported in the reaction of allyl isothiocyanate with cystine [2,3] and proved by NMR measurements [3]. Liquid chromatography–thermospray mass spectrometry (LC–TSP-MS) seemed to be to confirm this fact [4]; it has been demonstrated [4] that (i) reconstructed single-ion mass chromatograms corresponding to the protonated molecular ion for each PTC amino acid in the mixture, with a single exception, displayed a peak coinciding with the elution of the corresponding PTC amino acid and (ii) the exception was PTC-cystine, for which the largest ion observed within the scanned range was at m/z 255; this ion represents the monomer product formed from the PTC-derivatized cysteine dimer by fragmentation. Taking into consideration the forceful intervention of the LC–TSP-MS (thermospray nozzle and chamber at 320 and 340°C), the fragmentation can be presumed not only in the derivatization reaction but also in the thermospray evaporation process.

The aim of this study was to examine the composition and the behaviour of the different PTC-cyst(e)ine derivatives applying the well known mild conditions of API-MS.

2. Experimental

2.1. Materials

Triethylamine (TEA), PITC, amino acids and proteins were obtained from Sigma (St. Louis, MO, USA) and Serva (Heidelberg, Germany). HPLC-grade acetonitrile and methanol were purchased from Reanal (Budapest, Hungary). All other reagents of the highest purity available.

2.2. Apparatus

High-performance liquid chromatography (HPLC) with UV detection

The system used for the determination of the molar responses of the various racemates was a Liquochrom Model 2010 liquid chromatograph (Labor MIM, Budapest, Hungary), which consisted of a two-Liquopump 312/1 solvent-delivery system and a Type OE-308 UV detector with a wavelength range of 195–440 nm ("Liquochrom system"). Samples were injected in 20-μl volumes using an injector supplied by Labor MIM.

HPLC with diode-array detection

A Varian LC Star system was used, equipped with a Star 9020 workstation, a Star 9010 solvent-delivery system and a Polychrom 9065 diode-array detector (Varian, Walnut Creek Instrument Division, Walnut Creek, CA, USA). The same columns, eluents and elution programmes were applied as with the Liquochrom system.) The 150 mm × 4.0 mm I.D. columns (BST, Budapest, Hungary) contained Hypersil ODS bonded phase (5 μm; Shandon) ("Varian LC Star system").

Liquid chromatography–atmospheric pressure ionization mass spectrometry

The mass spectrometer used was an API III TAGA 6000 with an ionspray interface (Sciex, Thornhill, Toronto, Canada), with a Model 22 syringe infusion pump 22 (Harvard Apparatus, South Natick, MA, USA).

The HPLC column (100 × 2 mm I.D.) contained Nucleosil 120 C_{18} (5μm) (Grom, Herrenberg, Germany). The system consisted of a microbore HPLC pump, an ABI model 140A solvent-delivery system (Applied Biosystems, Foster City, CA, USA), Linear UV/VIS 204 Model 9550-0155 UV detector, (Linear Instruments, Reno, NV, USA), a C-R5A Chromatopac integrator, (Shimadzu, Analytical Instrument Division, Kyoto, Japan) and a Gilson Abimed Model 231 autosampler ("LC–API-MS system").

2.3. Hydrolysis system

A Pico Tag workstation (Millipore Waters, Milford, MA, USA) was used.

2.4. Hydrolysis of amino acids [simulated hydrolysis conditions ("hydrolysis")]

Authentic amino acids were dissolved in 0.1 *M* hydrochloric acid. Aliquots of 5 μl of stock solutions containing ca. 0.017 g of DL-, D- or L-cysteine · HCl or ca. 0.024 g of DL-, D- or L-cystine base per 10 cm^3 (weighed with 10^{-5} g accuracy) were pipetted into 50 × 6 mm I.D. tubes and up to twelve tubes were placed in a vacuum vial. The vial was then attached to the work station manifold and the solvent removed under vacuum. After drying, the vacuum was released and 200 or 900 μl of constant-boiling hydrochloric acid were pipetted into the bottom of the vacuum vial. The vacuum vial was then reattached to the manifold and, after treatment as recommended in the workstation manual, they were hydrolysed in the workstation at 145°C for 4 h. After this hydrolysis, the sample tubes were carefully removed from the vial and the hydrochloric acid wiped from the outside of each tube. The tubes were then transferred to a fresh reaction vial, attached to the workstation and evaporated to the constant minimal reading (about 65 mTorr). The hydrolysed samples were then ready for derivatization.

2.5. Derivatization of amino acids with PITC

Standards of individual cyst(e)ine samples (containing ca. 50.0 nmol of each amino acid), were placed in the 50 × 6 mm I.D. tubes and dried under vacuum. Free amino acids and hydrolysed proteins were redried after adding 10 μl of ethanol–water–TEA (2:2:1) to each tube. Thereafter, to each redried sample, 20 μl of derivatization reagent [ethanol–TEA–H_2O–PITC (7:1:1:1)] was added and mixed by vortex mixing. The test-tubes containing the derivatized samples were then transferred in to the vial, installed again in the workstation, evaporated to a minimum reading of about 65 mTorr and held at this constant reading for 20 min. The derivatized standards were dissolved, in order of listing, in 50 μl of acetonitrile, 50 μl of water and 500 μl of 0.05 *M* sodium acetate solution with a pH of 7.2. Thus, the 20-μl aliquots of standards contained ca. 1700 pmol of each amino acid.

2.6. Separation of the PTC-amino acids by HPLC

The solvent system consisted of two eluents: (A) 0.05 *M* sodium acetate (pH 7.2) and (B) 0.1 *M* sodium acetate–acetonitrile–methanol (46:44:10) (mixed in volume proportions and titrated with glacial acetic acid or 50% sodium hydroxyde to pH 7.2). A gradient, which was optimized for the separation, from 0% to 100% B in 22 min was applied. After a 5-min washing step with 100% B, the eluent was programmed to 100% in 2 min. After an additional 3 min, elution with 100% A was performed. Thereafter the system was ready for the next injection.

3. Results and discussion

The new approach presented recently for the HPLC of DL- and L-cystine and -cysteine as their PTC derivatives [1] has been completed, in order to have a comprehensive overview, by a study of the D-racemates.

The reaction of all six racemates with PITC resulted in four derivatives both before and after hydrolysis (Figs. 1A and 2A, peaks a, b, c and d). The ratios of these four derivatives are characteristic of the initial compound.

Without any pretreatment, i.e., immediately after derivatization (Figs. 1A and 2A), the PTC derivatives of D- and L-cystine and -cysteine all elute as a main single peak (Figs. 1 and 2, peaks b) and as a minor accompanying peak (Figs. 1 and 2, peaks c). The trace amounts of compounds a and d, with D- and L-cystine and -cysteine are of negligible importance (Figs. 1A and 2A).

The DL-racemates reacted directly with PITC (Figs. 1A and 2A) furnished without exception all four derivatives with different distributions. The ratios of peaks a and b are characteristic of DL-cystine and DL-cysteine, respectively (Table 1, peak-area ratios, in order of listing: $a/b \approx 1.9$ and 1.17).

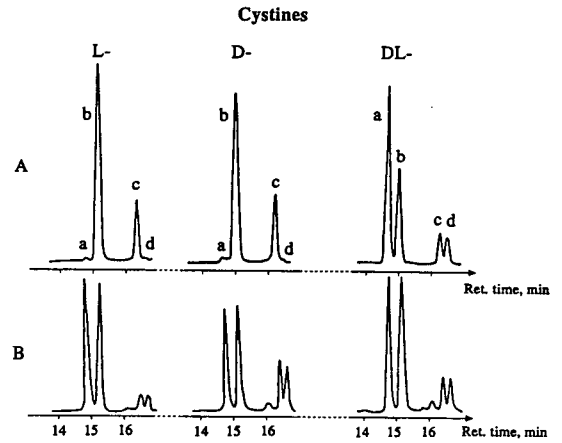

Fig. 1. HPLC of PTC-cystines derivatized (A) immediately and (B) after hydrolysis obtained with the Liquochrom system. Detailed data are given in Table 1.

After simulating the hydrolysis conditions (Figs. 1B and 2B), independently (a) of the parameters applied (varying the amount of HCl, reaction time and temperature) and (b) of the initial racemate form of cystines and cysteines reacted, the ratios of the two first-eluting PTC derivatives (Figs. 1B and 2B, peaks a and b, Table 1, peak-area ratios, column B) proved to be nearly the same ($a/b \approx 1$). The identity of the peak-area ratios after hydrolysis in all six cases ($a/b \approx 1$) can probably be attributed to the racemization of the D- and L-cystine and cysteine.

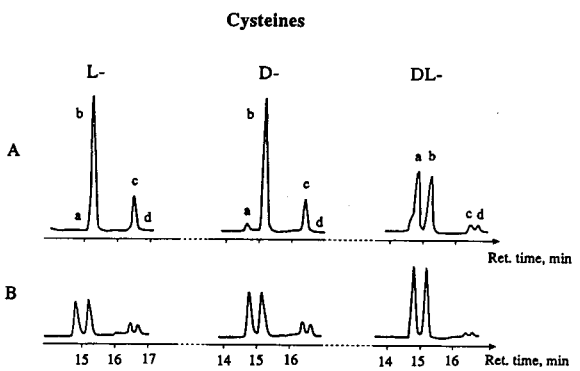

Fig. 2. HPLC of PTC-cysteines derivatized (A) immediately and (B) after hydrolysis, obtained with the Liquochrom system. Detailed data are given in Table 1.

Evaluating the detector responses of all six cyst(e)ines (Table 1, integration units/pmole amino acids), they are acceptable, with an experimental error of 7.2% or less (relative standard deviation). The same reproducibility can be calculated from the differences in the main values of the various racemates obtained before (Table 1, from the values in column A: 5.6%) or after hydrolysis (Table 1, from the values in column B 7.2%). It is worth mentioning that after hydrolysis the averages of the detector responses are smaller, probably owing to the destruction of cyst(e)ines. This effect can be avoided by the use of 3-(2-aminoethyl)indole as an additive in the HCl hydrolyses [5–7]. On the basis of the reproducibility data detailed above and published recently [1], the analytical applicability the proposed method has been demonstrated.

The characteristics of the spectra of PTC-cyst(e)ines in the UV region between 200 and 350 nm were analysed by diode-array detection (Table 2, Fig. 3). As can be seen, the maximum values of the absorbances of the corresponding PTC derivatives [Table 2, PuP (purity parameter) values for peaks a–d], independently of their origin, and within the experimental error of the measurements, are the same: the PuP of absorbances for peaks a and b varied from 254.63 to 254.84 nm, whereas for peaks c and d the corresponding values were higher, providing maximum absorbances between 255.60 and 256.19 nm. The small differences in the maximum values between the earlier (peaks a, b) and later eluting derivatives (peaks c and d) are probably due to the slightly different spectral characteristics of the two stereoisomer pairs, assuming that in addition to the NH_2 group, partly also the SH group can take part in any reaction.

Concerning the structure of the PTC-derivatives, it is obvious that we are measuring in all six cases either (i) the PTC-cystines (assuming that under hydrolysis/derivatization conditions the monomeric cysteines were oxidized to –S–S– bond-containing dimeric cystines) or (ii) the

Table 1
Distribution of the PTC derivatives of cystines and cysteines, measured by HPLC, derivatized (A) immediately and (B) after hydrolysis

Compound	Peak areas: integration units/ pmol amino acids (in total)[a]		Peak-area ratios: peak a/ peak b	
	A	B	A	B
DL-Cystine $\bar{X}$[b]	138	127	1.91/1	0.99/1
S.D.	4.6	1.0	0.11	0.068
R.S.D. (%)	3.3	0.8	3.9	6.8
DL-Cysteine $\bar{X}$[b]	125	110	1.17/1	1.01/1
S.D.	3.0	5.9	0.255	0.031
R.S.D. (%)	2.4	3.3	2122.8	3.1
D-Cystine $\bar{X}$[b]	137	123	0/1	0.96/1
S.D.	9.6	4.2		0.027
R.S.D. (%)	7.2	3.4		2.8
D-Cysteine $\bar{X}$[b]	121	114	0.1/1[c]	1.01/1
S.D.	7.0	2.8	0.576	0.079
R.S.D. (%)	5.8	2.5	58	7.8
L-Cystine $\bar{X}$[b]	133	129	0/1	0.95/1
S.D.	9.4	4.5		0.034
R.S.D. (%)	7.1	3.5		3.6
L-Cysteine $\bar{X}$[b]	124	110	0.1/1[c]	1.00/1
S.D.	4.1	6.2	0.098	0.056
R.S.D. (%)	3.3	5.3	98	5.6
Means of A and B $\bar{X}$	130	119		
S.D.	7.2	8.6		
R.S.D. (%)	5.6	7.2		

[a] In total: taking into account peaks a, b, c, d at (a) 936 s, (b) 966 s, (c) 1036 and (d) 1050 s (see also Fig. 1).
[b] $\bar{X}$: average of six separate tests.
[c] Averages obtained from the ratios of D- or L-cyteines, in order of listing, 0.072/1, 0.0065/1, 0.10/1, 0.23/1 (for D-cysteine) and 0.03/1, 0.003/1, 0.18/1, 0.19/1 (for L-cysteine), respectively.

Table 2
Evaluation of the spectra of various cyst(e)ines obtained by diode-array detection

Sample	Spectral analyses over of 200–350 nm for derivatives of peaks							
	Peak a		Peak b		Peak c		Peak d	
	PuP	S.D.	PuP	S.D.	PuP	S.D.	PuP	S.D.
DL-Cystine	254.84	0.047	254.78	0.050	255.87	0.507	255.60	0.195
L-Cystine	–	–	254.63	0.11	–	–	255.62	0.140
D-Cystine	–	–	254.68	0.073	–	–	255.62	0.086
D-Cysteine	254.79	0.006	254.65	0.122	255.72	0.045	256.19	0.138
D-Cysteine	253.96	0.028	254.68	0.112	–	–	–	–

Spectral Overlay Report

No.	Name PuP (nm)	tR (min)	Spectrum Type	Correction	Filename
1	DL-Cystine 311				
	254.831	17.092	Spectral Sum	--------	v0707003.run
2	DL-Cystine 311				
	254.700	17.534	Spectral Sum	--------	v0707003.run
3	D-Cystine 253				
	254.659	17.539	Spectral Sum	--------	v0707004.run
4	L-Cystine 338				
	254.610	17.506	Spectral Sum	--------	v0707005.run
5	DL-Cysteine 4				
	254.789	17.016	Spectral Sum	--------	v0707007.run
6	DL-Cysteine 4				
	254.639	17.432	Spectral Sum	--------	v0707007.run
7	D-Cysteine 113				
	254.681	17.262	Spectral Sum	--------	v0707009.run

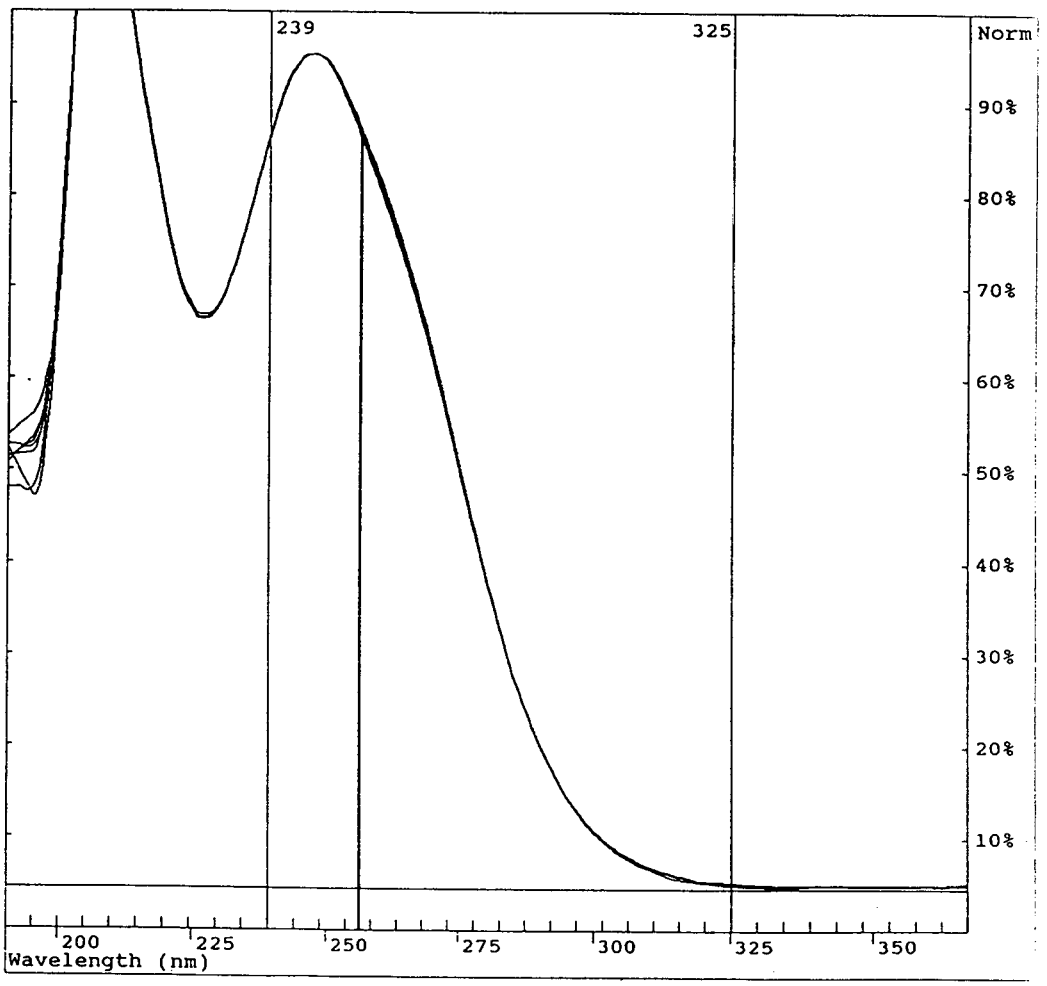

Fig. 3. Spectral overlay report on the PuP conditions of peaks a and b, obtained with the Varian LC Star system. Detailed data are given in Table 2.

PTC-cysteines. In accordance both with our spectrophotometric results [1] and with literature data [2–4], (a) we proved [1] that the characteristic shoulder peak of cysteines does not show any changes after hydrolysis conditions (oxidation to cystine under the hydrolysis conditions can be excluded); (b) Kawakishi and Namiki [2,3] verified by NMR spectrometry that the electrophilic attack of allyl isothiocyanate on cystine resulted in the scission of the disulphide bond yielding 2 mol of cysteine derivatives and, in addition to all of the above, (c) LC–MS studies [4], applying thermospray ionization, proved that the PTC derivative formed from cystine is a monomeric species of particularly high stability; Pramanik et al. [4] found "evidence for a pyrolytic cleavage process that yielded PTC and the free amino acid. . . in all cases except PTC-cys". All these results indicate that very likely with cysteine the composition of this PTC derivative must differ considerably from all others.

In order to determine the composition of the six PTC-cyst(e)ine derivatives, also in comparison with all other PTC-amino acids, a detailed LC-MS study was performed applying the very soft conditions of the API technique. Fragmentation patterns obtained both with seventeen PTC-amino acids (Table 3, Fig. 4) and with all six PTC-cyst(e)ines (Table 4, Fig. 5) derivatized immediately and after 'hydrolysis' conditions showed that concerning the components of the calibration standard (Table 3, Fig. 4), the main fragment proved to be, in all cases investigated, the protonated molecular ion. Chosen representatives, such as (A) methionine, (B) leucine, (C) phenylaline and (D) tryptophane, provided monomeric fragments of m/z 284.8, 266.8, 301.0 and 340.4, instead of the calculated M + 1 = $m/$

Table 3
Fragment patterns of PTC-amino acids obtained from full-scan LC–MS background-subtracted total ion current (TIC) chromatogram and positive-ion API mass spectra

Amino acid	Retention time[a] (min)	Molecular mass			
		M + 1		M + 1/D + 1	%D + 1[b]
		Calculated	Measured		
Aspartic acid	5.43	269.4	269.0	–[c]	
Glutamic acid	6.18	283.1	283.0	–	
Hydroxy-proline	6.75	267.1	267.0	–	
Serine	7.70	241.1	240.0	–	
Glycine	8.06	211.1	211.0	–	
Histidine	9.26	291.2	291.0	291/581	5
Threonine	9.49	255.1	255.0	255/509	3
Alanine	9.99	225.1	225.9	225/449	3
Proline	10.20	251.1	251.0	251/501	10
Arginine	10.76	310.2	310.0	310/619	2
Tyrosine	14.21	317.2	317.2	317/633	10
Valine	14.53	253.2	253.0	253/505	13
Methionine	15.21	285.2	284.8	285/569	16
Isoleucine-leucine	17.01	267.2	266.8	266/533	20
Phenylalanine	18.96	301.2	301.0	301/601	13
Tryptophan	19.69	340.2	340.4	340/679	12
Lysine	20.57	417.2	417.4	Out of mass range	

[a] Taken from the detailed mass spectra.
[b] Expressed as the total of [(M + 1) + (D + 1)].
[c] Dashes indicate that no dimer (D) was found.

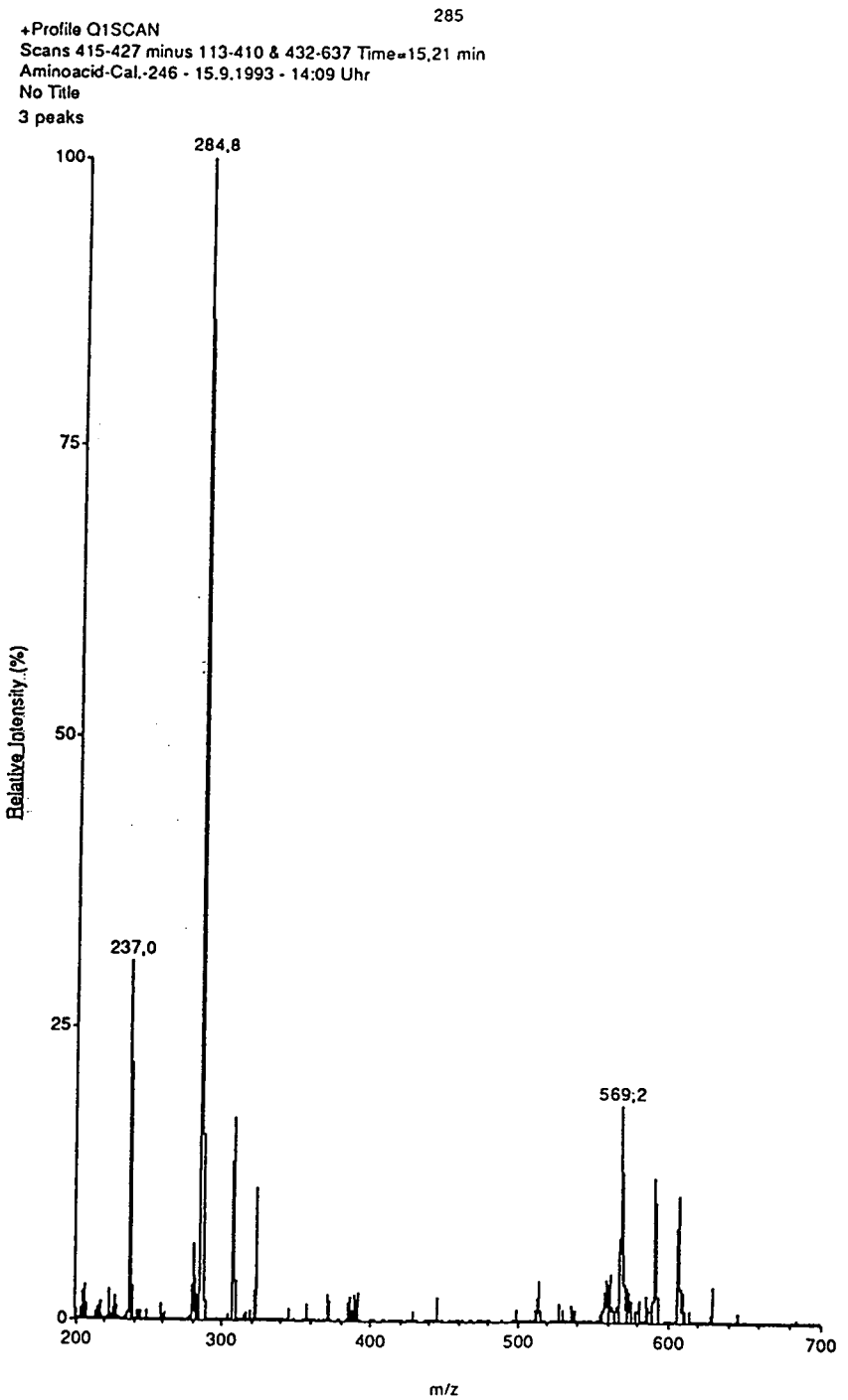

Fig. 4. Fragmentation patterns of PTC-leucine, obtained with the LC–API-MS system. Detailed data and also for all other amino acid derivatives are given in Table 3.

Table 4
Fragment patterns of the PTC-cyst(e)ines (DL-, D- and L-) derivatized before and after hydrolysis (H), obtained from peaks a, b, c and d by full-scan LC–MS background-subtracted total ion current (TIC) chromatograms and positive-ion API mass spectra

Initial compound	Mass fragments[a] expressed as % of the total obtained from peaks		
	Peak a (~15.6)[b] 255/511	Peak b (~16.0)[b] 255/511	Peaks c + d (~17.7–18.0)[b] 255/287/543
DL-Cysteine	85/15	85/15	44/38/18
DL-Cysteine (H)	85/15	85/15	45/44/11
DL-Cystine	83/17	92/8	0/78/22
DL-Cystine (H)	80/20	80/20	47/32/21
D-Cysteine		89/11	51/35/14
D-Cysteine (H)	87/13	85/15	46/41/13
D-Cystine		84/16	53/37/10
D-Cystine (H)	83/17	83/17	44/33/13
L-Cysteine		84/16	52/28/20
L-Cysteine (H)	87/13	87/13	41/41/18
L-Cystine		85/15	48/40/12
L-Cystine (H)	84/16	85/15	41/37/22

[a] Fragments: m/z 254.2–255, 286.6–287.2, 510.2–511.2 and 543.8–547.2, listed as 255, 511, 287 and 543.
[b] Retention times (min) are given in parentheses.

$z = 285.2$, 267.2, 301.2 and 340.2, respectively. The calculated and measured values (Table 3, columns 3 and 4) agree excellently, confirming that the API technique is a very low-energy process which does not induce fragmentations. In addition, the amounts of the protonated dimer ($2M + 1 = D + 1$), present in twelve cases out of seventeen, vary between 2 and 20%. The appearance of the dimers is probably attributable to the specificity of the PTC-amino acid derivatives and it is of primary importance from the point of view of the composition of the PTC-cyst(e)ine derivatives (Table 4, columns for peaks a, b and c + d).

As seen, for PTC-cystines and-cysteines, the ratios of the monomers to the dimers, in peaks a and b equally, vary between 8 and 20% (Table 4, columns 2 and 3, not exceeding the amount of dimer fragments found with other PTC-amino acids. In peaks c and d the amounts of dimers proved to be higher: as maximum values, for DL- and L-cystines 22% of the total were obtained (Table 4, last column). These results confirmed unambigously our earlier assumption [1], supported also by literature evidence [2–4], that in the interaction of PITC with cystines, as a result of the oxidative scission of the disulphide bond, moneric PTC-cysteine derivatives are formed.

A further question to be answered is to establish the exact composition of peaks a, b, c and d). Fragment patterns of the earlier eluting peak pair a and b, differ from that of the later pair c and d, providing the same fragments within the given pair. Thus, a and b and also c and d assumed to be diastereoisomer derivatives. Peaks a and b (instead of the calculated m/z 257 i.e., $M + 1 = 256 + 1$), furnished fragments of $m/z \approx 255$ (Table 4, columns 2 and 3), corresponding to the formula $C_{10}H_{10}N_2O_2S_2$. To describe the structure of this compound, containing two fewer protons than the regular PTC-cysteine, even with the knowledge of its outstandingly high stability [4], needs further study. (In contrast with all other PTC-amino acids, also under the extremely strong evaporation parameters of the thermospray ionization technique [4], the fragment of m/z 255, originating from cystine, proved to remain intact.)

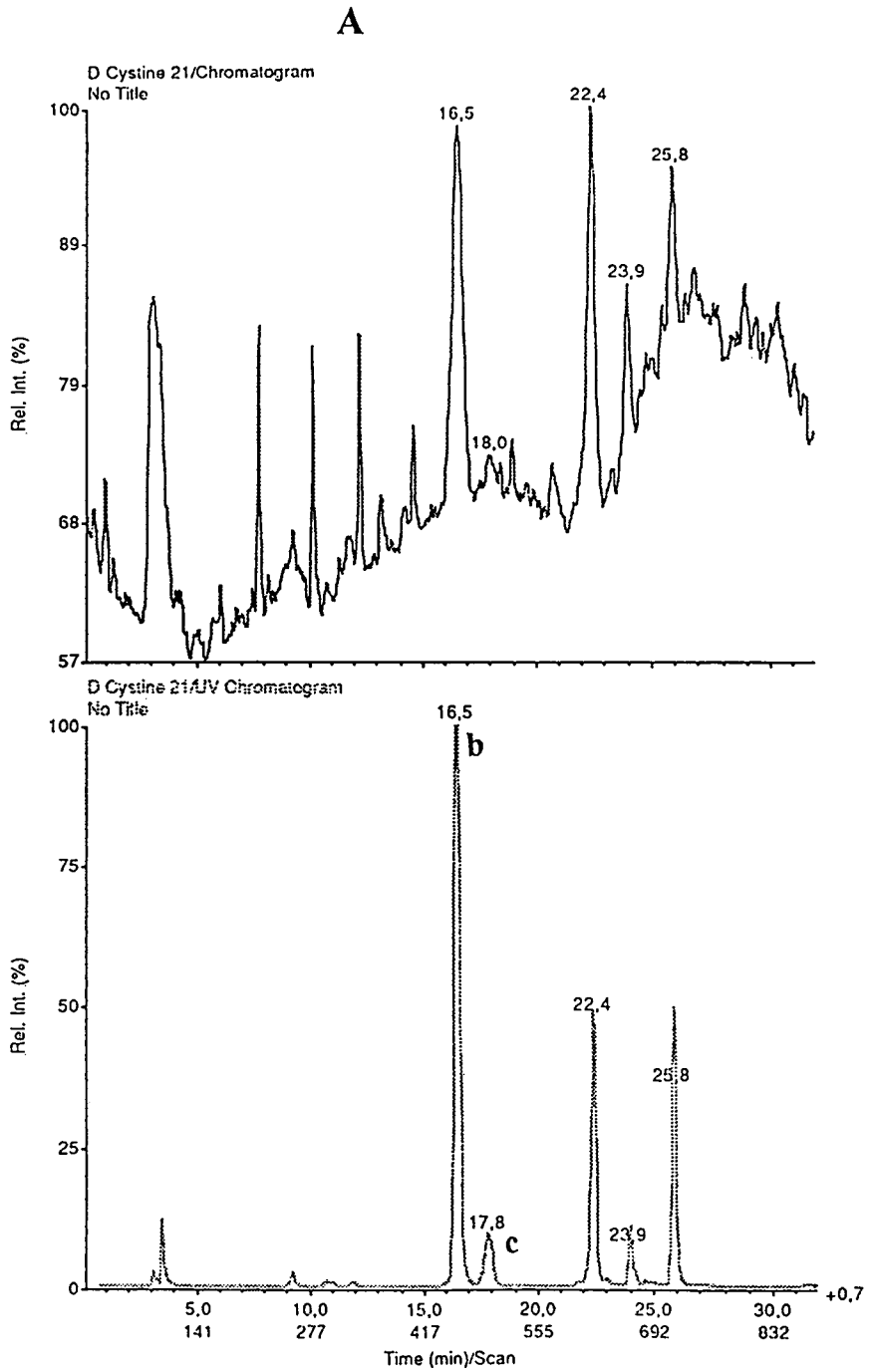

Fig. 5. (A,C) Ultraviolet absorption (254 nm) and total ion current (m/z 200–850) chromatograms and (B–D) fragmentation patterns of PTC-D-cystines. (A,B) Derivatized immediately. (A) Chromatograms of peaks b and c, retention times 16.5 and 17.8–18.0 min; (B) API-MS of peaks b and c. (C,D) Derivatized after simulating hydrolysis conditions. (C) chromatograms of peaks a, b, c and d, retention times 16.0, 16.4, 17.9 and 18.1–18.3 min; (D) API-MS of peaks a, b and c + d. Detailed data are given in Table 4. Chromatograms and mass spectra were obtained with the LC–API-MS system.

B

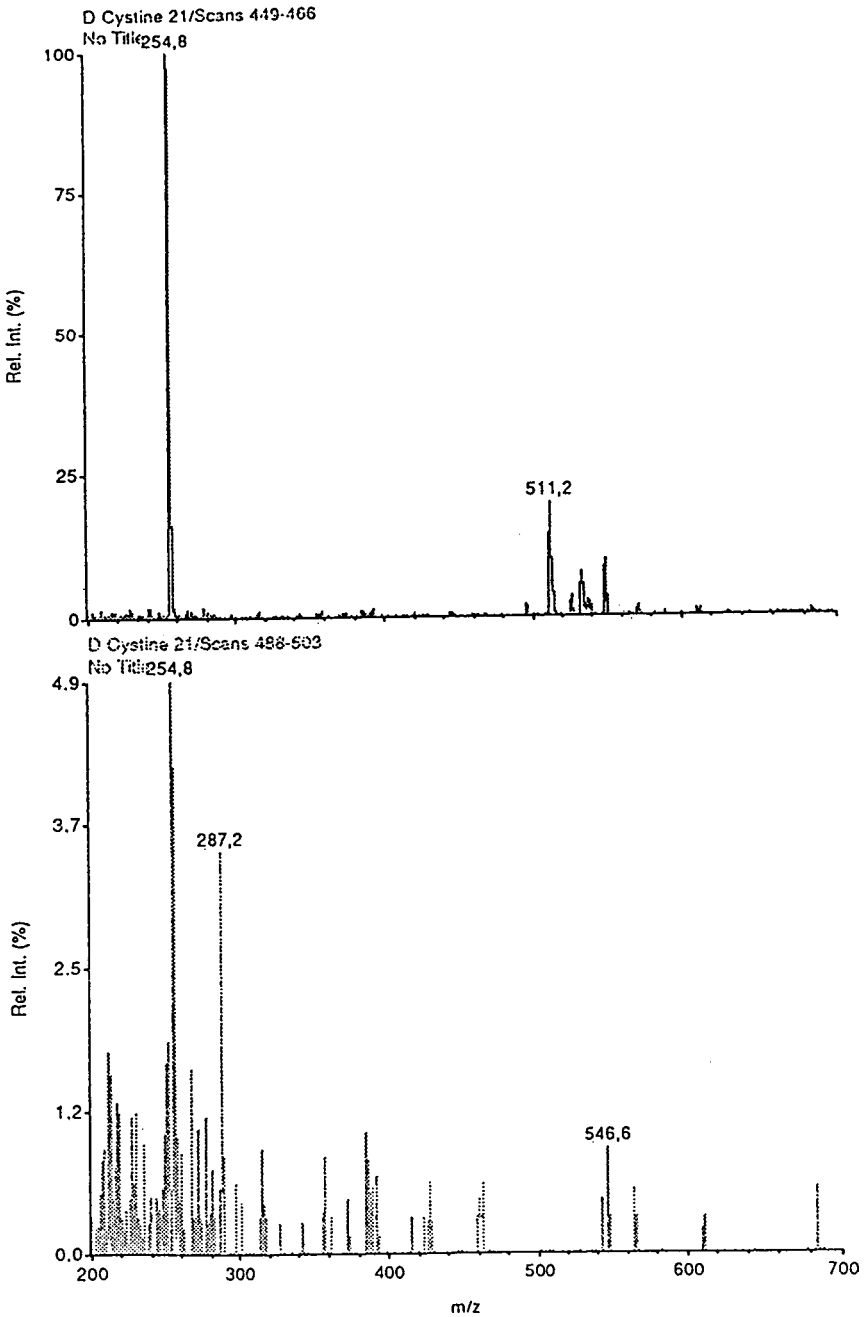

Fig. 5. (*Continued on p. 296*)

C

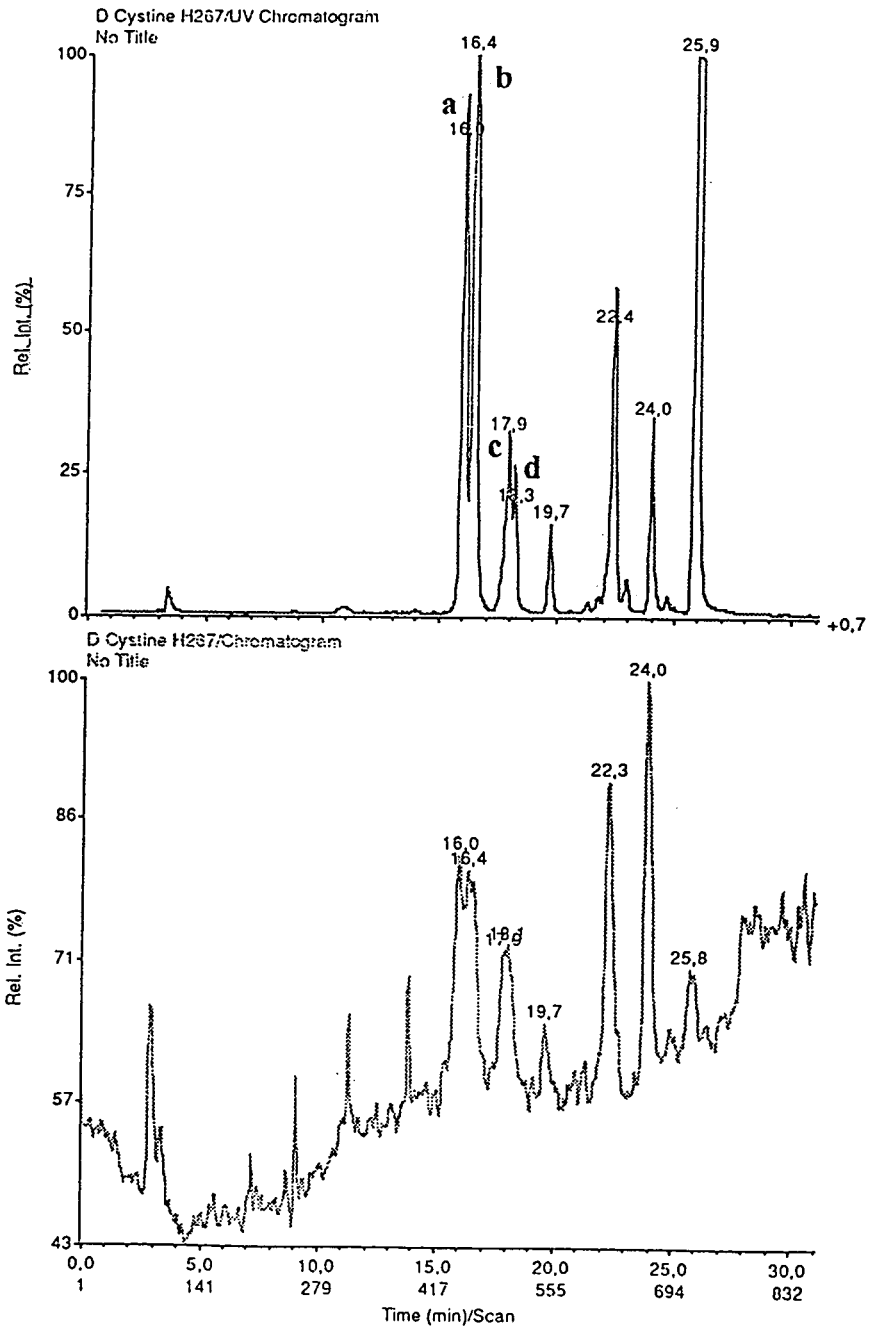

Fig. 5. (*Continued*)

D

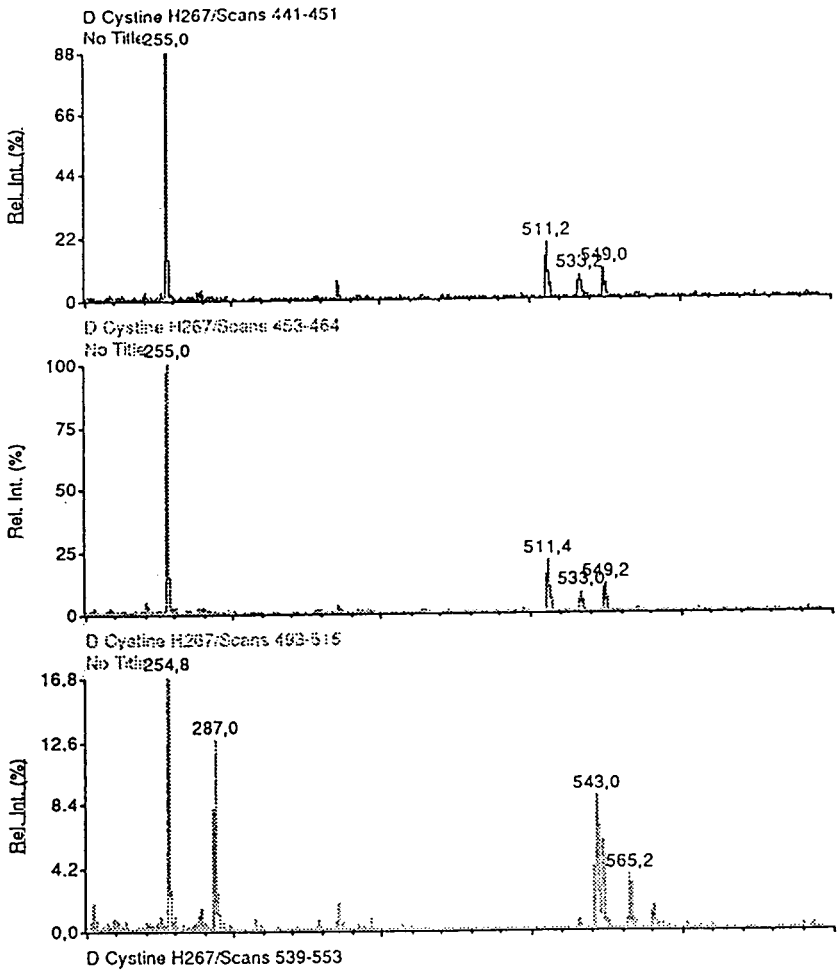

Fig. 5. (*Continued*)

Concerning the calculated masses of the monomeric (m/z 256 + 1) and dimeric (m/z 512 + 1) fragments of PTC-cyst(e)ines, shown by a detailed fragmentation profile of peak a obtained from derivatized L-cystine [Fig. 6A (monomers) and B (dimers)], they also exist, representing ca. 5–6% of the total, in case of both the monomeric (Fig. 6A, $M + 1 = m/z \approx$ 257) and the dimeric (Fig. 6B, $2M + 1 = m/z \approx$ 513) derivatives. Moreover, fragments with one proton less, indicating an intermediate position between the calculated (m/z 257) and abundant fragments (m/z 255), are also present (Fig. 6A, m/z 256; Fig. 6B, m/z 512), providing also 5–6% of the total of cyst(e)ine derivatives.

Regarding the composition of the c and d peak pair (Table 4, last column), they consist of a compound providing three fragments: such as

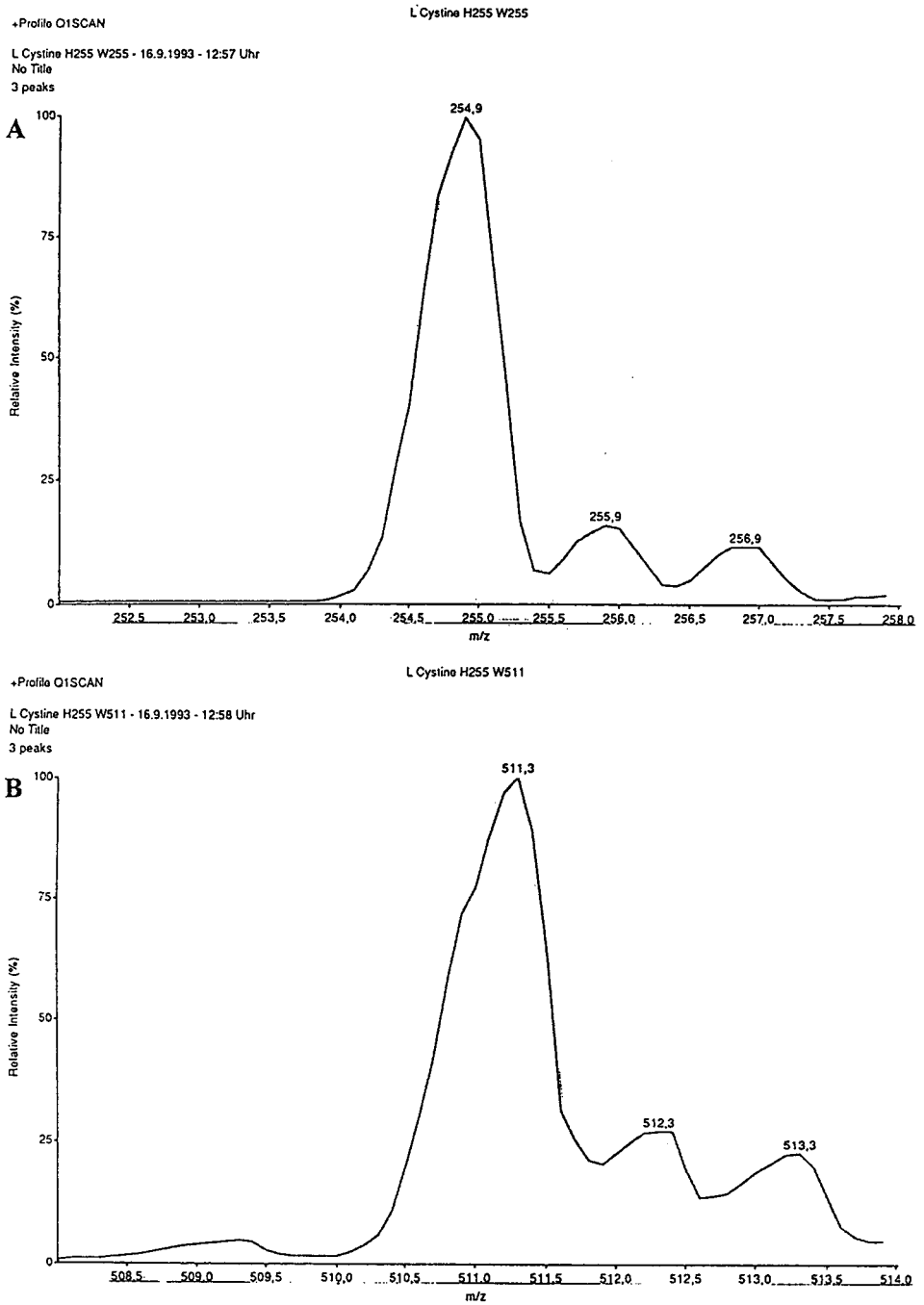

Fig. 6. Detailed fragmentation profile provided by (A) the monomeric and (B) the dimeric fragments obtained from peak a of PTC-L-cystine.

m/z 255, $m/z = 287$ (which corresponds to the protonated PTC cysteine sulphone), as well as their protonated dimer, $m/z = 543$.

4. Conclusions

On the basis of the fragmentation patterns of seventeen PTC-amino acids and six PTC-cyst(e)ines, obtained under the very soft conditions of the LC–API-MS procedure), we can state that two characteristic monomer PTC derivatives are formed. The PTC-cysteine monomers appear as two stereoisomer pairs: (i) the main product (a and b diastereoisomers, >80% of the total) proved to be a fragment of $m/z = 255$, a monomeric cysteine derivative; and (ii) the other characteristic constituent (c and d stereoisomers, <20% of the total) consisting of a fragment of $m/z = 255$ and its oxidized version of $m/z = 287$.

Taking into account all the literature data and our results detailed above, it can be concluded that the electrophilic attack of PITC on cystine results in oxidative scission of the disulphide bond, giving two PTC-cysteine derivatives.

In addition to the unambiguous evidences of the mechanism regarding the phenylthiocarbamylation of cyst(e)ines, the analytical utility of this work can be emphasized: the identical molar response values of the PTC derivatives of cystine and cysteine provide a simple approach for their determination in protein hydrolysates, without any special, previous pretreatment.

Acknowledgements

This work was supported by the Hungarian Academy of Sciences (Projects Nos. OTKA I/3 2284 and I/4, T5053). The authors thank Christoph Kempter, Ingrid Enss and Konrad Bleicher for their valuable assistance.

References

[1] I. Molnár-Perl and M. Morvai, *Chromatographia*, 34 (1992) 132.
[2] S. Kawakishi and M. Namiki, *Agric. Biol. Chem.*, 33 (1969) 452.
[3] S. Kawakishi and M. Namiki, *J. Agric. Food Chem.*, 30 (1982) 618.
[4] B.C. Pramanik, C.R. Moomaw, C.T. Evans and S.A. Cohen, *Anal. Biochem.*, 176 (1989) 269.
[5] I. Molnár-Perl, M. Pintér-Szakács and M. Khalifa, *J. Chromatogr.*, 632 (1993) 57.
[6] I. Molnár-Perl and M. Khalifa, *Chromatographia*, 36 (1993) 43.
[7] I. Molnár-Perl, *J. Chromatogr. A*, 661 (1994) 43.

ELSEVIER

Journal of Chromatography A, 691 (1995) 301–315

JOURNAL OF CHROMATOGRAPHY A

Sensitivity and selectivity of the electrochemical detection of the copper(II) complexes of bioactive peptides, and comparison to model studies by rotating ring-disc electrode

Jian-Ge Chen, Steven J. Woltman, Stephen G. Weber*

Department of Chemistry, University of Pittsburgh, Pittsburgh, PA 15260, USA

Abstract

Post-column reaction of peptides with Cu(II) can be used for the electrochemical detection of peptides as their biuret complexes. Understanding of the behavior (sensitivity at the anode and cathode in the dual-series electrochemical detector) of the system is facilitated through the observation of the rotating ring disc voltammetry of some model compounds. In operation, the anodic signal from the oxidation of the Cu(II)–peptide to the Cu(III) form can be used to detect peptides, or the downstream cathode can be used to detect the Cu(III) form. The signals appear at about 0.4 V (anode) for tetra- and longer peptides, 0.65 V for tripeptides. The anode signal is augmented by tyrosine (oxidation at 0.4–0.5 V) and tryptophan (0.5–0.6 V). If the cathode is used as the detector in a two working electrode cell, the sensitivity depends on the stability of the Cu(III) product. This is peptide dependent, but the signal is significant and useful analytically. Twenty-three bioactive peptides in two groups, naturally electrochemically active and naturally electrochemically silent, and several model compounds have been studied.

Both naturally electrochemically active peptides (contain tyrosine and/or tryptophan) and naturally electrochemically silent peptides have been studied. Chromatography with an acetonitrile gradient has been used to separate the peptides in each group. Detection limits are for non-electroactive peptides in the range of 16–100 fmol (10- μl injection 1.6–10 nM, 100 μl injection 0.16–1.0 nM), and for electroactive peptides in the range of 6–40 fmol (0.6–4.0 nM for a 10- μl injection and 60–400 pM for a 100- μl injection). A tryptic digest of bovine cytochrome *c* is easily seen at 100 nM.

1. Introduction

Peptides carry critical information in living systems [1]. Their quantitative determination represents a considerable challenge. Antibody-based binding assays are challenged by the homology of peptides that originate in the same propeptide or prepropeptide [2]. Reversed-phase liquid chromatography [3] and capillary electrophoresis [4] have the capability to separate peptides, but routine, commercially available detectors are often not capable of detecting at the concentrations required. Thus, separations methods are challenged by the detection problem.

For work around μM concentrations, a UV photometer or spectrophotometer at around 210 nm is a good detector. It has the advantage of being able to detect any peptide, for the absorbance transition on which it works is due to

* Corresponding author.

0021-9673/95/$09.50
SSDI 0021-9673(94)00843-4

the amide bond. Of course, many other species absorb at that wavelength, so selectivity is poor. For lower concentrations, fluorescence of derivatized peptides, e.g., *o*-phthalaldehyde (OPA) [5] and naphthalene-2,3-dicarboxaldehyde/CN^- (NDA) [6], have been successful. An optimized detector using an Ar^+ laser-based detector and a 150×1 mm reversed-phase column demonstrated a detection limit for OPA derivatives of sulfur-containing amino acids of about 10^{-10} *M* in 10 μl (1 fmol) [7]. The peptide derivatives do not yield as high a sensitivity as the amino acids because of differences in the photophysical properties of the isoindole derivatives [8]. These successful fluorescent reagents rely on the presence of the primary amine for their success. A significant fraction of peptides do not have primary amines, for example they may be cyclic, N-acylated, or pyroglutamate may be the amine terminus. Thus, while fluorescence derivatization has certainly established itself as a useful and robust approach, it will not permit detection of peptides without reactive amines.

We [9–11] have been developing electrochemical detection [12] with the goal of providing useful detection limits and universal applicability to peptides [9], especially those without electroactive functional groups, W (Trp) and Y (Tyr) [10,11]. We use the biuret reaction, in which basic copper tartrate reacts with the peptides, and then take advantage of the reversible electrochemistry of the Cu(II)/Cu(III) couple [9]. Peptides with Y and W are detectable without derivatization [13], however the reaction with Cu(II) leads to increases in sensitivity for Y- [14] and W- [15] containing peptides.

One of the goals in the overall development of this approach to detection is to understand and predict the sensitivity of the method to various peptides. There are two general issues. One is whether the peptides in which one is interested react with the Cu(II) and give a signal under useful conditions, while the other is whether there are particular conditions that allow for the detection of desired peptides with selectivity over other peptides. Incidentally, in contrast to the amine-reactive fluorescence reagents, the biuret reaction does not occur with amino acids. It is impossible to determine the detection properties of every peptide because of the number of them, and because of differences among peptides, it is not possible to generalize with certainty concerning individual peptides that carry a similarity. Nonetheless, we must, in order for the technique to be useful, provide some basis for understanding the above mentioned pair of issues. Our approach is to study model peptides by rotating ring-disc voltammetry [16], and to determine the detection properties of bioactive peptides independently. In this paper, the first using this approach, we have examined several bioactive peptides, and we have developed a core understanding for the basic electrochemistry of the Cu(II)–peptide complex. Each bioactive peptide has not been investigated in detail, so there are some results for which a satisfying chemical interpretation is not in hand. However, taken together, the results for the electrochemical detection of the bioactive peptides represents a survey that gives a broad feeling for the potential of the approach.

2. Experimental

2.1. HPLC with post-column reagent addition

We used reversed-phase chromatography (Hypersil C_{18}, 3 μm, 100×1 mm, Keystone Scientific, Bellefonte, PA, USA) with gradient elution (Waters 600 MS pump, Bedford, MA, USA). The binary gradient used as solvent A 0.1% trifluoroacetic acid (TFAA) (HPLC grade; Sigma, St. Louis, MO, USA), 3% 1-propanol (HPLC grade, Sigma) (except for the tryptic digest analysis); B was 0.1% TFAA, 3% 1-propanol (except for the tryptic digest analysis), 60% acetonitrile (HPLC grade; EM Science, Gibbstown, NJ, USA) in water. Timing details are provided in the figures. The post-column phase, 1.2 *M* carbonate buffer [0.6 *M* each of $NaHCO_3$ (Mallinckrodt, Paris, KY, USA) and Na_2CO_3 (Fisher, Pittsburgh, PA, USA)], pH 9.8, 3% 1-propanol (except for the tryptic digest analysis), copper sulfate (Fisher) at around m*M* (exact concentrations given in the figures), and sodium potassium tartrate (Fisher) at 6 times the Cu(II) concentration was pumped with an ISCO (Lincoln, NE, USA) syringe pump. The sodium

potassium tartrate used for HPLC was recrystallized from water. The temperature of both the post-column phase and the column were controlled. Typical volume flow-rates were column: 50 μl/min and post-column 20 μl/min. The post-column reactor was PTFE tubing that had been woven through a nylon net. Its volume was 105 μl which resulted in a reaction time of 1.5 min. All data in the tables have been obtained with 1.0 m*M* copper sulfate in the post-column reagent. Reagent sources are listed below.

2.2. Electrochemical detection

A BAS (W. Lafayette, IN, USA) Model LC-4C dual-electrode controller, and dual-series glassy carbon cell were used as the detector. The thermal equilibration unit, ordinarily positioned just before the cell, was removed from the system. Signals from the detector were acquired at 1 point/s by EZChrom (Scientific Software, San Ramon, CA, USA). Areas were determined after manually specifying the limits of integration for each peak. Noise measurements were made by picking a segment of baseline where there were no peaks, amplifying a 1-min section, taking the maximum signal in this window minus the minimum as the peak-to-peak noise, and dividing by 5 to estimate root mean square (rms) noise.

Bioactive peptides, cytochrome *c* and trypsin were all purchased from Sigma. All solutions were made in Milli-Q laboratory-deionized water, except N-formyl-MLFF (DMF), N-formyl-MLF, fibrinopeptide A, and ACTH 1–10 were prepared in 0.1 *M* acetic acid (Fisher), and octadecaneneuropeptides in 0.1 *M* NaOH (EM Science) solution. One-letter abbreviations are used for amino acids.

2.3. Tryptic digest

A 5.0-ml volume of a 2.0 mg/ml solution of bovine cytochrome *c* (Sigma) in 0.1 *M* pH 8.0 ammonium carbonate buffer was mixed with 5.0 ml of a 0.1 mg/ml solution of trypsin in the same buffer. The solution was incubated for 24 h at 37°C, and then frozen. Before injection, the solution was diluted by a factor of 810 to yield 100 n*M* injected protein.

2.4. Rotating ring-disc electrode (RRDE) studies

RRDE studies employed a DT-29 glassy carbon disc/glassy carbon ring electrode, ASR-2 rotator and RDE-3 potentiostat (all from Pine Instrument Co., Grove City, PA, USA). A platinum grid counter-electrode and Ag/AgCl (3 *M* NaCl) reference electrode were used. All potentials are reported relative to the reference electrode.

Peptides (GGG, GGGG, GGY, GYG, YGG, GGFL and YGGFL; all from Sigma), analytical-grade sodium hydroxide, boric acid and sodium hydrogencarbonate (Mallinckrodt), ACS-grade copper sulfate pentahydrate (Fisher), and ACS-grade disodium tartrate dihydrate (Baker, Phillipsburg, NJ, USA) were used without further purification.

Carbonate buffer, pH 9.80, was prepared by dissolving sodium hydroxide and sodium hydrogencarbonate to concentrations of 0.10 and 0.20 *M*, respectively; the pH was confirmed with a meter before use. Borate buffer, pH 10.0, was prepared by titration of 0.10 *M* boric acid/0.10 *M* KCl with solid sodium hydroxide. Copper–peptide solutions were prepared by first mixing peptide stock solution with copper sulfate solution. For copper–peptide (1:1) solutions, equimolar copper sulfate was used; otherwise, copper sulfate–tartrate (1:3) solution was mixed with peptide solution to give a peptide–copper–tartrate molar ratio of 1:5:15. Sufficient deionized water was then added to reach 10% of the final solution volume. Buffer was introduced to the solution initially dropwise with mixing, then rapidly after the characteristic color change indicated development of the complex.

RRDE data were collected with EZChrom chromatography software. Potentiostat voltage was switched on simultaneously with manual triggering of data collection. To plot hydrodynamic voltammograms, EZChrom files were converted to ASCII format using the data export utility, then processed with Stata statistical software (Computing Resource Center, Santa Monica, CA, USA).

In all RRDE experiments, the ring (collector) electrode was maintained at a potential of 0 mV. Background runs were performed in buffer for

copper–peptide (1:1) solutions, and in biuret reagent mixed with buffer for peptide solutions with excess copper. The background signal was found not to have rotation speed dependence at the potentials used. The electrode surface was conditioned before each run by wet polishing with 0.05-μm alumina, rinsing with a stream of deionized water, and then pretreating at a potential of 800 mV disc, 0 mV ring in carbonate buffer for 1 min.

To perform hydrodynamic voltammetry, the disc potential was swept linearly from 0 to 900 mV, using the sweep generator of the RDE-3 potentiostat. The usual sweep rate of 600 mV/min was reduced to 80 mV/min for the lowest rotation speed runs to preserve steady state electrochemical behavior.

Each rotation speed study was conducted with the disc maintained at a constant potential previously identified as being in limiting current regions based upon the voltammetry. In each run, the electrode was rotated initially at a constant moderate speed (500 to 1000 rpm) and then potential was applied to the disc. The non-faradaic charging current was allowed to decay for one min, then the rotation speed was varied manually in a random sequence. Data collected in the first minute were ignored. The rotation speed was maintained at each value long enough for the signal to stabilize; this ranged from a few seconds at the highest rotation speeds to tens of seconds at the lowest. Rotation speeds ranged from 15 to 10 000 rpm, with ten to fifteen different rotation speeds per run. The low speed pully of the ASR rotator was used at the low end of this range.

3. Results and discussion

3.1. Equivalence of time scales between RRDE and electrochemical detection

By comparison of mass transfer rates calculated from theory [16,17], we have found that the conditions used in the HPLC experiment correspond to low rotation speeds, on the order of 15 rpm. For detection at the higher flow-rates typical of larger columns, the correspondence occurs at higher rotation speeds. For example, at 3.0 ml/min and a 25-μm thick spacer in the electrochemical detector, the equivalent rotation speed is about 1000 rpm.

3.2. Peptide backbone by RRDE

A considerable body of work on the stability of, and kinetics and mechanism of the reactions of Cu(II)–peptide complexes exists [18]. We draw on this work heavily in the interpretation of the voltammetry of these compounds, which is much less investigated than the homogeneous chemistry of these compounds. Figs. 1 and 2 show representative anodic (disc) and cathodic (ring) voltammograms for the simple peptides GGG and GGGG. At high rotation velocities, the voltammogram of GGG shows a single wave at 0.67 V. The stability of the Cu(III)–GGG complex is evidenced by the large cathodic current. The theoretical maximum cathodic current as a fraction of the anodic current for our electrode pair is 0.37. This ratio, called the collection efficiency, N_{coll}, is 0.32 for GGG at 10 000 rpm. Comparison to the standard (GGGG at pH 11.6) shows that there is one electron transferred, as expected for the reaction Cu(II)–GGG → Cu(III)–GGG. At lower rotation velocities there is a simultaneous increase in anodic current and decrease in cathodic current. This indicates an instability in the Cu(III)–GGG complex at this longer time. The products of the reaction that removes Cu(III) from the system are oxidized at the anode, leading to a higher current, and the depletion of the Cu(III) form of the complex leads to a reduction in cathodic current. Chemical studies on the stability of Cu(III)–peptides [19] indicates that the more α hydrogens a tripeptide has, the less stable the complex. Clearly GGG has the maximum number of α hydrogens, so it represents the minimum stability. Investigations of the peptides FGG, GFG, GGF have shown virtually identical behavior to GGG at the RRDE (data not shown).

GGGG (Fig. 2) shows two waves, more distinctly the higher the rotation velocity. The first

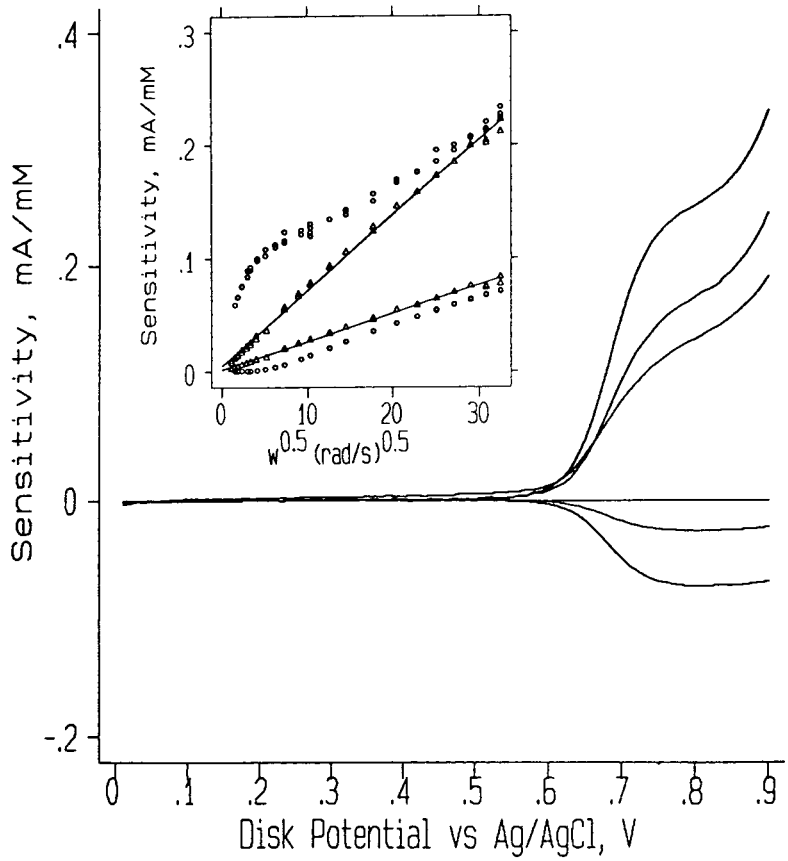

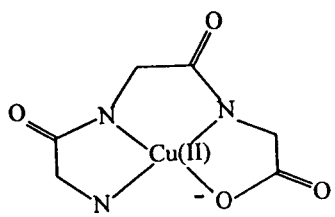

I

Fig. 1. RRDE voltammograms at pH 9.8 and structure of the Cu(II)–GGG complex. Anode (upward going) and cathode (downward going) traces are shown for (lowest to highest) 150, 2000, 10 000 rpm. In the inset is shown rotation speed dependent data for the anode at 0.7 V (upper set of points), and the cathode at 0.0 V (lower set of points). The cathode signal at the lowest rotation speed is negligible. The points associated with the regression lines are anode and cathode data for a standard one electron transferring species, Cu(II)–GGGG at pH 11.6.

wave at 0.42 V represents the more easily oxidized complex $Cu(H_{-3}GGGG)$, shown in the figure as **II**. The negative subscript on H in the formula indicates that the loss of three protons from the neutral ligand was required to form the complex. The second wave at 0.67 V is from the $Cu(H_{-2}GGGG)$ complex, **III**, which has around the Cu(II) the same atoms as the Cu(GGG)

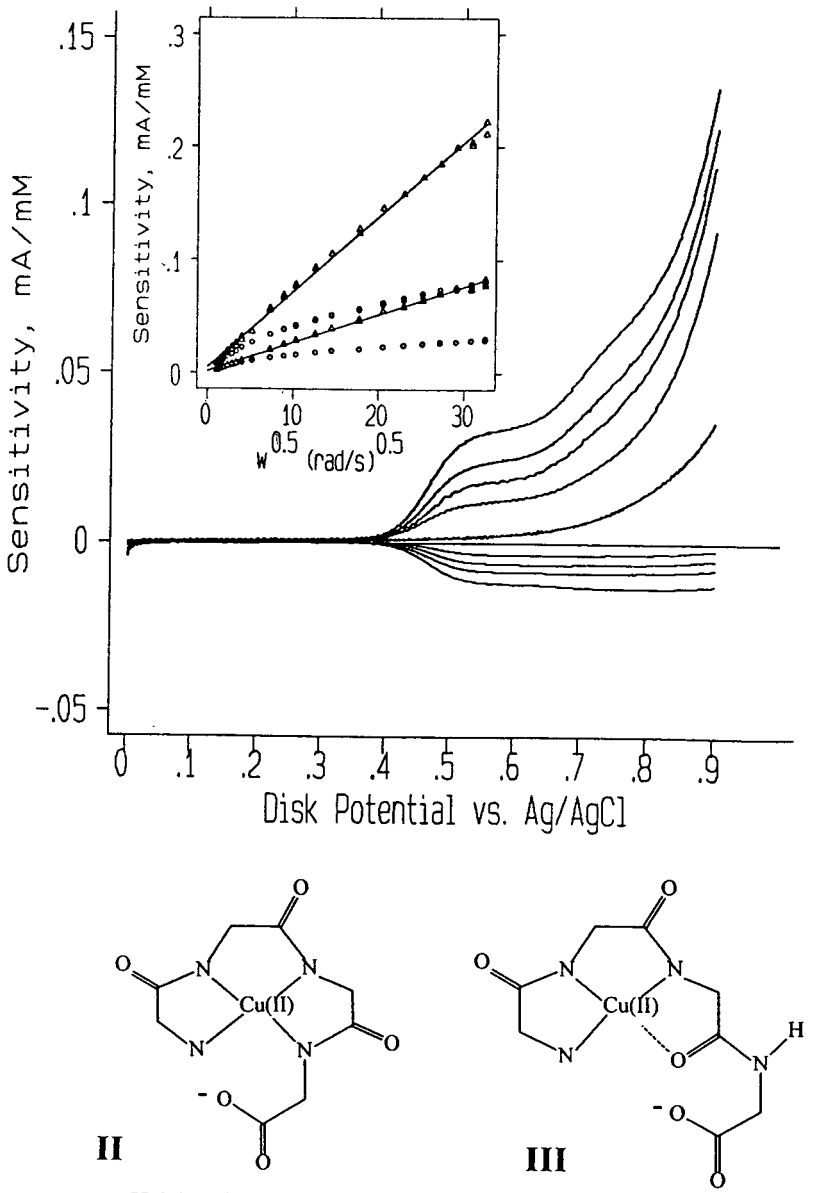

Fig. 2. RRDE voltammograms at pH 9.8 and structure of the Cu(II)–GGGG complex. Anode (upward going) and cathode (downward going) traces are shown for (lowest to highest) 15, 50, 100, 250 rpm plus anodic background (for all rotation speeds). The cathodic background is negligible. In the inset is shown rotation speed dependent data for the anode at 0.52 V (upper set of points), and the cathode at 0.0 V (lower set of points). The points associated with the regression lines are anode and cathode data for a standard one electron transferring species, Cu(II)–GGGG at pH 11.6.

complex (compare structures **III** and **I**). The near identity of the potentials is due to this homology. The appearance of two waves, with the second beginning to dominate the first, at higher rotation speeds is due to the slow interconversion between the H_{-3} and the H_{-2} forms of the complex [20]. Oxidation on the lower potential plateau removes Cu(II)(H_{-3}GGGG) from the solution, and by mass action the reaction:

Table 1
Sensitivities of small peptides at 0.55 and 0.80 V upstream anodic potentials and at 0.10 V of their corresponding downstream cathodic potentials (nC/pmol)

Peptide	Electrode potential (V)			
	0.55	0.10	0.80	0.10
GGF	0.14	0.00	54	0.82
GGFL	15	7.1	20	8.6
N-f-MLF	9.6	3.2	18	3.9
N-f-MLFF	2.4	0.61	2.5	1.2

$$\mathrm{Cu(II)(H_{-2}GGGG)} \rightarrow \mathrm{Cu(II)(H_{-3}GGGG)} \quad pK_a = 9.15 \qquad (1)$$

occurs. Thus, while the solution contains both forms, all of the complex can be oxidized at 0.55 V if the timescale is long enough. Of course, all of the complex is oxidized at 0.8 V, or at lower potentials and higher pH values; this reaction is not inhibited by homogeneous reaction kinetics. For both waves there is a substantial cathodic signal. A full study of the kinetics and mechanism of this electrochemical reaction is in progress. The equilibrium constant and rate constants for reaction 1 depend on the peptide, so the magnitude of the difference in anodic response depends on both the peptide and the time scale.

3.3. Electrochemical detection

First, the results discussed above will be used to understand the behavior of four small peptides. Following that, we will take a look at several peptide classes, and rationalize, where we can, the behavior based on the chemistry of the peptides.

Small peptides

Sensitivities for four small peptides may be found in Table 1. Of these, only two are "simple" peptides, two are N-formylated. The leu-enkephalin fragments, GGF and GGFL behave differently, as expected from the RRDE studies. At 0.8 V the signal from GGF exceeds that of GGFL by a factor of 2.7, while N_{coll} for GGFL is several-fold higher than for GGF. These results are qualitatively consistent with the RRDE studies. At 0.55 V the GGFL signal is somewhat lower, while that of GGF is significantly lower, again as expected from the RRDE work. As GGFL shows uncomplicated RRDE behavior that is in good qualitative agreement with the hydrodynamic voltammogram obtained by changing the potential at the electrochemical detector (Fig. 3), we accept that a sensitivity of about 20 nC/pmol represents a single electron transfer for a small peptide. Theory [17] predicts about 30 nC/pmol, however there are uncertainties in the actual diffusion coefficient, the actual

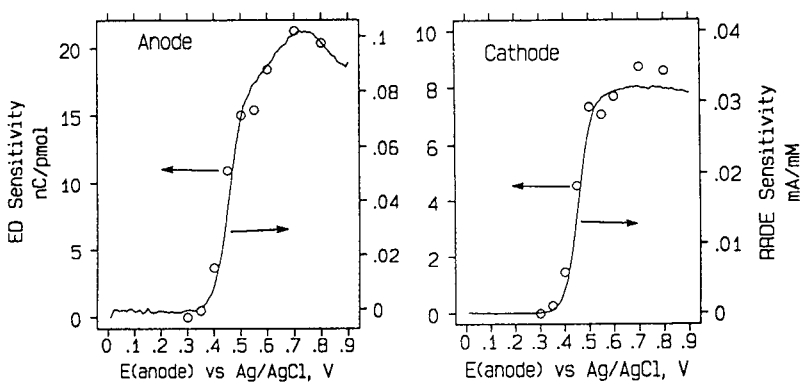

Fig. 3. Superimposition of RRDE voltammograms (solid line) and hydrodynamic voltammograms (HDV, O) from HPLC with electrochemical detection (ED). The vertical scales have been adjusted arbitrarily to give a fit pleasing to the eye.

cell thickness, nominally 12.5 μm, and in the actual velocity distribution across the channel, which is a full 6 mm wide. These uncertainties in the parameters that go into calculating the signal lead us to accept conditionally the experimental result, so we will use 20 nC/pmol as a benchmark for analysis of the results.

N-Blocked peptides

The N-formylated peptides react with the biuret reagent, but at 0.8 V only the N-f-MLF yields a signal approaching what would be expected for a straightforward one-electron transfer. Previous work on N-acetylated peptides [12] in flow injection analysis has pointed out the need for higher pH in the determination of these. Visible spectroscopic investigation of MLF, N-f-MLF, and N-acetyl-MLF at pH 9.8 (same as post-column reactor) shows that there is no formation of the N-acetyl-MLF complex, and partial formation of the N-f-MLF complex. Though a complete dependence study has not been carried out, we have noted that the sensitivity of the N-formylated peptides is very dependent on the Cu(II) concentration in the post-column reactor.

Another example of N-blocked peptides are those in which the amine terminal glutamate exists as the γ-lactam; this is pyroglutamate, pE. Table 2 compares sensitivities for substance P fragments pEFFGLM–NH_2, and QFFGLM–NH_2 (Q is Gln). They are very similar at both the cathode and the anode, and they are in the same range as the N-f peptides. We have established that the N-f and pE peptides are detectable, but further work to understand the reasons for the suppressed sensitivity is required.

Effect of peptide length

Data for a series of peptides are given in Table 2. Two of the peptides, lengths 4 and 8, show the full sensitivity that we expect. The other peptides (lengths 4, 6, 10, 13, 16, 18) show somewhat reduced sensitivity, but there is no distinct correlation with length. We can say, recalling the caveat about generalization stated above, that peptides up to 18 amino acids in length give acceptable signals. Lower sensitivity, where it occurs, is likely to be kinetic in origin, so reaction time, reaction temperature, and Cu(II) concentration can be used for improving the reaction rates.

Peptides with electroactive amino acids

At pH 9.8, Y is slightly easier to oxidize than W (0.56 vs. 0.67 V [21]). I is more easily oxidized than either. Neither W nor Y has a reversible redox wave, so we do not anticipate a useful cathode signal from peptides that have W and Y in the absence of Cu(II). In the presence of Cu(II), the anode signal may be the sum of the electroactive amino acid signal and the

Table 2
Sensitivites of non-electroactive bioactive peptides at 0.80 V upstream anode and 0.10 V downstream cathode (nC/pmol)

No.	Peptide	Amino acid sequence	Electrode potential (V)	
			0.80	0.10
1	RFDS	RFDS	14	6.4
2	Speract	GFDLNGGGVG	10	3.2
3	Des-Y-L-enkephalin	GGFL	20	8.6
4	Fibrinopeptide A	ADSGEGDFLAEGGGVR	14	5.1
5	Octadecaneuropeptide	QATVGDVNTDRPGLLDLK	7.51	2.2
6	N-Formyl-MLF	N-f-MLF	18	3.9
7	SPF 6–11[a]	QFFGLM–NH_2	8.7	2.3
8	pE^6–SPF 6–11[a]	pEFFGLM–NH_2	5.8	2.8
9	ALILTLVS	ALILTLVS	21	9.3
10	HPPGRHF 14–26	DAENLIDSFQEIV	8.2	2.2
11	N-Formyl-MLFF	N-f-MLFF	2.5	0.46

[a] SPF = Substance P fragment.

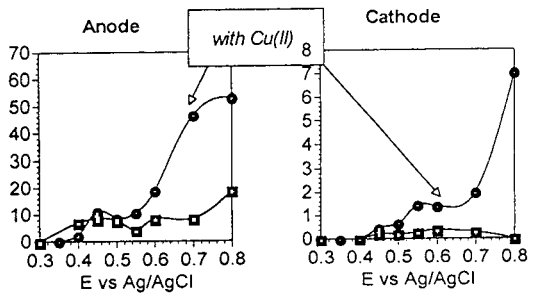

Fig. 4. HDV with and without Cu(II) for the tyrosine-containing peptide α-endorphin. Vertical scale nC/pmol. Lines are a cubic spine fit to the points. pH 9.8.

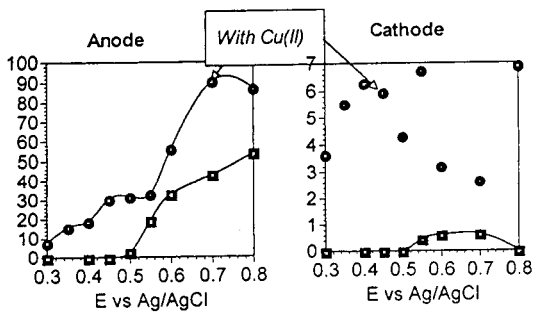

Fig. 5. HDV with and without Cu(II) for the tryptophan-containing peptide leucokinin II. Vertical scale nC/pmol. Lines are a cubic spine fit to the points. pH 9.8.

Cu(II) signal [14]. The cathode signal in this case is depressed in small Y-containing peptides [14]. Plots of the anodic and cathodic sensitivities as a function of potential at the anode are shown in Figs. 4 and 5 for representative peptides containing only W (leukokinin II, DPGFSSWG–NH_2) and only Y (α-endorphin, YGGFMTSEKSQTPLVT), and Table 3 gives sensitivities at the anode at 0.5 V and at the cathode (0.0 V) while the anode is at 0.8 V in the presence and absence of Cu(II) for several bioactive electroactive peptides. Before discussion we point out that the baseline at the cathode is more stable at 0.1 V, and sensitivities, where we have tested them, are the equivalent or higher than those at 0.0 V, however we have more complete data for more peptides at 0.0 V, thus we will concentrate on them. The increased baseline at 0.0 V is caused by the stabilizing influence of acetonitrile on Cu(I). As the acetonitrile content of the mobile phase increases, it becomes easier to reduce Cu(II) to Cu(I), and that reduction becomes background current.

The anodic voltammograms of the electroactive peptides without Cu(II) show behavior similar to that of model compounds (Figs. 6 and 7). In the absence of Cu(II), Y is more easily oxidized than W, the wave of YGGFL precedes that of GWGG, and the wave of the Y-con-

Table 3
Sensitivites of electroactive bioactive peptides at 0.50 and 0.0 V while the upstream anodic potential is at 0.80 V with (w/) and without (w/o) Cu^{2+} (nC/pmol)

No.	Peptide	Amino acid sequence	Electrode potential (V)			
			0.50 (w/)	0.00 (w/)	0.50 (w/o)	0.00 (w/o)
1	DSIP	WAGGDASGE	32	4.3	5.6	1.0
2	RKDVY	RKDVY	11	2.5	8.6	0.49
3	Lys^8-vasopressin	C(YFQN)CPLG–NH_2	36	1.6	20	0.71
4	Leucokinin II	DPGFSSWG–NH_2	32	6.9	2.9	0.0
5	Oxytocin	C(YIQN)CPLG–NH_2	40	3.1	9.5	0.21
6	Leu-enkephalin	YGGFL	60	10	21	0.58
7	WMDF-NH_2	WMDF-NH_2	29	7.3	8.2	1.0
8	Angiotensin II	DRVYIHPF	33	7.1	7.7	0.08
9	ACTH 1–10	SYSMEHFRWG	50	9.3	36	0.62
10	Neurotensin	pELYENKPRRPYIL	55	11	13	0.26
11	α-Endorphin	YGGFMTSEKSQTPLVT	56	8.3	36	2.3
12	Tyr-somatostatin	YAGC(KNFFWKTFTS)C	8.8	7.0	7.9	0.0

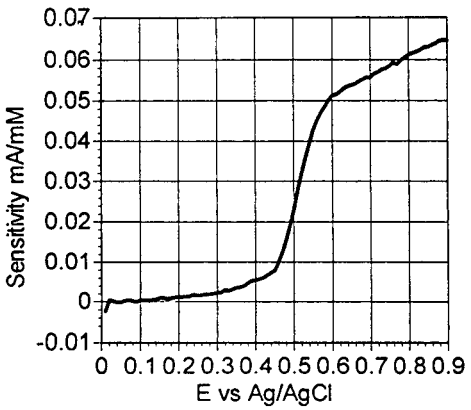

Fig. 6. RRDE voltammogram of YGGFL in the absence of Cu(II). pH 9.8.

taining α-endorphin is negative of that of the W-containing leucokinin II. The sensitivity suggests up to 2 electrons are transferred in the oxidation, which agrees with observations on the amino acids themselves. The cathode signals are lower than what is expected for a reversible reaction befitting the irreversible nature of the oxidations. The nominal two electron oxidation of Y- and W-containing peptides is most likely a sequence of reactions, an electron transfer followed by a chemical reaction, and then another electron transfer [14,15]. The rate of the chemical reaction dictates the lifetime of the first electron transfer product. This rate may certainly be peptide dependent, thus we may expect some peptides to give more significant cathodic signals than others as seen in Table 3. The examples shown in Figs. 4 and 5 represent extremes in this regard. The α-endorphin has a significant cathode signal, while that of the leukokinin II is zero.

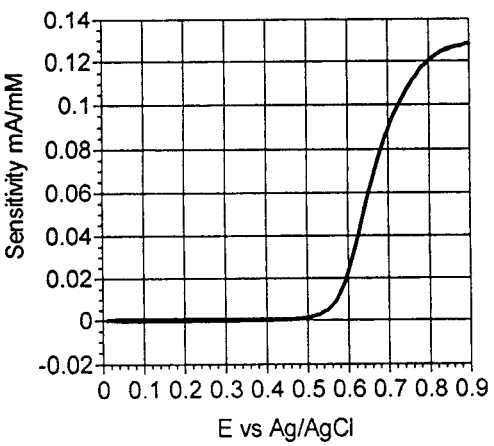

Fig. 7. RRDE voltammogram of GWGG in the absence of Cu(II). pH 9.8.

In the presence of the biuret reagent there is a considerable improvement in sensitivity, both at the anode at 0.5 V and at the cathode at 0.0 V (anode 0.8 V). The increase in sensitivity at 0.5 V is about 15–40 nC/pmol (Table 3) except for RKDVY and Y-somatostatin. Discussion of these is deferred. For the bulk of the peptides, the Cu chemistry expresses itself at a low potential as an additive factor. Furthermore, at the cathode, when the anode is at 0.8 V the sensitivities are the equal of those for typical non-electroactive peptides. This result is not the same as results for shorter peptides in which the cathode sensitivities are compromised by the presence of Y [14]. Let us consider the exceptions. The RKVDY will be discussed below, however for the somatostatin we must consider that the sensitivity of its detection without Cu is abnormally low (it contains W and Y) and its sensitivity at 0.5 V in the absence of Cu(II) is 7.9 nC/pmol. It may have a structure that inhibits electron transfer; it is highly basic. At 0.8 V, the sensitivity of the biuret complex of the Y-somatostatin is more normal. There is the possibility as well that the reaction analogous to reaction 1 above is slow, or the pK_a is very basic, which minimizes the H_{-3} wave and emphasizes the H_{-2} wave. This explanation, however, does not explain the low sensitivity to the Y and W in the peptide under Cu-free conditions.

Peptide structure

We have previously shown that bradykinin reacts slowly with the biuret reagent [10]. We rationalized this in terms of the limitations caused by proline on the accessible structures, which in turn limits the chance that the peptide is in an appropriate conformation to react with

Cu(II). Here, under different conditions of mobile phase, we have found the same result; anodic sensitivity (nC/pmol) is only 1.9 at 0.50 V and 0.39 for the corresponding cathode at 0.1 V. Substance P, which has 2 proline residues, appears to behave similarly; it only gives 0.72 and 0.14 nC/mol at the same applied potentials given for bradykinin.

Pre-column derivatization with Cu(II) was found to be an effective method for bradykinin [10]. A fuller study of highly constrained peptides is certainly warranted.

Many bioactive peptides are cyclic disulfides as a result of the formation of intramolecular S–S bridges by a pair of cysteines. Table 3 has data for Y-somatostatin, which has been discussed, and oxytocin and lys^8-vasopressin, all of which have cyclic, S–S bridged structures. A model RRDE voltammogram of CAAGVC is shown in Fig. 8. Clearly, this cyclical structure does not inhibit the formation of the complex. Once again, it is worth remembering the caveat concerning generalization, but at least one can say that the restrictions on structure due to the S–S bridge do not interfere with the detection of these peptides.

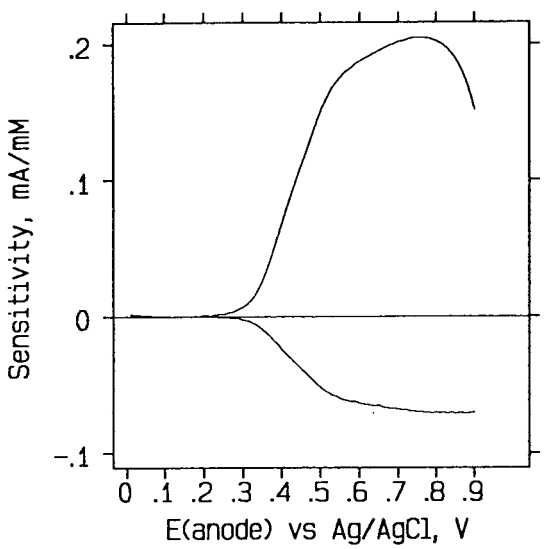

Fig. 8. RRDE voltammogram of CAAGVC at pH 9.8, 10 000 rpm.

RGD peptides are an important class of cell adhesion mediators [22]. It has been reported that the Cu(II) complexes of peptides with an aspartate in the third position from the amine terminus, which will be written as XXD, are very stable [23]. The stability arises because the β-carboxy group of the D is a ligand for the Cu(II); even in a tetrapeptide, the carboxy group is the fourth ligand in the complex, not the amide between the third and fourth amino acid. As we have seen above for the pair GGG and GGGG, the effect of the carboxy group on the electrochemistry is dramatic. Table 4 shows data from three peptides with the sequence XXDX.... Clearly the signal from Cu(II)–XXDX.. is low at 0.55 V, and higher at 0.8 V. This pattern reflects the chemistry of the tripeptide as expected for the purported structure of the complex. Though it has not yet been done, it can be predicted that these Cu(II) complexes will be stable even in mildly acidic conditions, and that rather selective detection of them at an anode will be possible because ordinary biuret complexes lose Cu(II) at such low pH values.

3.4. Example chromatograms

Fig. 9 shows the gradient separation of 100 μl of 50 n*M* non-electroactive peptides. The best signal-to-noise ratio comes from the cathode. The inserts show noise from two segments of the cathode voltammogram; the peak-to-peak noise is $6 \cdot 10^{-4}$–$8 \cdot 10^{-4}$ V, while the peak heights

Table 4
Sensitivities of XXDX.. peptides at 0.50 and 0.80 V (nC/pmol)

Peptide	Electrode potential (V)	
	0.50	0.80
RKDVY	11	57
RFDS	0.48	14
GFDLNGGGVG	0.24	10

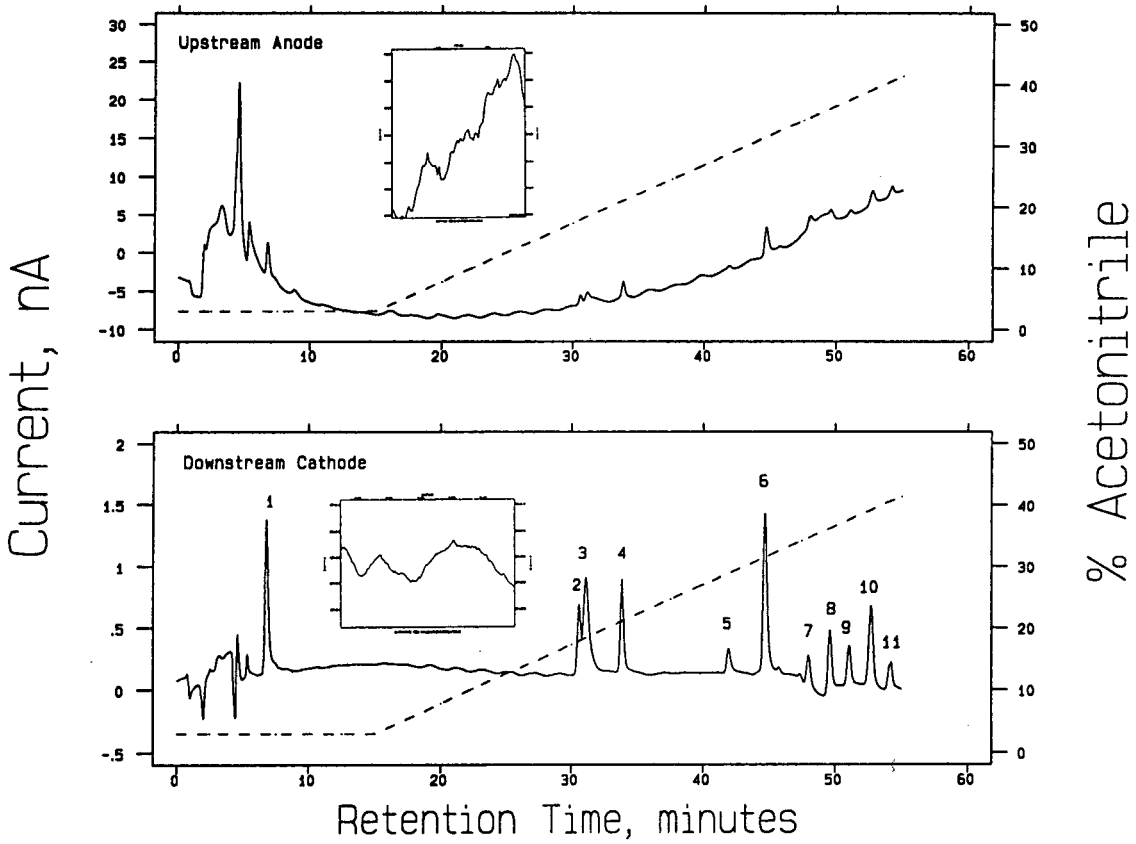

Fig. 9. Gradient elution chromatogram of the peptides in Table 2 (to which the numbers refer). Solvents A and B both have 0.1% TFAA and 3% 1-propanol; B also contains 60% acetonitrile. Gradient timing is shown with the dotted line. Post-column reagent: 0.5 m*M* Cu(II). Column and post-column temperatures 50°C. Upper chromatogram, anode 0.80 V, sensitivity 200 nA/V. Inset on upper, anode, trace is an expansion of the cathode trace's baseline at 40 min. It is 0.0006 V peak-to-peak. Lower chromatogram, cathode 0.09 V, sensitivity 10 nA/V. Inset is an expansion of the cathodic baseline at 38 min. It is 0.0008 V peak-to-peak.

range from about $2 \cdot 10^{-2}$ to 0.1 V. The signal to rms noise ratio is 3 when the signal is about $4 \cdot 10^{-4}$ V, which corresponds to the range of 20–100 fmol injected. Fig. 10 shows the anodic voltammogram (0.55 V) from the electroactive peptides. In this experiment, both electrodes were used as anodes at 0.55 V. The signal-to-noise ratio is better at the upstream electrode, ranging from 6–40 fmol injected. Table 5 shows linear regression results of calibration curves (0.5 V anode) for the electroactive peptides except for 1 and 2 which were not well-retained. Other than Tyr-somatostatin, which has been discussed and gives good sensitivity at 0.8 V, the curves are acceptable. It is hard to see in the curves, but there is some tendency among several peptides to lose sensitivity at low concentrations. This is undoubtedly due to adsorptive loss of the peptides which we have done nothing to prevent.

Fig. 11 shows the injection of 100 μl of 100 n*M* of a cytochrome *c* tryptic digest. Eleven peaks are expected; Fig. 11 shows clearly 10

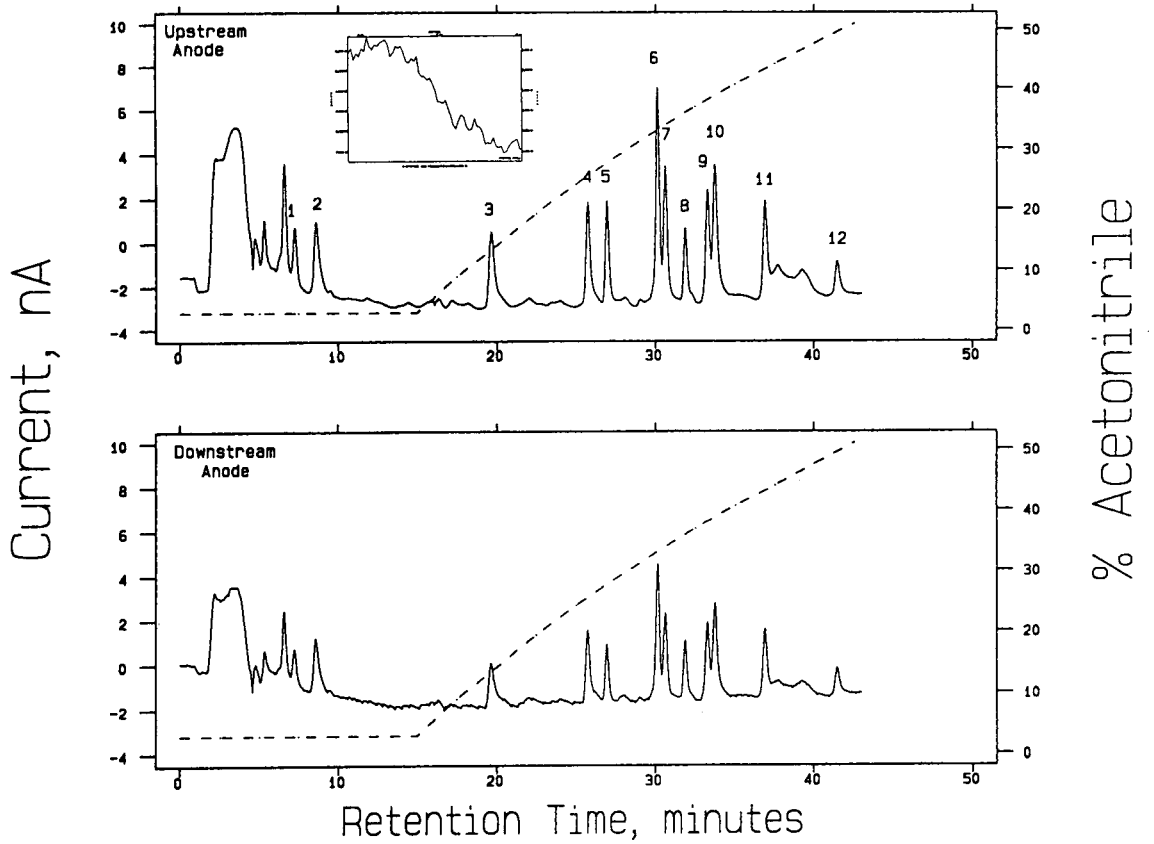

Fig. 10. Gradient elution chromatogram of the peptides in Table 3 (to which the numbers refer). Both solvents A and B have 0.1% TFAA and 3% 1-propanol; B also contains 60% acetonitrile. Gradient timing is shown with dotted line. Post-column reagent: 0.2 m*M* Cu(II). Column and post-column temperatures 50°C. Upper chromatogram, anode 0.55 V, sensitivity 100 nA/V. Inset on upper, anode, trace is an expansion of the anode trace's baseline at 11 min. It is 0.0005 V peak-to-peak. Lower chromatogram, also an anode at 0.55 V, sensitivity 100 nA/V.

Table 5
Linear regression results of some electroactive peptides obtained with an anodic applied potential of 0.55 V

Compound	Slope (nC/pmol)	*y*-Intercept (nC)	R^2
Lys^8-vasopressin	49	−4.7	0.995
Leucokinin II	36	1.6	0.985
Oxytocin	42	−3.2	0.999
Leu-enkephalin	88	−1.6	0.996
WMDF–NH_2	61	−5.1	0.999
Angiotensin II	32	−7.4	0.991
AHF 1–10	37	5.6	0.991
Neurotensin	72	−2.9	0.981
α-Endorphin	38	−9.1	0.997
Tyr-somatostatin	6.1	14	0.906

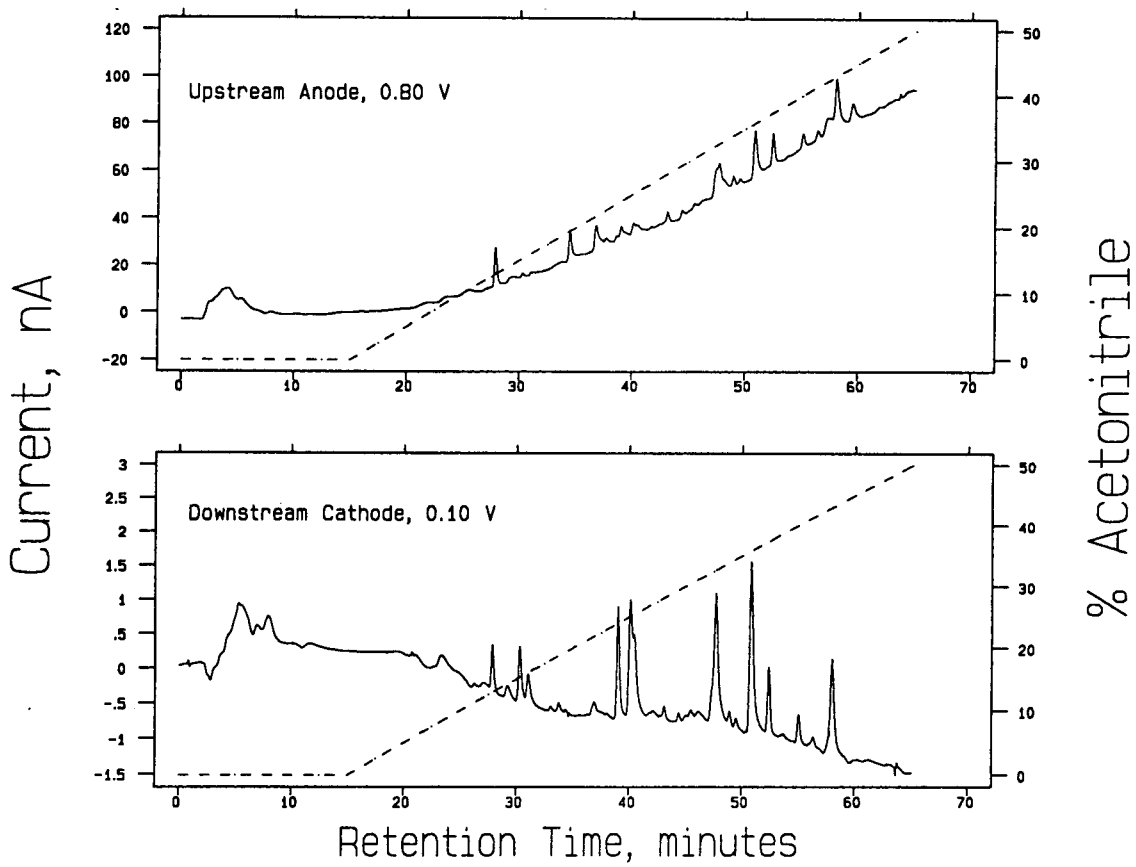

Fig. 11. Gradient elution of 100 n*M* tryptic digest fragments of cytochrome *c*. Both solvents A and B contain 0.1% TFAA; B also contains 3% 1-propanol and 60% acetonitrile. Gradient timing is shown with the dotted line. Post-column reagent: 0.5 m*M* Cu(II). Column and post-column temperatures 50°C. Top: anode at 0.8 V; bottom: Cathode at 0.10 V.

(cathode) one which, at about 48 min, is certainly a pair of peaks.

4. Conclusions

We have demonstrated the application of the biuret reaction for peptide detection with post-column reaction. Peptide sensitivities for electrochemical detection were predicted by model compound studies with the rotating ring-disc electrode. The Cu(II)–peptide electrochemistry of several classes of peptides has been characterized. The response of this detection technique was shown to be linear and to exhibit low detection limits for the oligopeptides studied, ranging from 0.16 to 4 n*M* for a 100-μl injection. Finally, the technique was applied to a tryptic digest of cytochrome *c*.

Acknowledgement

We are pleased to thank NIGMS for financial support through grant 44842.

References

[1] T. Hökfelt, *Neuron*, 7 (1991) 867.
[2] D. Liu, C. Dass, G. Wood and D.M. Desiderio, *J. Chromatogr.*, 500 (1990) 395.

[3] W.S. Hancock and D.R.K. Harding, in W.S. Hancock (Editor), *Handbook of HPLC for the Separation of Amino Acids, Peptides, and Proteins*, Vol. II, CRC Press, Boca Raton, FL, 1984, p. 3.
[4] J.R. Mazzeo and I.S. Krull, in N.A. Guzman (Editor), *Capillary Electrophoresis Technology*, Marcel Dekker, New York, 1993, p. 795.
[5] O. Orwar, S. Folestad, S. E. Einarsson, P. Andiné and M. Sandberg, *J. Chromatogr.*, 566 (1991) 39.
[6] R.G. Carlson, R.S. Srinivasachar and B.K. Matuszewski, *J. Org. Chem.*, 51 (1986) 3978.
[7] O. Orwar, M. Sandberg, M. Sundahl, S. Folestad and I. Jacobson, *Anal. Chem.*, in press.
[8] O. Orwar, M. Sandberg, S. Folestad, A. Tivesten, S.G. Weber and M. Sundahl, *J. Chromatogr.*, in press.
[9] A.M. Warner and S.G. Weber, *Anal. Chem.*, 61 (1989) 2664.
[10] H. Tsai and S.G. Weber, *J. Chromatogr.*, 542 (1991) 345.
[11] H. Tsai and S.G. Weber, *J. Chromatogr.*, 515 (1990) 451.
[12] L. Dou, J. Mazzeo and I.S. Krull, *BioChromatography*, 5 (1990) 74.
[13] L.H. Fleming and N.C. Reynolds, Jr., *J. Chromatogr.*, 431 (1988) 65.
[14] H. Tsai and S.G. Weber, *Anal. Chem.*, 64 (1992) 2897.
[15] H. Tsai and S.G. Weber, in preparation.
[16] W.J. Albery and M.L. Hitchman, *Ring-Disc Electrodes*, Clarendon Press, Oxford, 1971, p. 17.
[17] S.G. Weber and W.C. Purdy, *Anal. Chim. Acta*, 100 (1978) 531.
[18] D.W. Margerun, *Pure Appl. Chem.*, 55 (1983) 23.
[19] F.P. Bossu, K.L. Chellappa and D.W. Margerum, *J. Am. Chem. Soc.*, 99 (1977) 2195.
[20] M.P. Youngblood, K.L. Chellappa, C.E. Banniser and D.W. Margerum, *J. Am. Chem. Soc.*, 20 (1981) 1742.
[21] M.R. DeFelippis, C.P. Murthy, M. Faraggi and M.H. Klapper, *Biochemistry*, 28 (1989) 4847.
[22] S. Cheng, W.S. Craig, D. Mullen, Juerg. F. Tschopp, D. Dixon and M.D. Pierschbacher, *J. Med. Chem.*, 37 (1994) 1.
[23] B. Decock-Le Reverend, A. Lebkiri, C. Livera and L.D. Pettit, *Inorg. Chim. Acta.*, 124 (1986) L19.

ELSEVIER

Journal of Chromatography A, 691 (1995) 317–323

JOURNAL OF CHROMATOGRAPHY A

Separation of amino acids, peptides and proteins on molecularly imprinted stationary phases

Maria Kempe[1], Klaus Mosbach*

Pure and Applied Biochemistry, University of Lund, P.O. Box 124, S-221 00 Lund, Sweden

Abstract

Stationary phases, to be used in high-performance liquid chromatography, were tailor-made for the separation of amino acids, peptides and proteins. The stationary phases were prepared by molecular imprinting, applying two different approaches. Low-molecular-mass compounds were imprinted in bulk polymers by copolymerization of functional monomers and cross-linkers in the presence of the compound of interest, the print molecule. These polymers were, after extraction of the print molecule, successfully applied as chiral stationary phases, showing high resolution and load capacity. The development of a surface-imprinting approach for the preparation of stationary phases selective for proteins is also discussed.

1. Introduction

Molecular recognition plays a central role in interactions between biochemically important species. These interactions rely on selective binding between the recognition sites and the ligands. The aim in the design of synthetic receptors or binding sites has been to construct host systems possessing steric and electronic features complementary to those of the guest to be bound by the host. This has resulted in hosts such as crown ethers, cyclodextrins, cyclophanes and various molecular clefts and cavities [1–3].

Another approach to create receptor-like binding sites is molecular imprinting, sometimes referred to as template polymerization [4–6]. The binding sites are tailor-made by the copolymerization of functional monomers and cross-linkers in the presence of a print molecule. The print molecule is subsequently removed from the polymer, leaving recognition sites complementary to the print molecule in shape and in the positioning of functional groups. The polymer is able to selectively recognize and rebind the print molecule (Fig. 1). Molecularly imprinted polymers prepared according to this approach have proven to be useful as chiral stationary phases (CSPs) [7–15].

The technique of molecular imprinting can be applied to macromolecules too [16,17]. Glad et al. [18] published in 1985 a surface-imprinting approach for the preparation of adsorbents selective for the glycoprotein transferrin. In a more recent approach we have developed a method for the imprinting of proteins containing surface-exposed histidines [19].

Some aspects of the separation of amino acid

* Corresponding author.

[1] Present address: Department of Chemistry, University of Minnesota, 207 Pleasant Street S.E., Minneapolis, MN 55455, USA.

0021-9673/95/$09.50
SSDI 0021-9673(94)00820-5

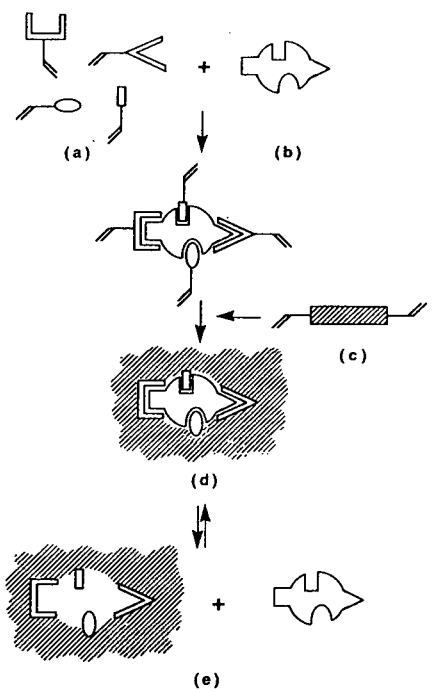

Fig. 1. Schematic representation of the concept of molecular imprinting. Functional monomers (a) interact non-covalently with a print molecule (b). Cross-linker (c) is added and the polymerization is initiated. The interactions between the functional groups of the polymer and the functional groups of the print molecule are maintained in the rigid bulk polymer (d). The print molecule is extracted from the polymer, leaving specific recognition sites, complememtary to the print molecule in the positioning of the functional groups and in shape (e). The polymer is able to selectively rebind the print molecule.

derivatives, peptides and proteins on molecularly imprinted stationary phases are detailed in this paper.

2. Experimental

2.1. Chemicals

Amino acid derivatives and peptides were purchased from Sigma (St. Louis, MO, USA), Bachem (Bubendorf, Switzerland), Nova Biochem (Läufelfingen, Switzerland) or synthesized according to König and Geiger [20] using N,N′-dicyclohexylcarbodiimide (DCC) and 1-hydroxybenzotriazole (HOBt) as coupling reagents. Methacrylic acid (MAA) and 2,2′-azoisobutyronitrile (AIBN) were obtained from Janssen Chimica (Geel, Belgium). Ethylene glycol dimethacrylate (EDMA) and 4-vinylpyridine (4VPy) were from Merck–Schuchardt (Germany). Trimethylolpropane trimethacrylate (TRIM) was from Aldrich (Steinheim, Germany). Bovine pancreas ribonuclease A (RNase A) and bovine serum albumin (BSA) were obtained from Sigma.

2.2. Preparation of bulk polymers

MAA and 4VPy were used as functional monomers. EDMA or TRIM were used as cross-linkers. Print molecule, functional monomer, cross-linker and solvent (according to the amounts given in Table 1) were mixed with the initiator AIBN. The mixtures were deoxygenated with a stream of nitrogen for 10 min and then irradiated at 366 nm for 24 h in 4°C (polymers 1, 2, 5 and 6) or −20°C (polymers 3 and 4). The bulk polymers were ground in an end runner mill Model RM O (Retsch, Haan, Germany) and wet-sieved by hand with water

Table 1
Polymer compositions

Polymer	Print molecule, mmol	Functional monomer, mmol	Cross-linker, mmol	Polymerization solvent, ml
1	Boc–L-Phe–OH, 2.5	MAA, 10	EDMA, 50	Chloroform, 15
2	Z–L-Phe–OH, 2.5	MAA, 10	EDMA, 50	Chloroform, 15
3	Z–L-Asp–OH, 1.0	4VPy, 12	EDMA, 60	Tetrahydrofuran, 18
4	Z–L-Glu–OH, 1.0	4VPy, 12	EDMA, 60	Tetrahydrofuran, 18
5	Z–L-Ala–L-Ala–OMe, 5.0	MAA, 30	TRIM, 30	Chloroform, 20
6	Z–L-Ala–Gly–L-Phe–OMe, 3.75	MAA, 30	TRIM, 30	Chloroform, 20

and ethanol through a 25-μm sieve (Retsch). The particles which passed the sieve were collected and dried on a sintered glass funnel. The particles were sedimented in acetone and the fines were removed by decantation.

2.3. High-performance liquid chromatography

The sieved and sedimented particles were slurried in chloroform–acetone (17:3, v/v) and packed with acetone as solvent into stainless-steel HPLC columns at 300 bar using an air-driven fluid pump (Haskel, Burbank, USA). The print molecules were extracted from the polymers by eluting with methanol–acetic acid (9:1, v/v) (polymers 1 and 2), tetrahydrofuran–acetic acid (7:3, v/v) (polymers 3 and 4) or methanol–acetic acid (7:3, v/v) (polymers 5 and 6). The HPLC analyses were performed using a Kontron HPLC comprising a Model 420 HPLC pump, a Model 425 gradient former and a Model 432 variable-wavelength absorbance detector. The pump was controlled by a Toshiba T 1000 personal computer. The elutions were performed at ambient temperature and monitored spectrophotometrically at 260–265 nm.

2.4. Preparation of protein-imprinted silica particles

Methacrylate silica and N-(4-vinyl)-benzyl iminodiacetic acid were prepared as previously described [19]. The RNase A-imprinted silica (prepared in the presence of RNase A) and the reference silica (prepared in the presence of BSA) were also prepared as previously described [19].

2.5. Chromatographic evaluation of protein-imprinted stationary phases

The silica particles were slurried in water–N,N-dimethylformamide (7:3, v/v) and packed at 200 bar into PTFE-coated stainless-steel columns (50 × 4.6 mm) with water–N,N-dimethylformamide (7:3, v/v) as packing solvent. The chromatographic evaluation was performed in the HPLC mode using the same HPLC system as described above. The flow-rate was 0.5 ml/min and the elution was monitored spectrophotometrically at 280 nm. The columns were washed by injecting 5 ml 0.1 *M* EDTA and 5 ml 6 *M* urea, repeated five times each. The eluents for the separation studies were [20 m*M* 4-(2-hydroxyethyl)-1-piperazineethanesulphonic acid (HEPES) pH 7.0, 0.5 *M* NaCl]–N,N-dimethylformamide (7:3, v/v) with and without 0.5 m*M* $ZnCl_2$.

3. Results and discussion

3.1. Molecularly imprinted bulk polymers

Molecularly imprinted bulk polymers, selective for various amino acid derivatives and peptides were prepared by copolymerization of functional monomers and cross-linkers in the presence of the print molecules (Table 1). The functional monomers were chosen so as to interact non-covalently with the functional groups of the print molecules. The polymers were prepared with varying molar ratios of monomers to print molecules. The ground, sieved and extracted polymers were used as stationary phases in HPLC. The polymers described in Table 1 resulted in the highest separation factors of the polymers prepared.

A MAA–EDMA copolymer imprinted with the N^{α}-protected amino acid Boc–L-Phe–OH (Boc = *tert.*-butyloxycarbonyl) (polymer 1, Table 1) was investigated by frontal chromatography [9]. The dissociation constant for Boc–L-Phe–OH was determined to be lower than for Boc–D-Phe–OH (6.3 and 8.1 m*M*, respectively). This shows that the affinity for the L-enantiomer was higher than for the D-enantiomer, as was expected since the L-enantiomer was used as print molecule. The number of binding sites giving rise to these dissociation constants were equal for both enantiomers (28 μmol/g dry polymer).

To obtain a stereospecific recognition, a "three-point" interaction is required [21]. In the case of a polymer imprinted with an N^{α}-protected amino acid and prepared using MAA as the functional monomer, it is believed that the

carboxy and carbamate functions of the print molecule interact via hydrogen bonds with the positioned carboxy groups of the polymer (Fig. 2). This gives, however, only two interaction points. Therefore, at least one additional interaction must exist to explain the observed stereospecific recognition. A polymer imprinted with Z–L-Phe–OH (Z = benzyloxycarbonyl) (polymer 2, Table 1) was able to resolve racemic Z–Phe–OH with a separation factor (α) of 1.84 (Table 2). Changing the N^{α}-protecting group of the racemic phenylalanine derivative to be separated on the CSP to Boc, 9-fluorenylmethyloxycarbonyl (Fmoc) or acetyl (Ac), instead of Z, resulted in lower separation factors (Table 2). The same trend, i.e. low separation factors with non-imprinted molecules, was seen when these racemates were separated on Boc–L-Phe–OH- and Fmoc–L-Phe–OH-imprinted polymers. Changing the amino acid side chain of the racemate to be separated on the Z–L-Phe–OH-imprinted stationary phase from that of phenylalanine (Z–Phe–OH) to that of alanine (Z–Ala–OH) also resulted in a lower separation factor (Table 2). This shows that both the N^{α}-protecting group and the amino acid side chain interacts with, and are recognized by the binding sites in the polymer [12].

A Boc–L-phenylalanine anilide-imprinted MAA–EDMA copolymer was able to resolve the racemate of the print molecule efficiently ($\alpha = 2.95$). Racemic Boc–phenylalanine *p*-nitroanilide and racemic Boc–phenylalanine glycine ethyl ester were less well resolved on this CSP ($\alpha = 1.68$ and 1.52, respectively), showing that also the C^{α}-protecting group of the amino acid is of importance for the recognition [12].

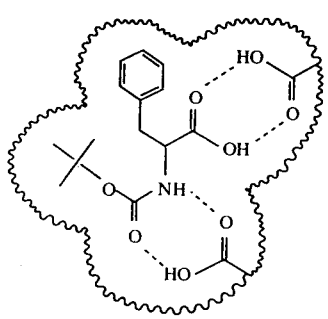

Fig. 2. Schematic representation of Boc–Phe interacting with the carboxyl groups of the polymer via hydrogen bonds.

Table 2
The influence of the N^{α}-protecting group and the amino acid side chain in the recognition

Separated species	Separation factor (α)[a]
Z–D,L-Phe–OH	1.84
Boc–D,L-Phe–OH	1.31
Fmoc–D,L-Phe–OH	1.21
Ac–D,L-Phe–OH	1.21
Z–D,L-Ala–OH	1.28

Separation of 80 nmol of the indicated racemates on a Z–L-Phe–OH-imprinted CSP (polymer I) using isocratic elution with chloroform as the eluent at 0.5 ml/min (column size: 100 × 4.5mm).

[a] The separation factor (α) was calculated as $\alpha = (t_L - t_0)/(t_D - t_0)$, where t_L and t_D are the retention times of the L- and the D-enantiomer, respectively, and t_0 is the void volume.

The most widely applied functional monomer in non-covalent molecular imprinting is MAA. It has been shown to interact via ionic interactions with amines on the print molecules and via hydrogen bonds with amides, carbamates and carboxyls on the print molecules. The introduction of 4VPy as a functional monomer in non-covalent molecular imprinting made ionic interactions between the recognition sites of the polymers and print molecules containing the carboxy group possible [10]. 4VPy–EDMA copolymers prepared in the presence of Z–L-Asp–OH (polymer 3, Table 1) or Z–L-Glu–OH (polymer 4, Table 1) were able to resolve racemic mixtures of their respective print molecules. Resolution of the racemate of Z–Glu–OH on the Z–L-Asp–OH-imprinted polymeric CSP was not possible. The reverse was also not possible, namely the separation of Z–D,L-Asp–OH on the Z–L-Glu–OH-imprinted stationary phase. Z–Asp–OH and Z–Glu–OH differ by only one methylene group. Despite this small

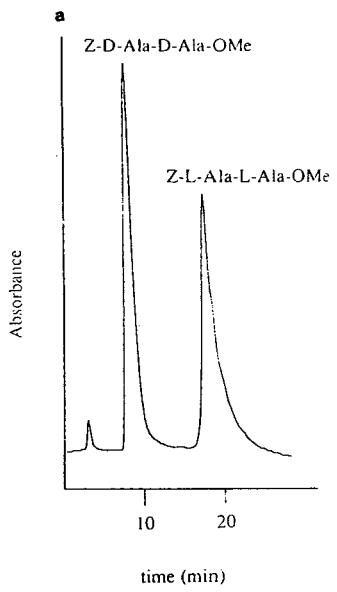

Fig. 3. Separation of mixtures of Z–L-Ala–L-Ala–OMe and Z–D-Ala–D-Ala–OMe on a Z–L-Ala–L-Ala–OMe-imprinted CSP (polymer 5) packed into an HPLC-column (250 × 4.6 mm). (a) A 100-μg amount was separated using gradient elution at 1 ml/min with chloroform–acetic acid (99.75:0.25) and chloroform–acetic acid (8:2) (A) as the eluents (gradient: 0–10 min, 0% A; 10–18 min, 0–5% A; 18–22 min, 5% A; 22–24 min, 5–0% A). (b) A 1-mg amount was separated using isocratic elution at 1 ml/min with chloroform–acetic acid (99.75:0.25) as the eluent.

difference, the imprinted polymers are able to discriminate between the species.

Molecularly imprinted polymers with high load capacity and excellent resolving capability were prepared using the branched cross-linker TRIM [13,14]. Fig. 3a shows the resolution of 100 μg of a racemic mixture of the dipeptide Z–Ala–Ala–OMe on a Z–L-Ala–L-Ala–OMe-imprinted MAA–TRIM copolymer (polymer 5, Table 1) packed into an analytical column (250 × 4.6 mm). Gradient elution was used to enhance the elution rate of the enantiomer used as print molecule, since it was much more retarded than the non-imprinted optical antipode. The separation factor was 3.2 and the resolution factor was 4.5. The load capacity of MAA–TRIM copolymers are higher than what has been reported for MAA–EDMA copolymers. Fig. 3b shows the elution profile when 1 mg was sepa-

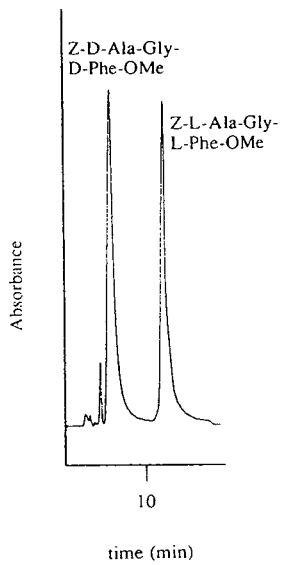

Fig. 4. Separation of 100 μg of a mixture of Z–L-Ala–Gly–L-Phe–OMe and Z–D-Ala–Gly–D-Phe–OMe on a Z–L-Ala–Gly–L-Phe–OMe-imprinted CSP (polymer 6) packed into an HPLC column (250 × 4.6 mm) using gradient elution at 1 ml/min with chloroform–acetic acid (99:1) and chloroform–acetic acid (9:1) (A) as the eluents (gradient: 0–7 min, 0% A; 7–9 min, 0–100% A; 9–17 min, 100% A; 17–22 min, 100–0% A).

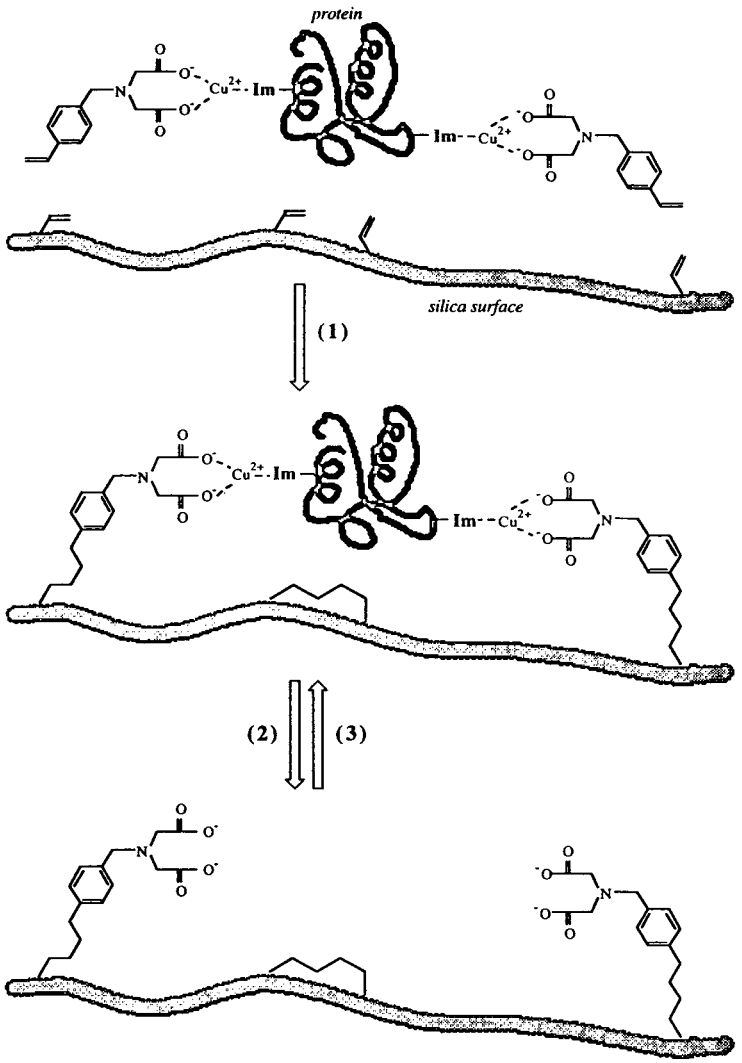

Fig. 5. Schematic representation of protein imprinting on silica-surfaces derivatized with methacrylate groups. Imidazole groups (Im) of surface-exposed histidines on the protein and the monomer N-(4-vinyl)-benzyl iminodiacetic acid coordinate metal ions. The derivatized silica particles are added and the polymerization is initiated (1). The protein and the metal ions are subsequently removed, e.g. by treatment with EDTA (2). The metal-binding ligands are positioned so as to, in the presence of metal ions, selectively recognize and rebind the protein (3).

rated using isocratic elution. The enantiomers were resolved with almost baseline resolution.

Another example of a chiral separation on an imprinted MAA–TRIM copolymer is shown in Fig. 4. A mixture of Z–L-Ala–Gly–L-Phe–OMe and Z–D-Ala–Gly–D-Phe–OMe was resolved on a CSP imprinted against Z–L-Ala–Gly–L-Phe–OMe (polymer 6, Table 1) with a separation factor of 3.6 and a resolution factor of 4.1.

3.2. Surface imprinting of proteins

A metal-binding monomer, N-(4-vinyl)-benzyl iminodiacetic acid, and the imidazole groups of the surface-exposed histidines of RNase A were allowed to coordinate metal ions, as shown schematically in Fig. 5 [19]. Silica particles, derivatized with methacrylate groups, were added and the polymerization was initiated. The

protein was subsequently removed by treatment with EDTA and urea. The resulting silica particles were used as a stationary phase in HPLC. This RNase A-imprinted stationary phase was compared with a stationary phase consisting of silica particles prepared in the presence of BSA instead of RNase A. It was concluded that the RNase A-imprinted stationary phase showed, in the presence of metal ions, higher affinity for RNase A than what the reference stationary phase did.

4. Conclusions

Molecular imprinting has proven to be a useful technique for the preparation of stationary phases selective for amino acid derivatives, peptides and proteins. The technique can also be applied to other types of compounds, exemplified by β-adrenergic blockers [15] and non-stereoidal anti-inflammatory drugs [11]. The polymers are easily prepared, inexpensive and possess excellent chemical, physical and mechanical stability.

References

[1] J.-M. Lehn, *Angew. Chem., Int. Ed. Engl.*, 27 (1988) 89.
[2] J. Rebek, Jr., *Angew. Chem., Int. Ed. Engl.*, 29 (1990) 245.
[3] D.J. Cram, *Nature*, 356 (1992) 29.
[4] B. Ekberg and K. Mosbach, *Trends Biotechnol.*, 7 (1989) 92.
[5] G. Wulff, *Trends Biotechnol.*, 11 (1993) 85.
[6] K. Mosbach, *Trends Biochem. Sci.*, 19 (1994) 9.
[7] D.J. O'Shannessy, B. Ekberg, L.I. Andersson and K. Mosbach, *J. Chromatogr.*, 470 (1989) 391.
[8] L.I. Andersson and K. Mosbach, *J. Chromatogr.*, 516 (1990) 313.
[9] M. Kempe and K. Mosbach, *Anal. Lett.*, 24 (1991) 1137.
[10] M. Kempe, L. Fischer and K. Mosbach, *J. Mol. Recogn.*, 6 (1993) 25.
[11] M. Kempe and K. Mosbach, *J. Chromatogr. A*, 664 (1994) 276.
[12] M. Kempe and K. Mosbach, *Int. J. Pept. Prot. Res.*, in press.
[13] M. Kempe and K. Mosbach, submitted for publication.
[14] M. Kempe, in preparation.
[15] L. Fischer, R. Müller, B. Ekberg and K. Mosbach, *J. Am. Chem. Soc.*, 113 (1991) 9358.
[16] M. Glad, M. Kempe and K. Mosbach, *Pat. Appl. Sweden*, SE 9102622-9.
[17] M. Glad, M. Kempe and K. Mosbach, *Pat. Appl.*, PCT/SE92/00610.
[18] M. Glad, O. Norrlöw, B. Sellergren, N. Siegbahn and K. Mosbach, *J. Chromatogr.*, 347 (1985) 11.
[19] M. Kempe, M. Glad and K. Mosbach, *J. Mol. Recogn.*, (1994) in press.
[20] W. König and R. Geiger, *Chem. Ber.*, 103 (1970) 788.
[21] C.E. Dalgliesh, *J. Chem. Soc.*, 137 (1952) 3940.

ELSEVIER

Journal of Chromatography A, 691 (1995) 325–330

JOURNAL OF CHROMATOGRAPHY A

Separation and analysis of proteins by perfusion liquid chromatography and electrospray ionization mass spectrometry

J. Fred Banks, Jr.

Analytica of Branford, Inc., 29 Business Park Drive, Branford, CT 06405, USA

Abstract

Perfusion LC has been interfaced with electrospray ionization mass spectrometry (ESI-MS) for the rapid separation and molecular mass determination of proteins. The combination of this unique chromatographic system and the multiply charged envelope of the ESI-MS data allows this analysis to be accomplished in just a few minutes when using the optimum conditions determined. The performance of the perfusion system has been compared to both 1 mm I.D. and 320 μm I.D. columns packed with conventional C_{18} media.

1. Introduction

The use of electrospray ionization (ESI) for the interfacing of mass spectrometry (MS) and liquid chromatography (LC) as developed by Fenn and co-workers [1–3] has been proven to both desolvate and ionize fragile chemical species, such as proteins, peptides, nucleic acids and pharmacologically active compounds, from solution for transport to a mass analyzer.

One of the characteristic and unique features of this particular "soft" ionization technique when used for the analysis of proteins is the generation of a distribution of ions with a varying large number of charges. The number of charges can be as high as 1 per every 500 u of the protein's molecular mass and results in the production of a complex mass spectrum with a multiply charged envelope which has peaks appearing at many masses. Because the number of charges appearing on each ion population differs by an integral amount from any other population, these individual contributions to the total spectra can be "deconvoluted" to calculate the molecular mass of the entire protein molecule [4,5]. Since there is a great quantity of information contained within the multiply charged envelope, the accuracy of this calculation can be very high, such that a protein having a molecular mass of tens of thousands can be identified to within 1 u.

A second consequence of the appearance of highly charged ions, is that these species appear at a substantially reduced range on the m/z scale, and therefore fall within the range of most conventional mass analyzers. This result is also largely responsible for ESI's proven ability to determine accurately the molecular mass of proteins weighing over 100 000 u.

The promising combination of using on-line protein LC separations coupled with ESI-MS detection has been hampered, however, by an incompatibility between the LC mobile phase and solvent which can be electrosprayed. Specifically, the inclusion of 0.1% trifluoroacetic acid (TFA) in the LC mobile phase, a practice commonly used in protein and peptide separations, inhibits the electrospray process re-

0021-9673/95/$09.50
SSDI 0021-9673(94)01033-1

sulting in complete loss of ion signal. Also, the flow-rates used for LC are usually considerably higher than the optimum flow-rate of 1 μl/min or less required for optimum ESI-MS. Fortunately, this difficulty has been solved through the development of a number of assisted-ESI techniques, such as pneumatically assisted nebulization [6–8] and ultrasonically assisted nebulization [9].

Perfusion LC [10–13] is rapidly becoming a useful technique for the analysis of peptides and proteins. The unique chromatographic media used is characterized by both a primary liquid flow path through large internal pores (6000–8000 Å) and a secondary diffusive path through smaller pores (300 Å). Because the mobile phase carrying the analytes flows through the interior of the particles, instead of mostly around them, this medium is particularly beneficial when working with larger species which have smaller diffusion constants. The result of employing this chromatographic medium in a column format is the reduction by 5- to 10-fold of the total analysis time, as compared with a conventional column, required to successfully complete a peptide or protein separation. A related effect is the reduction of chromatographic peak widths so that under optimum conditions, proteins or peptides completely elute in 5–10 s.

This paper explores the performance obtained from the coupling of perfusion LC, a new type of high-performance liquid chromatography, with ESI-MS for the analysis of proteins. The investigations presented here focus on several areas. The first is the effect of LC conditions, i.e. mobile phase flow-rate, on performance followed by deconvolution of a protein LC peak and a sensitivity study. The second is a comparison of performance for the separation and detection of a protein mixture by ESI-MS between the perfusion LC column and 1 mm I.D. and 320 μm I.D. columns packed with conventional media. This particular comparison is interesting since the 320 μm I.D. column has the same physical dimensions as the perfusion column, while the 1 mm I.D. column operates at a similar flow-rate to the perfusion column.

2. Experimental

2.1. Apparatus

The pump used for mobile phase delivery in all cases was a dual-syringe type, Model ABI 140A from Applied Biosystems (Foster City, CA, USA). For the 320 μm I.D. perfusion column and the 1 mm I.D. "microbore" column, the pumping system was used without modification. However, in order to deliver linear gradients at low flow-rates suitable for the 320 μm I.D. "packed-capillary" column, a flow-splitting device consisting of a simple tee with a fused-silica restrictor was constructed. With this system, the pump was operated at 50 μl/min, and the resulting flow was measured at 4.7 μl/min optimum for this column. This system was rugged and provided reproducible results, so it was used for all these particular studies. Sample injection was accomplished for all columns with a Valco Instruments (Houston, TX, USA) CI4W valve having a 1-μl internal loop.

The microbore or 15 cm × 1 mm I.D. column was purchased from Vydak (Hesperia, CA, USA) and was packed with 5-μm C_{18} particles. The perfusion LC column was purchased from LC Packings (San Francisco, CA, USA) and was 15 cm × 320 μm I.D. This column was packed with 10-μm Poros II medium from Perceptive Biosystems (Cambridge, MA, USA). The packed-capillary column was fabricated from 320 μm I.D. fused-silica from Polymicro Technologies (Phoenix, AZ, USA) and was 15 cm in length as well. The reversed-phase packing material used was again the C_{18} 5-μm particle size from Vydak.

The electrospray ionization source was similar to that developed at Yale [1–3] except that an ultrasonic nebulizer [9] was substituted for the original needle assembly. This particular source design allowed independent control of the source potentials on the needle (V_{need}), cylindrical electrode (V_{cyl}), nosepiece (V_{nose}) and capillary entrance (V_{ent}). With this configuration, the system was always operated with V_{need} = ground in order to protect the user from electrical shock and isolate the LC system from high voltage. Drying-

gas temperature was always set to 300°C. The mass spectrometer (HP89A) was from Hewlett-Packard (Palo Alto, CA, USA).

2.2. Materials

Protein samples were obtained from Sigma (St. Louis, MO, USA). At the time of injection, these samples were dissolved at the appropriate concentration in a mobile phase composition which was identical to the beginning of the LC gradient used. All water was obtained from a Barnstead (Boston, MA, USA) NANOpure II system. Acetonitrile (ACN) was purchased from Mallinckrodt (Paris, KY, USA). All solvents were filtered through nylon 66 membranes from Anspec (Ann Arbor, MI, USA). TFA was also obtained from Mallinckrodt.

3. Results and discussion

3.1. Effect of mobile phase flow-rate on performance of a perfusion column

In order to determine the optimum mobile phase flow-rate for this system, a mixture of proteins containing ubiquitin, cytochrome *c* and myoglobin (30 pmol each) was injected on the column in a series of experiments where the flow-rate was varied from 25 to 125 μl/min in increments of 25 μl/min. While the flow-rate was increased, the identical gradient conditions were maintained as a linear ramp from 20 to 90% ACN in water (with 0.1% TFA) in 5 min. Total ion current (TIC) was recorded as the quadrupole mass analyzer was scanned from 500 to 1300 *m/z* units. This resulting series of TIC traces at increasing mobile phase flow-rates is shown in Fig. 1. Of the trends seen here, perhaps the most important and significant is the reduction in total analysis time required as the flow-rate was increased. At the maximum value used, 125 μl/min, the time required to complete this separation was just over 3 min, considerably less than the time required at 25 μl/min. Furthermore, the resolution between the first two eluting species (ubiquitin and cytochrome *c*)

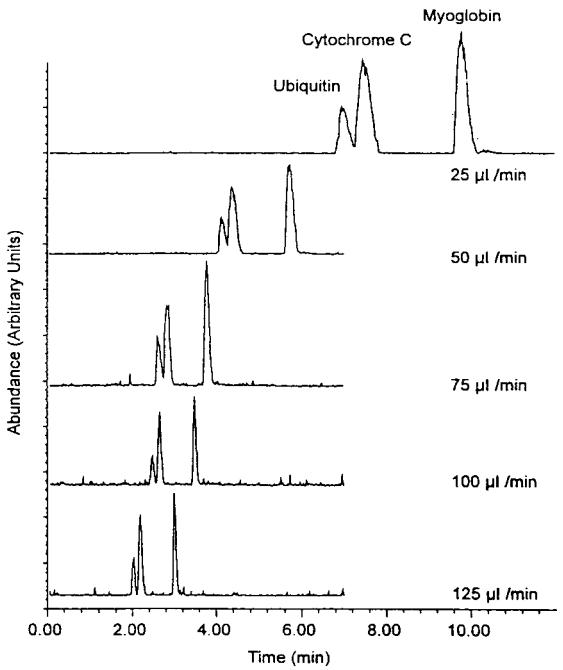

Fig. 1. Effect of mobile phase flow-rate on the TIC from a separation of a protein mixture. Gradient: 20–90% ACN in water (0.1% TFA) in 5 min.

and column efficiency was maintained at nearly the same value as the flow-rate was increased. This relatively "flat" Van Deemter response is one of the characteristics which makes perfusion LC so attractive and allows much higher than normal flow-rates to be employed. Proteins have especially low diffusion constants so these species are expected to benefit greatly from the large pore structure of the perfusion media.

Another notable effect of employing the perfusion material was a considerable reduction in chromatographic peak widths, which ranged from 5–10 s, depending on the protein, for the 125 μl/min separation. This and the overall analysis time might be improved with even higher flow-rates still, but the back pressure on this particular system was already precariously high at 2600 p.s.i. (1 p.s.i. = 6894.76 Pa), so no further increases in flow-rate were attempted. At a peak width of just 5 s, only five data points could be taken as a protein eluted when operating the mass analyzer at its maximum scan

speed, approximately 1 scan/s. Increasing the scan speed much beyond this point begins to degrade the mass spectral resolution due to ion statistics or ultimately, the flight time of an ion through the quadrupole rods. Scanning too fast causes the ion population being analyzed to be exposed to a changing radio frequency (rf) field. Because the quality of individual scans is good, five data points when averaged together seem sufficient to give good results. This is demonstrated in Fig. 2, which shows an average of the scans taken during the elution of the 5-s cytochrome *c* peak in the 125 μl/min separation from Fig. 1. It is important to note that further reduction in peak widths will mandate the use of a mass analyzer with faster scan rate capabilities, such as a time-of-flight mass spectrometer. Finally, the averaged spectra in Fig. 2 could be deconvoluted (Fig. 3) via a simple algorithm [4] to give the molecular mass of the protein. The value determined here, 12 359.51 u, is within 0.004% of the accepted molecular mass of cytochrome *c* at 12 360 u, thus differing by approximately 0.5 u.

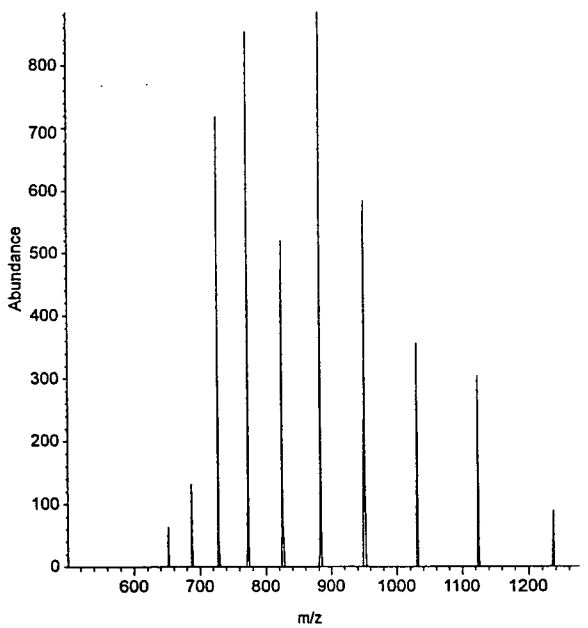

Fig. 2. Average of scans during the elution of cytochrome *c* at a mobile phase flow-rate of 125 μl/min on the perfusion column.

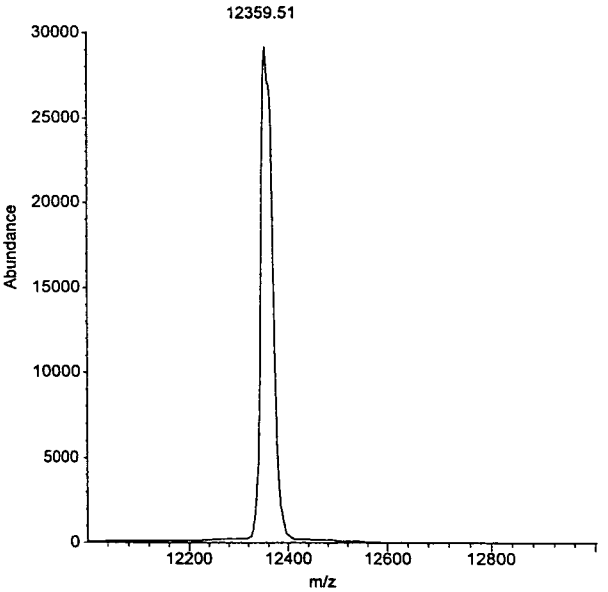

Fig. 3. Deconvolution of cytochrome *c* from MS data in Fig. 2.

3.2. Linear dynamic range and limit of detection of a perfusion column

Using the optimized flow-rate above, 125 μl/min, the linear dynamic range (LDR) for injections of cytochrome *c* with this system was determined both in scan mode (500–1300 *m/z*) and selected ion monitoring (SIM) mode (825 *m/z*). These data are shown in Fig. 4. The response in both scan and SIM were both linear until approximately 200 pmol, were injected. The limit of detection (LOD) in SIM mode was found to be 64 fmol while the LOD in scan mode was found to be 1600 fmol. The difference here is as expected and similar to other LC methods. The much higher LOD in scan mode is the result of both increased background noise, normally seen while scanning many more *m/z* channels, and greatly decreased signal averaging, also encountered in the scan mode of operation.

Future work will concentrate on the prepara-

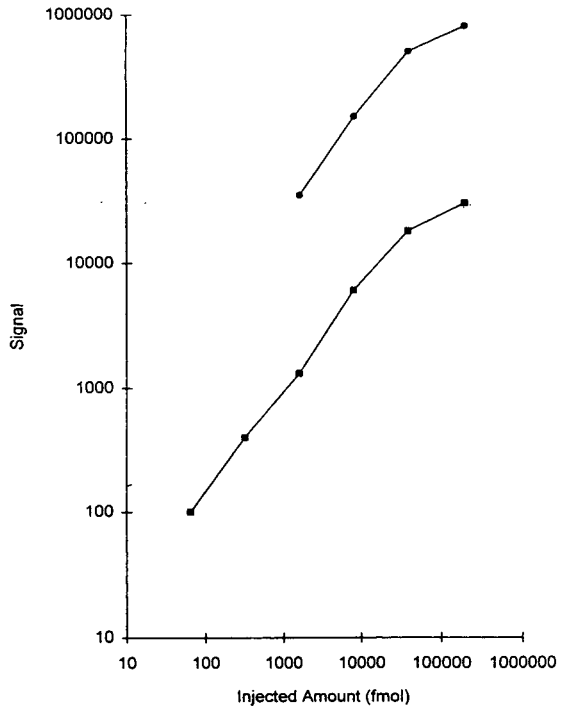

Fig. 4. Signal vs. concentration of cytochrome *c* from scan (●) and SIM (□) modes of MS operation using perfusion column.

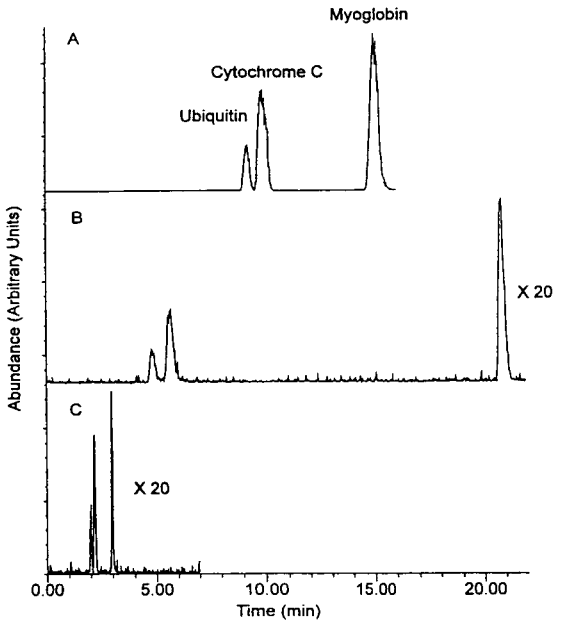

Fig. 5. Comparison of TIC from a protein mixture with different columns using best conditions for each: (A) 320 μm I.D. capillary column packed with conventional media, gradient: 30–90% ACN in water (0.1% TFA) in 30 min, (B) 1.0 mm I.D. microbore column also packed with conventional media, gradient: 25–90% ACN in water (0.1% TFA) in 15 min, (C) perfusion column, 20–90% ACN in water (0.1% TFA) in 5 min.

tion and use of even smaller column diameters and more sensitive detection in order to increase the linear dynamic range at the lower end.

3.3. Comparison of perfusion to packed-capillary and microbore LC with conventional packing media

In a final set of experiments, performance of this system was compared with both packed-capillary (320 μm I.D.) and microbore (1.0 mm I.D.) columns packed with conventional C_{18} media. This comparison is interesting, since the packed-capillary column has the same diameter as the perfusion column, while the 1 mm I.D. column has a similar optimum flow-rate as the perfusion LC column. Fig. 5 summarizes the results of these experiments where the same mixture of proteins (30 pmol each) was injected onto the columns under their respective ideal operating conditions. This figure shows the resulting TICs obtained when the quadrupole mass analyzer was scanned from 500–1300 m/z units.

Fig. 5A is the TIC from the 15 cm × 320 μm I.D. capillary column packed with the conventional Vydak C_{18} 5-μm particles. The total analysis time was approximately 15 min. Fig. 5B is the TIC from the 15 cm × 1 mm I.D. microbore column, also packed with the conventional Vydak C_{18} 5-μm particles. The analysis time, being approximately 21 min, does not differ markedly from the 320 μm I.D. microcolumn. However, the sensitivity of the 1.0 mm column is nearly 20-fold less than the 320 μm capillary column. This result is as expected, since the relative sensitivity of two LC columns of otherwise equal character, is known to vary by the

inverse of the square of the two radii. In this case, that calculation gives a gain of at least a factor of 10. Finally, Fig. 5C shows the TIC obtained from the 320 μm I.D. perfusion column. The sensitivity here is again approximately 20-fold less than the packed-capillary column yields yet is essentially equal to the sensitivity of the microbore column. Dramatically different, however, was the total analysis time required. With the perfusion column, the entire separation was completed in just 3 min. This is nearly 7 times faster than the 1 mm I.D. column and 5 times faster than the 320 μm I.D. columns packed with conventional media. These results are similar to those reported by Kassel et al. [14] where the performance of peptides on perfusion, packed-capillary and microbore LC–MS systems was evaluated.

4. Conclusions

In these studies, it has been shown that the use of the perfusion media in an LC column format allows for a reduction in analysis time for a protein mixture of at least a factor of 5, as compared to either a 1.0 mm I.D. column or a 320 μm I.D. column packed with conventional media. Care was taken in this study to maintain the chromatographic resolution between two of the eluting species across the range of columns used so that the comparisons would be fair. The optimum mobile phase flow-rate for the perfusion column was found to be 125 μl/min, which generated peak widths of between 5 and 10 s. This flow-rate is approximately 25-fold higher than would be expected from a column of the same diameter but packed with conventional media. Using the perfusion column, an average of five scans recorded during the elution of cytochrome *c* was sufficient to allow the deconvolution of the multiply charged envelope appearing in the mass spectrum and determine the molecular mass of this protein to within 1 u.

The results also show that both the 1 mm I.D. column packed with conventional media and the perfusion column suffer a signal loss of approximately 20-fold, compared to the 320 μm I.D. column packed with conventional media. For this reason, future work will focus on the development and use of even smaller-I.D. columns with the perfusion media in order to recover some of this sensitivity.

References

[1] M. Yamashita and J.B. Fenn, *J. Phys. Chem.*, 88 (1984) 4671.
[2] M. Yamashita and J.B. Fenn, *J. Phys. Chem.*, 88 (1984) 4451.
[3] C.M. Whitehouse, R.N. Dreyer, M. Yamashita and J.B. Fenn, *Anal. Chem.*, 57 (1985) 675.
[4] M. Mann, C. Meng and J.B. Fenn, *Anal. Chem.*, 61 (1989) 1702.
[5] M. Labowski, C. Whitehouse and J. Fenn, *Rapid Commun. Mass Spectrom.*, 7 (1993) 71.
[6] E.D. Lee, W. Muck, T.R. Covey and J.D. Henion, *Anal. Chem.*, 18 (1989) 844.
[7] A.P. Bruins, L.O.G. Weidolf, J.D. Henion and W.L. Budde, *Anal. Chem.*, 59 (1987) 2647.
[8] A.P. Bruins, T.R. Covey and J.D. Henion, *Anal. Chem.*, 59 (1987) 2642.
[9] J.F. Banks, S. Shen, C.M. Whitehouse and J.B. Fenn, *Anal. Chem.*, 66 (1994) 406.
[10] N.B. Afeyan, S.P. Fulton and F.E. Regnier, *LC·GC*, 9 (1991) 824.
[11] N.B. Afeyan, S.P. Fulton and F.E. Regnier, *J. Chromatogr.*, 544 (1991) 267.
[12] S.P. Fulton, N.B. Alfeyan, N.F. Gordon and F.E. Regnier, *J. Chromatogr.*, 547 (1991) 452.
[13] F.E. Regnier, *Nature*, 350 (1991) 634.
[14] D.B. Kassel, B. Shushan, T. Sakumua and J.P. Salzmann, *Anal. Chem.*, 66 (1994) 236.

ELSEVIER

Journal of Chromatography A, 691 (1995) 331–336

JOURNAL OF CHROMATOGRAPHY A

High-performance liquid chromatographic assay of glycosyltransferases using flavonoids as substrate

Mario Pace*, Dario Agnellini, Claudio Gardana, Pier Luigi Mauri, Pier Giorgio Pietta

Dipartimento di Scienze e Tecnologie Biomediche, Sez. Chimica Organica, Università di Milano, Via G. Celoria 2, 20133 Milan, Italy

Abstract

An HPLC method for the determination of glycosyltransferase activity, alternative to the radioactive assay, is proposed. The method is suitable for following the kinetics of consecutive enzymes that yield monoglucosides, diglucosides and triglucosides, as demonstrated with a pea seedling extract containing a mixture of three glucosyltransferases using flavonoids as substrate and UDP-glucose as carbohydrate donor. In this instance the HPLC determination of the three glucosides could be accomplished after separation of the aglycones by solid extraction on a Sep-Pak C_{18} microcolumn. After isolation of the enzyme catalysing the production of the monoglucoside of quercetin (isoquercitrin) or kaempferol (astragalin), the kinetics of the reaction were determined by HPLC, following both the increase of the product and the disappearance of the substrate. The increasing amounts of isoquercitrin and astragalin were consistent with the decrease in the amount of aglycone measured after direct injection of the reaction mixture into the HPLC system and its elution with a less polar solvent.

1. Introduction

Flavonoids are pigments widely found in plant tissues which are involved in a protection mechanism against predatory insects but can work also as a lure for pollinating agents. The technological uses of flavonoids concern mainly their antioxidant activity as radical scavengers, which inhibits the peroxidation of lipids [1–3], and the therapeutic properties of many glycosides derived from this kind of aglycone [4–7]. The glycosylation of flavonoids is very important not only for the latter purpose but mainly because the glycosides are much more soluble than the aglycones and therefore can be easily conveyed through physiological fluids. The enzymes that catalyse the glycosylation of flavonoids (O-glycosyltransferases) use uridine diphosphate as carbohydrate donor and are often specific for the sugar and the position of binding.

The most common assay of the enzyme activity involves the use of radioactive sugars and the determination of the products by TLC or paper chromatography [8–13], although a few methods using an HPLC linear gradient have been mentioned [14,15]. We have developed an improved HPLC procedure, employing isocratic elution, able to determine the activity of O-glycosyltrans-

* Corresponding author.

0021-9673/95/$09.50
SSDI 0021-9673(94)00943-0

ferases even when various enzymes of this kind are present in the same sample. After isolation of three 3-O-glucosyltransferases from pea seedling, according to the method described by Jourdan and Mansell [16], their activity was determined by isocratic HPLC elution, measuring the products formed and/or the substrate left over. The enzymes present in pea seedlings work in sequence, yielding a monoglucoside, a diglucoside and a triglucoside of flavonoids, and therefore a prior separation of the glucosides from the aglycones by means of solid-phase extraction might sometimes be needed.

2. Experimental

2.1. Materials

Kaempferol (K), quercetin (Q) and uridine-5′-diphosphoglucose (UDP-G), used as enzyme substrates, were obtained from Sigma (St. Louis, MO, USA). Kaempferol, quercetin, kaempferol-3-O-glucoside (K-G) and quercetin-3-O-glucoside (Q-G) used as standards were purchased from Extrasynthese (Genay, France). Methanol, tetrahydrofuran (THF), 1-propanol and 2-propanol were of HPLC grade (Baker, Deventer, Netherlands) and water was distilled twice before use. All other reagents were of analytical-reagent grade.

O-Glucosyltransferases were extracted from pea seedlings grown for 1 week under continuous light at 25°C. After harvesting, the seedlings were stored at −80°C until used. The enzymes were purified according to the procedure of Jourdan and Mansell [16]. Frozen seedlings were ground in a Waring blender together with dry-ice and extracted with borate buffer (pH 7.7) containing 20 m*M* 2-mercaptoethanol at 4°C. After double precipitation with 40% and 70% ammonium sulfate, the salts in excess were removed by gel filtration on Sephadex G-25 and the solution containing the O-glucosyltransferases was used for the simultaneous assay of the three enzymes by HPLC. The 3-O-glucosyltransferase which catalyses the production of the monoglucoside was purified from the mixture of the three enzymes by ion-exchange chromatography on cellulose DE-52 equilibrated with 0.05 *M* phosphate buffer (pH 7.3) containing 20 m*M* 2-mercaptoethanol and eluted with a linear gradient (0–0.1 *M*) of KCl.

2.2. Assay of enzyme activity

The reaction mixture used for the assay of glucosyltransferase activity consisted of 10 μl of substrate (3 m*M* kaempferol or quercetin, dissolved in ethylene glycol monomethyl ether) added to 900 μl of 25 m*M* phosphate buffer (pH 7.3) containing 60 μ*M* acceptor (UDP-G) incubated at 25°C. The reaction was started by addition of 100 μl of enzyme solution. At fixed times an aliquot of the reaction mixture was assayed by HPLC for the amounts of substrate and product(s). When purified O-glucosyltransferase catalysing the monoglucosylation was used, 20 μl of reaction mixture were injected in the HPLC system equilibrated with the aglycones eluent as described in Section 2.3. Otherwise, 200 μl of sample containing a mixture of the three glucosyltransferases were loaded on a Sep-Pak C_{18} microcolumn (Waters, Milford, MA, USA) previously washed with methanol (5 ml) and water (10 ml), and successively eluted with 5 ml of water, 5 ml of 50% methanol and 5 ml of pure methanol. The fraction in 50% methanol was dried under reduced pressure, dissolved in 200 μl of methanol and 20 μl of this solution were injected in the HPLC system equilibrated with the glucosides eluent (see Section 2.3).

2.3. Chromatographic conditions

HPLC analyses of the reaction mixture were performed with a Gilson apparatus (Gilson Medical Electronics, Middleton, WI, USA) equipped with Model 712 HPLC system controller or with a Waters apparatus supplied with a

Model 1040 A photodiode-array detector (Hewlett-Packard, Waldbronn, Germany). Separations were carried out on a C_8 (7-μm) Aquapore RP 300 column (220 × 2.1 mm I.D.) or a C_8 (5-μm) Hypersil MOS column (200 × 4.6 mm I.D.) with a precolumn of the same type, using a flow-rate of 1.5 ml/min at a pressure of 20.68 MPa. The aglycones eluent, used for the determination of the activity of O-monoglucosyl transferase, consisted of THF–1-propanol–0.6% citric acid (7.5:12.5:80) and the glycosides eluent consisted of THF–2-propanol–water (5:10:85) and was used for the assay of the mixture of the three enzymes when the three glucosides produced were previously separated from the aglycones after solid-phase extraction with Sep-Pak C_{18}. Calibration graphs for aglycones (kaempferol and quercetin) and their glucosides (kaempferol 3-O-glucoside and quercetin 3-O-glucoside) were established in presence and absence of rutin (quercetin-3-rutinoside) as an internal standard.

3. Results and discussion

Glucosyltransferases from pea seedlings were chosen because their purification is simple and, at the same time, three different enzymes could be obtained with a minimum time consumption [16]. These enzymes (OGT-1, OGT-2 and OGT-3) catalyse the consecutive glucosylation of flavonoids (F) according to the following reactions:

$$F \xrightarrow{\text{OGT-1+UDP-G}} F\text{-}G \xrightarrow{\text{OGT-2+UDP-G}}$$

$$F\text{-}GG \xrightarrow{\text{OGT-3+UDP-G}} F\text{-}GGG$$

where OGT = 3-O-glucosyltransferase (OGT-1 uses an aglycone as substrate; OGT-2 uses a monoglucoside as substrate and OGT-3 uses a diglucoside as substrate), and -G, -GG and -GGC represent mono-, di- and triglucoside, respectively.

By means of HPLC it was possible to de-

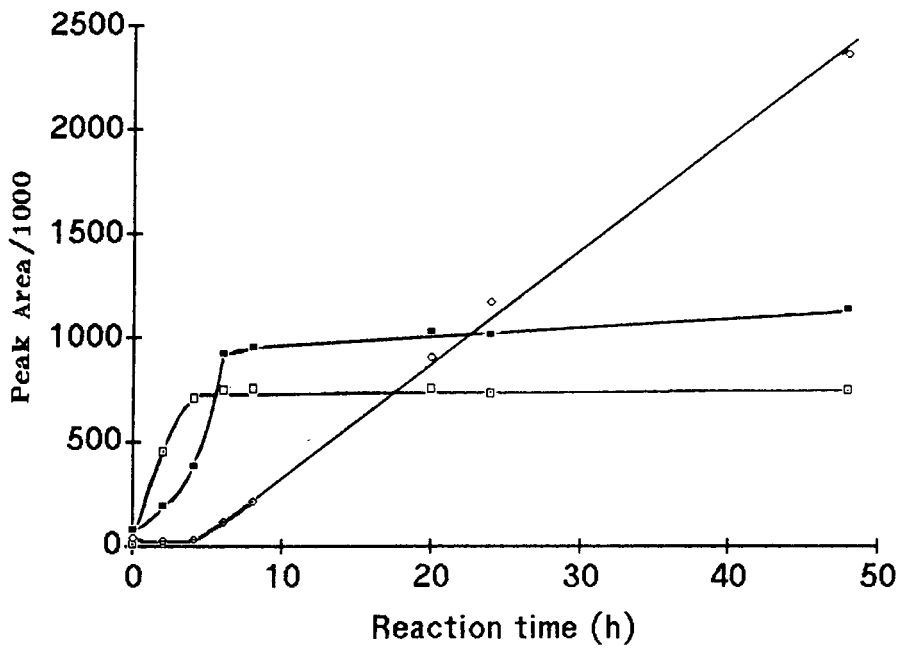

Fig. 1. Kinetics of consecutive glucosylation of kaempferol by the mixture of three O-glucosyltransferases from pea seedlings. □ = Kinetics of monoglucoside-producing enzyme (OGT-1); ■ = OGT-2; ○ = OGT-3.

termine simultaneously the products of the consecutive reactions in the mixture of the three enzymes. The kinetics of the consecutive reactions are reported in Fig. 1, where kaempferol was used as substrate.

As the aglycones and the glucosides have distinct polar properties, the three glucosides could be characterized after solid-phase extraction with Sep-Pak C_{18} and HPLC elution with the glucosides eluent, THF–2-propanol–water (5:10:85). This eluent required too long a time for the complete elution of the mixture of glucosides and aglycones, whereas the aglycones eluent, THF–1-propanol–0.6% citric acid (7.5:12.5:80), although faster, caused overlapping of the peaks of the glucosides, which therefore could not be individually identified.

Among the products of the three O-glucosyl transferases, only the monoglucosides (K-G, astragalin; Q-G, isoquercitrin) were available as standards, therefore the diglucosides and the triglucosides of kaempferol and quercetin were identified by the typical flavonoid spectrum obtained with the diode-array detector from the HPLC peaks (Fig. 2). The correlation between the peak areas of the substrate (aglycone) or product (monoglucoside) and their amounts (nanomoles or micrograms) was assessed by means of a calibration graph and used for the determination of the activity of the O-glucosyltransferase catalysing the first reaction (OGT-1). The relationship between peak area and amount was linear both for aglycones (quercetin, $R = 0.989$; kaempferol, $R = 0.999$) and glucosides (isoquercitrin, $R = 0.976$; astragalin, $R = 0.996$).

The assay of the isolated enzyme catalysing the monoglucosylation of kaempferol and quercetin (OGT-1) was simply carried out with the aglycones eluent without solid-phase extraction, as the only product obtained could be easily identified from the substrate (Fig. 3). In this way it was possible to obtain the enzyme kinetics through the disappearance of the substrate and the corresponding increase in the product. Fig. 4 shows typical kinetics where the decrease in the substrate (kaempferol) is in good agreement with the increase in the product (kaempferol-3-O-glucoside). In this case a consumption of 7.3 nmol of substrate per hour ($R = 0.989$) corresponds to the production of 7.6 nmol per hour of kaempferol-3-O-glucoside ($R = 0.955$).

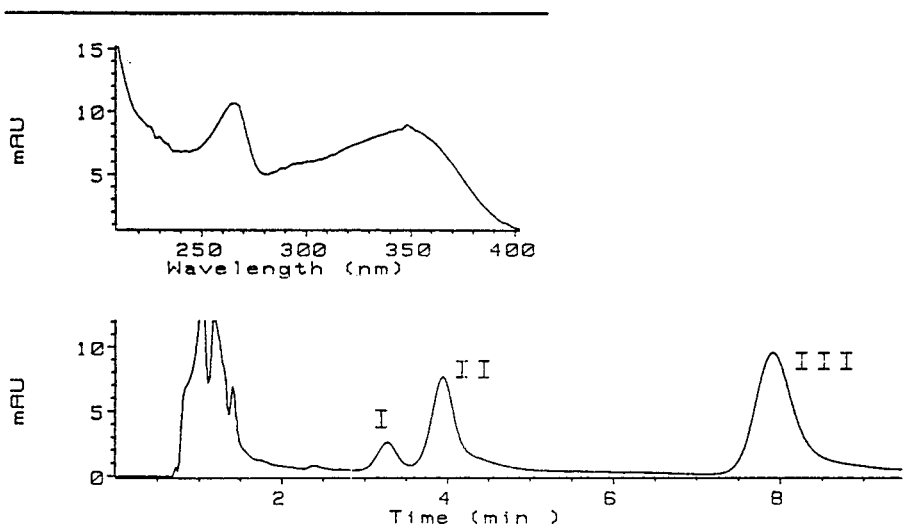

Fig. 2. Bottom: HPLC profile of the three glucosides of kaempferol after 8 h of reaction with the mixture of the three enzymes. Peaks I, II and III correspond to triglucoside, diglucoside and monoglucoside, respectively. Top: spectrum of peak II in the bottom trace. The elution was accomplished with the glucosides eluent, THF–2-propanol–water (5:10:85) after solid-phase extraction with Sep-Pak C_{18} as described in the text.

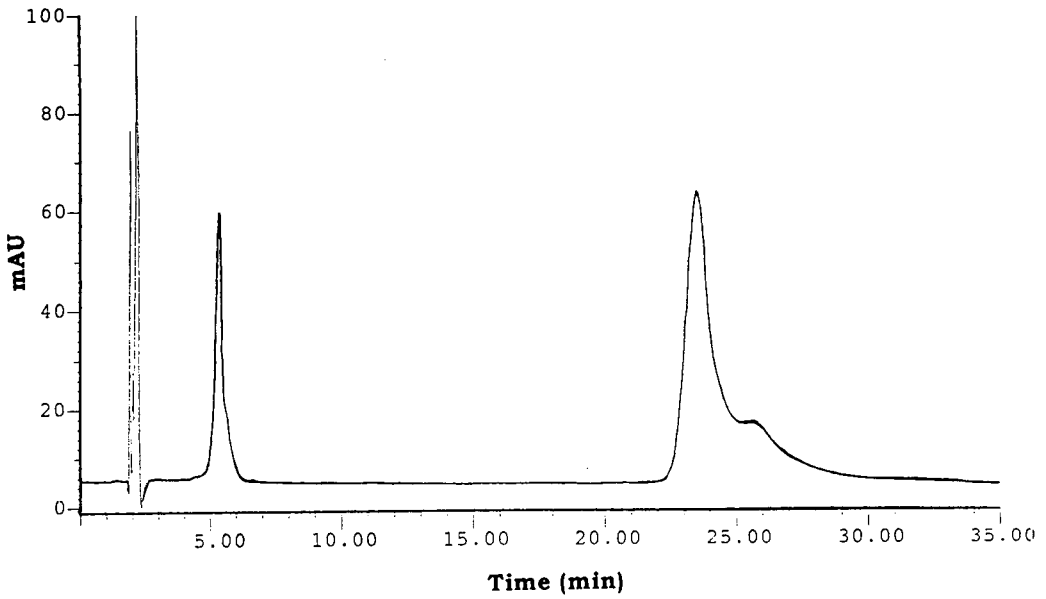

Fig. 3. Elution pattern of kaempferol (I, right peak) and astragalin (kaempferol-3-O-glucoside) (II, left peak) with the aglycones eluent, THF–1-propanol–0.6% citric acid (7.5:12.5:80) as described in the text.

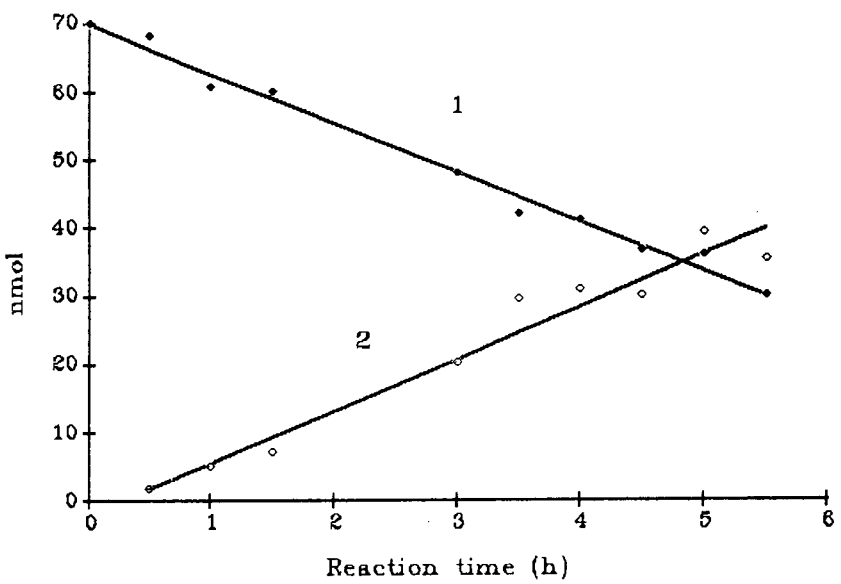

Fig. 4. Assay of 3-O-glucosyl transferase with kaempferol as a substrate. Simultaneous determination of substrate (◆) and product (◇). The kinetics of the disappearance of kaempferol are in good agreement with that of the increase in astragalin.

Acknowledgement

This work was supported by the Target Project on Biotechnology and Bioinstrumentation of the Italian National Council of Research (CNR).

References

[1] R. Brouillard and A. Cheminat, *Prog. Clin. Biol. Res.*, 280 (1985) 93.
[2] N.P. Das and L. Ramanathan, in A.S.H. Ong and L. Packer (Editors), *Lipid-Soluble Antioxidants: Biochemistry and Clinical Applications*, Birkhauser, Basle, 1992, p. 295.
[3] H.M. Dani, S. Sharma, Neelam and Harkirat, in A.S.H. Ong and L. Packer (Editors), *Lipid-Soluble Antioxidants: Biochemistry and Clinical Applications*, Birkhauser, Basle, 1992, p. 320.
[4] M. Gabor, in J.R. Vane and S.H. Ferreira (Editors), *Handbook of Experimental Pharmacology: Anti-Inflammatory Drugs*, Vol. 50/II, Springer, New York, 1979, p. 698.
[5] A.M. Pamukeu, S. Yalciner, J.F. Hatcher and G.R. Bryan, *Cancer Res.*, 40 (1980) 3468.
[6] E. Middleton, Jr., G. Drzewiecki and D. Krishnarao, *J. Immunol.*, 127 (1981) 546.
[7] M. Lonchampt, B. Guardiola, N. Sicot, M. Bertrand, M. Perdix and J. Duhault, *Arzneim. Forsch./Drug Res.*, 39 (1989) 882.
[8] E. Wellmann, D. Baron and H. Grisebach, *Biochim. Biophys. Acta*, 244 (1971) 1.
[9] G. Hrazdina, G.J. Wagner and H.W. Siegelman, *Phytochemistry*, 17 (1978) 53.
[10] J. Köster and W. Barz, *Arch. Biochem. Biophys.*, 212 (1981) 98.
[11] U. Matern, W. Heller and K. Himmelspack, *Eur. J. Biochem.*, 133 (1983) 439.
[12] K.L. Bajaj, V. De Luca, H. Khouri and R.K. Ibrahim, *Plant Physiol.*, 72 (1983) 891.
[13] R.R. Drake, Jr., G.P. Kaushal, I. Pastuszak and A.D. Elbein, *Plant Physiol.*, 97 (1991) 396.
[14] D. Strack, J. Heilemann, V. Wray and H. Dirks, *Phytochemistry*, 28 (1989) 2071.
[15] J. Heilemann and D. Strack, *Phytochemistry*, 30 (1991) 1773.
[16] P.S. Jourdan and R.L. Mansell, *Arch. Biochem. Biophys.*, 213 (1982) 434.

ELSEVIER

Journal of Chromatography A, 691 (1995) 337–347

JOURNAL OF CHROMATOGRAPHY A

Selectivity optimization of reversed-phase high-performance liquid chromatographic peptide and protein separations by varying bonded-phase functionality

Barry E. Boyes[a,*], Douglas G. Walker[b]

[a]*Rockland Technologies Inc., 538 First State Boulevard, Newport, DE 19804, USA*

[b]*Kinsmen Laboratory of Neurological Research, University of British Columbia, 2255 Wesbrook Mall, Vancouver, British Columbia V6T 1W5, Canada*

Abstract

Several chemical bonded-phase modified silicas were prepared using sterically protected monofunctional silane reagents which varied widely in structure and polarity. Since some of these bonded-phase packing materials are highly polar (hydrophilic), resistance to acid-catalyzed bonded-phase loss by hydrolysis was examined, and observed to remain high even for the highly polar Diol bonded-phase functionality. Modification of the surface of 300 Å pore size, fully hydroxylated and base-deactivated silica microspheres with these sterically protected silanes yielded HPLC column packing materials for examination of separation selectivities in reversed-phase separations of peptide and protein mixtures. Distinct separation selectivities were apparent for each bonded-phase functionality. Selectivity differences ranged from limited band spacing changes for steric-protected C_{18} and C_8 bonded-phases, to reversal of elution order for the more polar C_3 and CN bonded phases. The use of column-based selectivity differences between sequential reversed-phase separation steps is used for the two-step HPLC isolation of a recombinant human amyloid precursor polypeptide fragment from a crude bacterial extract.

1. Introduction

Separation of peptide and polypeptide mixtures by reversed-phase high-performance liquid chromatography (RP-HPLC) is a widely used protein chemical separation technique, due to the very-high-resolution separations that can be obtained. Such high-resolution separations can be performed because of the ready availability of small-particle, high-performance RP-HPLC column packings. Additionally, high-resolution separations result from using elution conditions which reduce peak tailing, band broadening, peak ghosting, etc. Specifically, many RP-HPLC separations of peptides and polypeptides use a low-pH mobile phase with an elevated column temperature, using gradient elution with an organic modifier, usually acetonitrile. Trifluoroacetic acid (TFA) is widely favored as the acidic mobile phase modifier due to its high available purity, excellent solubilizing properties, and low UV absorbance. Octadecyl silane-modified silicas (ODS or C_{18}) are commonly used for peptide HPLC, and butyl- (C_4) or propyl- (C_3) silane-modified silicas for protein separations.

Optimization of selectivity, or band spacing, in the RP-HPLC separation of small molecules is generally achieved by systematic changes in

* Corresponding author.

0021-9673/95/$09.50
SSDI 0021-9673(94)00948-8

mobile phase composition [1,2]. In gradient elution this includes optimizing gradient steepness of the organic solvent modifier [2]. Significant changes in separation selectivity can also be obtained by manipulating column temperature, although relatively few workers take advantage of this useful procedure. A further source of changing separation selectivity results from varying the stationary phase interactive surface [3,4]. In this approach, practitioners often optimize separation selectivity by varying the interactive surface of C_{18} columns, by using columns from various manufacturers. Unfortunately, this approach to separation optimization often produces a method with limited robustness [3].

Reversed-phase separations of peptides and polypeptides permit fewer options for mobile phase optimization. Problems associated with sample solubility, aggregation, unfavorable silanol interactions, eluent transparency at low wavelengths, and eluent viscosity, limit the ability to change the mobile phase. Therefore, in some circumstances, it is desirable to use a favorable mobile phase, such as TFA–acetonitrile–water, then manipulate separation selectivity by varying the stationary phase functionality. While there has been limited systematic investigation of the effects of bonded-phase functionality on selectivity manipulation of peptide and polypeptide separations, the advantages for separations of small organic molecule mixtures have been amply demonstrated [3,4].

It is generally acknowledged that peptide separations exhibit selectivity differences with different bonded phases. However, this effect is infrequently employed for method development. This probably is a result of experience with the poor stability of short-chain, polar, bonded-phase silicas in reversed-phase operation at low pH. Literature reports on the selectivity effects of bonded-phase chemistry for protein separations are more sparse. Comparisons of bonded-phase mediated selectivity effects should be approached with caution, using the same base silica support to minimize the potentially confounding effects of varying silanol contributions to retention processes. Early studies by Cooke et al. [5] demonstrated significant selectivity differences for protein separations on C_8 and C_3 bonded-phase porous silica columns. In contrast, significant selectivity differences were not observed for protein mixtures separated on nonporous silica particles modified with C_{18}, C_8, C_4, C_2 and phenyl bonded-phases [6]. Several studies have noted selectivity differences for proteins separated on *n*-alkyl bonded-phase porous silica columns, when compared to the cyanopropyl and/or phenyl bonded phases [7–12]. Recently, Hanson et al. [13] observed significant protein separation selectivity differences when comparing several polymethacrylate-based polymer- and copolymer-coated silica packings.

A variety of wide-pore, small particle silica column packings have been successfully prepared using the so-called steric-protected silane reagents [14,15]. These monofunctional silane reagents use bulky hydrophobic side chains (i.e. diisopropyl, diisobutyl) to protect the hydrolytically sensitive silica–siloxane bond. The loss of bonded-phase from the surface of conventional silica RP-HPLC column packings at low pH leads to progressive deterioration of polypeptide separations [16]. The marked hydrolytic stability of columns of steric-protected C_{18} and C_8 bonded-phase packing materials towards the aggressive mobile phase conditions used for peptide and protein separations (low pH, elevated temperature), has previously been described [15,17,18]. The bulky side groups on the bonded phase also affords steric protection of short-chain, more polar, bonded phases [15], resulting in much higher column stability. When such column packings are free of the complications associated with instability in low pH applications, then bonded-phase functionality can be widely varied to find surface properties to produce useful and stable selectivity characteristics for peptide and polypeptide RP-HPLC.

The purpose of the present study was to examine the potential for selectivity changes in peptide and polypeptide separations by using various steric-protected silica-based stationary phases, including short-chain bonded phases. These column packings differ only in the nature of the bonded-phase functionality, being uniformly produced on fully hydroxylated and base-

deactivated silica microspheres. Mixtures of small synthetic peptides and commercially available proteins were used as sample mixtures to study column selectivity.

There are few reports of the successful expression of the amyloid precursor polypeptides (APPs) in bacteria [19–21], and very limited information available on methods for the purification of recombinant APPs. Attempts to isolate an 400-amino acid C-terminal fragment of APP were complicated by low yield, and contamination of the ca. $50 \cdot 10^3$ molecular mass polypeptide by low-molecular-mass impurities [19]. Expression of sequences in the interior portion of the molecule, spanning regions as large as 572 residues (amino acids 20–591 of the APP695 sequence), have been successful [20]. At the time that the current work was in progress, Gardella et al. [21] reported on the successful bacterial expression of an 109-amino acid C-terminal fragment of APP fusion polypeptide. This recombinant polypeptide was partially purified by a combination of immobilized metal–chelate affinity chromatography, followed by RP-HPLC, both under denaturing conditions. In the current report, we describe the expression and purification of a 132-amino acid C-terminal fragment of APP, the so-called APP-C132 polypeptide. We examine the utility of column-based selectivity manipulation for the RP-HPLC purification of APP-C132, and demonstrate the use of sequential reversed-phase HPLC steps, differing in selectivity, for isolation of APP-C132.

2. Experimental

2.1. Apparatus

Analytical separations and column-stability studies were performed using an HP 1090 LC pump (Hewlett-Packard, Avondale, PA, USA). Preparative separations used an HP 1050 LC or DuPont Model 8800 pump fitted with 4 × flow pump heads. Data were acquired with PE-Nelson A/D converters using ChromPerfect software (Justice Innovations, Mountain View, CA, USA) with a personal computer.

2.2. Columns

Stationary phases were prepared in the laboratory by reacting steric-protected silanes with 300 Å pore size, 5 μm particle size, fully hydroxylated high-purity porous silica microspheres [22]. Silanes were obtained from Hüls America (Bristol, PA, USA), or prepared in the laboratory. Bound ligand concentration was determined by elemental analysis for C, H, N and F by Microanalysis (Wilmington, DE, USA). The monofunctional steric-protected silanes all yielded silica surface substitutions of 2.0 ± 0.2 μmol/m^2, which is the maximum theoretically available for these bulky silane reagents. Stainless-steel column blanks slurry-packed at high pressure by conventional techniques yielded > 10 000 plates for analytical columns (150 mm × 4.6 mm I.D.) or 18 500 plates for semi-preparative columns (250 mm × 9.4 mm I.D.). Similar columns designated as Zorbax 300 SB-C_{18}, 300 SB-C_8, 300 SB-CN and 300 SB-C_3 are commercially available in the USA from MacMod Analytical (Chads Ford, PA, USA) and in Canada from Chromatographic Specialties (Brockville, Canada). The Vydac C_4 column (part 214TP5415; The Separations Group, Hesperia, CA, USA) was obtained from the manufacturer, and had 5 μm particles with 300 Å pores in a 150 mm × 4.6 mm I.D. column format.

2.3. Samples

Commercially available standard proteins included; bovine ribonuclease A (RNase; Sigma Chemical, St. Louis, MO, USA), chicken egg white lysozyme (Lyso, Sigma), bovine cytochrome *c* (Cyt c, Sigma), bovine insulin (Ins, Sigma), bovine brain S-100A (S-100α/S-100β subunit heterodimer, Sigma), bovine brain S-100B (S-100β subunit homodimer, Sigma), equine myoglobin (Myo, Sigma), bovine erythrocyte carbonic anhydrase (CA, Sigma), rabbit muscle parvalbumin (Parv, Sigma) and bovine brain calmodulin (CDR; Calbiochem, San Diego, CA, USA). Solutions of standard proteins were prepared in 6 *M* guanidine–HCl/0.1 *M* phosphate buffer, pH 7.8, and kept at room

temperature (23°C) for at least 4 h before use. Synthetic peptides were obtained from Bachem (Philadelphia, PA, USA). The abbreviations used are as follows ($-NH_2$ refers to the modification of the carboxy-terminal to an amide): L1 = Leu–Gly–Leu; L2 = Leu–His–Leu; L3 = Leu–Arg–Leu; L4 = Leu–Leu–Leu–NH_2; L5 = Leu–Leu–Val–Tyr; L6 = Leu–Leu–Leu; L7 = Leu–Leu–Phe–NH_2; L8 = Leu–Leu–Phe; L9 = Leu–Leu–Val–Phe.

The recombinant amyloid precursor protein (APP) fusion polypeptide (APP-C132) is composed of 132 amino acids of the carboxy-terminal sequence of the human amyloid precursor protein sequence (amino acids 563–695, see ref. [23]), with an additional 38 amino acids at the amino-terminus. Twenty-nine residues of the N-terminal sequence can be released from APP-C132 by cleavage with enterokinase. The APP-C132 recombinant protein was prepared as follows: complementary DNA (cDNA) was prepared by reverse transcription of a sample of human brain mRNA, as described [24]. The APP-C132 coding sequence was isolated by polymerase chain reaction (PCR) amplification of human brain cDNA using a synthetic oligonucleotide with the sequence 5′-GCAAGCTTCAC – GATGGAAGTCGACCC-TGTTGATGCCCGCC-3′ as the sense primer and the sequence 5′-GACTCGAGTCCGCTG-TCCAACTTCAGAGGTGC-3′ as the antisense primer. PCR amplification was carried out as described previously [24]. The single amplified band of 468 base pairs (bp) was cleaved with the restriction enzymes Sal I and Xho I (Gibco-BRL, Gaithersburg, MD, USA) and directionally ligated to the Sal I/Xho I sites of the linearized plasmid pFLAG (International Biotechnologies, New Haven, CT, USA). Ligated plasmid was used to transform *Escherichia coli* (strain DH5α, Gibco-BRL). The DNA sequence of the cloned APP-derived insert was determined to confirm its identity and the absence of PCR generated mutations in the sequence. When following the supplier's recommended procedures, we were unable to isolate secreted, soluble APP-C132 from bacterial extracts, before or after induction of the bacteria by isopropylthiogalactoside (IPTG). Analysis of this expression system suggests that APP-C132 is recoverable only from dilute buffer-insoluble materials in the cells. It appears likely that the polypeptide is present in inclusion bodies, although this has yet to be directly examined.

Recombinant plasmid containing bacteria were grown in Luria Broth (LB) [5% tryptone (Difco; Fisher Scientific, Pittsburg, PA, USA), 2.5% yeast extract (Difco) and 5% sodium chloride] at 37°C, with vigorous shaking, until cultures had an optical density at 600 nm of 0.3. IPTG was added to a final concentration of 1.7 m*M* and cells were incubated for a further 4 h. The cells from 1 l of culture were lysed by treatment with lysozyme (1 mg/ml) in lysozyme buffer [50 m*M* Tris, 50 m*M* EDTA (pH 8.0), 8% sucrose, 100 mg/ml phenylmethylsulfonyl fluoride (PMSF), 1 mg/ml aprotinin, 1 mg/ml leupeptin] and sonication. The extract was centrifuged at 10 000 *g* for 10 min, the supernatant discarded and the pellet resuspended in 10 m*M* Tris–HCl/1 m*M* EDTA (pH 8.0) containing DNAase (100 mg/ml, Sigma) and RNAase (100 mg/ml, Sigma) for 30 min at room temperature. The insoluble material was collected by centrifugation (10 000 *g*, 15 min), resuspended in 100 m*M* NaCl/10 m*M* Tris–HCl/1 m*M* EDTA, pH 7.5, and again pelleted by centrifugation. The chromatographic feed stock was prepared by homogenization of the pellet with 6 *M* guanidine–HCl/0.02 *M* Tris–HCl, pH 8.0. The resulting extract was cleared by centrifugation (15 000 *g*, 60 min); the supernatant fraction typically contained 1.5–2 mg/ml of protein. The cleared extract was subjected to RP-HPLC on the 250 mm × 9.4 mm I.D. Zorbax 300 SB-C_8 column. Fractions of interest from the separation were lyophilized to dryness, then resolubilized using 5% acetic acid/6 *M* urea, at a protein concentration of 2–3 mg/ml. This protein solution was either used for further purification, or sampled for sodium dodecyl sulfate–polyacrylamide gel electrophoresis (SDS-PAGE).

2.4. Miscellaneous procedures

Protein determinations were carried out using the bicinchoninic acid (BCA) reaction, using reagents supplied by Pierce (Rockford IL,

USA). Discontinuous buffer SDS polyacrylamide gel electrophoresis (SDS-PAGE) was conducted on 12% or 10–20% polyacrylamide gradient minigels. Following electrophoresis, the gels were negatively stained with a copper stain kit (Bio-Rad, Hercules, CA, USA). A digital image was obtained of the gel using a UMAX 1260 scanner in the reflected light mode, and then the proteins were electrophoretically transferred to nitrocellulose membranes. The recombinant APP fragments were detected immunochemically on the membranes using a rabbit polyclonal antibody specific to the 14 C-terminal amino acids of APP (681–695) (antibody R37, Ref. [25]), and an alkaline phosphatase labeled anti-rabbit immunoglobulin secondary antibody. Immunoreactive bands were localized by reaction with 5-bromo-4-chloro-3-indoyl phosphate/Nitro-blue tetrazolium (BCIP/NBT) alkaline phosphatase substrate. Alternatively, gels were directly stained after electrophoresis using the Silver Stain Plus procedure and reagents from Bio-Rad. Electrophoretic analysis of protein samples containing guanidine–HCl required precipitation of proteins by cold 10% trichloroacetic acid. The resulting protein precipitate was collected by centrifugation, washed twice with cold ethanol–diethyl ether (50:50, v/v), lyophilized, and then resolubilized using 2% SDS/20 m*M* Tris–HCl, pH 7.5.

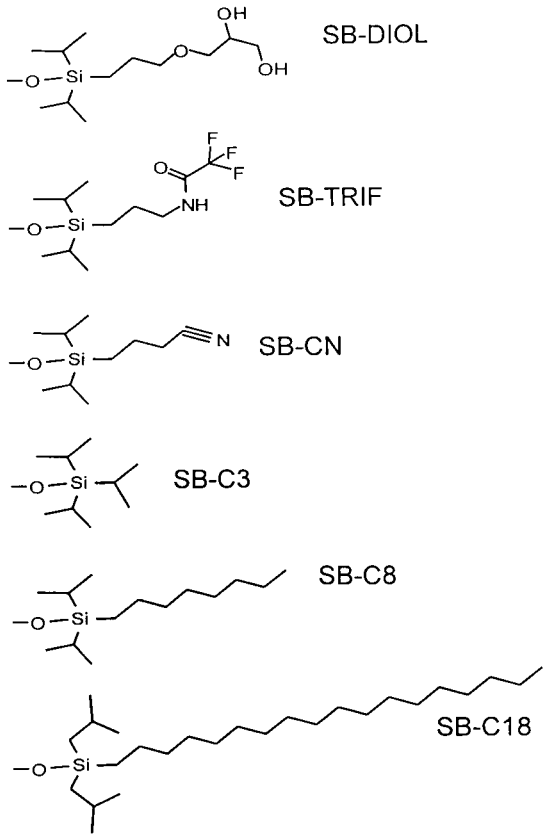

Fig. 1. Structures of the steric-protected silanes used in this study. The reagents are listed in the top-to-bottom order of increasing retention for small organic test molecules. SB-TRIF = [3-(trifluoroacetamido)propyl]-diisopropylsilane.

3. Results and discussion

A variety of organosilane reagents have been successfully prepared with bulky hydrophobic side chains that provide steric protection of the silica surface-bound silane [15,18]. Several examples of such reagents are illustrated in Fig. 1. These silica-based bonded phases have either the diisopropyl steric-protecting groups, or, in the case of the SB-C_{18} reagent, diisobutyl steric-protecting groups. As seen in this figure, a wide variety of bonded-phase surface chemistries are potentially available for changing selectivity in RP-HPLC separations. The corresponding stationary phases vary widely in polarity, as judged by retention of non-ionogenic hydrophobic organic compounds. A previous report [3] demonstrates the small molecule separation selectivity differences available with some of the bonded-phases shown in Fig. 1.

Hydrolysis of covalently attached bonded phases from the surface of silica occurs more rapidly at low pH and elevated temperatures [15,17]. At low pH, dimethyl-substituted bonded phases degrade more rapidly as the ligand chain is shortened, or the effective polarity of the bonded phase increases [15,18]. Highly stable peptide separations resulting from the use of steric-protected SB-C_8 and SB-C_{18} *n*-alkyl bonded phases have previously been reported [18]. Since some of the bonded phases listed in Fig. 1 are highly hydrophilic, there was a question that the protection afforded by bulky side groups may be insufficient to yield reasonable

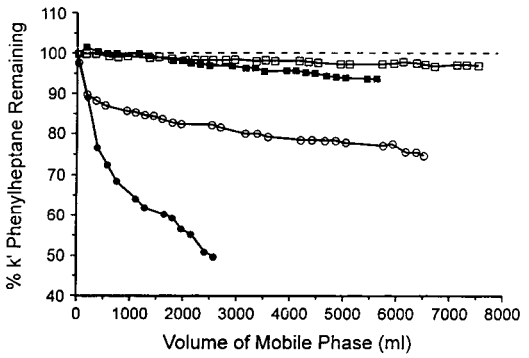

Fig. 2. Test of the stability of bonded-phase silica column packing materials. Loss of retention of phenylheptane as a function of volume of mobile phase passed through the column. Retention of phenylheptane was determined isocratically following 0–100% gradients of water to acetonitrile, both containing 0.5% TFA. The 150 mm × 4.6 mm I.D. columns were maintained at 60°C for the gradients, and tested isocratically at room temperature (ca. 22°C). □ = SB-C_3; ◘ = SB-TRIF; ○ = SB-Diol; ◘ = C_4 phase.

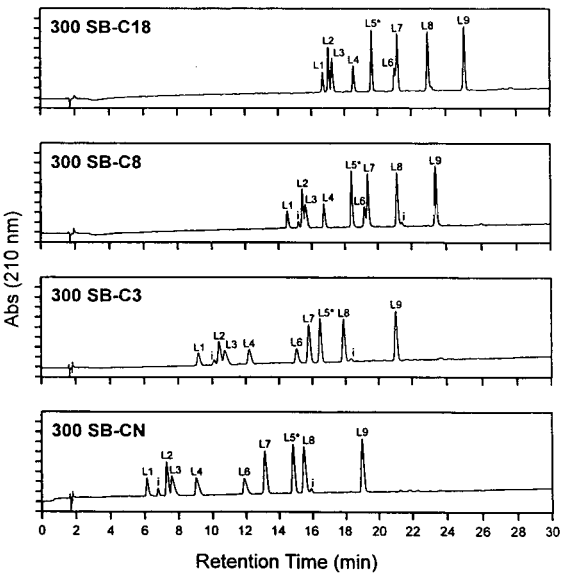

Fig. 3. Gradient RP-HPLC separations of a mixture of nine peptides on various bonded-phase column packings: columns, 150 mm × 4.6 mm I.D.; mobile phase gradient 0–36% water to acetonitrile, both with 0.1% TFA, over 30 min; flow-rate, 1 ml/min; temperature, 40°C; 2 μg of each peptide was injected in a volume of 20 μl. For L1–L9 see text; i = unidentified impurities.

stability for use under the aggressive conditions typical for peptide and polypeptide separations (pH 1–2, 20–60°C). Fig. 2 presents a comparison of bonded-phase stabilities for very polar steric-protected bonded phases versus a widely used, less polar, C_4 bonded-phase packing material. These plots show the retention of a neutral hydrophobic analyte (phenylheptane) as a function of the number of column volumes of the challenging mobile phase passing through the column. Loss of retention for this analyte has previously been shown to correlate with bonded-phase loss [15].

To investigate the potential for selectivity shifts with different bonded-phase functionalities, we compared peptide and polypeptide gradient RP-HPLC separations using columns packed with the SB-C_{18}, -C_8, -C_3 (triisopropyl) and -CN (cyanopropyl) bonded phases. Fig. 3 compares the elution profiles obtained for identical 30-min gradient separations of a nine-component mixture of 3- and 4-amino acid-residue peptides. Based on analyses of small organic molecules, retention decreased significantly, as expected, for all peptides when shifting from the longer-chain, more hydrophobic SB-C_8 and SB-C_{18} *n*-alkyl bonded phases, to the short-chain SB-C_3 and the nitrile-containing SB-CN bonded phase. For peptide L5, elution order shifts with bonded-phase type, with this peptide eluting between L4 and L6 on the *n*-alkyl bonded phases, and between L7 and L8 for the more polar SB-C_3 and SB-CN bonded phases. Less radical selectivity differences are noted for several band pairs when comparing the separations on each column, for example, band spacing for L6/L7, or L8/L9. The elution patterns were not completely reordered, however, as apparent by the similar selectivities of these packings for separating peptides L1, L2, L3 and L4.

Changes in gradient elution conditions lead to band spacing changes for separations such as those in Fig. 3 [26]. To define the dependence of gradient elution conditions on the selectivity differences between the bonded-phase packings, separations of the nine-component peptide mixture were conducted on each column at 20, 40 and 60 min. These retention data sets were used with DryLab software (LC Resources, Walnut

Creek, CA, USA) to predict optimum separations of this mixture both in bonded-phase functionality and gradient time. Fig. 4 presents the experimental verification of the predicted best separations of the nine-component peptide mixture on SB-CN and SB-C_{18} columns. The predicted and observed retention times were within 0.15 min. For this peptide mixture, the SB-CN bonded-phase column produced the best result, yielding baseline resolution in about 23 min. The SB-C_{18} bonded phase gave an acceptable separation, but required a longer gradient time with less resolution than obtained with the SB-CN or SB-C_3 bonded phases. The SB-C_3 column was also able to separate these components with near-baseline resolution ($R_s = 1.4$), but required a 35 min gradient time. Optimum separation with the SB-C_8 column required the least time (L9 elutes at 19.5 min), but gave poor resolution of bands L6/L7. The data in Fig. 4 show that judicious choice of bonded phase, combined with gradient optimization, yielded complete and rapid separation of all components of this peptide mixture.

Comparison of the separations for several polypeptides using the SB-C_{18}, -C_8, -C_3 and -CN bonded-phase columns demonstrated significant selectivity differences. Fig. 5 shows the elution profiles for a ten-component mixture of polypeptides using identical gradient conditions for each column. In this case nine standard proteins were denatured in 6 *M* guanidine–HCl before injection. As was observed previously for the small peptides, a general reduction in retention is apparent in shifting from the most hydrophobic SB-C_{18} bonded phase to the short-chain, more polar bonded phases. Significant selectivity differences are apparent with each of these bonded-phase packings for separating the ten polypeptides, as readily seen by comparing the

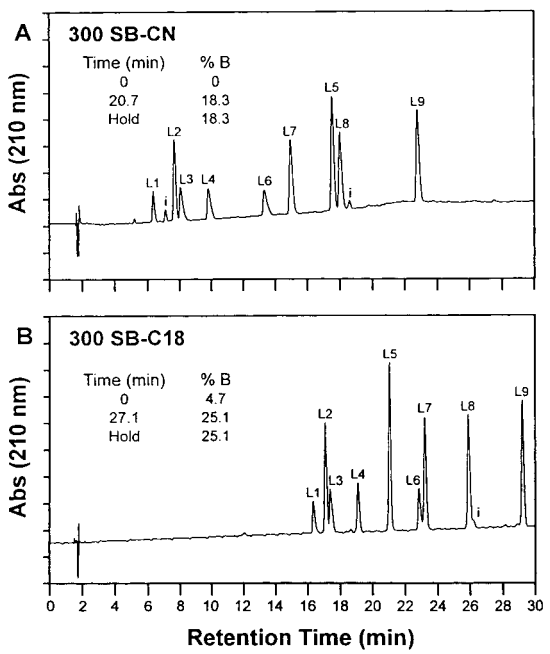

Fig. 4. Gradient RP-HPLC separations of a peptide mixture using gradient optimized elution conditions for two bonded-phase columns, packed with (A) SB-CN or (B) SB-C_{18} modified silicas: mobile phase gradients as indicated on the figure (solvent A = 0.1% TFA in water, solvent B = 0.1% TFA in acetonitrile); columns, 150 mm × 4.6 mm I.D.; flow-rate, 1 ml/min; temperature, 40°C; 2 μg of each peptide was injected in a volume of 20 μl.

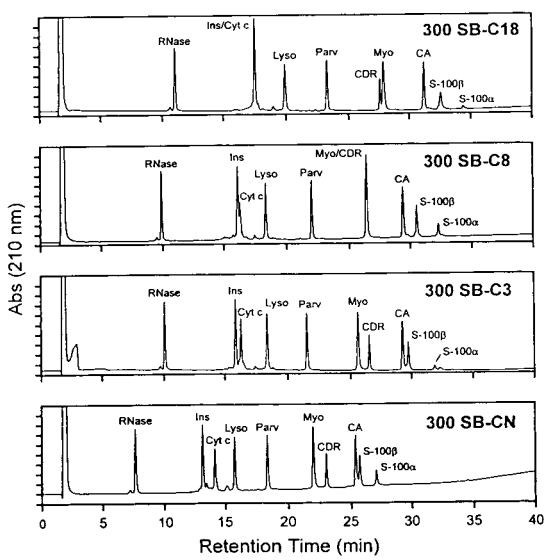

Fig. 5. Gradient RP-HPLC separations of a polypeptide mixture on various bonded-phase columns: columns, 150 mm × 4.6 mm I.D.; flow-rate, 1 ml/min; temperature, 60°C; gradient conditions, 25–70% B in 40 min, solvent A = 0.1% TFA in water, solvent B = 0.09% TFA in acetonitrile–water (80:20, v/v); 3 μg of each protein in 20 μl 6.0 *M* guanidine–HCl/0.1 *M* sodium phosphate, pH 7.8. For abbreviations, see text.

retentions of Ins and Cyt c, or Myo and CDR. Comparing the separations obtained on each column using gradients of 20, 40 and 60 min, as was described above for the peptide separations, confirmed that selectivity differences between bonded-phase types were not unique to the specific gradient conditions chosen for Fig. 5. The apparent differences in peak recovery between columns for the S-100 α-subunit is an artifact of the sample preparation buffer conditions. This polypeptide appears to slowly precipitate under the conditions used. No differences were noted in sample recovery between the columns for the ten polypeptides of this sample.

RP-HPLC separations of complex polypeptide samples can yield highly purified components. In some cases, insufficient selectivity differences exist to permit isolation of pure components in a single separation step. It becomes increasingly difficult, however, to isolate pure components from a complex sample as sample load increases, as is usually the case for preparative separations. Fig. 6 shows a semi-preparative-scale gradient RP-HPLC separation of proteins from a crude extract of recombinant protein expressing *E. coli* cells, using a 250 mm × 9.4 mm I.D. column packed with SB-C_8 bonded-phase silica (3.8 mg protein injected). The recombinant bacteria were engineered to express the fusion polypeptide APP-C132, which contains the carboxy-terminal sequence of the human amyloid precursor polypeptide. In this example of a complex sample separation, the target APP-C132 polypeptide (identified by western blot analysis in Fig. 7) is observed by gel electrophoresis to coelute with a variety of higher-molecular-mass polypeptides. Attempts to obtain pure material by gradient or temperature optimization of this separation provided insufficient resolution. The purity of the material produced by a single RP-HPLC step was, at best, 60–70% using the semi-preparative SB-C_8 column.

Fig. 8 compares separations of the partially purified APP-C132 preparation using SB-C_8 and SB-CN bonded-phase packings. Gradient conditions for these separations used the same rate changes in acetonitrile (0.36% acetonitrile/ml),

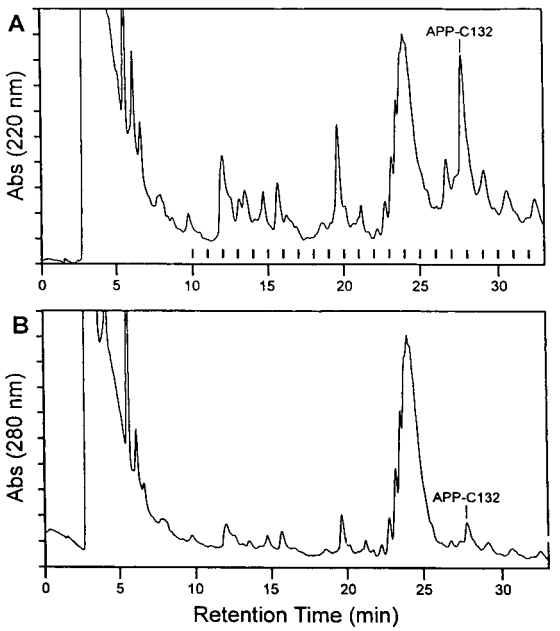

Fig. 6. Separation of APP-C132 from bacterial proteins: column, 250 mm × 9.4 mm I.D. Zorbax 300 SB-C_8; flow-rate, 4 ml/min; temperature, 40°C; gradient conditions, 35–47% B in 30 min, solvent A = 0.1% TFA in water, solvent B = 0.09% TFA in acetonitrile; sample, 2.5 ml of 6.0 *M* guanidine–HCl extract of recombinant protein expressing *E. coli* cells (3.8 mg protein); detection, absorbance at (A) 220 nm and (B) 280 nm. Fractions were collected at 1-min intervals starting at 10 min, as indicated in (A). The peak containing the $22 \cdot 10^3$ molecular mass immunoreactive APP-C132 polypeptide elutes at 28 min (see Fig. 7).

while yielding similar retention times of the peak of interest. This comparison shows that there are significant selectivity differences between these two bonded-phase functionalities for this sample. Most of the impurity peaks apparent for the SB-C_8 separation elute close to the APP-C132 peak, as expected, considering the source of the crude material (SB-C_8 semi-preparative separation). A major contaminant peak (labeled I in Fig. 8) is only partly resolved from the APP-C132 peak. In contrast, contaminants eluting from the SB-CN column are shifted considerably further from the target peak, for example, comparing the resolution of APP-C132 to the major contaminant peak I.

The purity of APP-C132 preparations isolated using the SB-CN and SB-C_8 columns, as de-

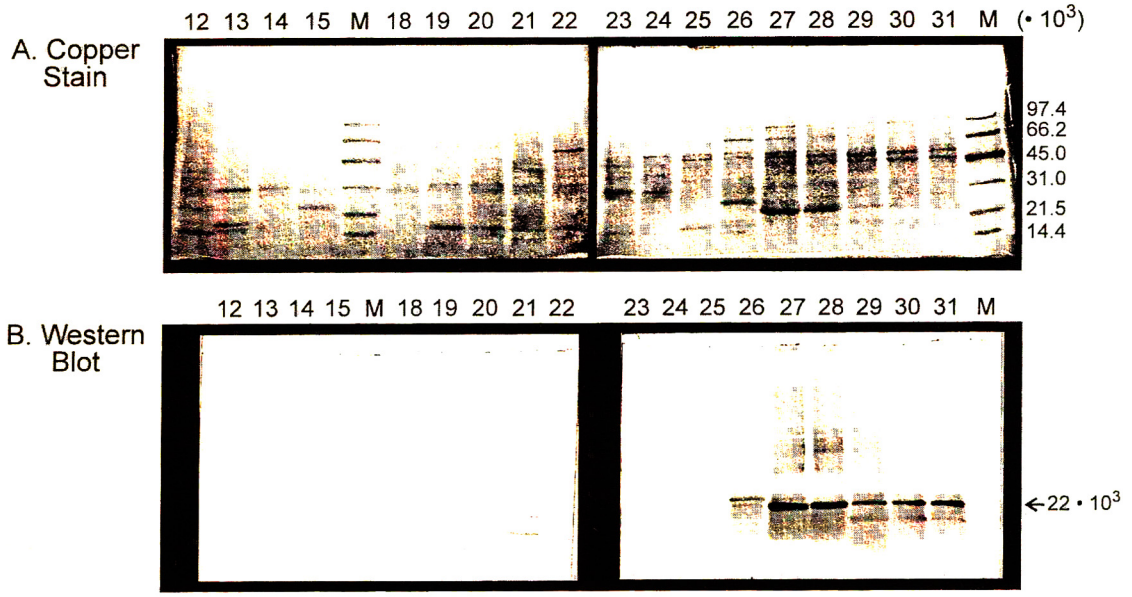

Fig. 7. SDS-PAGE analysis of fractions collected from the RP-HPLC separation of the bacterial extract (Fig. 6). Lyophilized samples obtained from RP-HPLC were submitted to SDS-PAGE separation on 10–20% gradient gels. Proteins were identified in the gels by the reversible copper stain (A), then transferred to nitrocellulose sheets for immunochemical staining (B). The immunoreactive APP-C132 band, eluting from the RP-HPLC column at 27–29 min, is identified on the immunoblot to migrate as an apparent $22 \cdot 10^3$ molecular mass band. M = Standard molecular mass marker proteins.

scribed above, were analyzed by reinjecting collected fractions on the opposite column. Fig. 9 shows the analysis of APP-C132 peaks from the SB-CN column, using SB-C_8 (A), and from the SB-C_8 column, using SB-CN (B). The separation shown in Fig. 9A reveals a single contaminant eluting at 11.8 min, representing about 2.5% of the area counts, compared to the APP-C132 peak. Fig. 9B shows that the APP-C132 isolate, obtained using the SB-C_8 column, is more contaminated, with several impurities eluting on the front of the target peak. Isolation of APP-C132 from the semi-purified sample by the use of the SB-CN column results in a material with higher purity than can be obtained using the SB-C_8 column.

Thus, the use of sequential reversed-phase steps, with a selectivity switch from the SB-C_8 to the SB-CN bonded-phase, yields highly purified APP-C132. Confirmation of the purity of APP-C132 produced by this scheme, and comparison with the intermediate purification steps, was carried out by SDS-PAGE analysis, as shown in Fig. 10. The final protein preparation appeared as a single band on the electropherogram.

4. Conclusions

Bonded-phase silica column packing materials were successfully prepared on 300 Å pore size fully hydroxylated, high-purity, silica microspheres with a variety of steric-protected silane reagents. In agreement with previous results [15,17,18], the sterically protected silane bonded phases exhibited excellent resistance to acid-catalyzed bonded-phase hydrolysis, even in cases where the bonded-phase moiety was highly hydrophilic (e.g., SB-Diol). Bonded-phase loss was minimal, even with highly aggressive mobile phase conditions (pH < 1, elevated temperature). Since the molar surface coverages of these monofunctionally reacted surfaces are highly

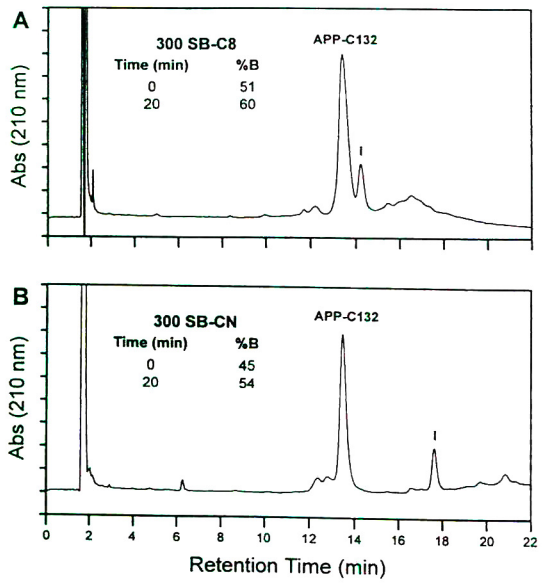

Fig. 8. Separation of partially purified APP-C132 from contaminants using the SB-C_8 (A) and SB-CN (B) bonded-phase columns: columns, 150 mm × 4.6 mm I.D.; flow-rate, 1 ml/min; temperature, 40°C; gradient conditions as described on the figure, solvent A = 0.1% TFA in water, solvent B = 0.09% TFA in acetonitrile–water (80:20, v/v); sample, 9 μg protein samples from the semi-preparative SB-C_8 separation were injected. I represents a major impurity peak.

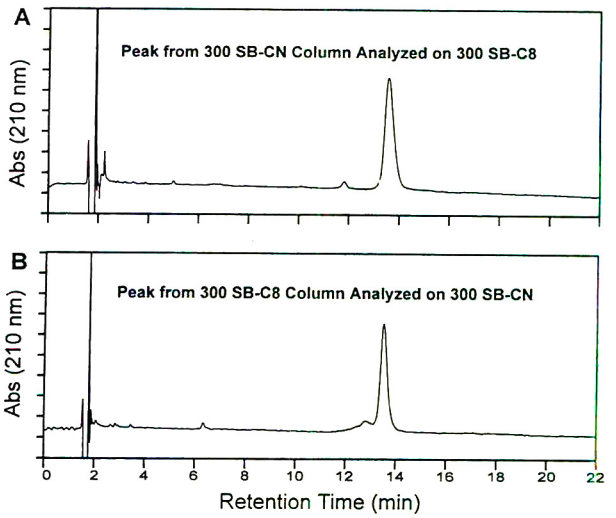

Fig. 9. Analysis of purified APP-C132 preparations. (A) Analysis of APP-C132 protein, obtained using the SB-CN column, as shown in Fig. 8B. This analysis used the SB-C_8 column, and conditions for the SB-C_8 column described in Fig. 8A. (B) Analysis of APP-C132 protein, obtained using the SB-C_8 column, as described in Fig. 8A. This analysis used the SB-CN column, and conditions for the SB-CN column, as described in Fig. 8B. For both analyses 4 μg of purified protein were injected.

similar (ca. 2.0 μmol/m^2), it is safe to assume that any selectivity changes observed between bonded-phase packings are not the result of surface changes resulting from use of the column, or due to gross differences in accessibility of the underlying silica silanol groups.

The present study has demonstrated significant differences in peptide and protein separation selectivities with bonded-phase functionality. The marked selectivity differences for separations on the sterically protected C_8 and CN bonded phases are in agreement with other recent studies [11,12], and extend these observations to a wider variety of stationary phases. Thus, columns of these short-chain bonded phases can be used to obtain favorable band-spacing changes because of their unique surface interactive properties, which result from varying the steric-protected silane functionality.

The utility of bonded-phase selectivity manipulation has been demonstrated by the two-step RP-HPLC purification of recombinant APP-C132 fusion polypeptide from a crude bacterial lysate. Although definitive proof of the purity of the APP-C132 preparation will require further independent methods of analysis, the use of column-based selectivity shifting between consecutive RP-HPLC steps yields a material of higher purity than could be obtained by using a single bonded-phase functionality. The recombinant construct used for expression of APP-C132 gave rather poor yields of the polypeptide, which resulted in a challenging sample for purification. Because the sequence of interest contains the amyloidogenic Aβ sequence [23], it was anticipated that poor expression efficiency might result, and that the resulting polypeptide would display inconvenient aggregation and solubility properties. Using the RP-HPLC approach described, APP-C132 fusion polypeptide could be prepared in a highly purified form, in a single working day. The successful isolation of APP-C132 will permit further analysis of the solubility

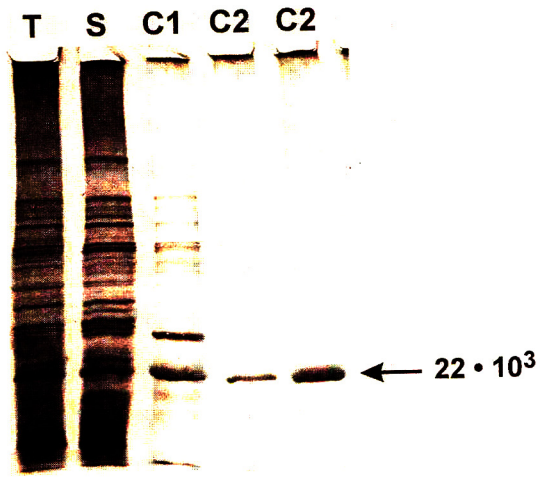

Fig. 10. Electrophoretic analysis following the purification of APP-C132. Samples were separated using a 12% SDS-PAGE gel, then visualized by silver staining. Sample identity: T = total protein in the lysed bacterial pellet (4 μg loaded); S = 6.0 *M* guanidine–HCl solubilized sample (4 μg loaded); C1 = pooled column eluate from the separation on Zorbax 300 SB-C_8 column (2 μg loaded); C2 = pooled column eluate from the separation of C1 on the Zorbax 300 SB-CN column, using conditions described in Fig. 8B (0.4- and 2.5-μg samples loaded).

and aggregation properties of the polypeptide, as well as supply material to characterize the biological role of APP and its fragments.

Acknowledgements

The authors would like to thank Drs. J.J. Kirkland, J.J. DeStefano and Professor E.G. McGeer for helpful discussion and encouragement and Mr. Bud Permar for his excellent technical assistance. Dr. Henry Leibu was of considerable help in the synthesis of the various surface modified silicas. D.G.W. was supported by a grant from the British Columbia Health Research Foundation.

References

[1] P.J. Schoenmakers, *Optimization of Chromatographic Selectivity*, Elsevier, Amsterdam, 1986.
[2] L.R. Snyder and J.J. Kirkland, *Introduction to Modern Liquid Chromatography*, Wiley, New York, 1979.
[3] J.J. DeStefano, J.A. Lewis and L.R. Snyder, *LC·GC*, 10 (1992) 130.
[4] J.L. Glajch, J.C. Gluckman, J.G. Charikofsky, J.M. Minor and J.J. Kirkland, *J. Chromatogr.*, 318 (1985) 23.
[5] N.H.C. Cooke, B.G. Archer, M.J. O'Hare, E.C. Nice and M. Capp, *J. Chromatogr.*, 255 (1983) 115.
[6] G. Jilge, R. Janzen, H. Giesche, K.K. Unger, J.N. Kinkel and M.T.W. Hearn, *J. Chromatogr.*, 397 (1987) 71.
[7] K. Titani, T. Sasagawa, K. Resing and K. Walsh, *Anal. Biochem.*, 123 (1982) 408.
[8] G.E. Tarr and J.W. Crabb, *Anal. Biochem.*, 131 (1983) 99.
[9] L.R. Gurley, D.A. Prentice, J.G. Valdez and W.D. Spall, *Anal. Biochem.*, 131 (1983) 465.
[10] W.G. Burton, K.D. Nugent, T.K. Slattery, B.R. Summers and L.R. Snyder, *J. Chromatogr.*, 443 (1988) 363.
[11] N.E. Zhou, C.T. Mant, J.J. Kirkland and R.S. Hodges, *J. Chromatogr.*, 548 (191) 179.
[12] B.A. Marchylo, D.W. Hatcher, J.E. Kruger and J.J. Kirkland, *Cereal Chem.*, 69 (1992) 371.
[13] M. Hanson, K.K. Unger, C.T. Mant and R.S. Hodges, *J. Chromatogr.*, 599 (1992) 65.
[14] J.L Glajch and J.J. Kirkland, *US Pat.*, 4 705 725 (1987).
[15] J.J.Kirkland, J.L. Glajch and R.D. Farlee, *Anal. Chem.*, 61 (1988) 2.
[16] J.L. Glajch, J.J. Kirkland and J. Köhler, *J. Chromatogr.*, 384 (1987) 81.
[17] J.L. Glajch and J.J. Kirkland, *LC·GC*, 8 (1990) 140.
[18] B.E. Boyes and J.J. Kirkland, *Peptide Res.*, 6 (1993) 249.
[19] D.J. Selkoe, M.B. Podlisny, C.L. Joachim, E.A. Vickers, G. Lee, L.C. Fritz and T. Ollersdorf, *Proc. Natl. Acad. Sci. U.S.A.*, 86 (1988) 3741.
[20] J.-M. Roche, I.P. Shapiro, M.P. Sundsmo, D.A.C. Otaro, L.M. Refolo, N.K. Robakis and T. Saito, *J. Biol. Chem.*, 267 (1992) 2214.
[21] J.E. Gardella, G.A. Gorgone, L. Candela, J. Ghiso, E.M. Castano, B. Frangione and P.D. Gorevic, *Biochem. J.*, 294 (1993) 667.
[22] J.J. Kirkland, C.H. Dilks and J.E. Henderson, *LC·GC*, 11 (1993) 290.
[23] J. Kang, H.G. Lemaire, A. Unterbeck, J.M. Salbaum, C.L. Masters, K.H. Grzechik, G. Multhaup, K. Beyreuther and B. Muller-Hill, *Nature*, 325 (1987) 733.
[24] D.G. Walker and P.L. McGeer, *Mol. Brain Res.*, 14 (1992) 109.
[25] P.L. McGeer, H. Akiyama, T. Kawamata, T. Yamada, D.G. Walker and T. Ishii, *J. Neurosci. Res.*, 31 (1992) 428.
[26] J.L. Glajch, M.A. Quarry, J.F. Vasta and L.R. Synder, *Anal. Chem.*, 58 (1986) 280.

ELSEVIER

Journal of Chromatography A, 691 (1995) 349–353

JOURNAL OF CHROMATOGRAPHY A

Insights into the role of the hydrogen bond and hydrophobic effect on recognition in molecularly imprinted polymer synthetic peptide receptor mimics

Ian A. Nicholls, Olof Ramström, Klaus Mosbach*

Department of Pure and Applied Biochemistry, Chemical Centre, University of Lund, Box 124, S-22100 Lund, Sweden

Abstract

Peptide antibody combining site mimics prepared by the molecular imprinting of N-Ac–L-Phe–L-Trp–OMe were used as highly efficient "tailor-made" chiral stationary phases and for the study of non-ionic non-covalent interaction-based recognition. The effect of water on recognition and the role of the hydrogen bonding and the hydrophobic effect on ligand selectivity are discussed.

1. Introduction

Molecular imprinting [1–3] provides a valuable tool for the modelling of the recognition processes observed in nature [4]. Non-covalent molecularly imprinted polymers (MIPs), in particular, have found application in areas as diverse as artificial antibody combining site mimics [5], artificial enzymes [6–9], synthesis mediators [10,11] and sensor components [12]. The most exploited area of application, however, is in tailor-made chiral chromatographic stationary phase development [3,13,14,15], where the high selectivity of these materials for a *predetermined* ligand makes them versatile systems for custom chromatographic method development.

The preparation of non-covalent molecularly imprinted polymers may be summarized as follows (Fig. 1). For a given imprint or template molecule, a functional monomer (or monomers) is selected with chemical functionality complementary to that of the imprint species. The complementarily interacting functionalities form predictable solution structures [16], the nature of which is captured through polymerization in the presence of a cross-linking monomer. After extraction of the imprint species, recognition sites of complementary steric and functional topography to the imprint molecule remain. Subsequent incubation of a mixture of the imprint molecule and related chemical species results in the selective rebinding of the imprint structure. The imprinting process thus engenders a cognitive capacity to the polymer. It is this selective recognition capability which is utilized in molecularly imprinted polymer-based chiral stationary phases (CSPs). MIP CSPs are distinguished from other CSPs by their predictable order of elution, whereby the application of a racemate of the imprint species always results in longer retention times for the imprinted enantiomer. Individual enantiomer dissociation constants reflect the differing affinities for MIP recognition sites.

* Corresponding author.

0021-9673/95/$09.50
SSDI 0021-9673(94)01067-6

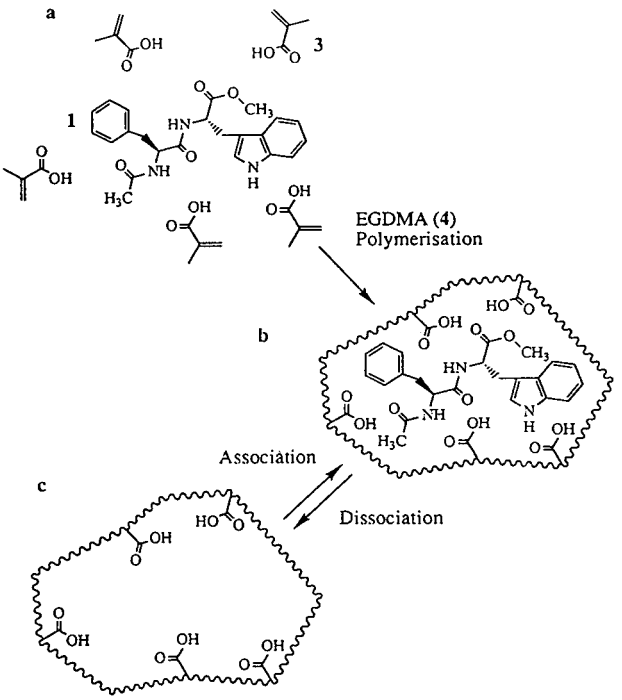

Fig. 1. Idealized molecular imprinting of N-Ac–L-Phe–L-Trp–OMe (**1**) in a methacrylic acid (**3**)–ethylene glycol dimethacrylate (**4**) copolymer. (a) Hydrogen-bonding interactions between functional monomers and the imprint species define solution adducts; (b) topographical relationship present in the solution adduct is captured by polymerization; (c) imprint species extraction yields a recognition site of complementary shape and functional topography.

A current goal in the development of new MIPs is the study of recognition in aqueous media. MIP receptor mimics selective for the dipeptide N-Ac–L-Phe–L-Trp–OMe (**1**) have recently [13] been shown to be capable of resolving racemic (Fig. 2) and diastereomeric mixtures of the imprint structure and racemates of a range of structurally related compounds. The unprecedented separations achieved with this system make it well suited to the study of recognition in solvent systems less favourable to the formation of hydrogen bonds, the strongest driving force for recognition in non-polar media [3]. Previous studies, with less selective MIPs based on methacrylic acid (MAA) (**3**)–ethylene glycol dimethacrylate (EGDMA) (**4**) copolymers, have

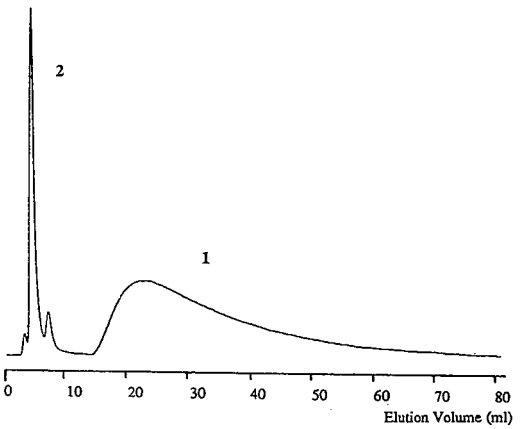

Fig. 2. Chromatogram of the resolution of a racemate of Ac–Phe–Trp–OMe (i.e., **1** and **2**), using chloroform (1% AcOH) as eluent (10 μg injected). The attenuation was increased ten-fold after 13 min to provide a more clear view of the peak of **1**.

been limited to the use of organic eluents. We report here the effect of aqueous–organic mixtures on recognition, which permits conclusions to be drawn regarding the role of the hydrogen bond and hydrophobic effect on recognition.

2. Experimental

2.1. General methods

Reagents and chemicals (Sigma, St. Louis, MO, USA), initiator [2,2′-azobis(2,4-dimethylvaleronitrile), Wako, USA] and solvents (Labscan, Malmö, Sweden) were of HPLC or analytical-reagent grade. Synthesis products were characterized by ^{1}H NMR (Varian XL 300 MHz) using tetramethylsilane as external reference, fast atom bombardment (FAB) mass spectrometry (Jeol SX-102, Xe as incident particle, positive-ion mode), TLC, HPLC (as detailed below) and optical rotation (AA-1000; Optical Activity, Cambridge, UK) with samples in methanol solution (c in g ml^{-1}). Monomers were purified prior to use [17] to remove inhibitors. Combustion analyses were performed by Mikrokemi (Uppsala, Sweden).

2.2. Dipeptide syntheses

Dipeptides were synthesized [18] by the coupling of the appropriate enantiomers of N-acetylphenylalanine and tryptophan methyl ester in the presence of N,N'-dicyclohexylcarbodiimide and 1-hydroxybenzotriazole. The products were purified by preparative TLC [Merck 5717 plates, chloroform–methanol (95:5) as eluent] followed by recrystallization from dry ethanol. Spectroscopic characterization of these materials has been described previously [13]. N-Ac–L-Phe–L-Trp–OMe (**1**), $[\alpha]_D^{20} = +11°$ (c = 0.010); N-Ac–D-Phe–D-Trp–OMe (**2**), $[\alpha]_D^{20} = -10°$ ($c = 0.010$).

2.3. Polymer preparation

Imprinted and blank polymers were prepared and characterized as described previously [13]. A mixture of N-Ac–L-Phe–L-Trp–OMe (**1**) (2.00 mmol), methacrylic acid (**4**) (5 equiv.) and ethylene glycol dimethacrylate (**5**) (30 equiv.) were dissolved in chloroform (redistilled, 16 ml) in a screw-capped borosilicate glass reaction vial. The mixture was treated with 2,2'-azobis(2,4-dimethylvaleronitile) (125 mg) then sonicated (3 min) to ensure total dissolution of reactants. After cooling to 0°C, the reaction mixture was sparged with dry nitrogen (7 min), then sealed and incubated at 45°C for 18 h. The resultant bulk polymer was ground in a Retsch Model RM0 mechanical mortar (Haan, Germany) and wet sieved (water and ethanol) through a 25-μm mesh filter. The material of ≤ 25 μm was sedimented (4×30 min) in acetone (400 ml). The MIP was packed (acetone, 300 bar) into stainless-steel HPLC columns (150×4.6 mm I.D.) and washed with methanol–acetic acid (7:3) for 18 h at 1.0 ml min^{-1}.

2.4. Polymer analysis

HPLC measurements were conducted on an LKB system consisting of two Model 2150 pumps, a Model 2152 gradient controller and a Model 2151 variable-wavelength detector coupled to a Waters WISP Model 710B autoinjector and interfaced with a Shimadzu C-R3A Chromatopac integrator–recorder. Analyses were run at flow-rates of 1.0 ml min^{-1} with detection at 260 nm. Capacity factors (k') were determined from $k' = (v - v_0)/v_0$, where v is the retention volume of a given species and v_0 is the void volume (determined by injection of acetone). Effective enantioseparation factors (α') were calculated from the relationship $\alpha' = k'_1/k'_2$, where k'_1 and k'_2 are the capacity factors of two individual species, 1 and 2, where 1 is the most retained species.

3. Results

The *anti*-N-Ac–L-Phe–L-Trp–OMe MIP was prepared [13] utilizing MAA (**3**) as the functional monomer, which is capable of acting as both a hydrogen bond donor and acceptor with the imprint species (Fig. 3). The bulk polymer was processed to render it suitable for use as a CSP for HPLC, packed into HPLC columns, then washed exhaustively under acidic conditions to remove residual imprint species. Combustion analysis data indicated a nitrogen content, in washed and dried polymer samples, consistent with extraction of $\geq 95\%$ of the print species. It was assumed that any residual print molecule was inaccessible to the bulk solvent.

The MIP's capacity for resolution of the imprint species (**1**) from its stereoisomer, N-Ac–D-Phe–D-Trp–OMe (**2**) was examined (Table 1) using pure acetonitrile and acetonitrile–water mixtures containing acetic acid. The relative insolubility of the dipeptides in aqueous mixtures

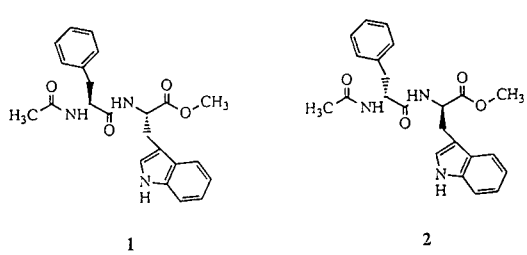

1 2

Fig. 3. Structure of the peptides separated.

Table 1
N-Ac-Phe-Trp-OMe enantiomeric recognition by the *anti*-N-Ac-L-Phe-L-Trp-OMe (**1**) MIP

Water (%, v/v)	k'_{DD} (**2**)	k'_{LL} (**1**)	α'
0	2.6	8.0	3.30
2	1.5	2.0	1.33
5	1.6	1.8	1.13
8	1.1	1.2	1.02

Chromatographic capacity factors (k') and *effective* separation factors (α') for the separation of LL-(**1**) and DD-(**2**) N-Ac-Phe-Trp-OMe (15 μg of dipeptide were injected in each run) using acetonitrile-based buffer systems.

precluded more than an 8% water content being used in the eluent. The acidic modifier was incorporated in the eluent mixtures to maintain polymer carboxylic acid residues in their protonated form and so preclude ion–dipole interactions between the polymer carboxylate moieties and the analytes. This was manifested as a sharpening of peak shape (reduction in tailing) corresponding to a reduction in non-specific binding modes. Analysis using a "blank" polymer, one prepared in the absence of the imprint species, afforded no evidence of stereo-differentiation in any instance. Solvent frontal analysis [19] (Table 2) demonstrates the enantiomer-dependent dissociation constants (k_{diss}) for **1** and **2** and provides estimates of the number of binding site populations for each enantiomer.

4. Discussion

Highly enantioselective separations have recently been reported utilising an *anti*-N-Ac-L-Phe-L-Trp-OMe MIP [13]. In organic media (chloroform), the selective recognition of the imprint species, the LL-dipeptide (**1**) relative to its DD-enantiomer (**2**), affords a clear baseline separation [Fig. 2, α-value 17.8 (note: 200 × 4.6 mm I.D. column and flow-rate 1.0 ml min^{-1}]. This is reflected in the different dissociation constants and binding site populations for the two enantiomers as determined by solvent frontal analysis (Table 2).

Table 2
Solvent frontal zone analysis of the *anti*-N-Ac-L-Trp-OMe MIP

Ligand	K_{diss} (mM)	L_t (μmol g^{-1})
LL-(**1**)	1.64 ± 0.07	20.8 ± 0.7
DD-(**2**)	2.00 ± 0.09	18.7 ± 0.7

Imprint species (**1**) and enantiomer (**2**) dissociation constants (K_{diss}) and site population densities (L_t) from solvent frontal analysis on MIP; flow-rates of 0.2 ml min^{-1} were employed.

Effective separation factors, α', calculated from the injection of individual enantiomers, rather than racemates, can be of use in evaluating stereoselective recognition in systems where small reproducible differences in retention times are present [13]. To investigate the role of water on recognition, an aqueous compatible organic solvent, acetonitrile, was selected. The α' values determined for **1** and **2** in acetonitrile were substantially lower than have previously been observed when using less polar eluents such as chloroform [13] (Table 1). On introduction of increasing amounts of water into the eluent mixture, a decrease in retention times was observed for both enantiomers, although most significantly for the imprint species. Enantiomeric differentiation, however, was still observed, on comparison of capacity factors and the calculation of *effective* separation factors.

The significance of hydrogen bonding has been enunciated in earlier discussions on recognition in MIP systems [3,4,16] and has been shown to be the major factor for recognition in MIPs prepared in non-polar solvents. The presence of water significantly lowers the effectiveness of the hydrogen bonding between ligand and receptor due to competition for hydrogen bond donor and acceptor sites. In accord with these facts, the effect of the presence of water was more pronounced in the case of the selective rebinding of the imprint species (**1**) than of its optical antipode (**2**). This suggests that the contribution of hydrophobic interactions for recognition in this system is mainly non-specific in character. This arises, we propose, from the fact that hydrophobic interactions [20], as distinct from Van der Waals complementarity [21], are not as significant in the defining of imprint recognition sites during the prearrangement phase of MIP prepa-

ration [4] in non-polar media. Thus, the hydrophobic binding of these ligands to the MIP is mainly non-specific, and applied similarly to both stereoisomers.

That **2** is partially recognized under conditions favourable to hydrogen bonding is a reflection of the heterogeneity of the receptor site population; analogy may possibly be drawn here to the recognition site distribution present in a polyclonal antibody sample. Undoubtedly, all sites do not possess the same array of interactions and steric complementarity, as illustrated by the broadness of the imprint species chromatographic response, the "primary recognition peak", hence conclusions reflect upon the nature of the "average site" rather than in terms of a uniform site population. Again, the dissociation constants determined for the imprint species (**1**) and its enantiomer (**2**) by solvent frontal zone analysis (Table 2) are indicative of the *average* specificity of the polymer receptor site population. This analysis afforded higher effective site populations for the print species (**1**) than for its optical antipode (**2**) in the MIP. Further, this technique provided a means of determining the binding site populations for the individual enantiomers. The difference between these two values provides a measure of the number of sites specific for **1**, *i.e.*, 2.1 μmol per gram (dry mass) of polymer under the conditions examined.

Molecular imprinting offers a means of constructing recognition sites of predetermined selectivity and is thus an extremely useful tool for the construction of "tailor-made" separation media and for the study of molecular recognition phenomena. The levels of enantioselectivity demonstrated by this *anti*-N-Ac-L-Phe-L-Trp-OMe MIP have previously only been observed for systems utilizing ionic interaction-facilitated recognition [3]. The dipeptide receptors have been used to investigate the influence of water on recognition in methacrylic acid–ethylene glycol dimethacrylate MIPs. Finally, MIP tailor-made recognition systems are now capable of racemate resolution on a par with the best commercially available CSPs and possess remarkable chemical and mechanical stability, as demonstrated by their repeated use, in many hundreds of runs, over several months.

Acknowledgements

The authors acknowledge the generous financial assistance of Norsk Hydro A/S and the Swedish Research Council for Engineering Sciences (TFR). IAN is most grateful to Wenner-Gren Centre-Foundation for Scientific Research (Stockholm, Sweden) for a travel award.

References

[1] K. Mosbach, *Trends Biochem. Sci.*, 19 (1994) 9.
[2] R. Arshady and K. Mosbach, *Makromol. Chem.*, 182 (1981) 687.
[3] L.I. Andersson, I.A. Nicholls and K. Mosbach, in G. Street (Editor), *Highly Selective Separation in Biotechnology*, Blackie, London, 1994, Ch. 9, p. 206.
[4] I.A. Nicholls, *Adv. Mol. Cel Biol.*, in press.
[5] G. Vlatakis, L.I. Andersson, R. Müller and K. Mosbach, *Nature (London)*, 361 (1993) 645.
[6] J. Matsui, I.A. Nicholls and K. Mosbach, *Angew. Chem., Int. Ed. Engl.*, submitted for publication.
[7] R. Müller, L.I. Andersson and K. Mosbach, *Makromol. Chem., Rapid Commun.*, 14 (1993) 637.
[8] J.V. Beach and K.J. Shea, *J. Am. Chem. Soc.*, 116 (1994) 379.
[9] D.K. Robinson and K. Mosbach, *J. Chem. Soc., Chem. Commun.*, (1989) 969.
[10] K. Mosbach, I.A. Nicholls and O. Ramström, *Swed. Pat. Appl.*, 9203914-0 (1992).
[11] S.E. Byström, A. Börje and B. Åkermark, *J. Am. Chem. Soc.*, 115 (1993) 2081.
[12] E. Hedborg, F. Winquist, I. Lundström, L.I. Andersson and K. Mosbach, *Sensors Actuators A*, 37–38 (1993) 796.
[13] O. Ramström, I.A. Nicholls and K. Mosbach, *Tetrahedron: Asymmetry*, 5 (1994) 649.
[14] L. Fischer, R. Müller, B. Ekberg and K. Mosbach, *J. Am. Chem. Soc.*, 113 (1991) 9358.
[15] M. Kempe and K. Mosbach, *J. Chromatogr. A*, 664 (1994) 276.
[16] B. Sellergren, M. Lepistö and K. Mosbach, *J. Am. Chem. Soc.*, 110 (1988) 5853.
[17] D.D. Perrin and W.L.F. Armarego, *Purification of Laboratory Chemicals*, Pergamon Press, Oxford, 3rd ed., 1988.
[18] M. Bodanszky and A. Bodanszky, *The Practice of Peptide Synthesis*, Springer, Berlin, 1984.
[19] M. Kempe and K. Mosbach, *Anal. Lett.*, 24 (1991) 1137.
[20] C. Tanford, *The Hydrophobic Effect Formation of Micelles and Biological Membranes*, Wiley, New York, 2nd ed., 1980.
[21] D.H. Williams, J.P.L. Cox, A.J. Doig, M. Gardner, U. Gerhard, P.T. Kaye, A.R. Lal, I.A. Nicholls, C.J. Salter and R.C. Mitchell, *J. Am. Chem. Soc.*, 113 (1991) 7020.

PUBLICATION SCHEDULE FOR THE 1995 SUBSCRIPTION

Journal of Chromatography A and *Journal of Chromatography B: Biomedical Applications*

MONTH	1994	J 1995	F 1995	M 1995	
Journal of Chromatography A	Vols. 683–688	689/1 689/2 690/1 690/2	691/1 + 2 692/1 + 2 693/1 693/2	694/1 694/2	The publication schedule for further issues will be published later.
Bibliography Section				713/1	
Journal of Chromatography B: Biomedical Applications		663/1 663/2	664/1 664/2	665/1 665/2	

INFORMATION FOR AUTHORS

(Detailed *Instructions to Authors* were published in *J. Chromatogr. A*, Vol. 657, pp. 463–469. A free reprint can be obtained by application to the publisher, Elsevier Science B.V., P.O. Box 330, 1000 AH Amsterdam, Netherlands.)

Types of Contributions. The following types of papers are published: Regular research papers (full-length papers), Review articles, Short Communications and Discussions. Short Communications are usually descriptions of short investigations, or they can report minor technical improvements of previously published procedures; they reflect the same quality of research as full-length papers, but should preferably not exceed five printed pages. Discussions (one or two pages) should explain, amplify, correct or otherwise comment substantively upon an article recently published in the journal. For Review articles, see inside front cover under Submission of Papers.

Submission. Every paper must be accompanied by a letter from the senior author, stating that he/she is submitting the paper for publication in the *Journal of Chromatography A* or *B*.

Manuscripts. Manuscripts should be typed in **double spacing** on consecutively numbered pages of uniform size. The manuscript should be preceded by a sheet of manuscript paper carrying the title of the paper and the name and full postal address of the person to whom the proofs are to be sent. As a rule, papers should be divided into sections, headed by a caption (*e.g.*, Abstract, Introduction, Experimental, Results, Discussion, etc.). All illustrations, photographs, tables, etc., should be on separate sheets.

Abstract. All articles should have an abstract of 50–100 words which clearly and briefly indicates what is new, different and significant. No references should be given.

Introduction. Every paper must have a concise introduction mentioning what has been done before on the topic described, and stating clearly what is new in the paper now submitted.

Experimental conditions should preferably be given on a *separate* sheet, headed "Conditions". These conditions will, if appropriate, be printed in a block, directly following the heading "Experimental".

Illustrations. The figures should be submitted in a form suitable for reproduction, drawn in Indian ink on drawing or tracing paper. Each illustration should have a caption, all the *captions* being typed (with double spacing) together on a *separate sheet*. If structures are given in the text, the original drawings should be provided. Coloured illustrations are reproduced at the author's expense, the cost being determined by the number of pages and by the number of colours needed. The written permission of the author and publisher must be obtained for the use of any figure already published. Its source must be indicated in the legend.

References. References should be numbered in the order in which they are cited in the text, and listed in numerical sequence on a separate sheet at the end of the article. Please check a recent issue for the layout of the reference list. Abbreviations for the titles of journals should follow the system used by *Chemical Abstracts*. Articles not yet published should be given as "in press" (journal should be specified), "submitted for publication" (journal should be specified), "in preparation" or "personal communication".

Vols. 1–651 of the *Journal of Chromatography*; *Journal of Chromatography, Biomedical Applications* and *Journal of Chromatography, Symposium Volumes* should be cited as *J. Chromatogr.* From Vol. 652 on, *Journal of Chromatography A* (incl. Symposium Volumes) should be cited as *J. Chromatogr. A* and *Journal of Chromatography B: Biomedical Applications* as *J. Chromatogr. B*.

Dispatch. Before sending the manuscript to the Editor please check that the envelope contains four copies of the paper complete with references, captions and figures. One of the sets of figures must be the originals suitable for direct reproduction. Please also ensure that permission to publish has been obtained from your institute.

Proofs. One set of proofs will be sent to the author to be carefully checked for printer's errors. Corrections must be restricted to instances in which the proof is at variance with the manuscript.

Reprints. Fifty reprints will be supplied free of charge. Additional reprints can be ordered by the authors. An order form containing price quotations will be sent to the authors together with the proofs of their article.

The right investment now

pays off big at collection time

Here are five fraction collectors that give you big advantages for your special HPLC or prep LC projects.

All save bench space with high density tube arrangement and minimal unused area. Important fractions are easy to find because they're in lift-off racks with straight rows. Collect in any 12 to 18 mm diameter tubes, or even 28 mm scintillation vials. Foxy® models also use microcollection trays and unlimited-volume remote containers.

You can program fraction size by time, drops, or directly in milliliters when using a Wiz® peristaltic pump. Isco LC systems put peaks in their own tubes, accurately detecting them by slope, level, or time windows.

To learn more about Isco's innovative, coldroom-proof fraction collectors and LC systems, call (800)228-4250. Outside the U.S.A. contact your distributor, or fax Isco U.S.A. (402)464-0318.

ISCO

• **Australia:** Australian Chromatography Co. • **Austria:** Neuber
• **Benelux:** Beun-de Ronde, B.V. • **Canada:** Canberra-Packard Canada, Ltd.
• **Denmark:** Mikrolab Aarhus • **Finland:** Ordior Oy Analytical
• **France:** Ets. Roucaire S.A. • **Germany:** Axel Semrau GmbH & Co.
• **Italy:** AlfaTech S.R.L. • **Japan:** Astech Corporation
• **Korea:** I WOO Scientific Corp. • **Norway:** Dipl. Ing. Houm a.s.
• **Portugal:** Emilio de Azevedo Campos • **Spain:** Izasa S.A.
• **Sweden:** SpectroChrom AB • **Switzerland:** Instrumenten-Gesellschaft AG
• **UK:** Jones Chromatography Ltd.

USA: Isco, Inc., P.O. Box 5347, Lincoln, NE 68505

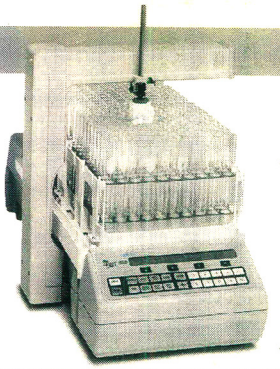

Foxy® 200

Foxy X-Y format provides sophisticated collection patterns to get the most out of your HPLC.

Foxy 200 is our smartest, highest capacity fraction collector; it controls valves and pumps to automate your entire system.

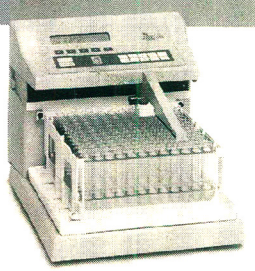

Foxy Jr.

Newest Isco smart fraction collector holds 144 tubes but fits anywhere in a crowded lab or coldroom.

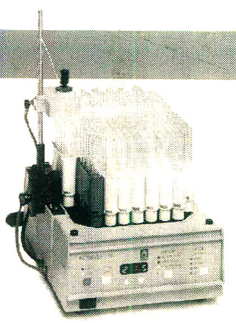

Retriever® 500

Retrievers have linear rack motion - they won't run you around in circles.

Budget Retriever 500 is the smallest collector that accommodates big tubes.

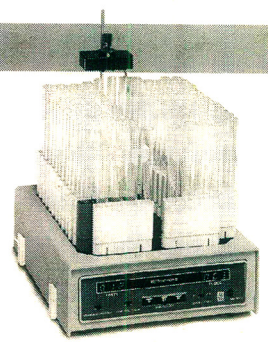

Retriever II

This classic fraction collector holds 174 tubes in a square foot.

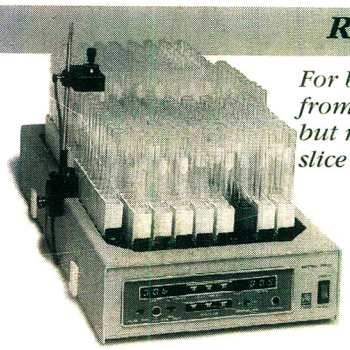

Retriever IV

For big jobs. Holds 9 liters from up to 10 columns, but needs only a 32 cm slice of your bench.